On the Implementation of Global Real-Time Schedulers*

Björn B. Brandenburg and James H. Anderson
Department of Computer Science, University of North Carolina at Chapel Hill

Abstract

An empirical study of implementation tradeoffs (choice of ready queue implementation, quantum-driven vs. event-driven scheduling, and interrupt handling strategy) affecting global real-time schedulers, and in particular global EDF, is presented. This study, conducted using UNC's Linux-based LITMUS$^{\mathrm{RT}}$ on Sun's Niagara platform, suggests that implementation tradeoffs can impact schedulability as profoundly as scheduling-theoretic tradeoffs. For most of the considered workloads, implementation scalability proved to not be a key limitation of global EDF on the considered platform. Further, a combination of a parallel heap, event-driven scheduling, and dedicated interrupt handling performed best for most workloads.

1 Introduction

The advent of multicore systems has resulted in renewed interest in real-time multiprocessor scheduling algorithms. In work on this topic, scheduling-theoretic issues have received the greatest attention. By comparison, only little attention has been devoted to the *actual implementation* of such algorithms within real OSs on real hardware, and consequently, only little is known about how implementation tradeoffs impact schedulability. This is surprising, as it is well established that such tradeoffs play a crucial role in real-time performance on uniprocessors [16].

In light of recent algorithmic research, a particularly relevant case in point is global scheduling algorithms, which use a single shared ready queue. Very little guidance can be found in the literature concerning how to *best* implement such algorithms. Should ready queues be implemented as lists or heaps? Should sequential queues with coarse-grained locking or parallel data structures be used? Should the scheduler rely on periodic timer ticks or follow an event-driven approach? On the surface, it may seem that any of these choices are viable. However, is this really true?

In this paper, we present an evaluation of these and other implementation tradeoffs as they arise in the implementation of a *global earliest-deadline-first* (G-EDF) scheduler. We show that different implementation choices—all seemingly plausible "in theory"—can have dramatically different effects on real-time schedulability.

Prior work. This is the third in a series of papers by our group investigating fundamental questions concerning the viability of supporting sporadic real-time workloads on SMP and multicore platforms *under consideration of real-world overheads*. To facilitate this line of research, our research group developed a Linux extension called LITMUS$^{\mathrm{RT}}$ (**LI**nux **T**estbed for **MU**ltiprocessor **S**cheduling in **R**eal-**T**ime systems), which allows different (multiprocessor) scheduling algorithms to be implemented as plugin components [9, 13]. To the best of our knowledge, LITMUS$^{\mathrm{RT}}$ is the only (published) real-time OS in which global real-time schedulers are supported.

In the initial study [9], Calandrino *et al.* evaluated several well-known multiprocessor real-time scheduling algorithms on a four-processor 2.7 GHz Intel Xeon SMP (not multicore) platform. On this platform with *few and fast processors*, *relatively large, private L2 caches*, and *fast memory*, each tested algorithm was found to be a viable choice in some of the tested scenarios, and global algorithms excelled at supporting soft real-time workloads.

In the second study [7], Brandenburg *et al.* explored the relative *scalability* of different real-time schedulers as implemented in LITMUS$^{\mathrm{RT}}$. To do so, they ported LITMUS$^{\mathrm{RT}}$ to a radically different, and much larger, multicore platform: a Sun Niagara with 32 logical processors, each with an effective speed well below 1 GHz.[1] On this platform with *many slow processors*, *a relatively small, shared L2 cache*, and *slower memory*, a decrease in the competitiveness of G-EDF was noted, especially in the presence of many tasks. Clearly, this study had uncovered scalability limitations *in that particular implementation of* G-EDF, but does this imply that G-EDF-like algorithms are a "lost cause" on large multicore platforms? Could the G-EDF plugin be significantly improved, and, in terms of schedulability, would overhead reductions even matter?

Contributions. Both preceding studies [7, 9] considered several scheduling algorithms, but only one implementation per algorithm. In stark contrast, the study presented in this paper considers only one scheduling algorithm, G-

*Work supported by IBM, Intel, and Sun Corps., NSF grants CCF 0541056, and CNS 0615197, and ARO grant W911NF-06-1-0425.

[1] Eight 1.2 GHz cores with four hardware threads per core. A core's cycles are distributed among its hardware threads in a round-robin manner.

EDF, but twelve possible realizations of it, seven of which were implemented and evaluated in LITMUS$^{\mathrm{RT}}$. The objective of this study was to determine which of these implementations are viable. Our major findings are as follows: **(i)** implementation tradeoffs in global real-time schedulers such as G-EDF affect schedulability *significantly*; **(ii)** there is a "best" way to implement G-EDF that outperforms other approaches in most cases; **(iii)** on our Niagara, which is a large multicore platform by today's standards, implementation scalability is *not* a key limitation of G-EDF.

In the sections that follow, we provide needed background (Sec. 2), describe the various implementation alternatives that we considered (Sec. 3), present our study and findings (Sec. 4), and conclude (Sec. 5).

2 Background

We consider the problem of scheduling n independent[2] real-time tasks $T_1, \ldots, T_n$ on m identical processors $P_1, \ldots, P_m$. LITMUS$^{\mathrm{RT}}$ supports *sporadic tasks* with *implicit deadlines*,[3] wherein each task T_i is specified by its *worst-case execution time* e_i and its *period* p_i. The j^{th} job of T_i, denoted T_i^j and released at r_i^j (where $r_i^j \geq r_i^{j-1} + p_i$), should complete by its *deadline* $r_i^j + p_i$, otherwise it is *tardy*. Note that T_i^j being tardy does not alter r_i^{j+1}, but T_i^{j+1} cannot execute until T_i^j completes (tasks are sequential). T_i's *utilization* u_i is given by e_i/p_i; the sum $\sum_{i=1}^{n} u_i \leq m$ denotes the system's *total utilization*. A job is *pending* after its release until it completes.

To avoid confusion, we use the term "task" exclusively to refer to sporadic tasks, and use the term "process" when discussing OS implementation issues. In LITMUS$^{\mathrm{RT}}$, sporadic tasks are implemented as processes, and jobs are an accounting abstraction managed by the kernel.

Scheduling. A *hard* real-time (HRT) system is considered to be *schedulable* iff it can be shown that no job is ever tardy. A *soft* real-time (SRT) system is considered (in this paper) to be *schedulable* iff it can be shown that tardiness is bounded.

We investigate G-EDF as a representative of the class of global, preemptive, priority-driven, work-conserving scheduling policies, *i.e.*, all processors use a single shared *ready queue* sorted by non-decreasing deadlines and jobs (but not necessarily the OS!) can be preempted.

There are two fundamental ways to realize schedulers (see [10, 16] for overviews):

S1 *event-driven scheduling*, wherein a job is scheduled *immediately* when there are fewer than m higher-priority[4] jobs pending (either upon release or when a higher-priority job completes);

S2 *quantum-driven scheduling*, wherein real-time jobs are only scheduled at integer multiples of a *scheduling quantum* Q (hence, a job may be delayed by up to Q time units before being scheduled).

Both approaches are illustrated in Fig. 1. Inset (a) shows an ideal, event-driven schedule of three jobs on two processors. The schedule is "ideal" in the sense that releases and completions are processed immediately (and require no processing time), and preemptions are enacted in zero time across processors. For example, at time 6.5, T_1^x is released on P_1 and immediately scheduled on P_2 without incurring any delay. While unattainable in practice, most G-EDF analysis assumes ideal, event-driven scheduling.

The same scenario in the ideal, quantum-driven case for $Q = 1$ is shown in Fig. 1(b). Again, the system does not incur overhead, but jobs are delayed when awaiting the next quantum boundary. For example, T_3^z is released at $r_3^z = 1.5$, but not scheduled until time 2 when the next quantum starts. Similarly, the preemption on P_2 due to T_1^x's arrival at $r_1^x = 6.5$ does not take place until the start of the next quantum at time 7. Note that some quanta may only be partially used if jobs complete during a quantum (*e.g.*, P_1 is partially idle for this reason in quantum [8,9)). Analysis assuming ideal, event-driven G-EDF scheduling can be applied to ideal, quantum-driven scheduling by shortening periods by one quantum (to account for delays upon release) and by rounding execution times up to a quantum multiple (to account for partially-idle quanta) [10].

Historically, OSs have employed quantum-driven (or hybrid) designs to facilitate time keeping and reduce overhead [16]; the first version of LITMUS$^{\mathrm{RT}}$ also followed this approach [9]. The current version supports both event-driven and quantum-driven scheduling.

LITMUS$^{\mathrm{RT}}$. As mentioned in Sec. 1, LITMUS$^{\mathrm{RT}}$ is a real-time extension of the Linux kernel.[5] The stock Linux scheduler is organized as a static hierarchy of *scheduling classes*: when the scheduler is invoked, each scheduling class is queried in top-down order until a process to service next is found. LITMUS$^{\mathrm{RT}}$ installs its scheduling class at the top of the hierarchy and hence overrides the stock Linux scheduler whenever real-time work is pending.

The LITMUS$^{\mathrm{RT}}$ scheduling class does not implement any particular scheduling policy; instead it allows scheduling policy plugins to be activated at runtime. All scheduling decisions are delegated by invoking plugin-provided *event*

[2] While LITMUS$^{\mathrm{RT}}$ supports real-time synchronization among tasks, this study is focussed on synchronization requirements *within* the kernel.

[3] We expect the reader to be familiar with the sporadic task model; see [10, 16] for an overview and relevant citations.

[4] We assume that priorities are unique, *i.e.*, that deadline ties are broken arbitrarily but consistently. LITMUS$^{\mathrm{RT}}$ tie-breaks by lower task index.

[5] The current base version is Linux 2.6.24. We plan to rebase LITMUS$^{\mathrm{RT}}$ to the latest kernel version in the near future.

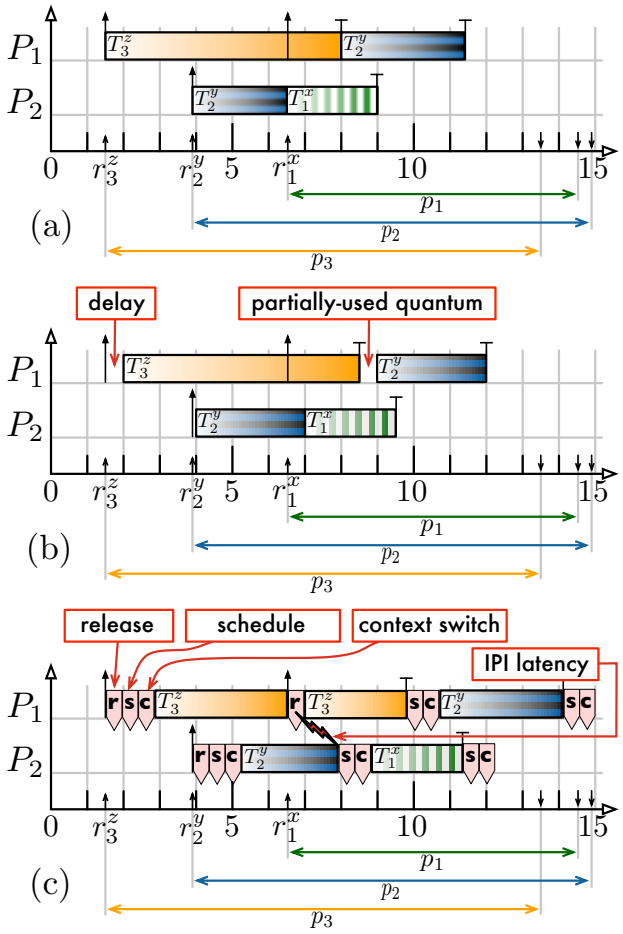

Figure 1: Example G-EDF schedules of three jobs (T_1^x, T_2^y, T_3^z), where $(e_i, p_i)_i = (2.5, 8)_1, (6, 11)_2, (6.5, 12)_3$, on two processors ($P_1$, P_2) illustrating delays introduced by quantum-driven scheduling and system overheads. Large up-arrows denote interrupts, small up-arrows denote job releases, down-arrows denote job deadlines, T-shaped arrows denote job completions, and wedged boxes denote overheads (which are magnified for clarity). Job releases occur at $r_3^z = 1.5$, $r_2^y = 3.9$, and $r_1^x = 6.5$. **(a)** Event-driven schedule and **(b)** quantum-driven schedule without overheads. **(c)** Event-driven schedule with overheads.

handlers, prominently among them the tick and schedule handlers. The tick handler is invoked, on each processor, each time a periodic timer interrupt occurs; this allows quantum-driven polices to be implemented. A typical tick period (*i.e.*, quantum length) is one millisecond. The schedule handler is invoked when traversing the scheduler class hierarchy to select the next process. Note that a quantum-driven plugin will make use of both the tick and schedule handlers—the tick handler assigns processes to processors and determines if preemptions are required, and the schedule handler, on each processor, enacts the desired changes. This split is required because the schedule handler, for technical reasons, *must* execute on the processor on which the preemption is to occur. In LITMUS$^{\mathrm{RT}}$'s event-driven plugins, the tick handler is usually only used for bookkeeping and overrun detection.

As a boot-time option, LITMUS$^{\mathrm{RT}}$ supports both *aligned* and *staggered quanta*. With aligned quanta, the per-processor tick interrupts are programmed to occur at the same time on all processors, whereas with staggered quanta, tick interrupts are spread out evenly across a full quantum. Staggering quanta may reduce bus and lock contention, but also delays job completions by up to $Q \cdot \frac{(m-1)}{m}$ time units. This can be accounted for by shortening periods.

Overheads. In LITMUS$^{\mathrm{RT}}$, processes are delayed by six major sources of overhead, four of which are illustrated in Fig. 1(c). *Release overhead* is incurred while handling an interrupt that releases a real-time job and involves making the corresponding process available for execution. If a preemption is required, then *scheduling overhead* is incurred while selecting the next process to execute and re-queueing the previously-scheduled process (which may be a background or the idle process). *Context-switching overhead* is incurred while switching the execution stack and processor registers. All three overhead sources occur in sequence in Fig. 1(c) on processor P_1 at time 1.5 when T_3^z is released, and again on P_2 at time 3.9 when T_2^y is released. A different scenario occurs at time 6.5 when T_1^x is released on P_1: release overhead is incurred on P_1 (where the interrupt occurred), but scheduling and context-switching overhead are incurred on P_2 where T_1^x preempts T_2^y (the lowest-priority scheduled job). To initiate the required preemption, P_1 sends an *inter-processor interrupt* (IPI) to P_2. Since IPIs are not delivered instantly, T_1^x incurs additional *IPI latency*.

For the sake of clarity, Fig. 1(c) omits the two additional sources of overhead. At the beginning of each quantum, *tick overhead* is incurred *on each processor* when the periodic timer interrupt is handled. Note that tick overhead also occurs, but to a lesser extent, under purely event-driven plugins as the periodic tick can currently not be disabled in Linux (while a process is executing). *Preemption* and *migration overhead* account for any costs due to a loss of cache affinity. Preemption (resp., migration) overhead is incurred when a preempted job later resumes execution on the same (resp., a different) processor.

Analysis that assumes ideal (*i.e.*, overhead-free), event-driven scheduling can be applied to real, overhead-impacted systems by inflating per-task worst-case execution costs. Accounting for overheads that only occur exactly before or after a job is scheduled is trivial as they are, from an analysis point of view, equivalent to extended execution: each job causes scheduling and context-switching overhead exactly twice [16], and causes preemp-

tion/migration overhead at most once.[6] Similarly, a job's completion time may be delayed by IPI latency and its *own* release overhead.

However, accounting for release overhead due to *other* jobs and tick overhead is more problematic as their occurrence is interrupt-based and hence not subject to G-EDF scheduling [8]. For example, in Fig. 1(c), T_3^z is delayed by release overhead at time 6.5 due to T_1^x's release even though T_3^z has higher priority than T_1^x. As the techniques for multiprocessor interrupt accounting are somewhat involved, a detailed discussion is unfortunately beyond the scope of this paper; the interested reader is referred to [8].

Given the preceding discussion, we can now refine the focus of this paper: we seek to understand how differences in the implementation of global policy plugins affect runtime overheads, and hence, after accounting for overheads, real-time performance (in terms of "schedulability"—see Sec. 4).

3 Plugin Implementation

Conceptually, a global scheduling policy implementation consists of three main components: a *release queue* holds not yet released jobs; a one-to-one *processor mapping* associates each of the currently-scheduled jobs with a processor; and pending jobs that are not currently scheduled are kept, sorted by descending priority, in a shared *ready queue*. Since these components are shared by all processors, the way in which *synchronization* is provided strongly impacts overheads. Next, we briefly describe some implementation and synchronization choices for these components.

Release queue. A release queue is required for two reasons: time-driven tasks (*e.g.*, video display) require job releases to occur at particular times, and interrupt-driven tasks (*e.g.*, sensor data acquisition) may have jobs triggered "too early" after the last job release, *i.e.*, the minimum job separation may have to be enforced by the OS. In both cases, a job must be made available for execution at a future point in time. In a quantum-driven implementation, the release queue can be implemented as a priority queue or timer wheel [18] that is polled by the tick handler to transfer all jobs with release times in the preceding quantum to the ready queue. Alternatively, hardware timers can be programmed to trigger future job releases with interrupts if sufficiently high-resolution hardware timers are available.

As our test machines have such timers, LITMUS$^{\mathrm{RT}}$ follows the latter approach. However, instead of using a timer for every job, our implementation uses a timer per release time to avoid unnecessary overhead, *i.e.*, if multiple job releases coincide (*e.g.*, on a hyperperiod boundary), then only one timer interrupt is required. Efficient timer sharing is accomplished by looking up future release times in a hash table. As a side effect, timer sharing enables the use of mergeable queues (see below).

Processor mapping. Since scheduling and switching between processes takes time, the notion of when a job is "scheduled" is not clear-cut. For example, consider a scenario in which a job T_i^j is one of the m highest-priority jobs when released, but a higher-priority job T_k^l arrives before the context switch to T_i^j's implementing process is complete. Now suppose that a third job T_x^y with priority less than T_k^l's but higher than T_i^j's arrives concurrently on another processor. Which job is "scheduled?" Is a preemption required? Should an IPI be sent?

In our experience, relying on the OS's notion of whether a particular *process* is scheduled (*i.e.*, is its stack in use?) for assigning *jobs* to processors is both difficult and error-prone, and tends to lead to priority inversions due to unanticipated corner cases and race conditions.[7] Instead, in LITMUS$^{\mathrm{RT}}$, we use the processor mapping to split *job scheduling*, which is at the level of the sporadic model and is only concerned with assigning abstract jobs to abstract processors, from *process scheduling*, which is concerned with address spaces, stacks, register sets, and other hardware peculiarities.

This simplifies the real-time scheduling logic since any processor's job assignment can be updated on any processor by any event handler (in contrast to performing context switches, which can be only done in one specific code path on the target processor). Process scheduling is then reduced to tracking which process *should* be executing based on the current job-to-processor mapping; any delay in tracking is captured by the various overhead terms.

Since the most common operation involving the processor mapping is to check whether a preemption is required, which requires identifying the lowest-priority scheduled job, the processor mapping is realized as a min-heap with processors ordered by the priority of their assigned jobs (if any—idle processors have the lowest priority).

Ready queue. In earlier versions of LITMUS$^{\mathrm{RT}}$, ready queues were realized as ordered linked lists. Not surprisingly, this simple approach did not scale well, and binomial heaps were employed instead [7]. Binomial heaps were chosen since they, together with timer sharing, support releasing jobs with coinciding release times in $O(\log n)$ time by means of a queue-merge operation.

However, since a binomial heap is a sequential data structure, it suffers from two inherent weaknesses when used as a shared queue on a multiprocessor: first, all ac-

[6] Since jobs starting to execute do not have cache affinity, only the preempted job (if any) must be considered.

[7] This is especially true when jobs may self-suspend for short durations (due to blocking on semaphores or page faults, library loading, *etc.*). However, handling self-suspensions is beyond the scope of this paper.

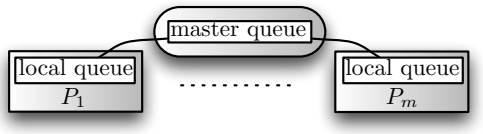

Figure 2: Illustration of hierarchical queues.

cesses must be synchronized through the use of a lock, which is likely to incur high contention; and, second, accesses are likely to cause significant cache-coherency traffic due to cache lines "bouncing" among processors.

To investigate the impact (if any) of these shortcomings, we consider two alternate priority-queue designs in this paper. With regard to lock contention, we implemented Hunt *et al.*'s concurrent heap [14, 15], which relies on fine-grained locking to increase parallelism. To address "cache line bouncing," we implemented a simple hierarchical priority queue that relies on (mostly) local per-processor queues to increase cache locality. The local queues contain the bulk of the jobs, and the global queue only consists of the highest-priority job on each processor (illustrated in Fig. 2). Under this scheme, insertion and merge operations are always performed on the cache-local queue, and an update of the global queue is only required if the highest-priority job changes in the local queue. However, removal of the highest-priority job from the global queue may require non-cache-local updates. Obviously, this algorithm is closely tied to the assumption that insertion and merge operations are evenly distributed across processors. (We used binomial heaps for both local and global queues.)

Another approach to avoiding lock contention is to employ *non-blocking* data structures, which allow accesses to occur concurrently (see [14] for an overview and relevant citations). We did not implement non-blocking priority queues for this study since, to the best of our knowledge, all such published algorithms only support bounded priority ranges (G-EDF requires unbounded priorities) or rely on problematic techniques such as multi-word compare-and-swap instructions (not supported by our hardware), frequent copying (excessive overheads), and probabilistic algorithms (ill-suited to real-time computing).

To summarize, the three ready-queue choices considered in this paper are:

- **R1** a sequential binomial heap (coarse-grained locking);
- **R2** Hunt *et al.*'s fine-grained heap [15];
- **R3** a simple, hierarchical "queue of queues" scheme (two-level locking with cache-local insertions).

Synchronization. In the latest publicly-available LITMUS$^{\mathrm{RT}}$ version (2008.2), implementation R1 is used. In this version, the processor mapping is protected by a lock that serves a dual purpose: it protects the (sequential) heap against concurrent updates, and it serves as the *linearization point* (see [14]) for the scheduler. Hence, it is acquired when the processor mapping itself is modified and whenever process state is observed or changed (*e.g.*, on process self-suspension, on job completions, and when comparing job priorities). This strategy also indirectly supports R1: all ready-queue accesses occur together with preemption checks, which require the processor mapping lock to be held.

However, to support R2 and R3, significant changes were required, as the processor mapping lock must be released before performing queue operations under these schemes. In making these changes, various complex race conditions had to be addressed. For example, both the ready queue and processor mapping must be locked to check whether a preemption is required. If a preemption is indeed required, then the processor mapping lock must be dropped before dequeuing the preempting job under R2 and R3. However, this allows the set of scheduled jobs to change while the preempting job is dequeued, which might lead to conflicts with other updates. To avoid this, the processor to be updated is temporarily removed from the processor mapping. Priorities are checked again upon re-insertion, otherwise, preemptions could be missed.

Ideally, the processor mapping lock should be held as little as possible to reduce contention. Unfortunately, the need to serialize (complex) process state updates makes a switch to fine-grained locking or non-blocking solutions non-trivial.

The release queue is also protected by a lock. However, contention for it is infrequent (it is only held briefly during job releases, after job completions, and possibly when a process resumes).

Interrupt handling. Two interrupt handling choices are considered in this paper:

- **I1** *global interrupt handling*, wherein each processor both handles interrupts and schedules jobs, and
- **I2** *dedicated interrupt handling*, wherein a single processor is reserved for interrupt processing [17].

By default, interrupts may occur on all processors in Linux. In fact, an even distribution of interrupts can help to improve throughput in non-real-time workloads. However, this implies that all real-time tasks are subject to release overhead (and delays by other interrupt sources, such as I/O devices). Since interrupt accounting can be severely pessimistic [8], it may be desirable to shield tasks from interrupts by dedicating a processor that does *not* serve tasks to handling job releases (and other interrupts).

While simple in concept, this approach can be difficult to implement if some hardware is only accessible from a particular processor. For example, in our test platform (see

Plugin	Ready Queue	Scheduling	Interrupts	Capacity
CQm	coarse-grained	quantum-driven	m	m
CEm	coarse-grained	event-driven	m	m
FEm	fine-grained [15]	event-driven	m	m
HEm	hierarchical	event-driven	m	m
CQ1	coarse-grained	quantum-driven	1	$m-1$
CE1	coarse-grained	event-driven	1	$m-1$
FE1	fine-grained [15]	event-driven	1	$m-1$

Table 1: Policy plugins evaluated in this paper. The letters of each plugin name refer to columns 2–4 in this table. An "Interrupts" value of 1 denotes the use of a dedicated interrupt processor. "Capacity" is the number of processors that schedule real-time tasks.

Sec. 4), each processor has a private, integrated hardware timer that is not accessible to other processors. This is resolved by sending IPIs to the dedicated processor to initiate the programming of hardware timers.

Implemented approaches. We implemented seven of the twelve possible combinations of choices S1, S2, R1–R3, I1, and I2 in LITMUS$^{\mathrm{RT}}$, as listed in Table 1. Under event-driven scheduling, we considered all three queue variants with global interrupt handling (CEm, FEm, and HEm), and coarse- and fine-grained queues with dedicated interrupt handling (CE1 and FE1). Hierarchical queues were not considered in combination with dedicated interrupt handling since they rely on insertions occurring on all processors. Only coarse-grained queues were considered under quantum-driven scheduling (CQm and CQ1) because quantum boundaries act as implicit barriers and ready queues are only accessed at quantum boundaries. Hence, parallel access would only yield minimal gains (if any).

4 Experiments

To evaluate the implemented approaches, we conducted extensive schedulability experiments under consideration of runtime overheads as incurred in LITMUS$^{\mathrm{RT}}$ on a Sun UltraSPARC T1 "Niagara" multicore platform. The Niagara is a 64-bit machine containing eight cores on one chip running at 1.2 GHz. Each core supports four hardware threads,[8] for a total of 32 logical processors. On-chip caches include a 16K (resp., 8K) four-way set associative L1 instruction (resp., data) cache per core, and a shared, unified 3 MB 12-way set associative L2 cache. Our test system is configured with 16 GB of off-chip main memory. In contrast to Sun's proposed Niagara-successor "Rock," our first-generation Niagara does not employ advanced cache-prefetching technology.

While the Niagara is clearly not an embedded systems processor, it is nonetheless an attractive platform for forward-looking real-time systems research. Its power-friendly combination of many simple and slow cores, predictable hardware multi-threading, and a small shared cache is likely indicative of future processor designs targeting computationally-demanding embedded systems.[9] Thus, we believe any limitations exposed on the enterprise-class Niagara today to be of value as guidance to future embedded system designs. However, note that specific results, as with all implementation-based studies, only apply directly to the tested configuration.

Next, we briefly discuss how we measured overheads, and then present our study in detail.

4.1 Runtime Overheads

We used the same methodology to determine overheads as in earlier LITMUS$^{\mathrm{RT}}$-based studies (*e.g.*, [7]). Runtime overheads were obtained by enabling aligned quanta and measuring the system's behavior for periodic task sets consisting of between 50 and 450 tasks in steps of 50. For each plugin and task-set size, we measured ten task sets generated randomly (with uniform light utilizations and moderate periods; see Sec. 4.2 below), for a total of 90 task sets per scheduling algorithm. Each task set was traced for 30 seconds. We repeated the same experiments with staggered quanta. In total, more than 100 GB of trace data and 640 million individual overhead measurements were obtained during more than ten hours of tracing. After removing outliers, we computed for each plugin average and worst-case overheads as a function of task set size (for both aligned and staggered quanta), which resulted in 20 graphs. Due to space constraints, we only discuss the three representative graphs shown in Fig. 3 here; all graphs and per-plugin overheads are provided in an extended version of this paper [6].

Fig. 3(a) shows average release overhead under staggered quanta. One can clearly distinguish between the quantum-driven plugins CQm and CQ1, which incur only very little, constant overhead, and the other event-driven plugins, which suffer the effects of increasing contention and ready-queue lengths. Releases encounter less contention in quantum-driven plugins because released jobs are placed in a temporary queue that is merged at the next quantum boundary by the tick handler [10]. Note that the FEm and FE1 plugins incur significantly higher release overhead than the CEm and CE1 plugins. This is likely due to Hunt *et al.*'s fine-grained heap not supporting efficient queue-merge operations (*i.e.*, merges require $O(n \log n)$ time), increased cache protocol traffic (as queue elements are being accessed concurrently), and frequent locking operations. Similar reasoning applies to the HEm plugin.

Fig. 3(b) shows average scheduling overhead under stag-

[8] The Niagara's hardware threads are real-time-friendly because each core distributes cycles in a round-robin manner—in the worst case, a hardware thread can utilize every fourth cycle.

[9] Similarly, 32-bit processors with L2 caches and speeds in excess of 100 MHz, once firmly associated with enterprise-class servers, are now routinely deployed in embedded systems.

gered quanta. Again, quantum-driven plugins incur only little overhead because staggering helps to avoid contention, and because jobs are assigned to processors in the tick, and not the schedule, handler. Staggering does not affect when event-driven plugins schedule, so contention remains high. Note that the FEm, FE1, and HEm plugins incur only a fraction of the CEm plugin's average scheduling overhead because the processor mapping lock is relinquished during queue operations. The trends are reversed in Fig. 3(c), which depicts average tick overhead under staggered quanta: event-driven plugins only perform bookkeeping activities in the tick handler and hence incur only little overhead, whereas the CQm and CQ1 curves reveal that job scheduling costs increase with the number of tasks.

We used monotonic piece-wise linear interpolation to derive upper-bounds for each plugin and each overhead as a function of task set size. These upper bounds were used in the schedulability experiments described next.

4.2 Experimental Setup

To assess schedulability trends, we generated random task sets (similarly to [7, 9]) using three period and six utilization distributions similar to those proposed by Baker [2], for a total of 18 scenarios. Task utilizations were distributed differently for each experiment using three uniform and three bimodal distributions. The ranges for the uniform distributions were [0.001, 0.1] (*light*), [0.1, 0.4] (*medium*), and [0.5, 0.9] (*heavy*). In the three bimodal distributions, utilizations were distributed uniformly over either [0.001, 0.5) or [0.5, 0.9] with respective probabilities of 8/9 and 1/9 (*light*), 6/9 and 3/9 (*medium*), and 4/9 and 5/9 (*heavy*). Similarly, we considered three uniform task period distributions with ranges $[3ms, 33ms]$ (*short*), $[10ms, 100ms]$ (*moderate*), and $[50ms, 250ms]$ (*long*). Note that all periods were chosen to be integral.

Task execution costs excluding overheads were calculated from periods and utilizations (and may be non-integral). Each task set was created by generating tasks until a specified cap on total utilization (that varied between 1 and 32) was reached and by then discarding the last-added task, thereby allowing some slack for overheads. Sampling points were chosen such that sampling density is high in areas where curves change rapidly. For each scenario and each sampling point, we generated 1,000 task sets, for a total of over 5.5 million task sets.

Schedulability tests. After a task system was generated, its schedulability under each of the plugins listed in Table 1 was tested as follows.

Prior to testing schedulability, we adjusted task parameters to account for overheads and quantum-driven scheduling as described in Sec. 2. Given Linux's roots as a general-purpose OS and our use of measured overheads (which are unlikely to capture true worst-case behavior), we interpret task execution costs in a way that is reasonable for a Linux-based system. Our main concern here (since this is not a paper on timing-analysis tools for determining execution costs) is to capture major differences in plugin implementations. Thus, in reality, we interpret "hard real-time" to mean deadlines should *almost never* be missed and "soft real-time" to mean that deadline tardiness *on average* remains bounded. Consequently, we assumed worst-case overheads and aligned quanta when testing HRT schedulability and average-case overheads and staggered quanta when testing SRT schedulability. Additionally, we also considered

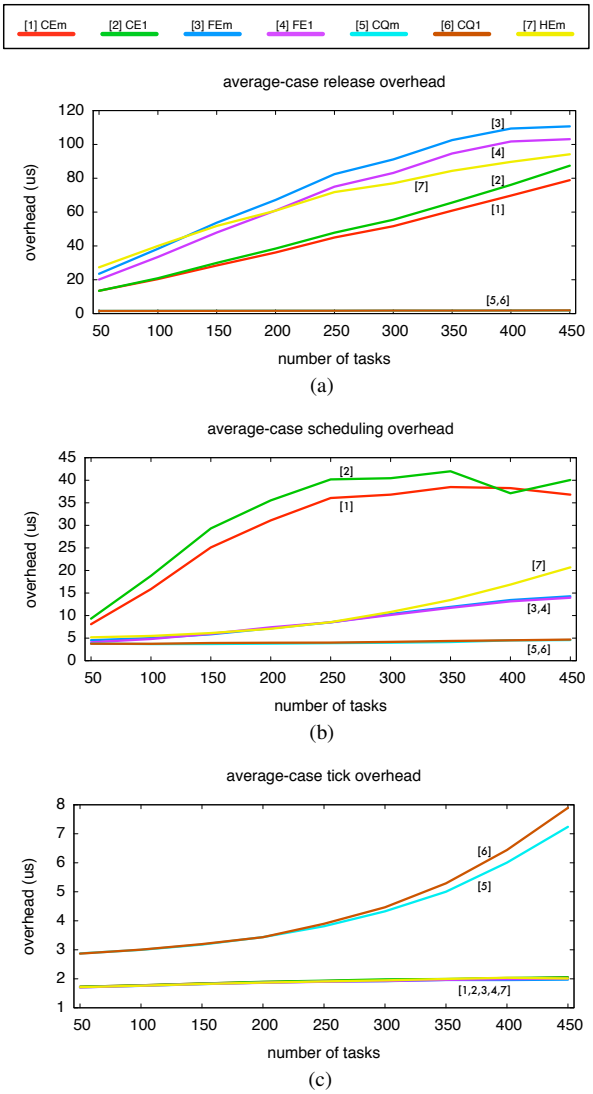

Figure 3: Sample average-case overhead measurements. The graphs show average-case measured per-event execution time (in microseconds) as a function of task set size (under staggered quanta). **(a)** Release overhead. **(b)** Scheduling overhead. **(c)** Tick overhead. Note the different scale of the Y-axis in each inset. The complete worst-case and average-case overhead measurements are reported in [6].

HRT schedulability under the CQm and CQ1 plugins assuming worst-case overheads under staggered quanta; those two cases are denoted S-CQm and S-CQ1 respectively.[10] (Note that periods are not modified in the SRT case under quantum-driven scheduling as quantum-based delays cause only constant tardiness.)

We used all major published sufficient (but not necessary) HRT schedulability tests for G-EDF [1, 3, 4, 5, 12] and deemed a task set schedulable if it passed at least one of these five tests. A notable exception is the light uniform utilization distribution: we had to disable Baruah's test [3] for these scenarios since it failed to terminate in reasonable time due to the large number of tasks involved and the test's pseudo-polynomial nature.[11]

For SRT schedulability, since G-EDF can guarantee bounded deadline tardiness if the system is not overloaded [11], only a check that total utilization (after inflation for overheads) is at most m is required.

4.3 Results

HRT schedulability results for the moderate period distribution are shown in Fig. 4. The first column of the figure (insets (a,c,e)) gives results for the three uniform distributions (light, medium, heavy) and the second column (insets (b,d,f)) gives results for the three bimodal distributions. The plots indicate the fraction of the generated task sets each plugin successfully scheduled, as a function of total utilization. Schedulability results for the SRT case are shown in Fig. 5, which is organized similarly to Fig. 4. Due to space constraints, other graphs (over 300) are not shown here but can be found in the extended version of the paper. [6]

The results clearly show that differences in plugin implementation and hence overheads can have a very significant impact on real-time performance. For example, in Fig. 5(a), the best-performing plugin (FE1) supports task systems of total utilization up to 26, whereas the worst-performing plugin (HEm) fails even for task systems with total utilization less than 5! Note that it is nearly impossible to predict such outcomes purely based on theoretical considerations. In fact, our initial assumption was that a hierarchical queue design should outperform any dedicated-interrupt scheme—surprisingly, the HEm plugin was consistently among the poorest-performing plugins. We will discuss this and other notable trends next.

Dedicated vs. global interrupt handling. The most remarkable trend is the superiority of dedicated interrupt handling. In virtually all tested scenarios, global interrupt handling is inferior in spite of its nominally larger system capacity, *i.e.*, CE1 outperforms CEm, FE1 outperforms FEm, and CQ1 outperforms CQm, in both the HRT and SRT cases, and usually by a significant margin (*e.g.*, Figs. 4(a,c,e) and 5(a–f)). Differences are less pronounced if periods are long (since overheads are proportionally small), or if performance is indistinguishably bad (*e.g.*, CQm/CQ1 for short periods).

Long periods with heavy, uniform utilizations is the only scenario in which global interrupt handling is consistently preferable—here, tasks are so few in number, periods so long, and overheads so low that release overhead becomes insignificant and system capacity is the deciding factor.

Staggered vs. aligned quanta. Another clear trend in the HRT results is that staggered quanta are generally preferable to aligned quanta, *i.e.*, S-CQm outperforms CQm and S-CQ1 outperforms CQ1 in most cases, as can be seen in Figs. 4(a,c,e). (This matches similar trends observed in the preceding scalability study [7].) Again, differences are less pronounced for high task count / short period scenarios (both plugins perform equally badly), and for heavy bimodal utilization / long periods (both plugins nearly reach the ideal G-EDF limit). As S-CQ1 is generally preferable to S-CQm (see above), the S-CQ1 plugin is the best-performing quantum-driven plugin in this study.

Quantum- vs. event-driven scheduling. In the HRT case, event-driven scheduling is mostly preferable. CQm outperforms CEm only in the cases of uniform light utilizations and moderate or long periods (Fig. 4(a)), and medium utilizations with moderate periods (Fig. 4(c)). Similarly, CQ1 is never preferable to CE1, though differences are small for some scenarios involving long periods. Further, S-CQm and S-CQ1 are inferior to CEm except for scenarios with many light tasks and long periods. Surprisingly, the trend is reversed in the SRT case. In Fig. 5, CQm is clearly preferable to CEm in every inset but (b), and similar findings apply to the case of short periods, too (but CEm remains superior for long periods). However, CE1 remains preferable to CQ1 for all period and utilization distributions, even in the SRT case. Hence, event-driven scheduling was found in our experiments to be the better choice for both HRT and SRT if (and only if) used in conjunction with a dedicated interrupt processor.

Fine-grained vs. coarse-grained vs. hierarchical queues. As mentioned above, hierarchical queues exhibited surprisingly poor performance in our experiments. In fact, in the SRT case, HEm is the worst-performing plugin in all tested scenarios, as can be readily seen in Fig. 5. It performs better in the HRT case (*e.g.*, Fig. 4(f)), but it is never preferable to the CEm plugin.

The FEm plugin is never preferable to the CEm plugin

[10] Only quantum-driven plugins were considered under staggering in the HRT case since neither overheads nor analysis are affected significantly by staggering under event-driven plugins.

[11] Regular compute jobs on UNC's research cluster are limited to 48 hours runtime. With, on average, over 150 sampling points per graph, 1,000 task sets per point, and 10 curves per HRT graph, *all five* HRT G-EDF schedulability tests must complete in ≈ 0.11 seconds per task set.

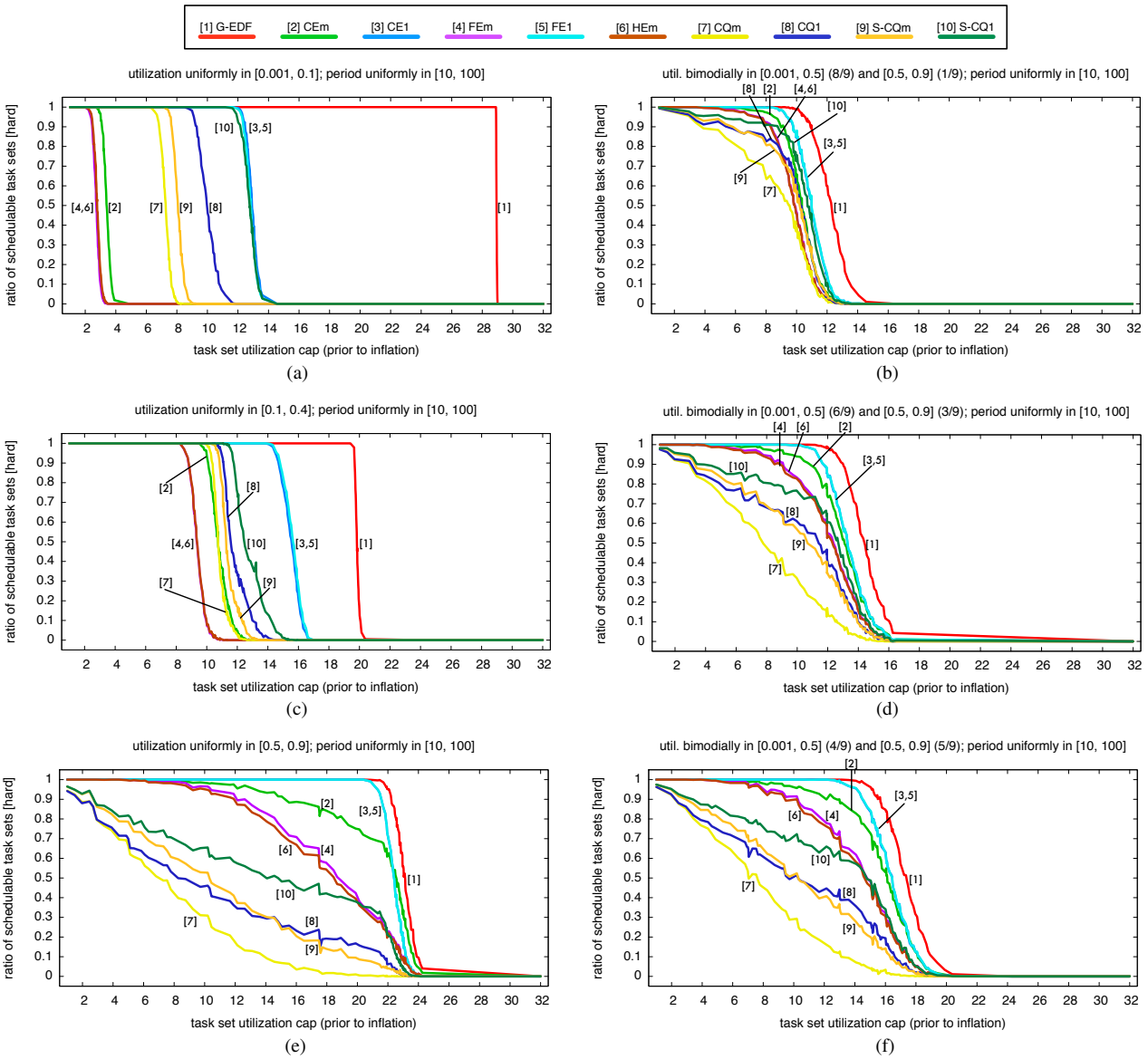

Figure 4: HRT schedulability (the fraction of generated task systems deemed HRT schedulable) for moderate periods as a function of task system utilization cap for various utilization distributions. **(a)** Uniform light. **(c)** Uniform medium. **(e)** Uniform heavy. **(b)** Bimodal light. **(d)** Bimodal medium. **(f)** Bimodal heavy. In each graph, the curve labeled "[1] G-EDF" indicates schedulability under an ideal event-driven system (zero overheads), the curves numbered 2–8 correspond to the plugins listed in Table 1, and the curves 9–10 correspond to curves 7–8 but assume staggered quanta. Recall from Sec. 4.2 that a task set is HRT schedulable if it can be shown to have *zero* tardiness under assumption of *worst-case* overheads.

in any of the tested scenarios. In the SRT case, the CEm plugin performs better by a significant margin in all scenarios, as is apparent in Fig. 5; in the HRT case, the difference is often less pronounced but still clear (*e.g.*, Fig. 4(f)). Interestingly, the FE1 plugin is very competitive—it never performs worse than the CE1 plugin, and in some scenarios marginally better. This highlights two points: reducing contention for the processor mapping lock is highly beneficial, but the lack of an efficient queue-merge operation penalizes FEm (see Fig. 3(a)).

Further observations. Overall, the FE1 and CE1 plugins performed best in our study. Their performance is promising in two regards. First, the disappointing G-EDF performance in [7] was shown here to be a correctable implementation artifact. Second, in many scenarios, FE1 and CE1 performance comes close to the limit imposed by current G-EDF schedulability analysis (*e.g.*, Fig. 4(b,d,e,f), and similarly Fig. 5(b–f)). This indicates that G-EDF in particular, and global scheduling in general, can be implemented efficiently on current multicore platforms.

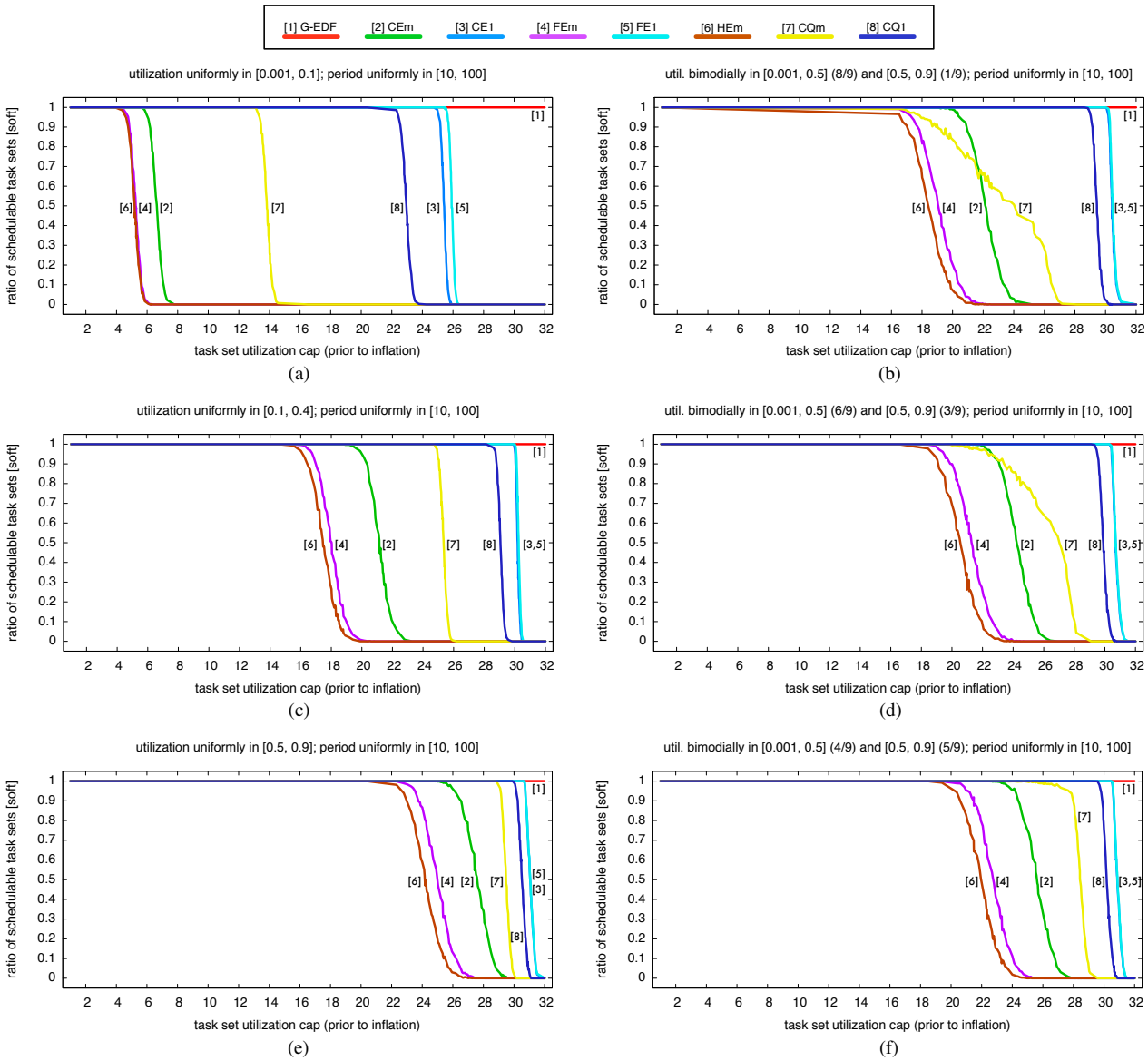

Figure 5: SRT schedulability (the fraction of generated task systems deemed SRT schedulable) for moderate periods as a function of task system utilization cap for various utilization distributions. **(a)** Uniform light. **(c)** Uniform medium. **(e)** Uniform heavy. **(b)** Bimodal light. **(d)** Bimodal medium. **(f)** Bimodal heavy. In each graph, the curve labeled "[1] G-EDF" indicates schedulability under an ideal event-driven system (zero overheads) and the curves numbered 2–8 correspond to the plugins listed in Table 1. Recall from Sec. 4.2 that a task set is SRT schedulable if it can be shown to have *bounded* tardiness under assumption of *average-case* overheads.

5 Conclusion

In this work, we explored several alternatives for implementing global real-time schedulers and conducted a large-scale implementation-based study. Our results indicate that implementation tradeoffs can impact schedulability as profoundly as scheduling-theoretic tradeoffs. On our test platform, the best performance was achieved in the majority of the tested scenarios by the combination of Hunt *et al.*'s fine-grained heap [15], event-driven scheduling, and dedicated interrupt handling (the FE1 plugin). In contrast, the simple hierarchical queue (the HEm plugin) performed significantly below expectation—this partially due to cache-affinity issues, which warrant further investigation generally. Additionally, we found that the scalability of global real-time scheduler implementations *is not the key limiting factor* in supporting sporadic real-time workloads on our—fairly large—multicore platform unless task counts are extremely high or most periods short.

Prior studies. Given this paper's conclusion that implementation choices can have a strong impact on schedulability, it is appropriate to re-visit the conclusions of the two preceding studies [7, 9]. Since the first study [9] was con-

ducted on a radically different hardware platform, its results are not directly comparable to this paper. However, its main conclusion that "for each tested scheme, scenarios exist in which it is a viable choice" [9] remains valid even with the improvements presented in this paper—while significantly better, G-EDF's HRT performance is still limited by pessimistic schedulability tests and contention under high task counts. Further, note that dedicated interrupt handling is likely less competitive on platforms with fewer processors.

The second study [7] is Niagara-based and hence readily comparable; the interested reader is encouraged to compare Figs. 4 and 5 above with Figs. 2 and 3 in [7]. As expected, the observation that "for global approaches, scheduling overheads are greatly impacted by the manner in which run queues are implemented" [7], which motivated the present study, has been validated. The relative performance of CQm vs. S-CQm (best seen in [6]) also confirms that "quantum-staggering can be very effective in reducing [preemption and migration] costs" [7], but the benefit observed in this study is less pronounced than that in [7].

Further, as noted above, G-EDF's HRT performance is still limited, and hence the observation that "for HRT workloads on the Niagara, [staggered Pfair] and [partitioned EDF] are generally the most effective approaches" [7] remains unchanged. However, [7] also stated that, "for SRT workloads on the Niagara, there is no single best overall algorithm, although [staggered Pfair] and [clustered EDF] seem to be less susceptible to pathological scenarios than the other tested algorithms." This statement has to be amended to include G-EDF, as the FE1 plugin is consistently among the top-performing choices (with regard to those in [7]) in the SRT case.

Future work. Our implementation efforts and the results of our study reveal four major open problems. From an analysis point of view, the two most-pressing concerns are the need for improved G-EDF HRT schedulability tests (ideally, both in accuracy and runtime requirements) and improved interrupt accounting techniques. Implementation-wise, better parallel priority queues that can be implemented efficiently in a kernel environment clearly have great potential. Ideally, such queues should efficiently support queue-merge operations. Further, fine-grained locking (or even non-blocking synchronization) for the processor mapping could improve performance in the presence of many tasks significantly. Especially with regard to the latter, we would like to investigate whether the hardware transactional memory support in Sun's proposed "Rock" processor can improve global schedulers.

References

[1] T. Baker. Multiprocessor EDF and deadline monotonic schedulability analysis. *Proceedings of the 24th IEEE Real-Time Systems Symposium*, pages 120–129, 2003.

[2] T. Baker. A comparison of global and partitioned EDF schedulability tests for multiprocessors. Technical Report TR-051101, Florida State University, 2005.

[3] S. Baruah. Techniques for multiprocessor global schedulability analysis. In *Proceedings of the 28th IEEE Real-Time Systems Symposium*, pages 119–128, 2007.

[4] M. Bertogna, M. Cirinei, and G. Lipari. Improved schedulability analysis of EDF on multiprocessor platforms. In *Proceedings of the 17th Euromicro Conference on Real-Time Systems*, pages 209–218, 2005.

[5] M. Bertogna, M. Cirinei, and G. Lipari. Schedulability analysis of global scheduling algorithms on multiprocessor platforms. *IEEE Transactions on Parallel and Distributed Systems*, 20(4):553–566, 2009.

[6] B. Brandenburg and J. Anderson. On the implementation of global real-time schedulers. Extended version of this paper. Available at http://www.cs.unc.edu/˜anderson/ papers.html.

[7] B. Brandenburg, J. Calandrino, and J. Anderson. On the scalability of real-time scheduling algorithms on multicore platforms: A case study. In *Proceedings of the 29th IEEE Real-Time Systems Symposium*, pages 157–169, 2008.

[8] B. Brandenburg, H. Leontyev, and J. Anderson. Accounting for interrupts in multiprocessor real-time systems. In *Proceedings of the 15th International Conference on Embedded and Real-Time Computing Systems and Applications*, pages 273–283, 2009.

[9] J. Calandrino, H. Leontyev, A. Block, U. Devi, and J. Anderson. LITMUS$^{\mathrm{RT}}$: A testbed for empirically comparing real-time multiprocessor schedulers. In *Proceedings of the 27th IEEE Real-Time Systems Symposium*, pages 111–123, 2006.

[10] U. Devi. *Soft Real-Time Scheduling on Multiprocessors*. PhD thesis, University of North Carolina, Chapel Hill, North Carolina, 2006.

[11] U. Devi and J. Anderson. Tardiness bounds under global EDF scheduling on a multiprocessor. *Real-Time Systems*, 38(2):133–189, 2008.

[12] J. Goossens, S. Funk, and S. Baruah. Priority-driven scheduling of periodic task systems on multiprocessors. *Real-Time Systems*, 25(2-3):187–205, 2003.

[13] UNC Real-Time Group. LITMUS$^{\mathrm{RT}}$ homepage. http://www.cs.unc.edu/ ˜anderson/litmus-rt.

[14] M. Herlihy and N. Shavit. *The Art of Multiprocessor Programming*. Morgan Kaufmann Publishers, 2008.

[15] G. Hunt, M. Michael, S. Parthasarathy, and M. Scott. An efficient algorithm for concurrent priority queue heaps. *Information Processing Letters*, 60(3):151–157, 1996.

[16] J. Liu. *Real-Time Systems*. Prentice Hall, 2000.

[17] J.A. Stankovic and K. Ramamritham. The Spring kernel: A new paradigm for real-time systems. *IEEE Software*, 8(3):62–72, 1991.

[18] G. Varghese and T. Lauck. Hashed and hierarchical timing wheels: data structures for the efficient implementation of a timer facility. *SIGOPS Operating Systems Review*, 21(5):25–38, 1987.

A Overheads

This appendix provides all measured overheads, in both visual (Sec. A.1) and tabular (Sec. A.2) forms. See Sec. 2 for an explanation of the various overheads. Note that *timer re-arming overhead* is conceptually part of the scheduling overhead, but is measured separately in LITMUS$^{\mathrm{RT}}$ due to implementation reasons (total scheduling overhead is composed of the overhead before and after a context switch, and timers are re-armed *after* performing a context switch for locking reasons). Further, note that IPI latency was not measured for quantum-driven plugins (CQm, CQ1) since such plugins do not employ IPIs. Please see [7] for a detailed discussion the measurement and filtering methodology used in LITMUS$^{\mathrm{RT}}$-based studies.

A.1 Overhead Graphs

The following 12 figures depict measured average and worst-case overheads under each of the implemented plugins, under both aligned and staggered quanta. Note that the Y-axis scale varies between graphs. The overhead graphs are organized as follows.

- Fig. 6 shows measured scheduling overhead under aligned quanta. Fig. 6 corresponds to Table. 2.
- Fig. 7 shows measured timer re-arming overhead under aligned quanta. Fig. 7 corresponds to Table. 3.
- Fig. 8 shows measured tick overhead under aligned quanta. Fig. 8 corresponds to Table. 4.
- Fig. 9 shows measured context-switching overhead under aligned quanta. Fig. 9 corresponds to Table. 5.
- Fig. 10 shows measured release overhead under aligned quanta. Fig. 10 corresponds to Table. 6.
- Fig. 11 shows measured IPI latency under aligned quanta. Fig. 11 corresponds to Table. 7.
- Fig. 12 shows measured scheduling overhead under staggered quanta. Fig. 12 corresponds to Table. 8.
- Fig. 13 shows measured timer re-arming overhead under staggered quanta. Fig. 13 corresponds to Table. 9.
- Fig. 14 shows measured tick overhead under staggered quanta. Fig. 14 corresponds to Table. 10.
- Fig. 15 shows measured context-switching overhead under staggered quanta. Fig. 15 corresponds to Table. 11.
- Fig. 16 shows measured release overhead under staggered quanta. Fig. 16 corresponds to Table. 12.
- Fig. 17 shows measured IPI latency under staggered quanta. Fig. 17 corresponds to Table. 13.

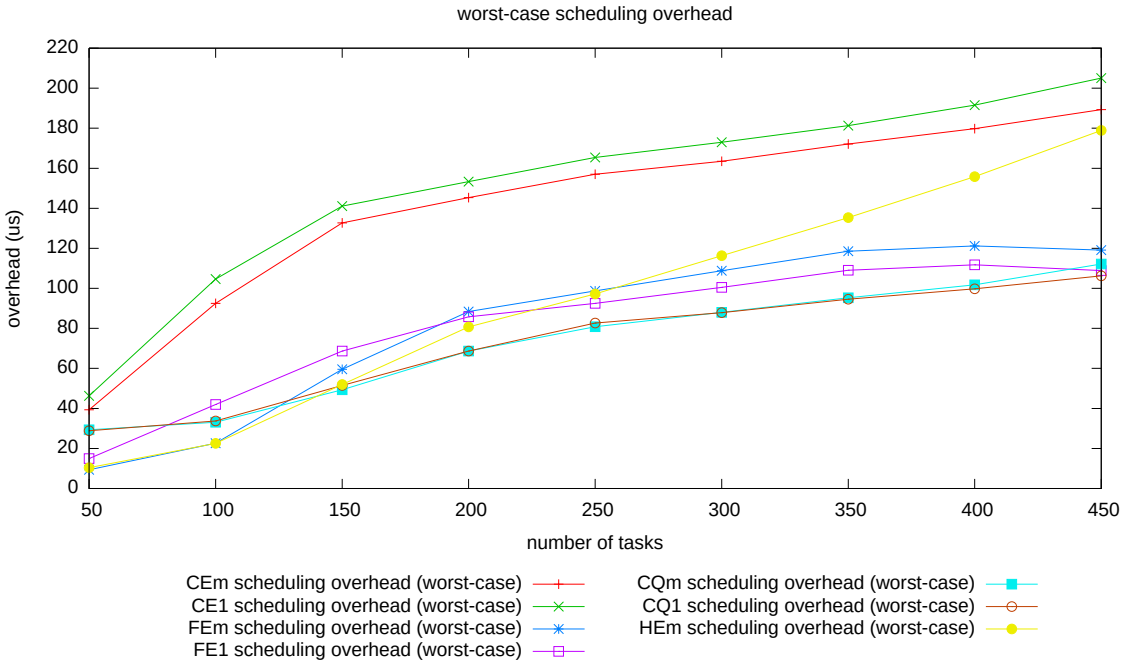

(a)

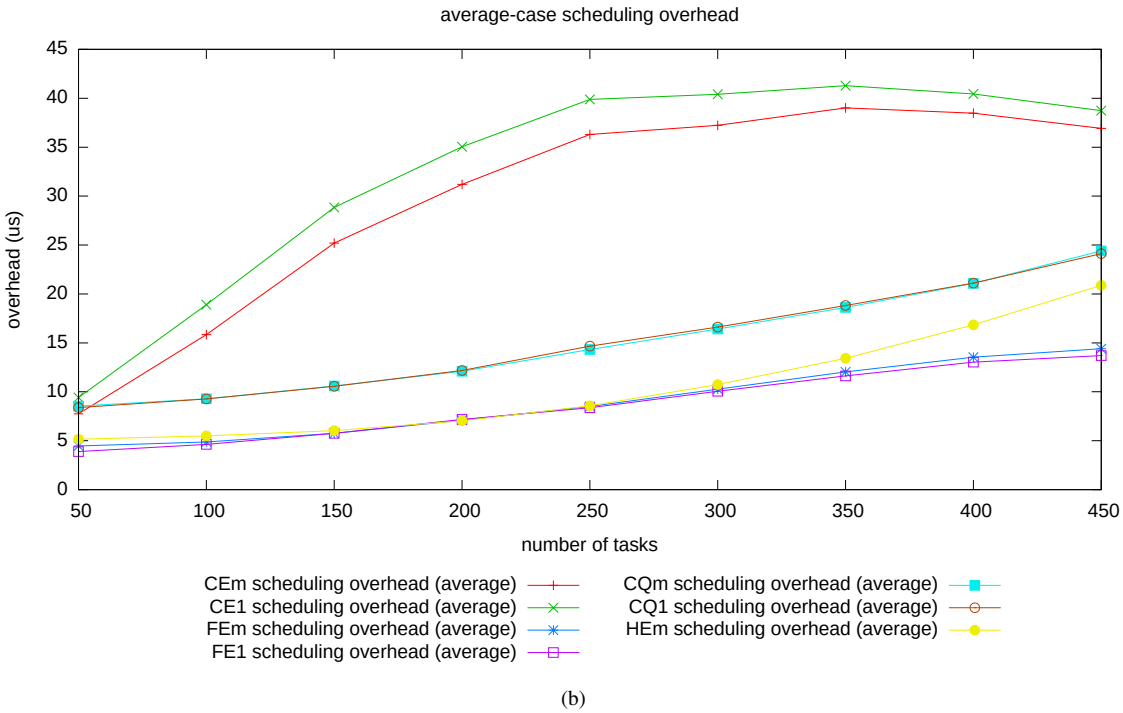

(b)

Figure 6: Measured scheduling overhead under aligned quanta. **(a)** Measured worst case. **(b)** Measured average case. Note that outliers were filtered before computing worst- and average-case values, as described in [7].

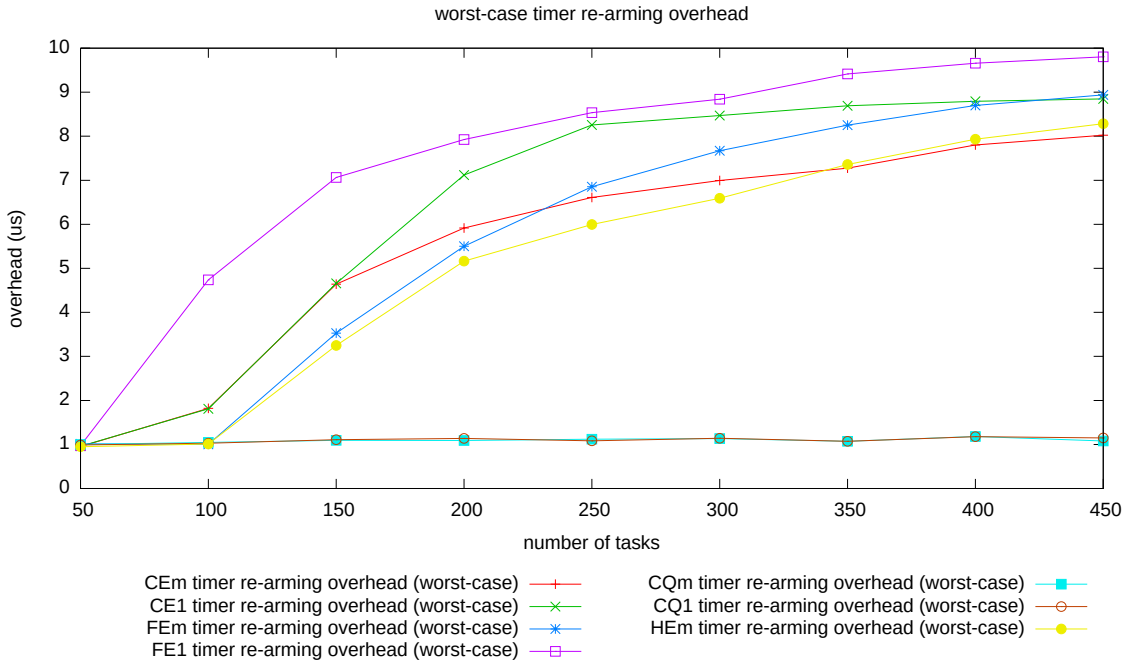

(a)

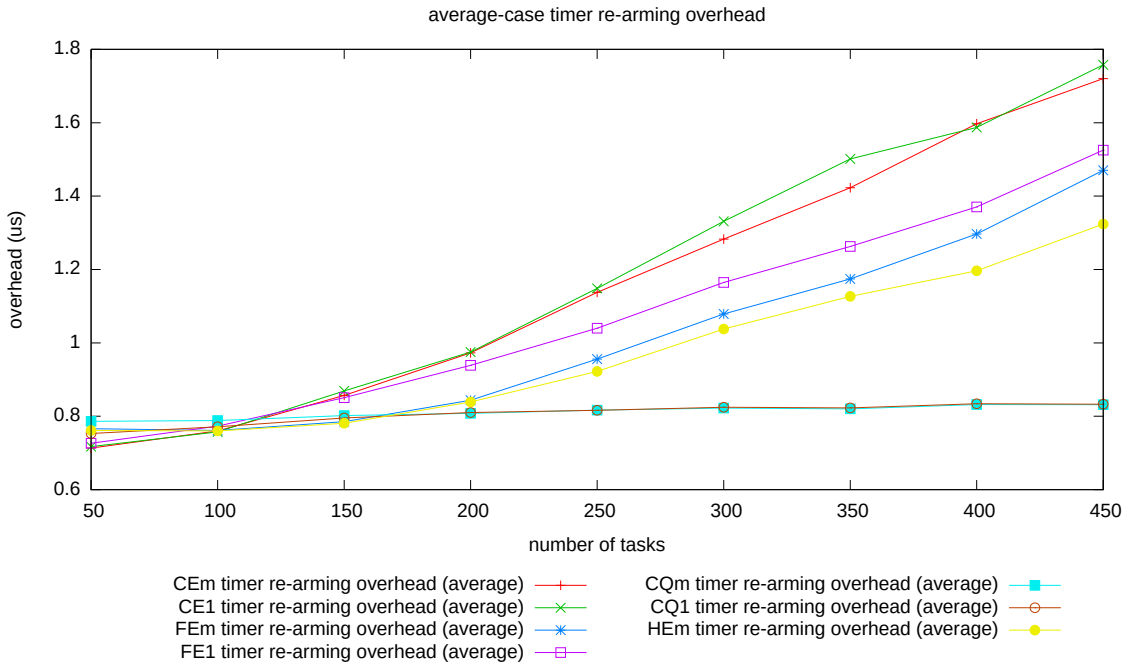

(b)

Figure 7: Measured timer re-arming overhead under aligned quanta. **(a)** Measured worst case. **(b)** Measured average case. Note that outliers were filtered before computing worst- and average-case values, as described in [7].

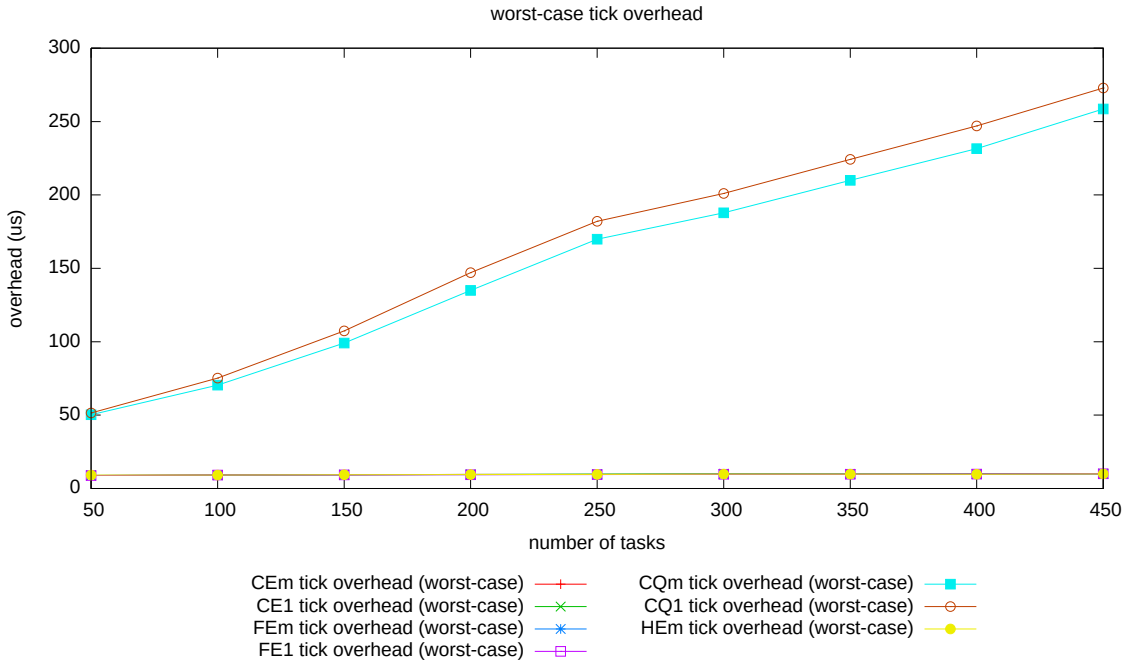

(a)

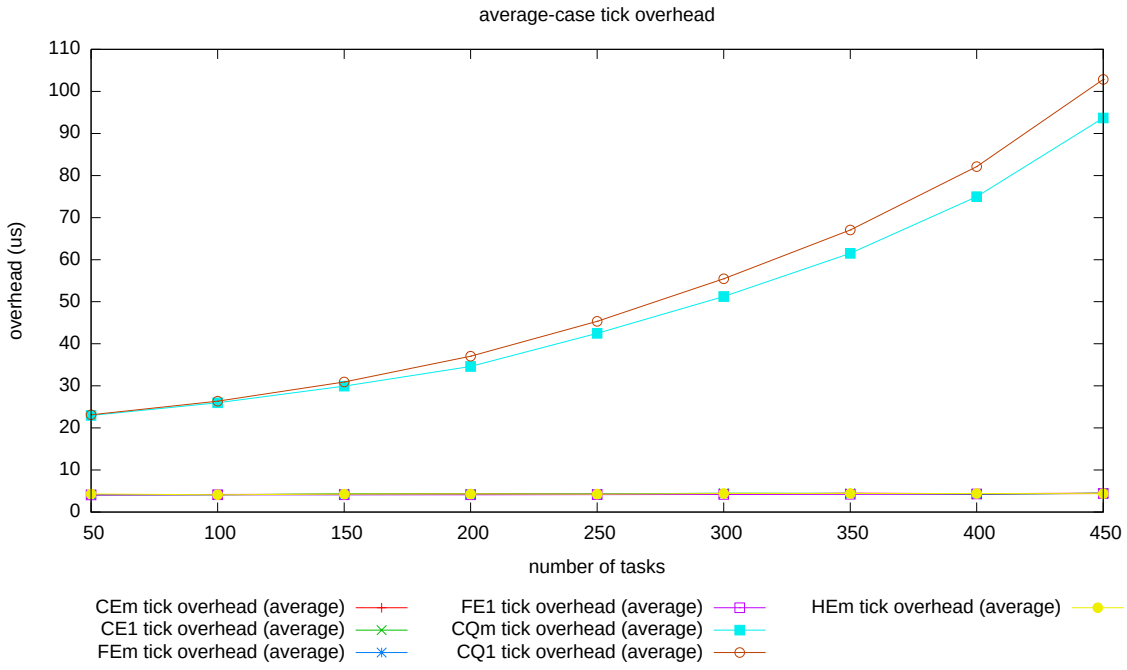

(b)

Figure 8: Measured tick overhead under aligned quanta. **(a)** Measured worst case. **(b)** Measured average case. Note that outliers were filtered before computing worst- and average-case values, as described in [7].

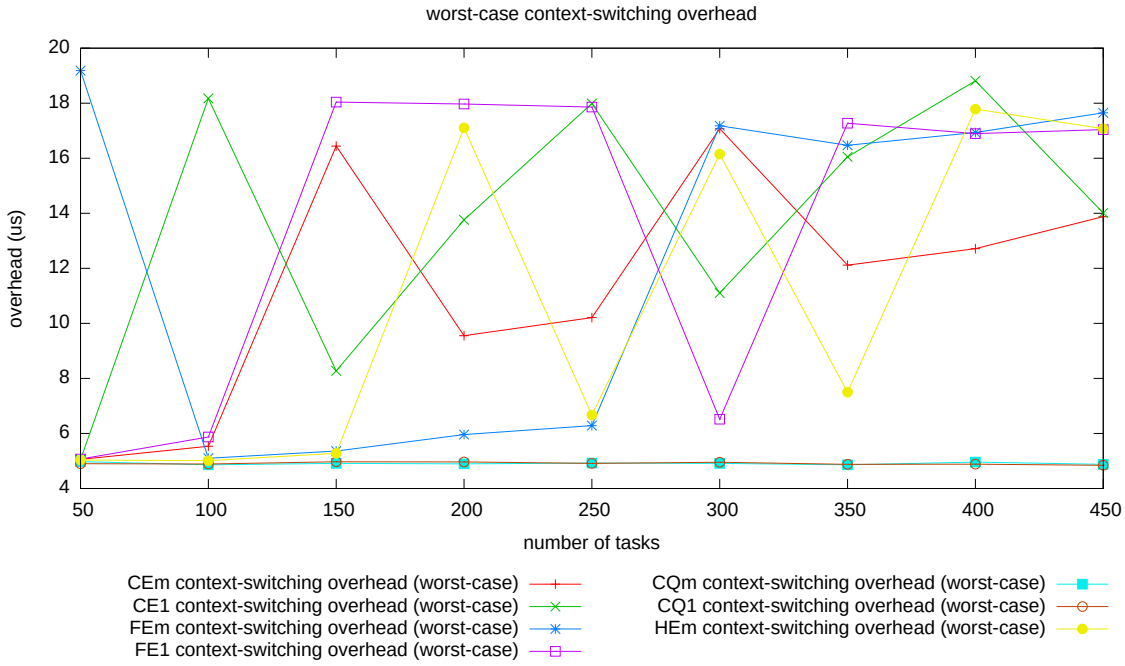

(a)

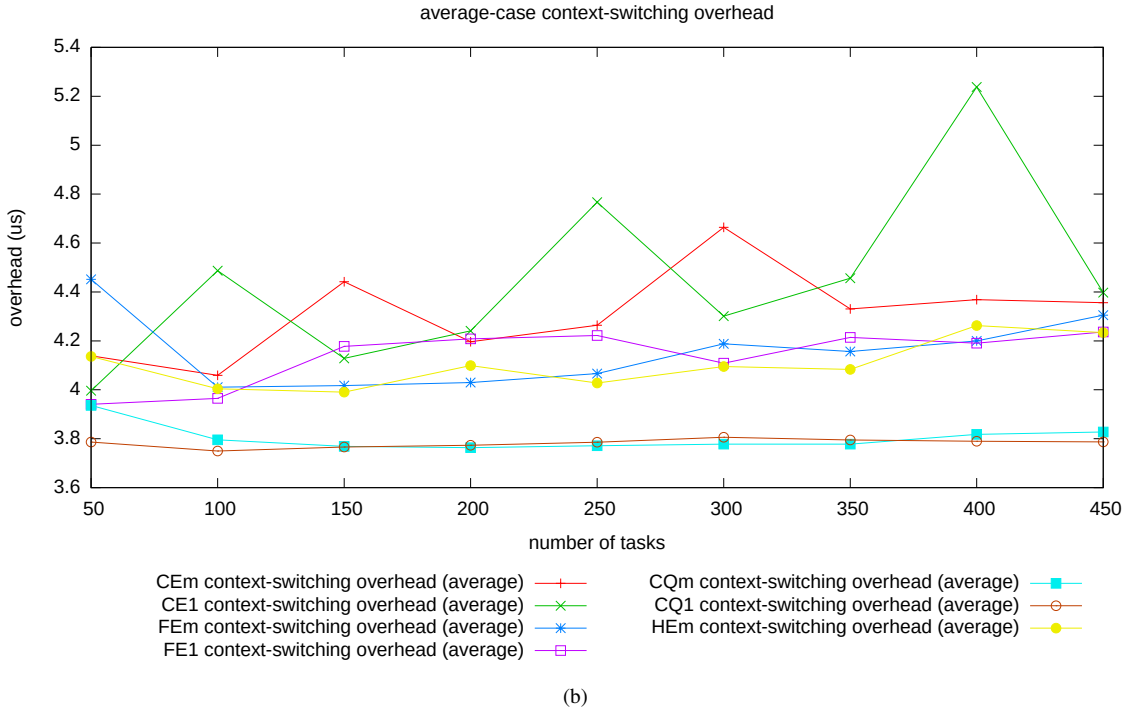

(b)

Figure 9: Measured context-switching overhead under aligned quanta. **(a)** Measured worst case. **(b)** Measured average case. Note that outliers were filtered before computing worst- and average-case values, as described in [7].

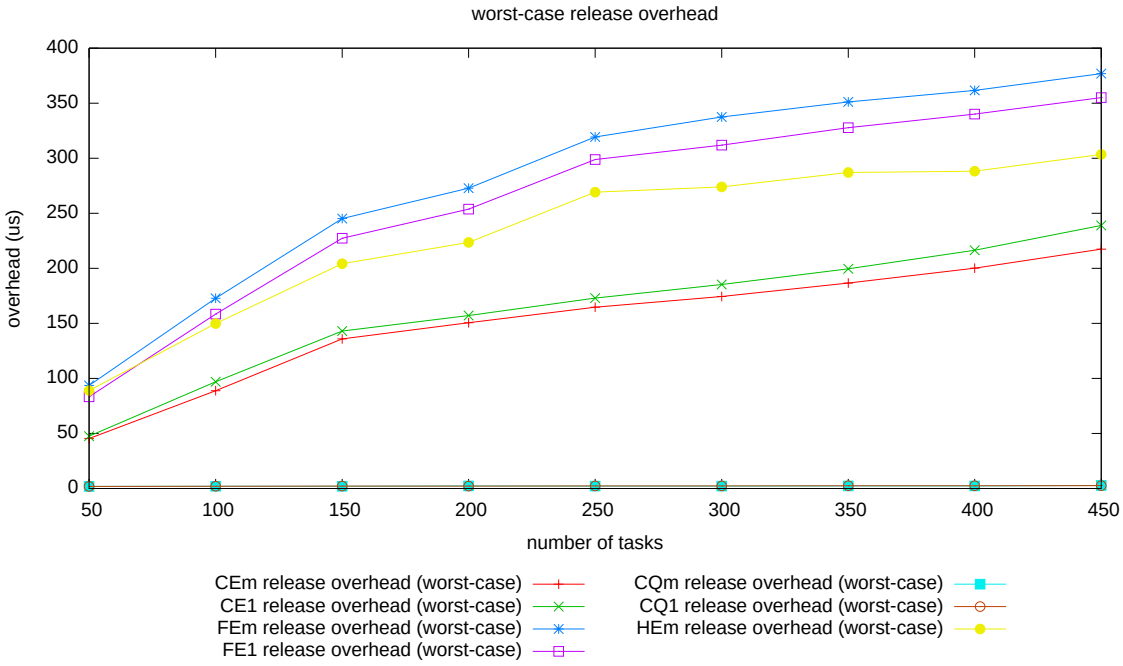

(a)

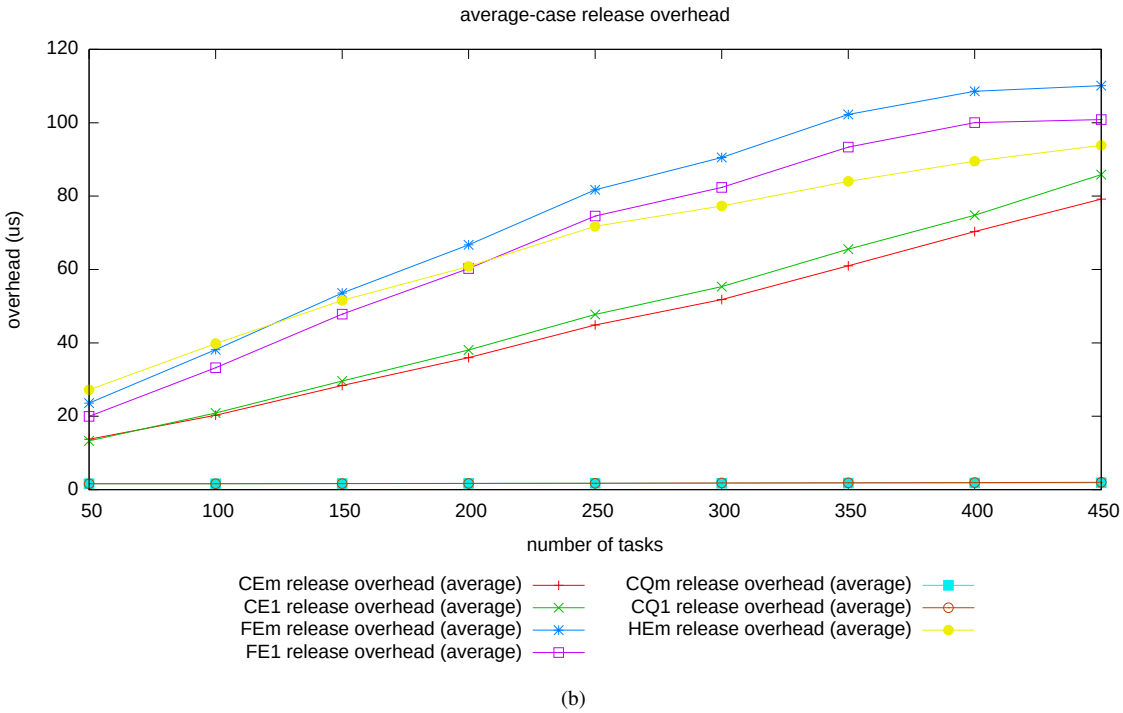

(b)

Figure 10: Measured release overhead under aligned quanta. **(a)** Measured worst case. **(b)** Measured average case. Note that outliers were filtered before computing worst- and average-case values, as described in [7].

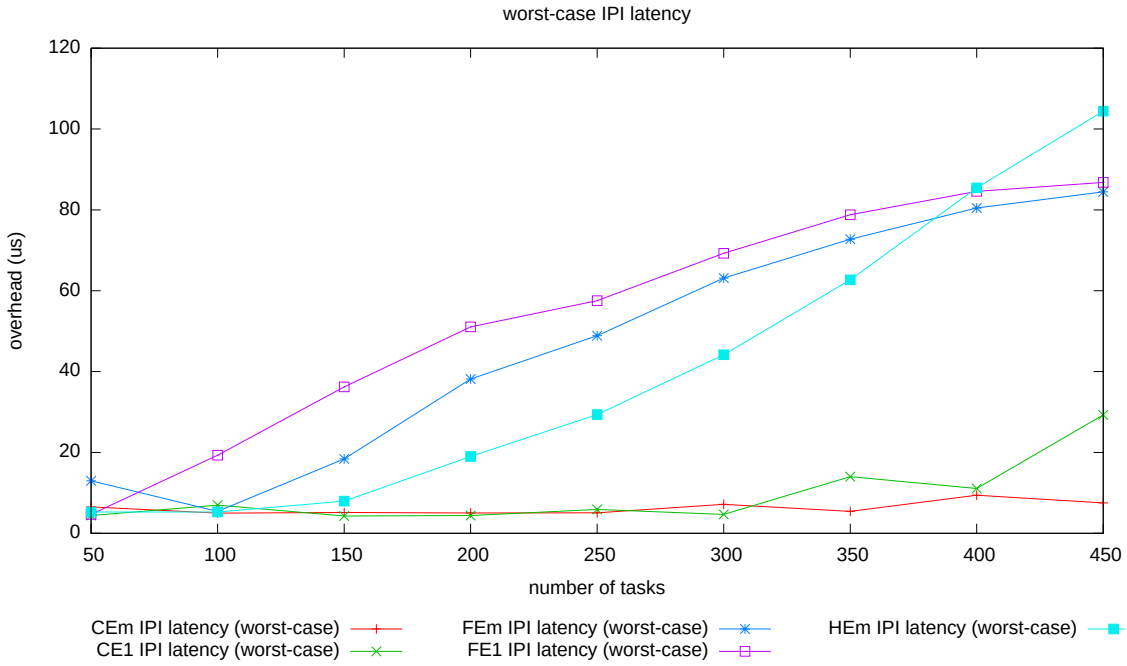

(a)

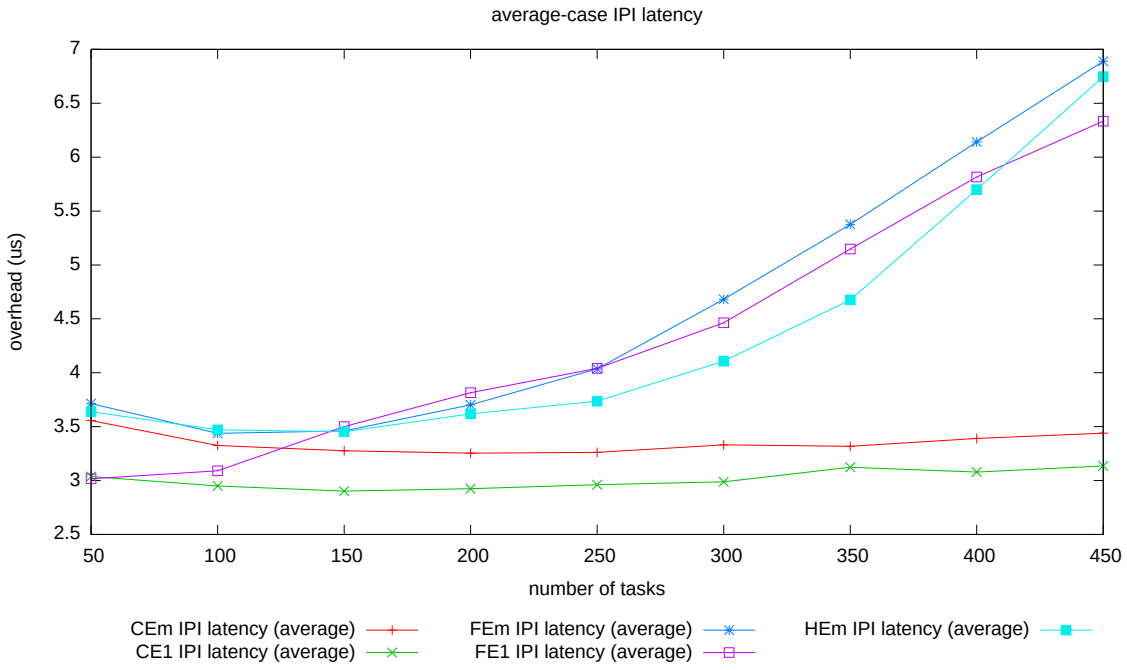

(b)

Figure 11: Measured IPI latency under aligned quanta. **(a)** Measured worst case. **(b)** Measured average case. Note that outliers were filtered before computing worst- and average-case values, as described in [7].

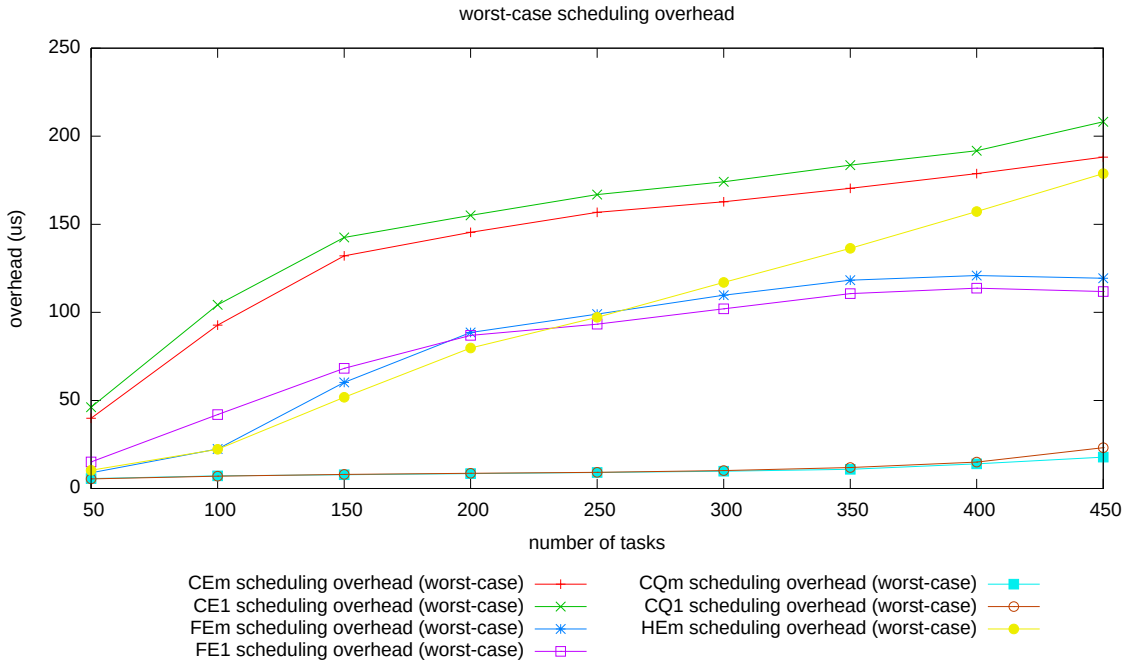

(a)

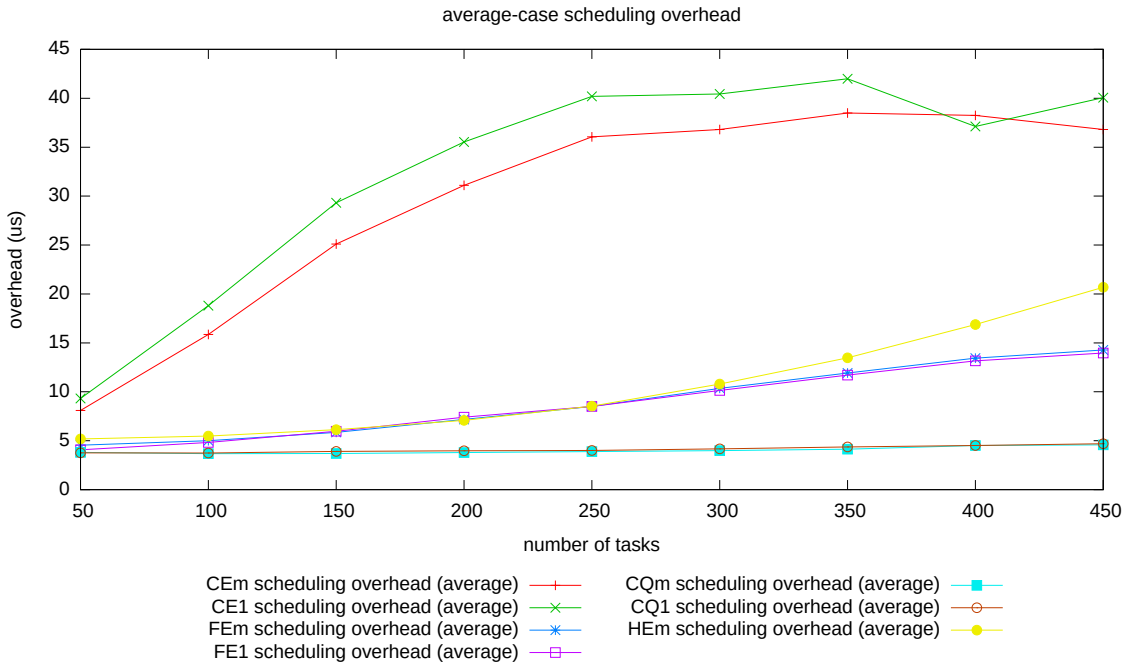

(b)

Figure 12: Measured scheduling overhead under staggered quanta. **(a)** Measured worst case. **(b)** Measured average case. Note that outliers were filtered before computing worst- and average-case values, as described in [7].

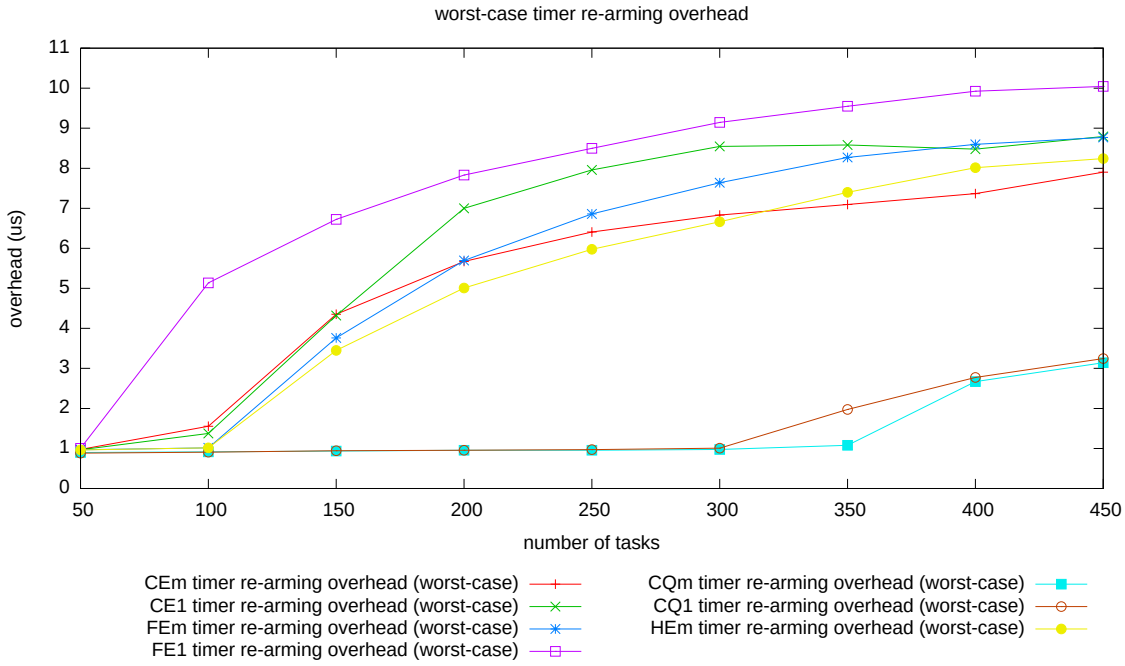

(a)

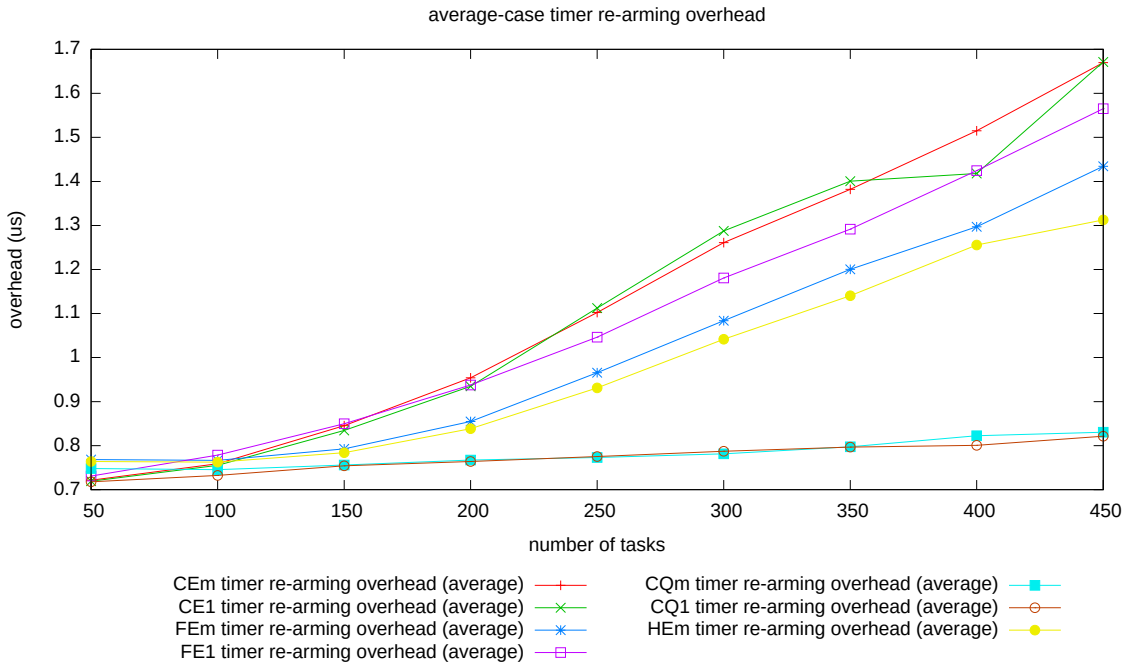

(b)

Figure 13: Measured timer re-arming overhead under staggered quanta. **(a)** Measured worst case. **(b)** Measured average case. Note that outliers were filtered before computing worst- and average-case values, as described in [7].

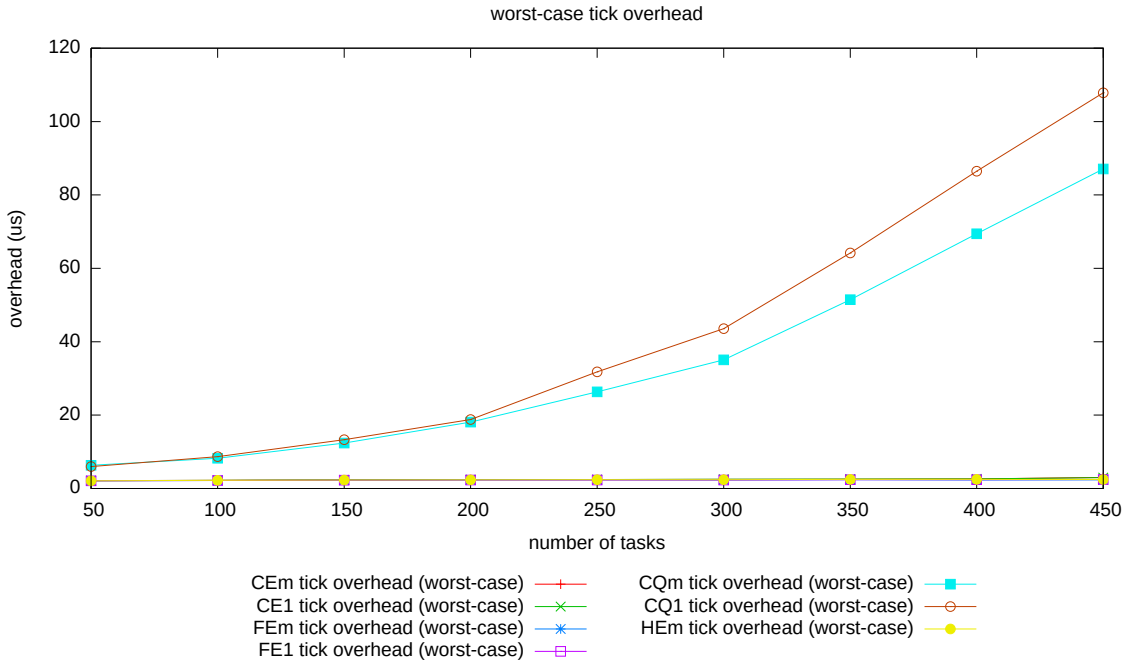

(a)

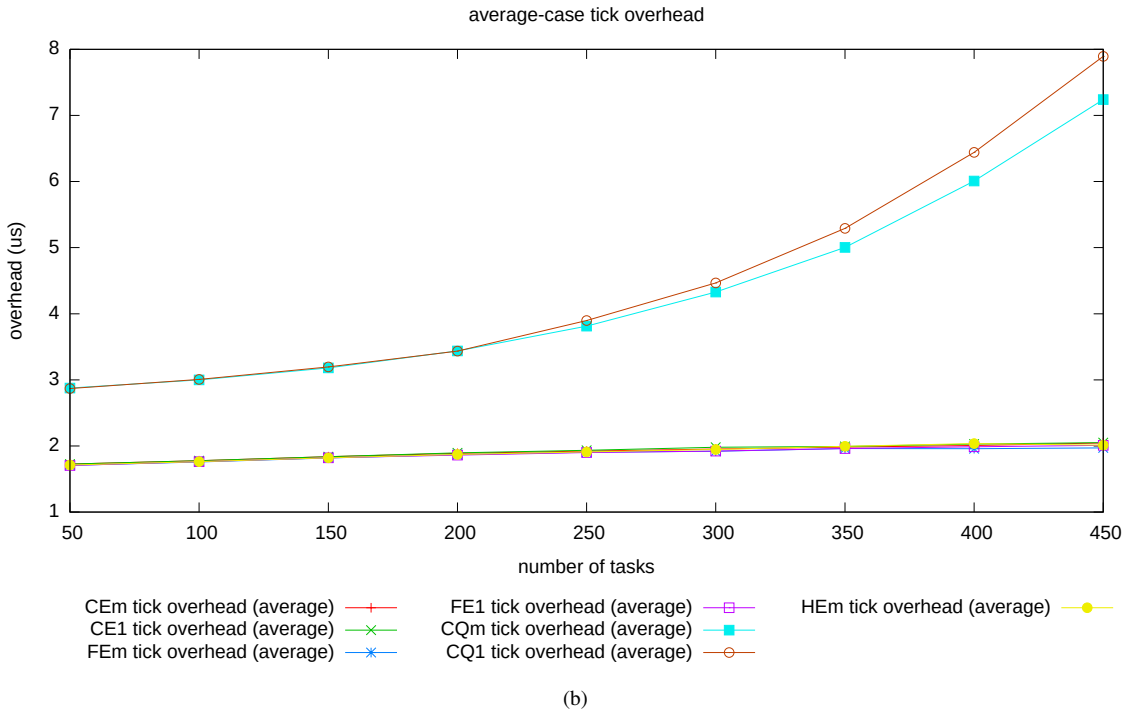

(b)

Figure 14: Measured tick overhead under staggered quanta. **(a)** Measured worst case. **(b)** Measured average case. Note that outliers were filtered before computing worst- and average-case values, as described in [7].

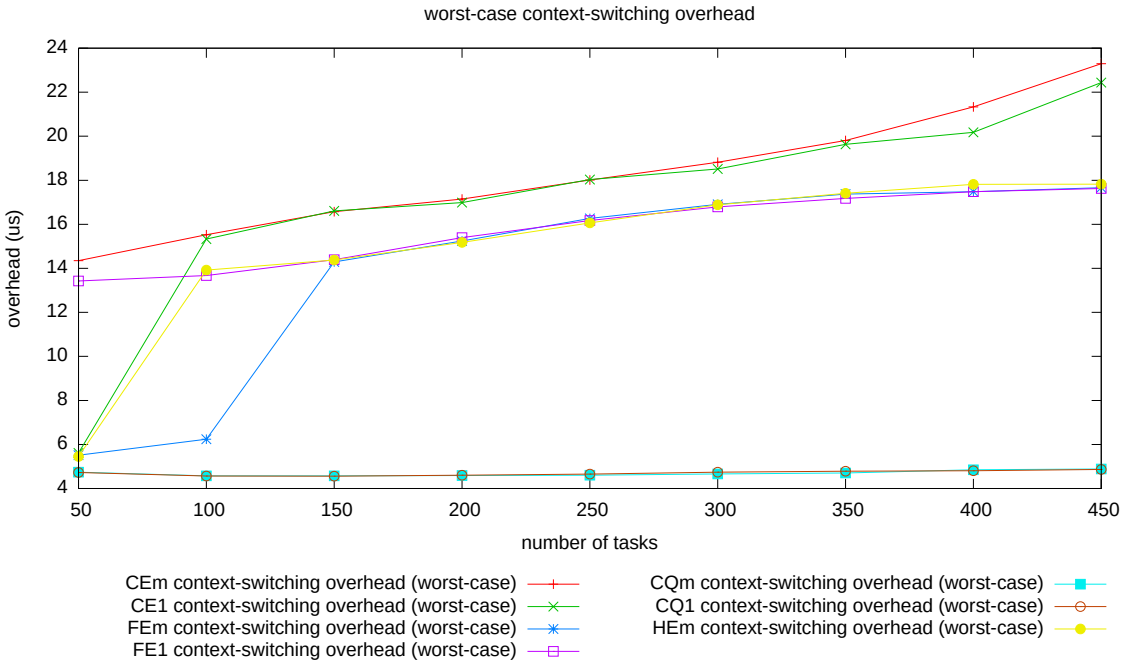

(a)

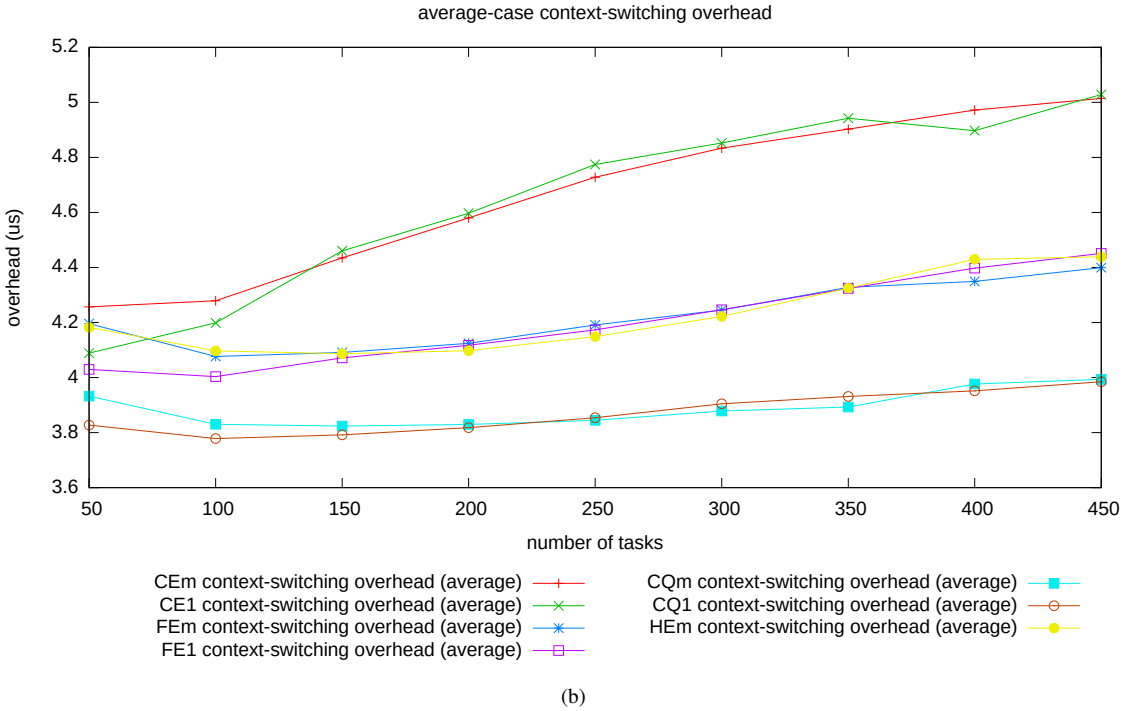

(b)

Figure 15: Measured context-switching overhead under staggered quanta. **(a)** Measured worst case. **(b)** Measured average case. Note that outliers were filtered before computing worst- and average-case values, as described in [7].

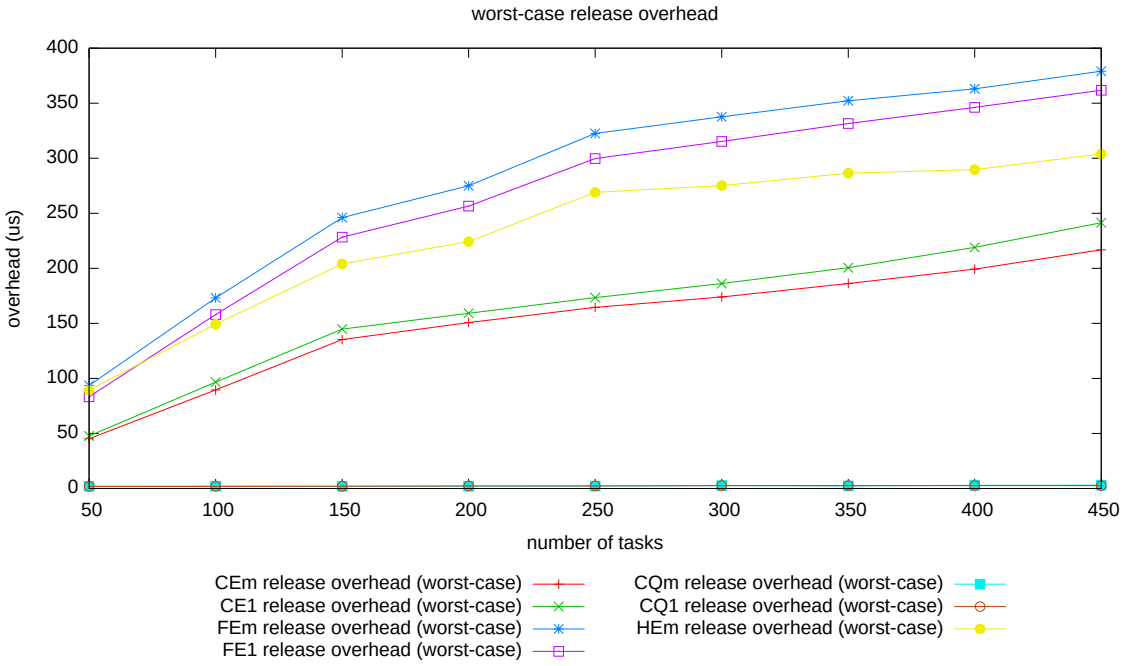

(a)

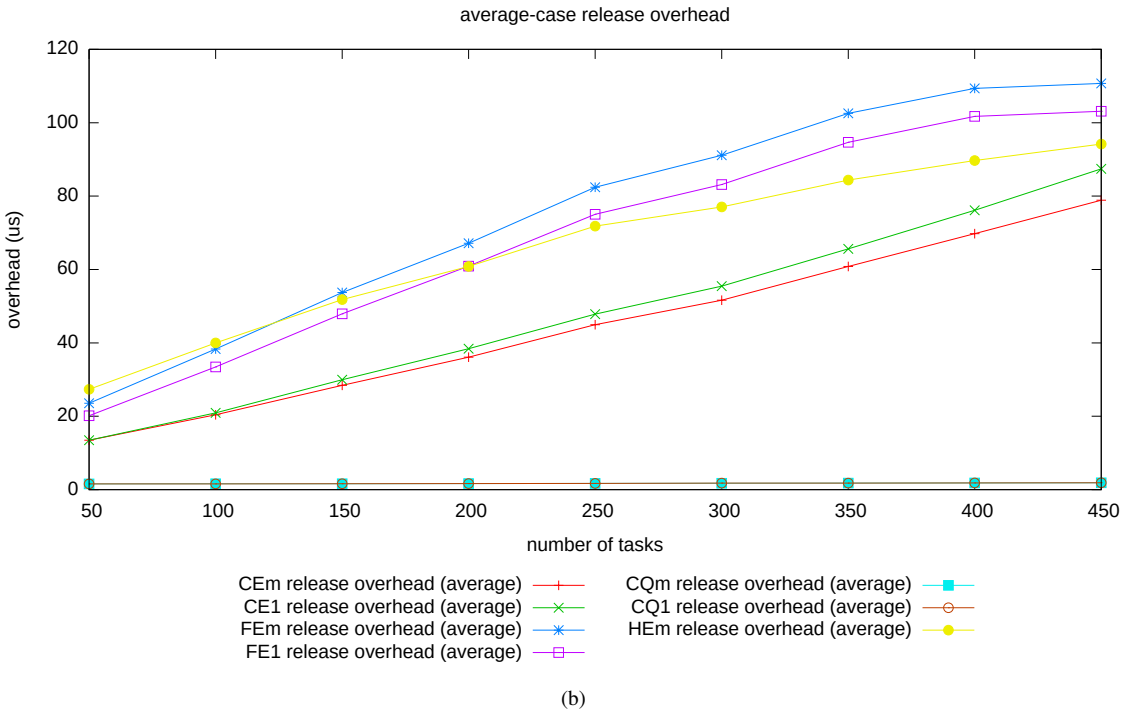

(b)

Figure 16: Measured release overhead under staggered quanta. **(a)** Measured worst case. **(b)** Measured average case. Note that outliers were filtered before computing worst- and average-case values, as described in [7].

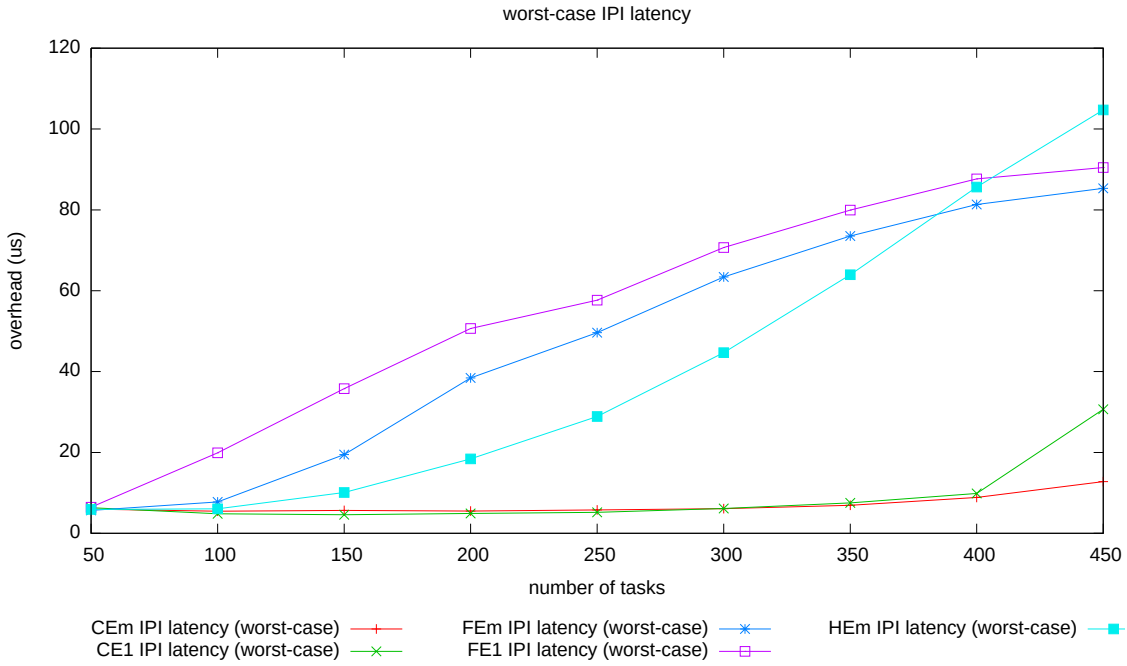

(a)

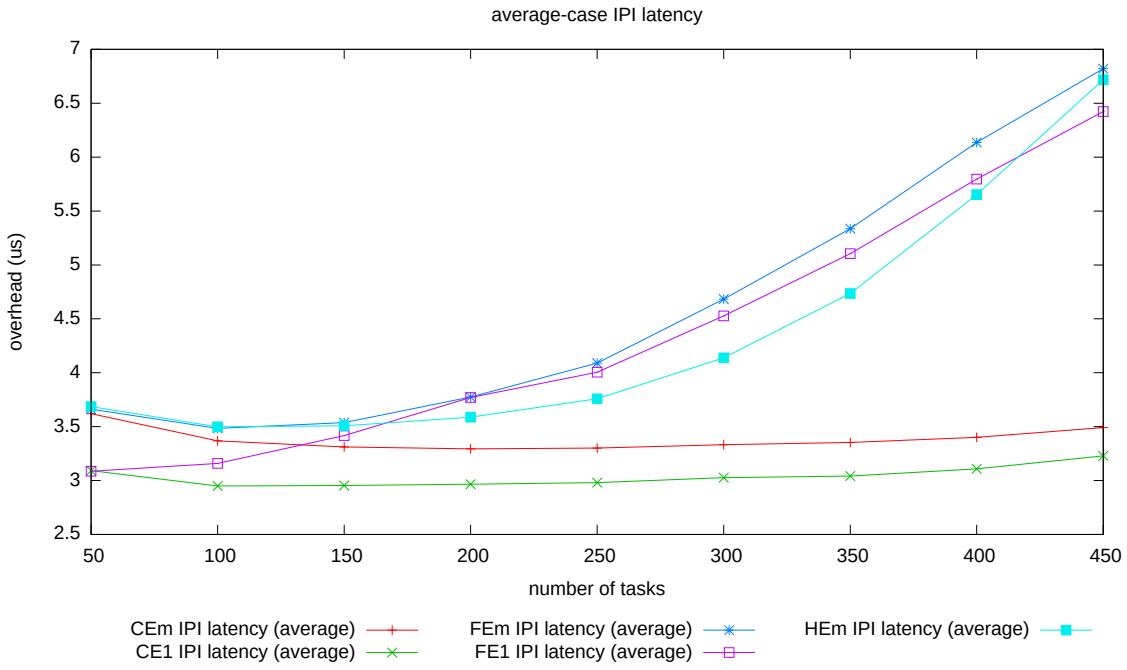

(b)

Figure 17: Measured IPI latency under staggered quanta. **(a)** Measured worst case. **(b)** Measured average case. Note that outliers were filtered before computing worst- and average-case values, as described in [7].

A.2 Overhead Tables

The following 12 tables list measured average and worst-case overheads under each of the implemented plugins, under both aligned and staggered quanta. The tables are organized as follows.

- Table 2 lists measured scheduling overhead under aligned quanta. Table 2 corresponds to Fig. 6.
- Table 3 lists measured timer re-arming overhead under aligned quanta. Table 3 corresponds to Fig. 7.
- Table 4 lists measured tick overhead under aligned quanta. Table 4 corresponds to Fig. 8.
- Table 5 lists measured context-switching overhead under aligned quanta. Table 5 corresponds to Fig. 9.
- Table 6 lists measured release overhead under aligned quanta. Table 6 corresponds to Fig. 10.
- Table 7 lists measured IPI latency under aligned quanta. Table 7 corresponds to Fig. 11.
- Table 8 lists measured scheduling overhead under staggered quanta. Table 8 corresponds to Fig. 12.
- Table 9 lists measured timer re-arming overhead under staggered quanta. Table 9 corresponds to Fig. 13.
- Table 10 lists measured tick overhead under staggered quanta. Table 10 corresponds to Fig. 14.
- Table 11 lists measured context-switching overhead under staggered quanta. Table 11 corresponds to Fig. 15.
- Table 12 lists measured release overhead under staggered quanta. Table 12 corresponds to Fig. 16.
- Table 13 lists measured IPI latency under staggered quanta. Table 13 corresponds to Fig. 17.

n	CEm	CE1	FEm	FE1	CQm	CQ1	HEm
50	39.346667	46.310000	9.380000	14.976667	29.340000	28.833333	10.400000
100	92.460000	104.620000	22.640000	41.996667	33.073333	33.733333	22.536667
150	132.733333	141.116667	59.523333	68.706667	49.310000	51.483333	51.993333
200	145.306667	153.336667	88.380000	85.810000	68.703333	68.643333	80.743333
250	156.976667	165.366667	98.723333	92.466667	80.796667	82.670000	97.243333
300	163.480000	173.026667	108.800000	100.523333	88.020000	87.850000	116.350000
350	172.140000	181.290000	118.536667	109.010000	95.270000	94.570000	135.303333
400	179.803333	191.580000	121.163333	111.720000	101.763333	99.806667	155.786667
450	189.310000	205.030000	119.146667	108.880000	112.146667	106.246667	178.926667

(a)

n	CEm	CE1	FEm	FE1	CQm	CQ1	HEm
50	7.752439	9.424788	4.470213	3.895430	8.533240	8.392539	5.156345
100	15.838610	18.902937	4.869468	4.623049	9.292148	9.269580	5.495724
150	25.204009	28.839955	5.753671	5.758967	10.592887	10.561661	6.034774
200	31.205482	35.036026	7.092584	7.185411	12.092571	12.186823	7.038922
250	36.303965	39.881126	8.510253	8.372861	14.317886	14.663960	8.575282
300	37.235267	40.398161	10.269631	10.061425	16.421629	16.613617	10.735403
350	39.022171	41.291210	12.030504	11.630174	18.616673	18.825374	13.429836
400	38.470626	40.443456	13.546267	13.027911	21.070269	21.103154	16.843601
450	36.919723	38.740216	14.408666	13.700526	24.395994	24.124089	20.877933

(b)

Table 2: Measured scheduling overhead under aligned quanta (in μs). **(a)** Measured worst case. **(b)** Measured average case. Note that outliers were filtered before computing worst- and average-case values, as described in [7]. These tables correspond to Fig. 6.

n	CEm	CE1	FEm	FE1	CQm	CQ1	HEm
50	0.953333	0.960000	1.013333	0.973333	1.000000	0.986667	0.950000
100	1.820000	1.810000	1.003333	4.740000	1.046667	1.030000	1.010000
150	4.640000	4.656667	3.526667	7.063333	1.093333	1.110000	3.250000
200	5.916667	7.116667	5.500000	7.926667	1.090000	1.136667	5.163333
250	6.610000	8.256667	6.853333	8.536667	1.120000	1.083333	5.996667
300	6.996667	8.470000	7.670000	8.840000	1.133333	1.140000	6.590000
350	7.273333	8.693333	8.253333	9.413333	1.073333	1.073333	7.360000
400	7.800000	8.793333	8.700000	9.660000	1.180000	1.176667	7.933333
450	8.023333	8.846667	8.940000	9.803333	1.080000	1.150000	8.283333

(a)

n	CEm	CE1	FEm	FE1	CQm	CQ1	HEm
50	0.713504	0.717220	0.766060	0.726614	0.786090	0.753023	0.761404
100	0.760120	0.757521	0.761278	0.772923	0.788185	0.771522	0.759820
150	0.856804	0.869075	0.785212	0.850755	0.801787	0.795528	0.781161
200	0.972993	0.975138	0.843885	0.938949	0.807965	0.810101	0.839040
250	1.137746	1.148415	0.955719	1.040132	0.816765	0.816219	0.922429
300	1.282820	1.331370	1.078885	1.164774	0.822374	0.824535	1.037595
350	1.422653	1.501239	1.174108	1.262720	0.820310	0.822704	1.126736
400	1.597441	1.587317	1.296925	1.370468	0.832053	0.834266	1.196564
450	1.720358	1.757886	1.470217	1.525324	0.831401	0.832972	1.323794

(b)

Table 3: Measured timer re-arming overhead under aligned quanta (in μs). **(a)** Measured worst case. **(b)** Measured average case. Note that outliers were filtered before computing worst- and average-case values, as described in [7]. These tables correspond to Fig. 7.

n	CEm	CE1	FEm	FE1	CQm	CQ1	HEm
50	8.876667	8.856667	8.950000	8.846667	50.280000	51.453333	9.106667
100	9.226667	9.096667	9.180000	9.113333	70.403333	75.266667	9.103333
150	9.380000	9.390000	9.326667	9.256667	99.060000	107.360000	9.376667
200	9.566667	9.610000	9.480000	9.376667	135.003333	147.030000	9.443333
250	9.613333	9.760000	9.580000	9.476667	169.886667	182.093333	9.573333
300	9.710000	9.990000	9.716667	9.660000	187.860000	201.036667	9.796667
350	9.850000	9.873333	9.843333	9.743333	209.936667	224.253333	9.803333
400	9.896667	9.836667	9.806667	9.846667	231.546667	247.013333	9.746667
450	10.033333	10.050000	9.923333	10.016667	258.543333	272.850000	9.880000

(a)

n	CEm	CE1	FEm	FE1	CQm	CQ1	HEm
50	4.123824	4.106791	4.108178	4.080642	22.961718	23.136902	4.283937
100	4.195850	4.102096	4.144745	4.112577	25.985758	26.355396	4.118961
150	4.228546	4.325074	4.160176	4.094020	29.916198	30.939934	4.249806
200	4.334438	4.287068	4.174363	4.091688	34.594384	37.057361	4.287678
250	4.316153	4.298950	4.263738	4.160574	42.483474	45.331352	4.243067
300	4.265730	4.498064	4.341251	4.173780	51.248863	55.455206	4.398583
350	4.496874	4.439727	4.340792	4.239454	61.488757	67.073086	4.420993
400	4.364132	4.175216	4.347097	4.288279	74.980141	82.111562	4.423725
450	4.507053	4.505451	4.445773	4.412984	93.698246	102.850925	4.367841

(b)

Table 4: Measured tick overhead under aligned quanta (in μs). **(a)** Measured worst case. **(b)** Measured average case. Note that outliers were filtered before computing worst- and average-case values, as described in [7]. These tables correspond to Fig. 8.

n	CEm	CE1	FEm	FE1	CQm	CQ1	HEm
50	5.060000	5.053333	19.186667	5.070000	4.976667	4.900000	5.036667
100	5.533333	18.176667	5.096667	5.870000	4.863333	4.886667	5.013333
150	16.443333	8.273333	5.363333	18.040000	4.910000	4.973333	5.276667
200	9.550000	13.760000	5.956667	17.973333	4.893333	4.963333	17.106667
250	10.210000	17.990000	6.283333	17.860000	4.926667	4.913333	6.666667
300	17.076667	11.106667	17.180000	6.520000	4.913333	4.953333	16.150000
350	12.116667	16.050000	16.470000	17.273333	4.860000	4.876667	7.500000
400	12.716667	18.816667	16.933333	16.893333	4.960000	4.883333	17.783333
450	13.876667	14.010000	17.653333	17.043333	4.876667	4.843333	17.076667

(a)

n	CEm	CE1	FEm	FE1	CQm	CQ1	HEm
50	4.138991	3.996073	4.451798	3.941008	3.936225	3.786728	4.136449
100	4.059153	4.486734	4.011071	3.964933	3.795740	3.749763	4.004124
150	4.441981	4.128498	4.017020	4.177519	3.769037	3.766105	3.990250
200	4.196506	4.241040	4.029879	4.208205	3.763583	3.773364	4.099085
250	4.263895	4.766770	4.066365	4.221872	3.771371	3.785994	4.027802
300	4.663931	4.301337	4.187729	4.108712	3.777913	3.805929	4.095264
350	4.330444	4.455888	4.156510	4.214278	3.777643	3.794741	4.083512
400	4.368608	5.237983	4.199495	4.190749	3.817717	3.789426	4.262767
450	4.356306	4.397440	4.304791	4.236237	3.827312	3.786919	4.233670

(b)

Table 5: Measured context-switching overhead under aligned quanta (in μs). **(a)** Measured worst case. **(b)** Measured average case. Note that outliers were filtered before computing worst- and average-case values, as described in [7]. These tables correspond to Fig. 9.

n	CEm	CE1	FEm	FE1	CQm	CQ1	HEm
50	45.376667	47.593333	93.643333	83.260000	1.916667	1.936667	88.910000
100	88.880000	96.990000	172.750000	158.453333	1.966667	2.060000	149.916667
150	135.913333	143.030000	245.166667	227.350000	2.053333	2.126667	204.256667
200	150.633333	157.190000	272.833333	253.710000	2.316667	2.230000	223.543333
250	164.733333	172.933333	319.290000	298.896667	2.220000	2.393333	269.206667
300	174.490000	185.276667	337.473333	311.986667	2.240000	2.393333	273.960000
350	186.636667	199.633333	351.213333	327.796667	2.283333	2.413333	287.126667
400	200.140000	216.396667	361.643333	340.100000	2.336667	2.490000	288.213333
450	217.460000	238.946667	376.903333	355.030000	2.713333	2.563333	303.420000

(a)

n	CEm	CE1	FEm	FE1	CQm	CQ1	HEm
50	13.722481	13.317044	23.592517	19.960966	1.600843	1.595411	27.209503
100	20.296912	20.889685	38.157151	33.235645	1.624723	1.627879	39.832092
150	28.401113	29.624356	53.569235	47.834889	1.663580	1.672091	51.603685
200	35.991031	38.081589	66.731202	60.265010	1.702945	1.715644	60.838567
250	44.851005	47.730453	81.711763	74.548864	1.727927	1.762242	71.786984
300	51.813998	55.353792	90.536651	82.364677	1.761089	1.819627	77.332104
350	60.994038	65.554669	102.245822	93.360484	1.793566	1.862089	84.035078
400	70.320794	74.796450	108.558637	100.009511	1.833770	1.929797	89.507775
450	79.184146	85.866271	110.095881	100.868910	1.891226	1.994778	93.858805

(b)

Table 6: Measured release overhead under aligned quanta (in μs). **(a)** Measured worst case. **(b)** Measured average case. Note that outliers were filtered before computing worst- and average-case values, as described in [7]. These tables correspond to Fig. 10.

n	CEm	CE1	FEm	FE1	CQm	CQ1	HEm
50	6.546667	4.403333	12.993333	4.676667	—	—	5.270000
100	5.000000	6.976667	5.403333	19.310000	—	—	5.246667
150	5.160000	4.293333	18.396667	36.196667	—	—	7.946667
200	5.016667	4.400000	38.133333	51.040000	—	—	19.013333
250	5.080000	5.916667	48.886667	57.543333	—	—	29.383333
300	7.150000	4.660000	63.120000	69.243333	—	—	44.160000
350	5.403333	14.023333	72.746667	78.793333	—	—	62.690000
400	9.433333	11.086667	80.480000	84.563333	—	—	85.463333
450	7.516667	29.290000	84.466667	86.813333	—	—	104.390000

(a)

n	CEm	CE1	FEm	FE1	CQm	CQ1	HEm
50	3.556947	3.036542	3.713910	3.017032	—	—	3.638669
100	3.324529	2.949595	3.438500	3.091216	—	—	3.470800
150	3.276622	2.901495	3.460304	3.500383	—	—	3.452193
200	3.253500	2.925008	3.702782	3.815593	—	—	3.619397
250	3.261812	2.961198	4.035601	4.039980	—	—	3.736179
300	3.330441	2.987722	4.681381	4.463799	—	—	4.106912
350	3.317120	3.123484	5.376778	5.148243	—	—	4.675227
400	3.390497	3.078722	6.141230	5.815550	—	—	5.698865
450	3.439381	3.135518	6.889130	6.333135	—	—	6.746458

(b)

Table 7: Measured IPI latency under aligned quanta (in μs). **(a)** Measured worst case. **(b)** Measured average case. Note that outliers were filtered before computing worst- and average-case values, as described in [7]. These tables correspond to Fig. 11.

n	CEm	CE1	FEm	FE1	CQm	CQ1	HEm
50	39.850000	46.170000	8.943333	15.110000	5.670000	5.446667	10.340000
100	92.726667	104.263333	22.423333	41.956667	7.133333	7.033333	22.276667
150	132.060000	142.516667	60.266667	68.220000	7.833333	7.980000	51.746667
200	145.480000	155.073333	88.613333	86.973333	8.493333	8.653333	79.763333
250	156.783333	166.880000	99.043333	93.326667	9.123333	9.213333	97.166667
300	162.796667	174.150000	109.706667	102.020000	9.780000	10.146667	116.983333
350	170.440000	183.586667	118.263333	110.620000	10.933333	11.920000	136.310000
400	178.783333	191.810000	120.953333	113.726667	13.993333	15.003333	157.220000
450	188.140000	208.173333	119.366667	111.810000	17.770000	23.176667	178.780000

(a)

n	CEm	CE1	FEm	FE1	CQm	CQ1	HEm
50	8.094222	9.319991	4.552216	4.078418	3.803485	3.762715	5.177300
100	15.868094	18.807846	5.004378	4.816280	3.679596	3.747637	5.485217
150	25.103310	29.322102	5.857759	5.968767	3.695616	3.914522	6.131576
200	31.101610	35.532560	7.176427	7.408112	3.791913	3.975425	7.078387
250	36.054611	40.184822	8.506393	8.509983	3.894480	4.012949	8.540165
300	36.809331	40.443841	10.342688	10.142849	3.989817	4.165312	10.799998
350	38.494031	41.986560	11.927195	11.712992	4.138575	4.369225	13.466103
400	38.254152	37.114869	13.446336	13.156129	4.508925	4.515190	16.872205
450	36.805547	40.057083	14.272900	13.959959	4.582703	4.687490	20.679590

(b)

Table 8: Measured scheduling overhead under staggered quanta (in μs). **(a)** Measured worst case. **(b)** Measured average case. Note that outliers were filtered before computing worst- and average-case values, as described in [7]. These tables correspond to Fig. 12.

n	CEm	CE1	FEm	FE1	CQm	CQ1	HEm
50	0.976667	0.966667	0.966667	1.003333	0.900000	0.883333	0.963333
100	1.556667	1.373333	1.013333	5.136667	0.916667	0.906667	1.013333
150	4.353333	4.320000	3.760000	6.723333	0.933333	0.943333	3.450000
200	5.673333	7.000000	5.696667	7.830000	0.953333	0.953333	5.010000
250	6.406667	7.960000	6.860000	8.496667	0.953333	0.970000	5.976667
300	6.830000	8.546667	7.636667	9.146667	0.976667	1.006667	6.663333
350	7.096667	8.583333	8.270000	9.550000	1.080000	1.973333	7.396667
400	7.366667	8.476667	8.596667	9.923333	2.670000	2.773333	8.013333
450	7.903333	8.793333	8.770000	10.043333	3.143333	3.246667	8.243333

(a)

n	CEm	CE1	FEm	FE1	CQm	CQ1	HEm
50	0.721284	0.719373	0.768484	0.730940	0.748132	0.717700	0.764010
100	0.758751	0.755307	0.766533	0.778376	0.745381	0.732346	0.762326
150	0.845318	0.834519	0.792729	0.849833	0.755979	0.754201	0.783979
200	0.954158	0.934839	0.854960	0.937816	0.767332	0.764130	0.838372
250	1.102249	1.112496	0.965707	1.046366	0.773118	0.775280	0.931207
300	1.261131	1.287508	1.083607	1.180734	0.781287	0.787279	1.041730
350	1.381913	1.400638	1.200222	1.291660	0.797554	0.796791	1.140392
400	1.515223	1.418092	1.296980	1.424485	0.822520	0.800558	1.255504
450	1.669743	1.671145	1.434209	1.565254	0.830449	0.821383	1.312786

(b)

Table 9: Measured timer re-arming overhead under staggered quanta (in μs). **(a)** Measured worst case. **(b)** Measured average case. Note that outliers were filtered before computing worst- and average-case values, as described in [7]. These tables correspond to Fig. 13.

n	CEm	CE1	FEm	FE1	CQm	CQ1	HEm
50	2.130000	2.116667	2.086667	2.080000	6.343333	5.990000	2.106667
100	2.236667	2.230000	2.190000	2.196667	8.236667	8.690000	2.210000
150	2.356667	2.333333	2.286667	2.276667	12.363333	13.293333	2.290000
200	2.423333	2.426667	2.320000	2.290000	18.090000	18.776667	2.336667
250	2.443333	2.456667	2.353333	2.313333	26.333333	31.766667	2.386667
300	2.473333	2.520000	2.306667	2.320000	35.053333	43.570000	2.406667
350	2.543333	2.560000	2.380000	2.383333	51.440000	64.206667	2.473333
400	2.630000	2.616667	2.330000	2.400000	69.436667	86.473333	2.506667
450	3.000000	2.973333	2.333333	2.426667	87.080000	107.853333	2.440000

(a)

n	CEm	CE1	FEm	FE1	CQm	CQ1	HEm
50	1.725689	1.725898	1.707446	1.703186	2.876093	2.868984	1.712122
100	1.776682	1.775776	1.757044	1.763110	2.998473	3.005491	1.763488
150	1.837533	1.837298	1.817713	1.821684	3.179663	3.196195	1.821727
200	1.888639	1.896777	1.869111	1.862838	3.436532	3.434289	1.870288
250	1.921243	1.934195	1.905806	1.899689	3.812870	3.896306	1.911194
300	1.953355	1.980133	1.918752	1.923040	4.328181	4.465542	1.945750
350	1.983651	1.992160	1.961229	1.961775	5.002456	5.291298	1.995029
400	2.007965	2.028137	1.959019	1.987410	6.007492	6.442091	2.035951
450	2.044645	2.050872	1.971021	2.009000	7.240790	7.894566	2.012400

(b)

Table 10: Measured tick overhead under staggered quanta (in μs). **(a)** Measured worst case. **(b)** Measured average case. Note that outliers were filtered before computing worst- and average-case values, as described in [7]. These tables correspond to Fig. 14.

n	CEm	CE1	FEm	FE1	CQm	CQ1	HEm
50	14.346667	5.610000	5.510000	13.423333	4.743333	4.723333	5.450000
100	15.526667	15.330000	6.236667	13.673333	4.576667	4.563333	13.923333
150	16.570000	16.610000	14.293333	14.393333	4.573333	4.556667	14.380000
200	17.146667	16.986667	15.243333	15.393333	4.586667	4.606667	15.176667
250	18.010000	18.030000	16.266667	16.173333	4.603333	4.656667	16.066667
300	18.816667	18.510000	16.910000	16.793333	4.660000	4.743333	16.886667
350	19.810000	19.630000	17.370000	17.173333	4.703333	4.783333	17.410000
400	21.333333	20.180000	17.483333	17.483333	4.850000	4.810000	17.813333
450	23.296667	22.436667	17.663333	17.630000	4.886667	4.866667	17.823333

(a)

n	CEm	CE1	FEm	FE1	CQm	CQ1	HEm
50	4.257116	4.088879	4.196198	4.029668	3.932774	3.827149	4.182817
100	4.279206	4.198589	4.076815	4.003217	3.830004	3.778489	4.097358
150	4.434866	4.460414	4.091428	4.071368	3.823897	3.791796	4.086779
200	4.580166	4.597347	4.124275	4.117165	3.829520	3.818305	4.097755
250	4.727793	4.774573	4.191172	4.173408	3.844619	3.853977	4.148575
300	4.833893	4.852097	4.245588	4.246263	3.878260	3.904391	4.222174
350	4.902915	4.942499	4.328150	4.323759	3.892930	3.931144	4.324972
400	4.972359	4.897116	4.349519	4.397633	3.976483	3.951878	4.429505
450	5.014317	5.028655	4.399700	4.451260	3.993735	3.984602	4.439013

(b)

Table 11: Measured context-switching overhead under staggered quanta (in μs). **(a)** Measured worst case. **(b)** Measured average case. Note that outliers were filtered before computing worst- and average-case values, as described in [7]. These tables correspond to Fig. 15.

n	CEm	CE1	FEm	FE1	CQm	CQ1	HEm
50	45.160000	47.710000	93.553333	83.270000	2.050000	1.900000	89.233333
100	89.496667	96.680000	173.153333	157.986667	2.136667	1.953333	149.223333
150	135.323333	144.700000	246.103333	228.286667	2.003333	2.060000	204.043333
200	150.733333	159.163333	274.986667	256.550000	2.090000	2.273333	224.243333
250	164.520000	173.416667	322.500000	299.726667	2.196667	2.306667	268.973333
300	174.040000	186.183333	337.590000	315.220000	2.600000	2.683333	275.200000
350	186.153333	200.590000	352.223333	331.483333	2.263333	2.613333	286.450000
400	199.260000	219.053333	363.106667	346.293333	2.903333	2.596667	289.636667
450	216.806667	241.460000	379.113333	361.786667	3.060000	2.593333	303.906667

(a)

n	CEm	CE1	FEm	FE1	CQm	CQ1	HEm
50	13.489388	13.458593	23.536775	20.139925	1.573317	1.561158	27.332953
100	20.400159	20.910676	38.318864	33.457051	1.605717	1.589809	39.973609
150	28.426785	29.948755	53.728555	47.915713	1.622647	1.633248	51.788456
200	36.111630	38.424155	67.164308	60.924967	1.661057	1.673685	60.815847
250	44.964809	47.840696	82.412810	75.037101	1.693608	1.713563	71.805802
300	51.642150	55.482255	91.122824	83.141689	1.752715	1.780821	77.028258
350	60.850067	65.605753	102.550111	94.652170	1.768444	1.801693	84.381160
400	69.746752	76.124222	109.369906	101.729210	1.833865	1.838063	89.684504
450	78.899514	87.408731	110.691870	103.121330	1.871730	1.895681	94.170941

(b)

Table 12: Measured release overhead under staggered quanta (in μs). **(a)** Measured worst case. **(b)** Measured average case. Note that outliers were filtered before computing worst- and average-case values, as described in [7]. These tables correspond to Fig. 16.

n	CEm	CE1	FEm	FE1	CQm	CQ1	HEm
50	5.986667	6.343333	5.646667	6.436667	—	—	5.900000
100	5.450000	4.813333	7.766667	19.910000	—	—	6.066667
150	5.660000	4.606667	19.486667	35.773333	—	—	10.106667
200	5.510000	4.893333	38.440000	50.673333	—	—	18.400000
250	5.783333	5.186667	49.633333	57.666667	—	—	28.873333
300	6.103333	6.130000	63.413333	70.686667	—	—	44.670000
350	6.916667	7.520000	73.523333	79.953333	—	—	63.946667
400	8.866667	9.853333	81.350000	87.680000	—	—	85.663333
450	12.783333	30.666667	85.346667	90.480000	—	—	104.726667

(a)

n	CEm	CE1	FEm	FE1	CQm	CQ1	HEm
50	3.620983	3.091875	3.662822	3.085628	—	—	3.685732
100	3.368507	2.949932	3.483586	3.158275	—	—	3.498932
150	3.311931	2.953710	3.538007	3.417121	—	—	3.507025
200	3.294768	2.965412	3.775435	3.770703	—	—	3.587282
250	3.301273	2.981535	4.090263	4.005280	—	—	3.758739
300	3.332466	3.026697	4.682636	4.527855	—	—	4.137825
350	3.353710	3.041287	5.336483	5.105332	—	—	4.734812
400	3.400673	3.109150	6.135478	5.796901	—	—	5.652826
450	3.492159	3.228440	6.820003	6.422823	—	—	6.717968

(b)

Table 13: Measured IPI latency under staggered quanta (in μs). **(a)** Measured worst case. **(b)** Measured average case. Note that outliers were filtered before computing worst- and average-case values, as described in [7]. These tables correspond to Fig. 17.

B Complete Schedulability Results

This appendix provides our complete schedulability results. To provide an overview, graphs showing curves for all plugins are provided in Sec. B.1. Graphs comparing individual plugins are provided in Sec. B.2 to better illustrate the tradeoffs between the considered approaches.

B.1 Overview

The following 12 figures depict schedulability for each considered scenario. They are organized as follows.

- Fig. 18 shows hard schedulability results under uniform light utilizations.
- Fig. 19 shows hard schedulability results under bimodal light utilizations.
- Fig. 20 shows hard schedulability results under uniform medium utilizations.
- Fig. 21 shows hard schedulability results under bimodal medium utilizations.
- Fig. 22 shows hard schedulability results under uniform heavy utilizations.
- Fig. 23 shows hard schedulability results under bimodal heavy utilizations.
- Fig. 24 shows soft schedulability results under uniform light utilizations.
- Fig. 25 shows soft schedulability results under bimodal light utilizations.
- Fig. 26 shows soft schedulability results under uniform medium utilizations.
- Fig. 27 shows soft schedulability results under bimodal medium utilizations.
- Fig. 28 shows soft schedulability results under uniform heavy utilizations.
- Fig. 29 shows soft schedulability results under bimodal heavy utilizations.

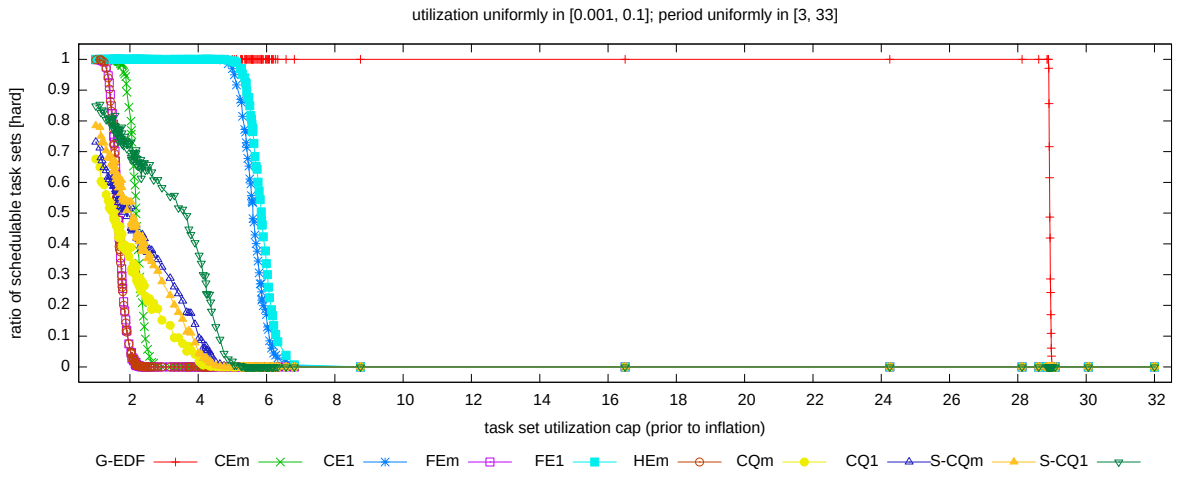

(a)

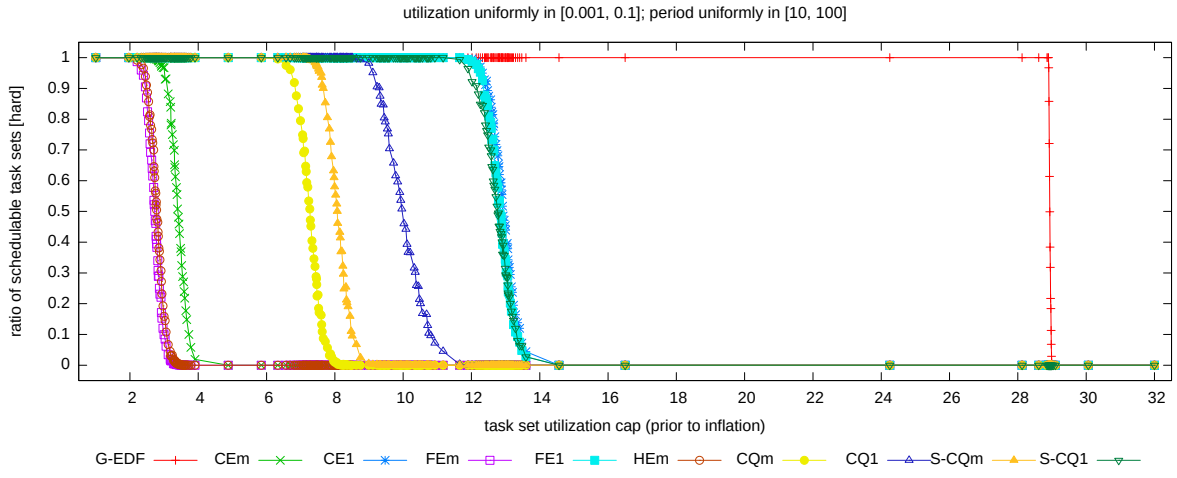

(b)

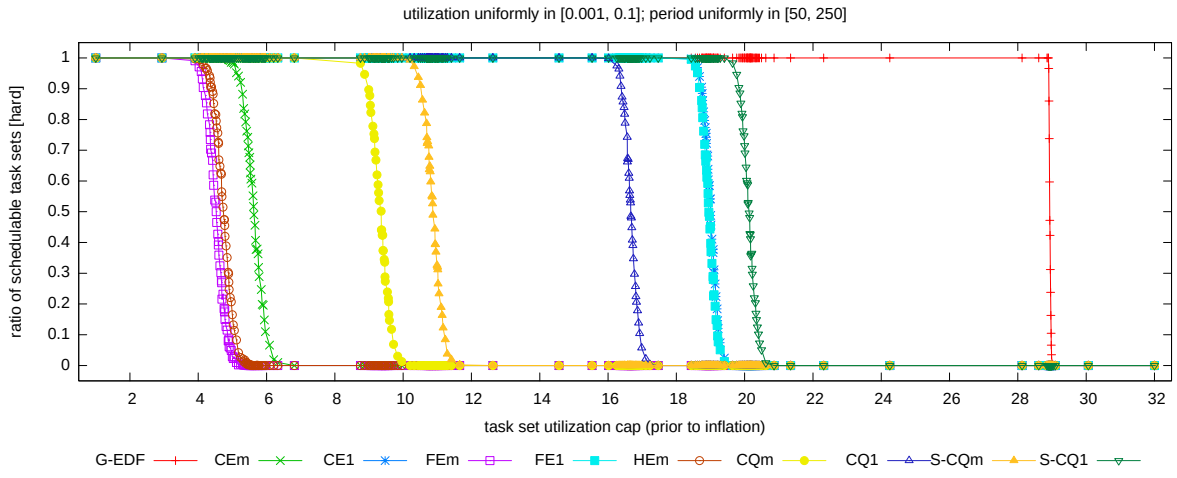

(c)

Figure 18: Hard schedulability of task sets with uniform light per-task utilizations and **(a)** short, **(b)** moderate, and **(c)** long periods.

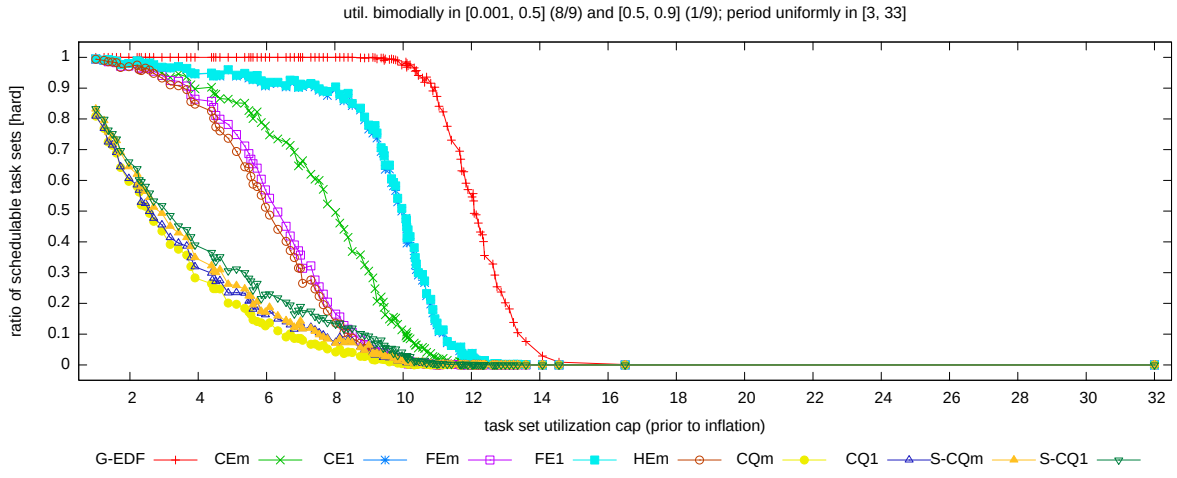

(a)

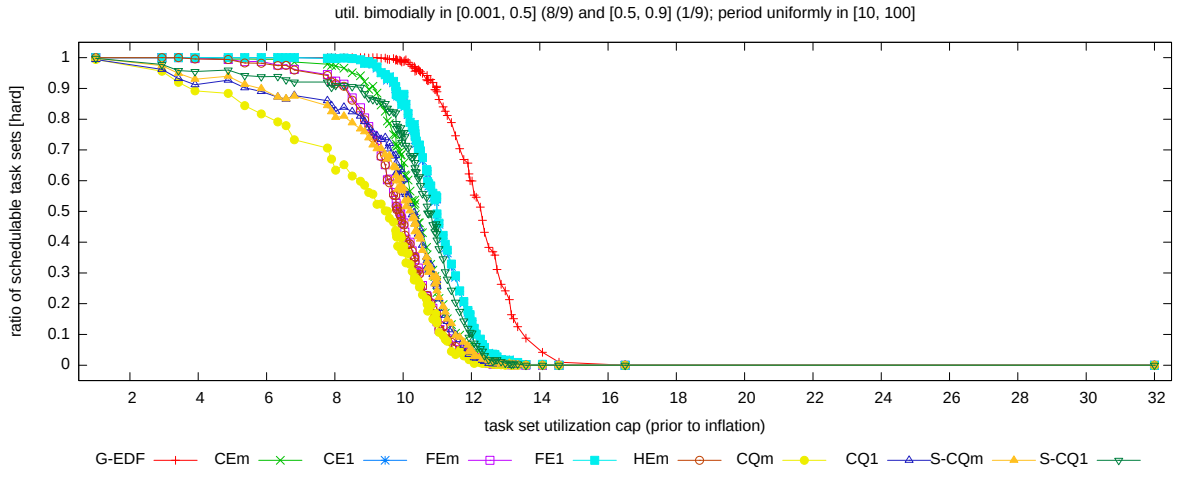

(b)

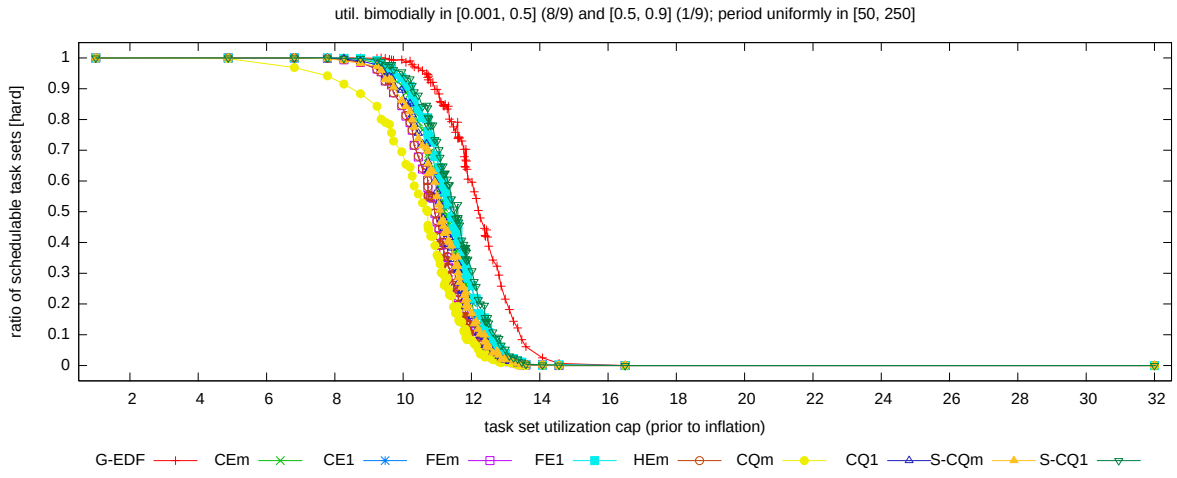

(c)

Figure 19: Hard schedulability of task sets with bimodal light per-task utilizations and **(a)** short, **(b)** moderate, and **(c)** long periods.

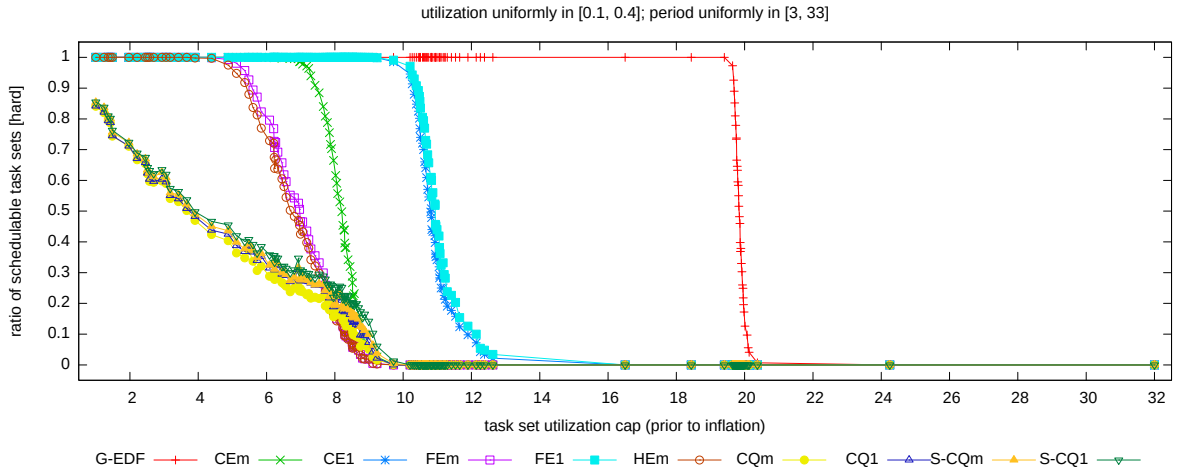

(a)

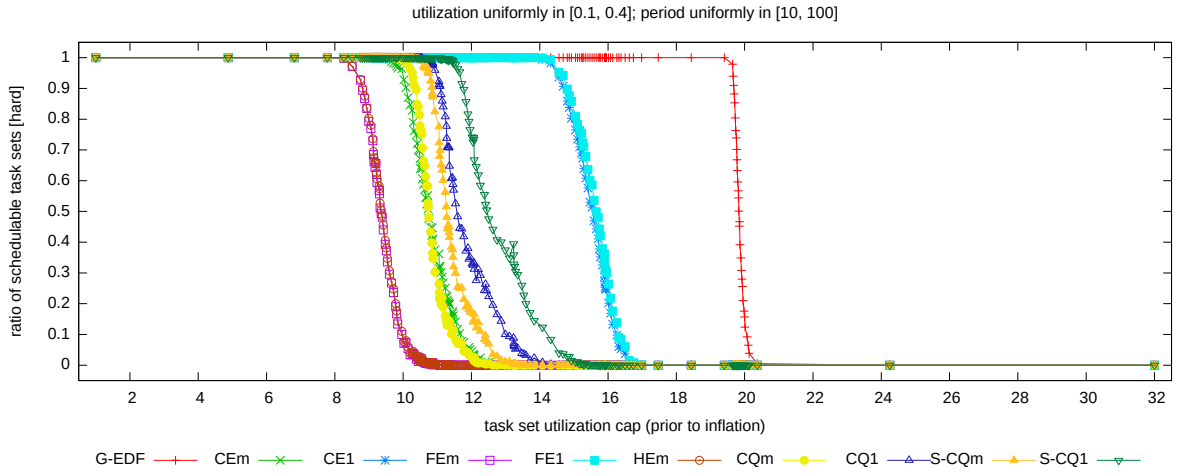

(b)

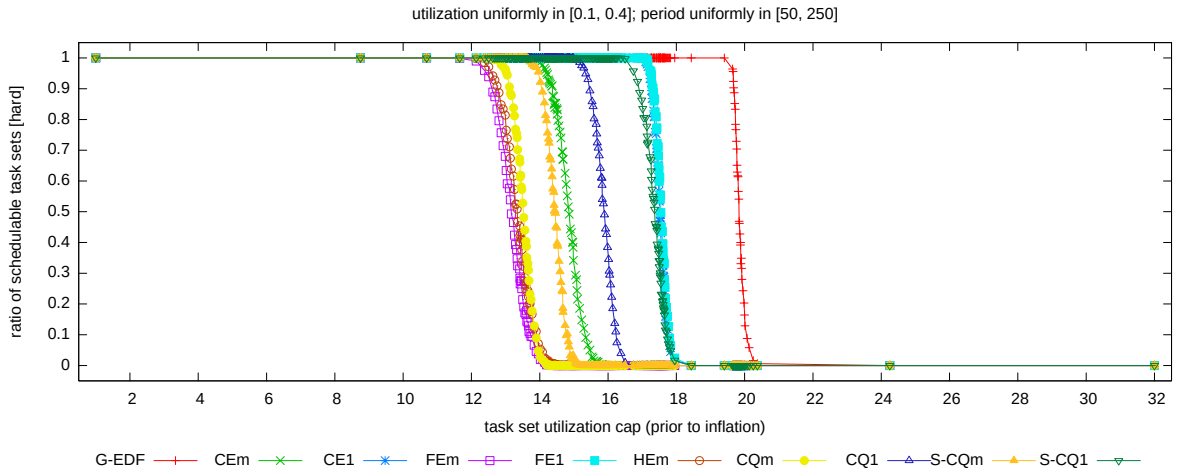

(c)

Figure 20: Hard schedulability of task sets with uniform medium per-task utilizations and **(a)** short, **(b)** moderate, and **(c)** long periods.

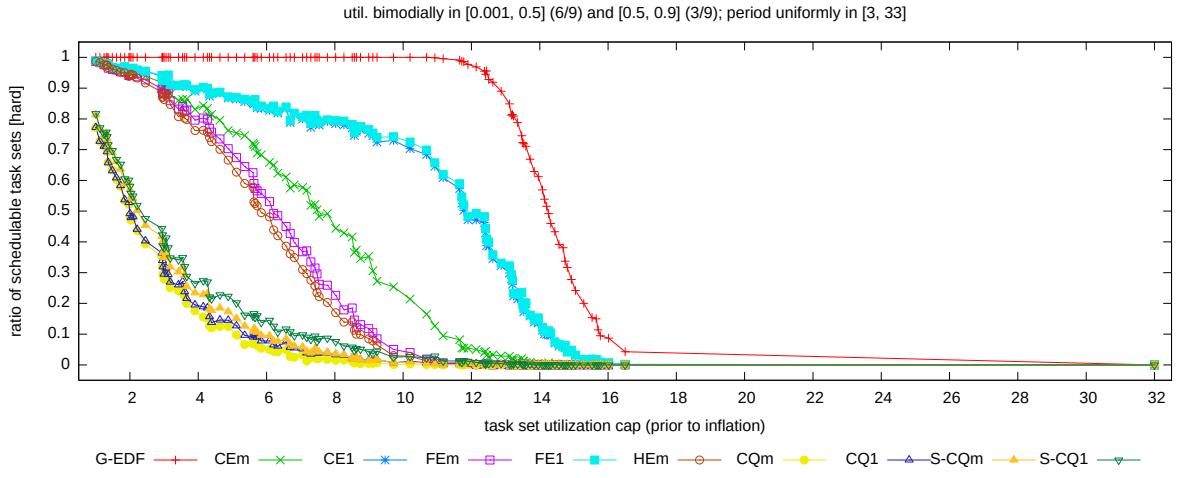

(a)

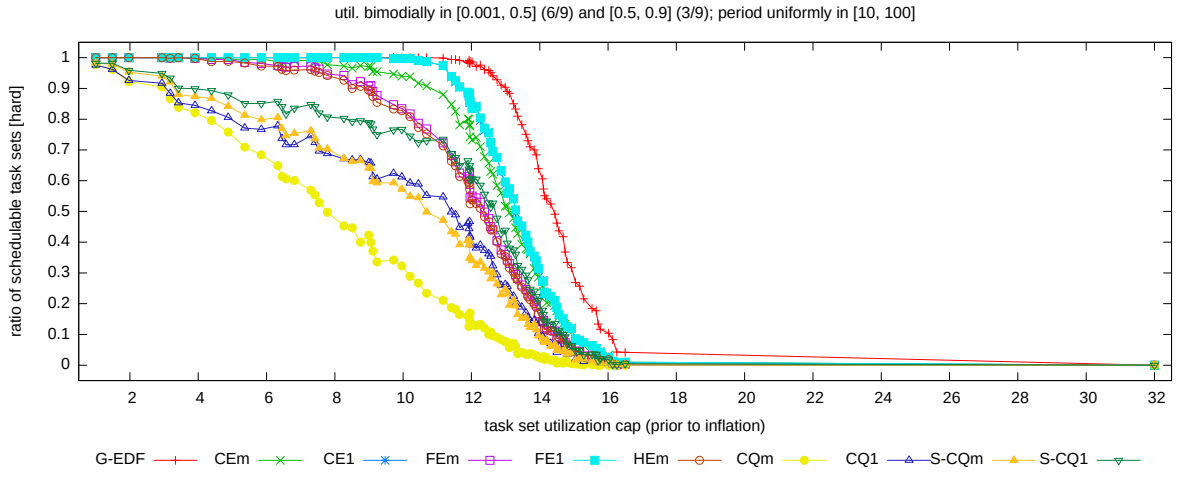

(b)

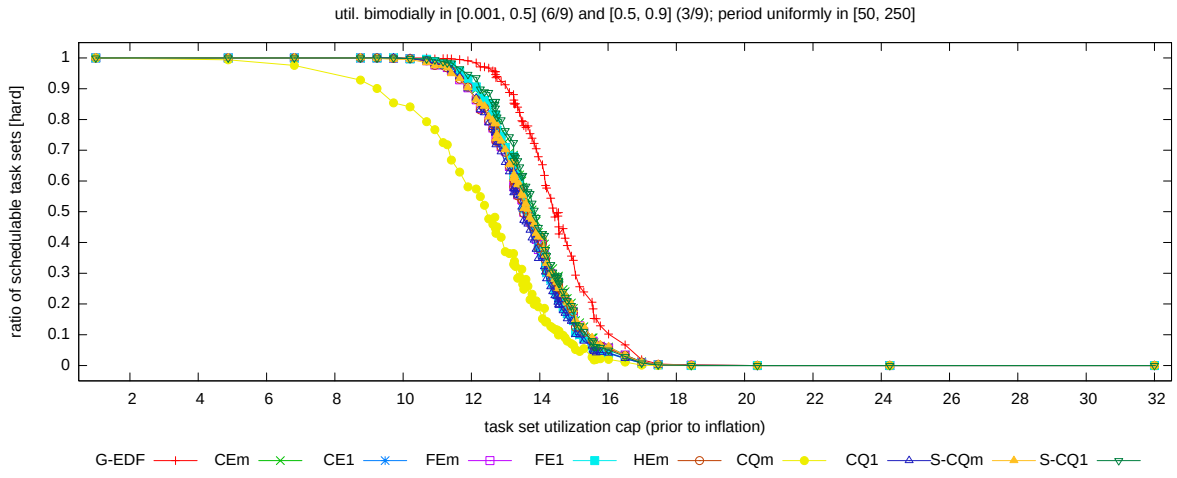

(c)

Figure 21: Hard schedulability of task sets with bimodal medium per-task utilizations and **(a)** short, **(b)** moderate, and **(c)** long periods.

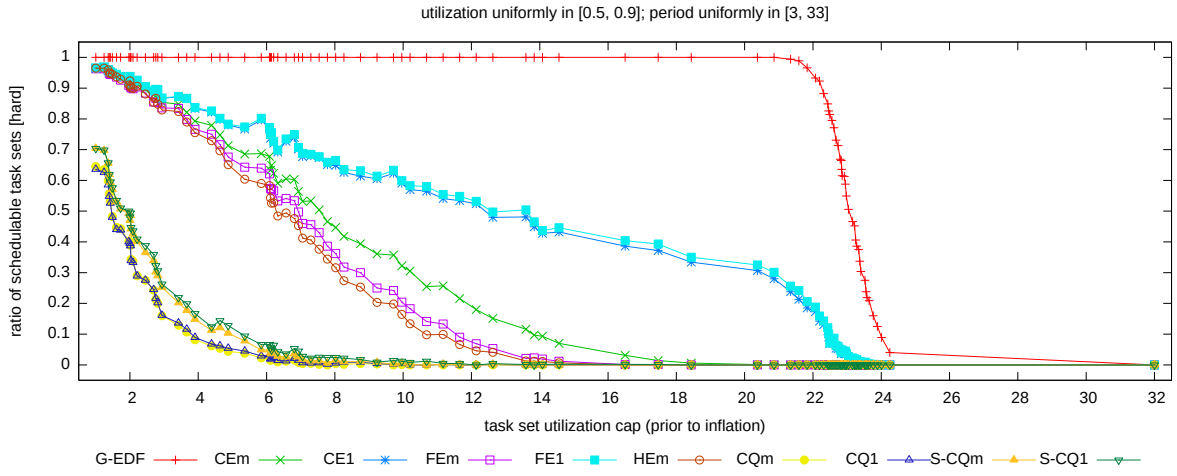

(a)

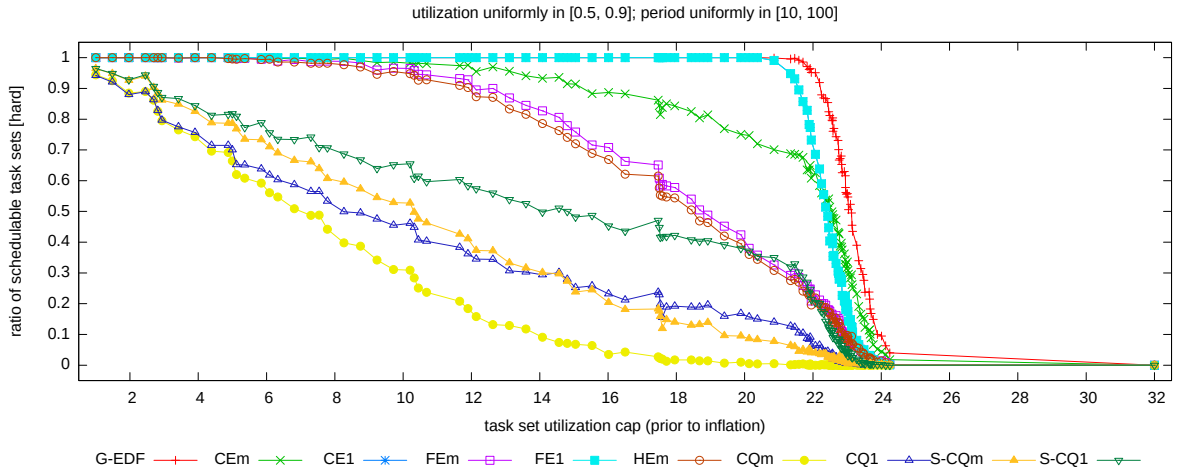

(b)

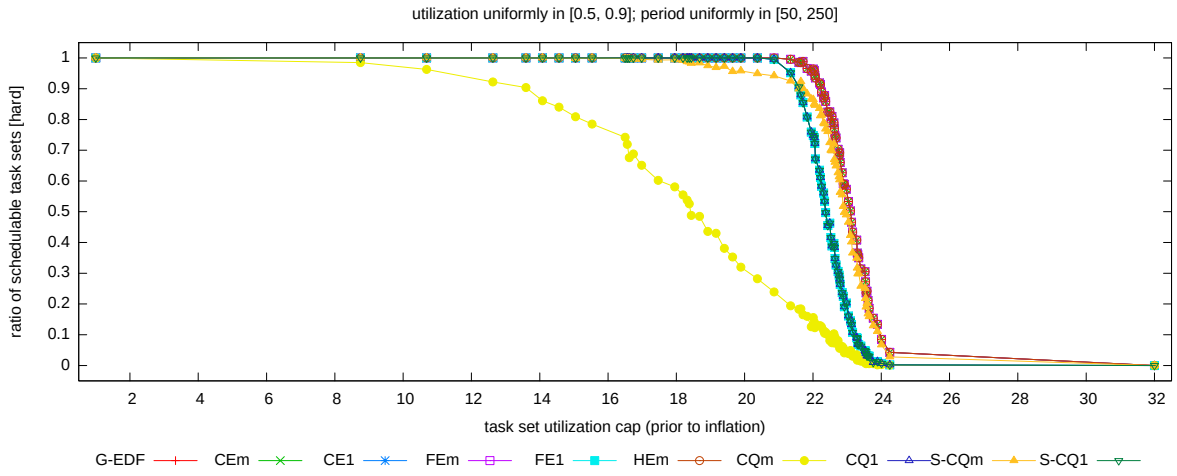

(c)

Figure 22: Hard schedulability of task sets with uniform heavy per-task utilizations and **(a)** short, **(b)** moderate, and **(c)** long periods.

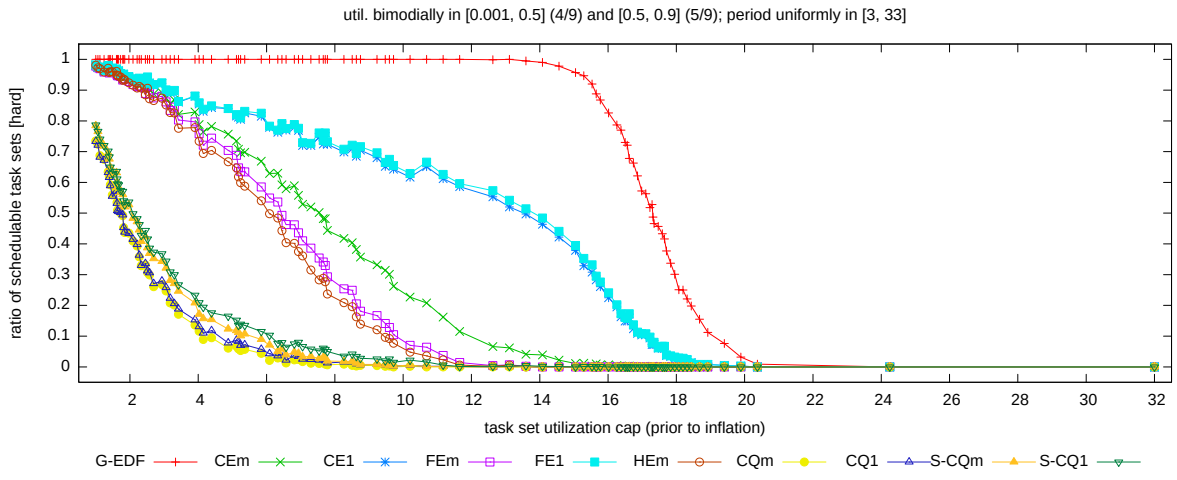

(a)

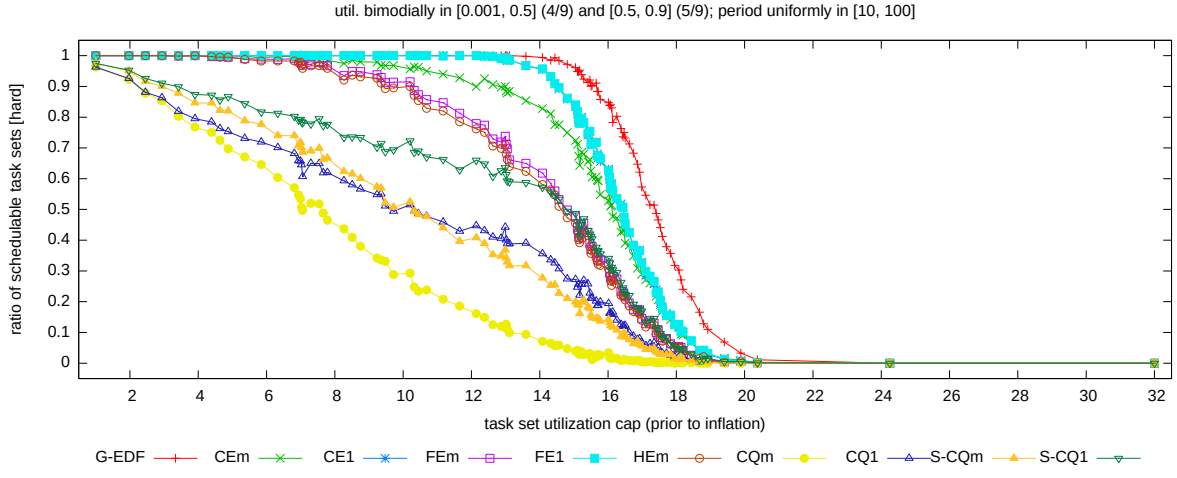

(b)

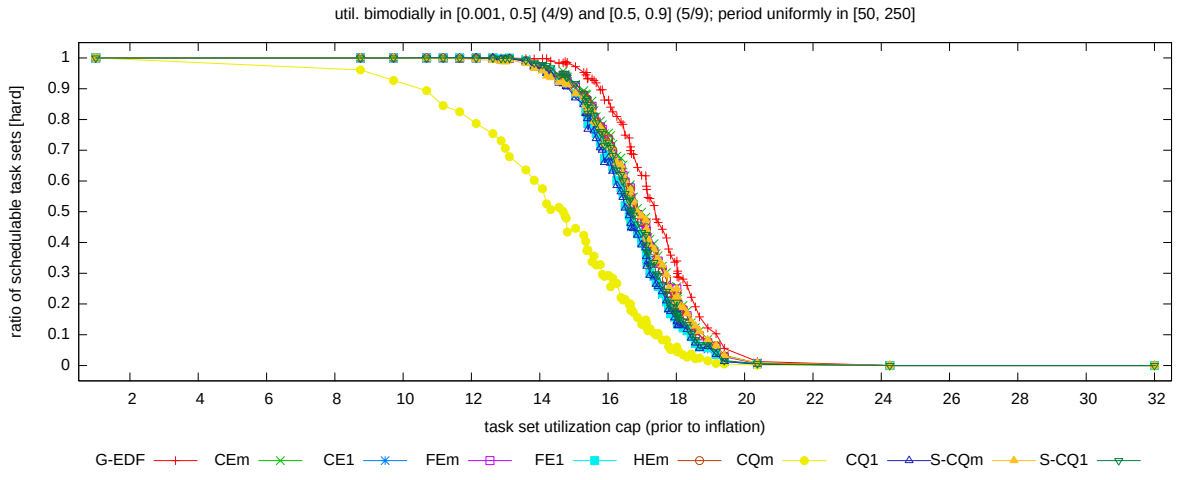

(c)

Figure 23: Hard schedulability of task sets with bimodal heavy per-task utilizations and **(a)** short, **(b)** moderate, and **(c)** long periods.

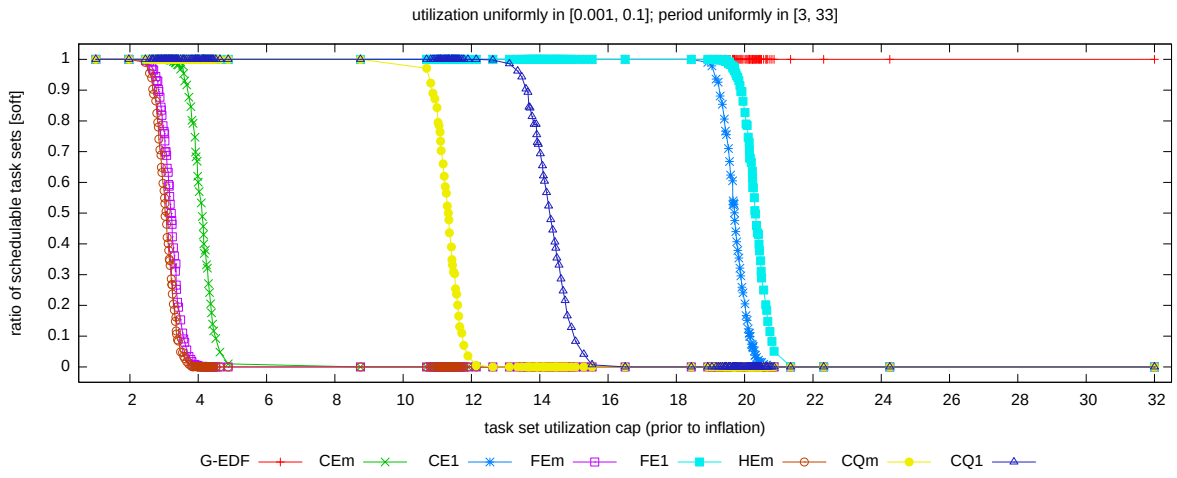

(a)

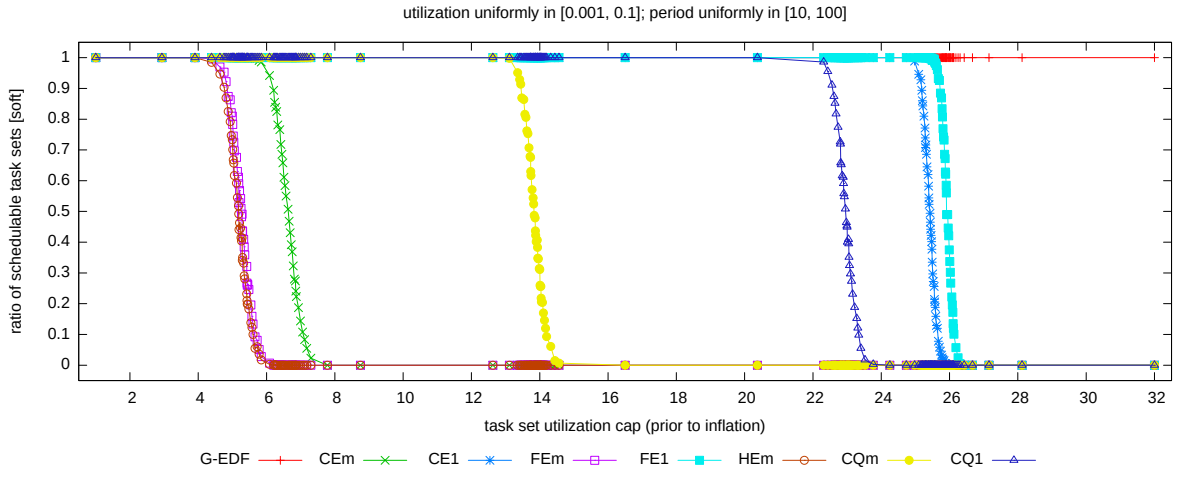

(b)

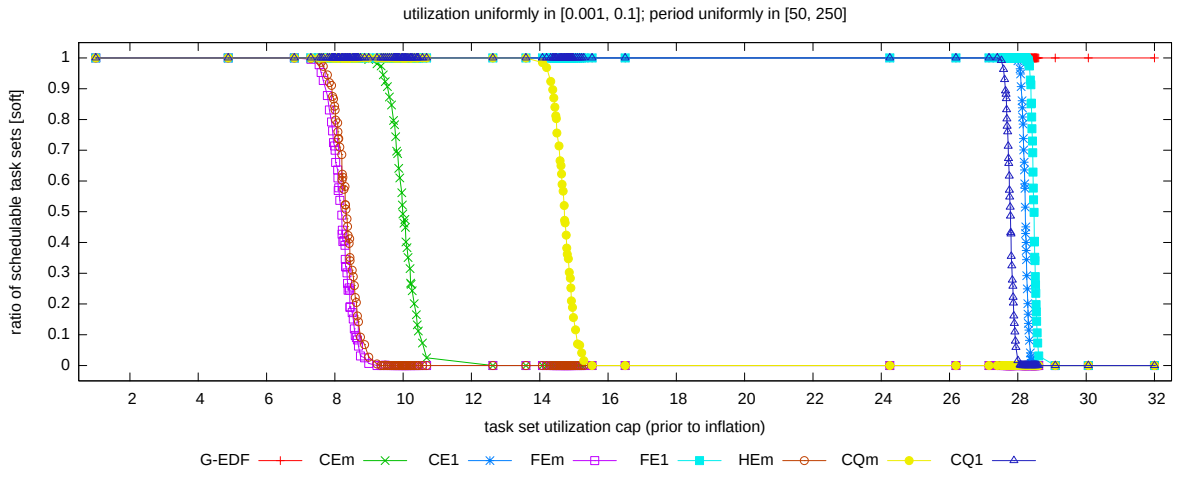

(c)

Figure 24: Soft schedulability of task sets with uniform light per-task utilizations and **(a)** short, **(b)** moderate, and **(c)** long periods.

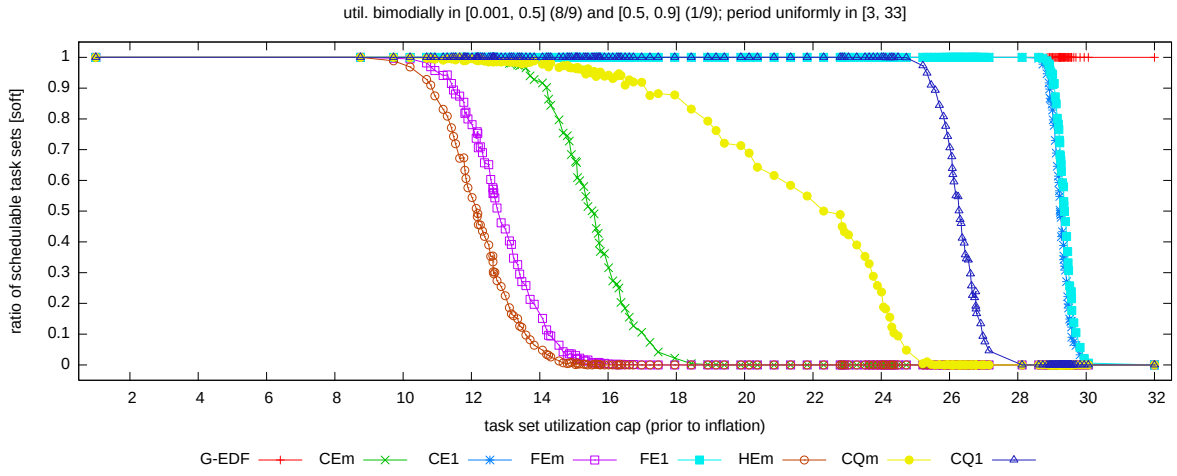

(a)

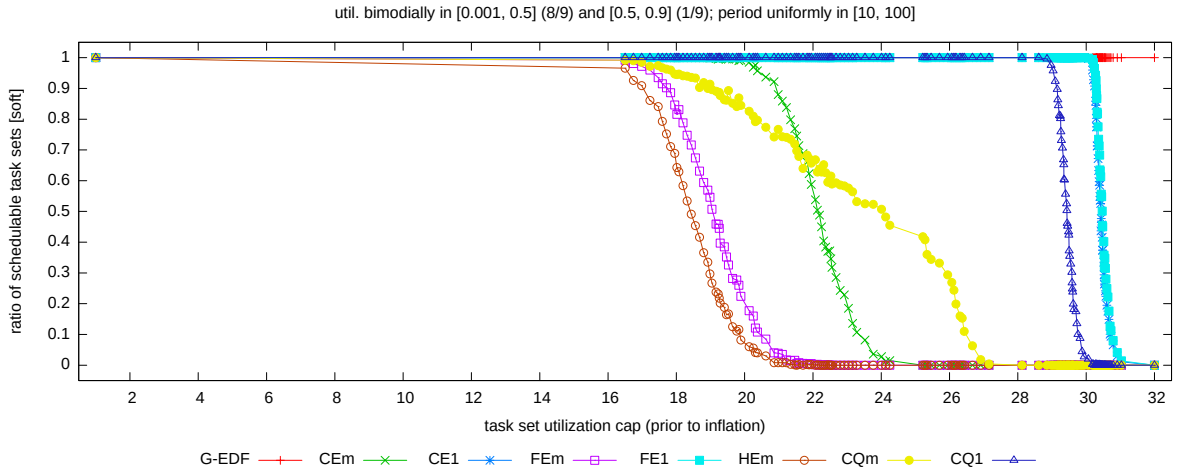

(b)

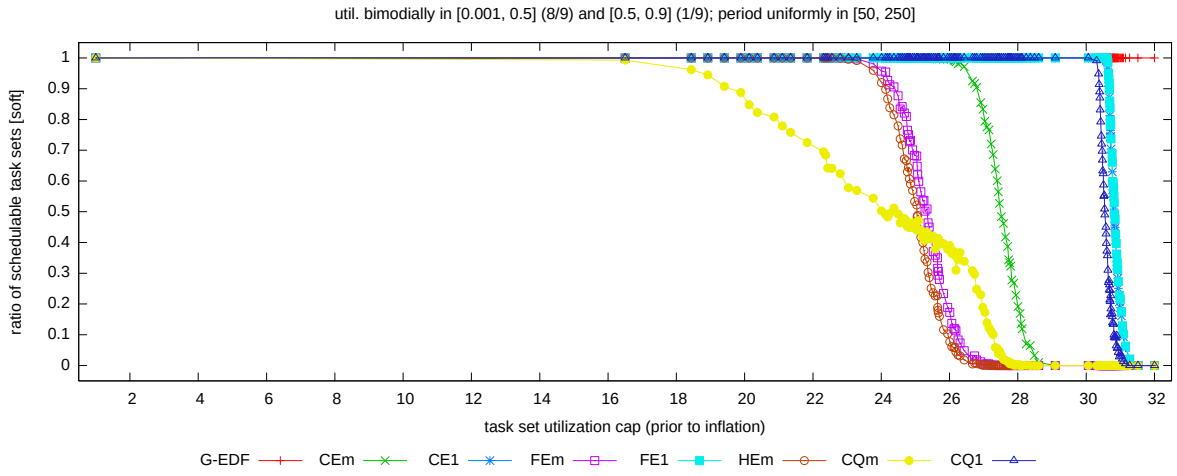

(c)

Figure 25: Soft schedulability of task sets with bimodal light per-task utilizations and **(a)** short, **(b)** moderate, and **(c)** long periods.

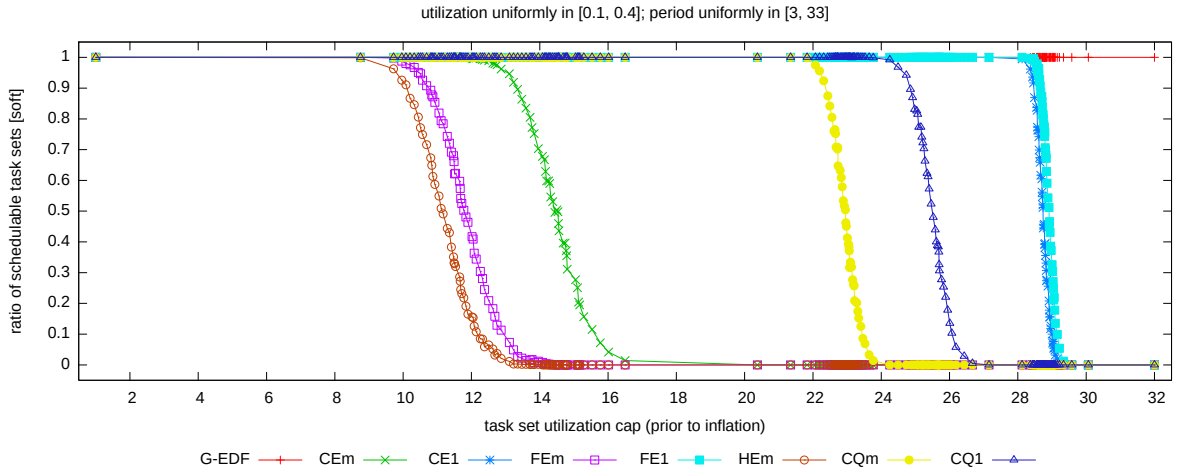

(a)

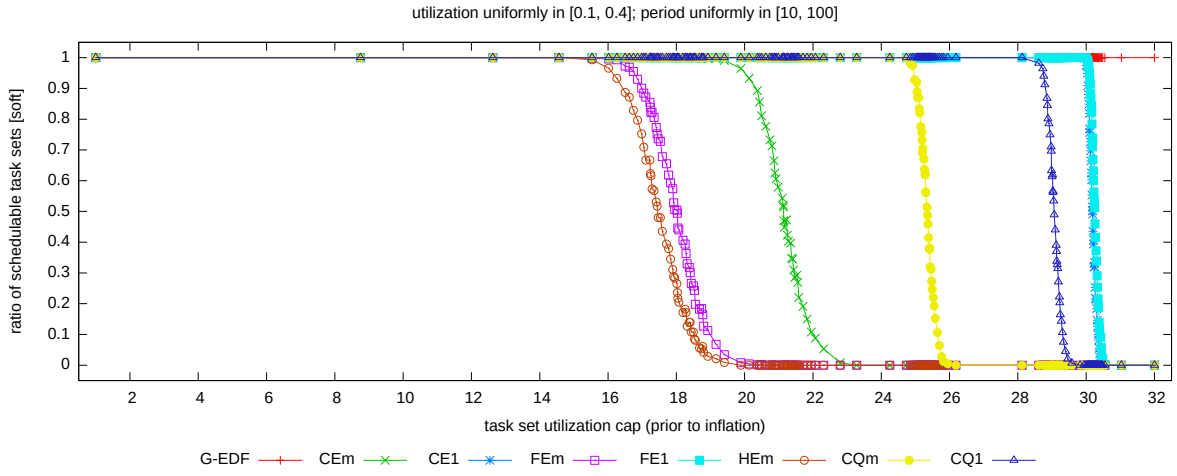

(b)

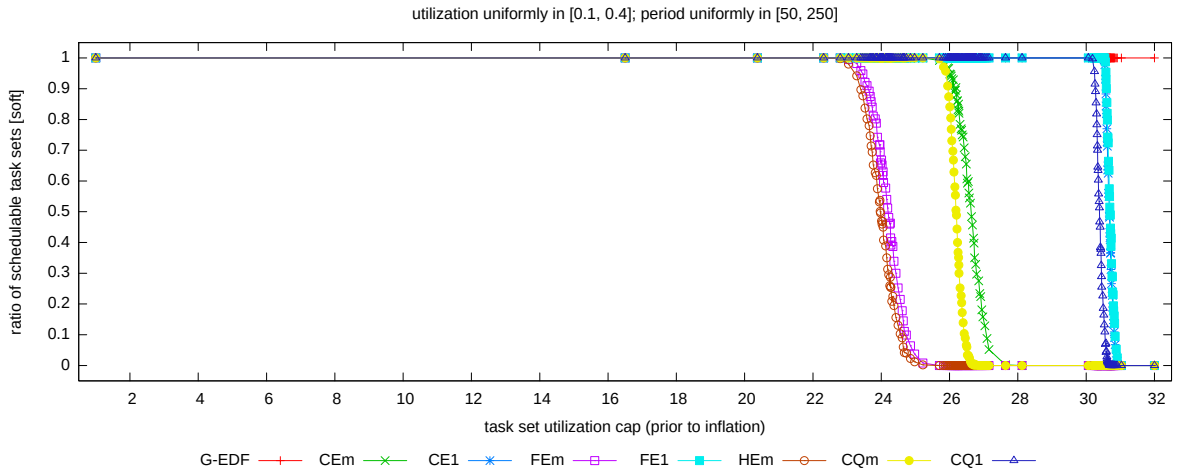

(c)

Figure 26: Soft schedulability of task sets with uniform medium per-task utilizations and **(a)** short, **(b)** moderate, and **(c)** long periods.

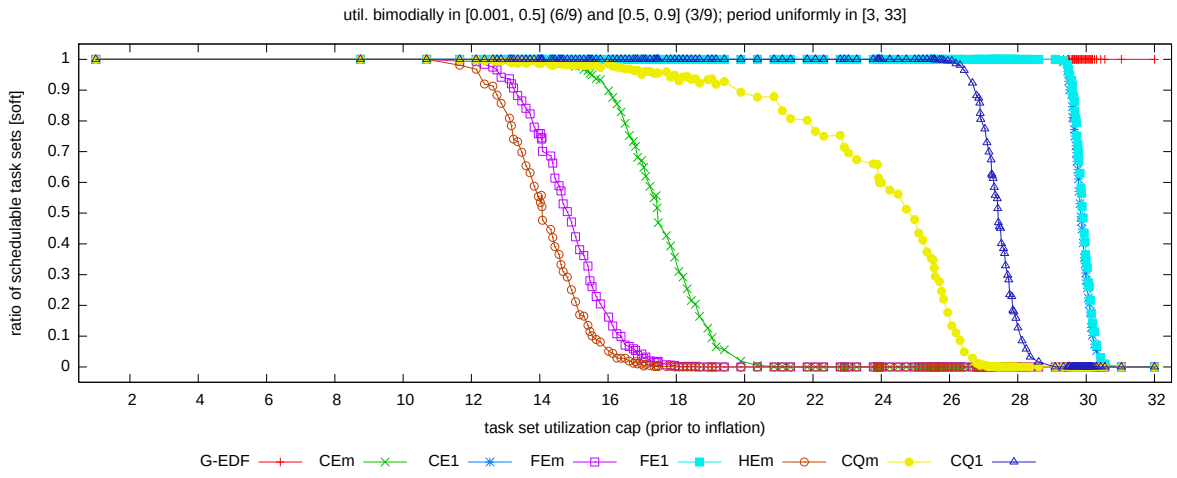

(a)

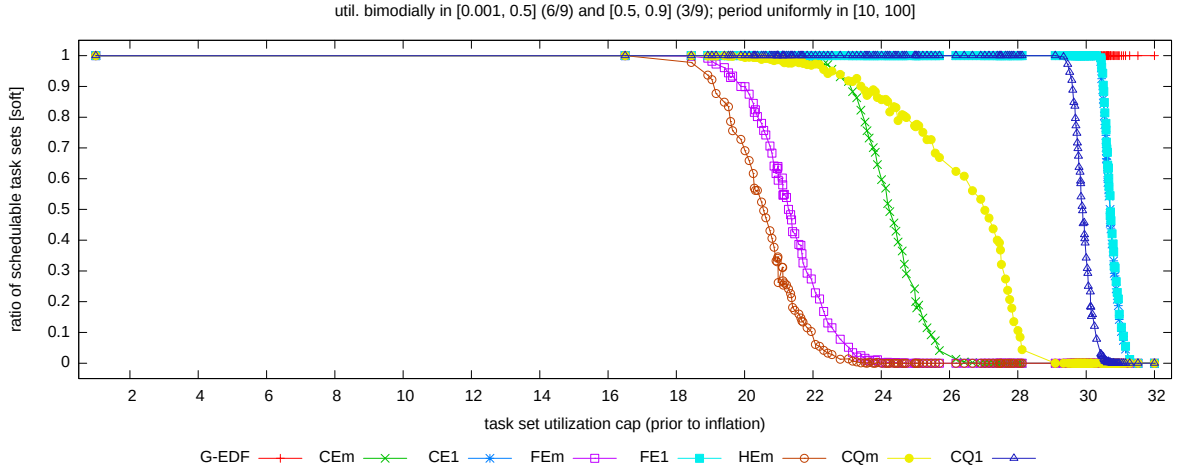

(b)

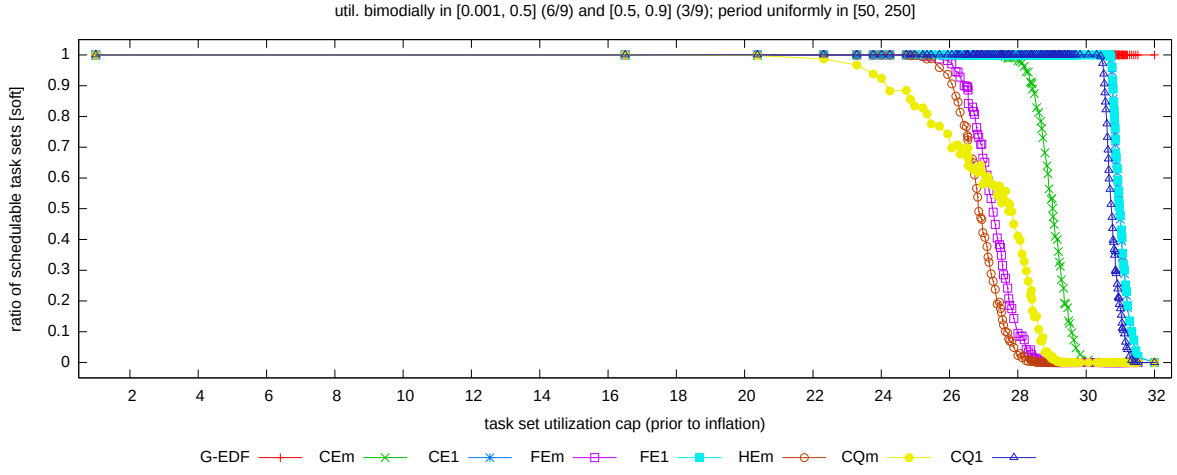

(c)

Figure 27: Soft schedulability of task sets with bimodal medium per-task utilizations and **(a)** short, **(b)** moderate, and **(c)** long periods.

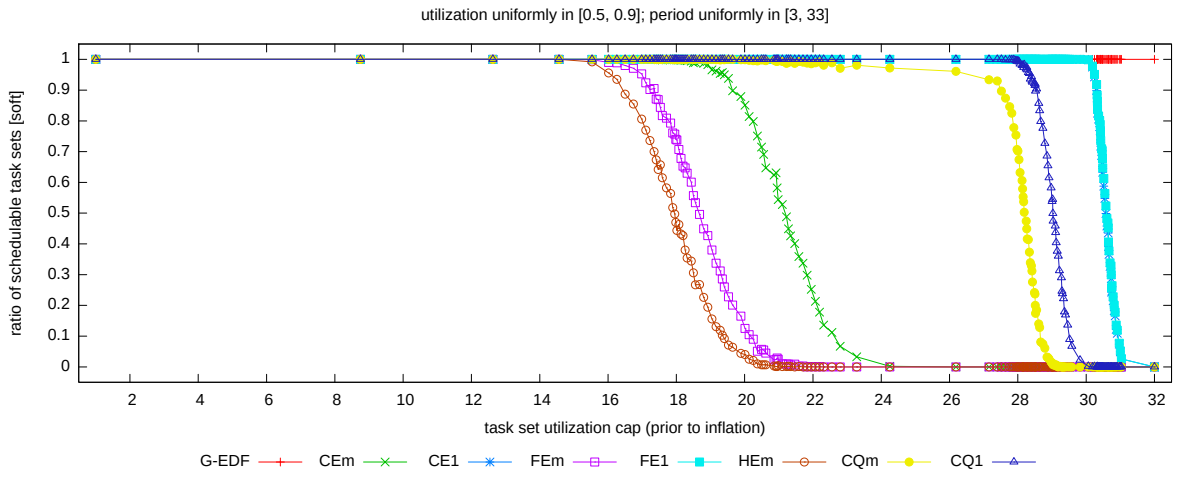

(a)

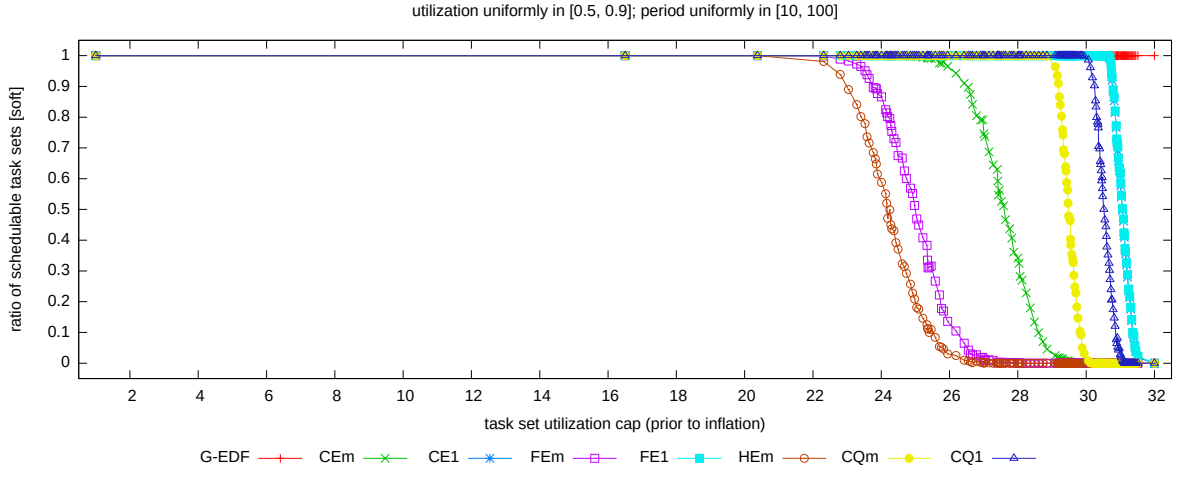

(b)

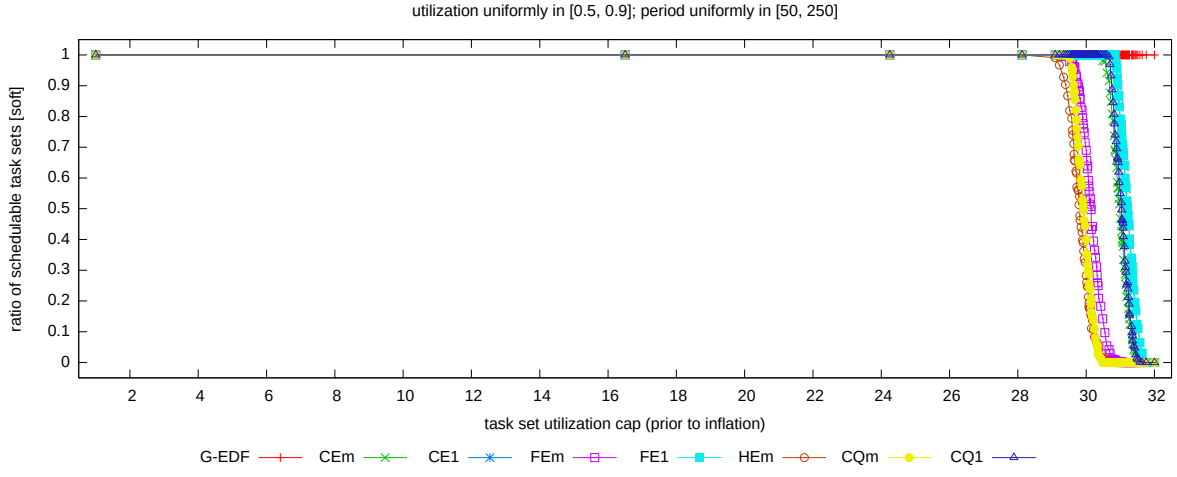

(c)

Figure 28: Soft schedulability of task sets with uniform heavy per-task utilizations and **(a)** short, **(b)** moderate, and **(c)** long periods.

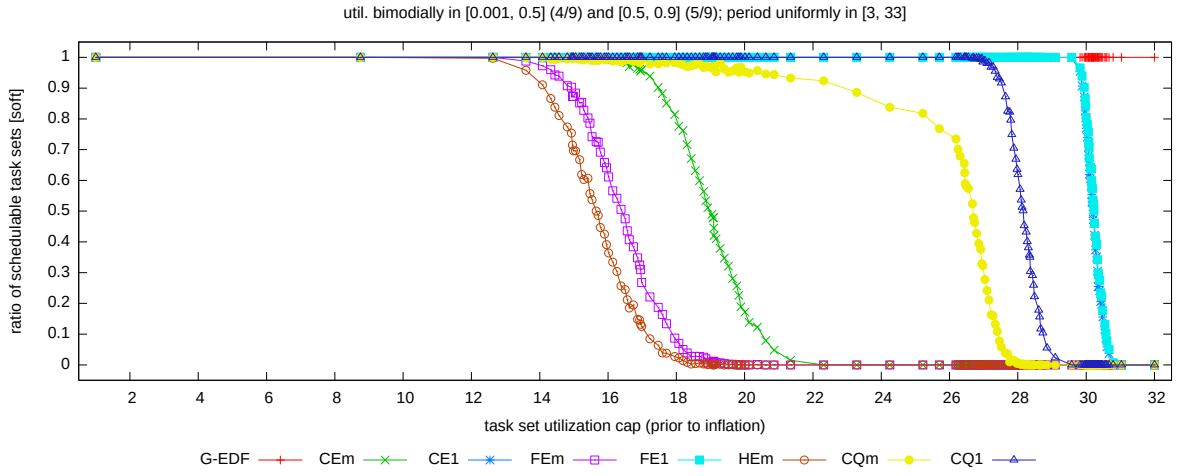

(a)

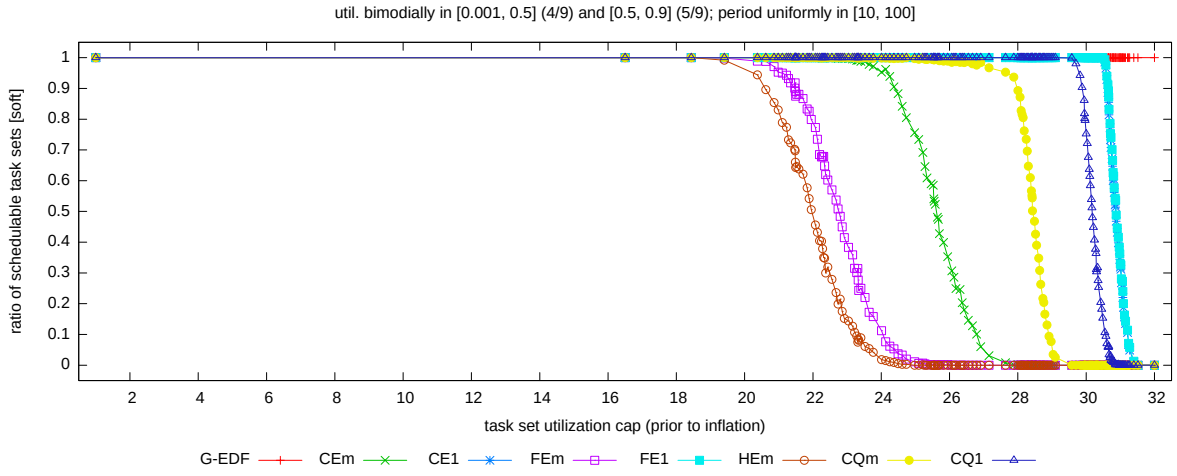

(b)

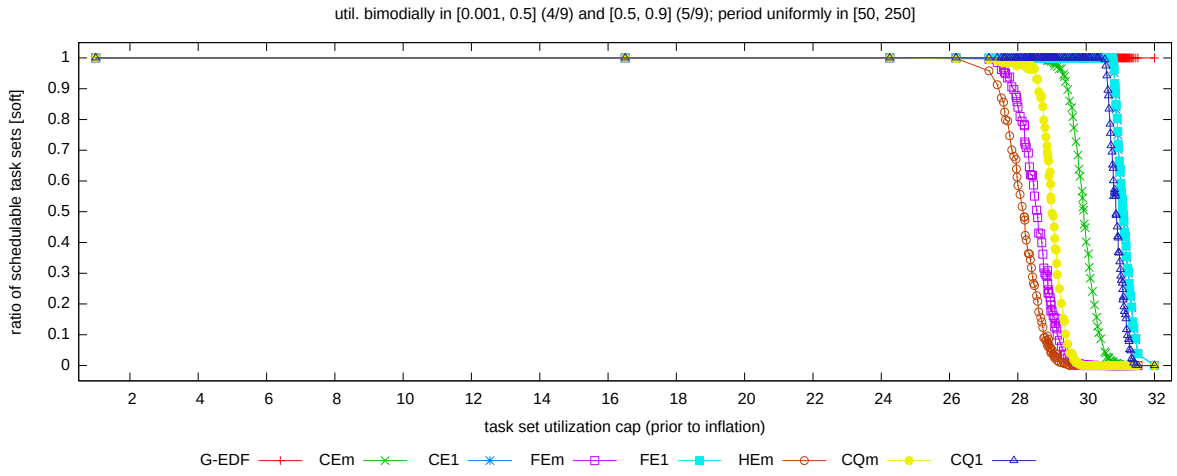

(c)

Figure 29: Soft schedulability of task sets with bimodal heavy per-task utilizations and **(a)** short, **(b)** moderate, and **(c)** long periods.

B.2 Individual Comparisons

Due to the large number of curves per graph in the preceding Sec. B.1, it is difficult to make out individual trends. To facilitate comparing the discussed tradeoffs individually, we provide the following 126 graphs that show only select curves per graph. They are organized as follows.

The following 12 figures compare CEm to CE1 (global vs. dedicated interrupt handling).

- Fig. 30 shows hard schedulability results under uniform light utilizations. Fig. 30 corresponds to Fig. 18.
- Fig. 31 shows hard schedulability results under bimodal light utilizations. Fig. 31 corresponds to Fig. 19.
- Fig. 32 shows hard schedulability results under uniform medium utilizations. Fig. 32 corresponds to Fig. 20.
- Fig. 33 shows hard schedulability results under bimodal medium utilizations. Fig. 33 corresponds to Fig. 21.
- Fig. 34 shows hard schedulability results under uniform heavy utilizations. Fig. 34 corresponds to Fig. 22.
- Fig. 35 shows hard schedulability results under bimodal heavy utilizations. Fig. 35 corresponds to Fig. 23.
- Fig. 36 shows soft schedulability results under uniform light utilizations. Fig. 36 corresponds to Fig. 24.
- Fig. 37 shows soft schedulability results under bimodal light utilizations. Fig. 37 corresponds to Fig. 25.
- Fig. 38 shows soft schedulability results under uniform medium utilizations. Fig. 38 corresponds to Fig. 26.
- Fig. 39 shows soft schedulability results under bimodal medium utilizations. Fig. 39 corresponds to Fig. 27.
- Fig. 40 shows soft schedulability results under uniform heavy utilizations. Fig. 40 corresponds to Fig. 28.
- Fig. 41 shows soft schedulability results under bimodal heavy utilizations. Fig. 41 corresponds to Fig. 29.

The following 12 figures compare FEm to FE1 (global vs. dedicated interrupt handling).

- Fig. 42 shows hard schedulability results under uniform light utilizations. Fig. 42 corresponds to Fig. 18.
- Fig. 43 shows hard schedulability results under bimodal light utilizations. Fig. 43 corresponds to Fig. 19.
- Fig. 44 shows hard schedulability results under uniform medium utilizations. Fig. 44 corresponds to Fig. 20.
- Fig. 45 shows hard schedulability results under bimodal medium utilizations. Fig. 45 corresponds to Fig. 21.
- Fig. 46 shows hard schedulability results under uniform heavy utilizations. Fig. 46 corresponds to Fig. 22.
- Fig. 47 shows hard schedulability results under bimodal heavy utilizations. Fig. 47 corresponds to Fig. 23.
- Fig. 48 shows soft schedulability results under uniform light utilizations. Fig. 48 corresponds to Fig. 24.
- Fig. 49 shows soft schedulability results under bimodal light utilizations. Fig. 49 corresponds to Fig. 25.
- Fig. 50 shows soft schedulability results under uniform medium utilizations. Fig. 50 corresponds to Fig. 26.
- Fig. 51 shows soft schedulability results under bimodal medium utilizations. Fig. 51 corresponds to Fig. 27.
- Fig. 52 shows soft schedulability results under uniform heavy utilizations. Fig. 52 corresponds to Fig. 28.
- Fig. 53 shows soft schedulability results under bimodal heavy utilizations. Fig. 53 corresponds to Fig. 29.

The following 12 figures compare CQm to CQ1 (global vs. dedicated interrupt handling).

- Fig. 54 shows hard schedulability results under uniform light utilizations. Fig. 54 corresponds to Fig. 18.
- Fig. 55 shows hard schedulability results under bimodal light utilizations. Fig. 55 corresponds to Fig. 19.
- Fig. 56 shows hard schedulability results under uniform medium utilizations. Fig. 56 corresponds to Fig. 20.

- Fig. 57 shows hard schedulability results under bimodal medium utilizations. Fig. 57 corresponds to Fig. 21.
- Fig. 58 shows hard schedulability results under uniform heavy utilizations. Fig. 58 corresponds to Fig. 22.
- Fig. 59 shows hard schedulability results under bimodal heavy utilizations. Fig. 59 corresponds to Fig. 23.
- Fig. 60 shows soft schedulability results under uniform light utilizations. Fig. 60 corresponds to Fig. 24.
- Fig. 61 shows soft schedulability results under bimodal light utilizations. Fig. 61 corresponds to Fig. 25.
- Fig. 62 shows soft schedulability results under uniform medium utilizations. Fig. 62 corresponds to Fig. 26.
- Fig. 63 shows soft schedulability results under bimodal medium utilizations. Fig. 63 corresponds to Fig. 27.
- Fig. 64 shows soft schedulability results under uniform heavy utilizations. Fig. 64 corresponds to Fig. 28.
- Fig. 65 shows soft schedulability results under bimodal heavy utilizations. Fig. 65 corresponds to Fig. 29.

The following 12 figures compare CEm to FEm (coarse- vs. fine-grained queues).

- Fig. 66 shows hard schedulability results under uniform light utilizations. Fig. 66 corresponds to Fig. 18.
- Fig. 67 shows hard schedulability results under bimodal light utilizations. Fig. 67 corresponds to Fig. 19.
- Fig. 68 shows hard schedulability results under uniform medium utilizations. Fig. 68 corresponds to Fig. 20.
- Fig. 69 shows hard schedulability results under bimodal medium utilizations. Fig. 69 corresponds to Fig. 21.
- Fig. 70 shows hard schedulability results under uniform heavy utilizations. Fig. 70 corresponds to Fig. 22.
- Fig. 71 shows hard schedulability results under bimodal heavy utilizations. Fig. 71 corresponds to Fig. 23.
- Fig. 72 shows soft schedulability results under uniform light utilizations. Fig. 72 corresponds to Fig. 24.
- Fig. 73 shows soft schedulability results under bimodal light utilizations. Fig. 73 corresponds to Fig. 25.
- Fig. 74 shows soft schedulability results under uniform medium utilizations. Fig. 74 corresponds to Fig. 26.
- Fig. 75 shows soft schedulability results under bimodal medium utilizations. Fig. 75 corresponds to Fig. 27.
- Fig. 76 shows soft schedulability results under uniform heavy utilizations. Fig. 76 corresponds to Fig. 28.
- Fig. 77 shows soft schedulability results under bimodal heavy utilizations. Fig. 77 corresponds to Fig. 29.

The following 12 figures compare CE1 to FE1 (coarse- vs. fine-grained queues).

- Fig. 78 shows hard schedulability results under uniform light utilizations. Fig. 78 corresponds to Fig. 18.
- Fig. 79 shows hard schedulability results under bimodal light utilizations. Fig. 79 corresponds to Fig. 19.
- Fig. 80 shows hard schedulability results under uniform medium utilizations. Fig. 80 corresponds to Fig. 20.
- Fig. 81 shows hard schedulability results under bimodal medium utilizations. Fig. 81 corresponds to Fig. 21.
- Fig. 82 shows hard schedulability results under uniform heavy utilizations. Fig. 82 corresponds to Fig. 22.
- Fig. 83 shows hard schedulability results under bimodal heavy utilizations. Fig. 83 corresponds to Fig. 23.
- Fig. 84 shows soft schedulability results under uniform light utilizations. Fig. 84 corresponds to Fig. 24.
- Fig. 85 shows soft schedulability results under bimodal light utilizations. Fig. 85 corresponds to Fig. 25.
- Fig. 86 shows soft schedulability results under uniform medium utilizations. Fig. 86 corresponds to Fig. 26.

- Fig. 87 shows soft schedulability results under bimodal medium utilizations. Fig. 87 corresponds to Fig. 27.
- Fig. 88 shows soft schedulability results under uniform heavy utilizations. Fig. 88 corresponds to Fig. 28.
- Fig. 89 shows soft schedulability results under bimodal heavy utilizations. Fig. 89 corresponds to Fig. 29.

The following 12 figures compare CEm to HEm (coarse-grained vs. hierarchical queues).

- Fig. 90 shows hard schedulability results under uniform light utilizations. Fig. 90 corresponds to Fig. 18.
- Fig. 91 shows hard schedulability results under bimodal light utilizations. Fig. 91 corresponds to Fig. 19.
- Fig. 92 shows hard schedulability results under uniform medium utilizations. Fig. 92 corresponds to Fig. 20.
- Fig. 93 shows hard schedulability results under bimodal medium utilizations. Fig. 93 corresponds to Fig. 21.
- Fig. 94 shows hard schedulability results under uniform heavy utilizations. Fig. 94 corresponds to Fig. 22.
- Fig. 95 shows hard schedulability results under bimodal heavy utilizations. Fig. 95 corresponds to Fig. 23.
- Fig. 96 shows soft schedulability results under uniform light utilizations. Fig. 96 corresponds to Fig. 24.
- Fig. 97 shows soft schedulability results under bimodal light utilizations. Fig. 97 corresponds to Fig. 25.
- Fig. 98 shows soft schedulability results under uniform medium utilizations. Fig. 98 corresponds to Fig. 26.
- Fig. 99 shows soft schedulability results under bimodal medium utilizations. Fig. 99 corresponds to Fig. 27.
- Fig. 100 shows soft schedulability results under uniform heavy utilizations. Fig. 100 corresponds to Fig. 28.
- Fig. 101 shows soft schedulability results under bimodal heavy utilizations. Fig. 101 corresponds to Fig. 29.

The following 12 figures compare CEm to CQm (event- vs. quantum-driven scheduling).

- Fig. 102 shows hard schedulability results under uniform light utilizations. Fig. 102 corresponds to Fig. 18.
- Fig. 103 shows hard schedulability results under bimodal light utilizations. Fig. 103 corresponds to Fig. 19.
- Fig. 104 shows hard schedulability results under uniform medium utilizations. Fig. 104 corresponds to Fig. 20.
- Fig. 105 shows hard schedulability results under bimodal medium utilizations. Fig. 105 corresponds to Fig. 21.
- Fig. 106 shows hard schedulability results under uniform heavy utilizations. Fig. 106 corresponds to Fig. 22.
- Fig. 107 shows hard schedulability results under bimodal heavy utilizations. Fig. 107 corresponds to Fig. 23.
- Fig. 108 shows soft schedulability results under uniform light utilizations. Fig. 108 corresponds to Fig. 24.
- Fig. 109 shows soft schedulability results under bimodal light utilizations. Fig. 109 corresponds to Fig. 25.
- Fig. 110 shows soft schedulability results under uniform medium utilizations. Fig. 110 corresponds to Fig. 26.
- Fig. 111 shows soft schedulability results under bimodal medium utilizations. Fig. 111 corresponds to Fig. 27.
- Fig. 112 shows soft schedulability results under uniform heavy utilizations. Fig. 112 corresponds to Fig. 28.
- Fig. 113 shows soft schedulability results under bimodal heavy utilizations. Fig. 113 corresponds to Fig. 29.

The following 12 figures compare FE1 to CQ1 (event- vs. quantum-driven scheduling).

- Fig. 114 shows hard schedulability results under uniform light utilizations. Fig. 114 corresponds to Fig. 18.
- Fig. 115 shows hard schedulability results under bimodal light utilizations. Fig. 115 corresponds to Fig. 19.

- Fig. 116 shows hard schedulability results under uniform medium utilizations. Fig. 116 corresponds to Fig. 20.
- Fig. 117 shows hard schedulability results under bimodal medium utilizations. Fig. 117 corresponds to Fig. 21.
- Fig. 118 shows hard schedulability results under uniform heavy utilizations. Fig. 118 corresponds to Fig. 22.
- Fig. 119 shows hard schedulability results under bimodal heavy utilizations. Fig. 119 corresponds to Fig. 23.
- Fig. 120 shows soft schedulability results under uniform light utilizations. Fig. 120 corresponds to Fig. 24.
- Fig. 121 shows soft schedulability results under bimodal light utilizations. Fig. 121 corresponds to Fig. 25.
- Fig. 122 shows soft schedulability results under uniform medium utilizations. Fig. 122 corresponds to Fig. 26.
- Fig. 123 shows soft schedulability results under bimodal medium utilizations. Fig. 123 corresponds to Fig. 27.
- Fig. 124 shows soft schedulability results under uniform heavy utilizations. Fig. 124 corresponds to Fig. 28.
- Fig. 125 shows soft schedulability results under bimodal heavy utilizations. Fig. 125 corresponds to Fig. 29.

The following 6 figures compare S-CQm to S-CQ1 (global vs. dedicated interrupt handling).

- Fig. 126 shows hard schedulability results under uniform light utilizations. Fig. 126 corresponds to Fig. 18.
- Fig. 127 shows hard schedulability results under bimodal light utilizations. Fig. 127 corresponds to Fig. 19.
- Fig. 128 shows hard schedulability results under uniform medium utilizations. Fig. 128 corresponds to Fig. 20.
- Fig. 129 shows hard schedulability results under bimodal medium utilizations. Fig. 129 corresponds to Fig. 21.
- Fig. 130 shows hard schedulability results under uniform heavy utilizations. Fig. 130 corresponds to Fig. 22.
- Fig. 131 shows hard schedulability results under bimodal heavy utilizations. Fig. 131 corresponds to Fig. 23.

The following 6 figures compare CQm to S-CQm (aligned vs. staggered quanta).

- Fig. 132 shows hard schedulability results under uniform light utilizations. Fig. 132 corresponds to Fig. 18.
- Fig. 133 shows hard schedulability results under bimodal light utilizations. Fig. 133 corresponds to Fig. 19.
- Fig. 134 shows hard schedulability results under uniform medium utilizations. Fig. 134 corresponds to Fig. 20.
- Fig. 135 shows hard schedulability results under bimodal medium utilizations. Fig. 135 corresponds to Fig. 21.
- Fig. 136 shows hard schedulability results under uniform heavy utilizations. Fig. 136 corresponds to Fig. 22.
- Fig. 137 shows hard schedulability results under bimodal heavy utilizations. Fig. 137 corresponds to Fig. 23.

The following 6 figures compare CQ1 to S-CQ1 (aligned vs. staggered quanta).

- Fig. 138 shows hard schedulability results under uniform light utilizations. Fig. 138 corresponds to Fig. 18.
- Fig. 139 shows hard schedulability results under bimodal light utilizations. Fig. 139 corresponds to Fig. 19.
- Fig. 140 shows hard schedulability results under uniform medium utilizations. Fig. 140 corresponds to Fig. 20.
- Fig. 141 shows hard schedulability results under bimodal medium utilizations. Fig. 141 corresponds to Fig. 21.
- Fig. 142 shows hard schedulability results under uniform heavy utilizations. Fig. 142 corresponds to Fig. 22.
- Fig. 143 shows hard schedulability results under bimodal heavy utilizations. Fig. 143 corresponds to Fig. 23.

The following 6 figures compare CEm to S-CQm (event- vs. quantum-driven scheduling).

- Fig. 144 shows hard schedulability results under uniform light utilizations. Fig. 144 corresponds to Fig. 18.
- Fig. 145 shows hard schedulability results under bimodal light utilizations. Fig. 145 corresponds to Fig. 19.
- Fig. 146 shows hard schedulability results under uniform medium utilizations. Fig. 146 corresponds to Fig. 20.
- Fig. 147 shows hard schedulability results under bimodal medium utilizations. Fig. 147 corresponds to Fig. 21.
- Fig. 148 shows hard schedulability results under uniform heavy utilizations. Fig. 148 corresponds to Fig. 22.
- Fig. 149 shows hard schedulability results under bimodal heavy utilizations. Fig. 149 corresponds to Fig. 23.

The following 6 figures compare FE1 to S-CQ1 (event- vs. quantum-driven scheduling).

- Fig. 150 shows hard schedulability results under uniform light utilizations. Fig. 150 corresponds to Fig. 18.
- Fig. 151 shows hard schedulability results under bimodal light utilizations. Fig. 151 corresponds to Fig. 19.
- Fig. 152 shows hard schedulability results under uniform medium utilizations. Fig. 152 corresponds to Fig. 20.
- Fig. 153 shows hard schedulability results under bimodal medium utilizations. Fig. 153 corresponds to Fig. 21.
- Fig. 154 shows hard schedulability results under uniform heavy utilizations. Fig. 154 corresponds to Fig. 22.
- Fig. 155 shows hard schedulability results under bimodal heavy utilizations. Fig. 155 corresponds to Fig. 23.

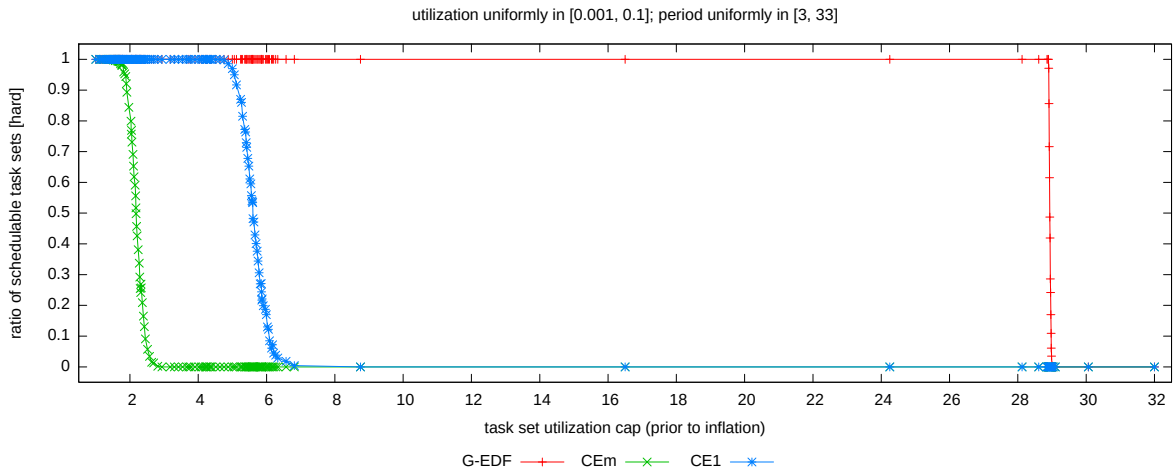

(a)

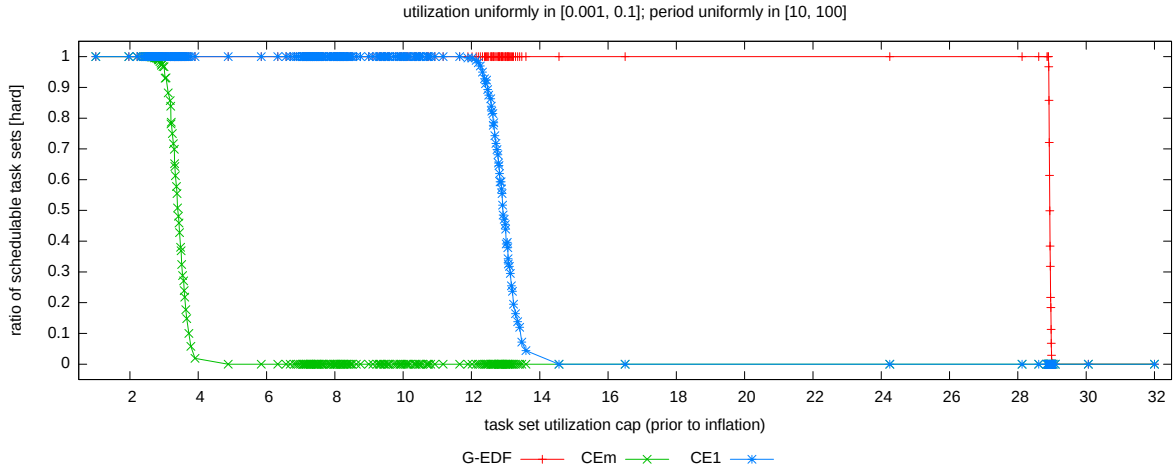

(b)

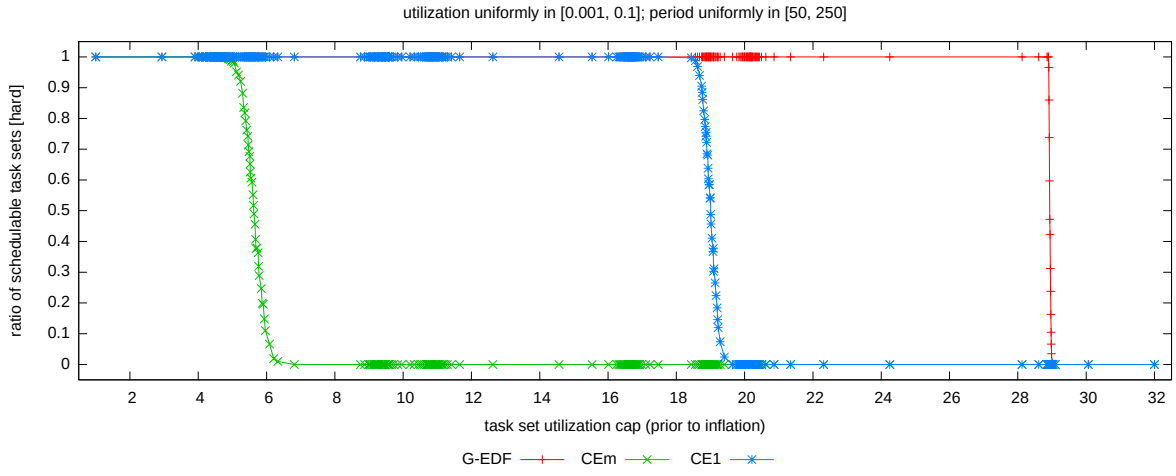

(c)

Figure 30: Comparison of CEm and CE1 (global vs. dedicated interrupt handling) in terms of hard schedulability of task sets with uniform light per-task utilizations and **(a)** short, **(b)** moderate, and **(c)** long periods. These graphs correspond to Fig. 18.

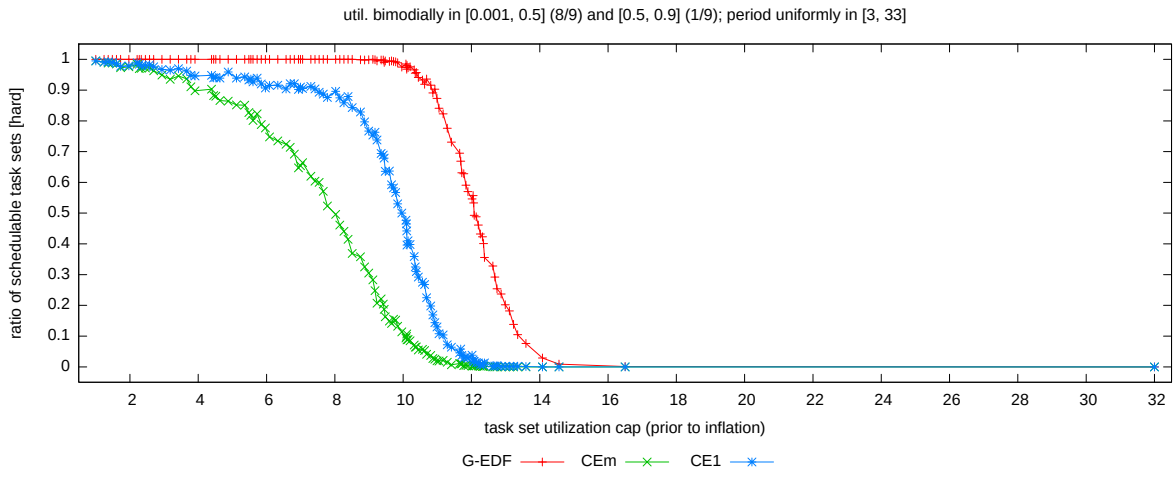

(a)

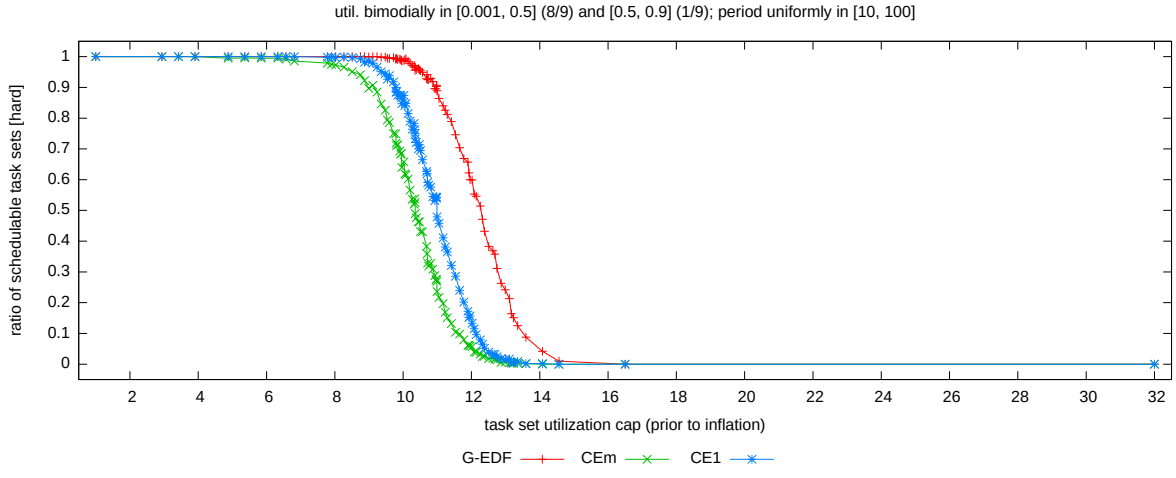

(b)

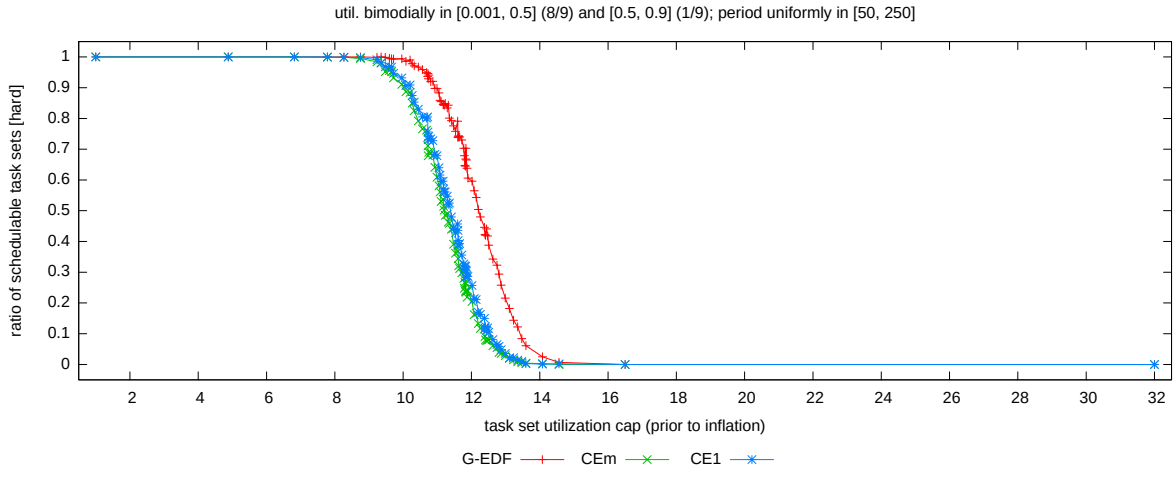

(c)

Figure 31: Comparison of CEm and CE1 (global vs. dedicated interrupt handling) in terms of hard schedulability of task sets with bimodal light per-task utilizations and **(a)** short, **(b)** moderate, and **(c)** long periods. These graphs correspond to Fig. 19.

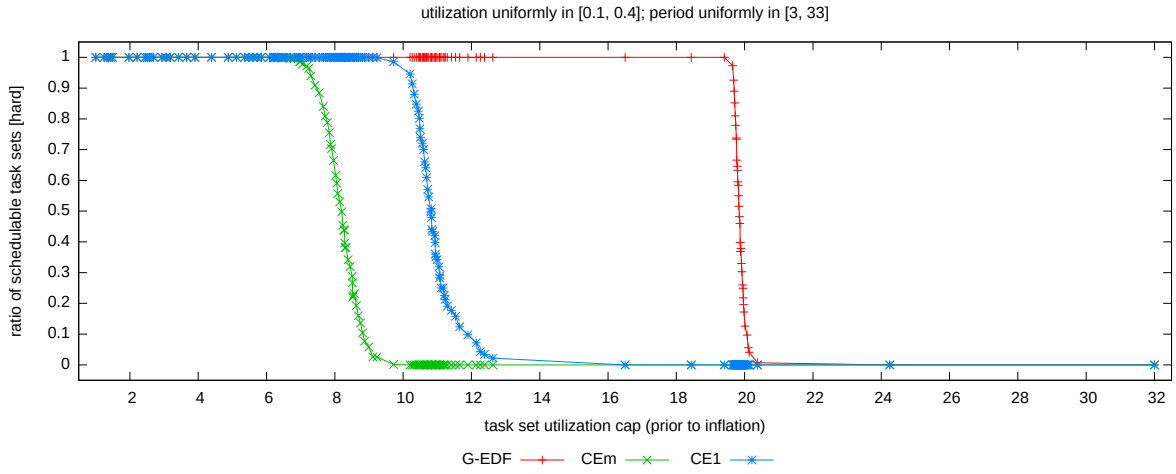

(a)

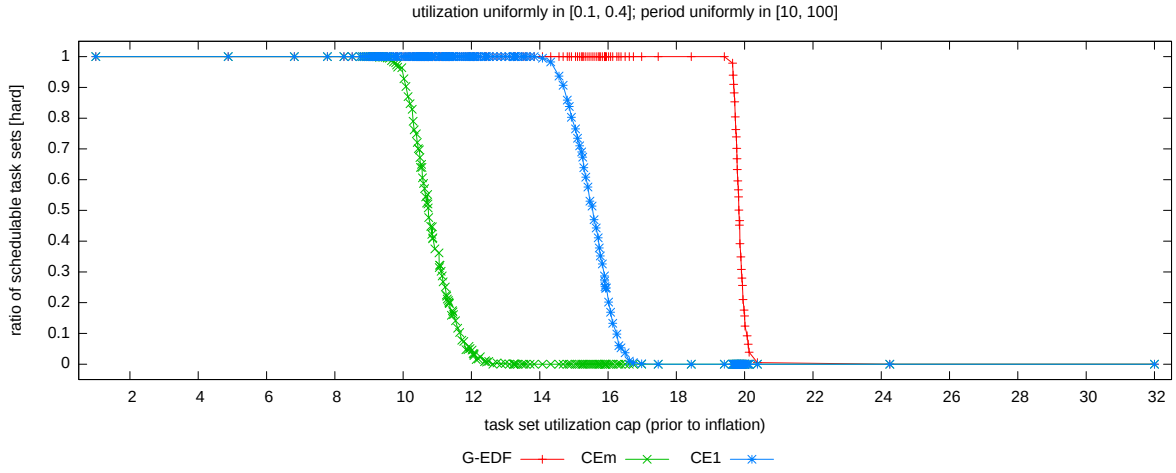

(b)

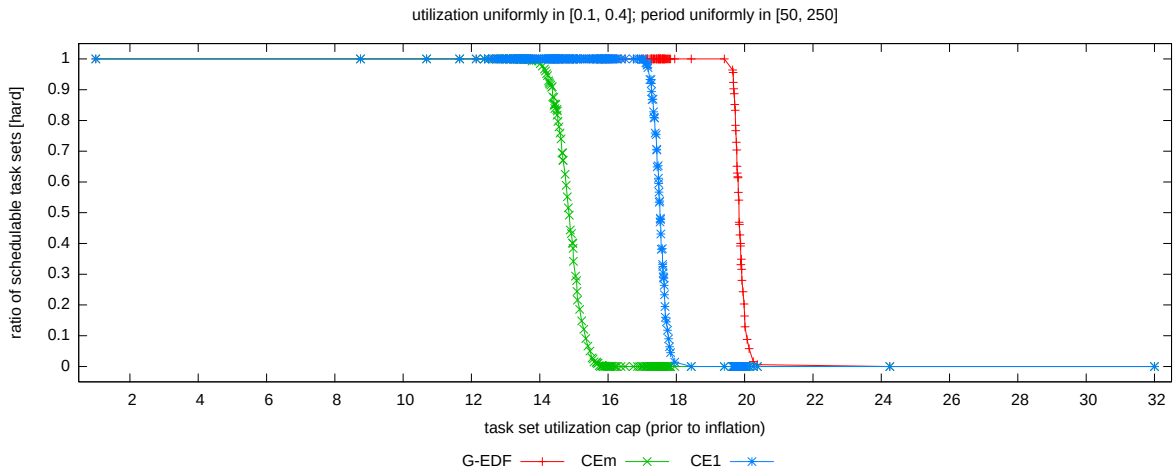

(c)

Figure 32: Comparison of CEm and CE1 (global vs. dedicated interrupt handling) in terms of hard schedulability of task sets with uniform medium per-task utilizations and **(a)** short, **(b)** moderate, and **(c)** long periods. These graphs correspond to Fig. 20.

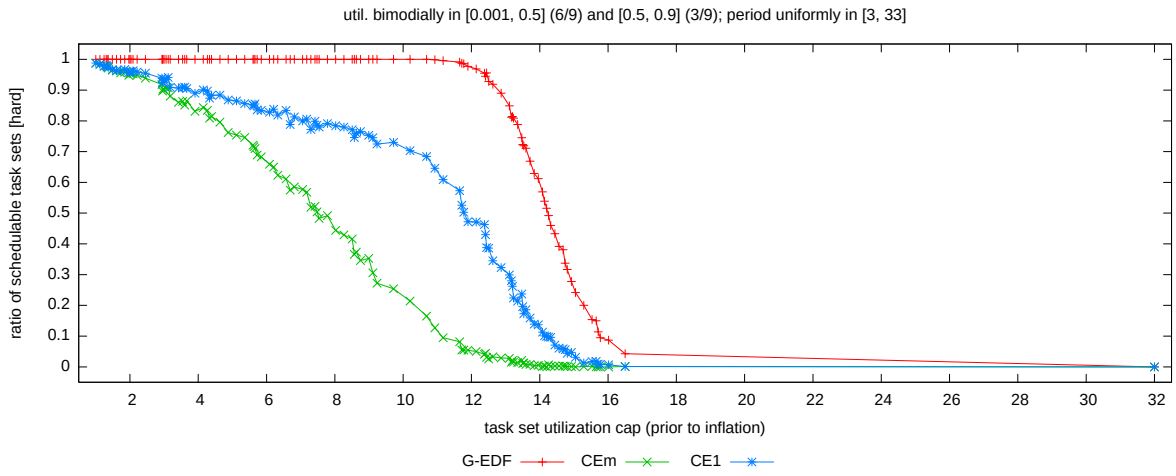

(a)

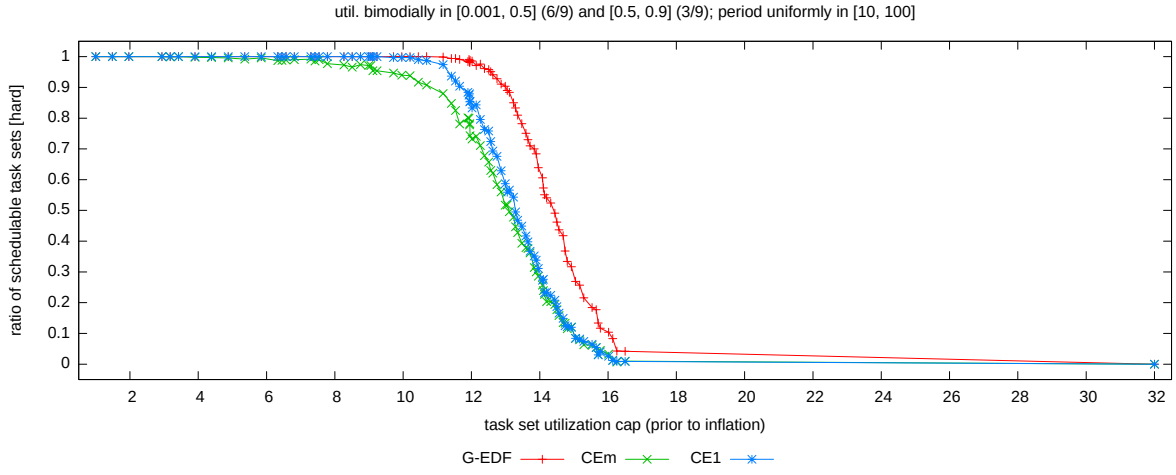

(b)

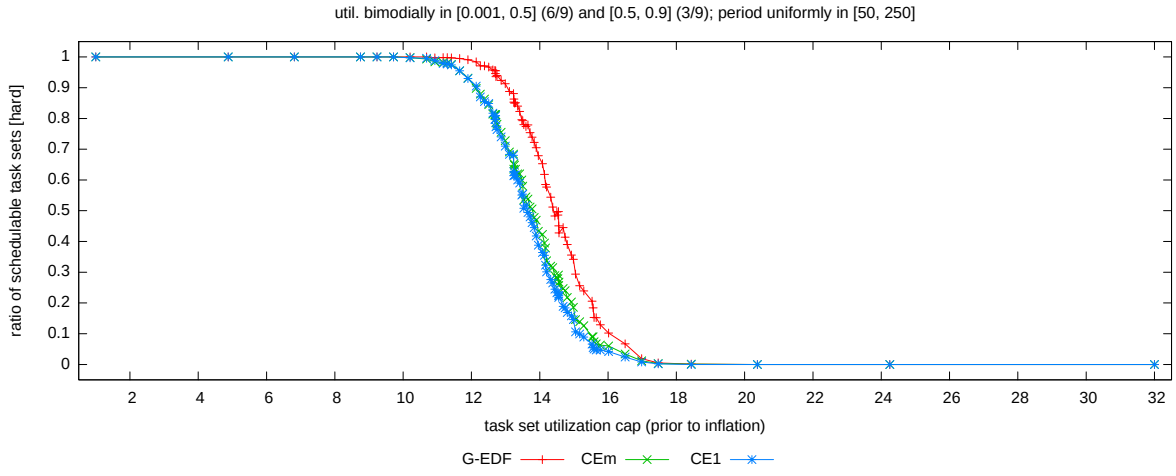

(c)

Figure 33: Comparison of CEm and CE1 (global vs. dedicated interrupt handling) in terms of hard schedulability of task sets with bimodal medium per-task utilizations and **(a)** short, **(b)** moderate, and **(c)** long periods. These graphs correspond to Fig. 21.

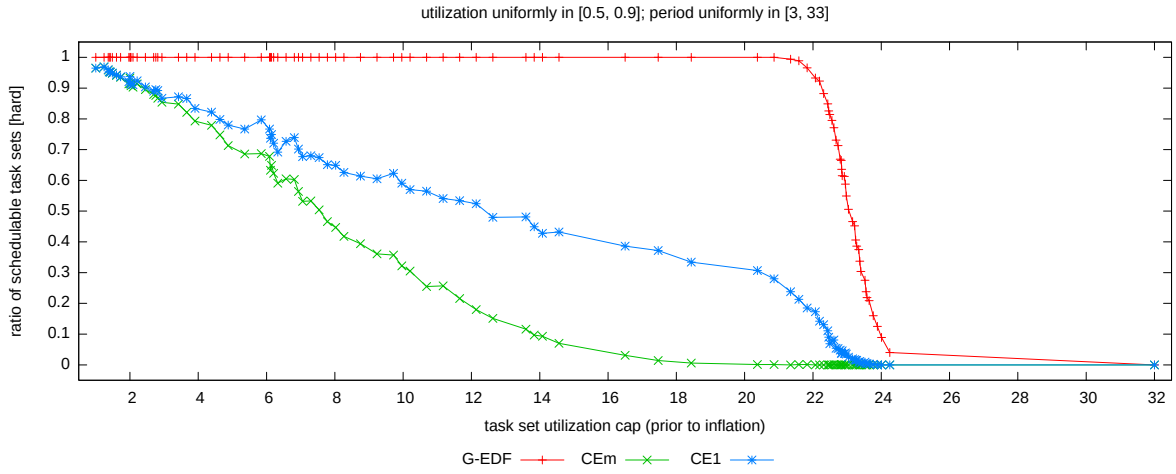

(a)

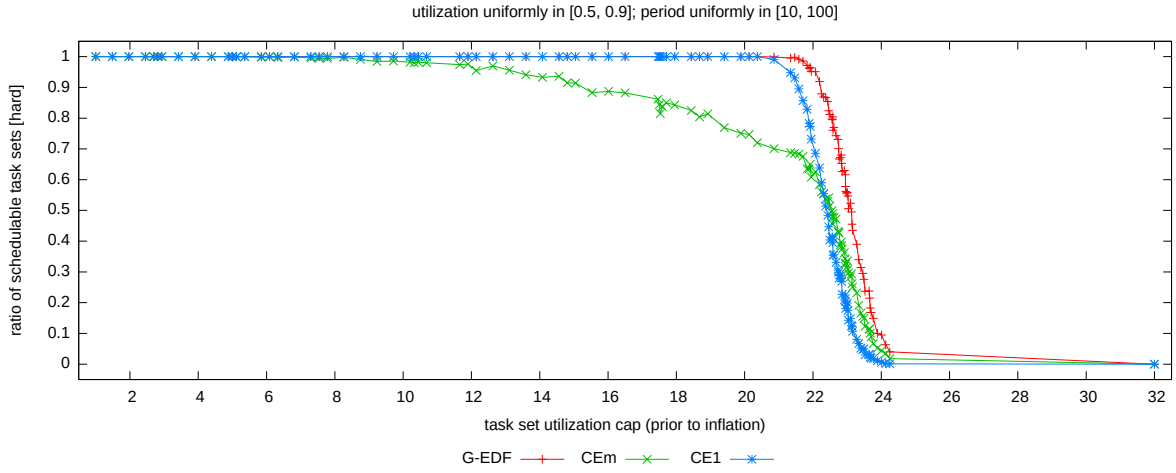

(b)

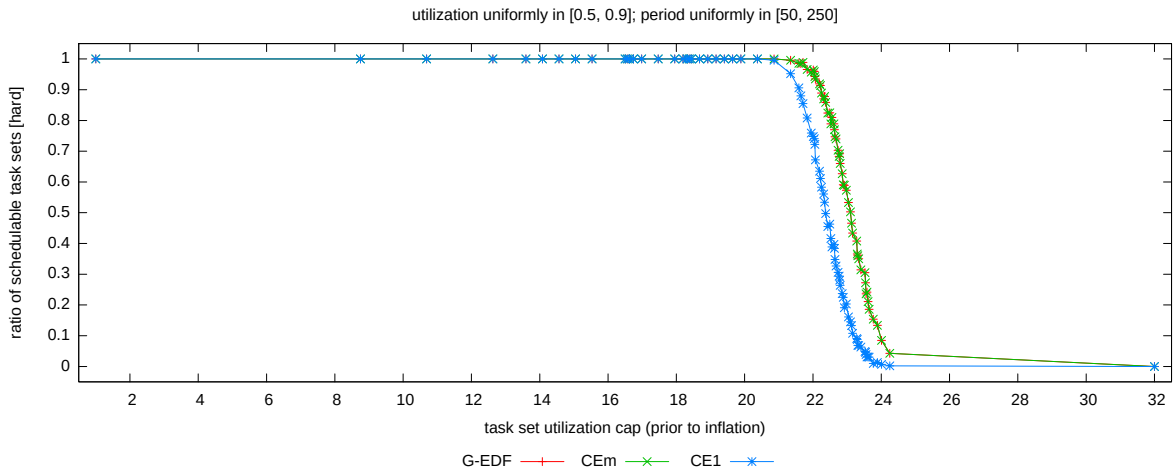

(c)

Figure 34: Comparison of CEm and CE1 (global vs. dedicated interrupt handling) in terms of hard schedulability of task sets with uniform heavy per-task utilizations and **(a)** short, **(b)** moderate, and **(c)** long periods. These graphs correspond to Fig. 22.

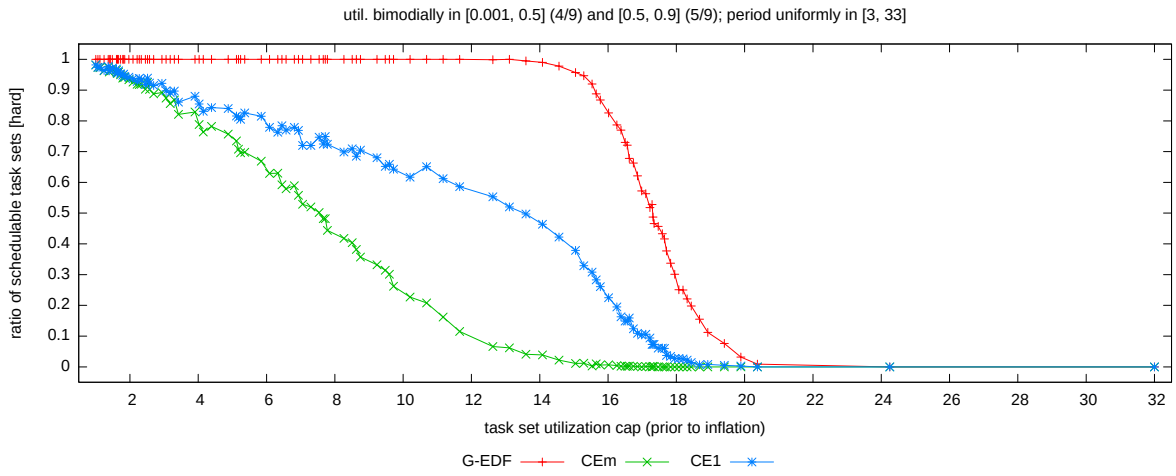

(a)

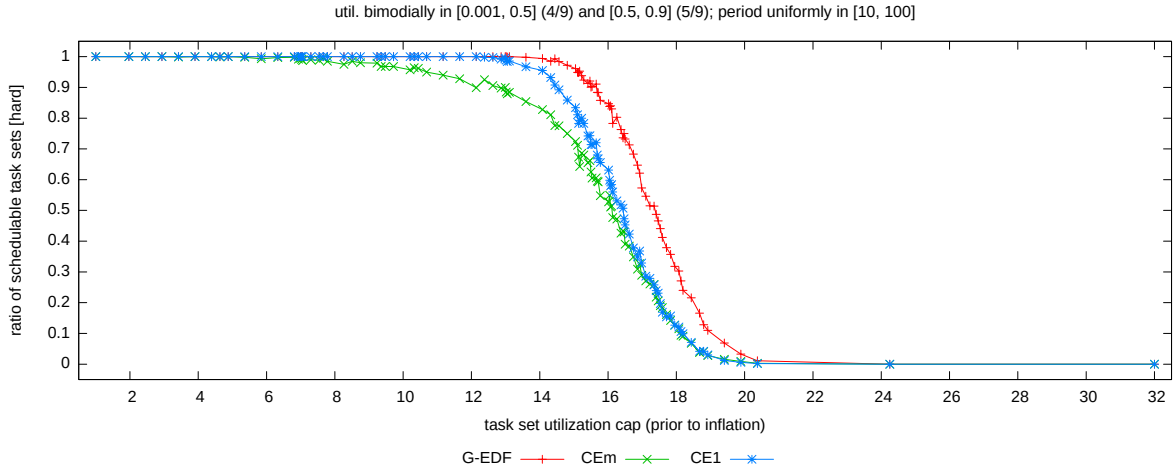

(b)

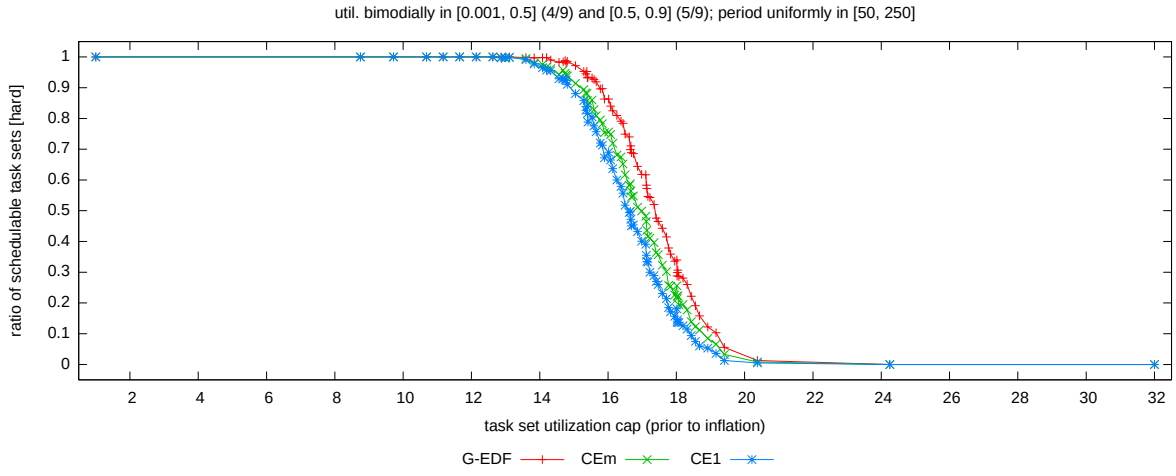

(c)

Figure 35: Comparison of CEm and CE1 (global vs. dedicated interrupt handling) in terms of hard schedulability of task sets with bimodal heavy per-task utilizations and **(a)** short, **(b)** moderate, and **(c)** long periods. These graphs correspond to Fig. 23.

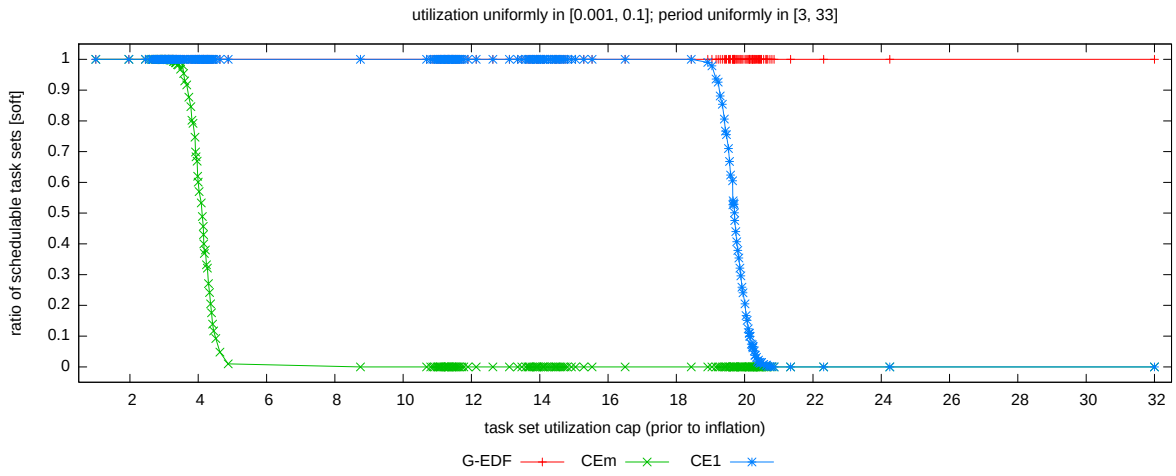

(a)

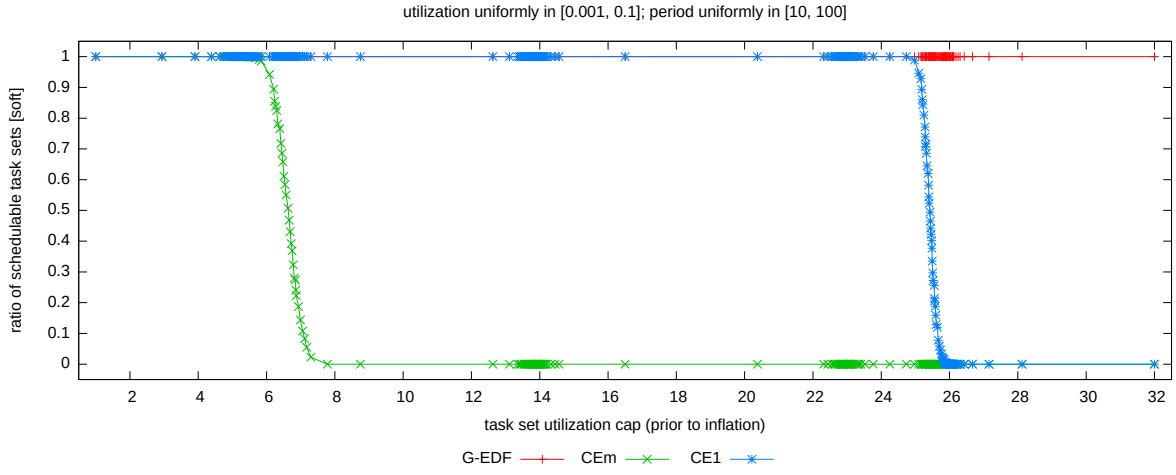

(b)

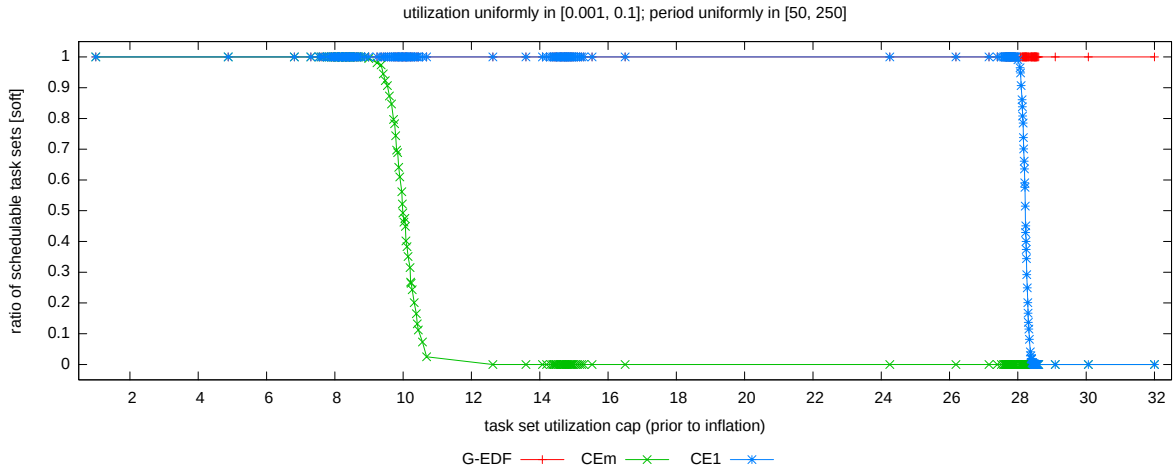

(c)

Figure 36: Comparison of CEm and CE1 (global vs. dedicated interrupt handling) in terms of soft schedulability of task sets with uniform light per-task utilizations and **(a)** short, **(b)** moderate, and **(c)** long periods. These graphs correspond to Fig. 24.

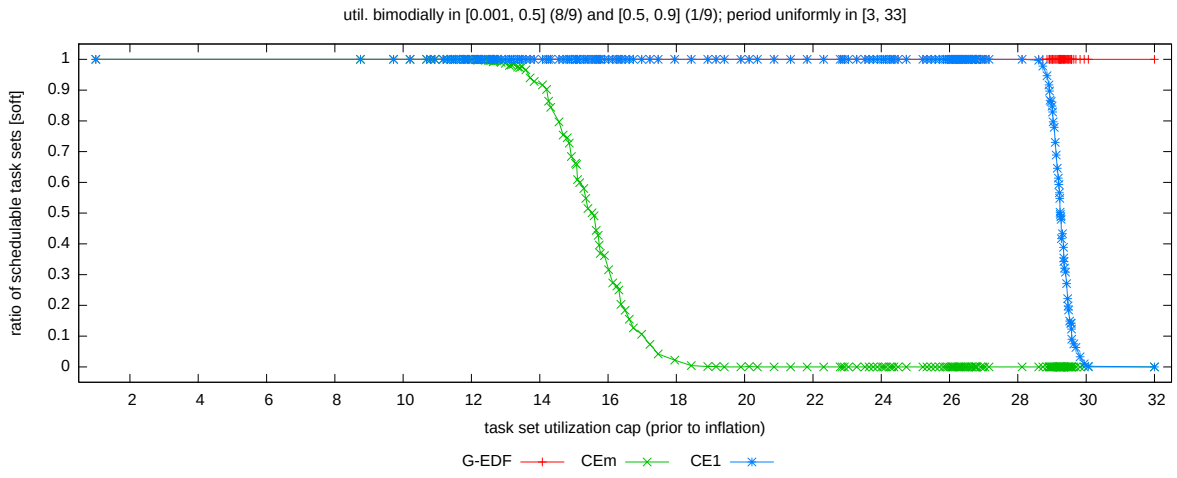

(a)

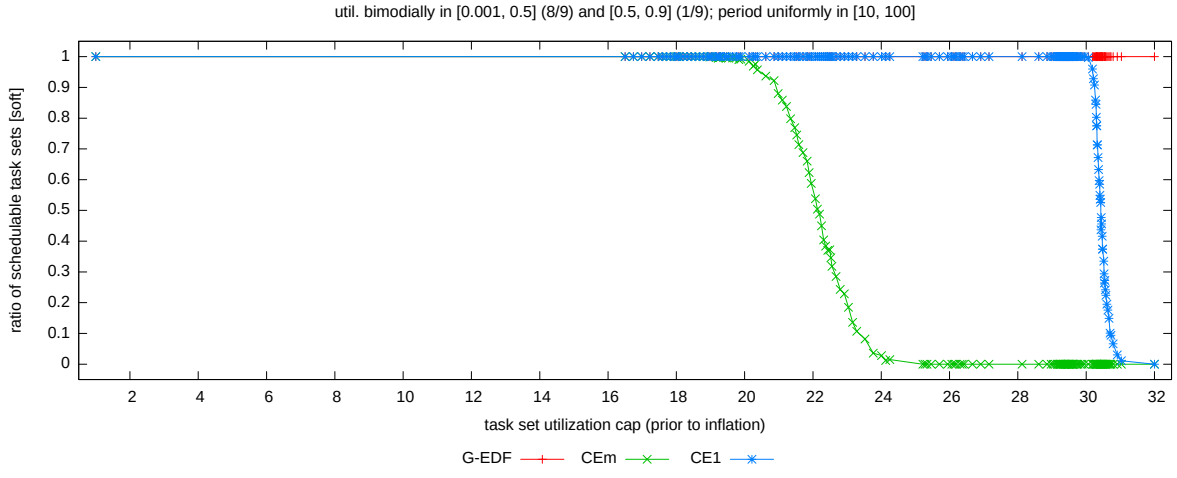

(b)

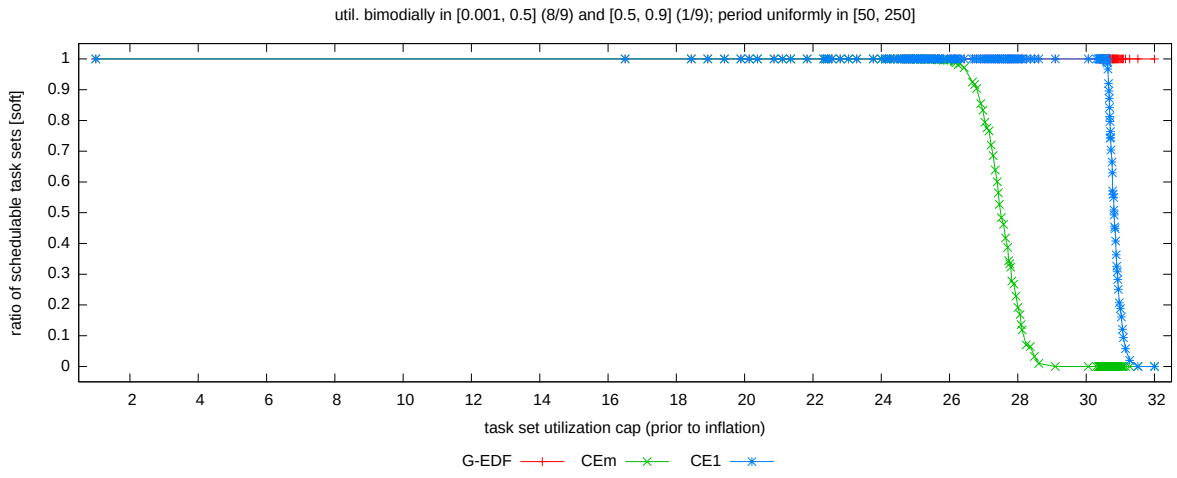

(c)

Figure 37: Comparison of CEm and CE1 (global vs. dedicated interrupt handling) in terms of soft schedulability of task sets with bimodal light per-task utilizations and **(a)** short, **(b)** moderate, and **(c)** long periods. These graphs correspond to Fig. 25.

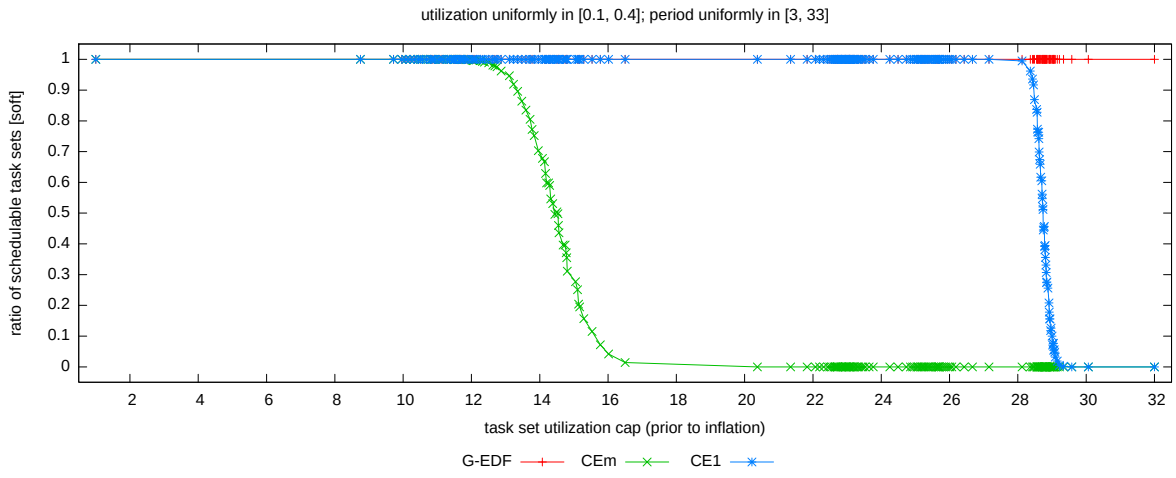

(a)

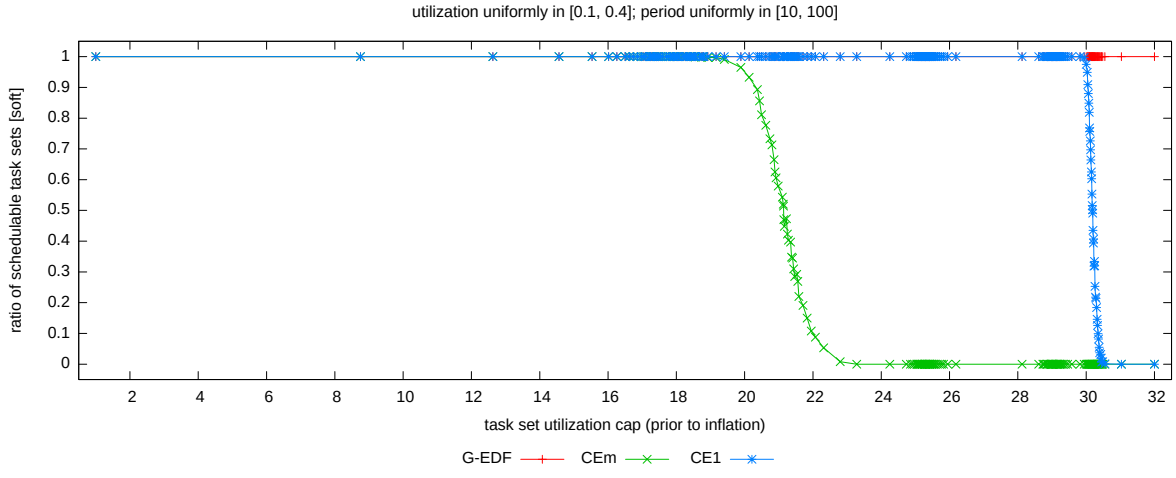

(b)

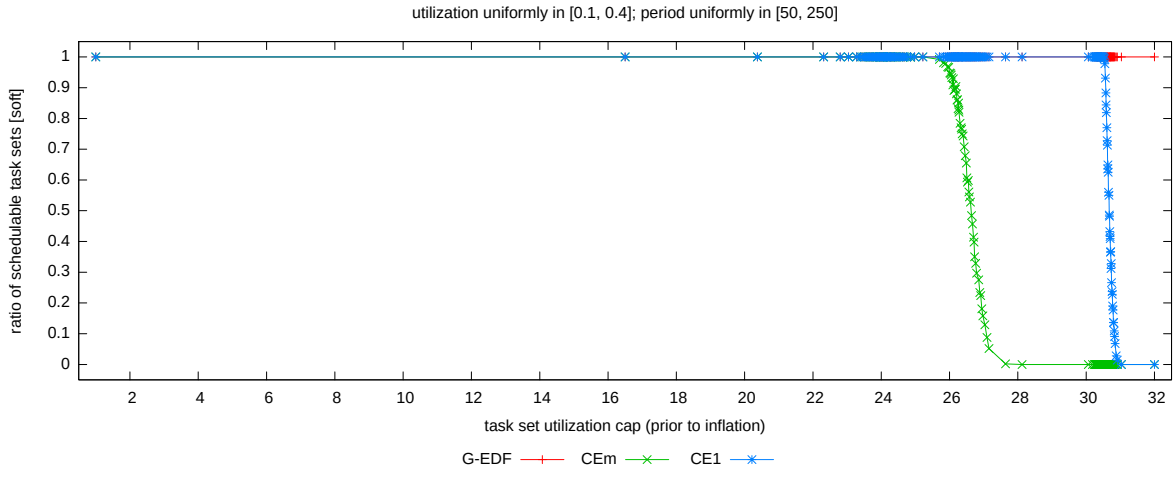

(c)

Figure 38: Comparison of CEm and CE1 (global vs. dedicated interrupt handling) in terms of soft schedulability of task sets with uniform medium per-task utilizations and **(a)** short, **(b)** moderate, and **(c)** long periods. These graphs correspond to Fig. 26.

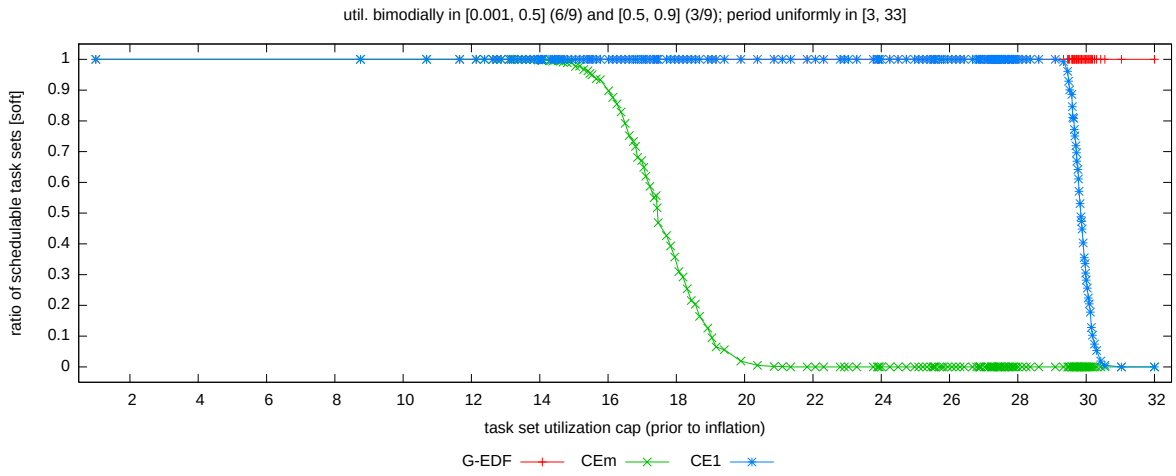

(a)

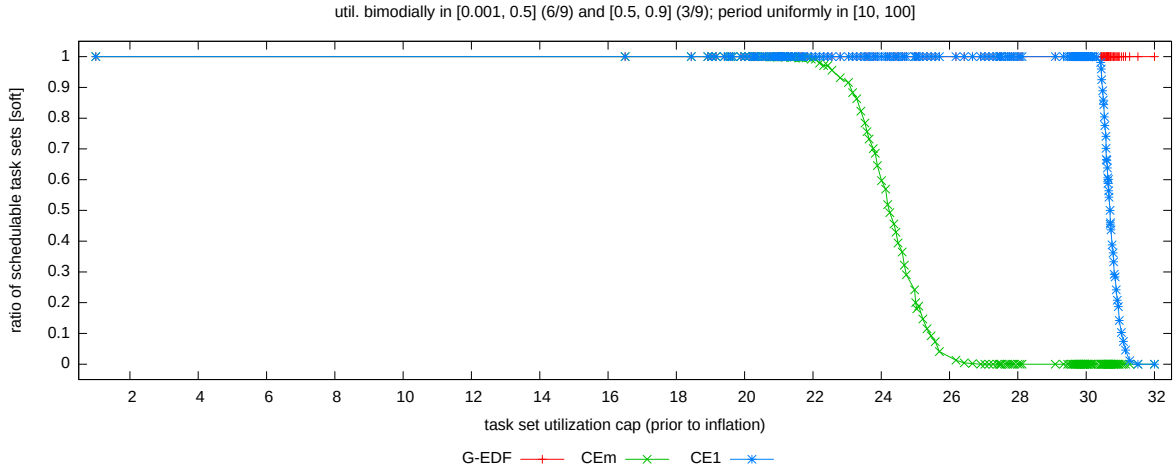

(b)

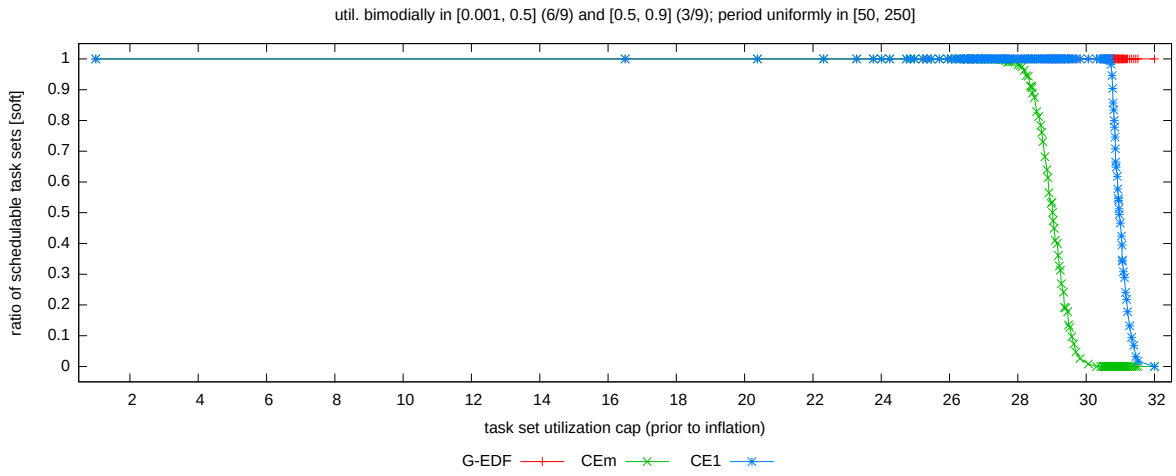

(c)

Figure 39: Comparison of CEm and CE1 (global vs. dedicated interrupt handling) in terms of soft schedulability of task sets with bimodal medium per-task utilizations and **(a)** short, **(b)** moderate, and **(c)** long periods. These graphs correspond to Fig. 27.

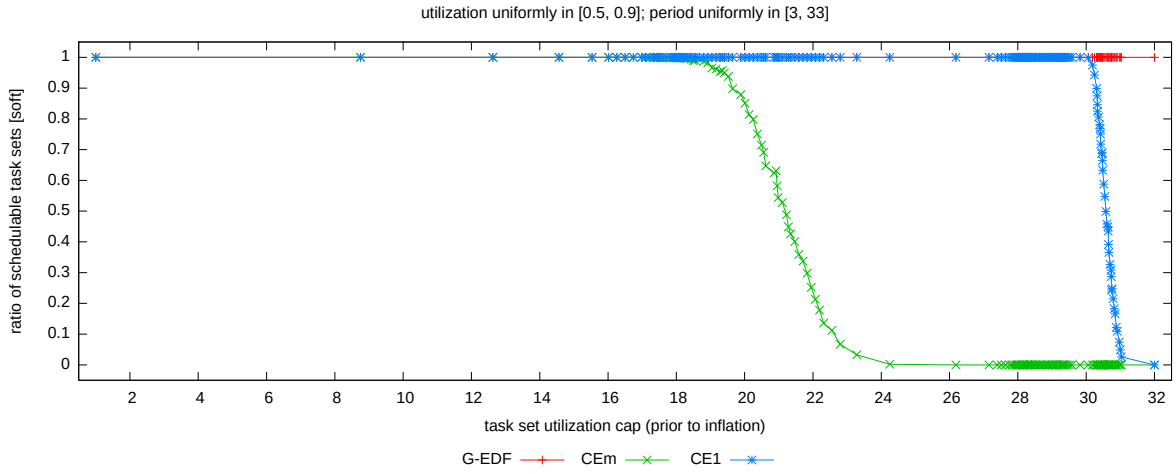

(a)

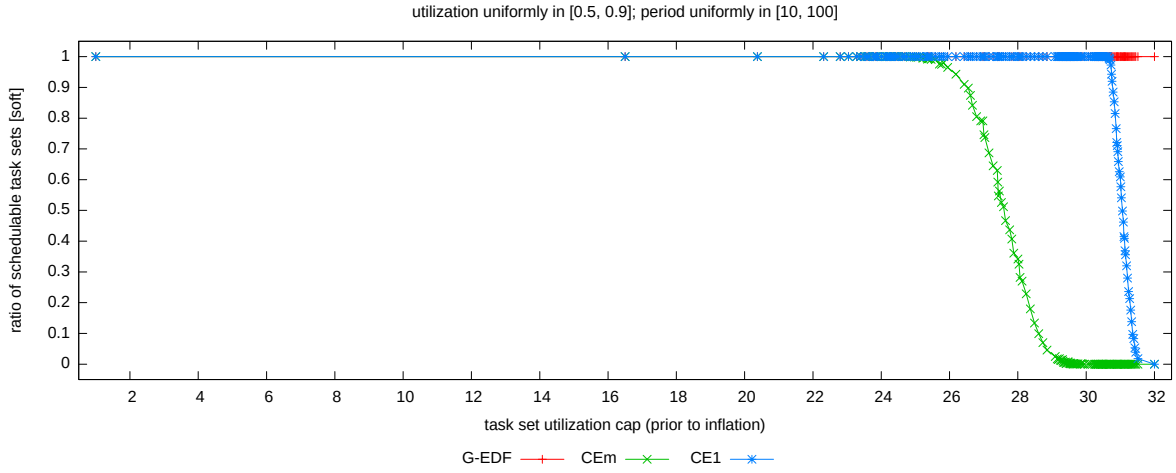

(b)

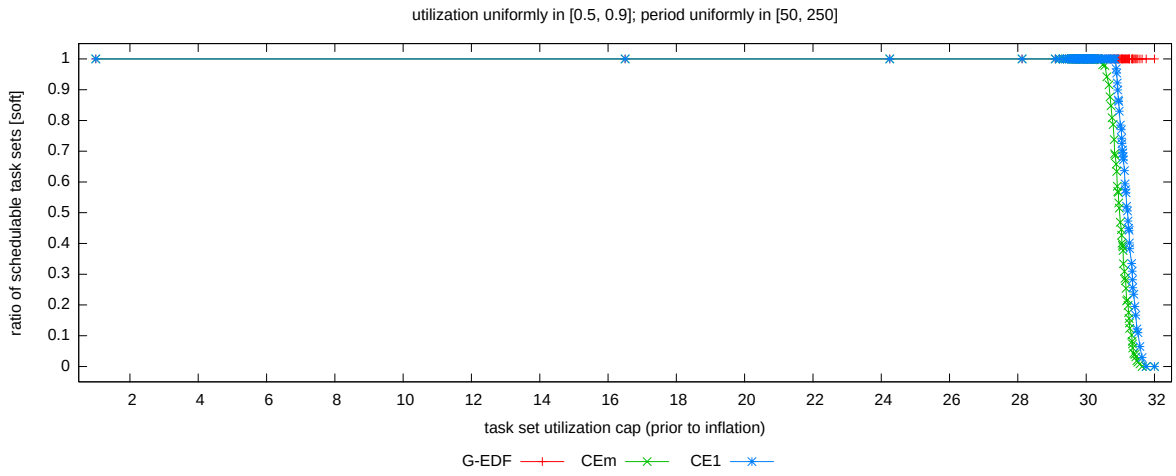

(c)

Figure 40: Comparison of CEm and CE1 (global vs. dedicated interrupt handling) in terms of soft schedulability of task sets with uniform heavy per-task utilizations and **(a)** short, **(b)** moderate, and **(c)** long periods. These graphs correspond to Fig. 28.

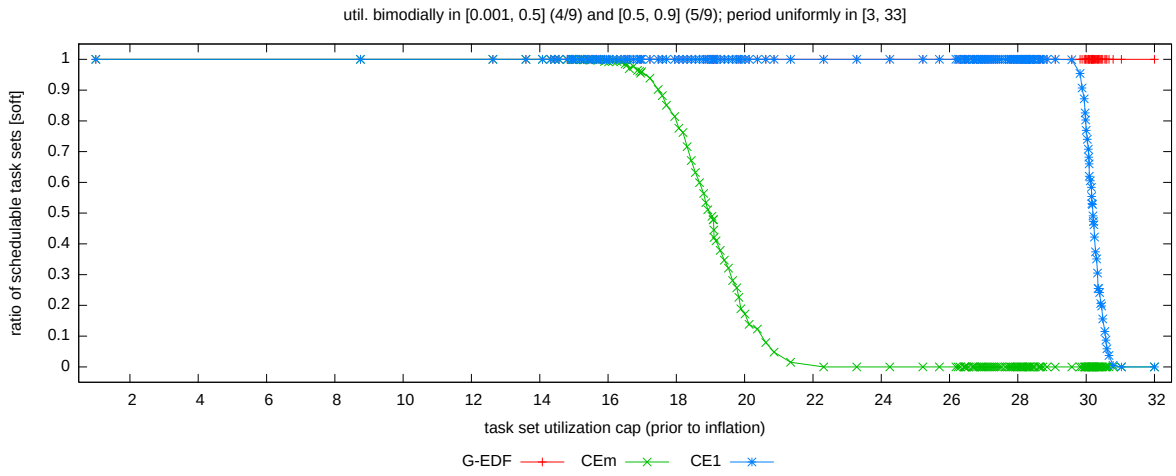

(a)

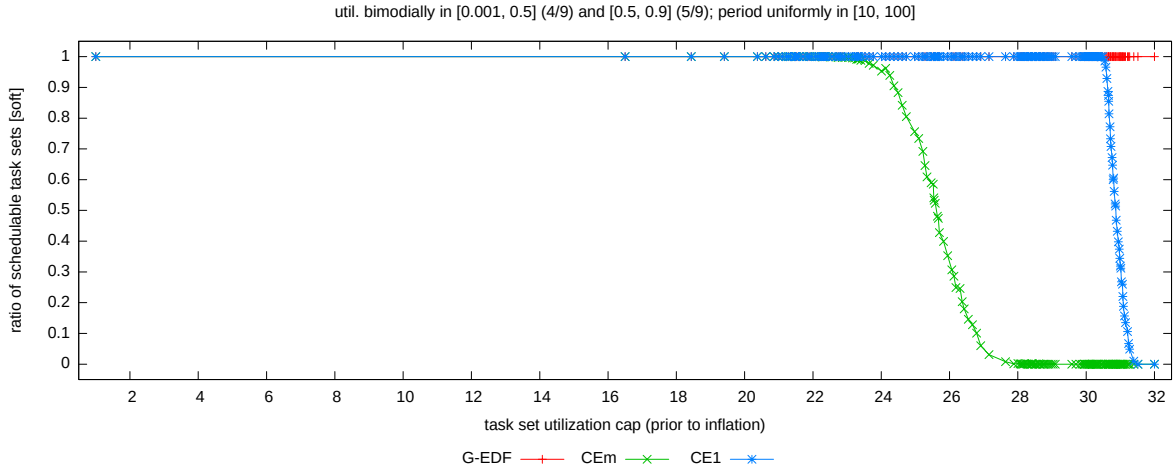

(b)

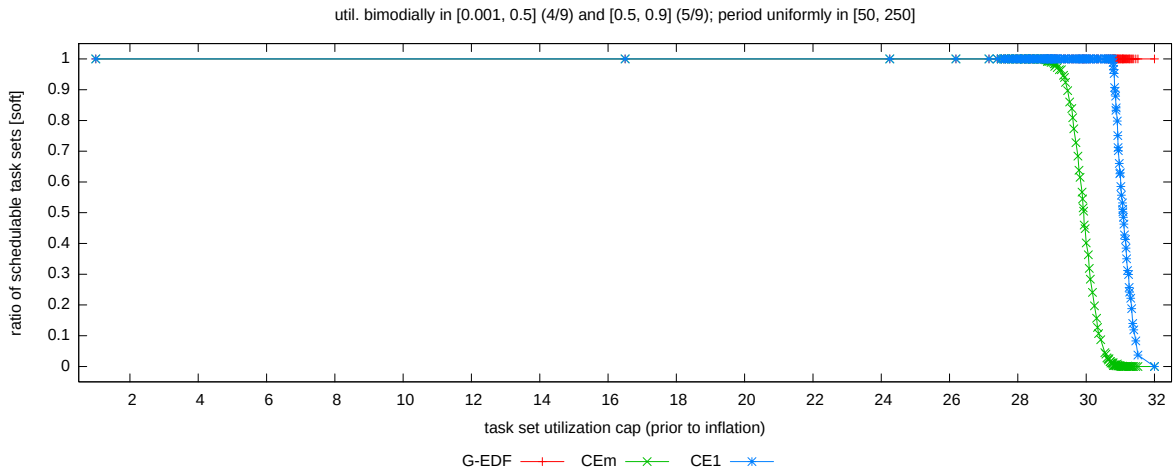

(c)

Figure 41: Comparison of CEm and CE1 (global vs. dedicated interrupt handling) in terms of soft schedulability of task sets with bimodal heavy per-task utilizations and **(a)** short, **(b)** moderate, and **(c)** long periods. These graphs correspond to Fig. 29.

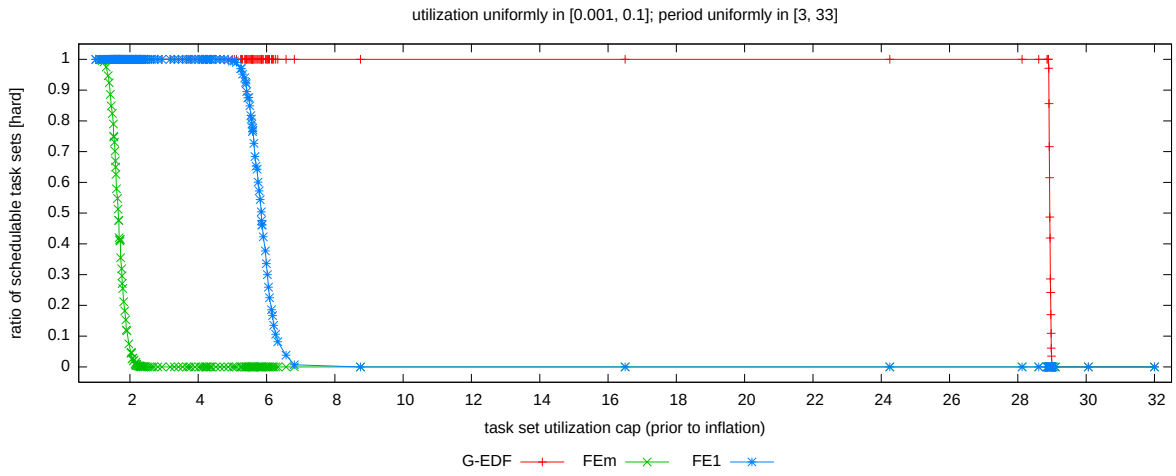

(a)

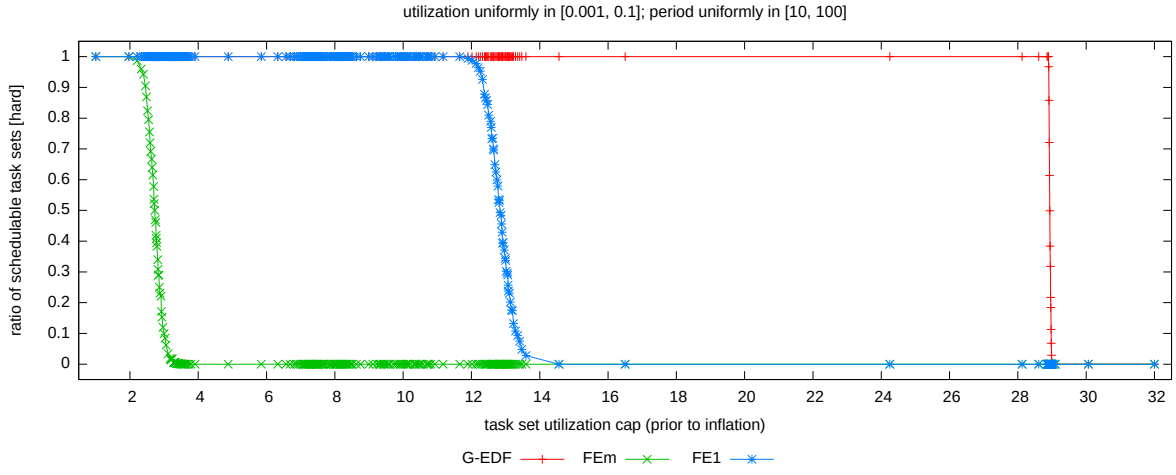

(b)

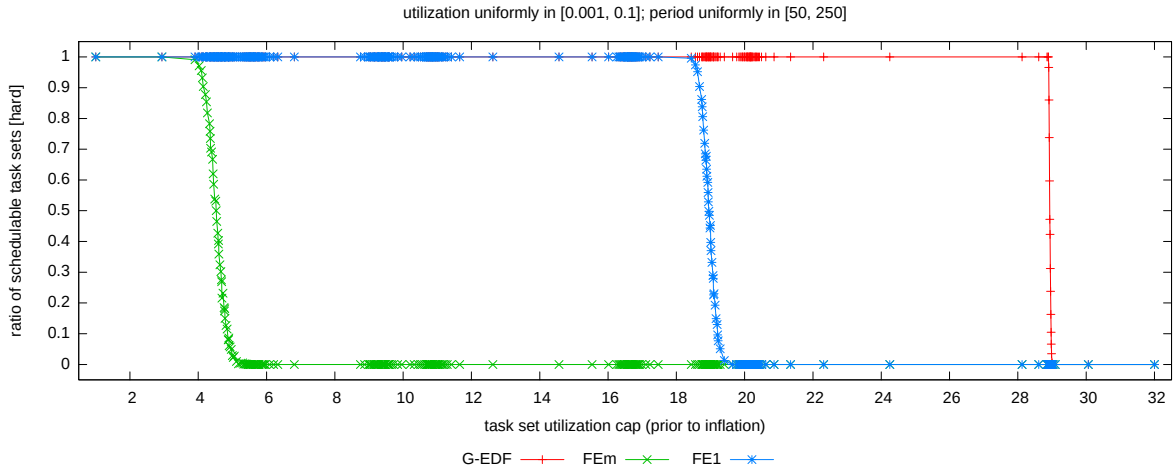

(c)

Figure 42: Comparison of FEm and FE1 (global vs. dedicated interrupt handling) in terms of hard schedulability of task sets with uniform light per-task utilizations and **(a)** short, **(b)** moderate, and **(c)** long periods. These graphs correspond to Fig. 18.

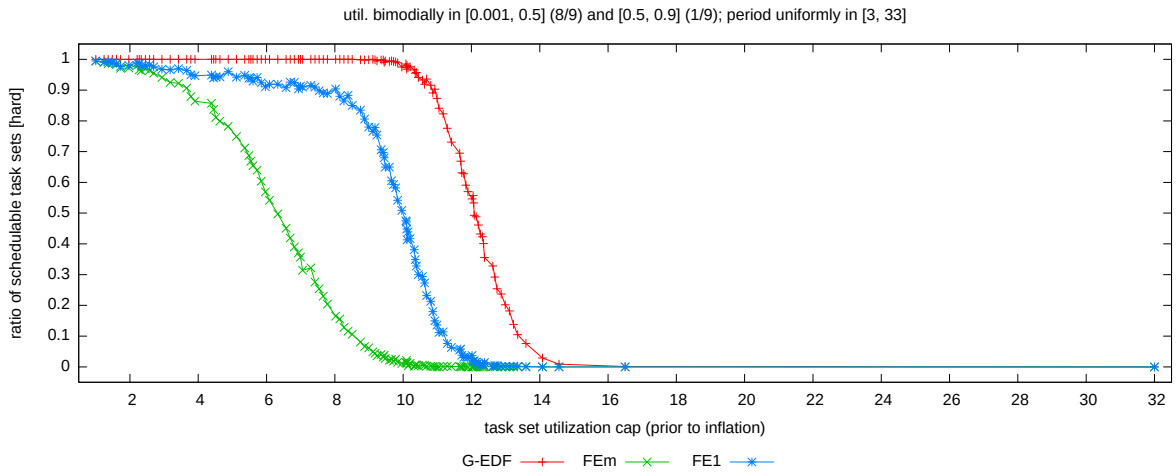

(a)

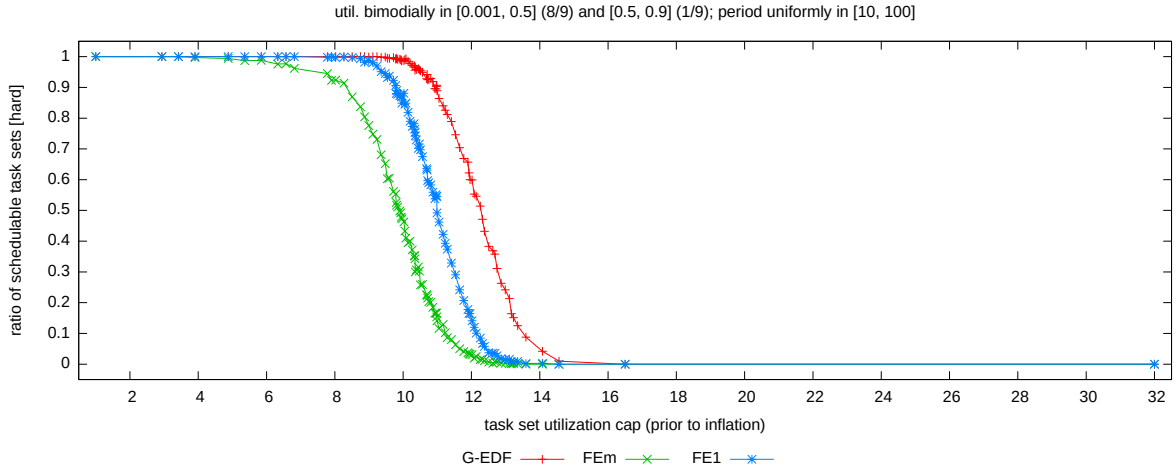

(b)

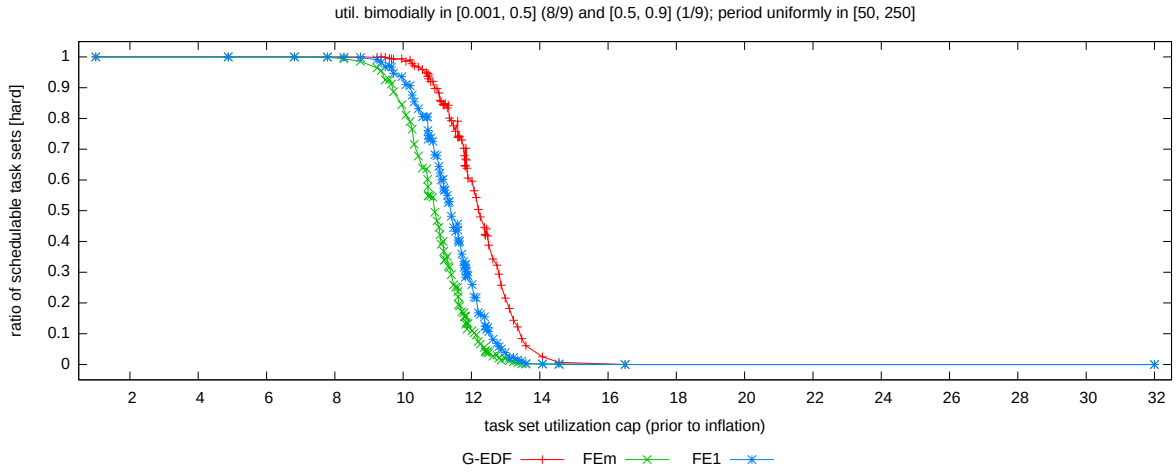

(c)

Figure 43: Comparison of FEm and FE1 (global vs. dedicated interrupt handling) in terms of hard schedulability of task sets with bimodal light per-task utilizations and **(a)** short, **(b)** moderate, and **(c)** long periods. These graphs correspond to Fig. 19.

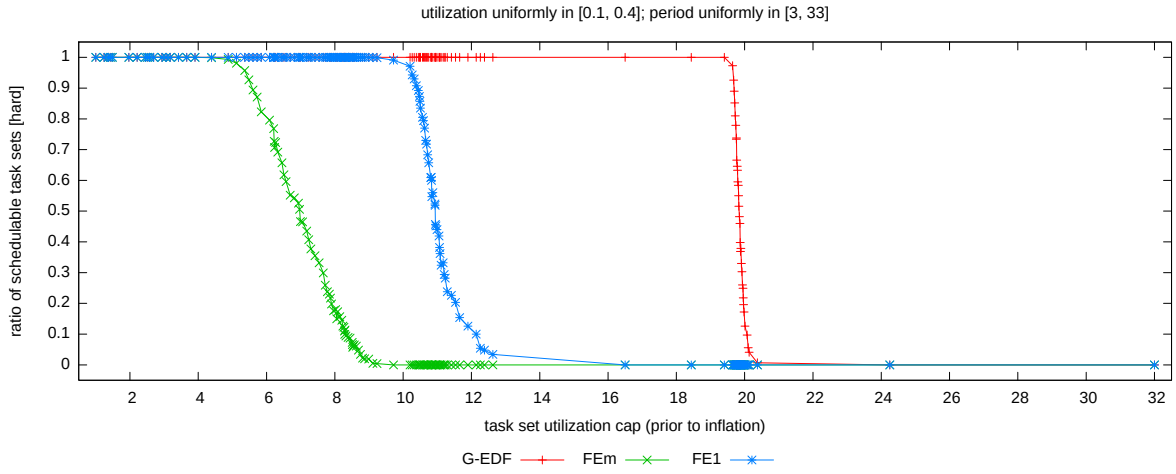

(a)

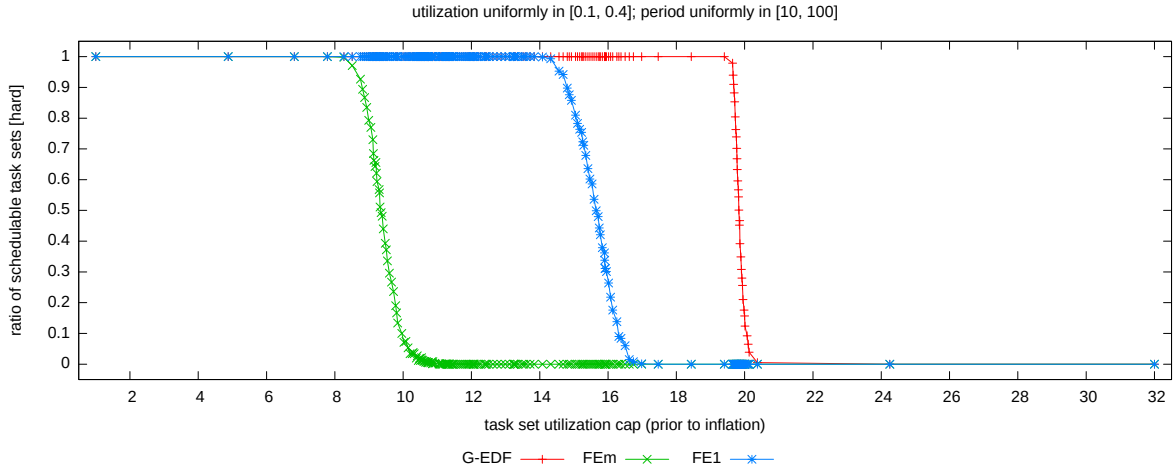

(b)

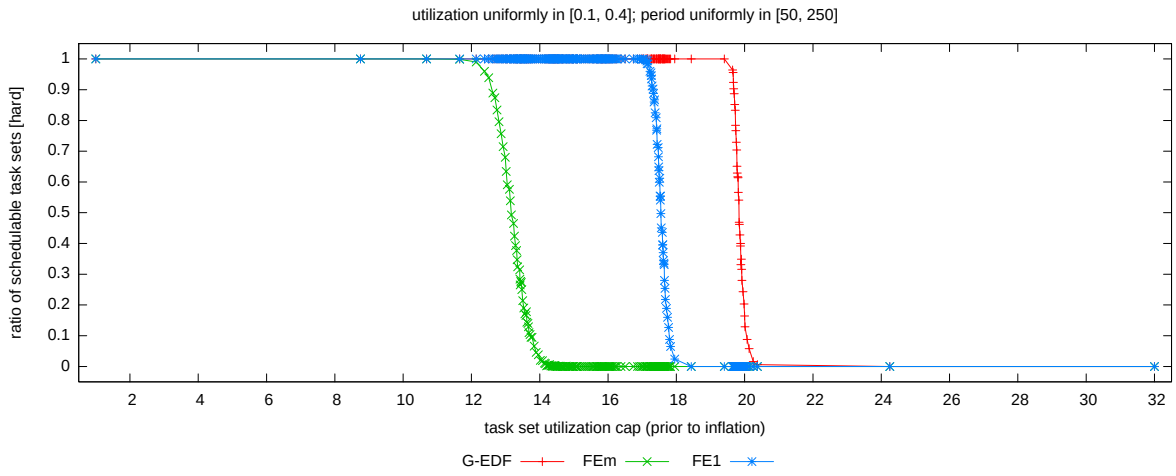

(c)

Figure 44: Comparison of FEm and FE1 (global vs. dedicated interrupt handling) in terms of hard schedulability of task sets with uniform medium per-task utilizations and **(a)** short, **(b)** moderate, and **(c)** long periods. These graphs correspond to Fig. 20.

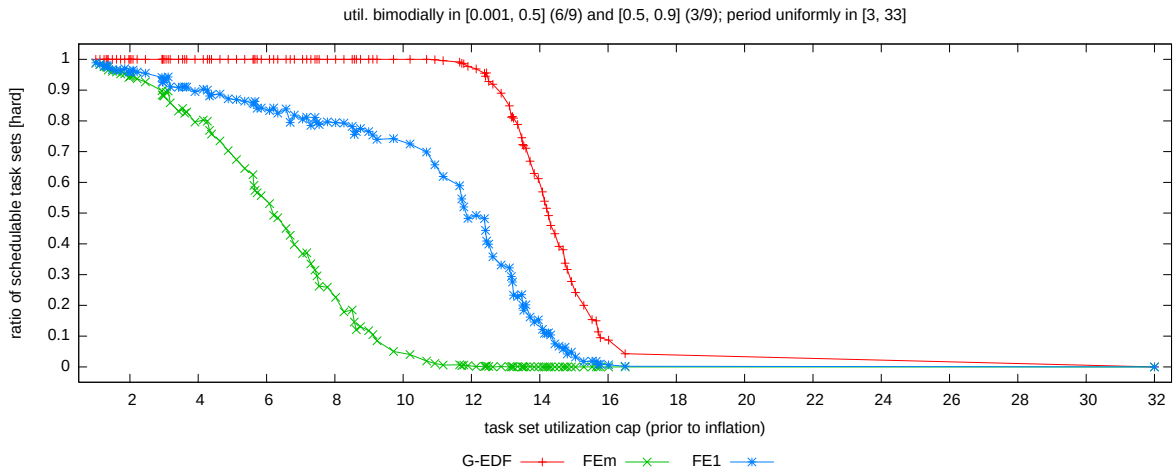

(a)

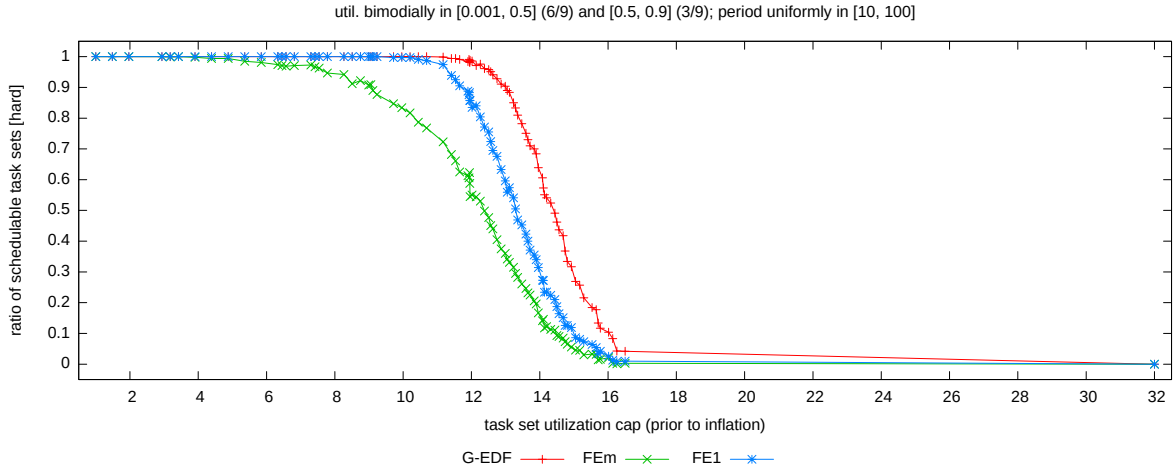

(b)

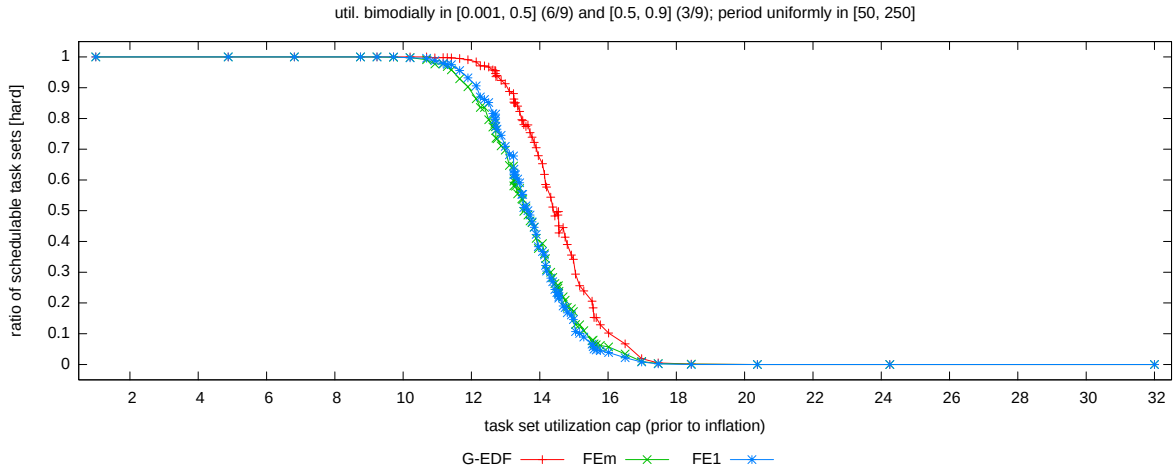

(c)

Figure 45: Comparison of FEm and FE1 (global vs. dedicated interrupt handling) in terms of hard schedulability of task sets with bimodal medium per-task utilizations and **(a)** short, **(b)** moderate, and **(c)** long periods. These graphs correspond to Fig. 21.

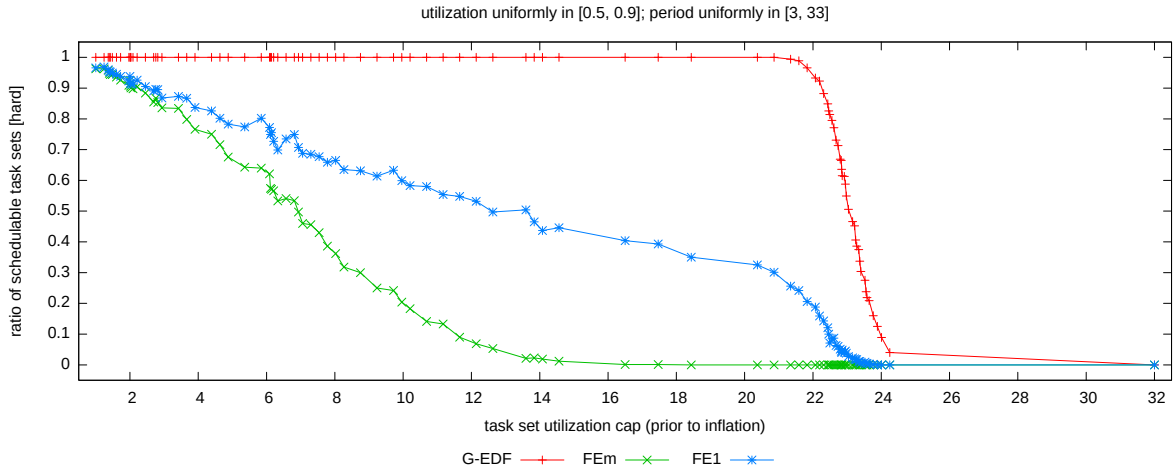

(a)

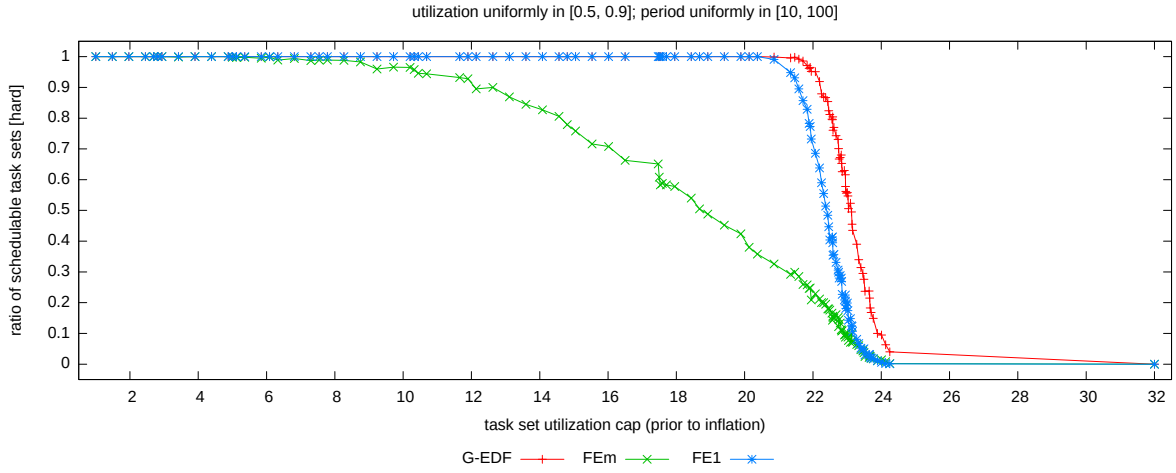

(b)

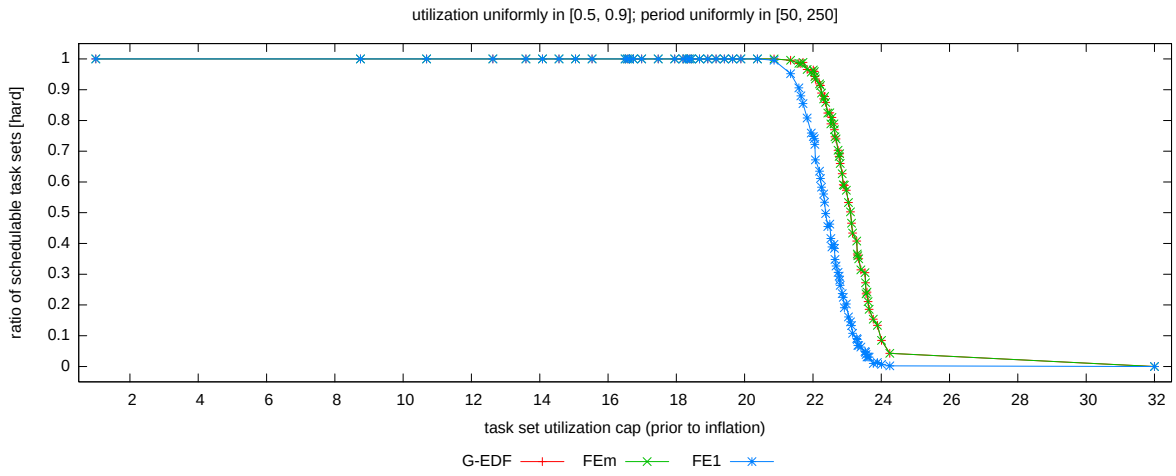

(c)

Figure 46: Comparison of FEm and FE1 (global vs. dedicated interrupt handling) in terms of hard schedulability of task sets with uniform heavy per-task utilizations and **(a)** short, **(b)** moderate, and **(c)** long periods. These graphs correspond to Fig. 22.

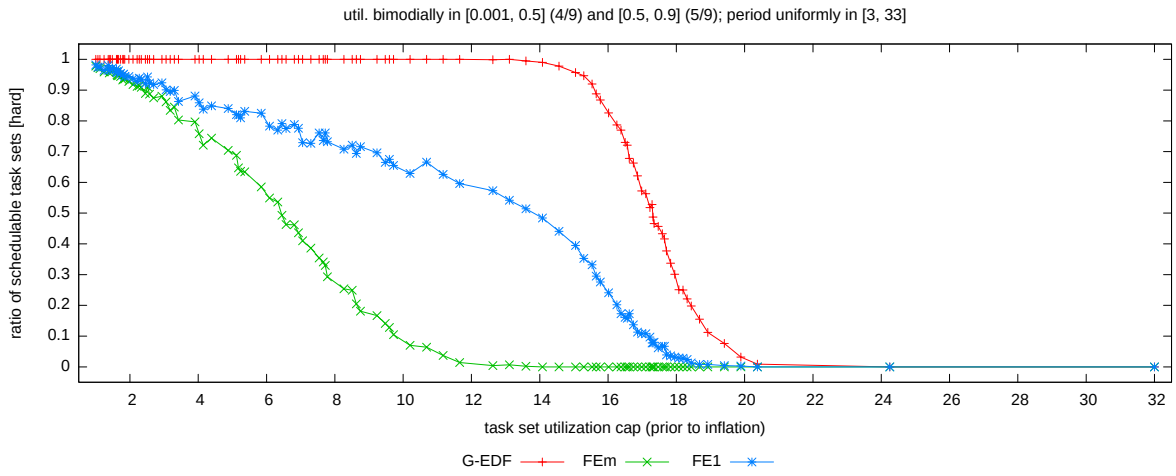

(a)

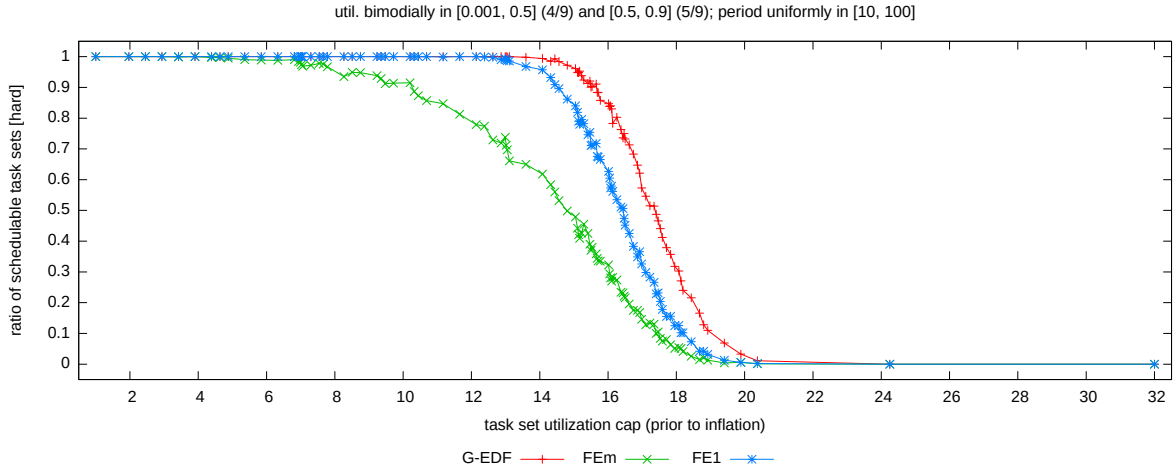

(b)

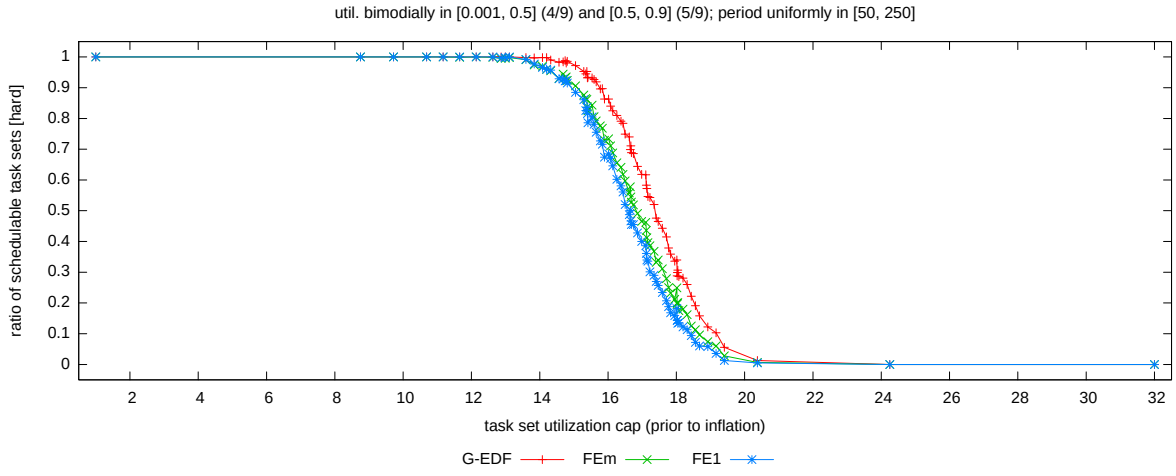

(c)

Figure 47: Comparison of FEm and FE1 (global vs. dedicated interrupt handling) in terms of hard schedulability of task sets with bimodal heavy per-task utilizations and **(a)** short, **(b)** moderate, and **(c)** long periods. These graphs correspond to Fig. 23.

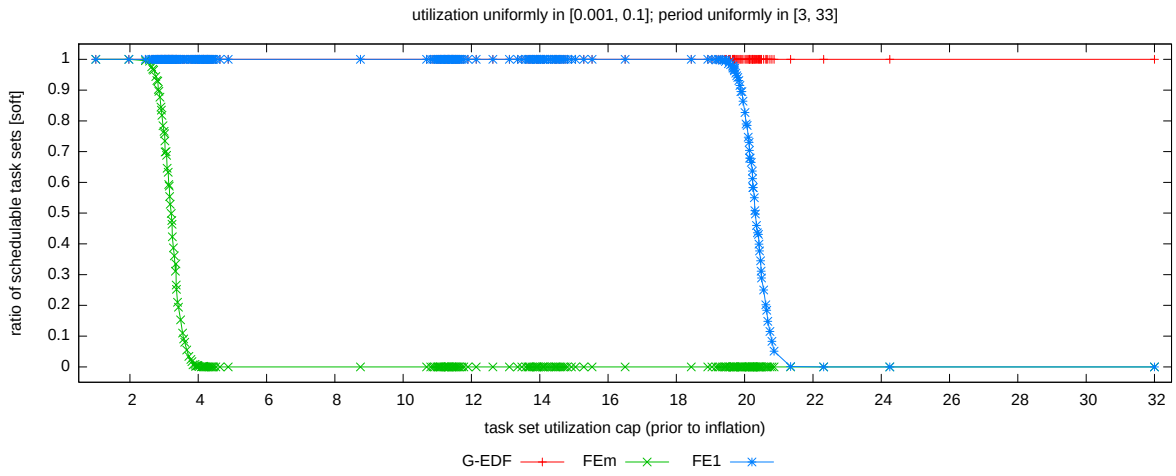

(a)

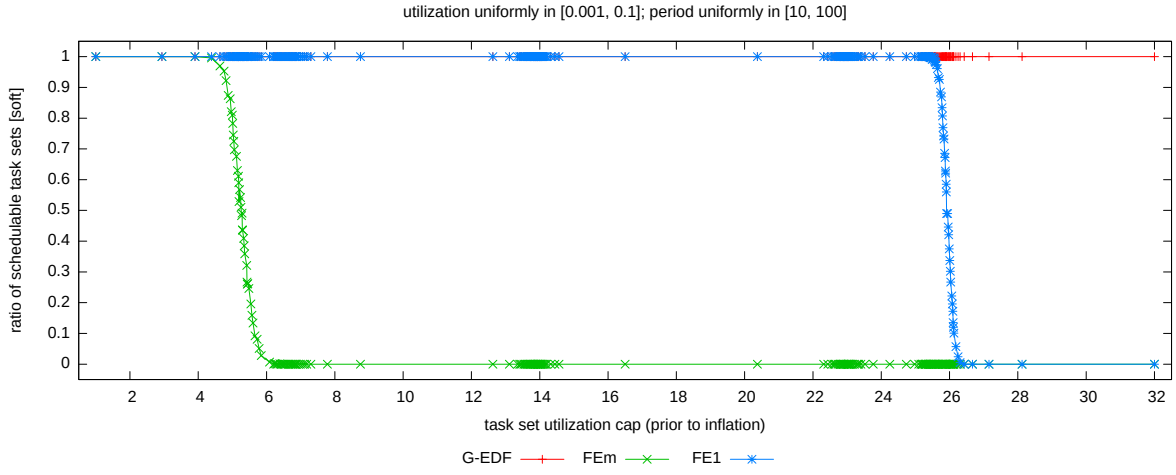

(b)

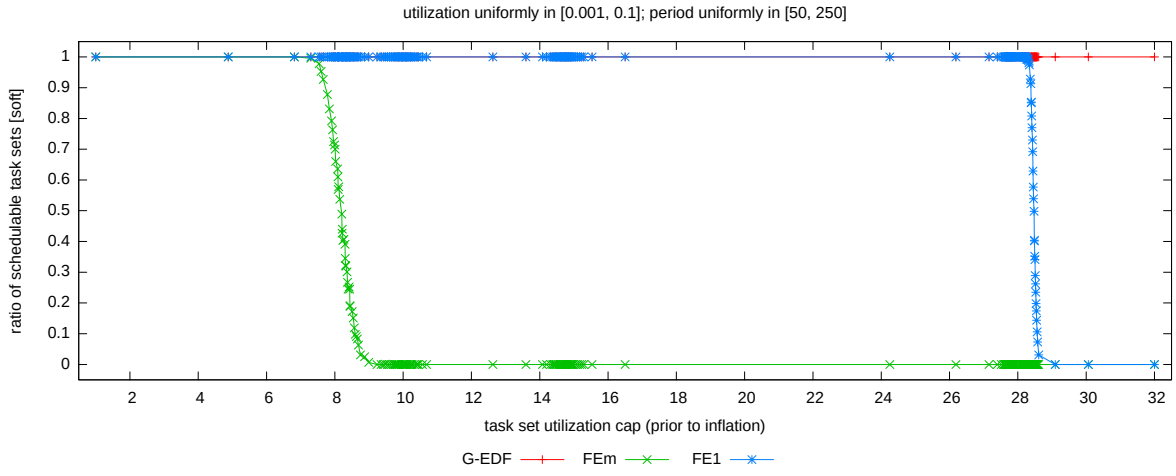

(c)

Figure 48: Comparison of FEm and FE1 (global vs. dedicated interrupt handling) in terms of soft schedulability of task sets with uniform light per-task utilizations and **(a)** short, **(b)** moderate, and **(c)** long periods. These graphs correspond to Fig. 24.

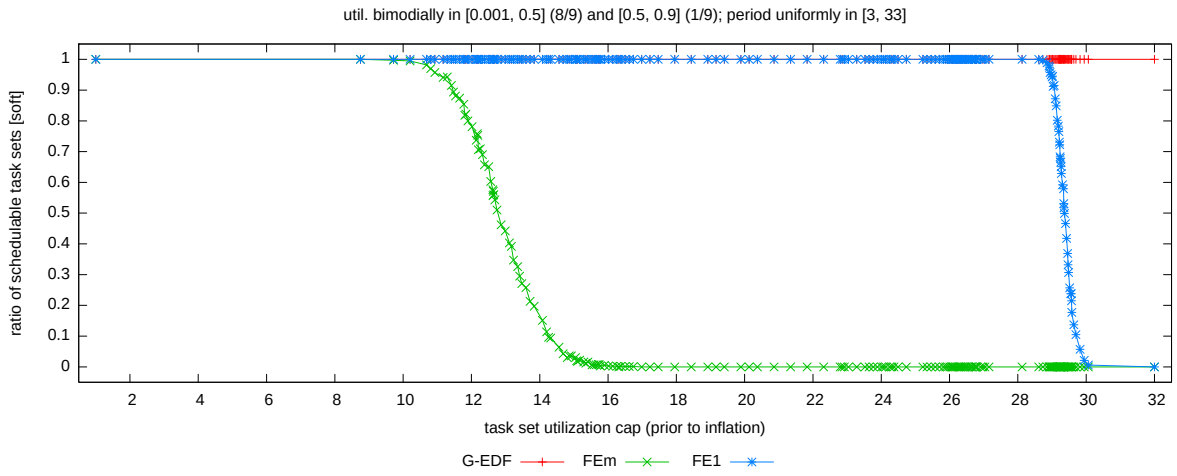

(a)

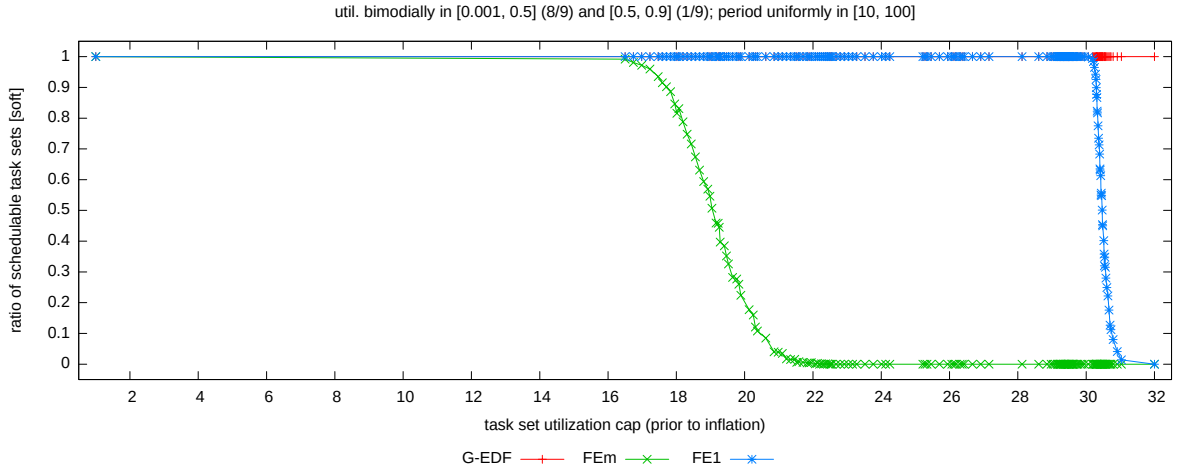

(b)

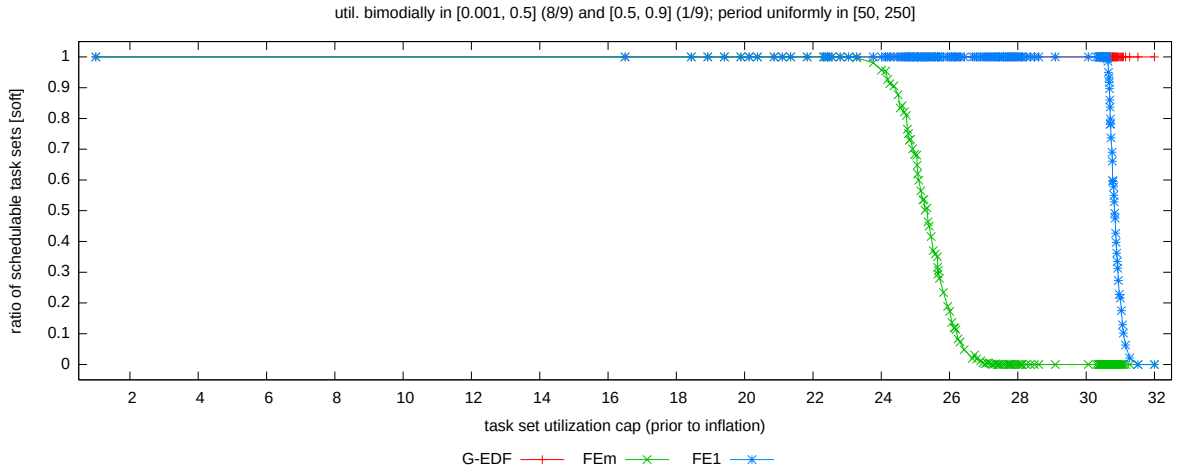

(c)

Figure 49: Comparison of FEm and FE1 (global vs. dedicated interrupt handling) in terms of soft schedulability of task sets with bimodal light per-task utilizations and **(a)** short, **(b)** moderate, and **(c)** long periods. These graphs correspond to Fig. 25.

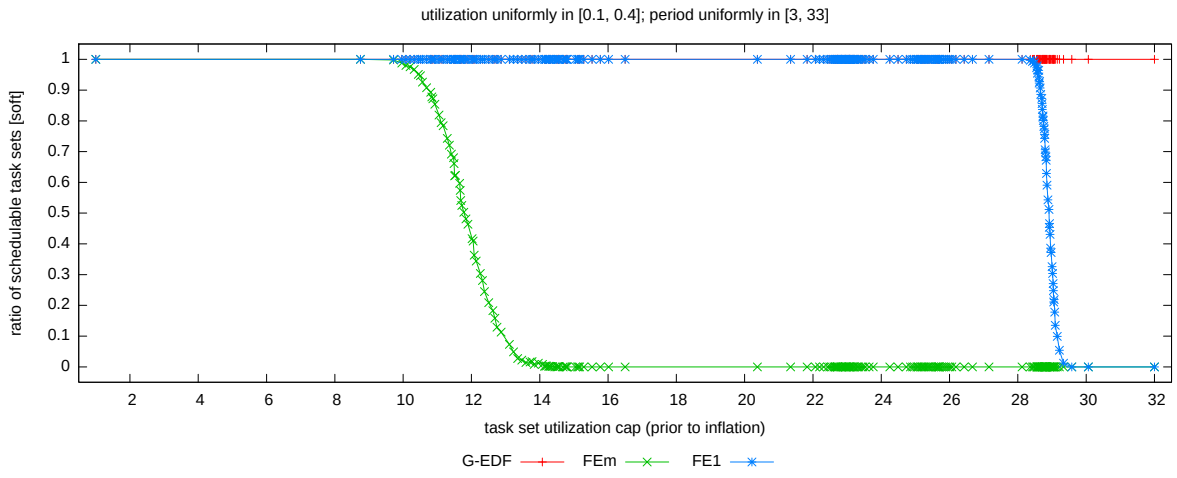

(a)

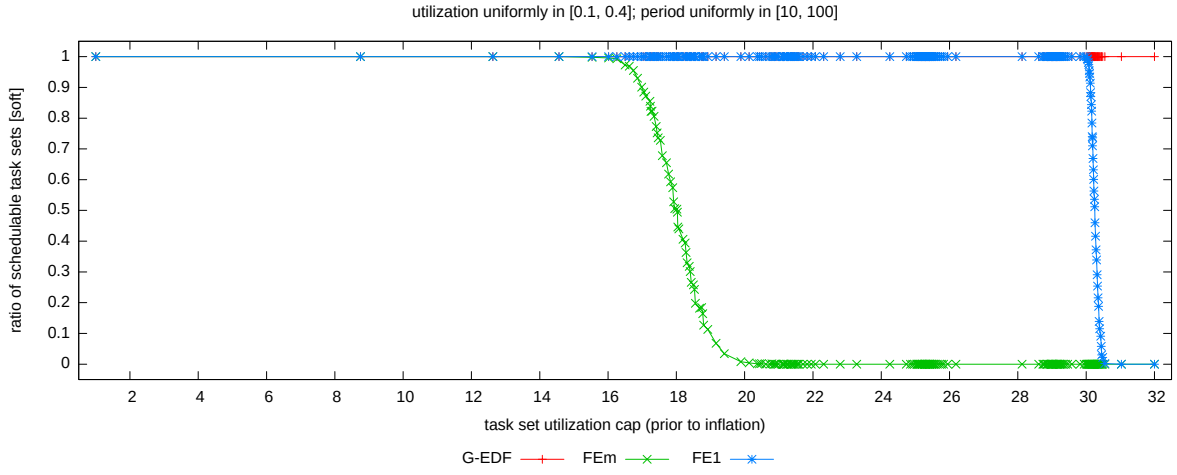

(b)

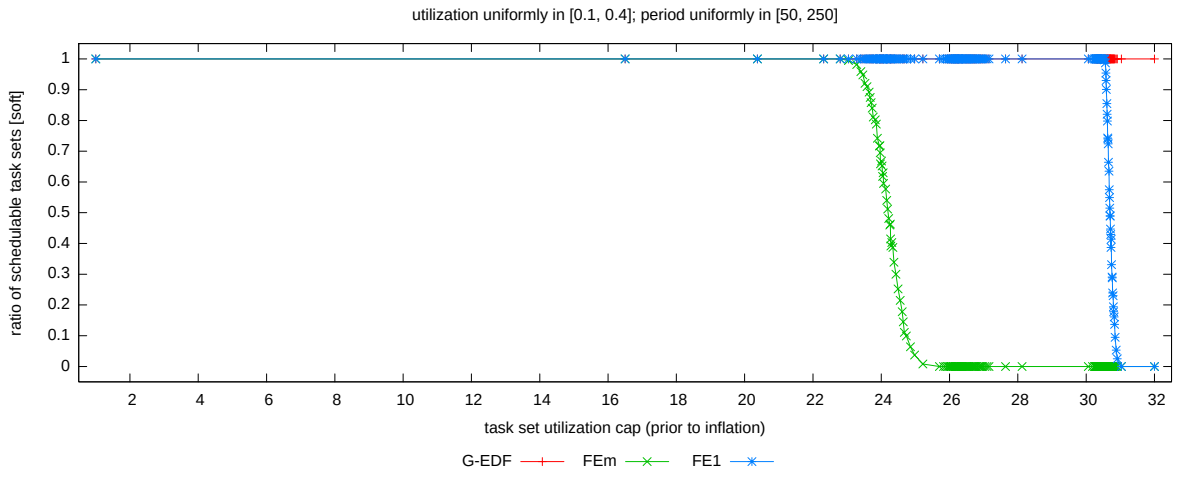

(c)

Figure 50: Comparison of FEm and FE1 (global vs. dedicated interrupt handling) in terms of soft schedulability of task sets with uniform medium per-task utilizations and **(a)** short, **(b)** moderate, and **(c)** long periods. These graphs correspond to Fig. 26.

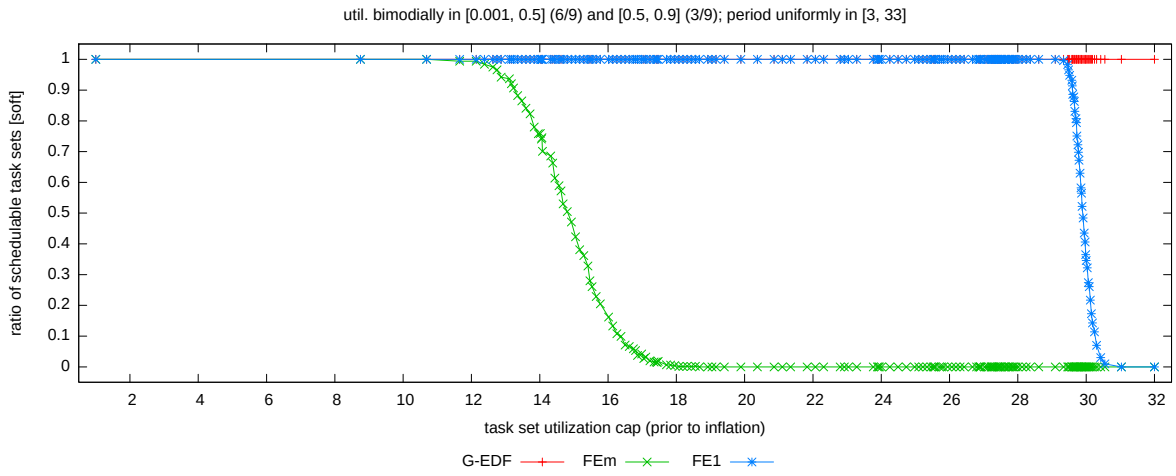

(a)

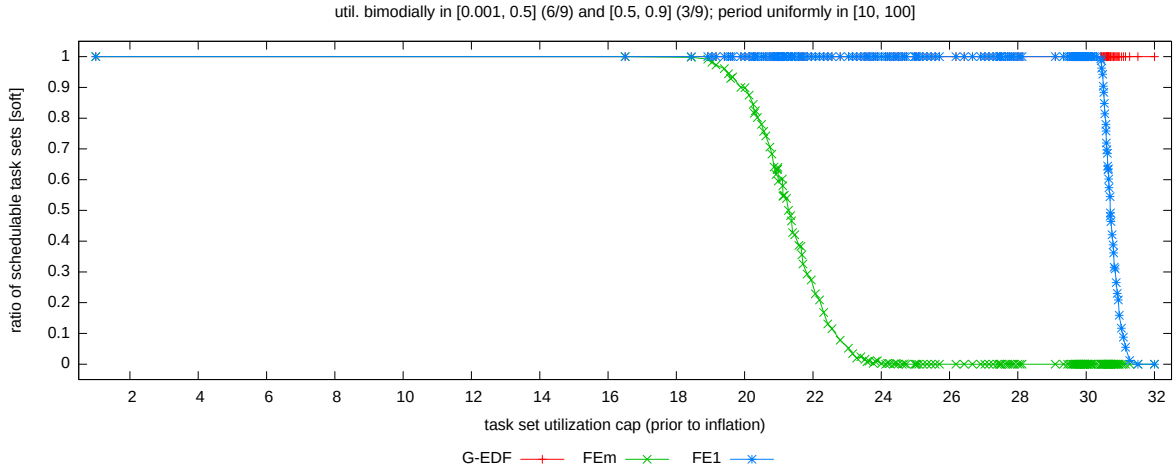

(b)

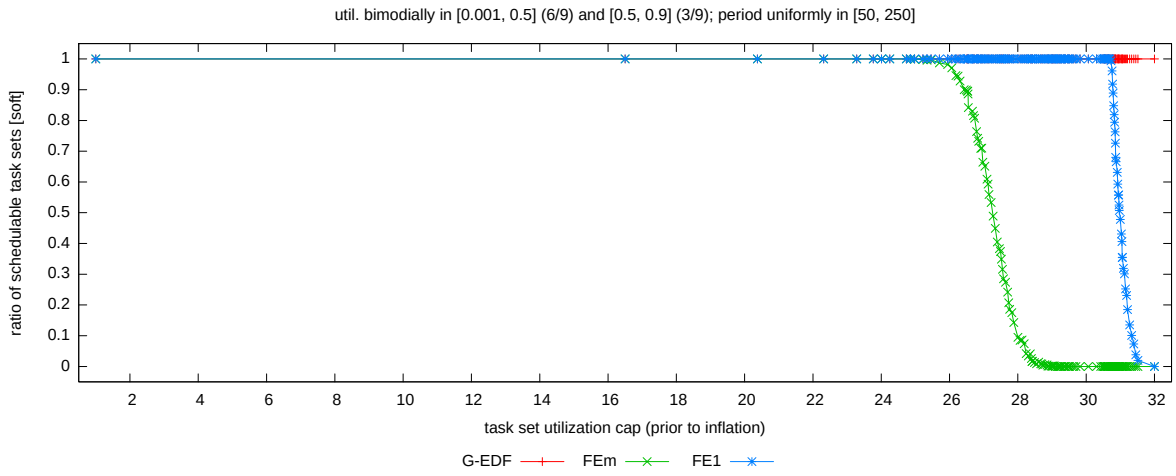

(c)

Figure 51: Comparison of FEm and FE1 (global vs. dedicated interrupt handling) in terms of soft schedulability of task sets with bimodal medium per-task utilizations and **(a)** short, **(b)** moderate, and **(c)** long periods. These graphs correspond to Fig. 27.

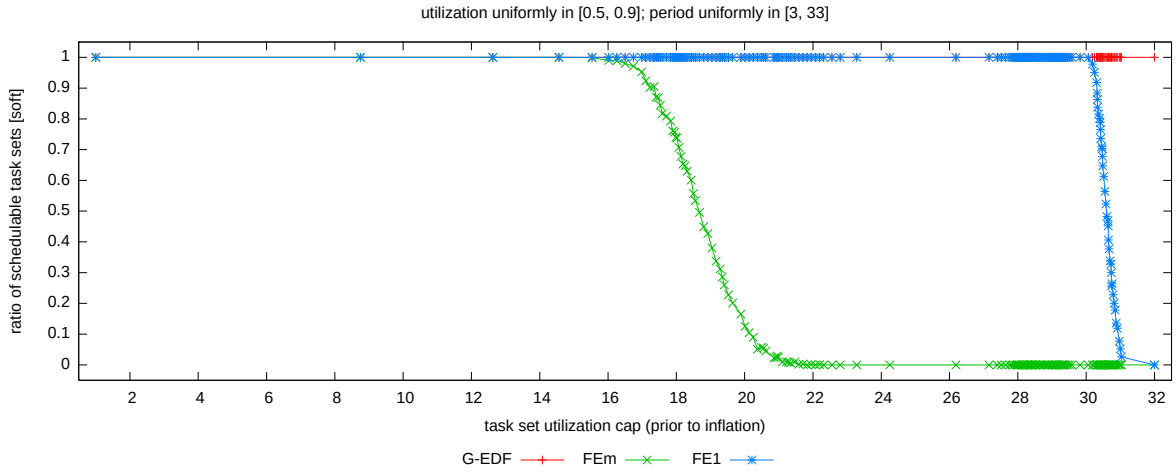

(a)

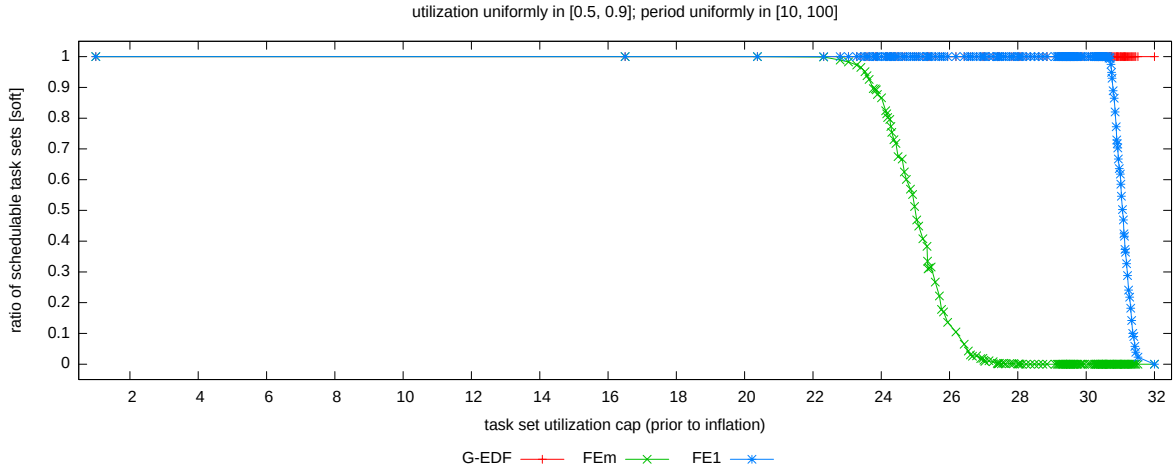

(b)

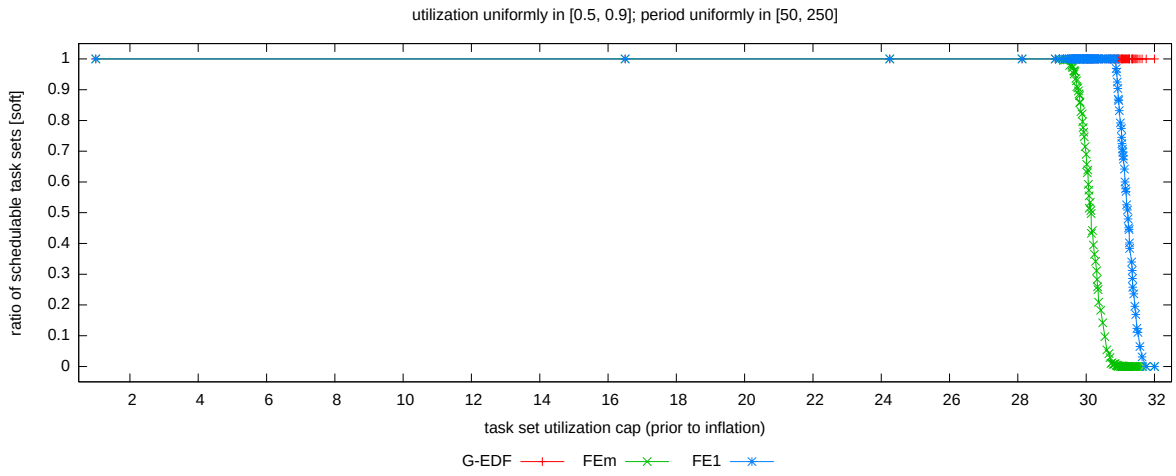

(c)

Figure 52: Comparison of FEm and FE1 (global vs. dedicated interrupt handling) in terms of soft schedulability of task sets with uniform heavy per-task utilizations and **(a)** short, **(b)** moderate, and **(c)** long periods. These graphs correspond to Fig. 28.

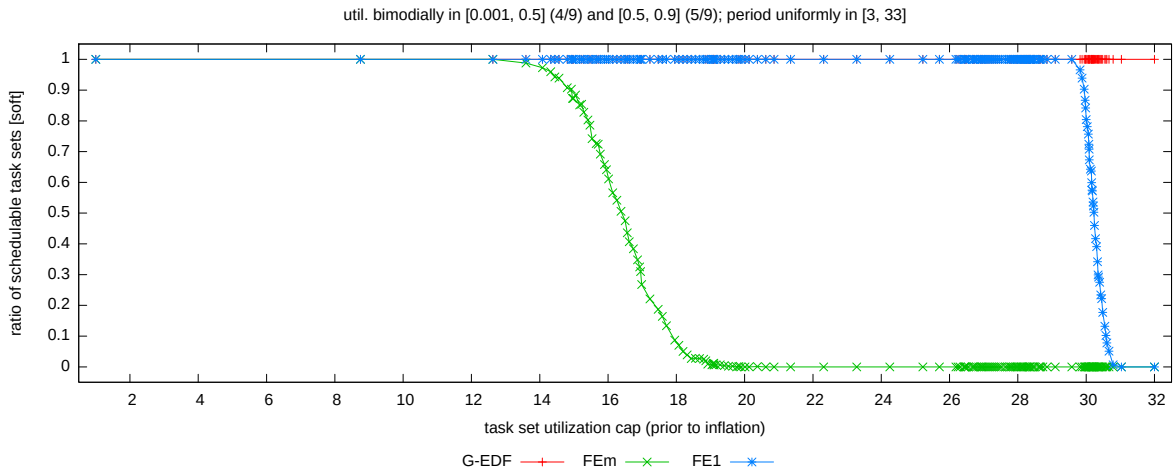

(a)

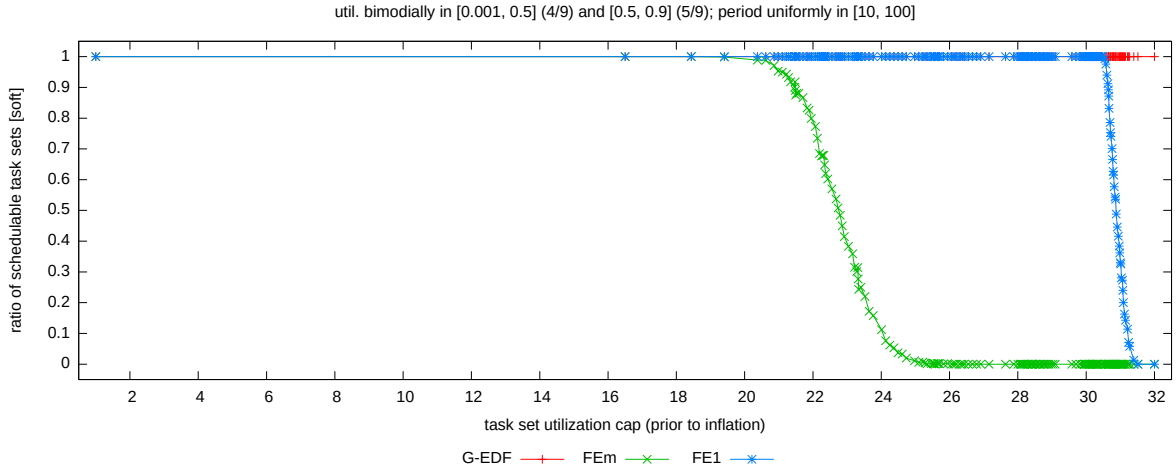

(b)

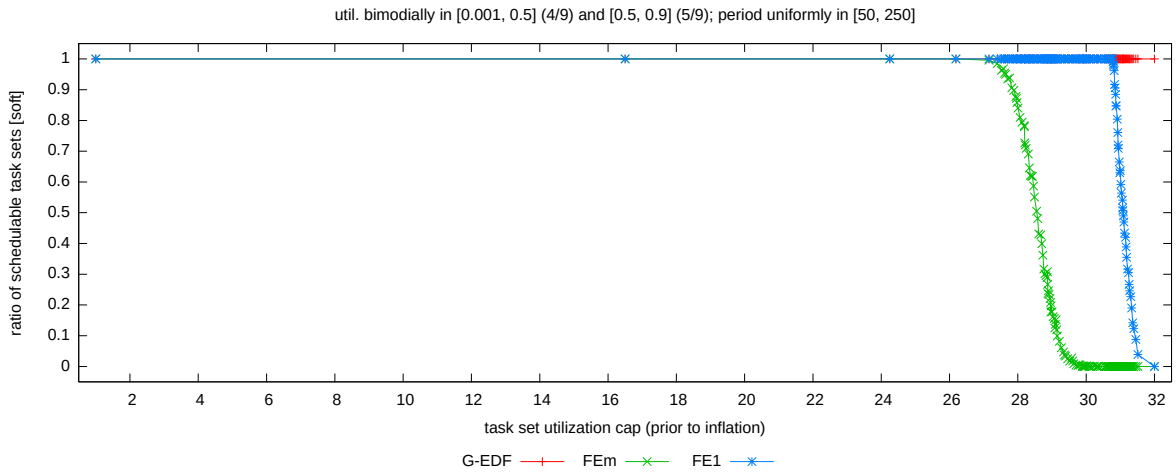

(c)

Figure 53: Comparison of FEm and FE1 (global vs. dedicated interrupt handling) in terms of soft schedulability of task sets with bimodal heavy per-task utilizations and **(a)** short, **(b)** moderate, and **(c)** long periods. These graphs correspond to Fig. 29.

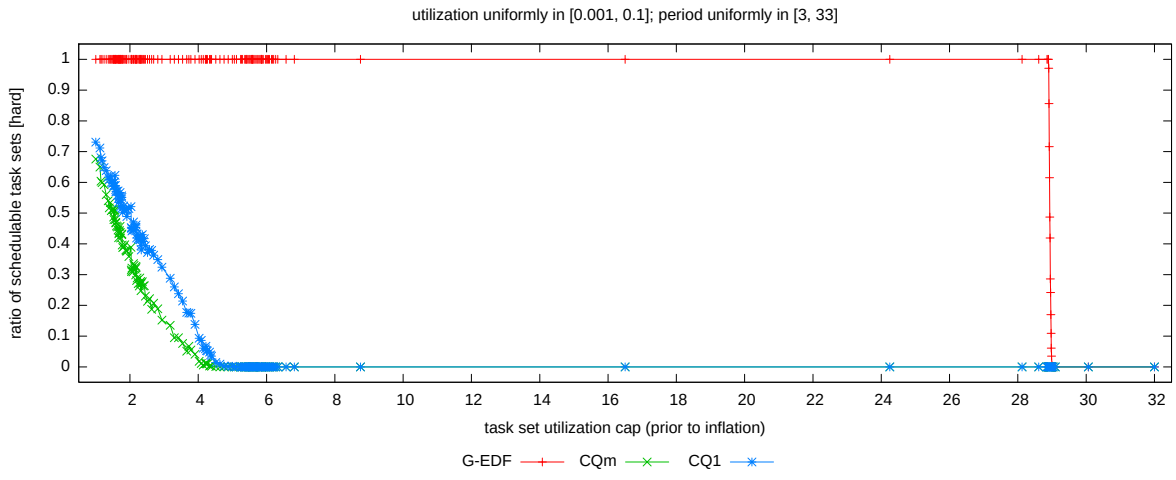

(a)

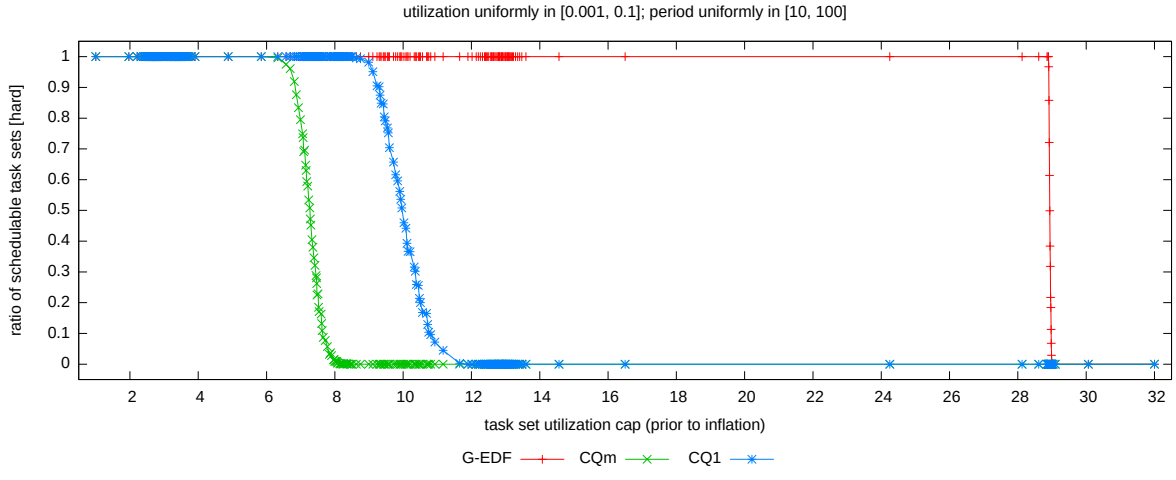

(b)

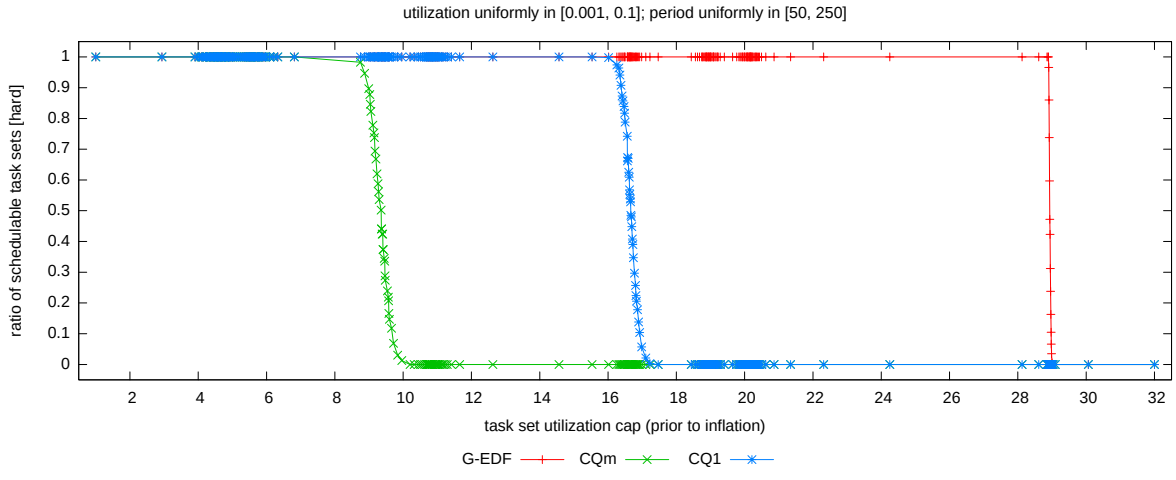

(c)

Figure 54: Comparison of CQm and CQ1 (global vs. dedicated interrupt handling) in terms of hard schedulability of task sets with uniform light per-task utilizations and **(a)** short, **(b)** moderate, and **(c)** long periods. These graphs correspond to Fig. 18.

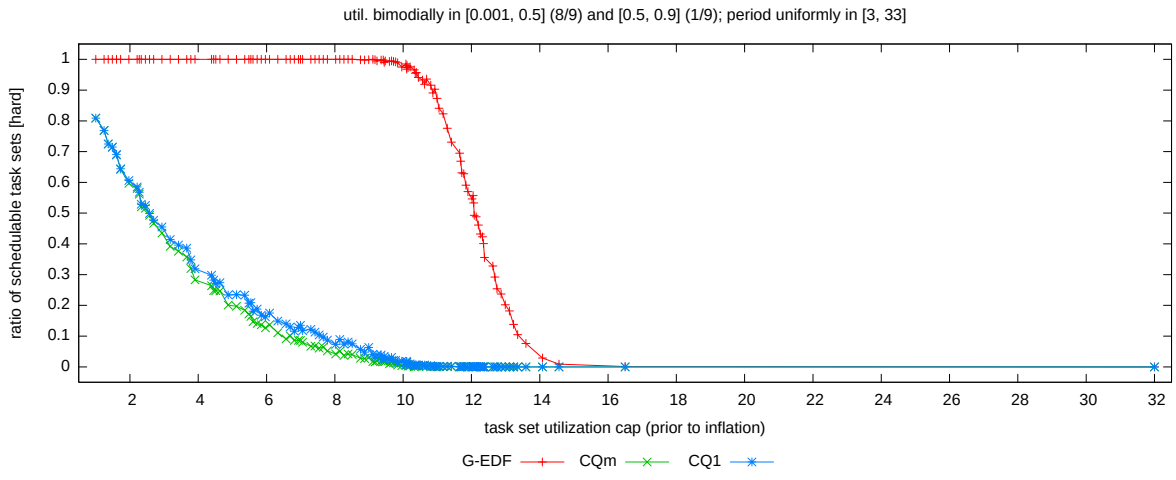

(a)

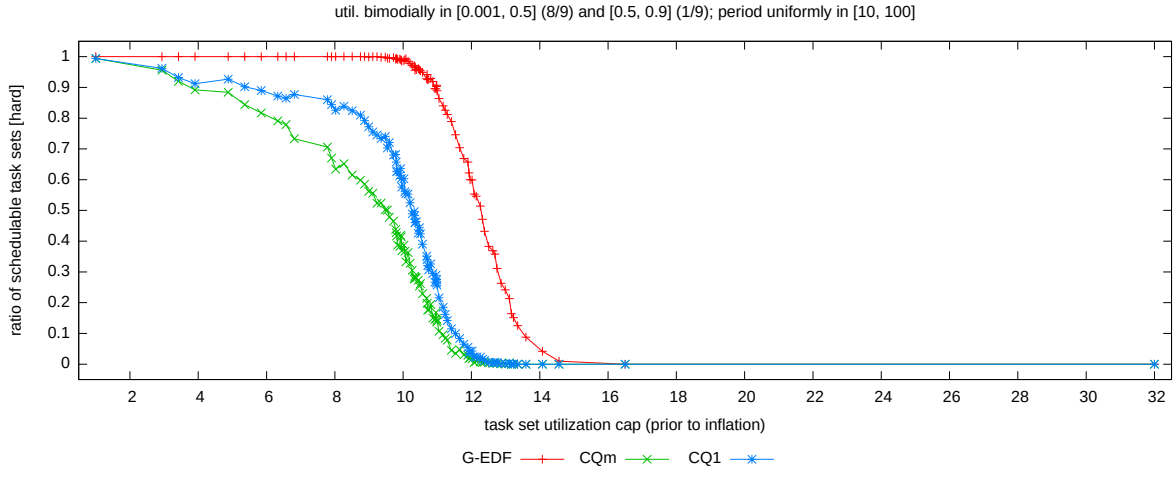

(b)

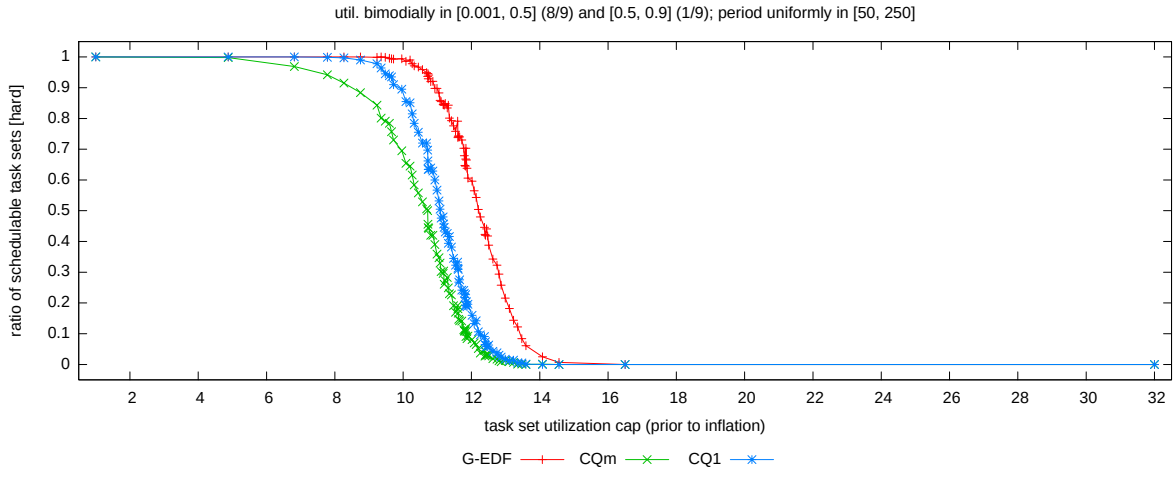

(c)

Figure 55: Comparison of CQm and CQ1 (global vs. dedicated interrupt handling) in terms of hard schedulability of task sets with bimodal light per-task utilizations and **(a)** short, **(b)** moderate, and **(c)** long periods. These graphs correspond to Fig. 19.

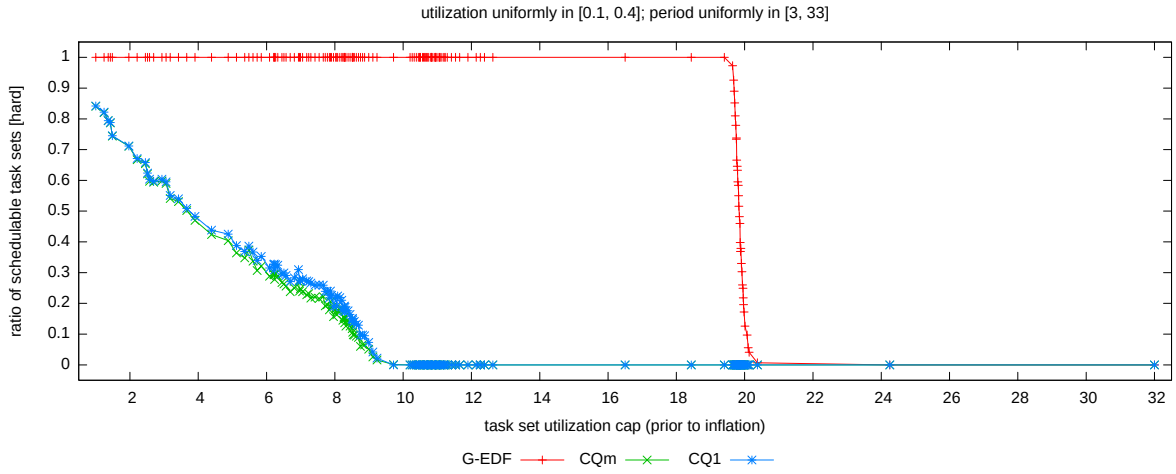

(a)

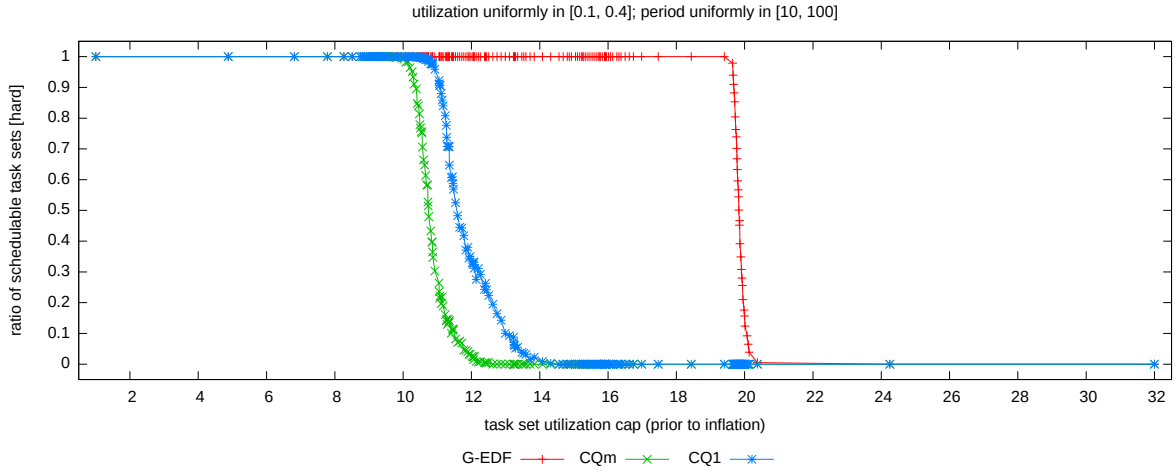

(b)

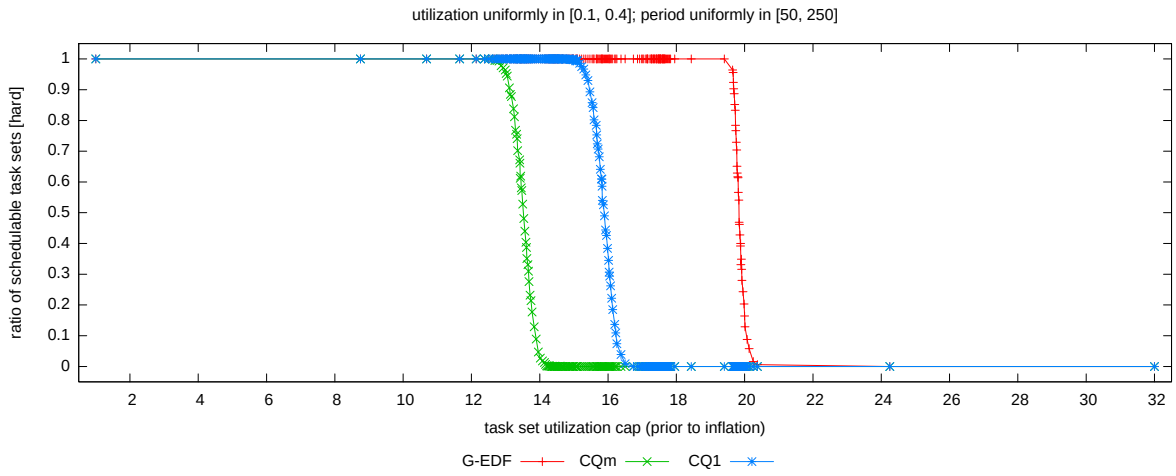

(c)

Figure 56: Comparison of CQm and CQ1 (global vs. dedicated interrupt handling) in terms of hard schedulability of task sets with uniform medium per-task utilizations and **(a)** short, **(b)** moderate, and **(c)** long periods. These graphs correspond to Fig. 20.

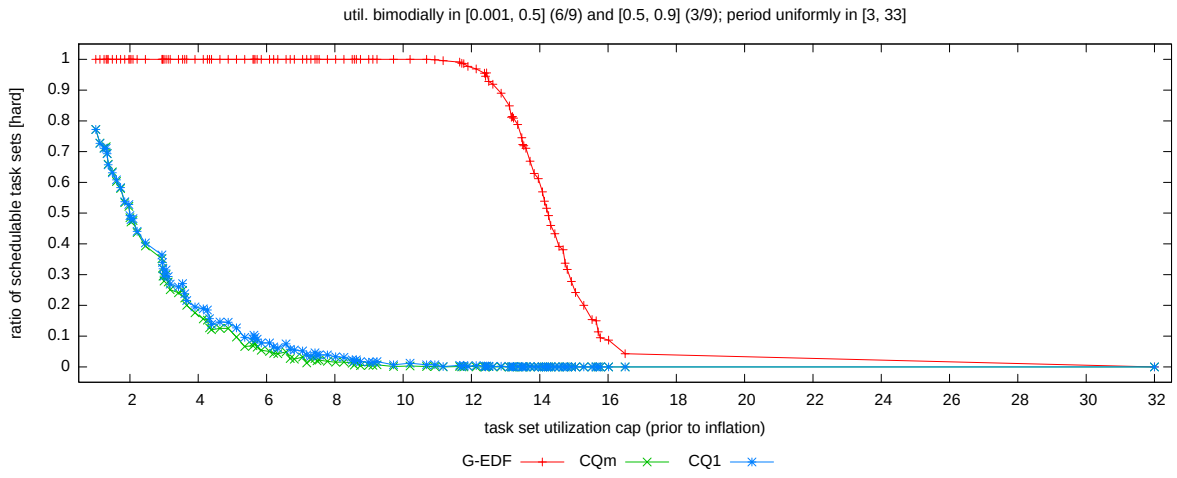

(a)

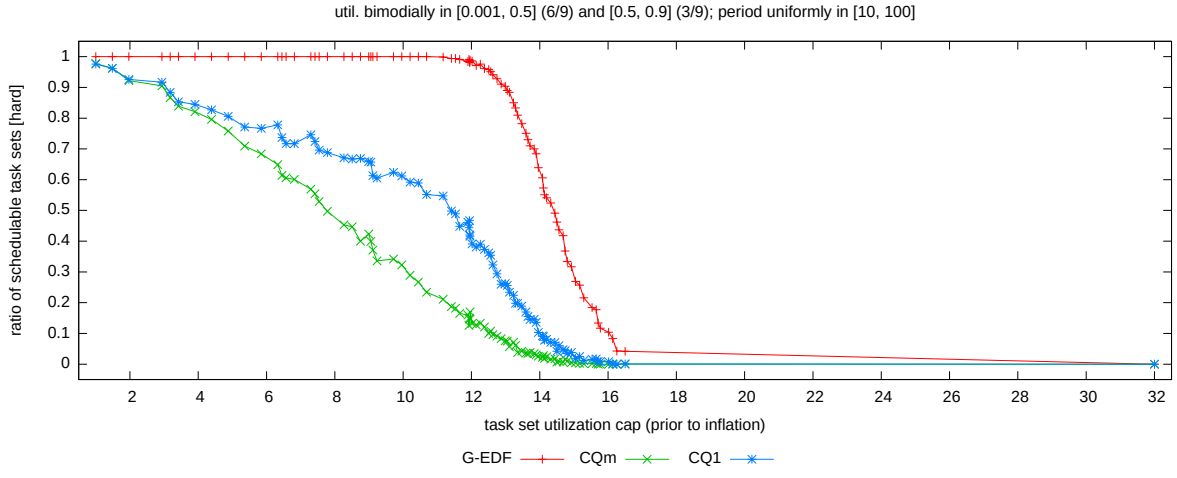

(b)

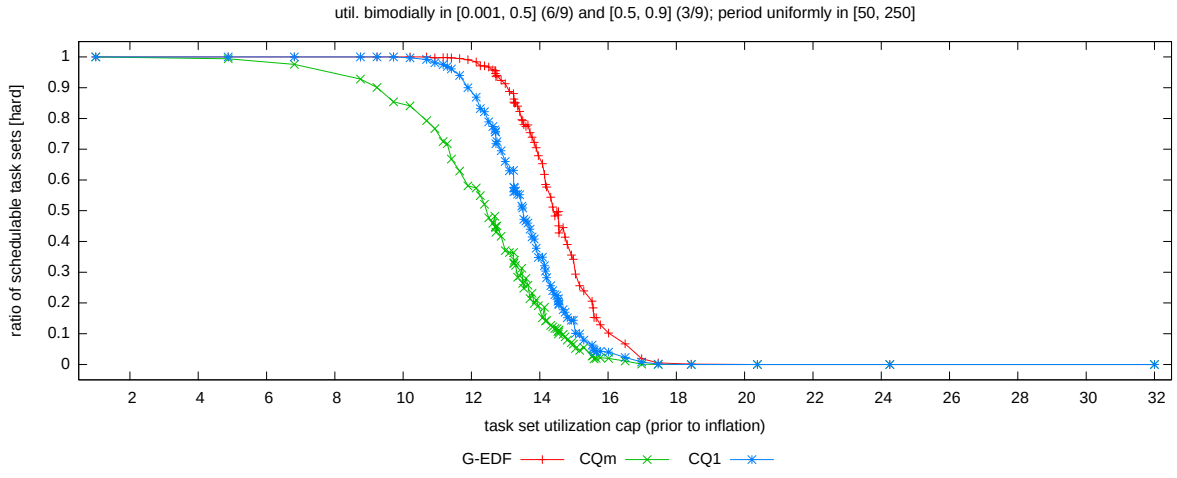

(c)

Figure 57: Comparison of CQm and CQ1 (global vs. dedicated interrupt handling) in terms of hard schedulability of task sets with bimodal medium per-task utilizations and **(a)** short, **(b)** moderate, and **(c)** long periods. These graphs correspond to Fig. 21.

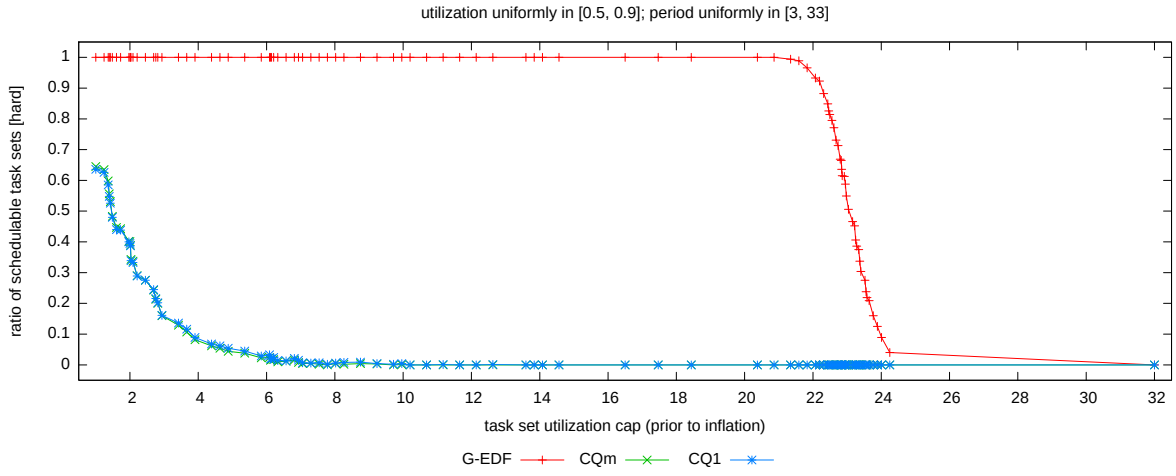

(a)

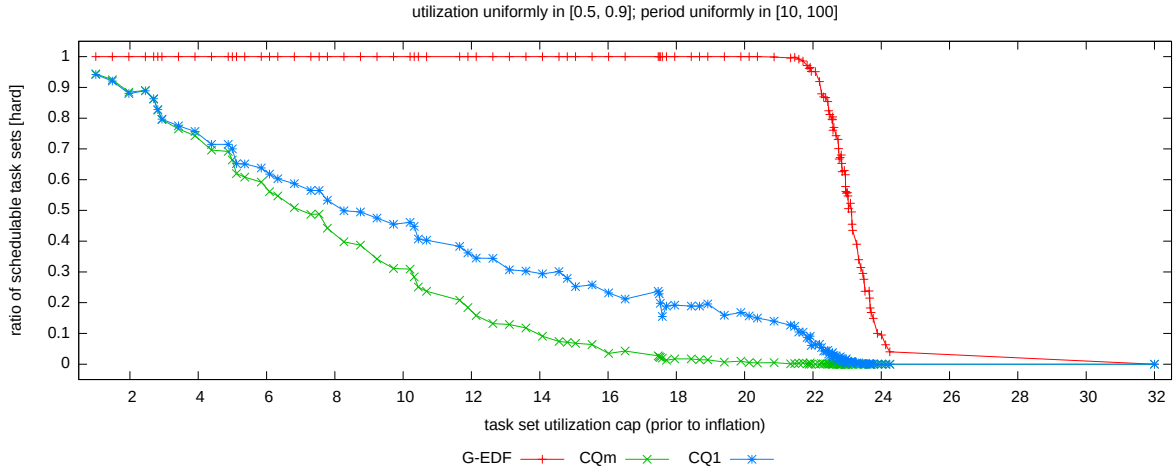

(b)

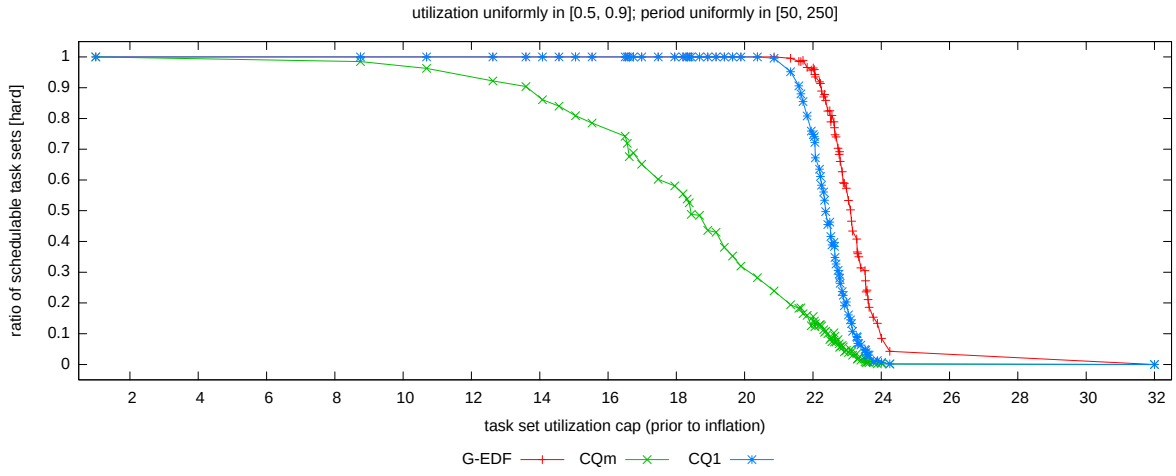

(c)

Figure 58: Comparison of CQm and CQ1 (global vs. dedicated interrupt handling) in terms of hard schedulability of task sets with uniform heavy per-task utilizations and **(a)** short, **(b)** moderate, and **(c)** long periods. These graphs correspond to Fig. 22.

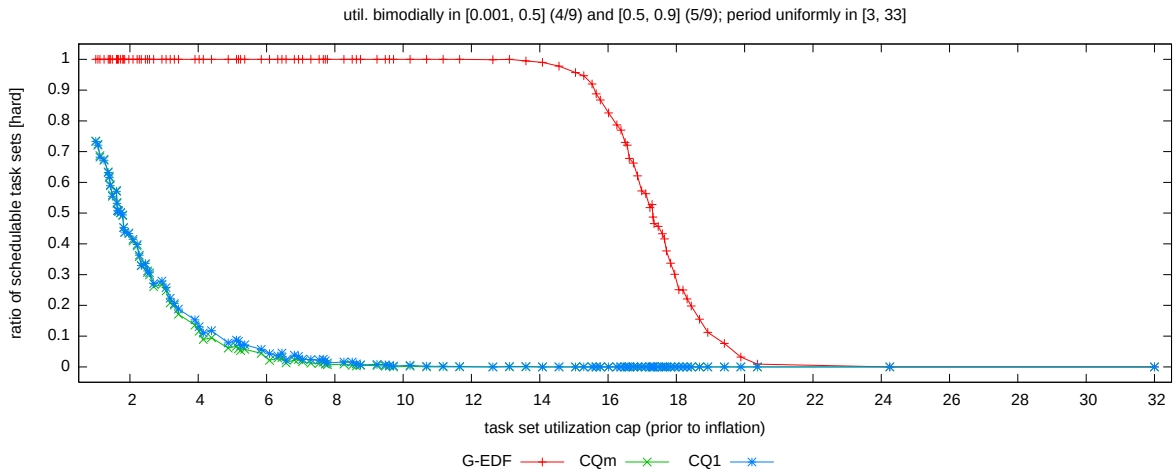

(a)

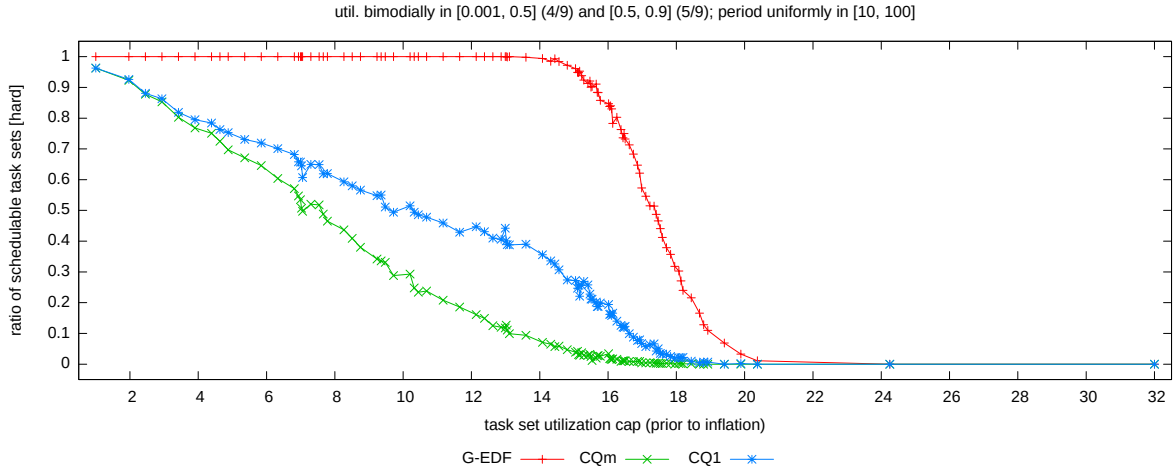

(b)

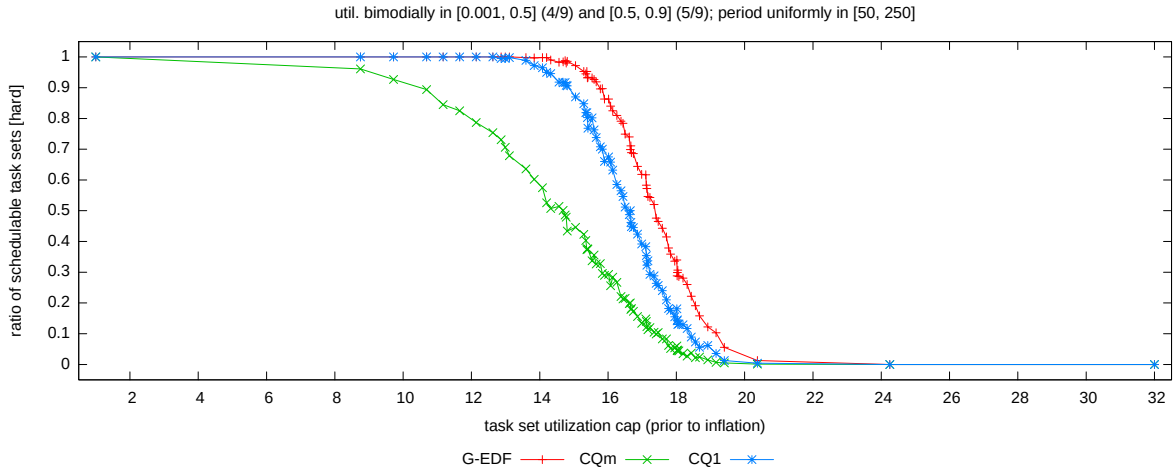

(c)

Figure 59: Comparison of CQm and CQ1 (global vs. dedicated interrupt handling) in terms of hard schedulability of task sets with bimodal heavy per-task utilizations and **(a)** short, **(b)** moderate, and **(c)** long periods. These graphs correspond to Fig. 23.

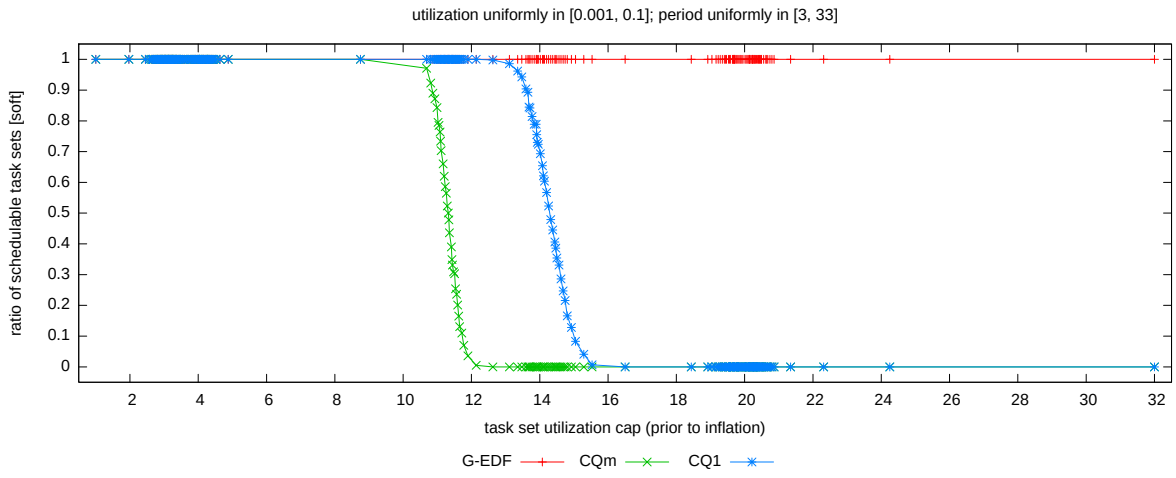

(a)

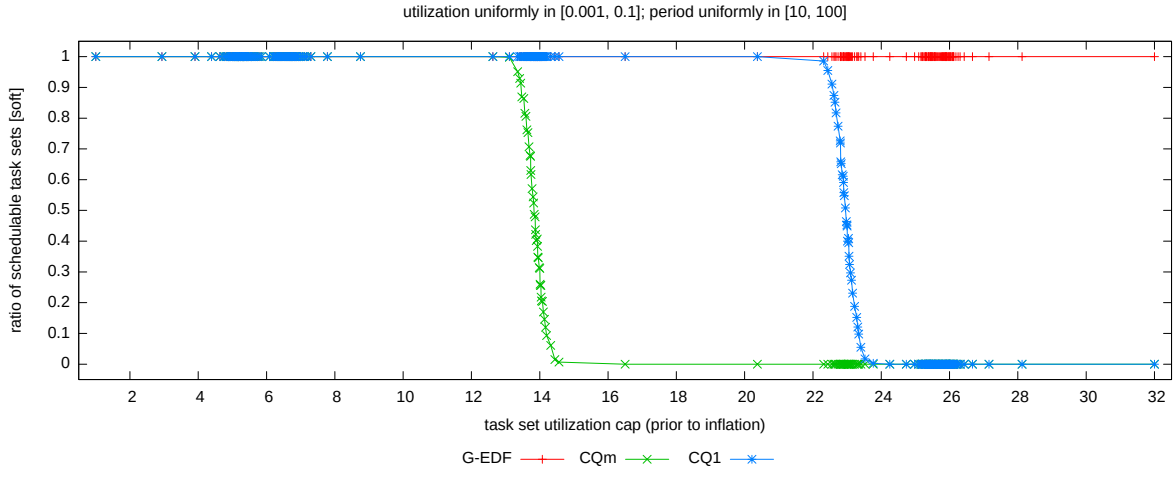

(b)

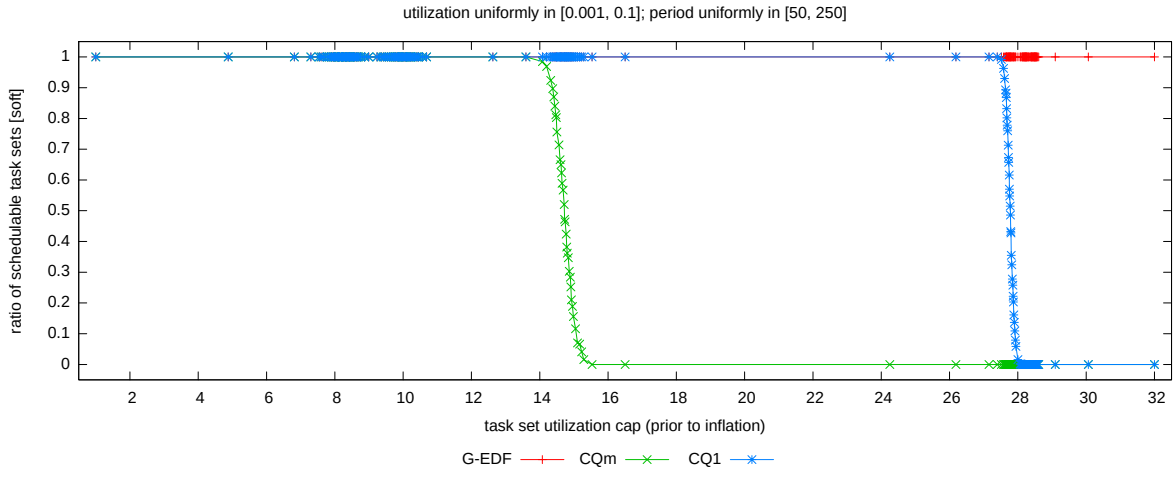

(c)

Figure 60: Comparison of CQm and CQ1 (global vs. dedicated interrupt handling) in terms of soft schedulability of task sets with uniform light per-task utilizations and **(a)** short, **(b)** moderate, and **(c)** long periods. These graphs correspond to Fig. 24.

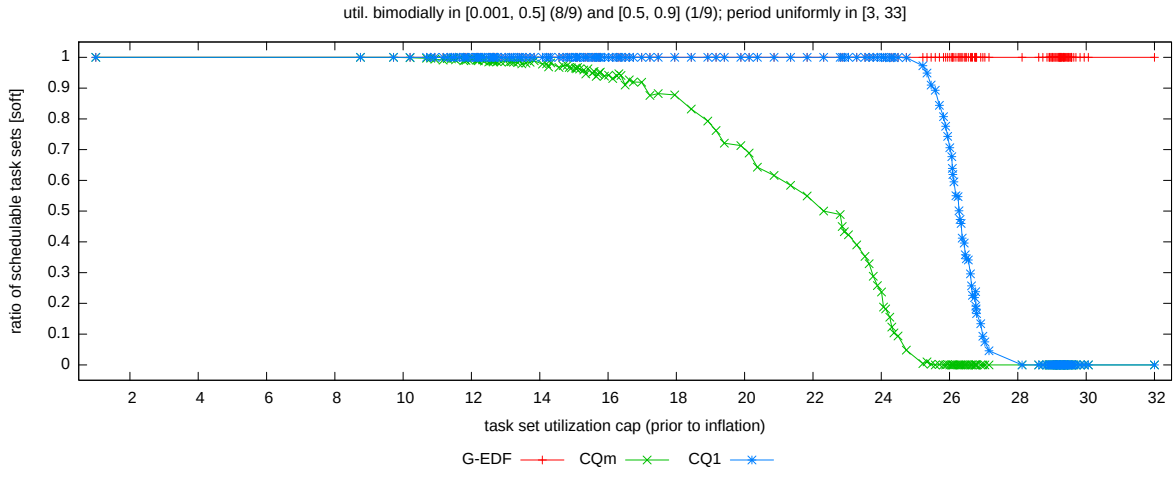

(a)

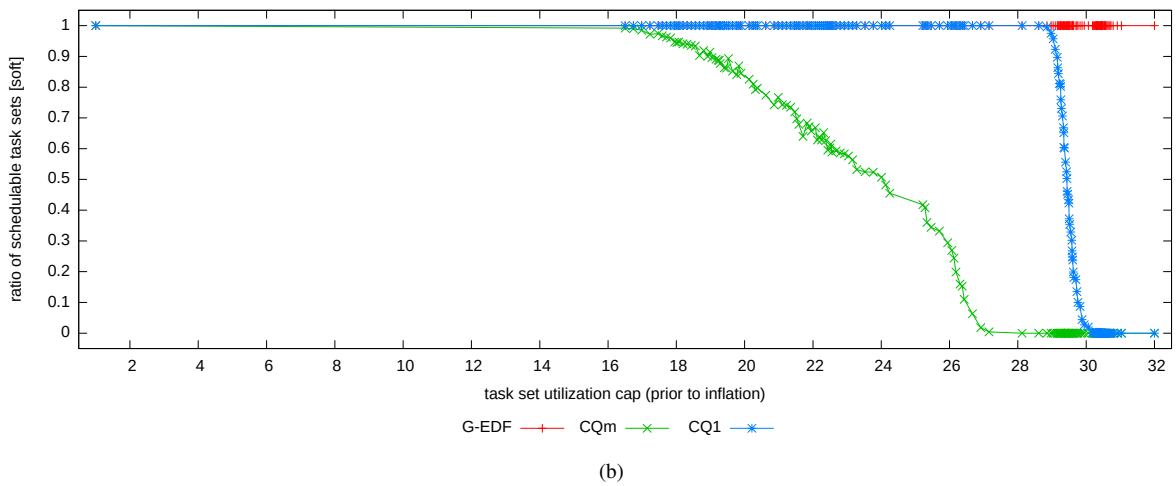

(b)

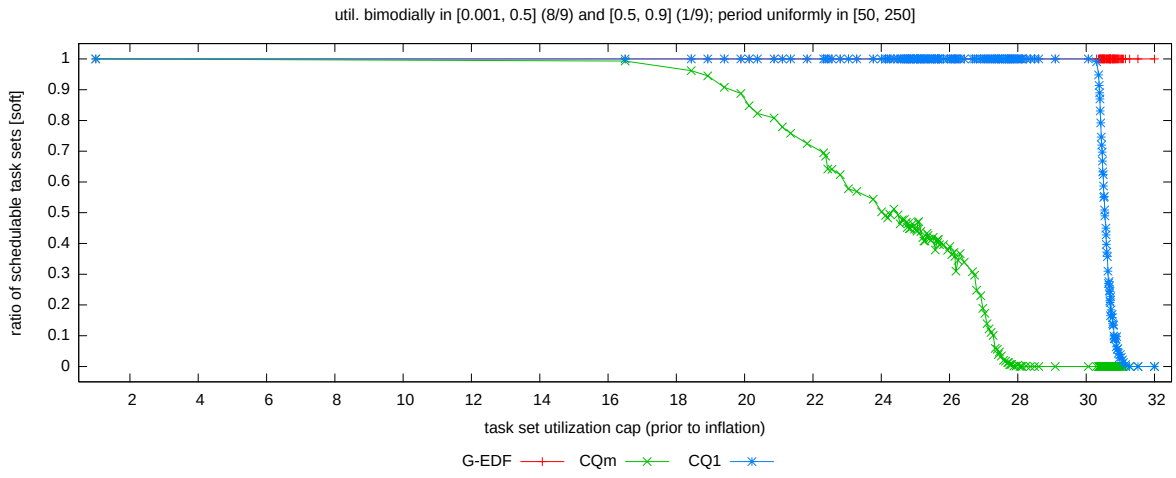

(c)

Figure 61: Comparison of CQm and CQ1 (global vs. dedicated interrupt handling) in terms of soft schedulability of task sets with bimodal light per-task utilizations and **(a)** short, **(b)** moderate, and **(c)** long periods. These graphs correspond to Fig. 25.

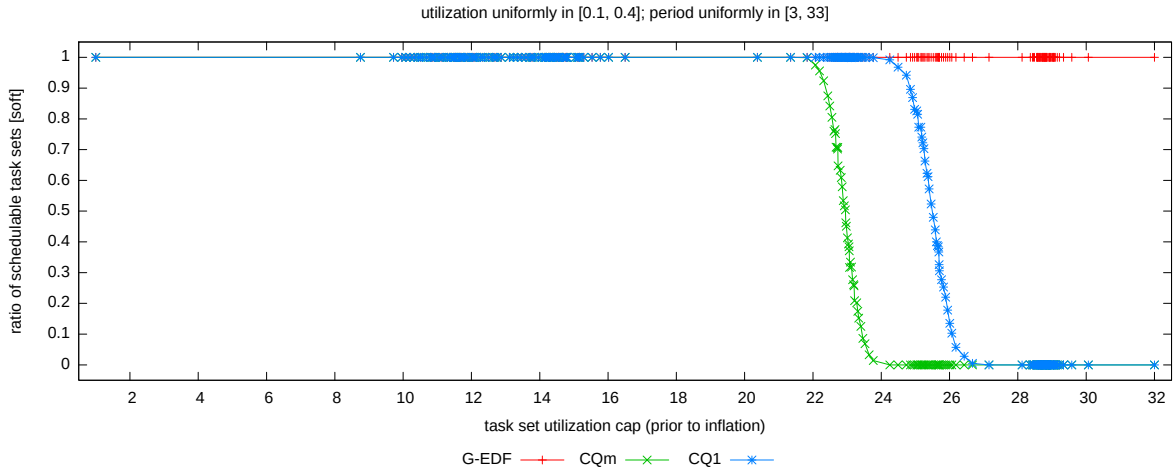

(a)

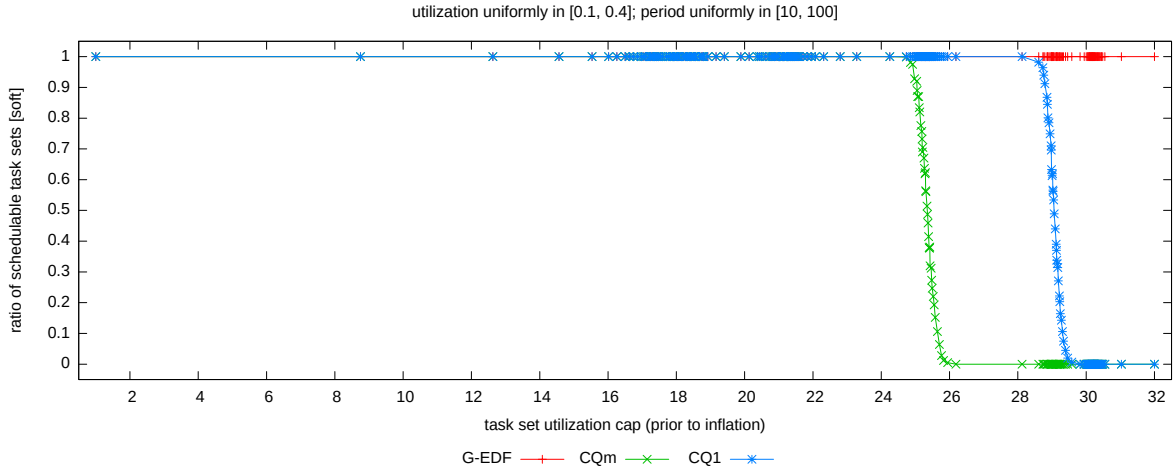

(b)

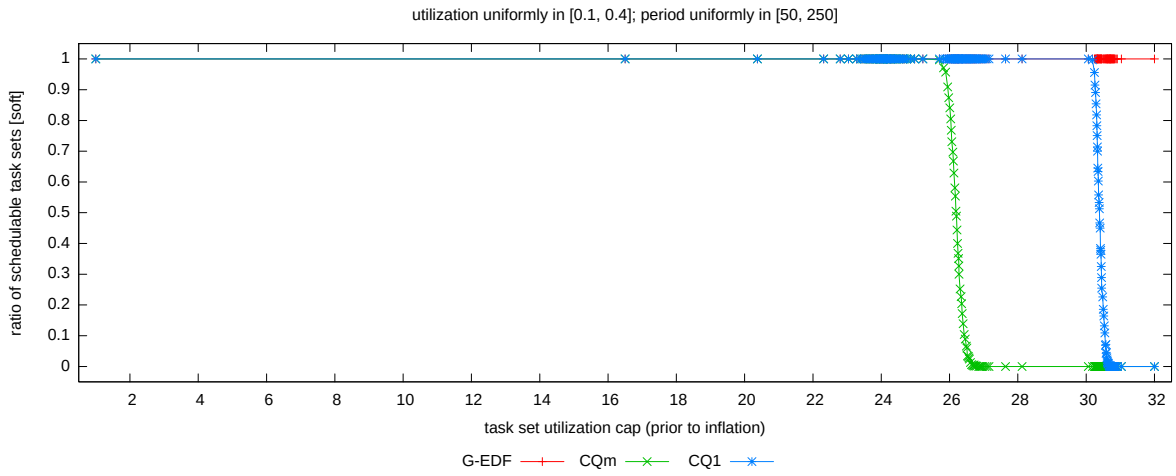

(c)

Figure 62: Comparison of CQm and CQ1 (global vs. dedicated interrupt handling) in terms of soft schedulability of task sets with uniform medium per-task utilizations and **(a)** short, **(b)** moderate, and **(c)** long periods. These graphs correspond to Fig. 26.

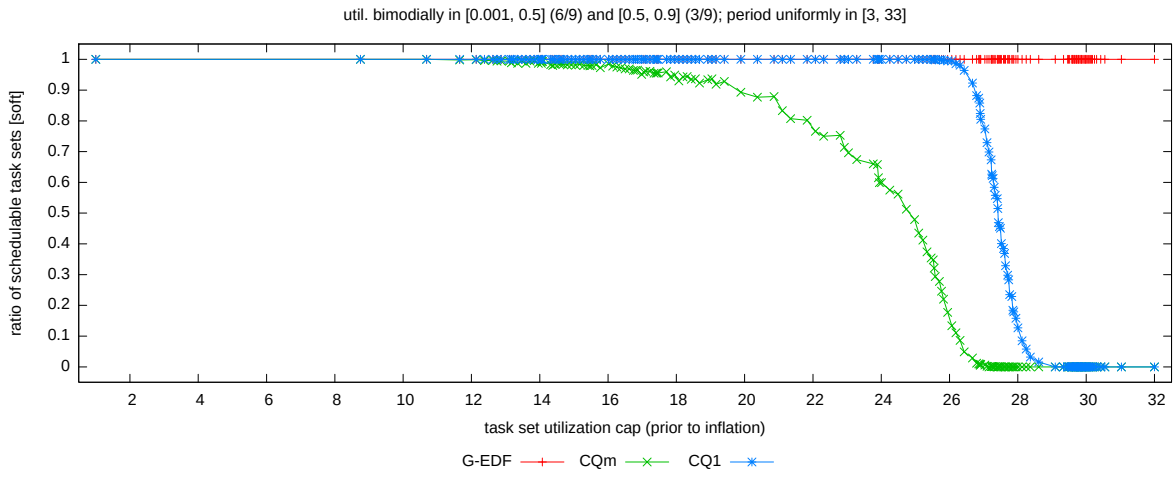

(a)

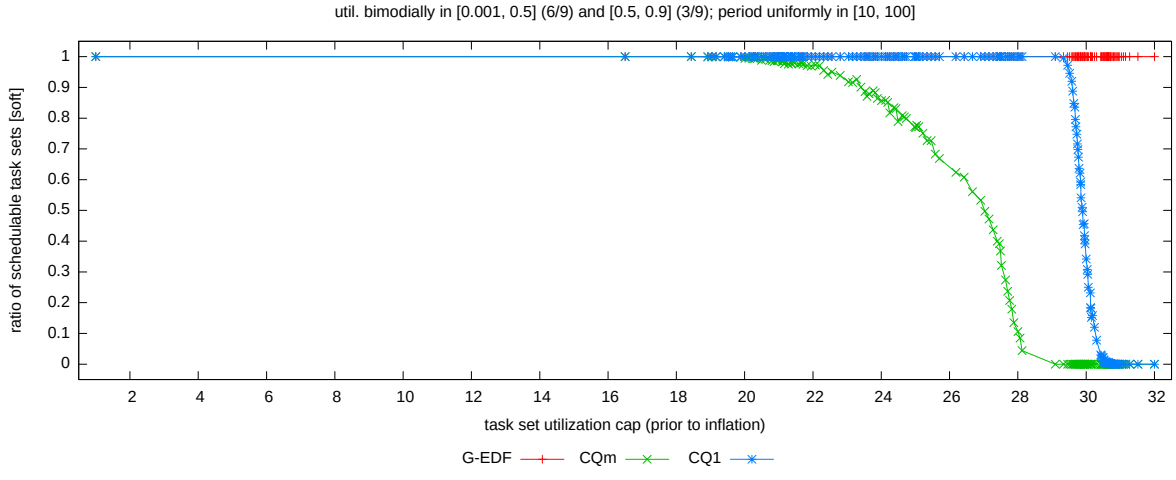

(b)

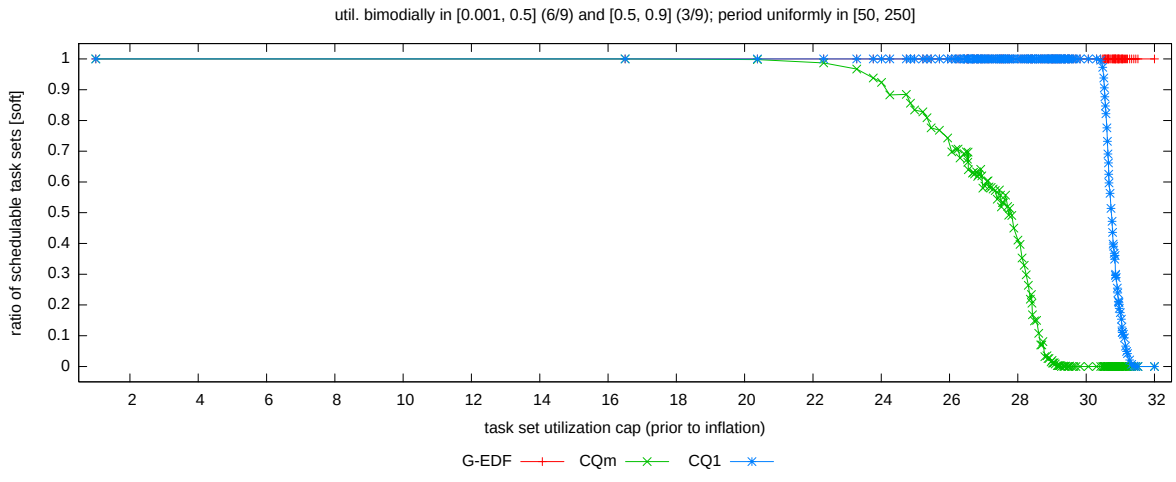

(c)

Figure 63: Comparison of CQm and CQ1 (global vs. dedicated interrupt handling) in terms of soft schedulability of task sets with bimodal medium per-task utilizations and **(a)** short, **(b)** moderate, and **(c)** long periods. These graphs correspond to Fig. 27.

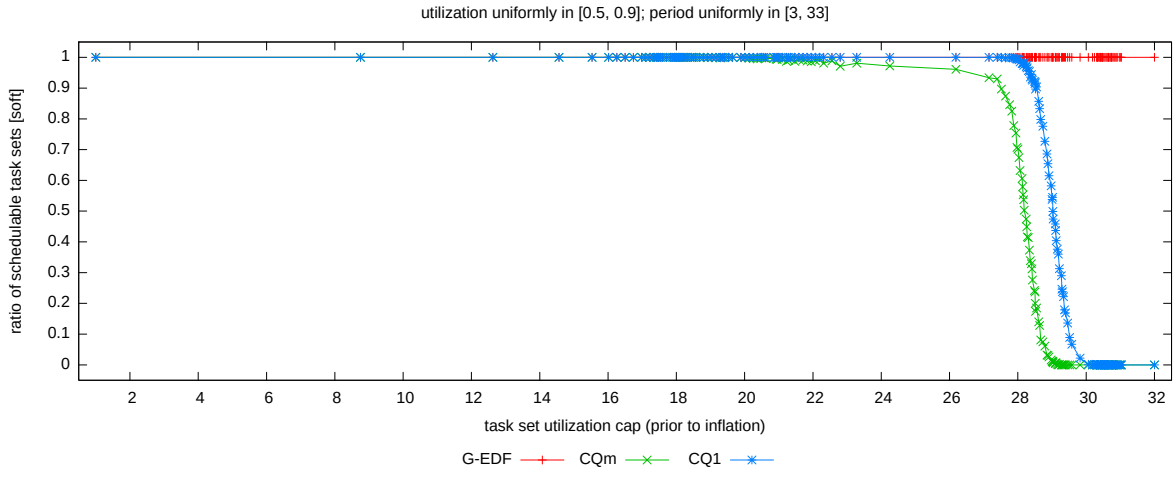

(a)

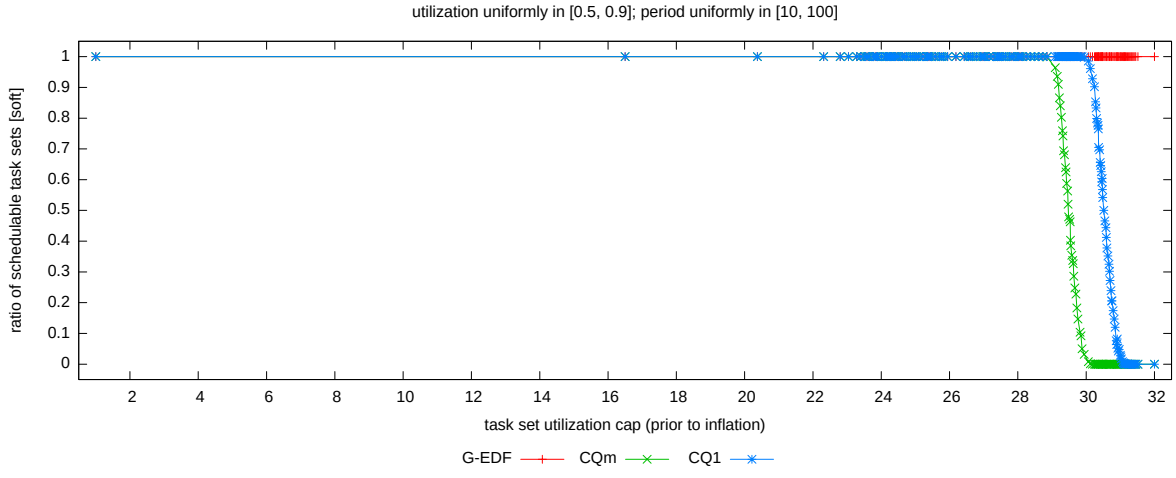

(b)

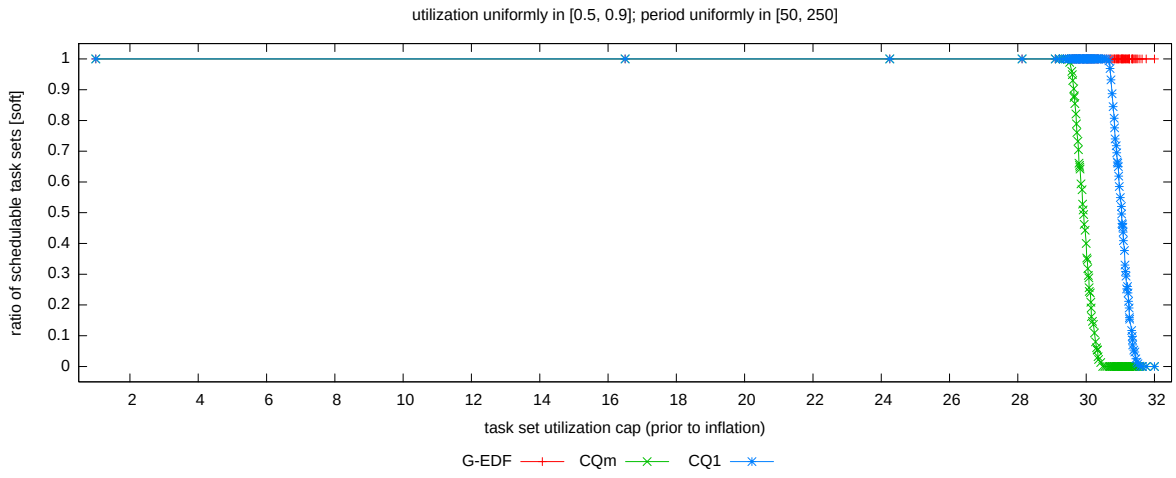

(c)

Figure 64: Comparison of CQm and CQ1 (global vs. dedicated interrupt handling) in terms of soft schedulability of task sets with uniform heavy per-task utilizations and **(a)** short, **(b)** moderate, and **(c)** long periods. These graphs correspond to Fig. 28.

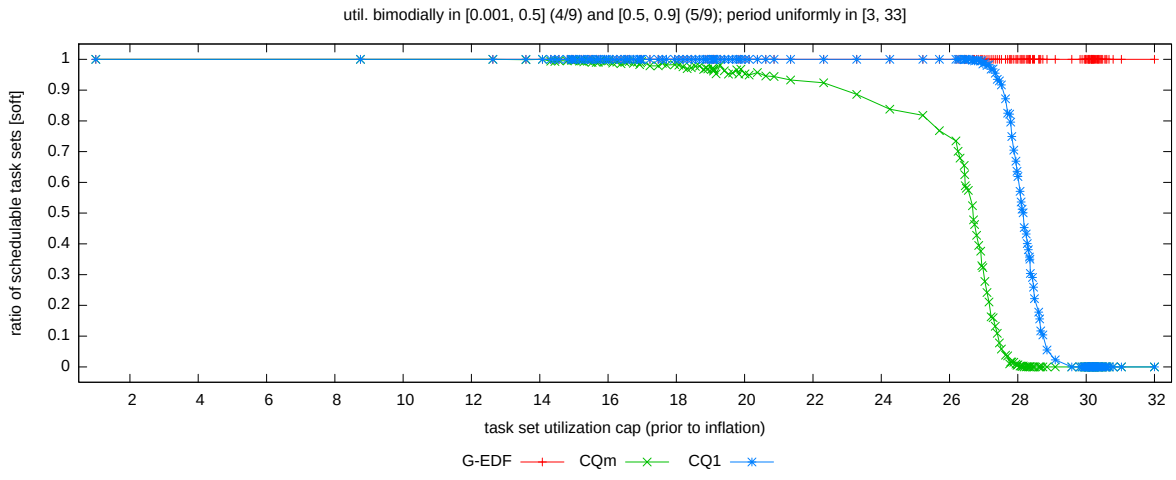

(a)

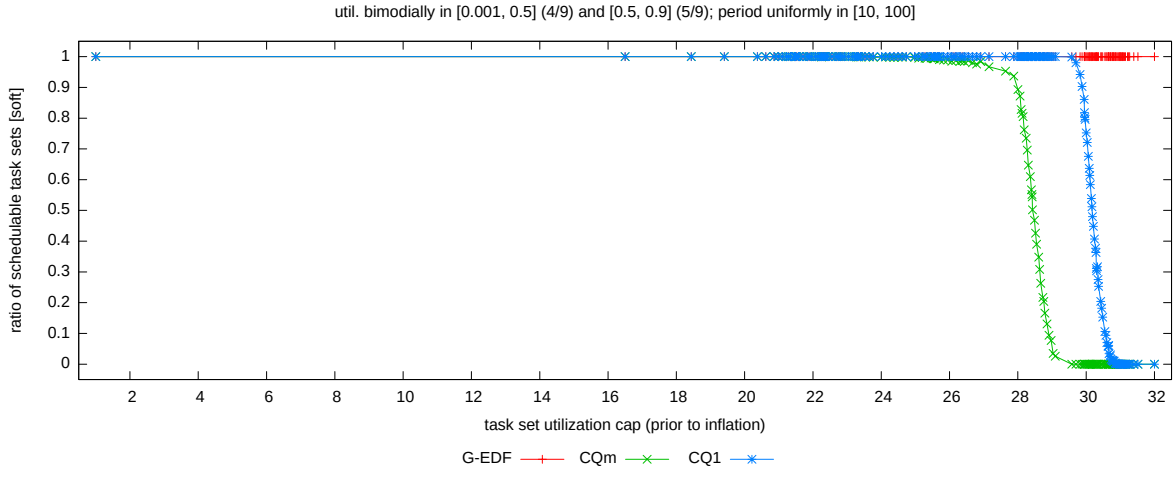

(b)

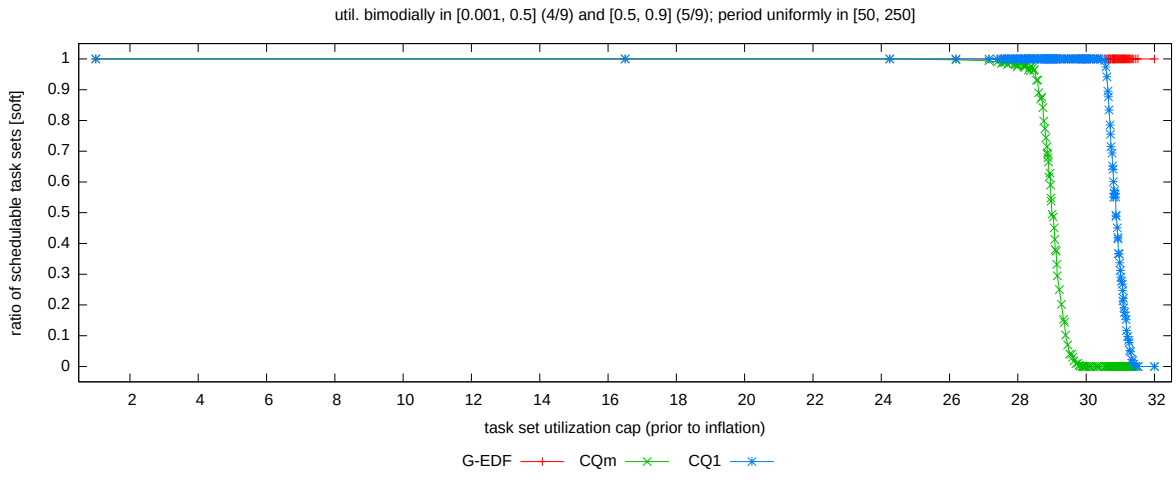

(c)

Figure 65: Comparison of CQm and CQ1 (global vs. dedicated interrupt handling) in terms of soft schedulability of task sets with bimodal heavy per-task utilizations and **(a)** short, **(b)** moderate, and **(c)** long periods. These graphs correspond to Fig. 29.

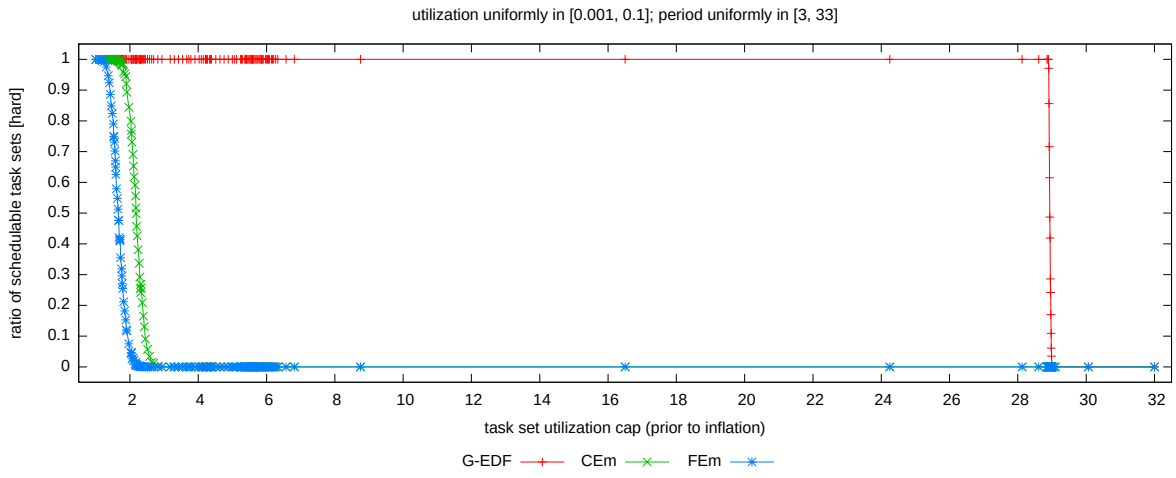

(a)

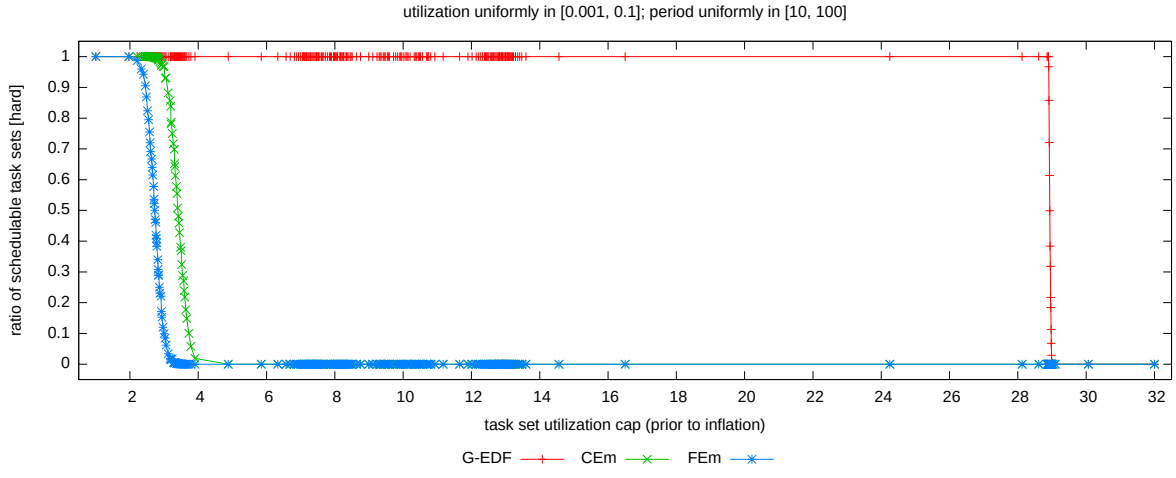

(b)

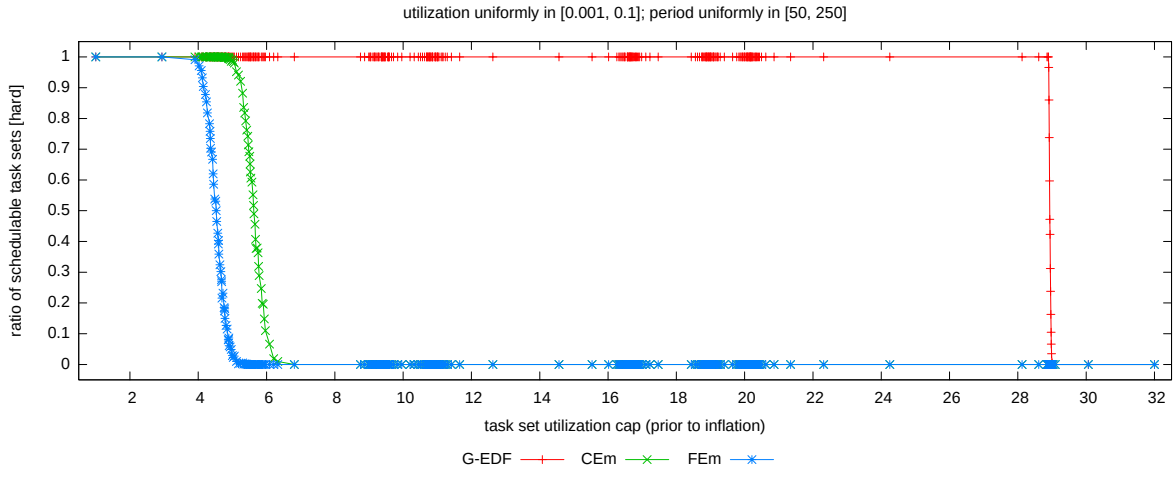

(c)

Figure 66: Comparison of CEm and FEm (coarse- vs. fine-grained queues) in terms of hard schedulability of task sets with uniform light per-task utilizations and **(a)** short, **(b)** moderate, and **(c)** long periods. These graphs correspond to Fig. 18.

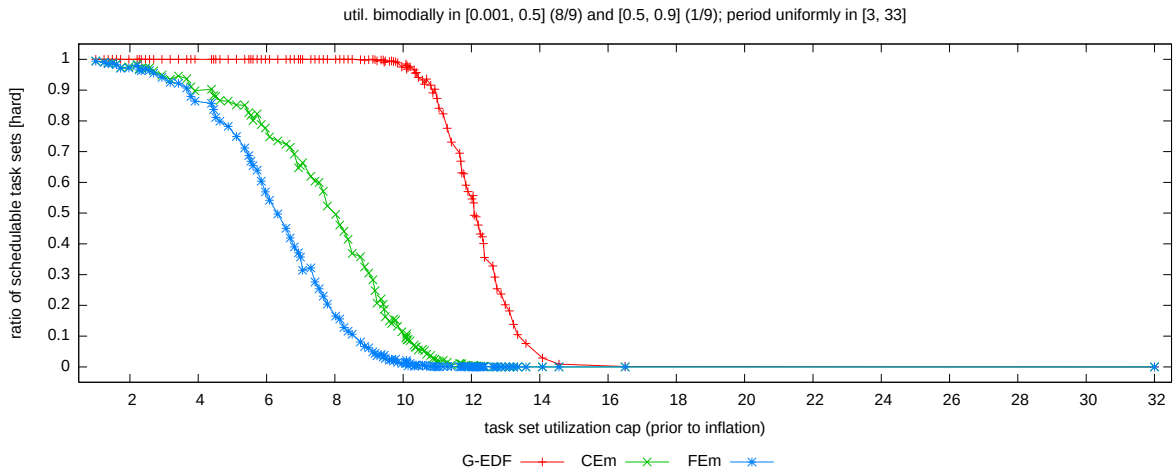

(a)

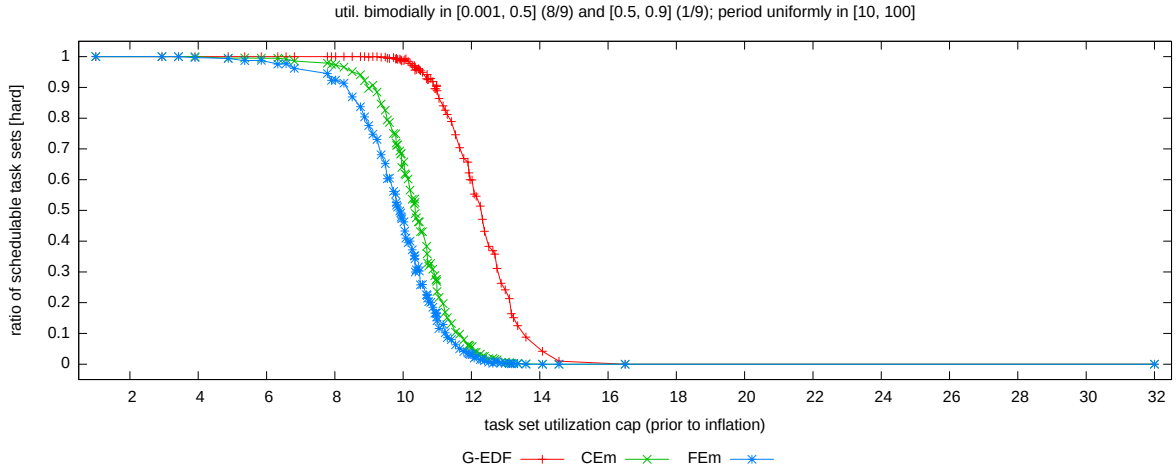

(b)

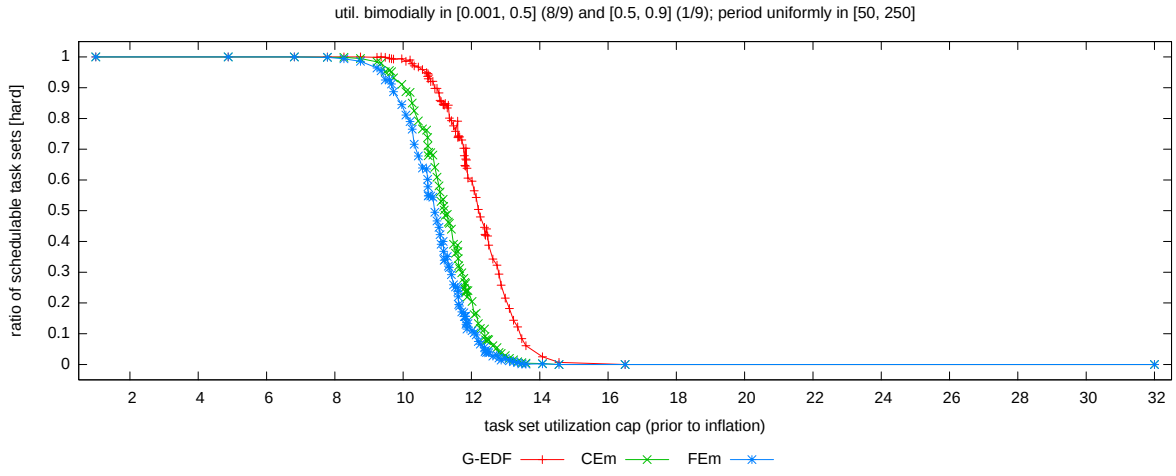

(c)

Figure 67: Comparison of CEm and FEm (coarse- vs. fine-grained queues) in terms of hard schedulability of task sets with bimodal light per-task utilizations and **(a)** short, **(b)** moderate, and **(c)** long periods. These graphs correspond to Fig. 19.

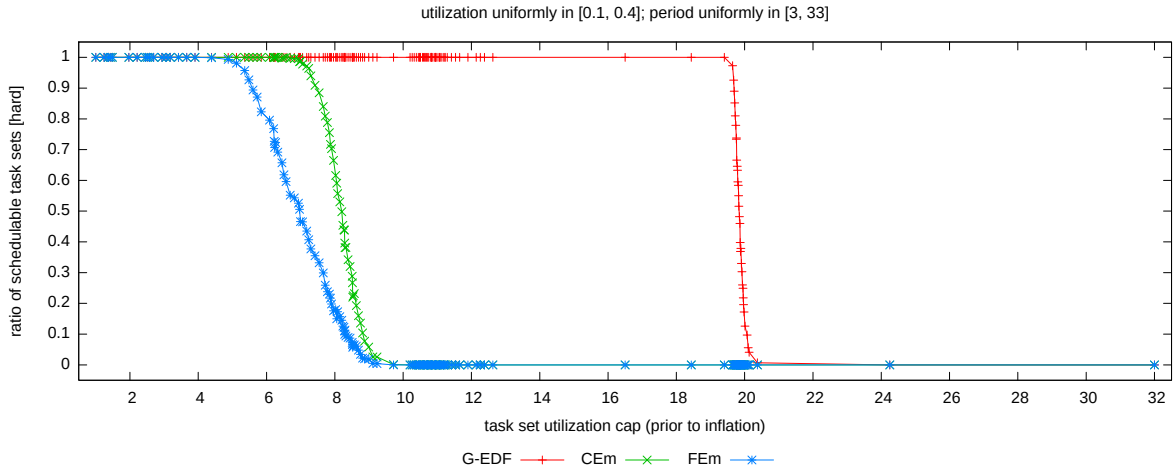

(a)

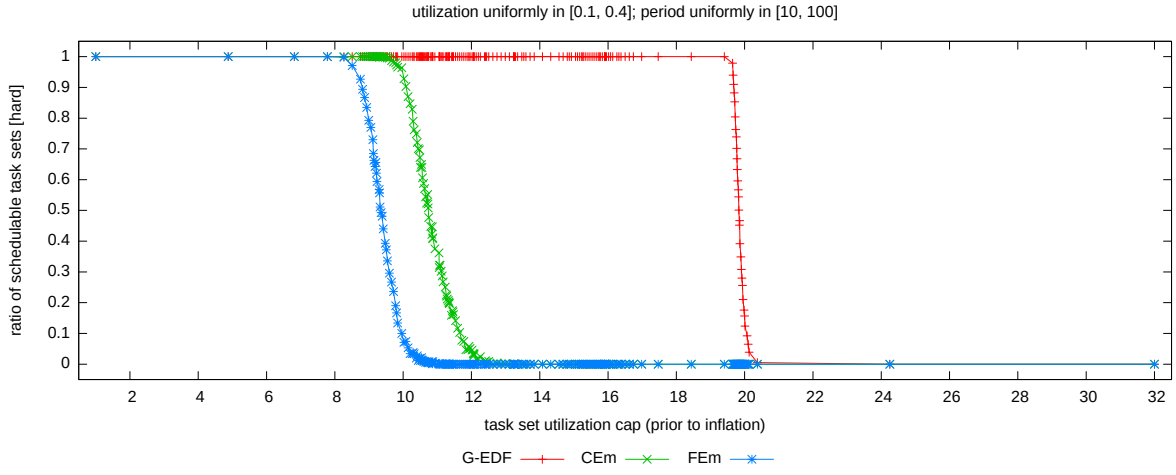

(b)

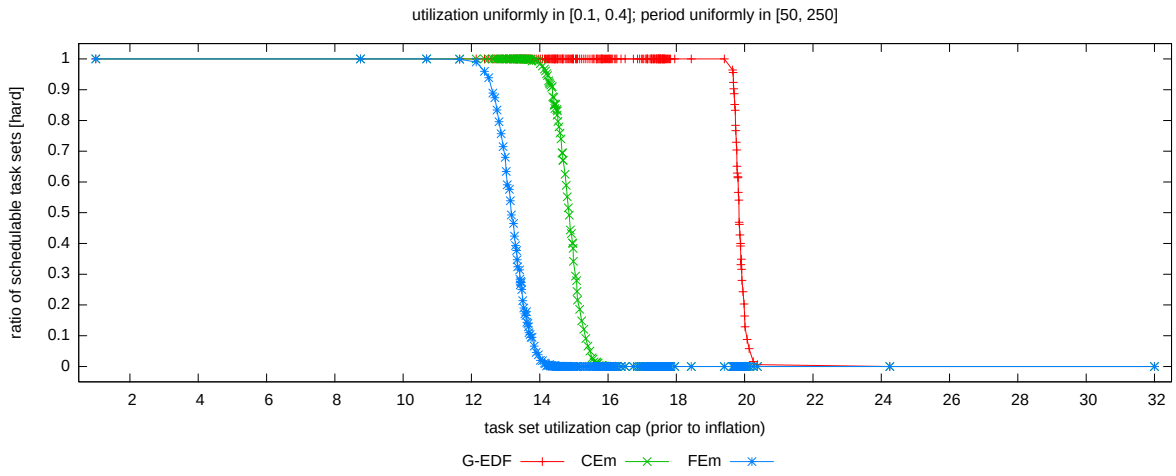

(c)

Figure 68: Comparison of CEm and FEm (coarse- vs. fine-grained queues) in terms of hard schedulability of task sets with uniform medium per-task utilizations and **(a)** short, **(b)** moderate, and **(c)** long periods. These graphs correspond to Fig. 20.

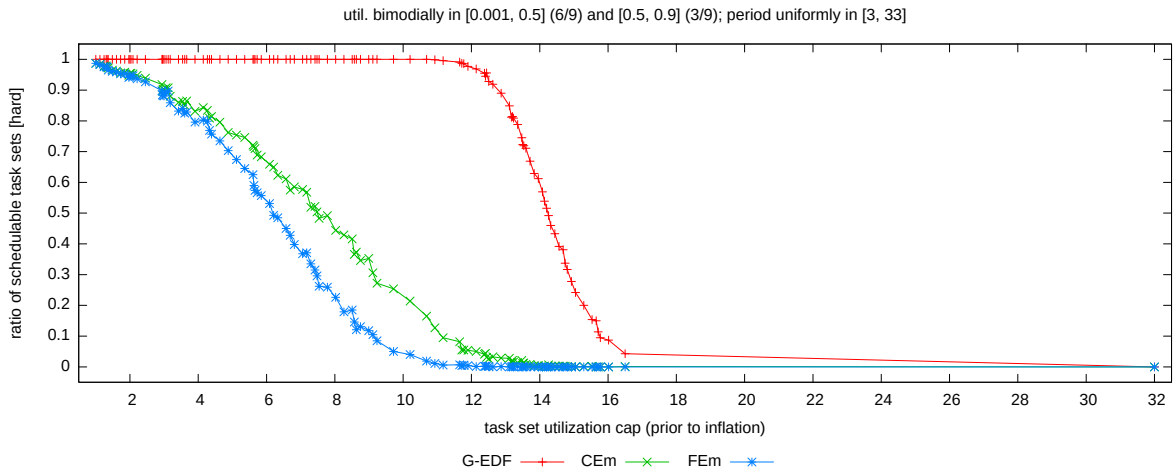

(a)

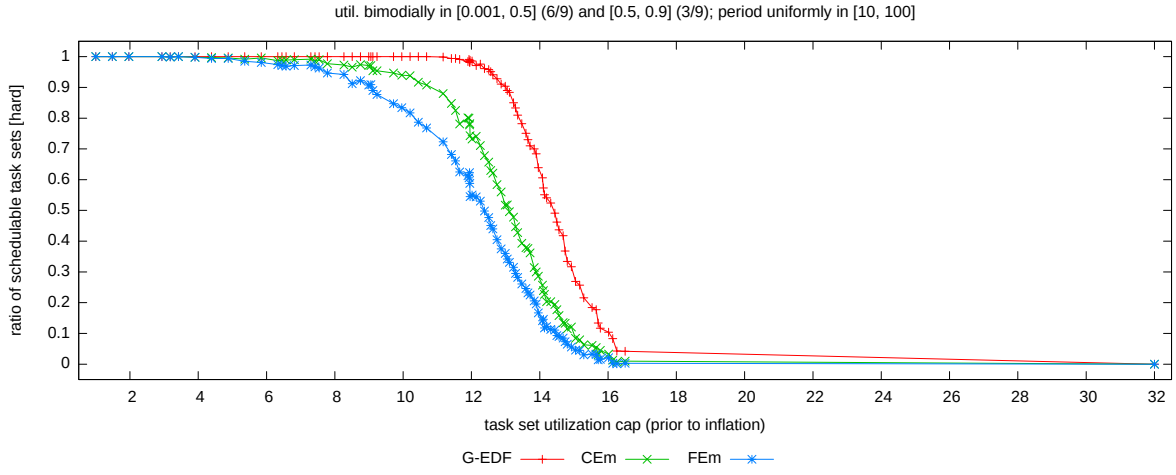

(b)

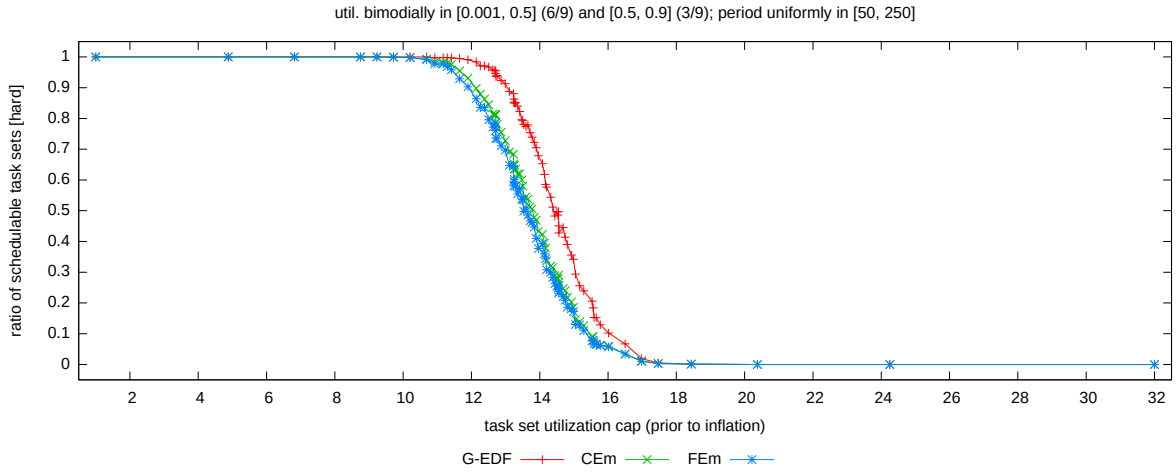

(c)

Figure 69: Comparison of CEm and FEm (coarse- vs. fine-grained queues) in terms of hard schedulability of task sets with bimodal medium per-task utilizations and **(a)** short, **(b)** moderate, and **(c)** long periods. These graphs correspond to Fig. 21.

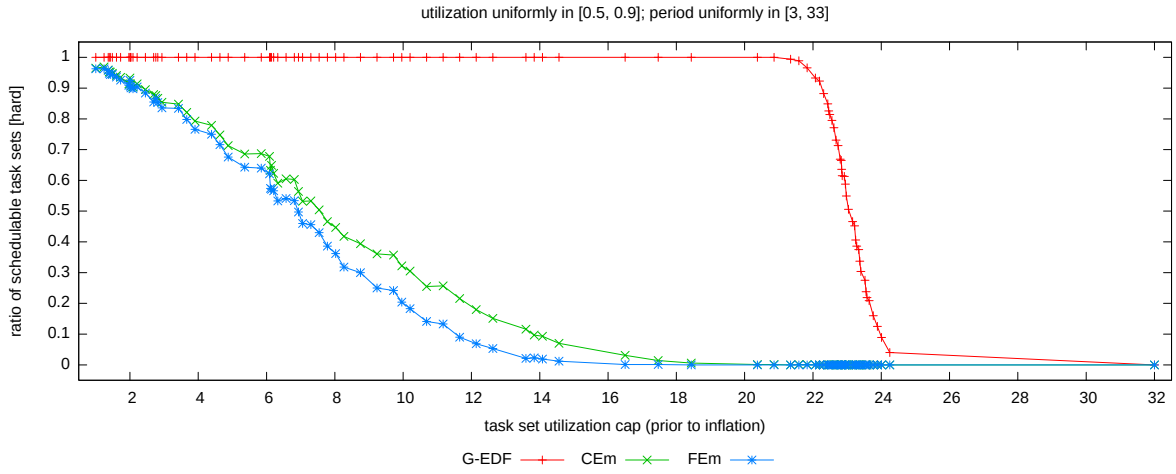

(a)

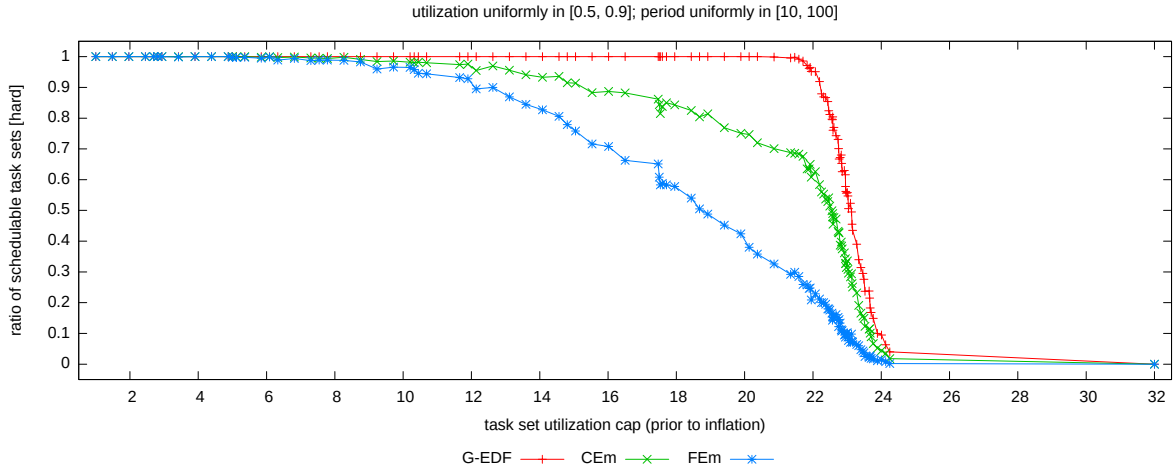

(b)

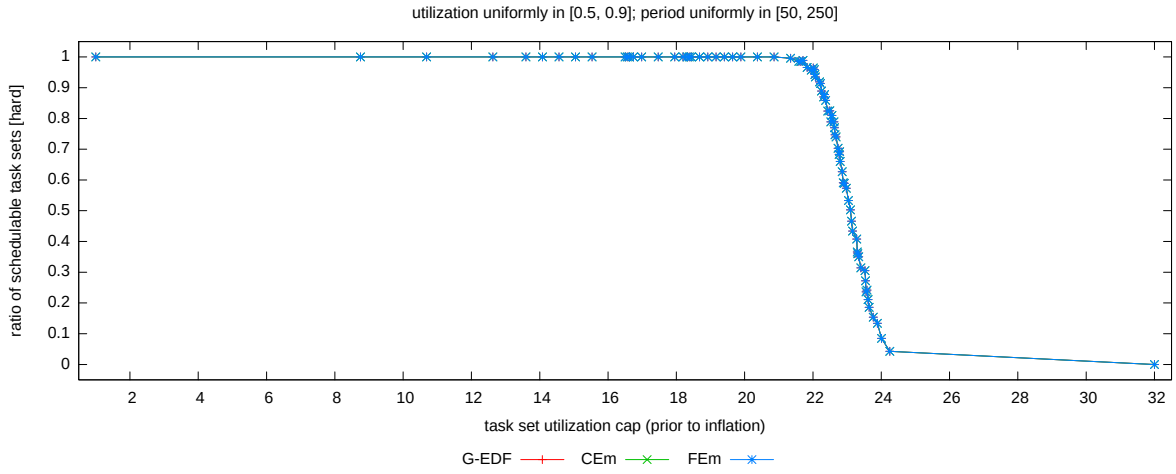

(c)

Figure 70: Comparison of CEm and FEm (coarse- vs. fine-grained queues) in terms of hard schedulability of task sets with uniform heavy per-task utilizations and **(a)** short, **(b)** moderate, and **(c)** long periods. These graphs correspond to Fig. 22.

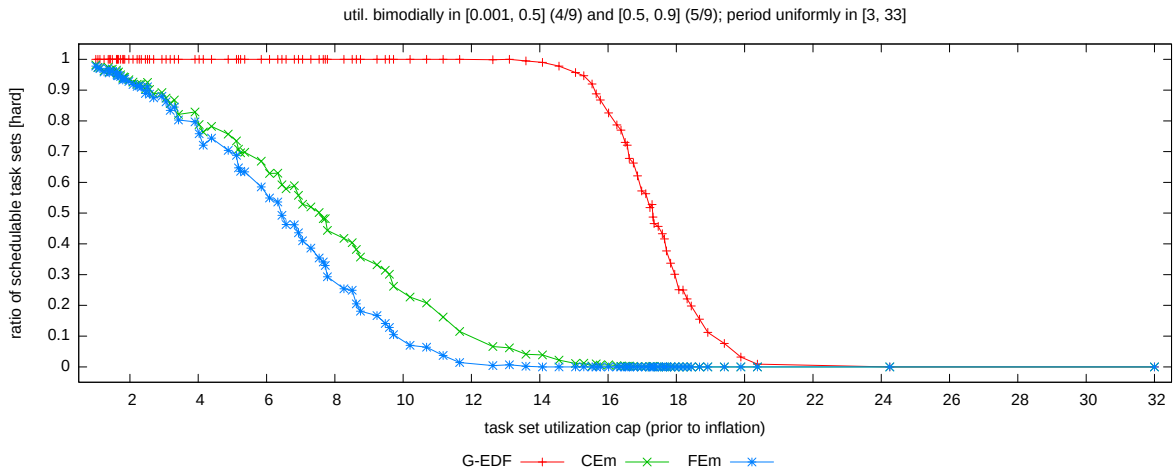

(a)

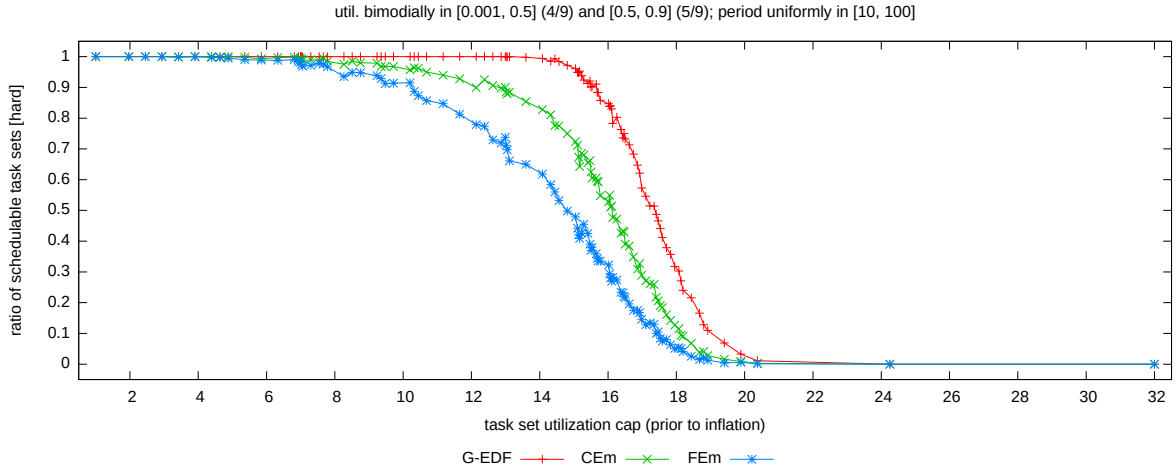

(b)

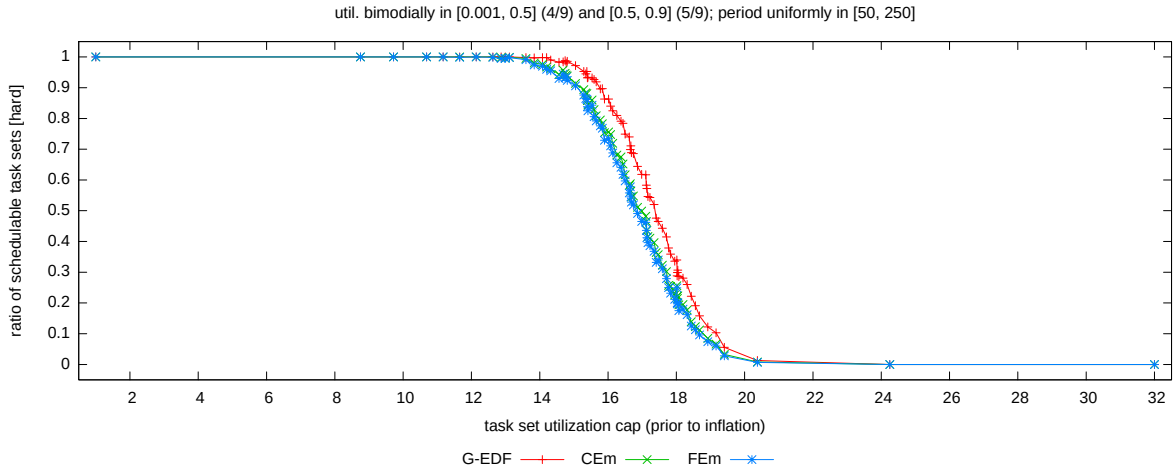

(c)

Figure 71: Comparison of CEm and FEm (coarse- vs. fine-grained queues) in terms of hard schedulability of task sets with bimodal heavy per-task utilizations and **(a)** short, **(b)** moderate, and **(c)** long periods. These graphs correspond to Fig. 23.

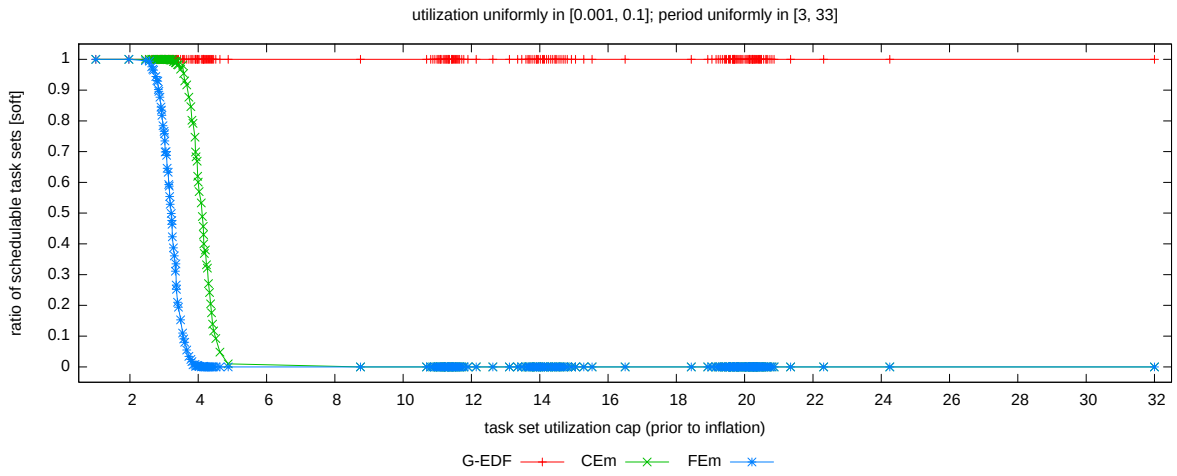

(a)

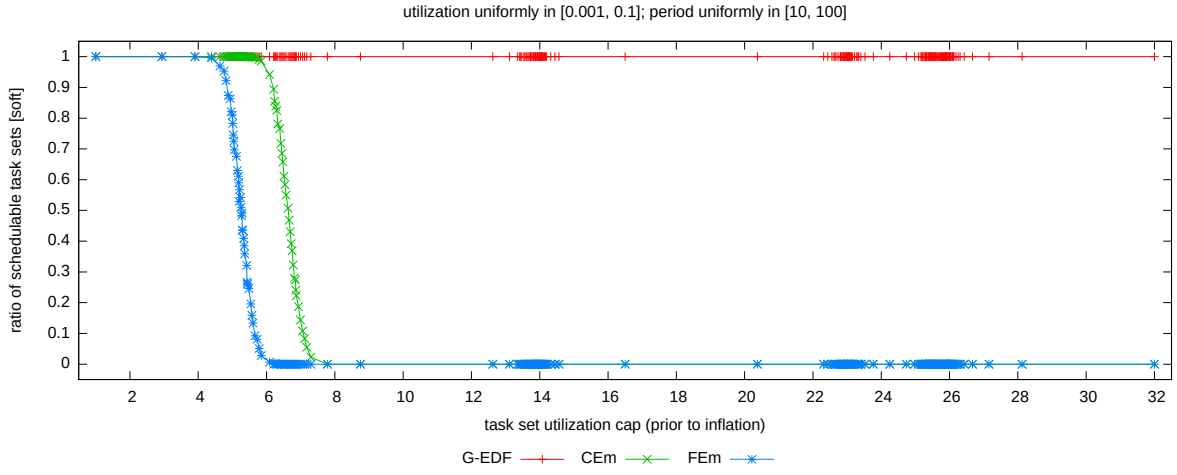

(b)

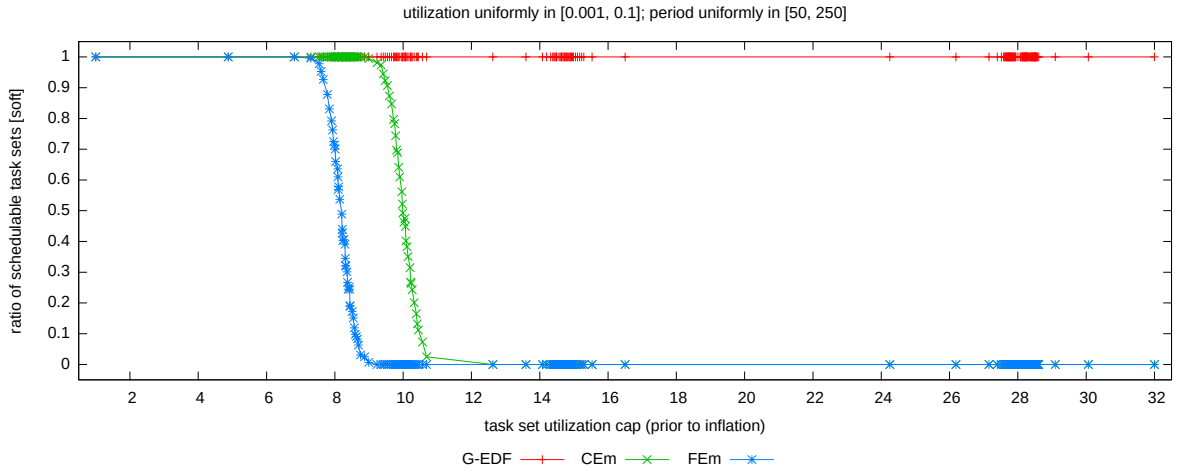

(c)

Figure 72: Comparison of CEm and FEm (coarse- vs. fine-grained queues) in terms of soft schedulability of task sets with uniform light per-task utilizations and **(a)** short, **(b)** moderate, and **(c)** long periods. These graphs correspond to Fig. 24.

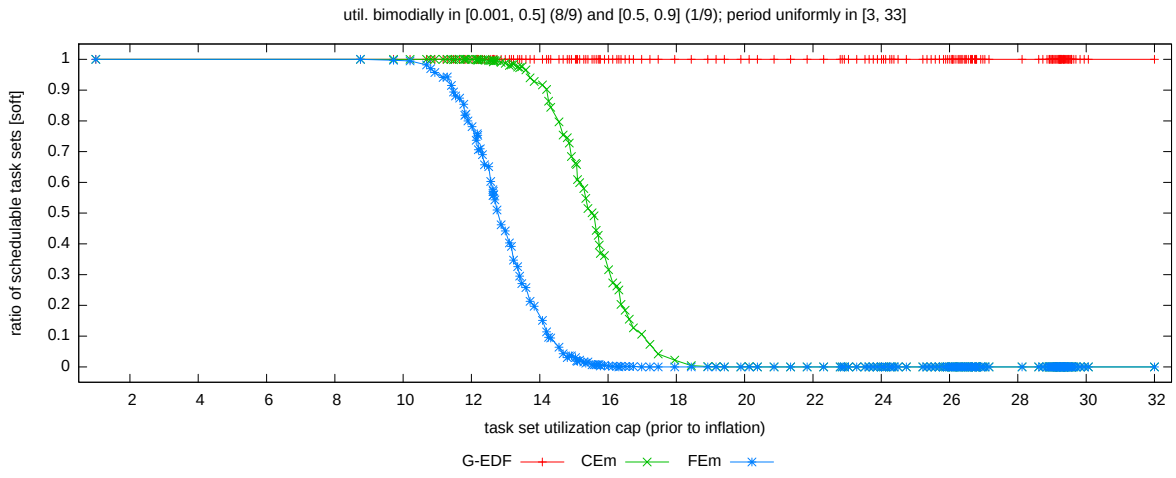

(a)

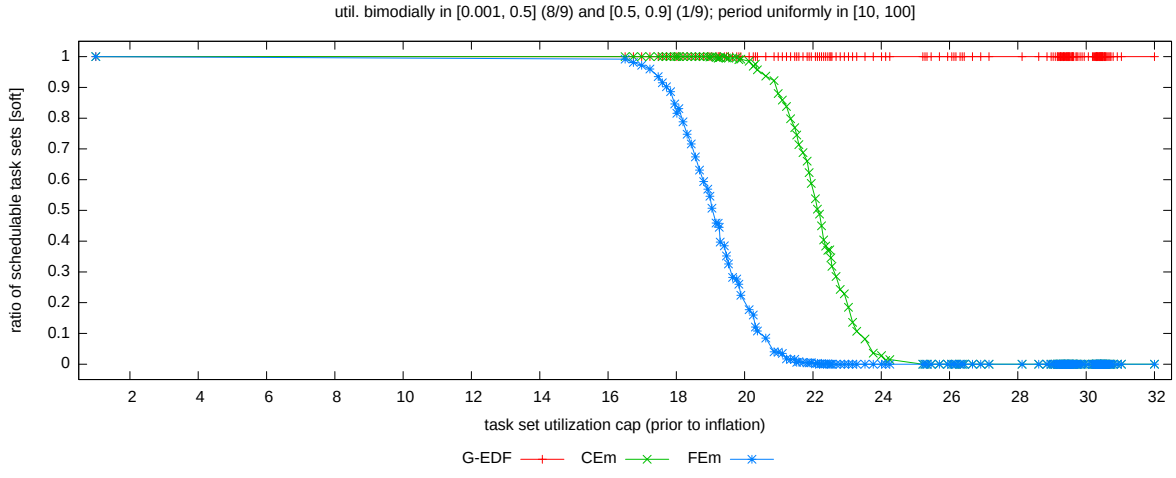

(b)

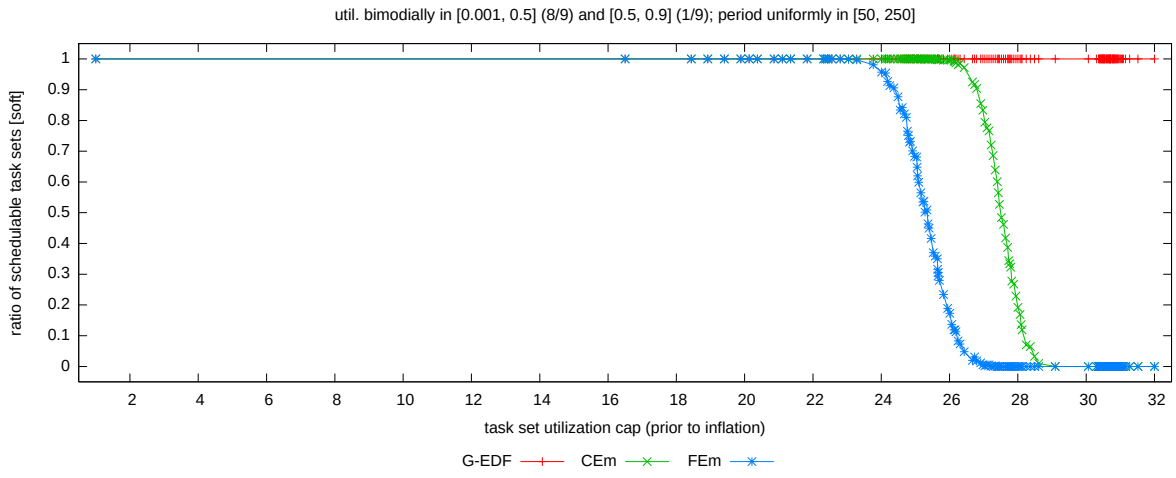

(c)

Figure 73: Comparison of CEm and FEm (coarse- vs. fine-grained queues) in terms of soft schedulability of task sets with bimodal light per-task utilizations and **(a)** short, **(b)** moderate, and **(c)** long periods. These graphs correspond to Fig. 25.

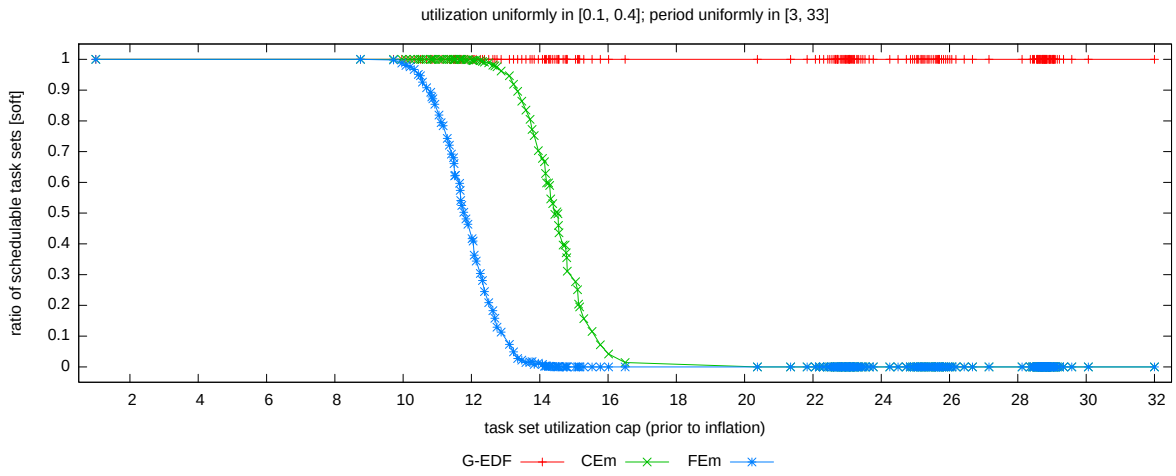

(a)

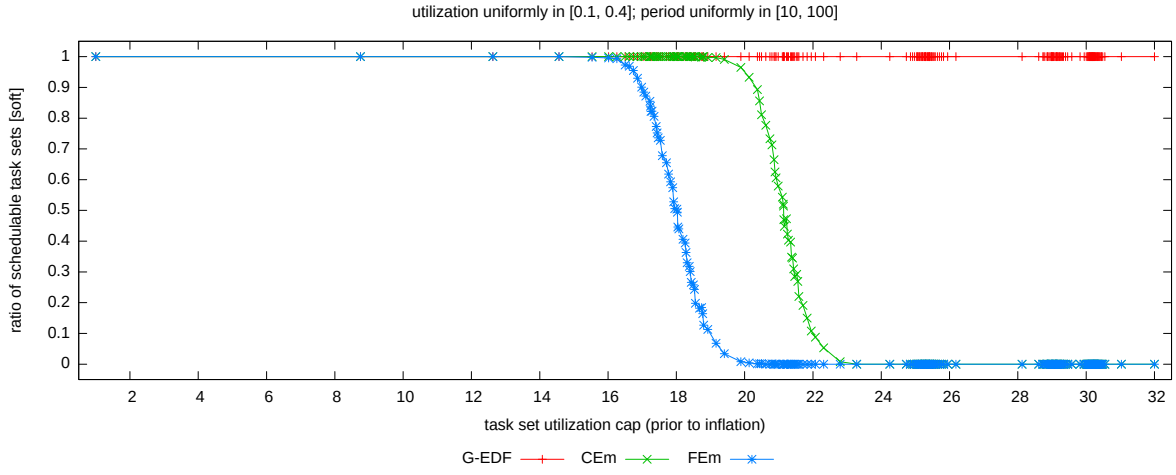

(b)

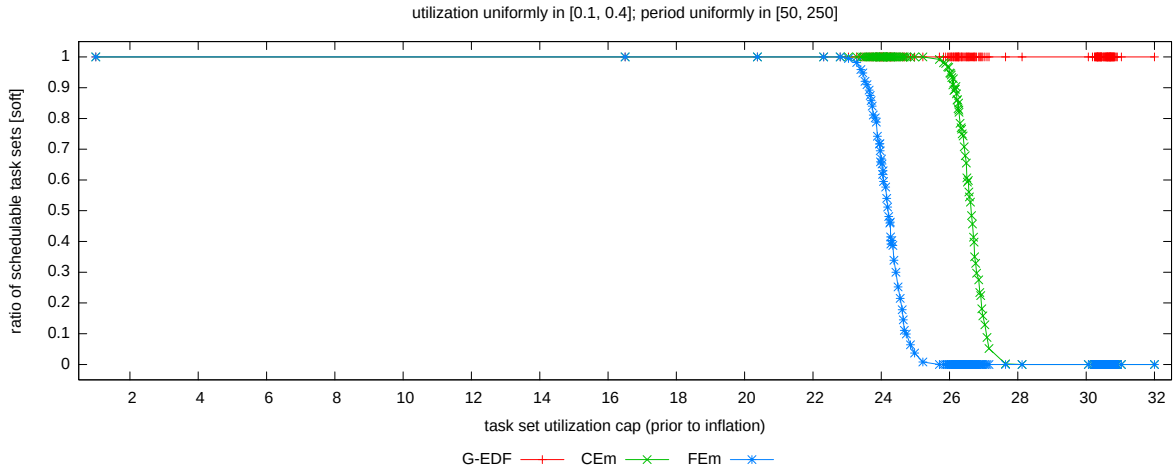

(c)

Figure 74: Comparison of CEm and FEm (coarse- vs. fine-grained queues) in terms of soft schedulability of task sets with uniform medium per-task utilizations and **(a)** short, **(b)** moderate, and **(c)** long periods. These graphs correspond to Fig. 26.

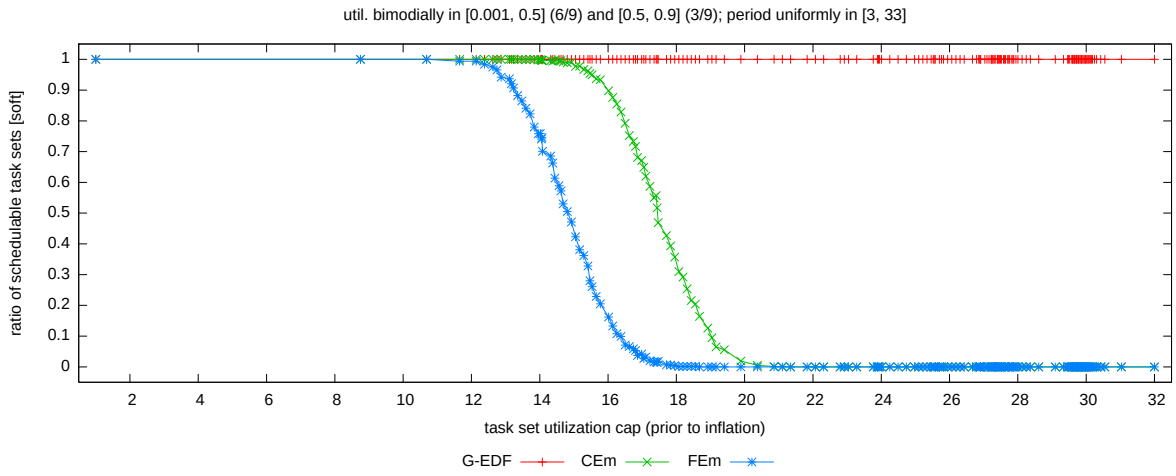

(a)

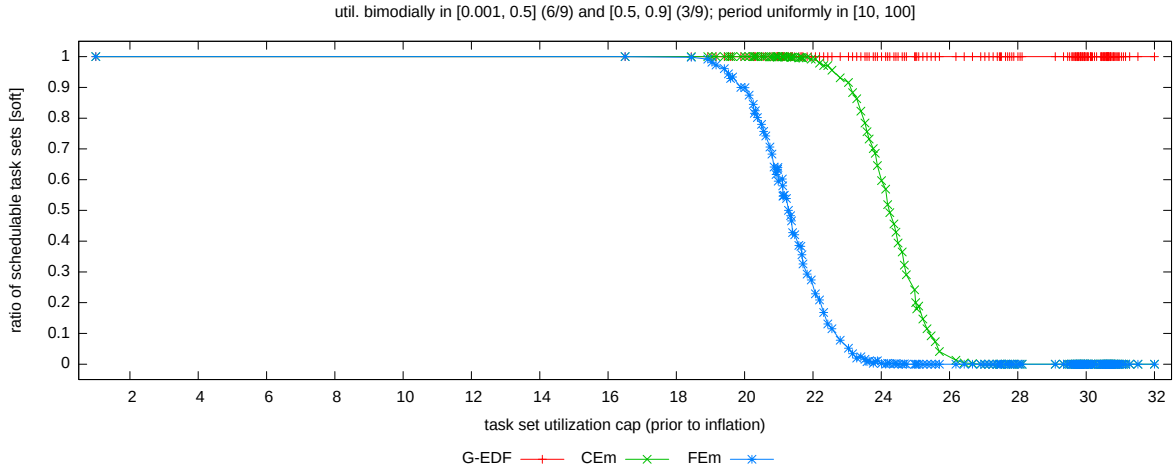

(b)

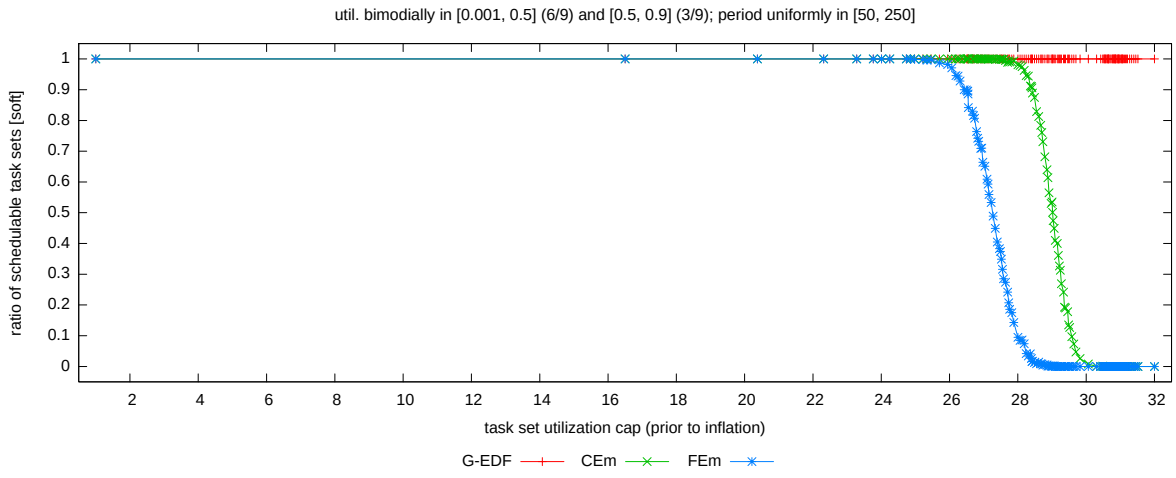

(c)

Figure 75: Comparison of CEm and FEm (coarse- vs. fine-grained queues) in terms of soft schedulability of task sets with bimodal medium per-task utilizations and **(a)** short, **(b)** moderate, and **(c)** long periods. These graphs correspond to Fig. 27.

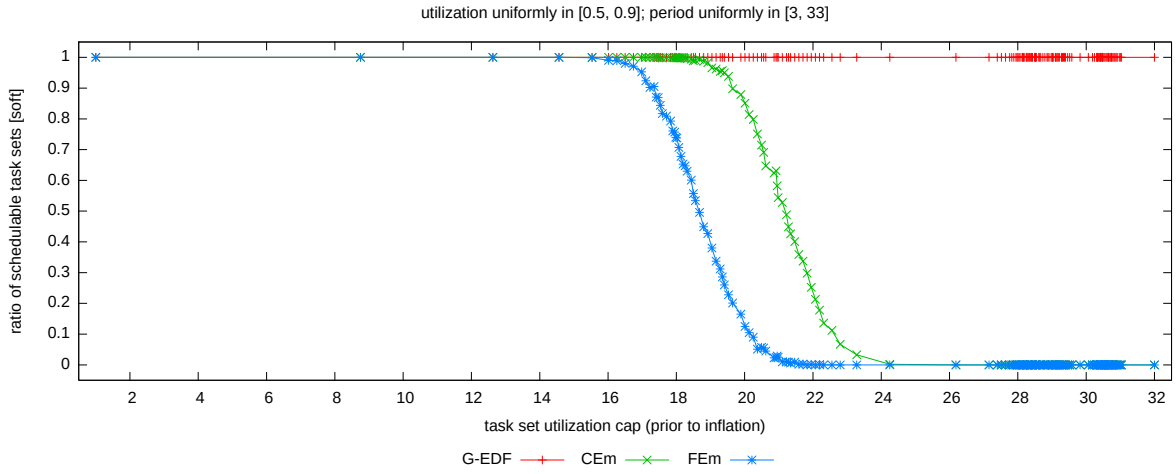

(a)

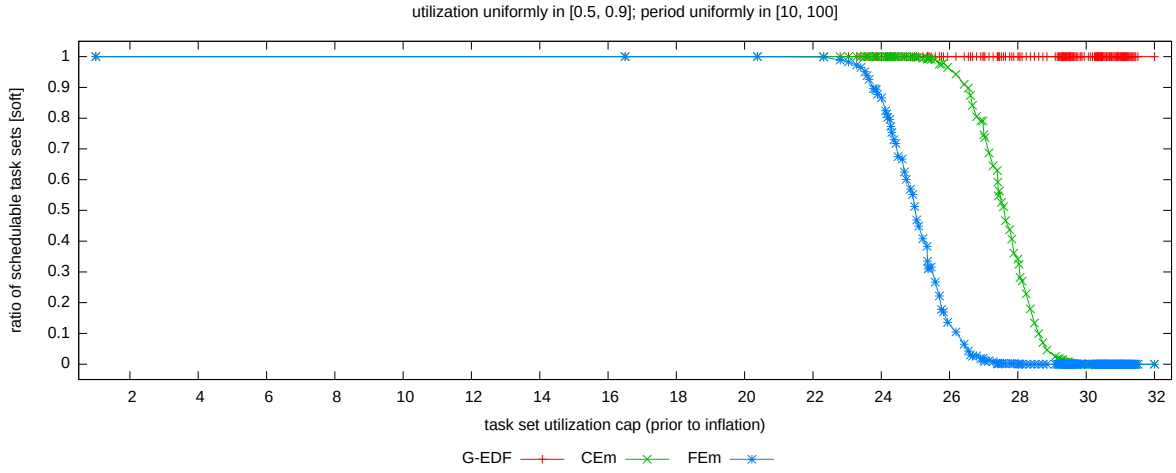

(b)

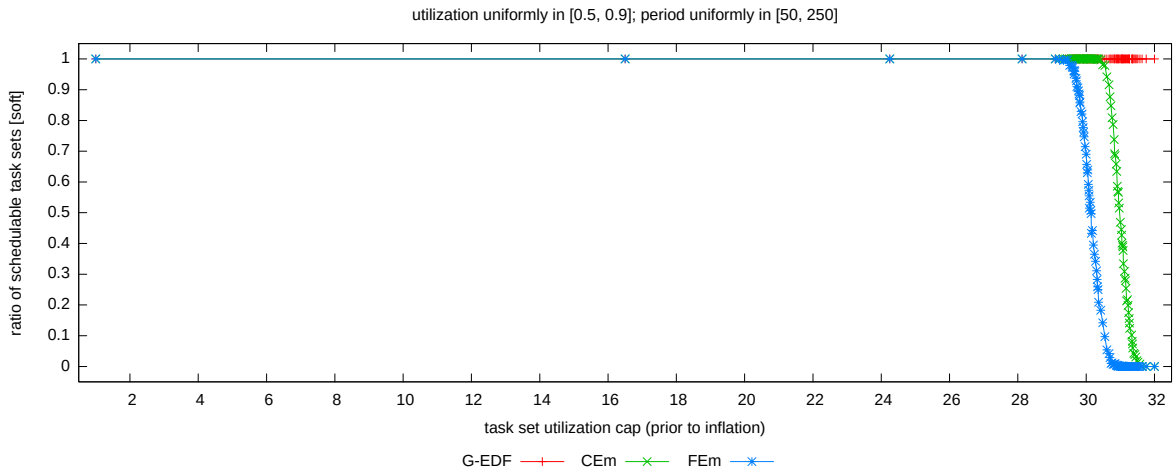

(c)

Figure 76: Comparison of CEm and FEm (coarse- vs. fine-grained queues) in terms of soft schedulability of task sets with uniform heavy per-task utilizations and **(a)** short, **(b)** moderate, and **(c)** long periods. These graphs correspond to Fig. 28.

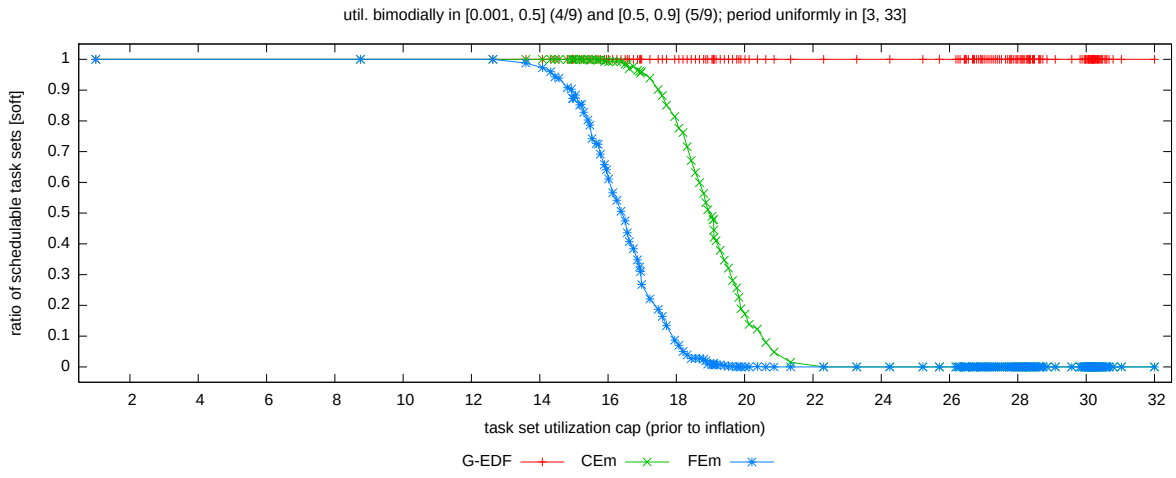

(a)

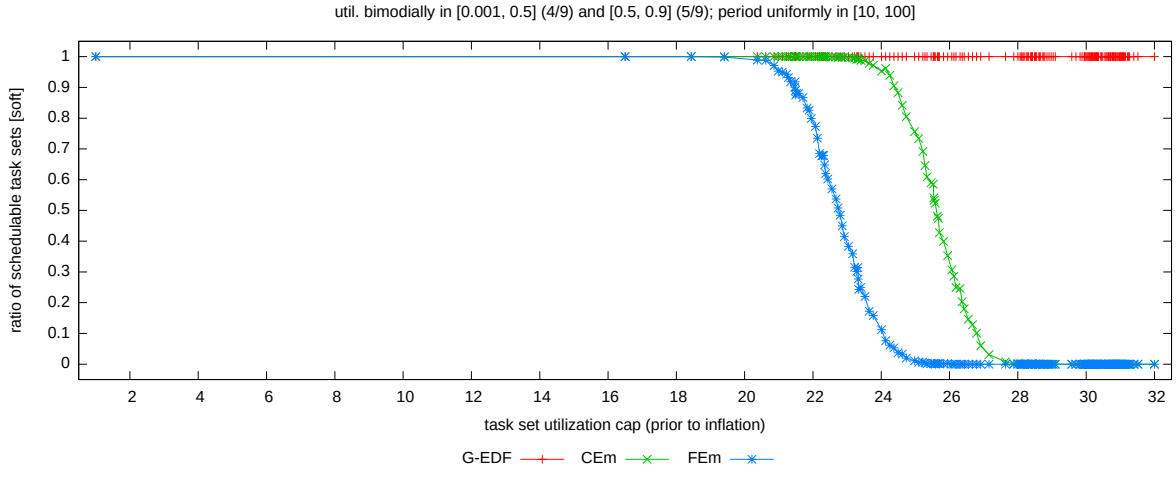

(b)

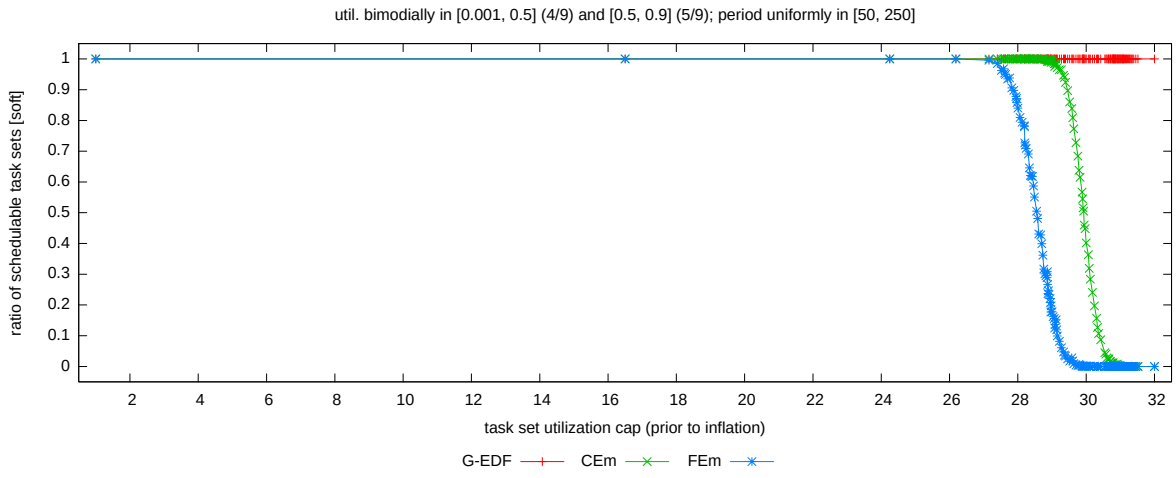

(c)

Figure 77: Comparison of CEm and FEm (coarse- vs. fine-grained queues) in terms of soft schedulability of task sets with bimodal heavy per-task utilizations and **(a)** short, **(b)** moderate, and **(c)** long periods. These graphs correspond to Fig. 29.

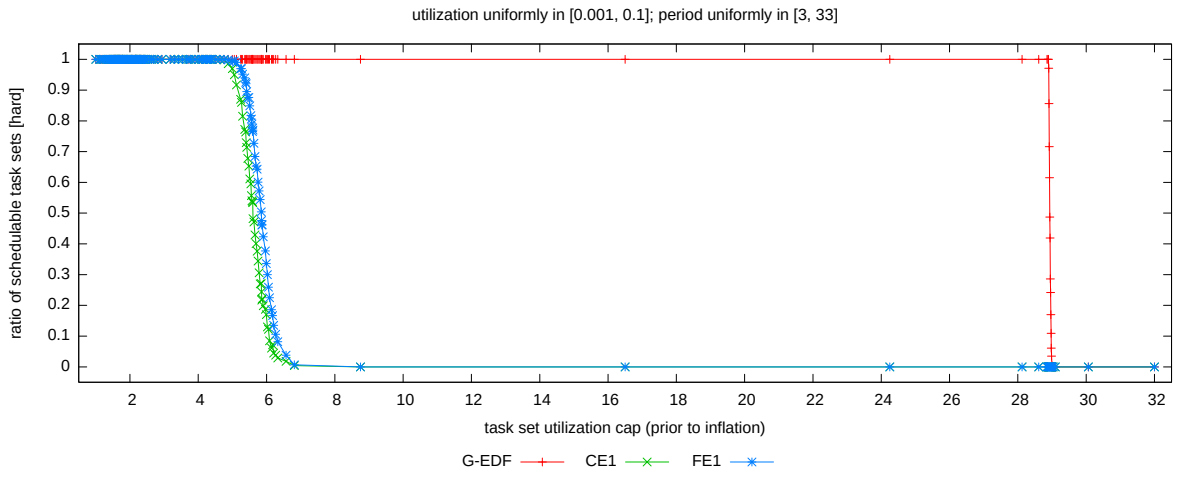

(a)

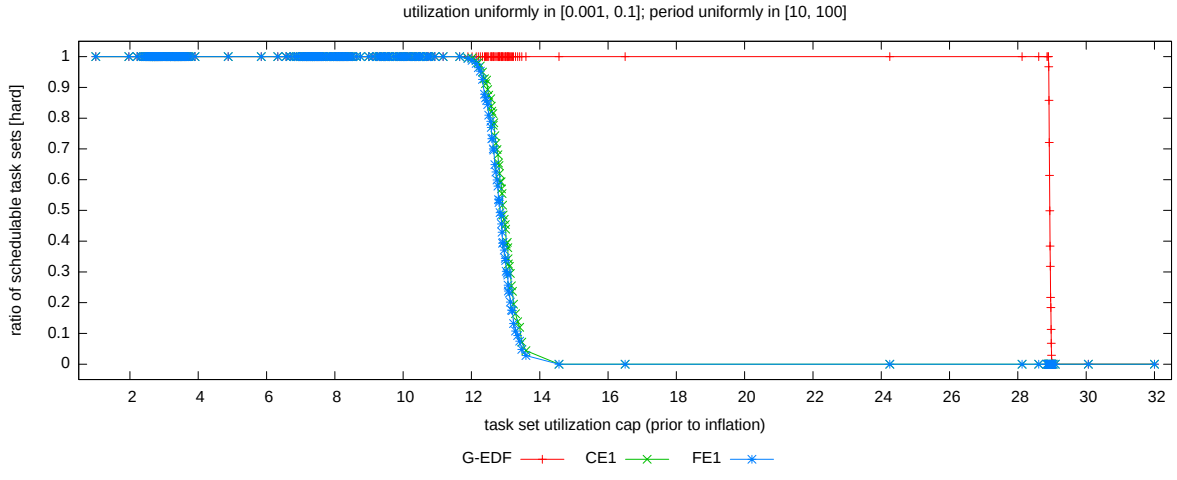

(b)

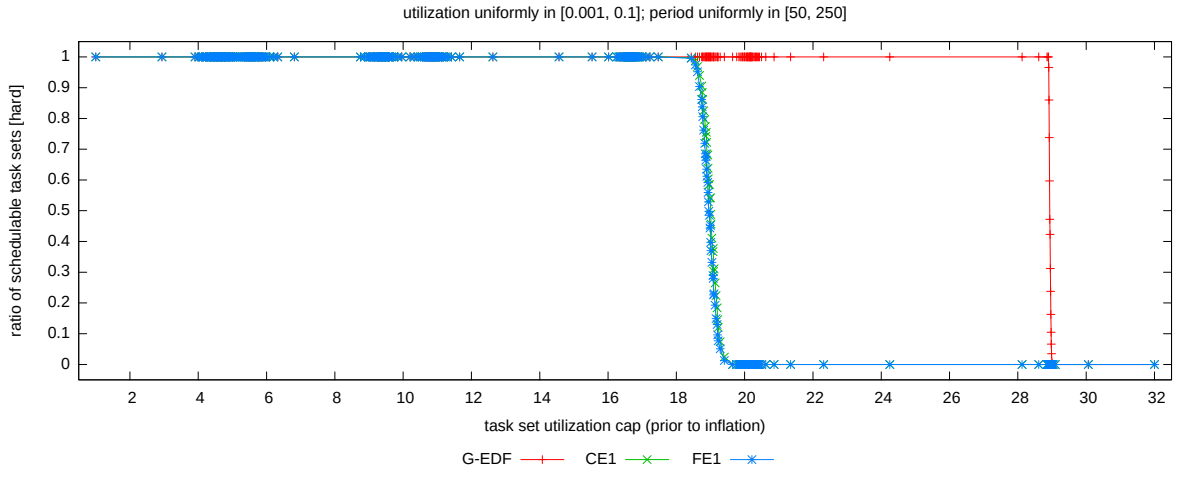

(c)

Figure 78: Comparison of CE1 and FE1 (coarse- vs. fine-grained queues) in terms of hard schedulability of task sets with uniform light per-task utilizations and **(a)** short, **(b)** moderate, and **(c)** long periods. These graphs correspond to Fig. 18.

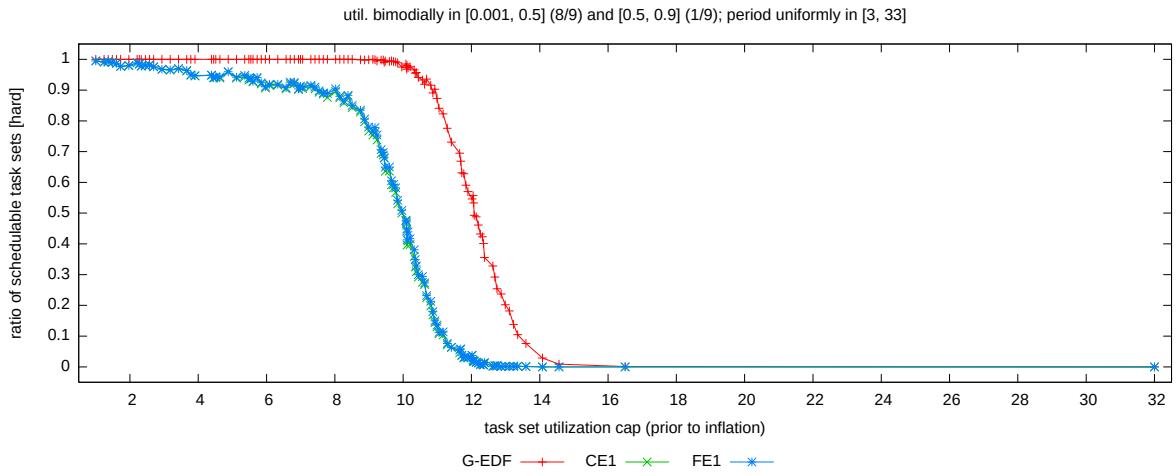

(a)

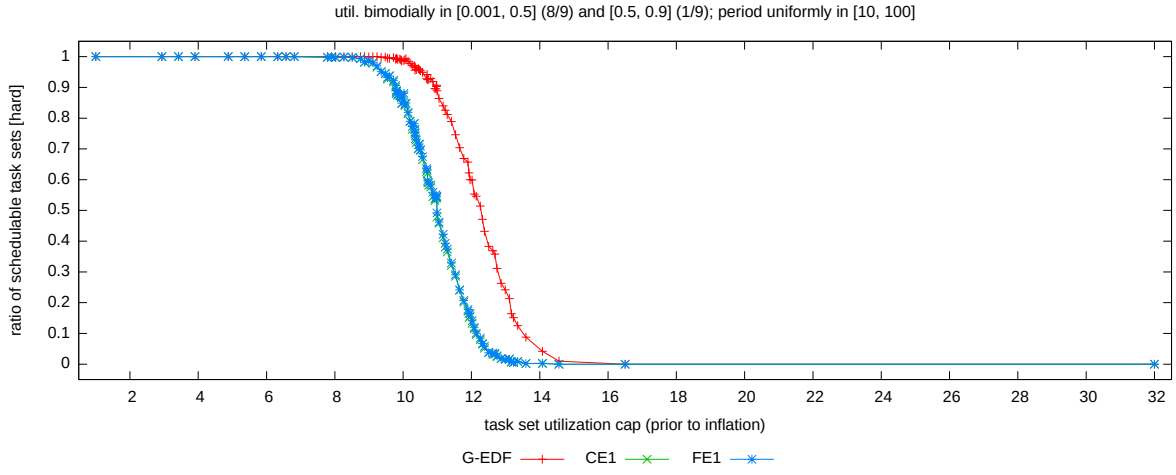

(b)

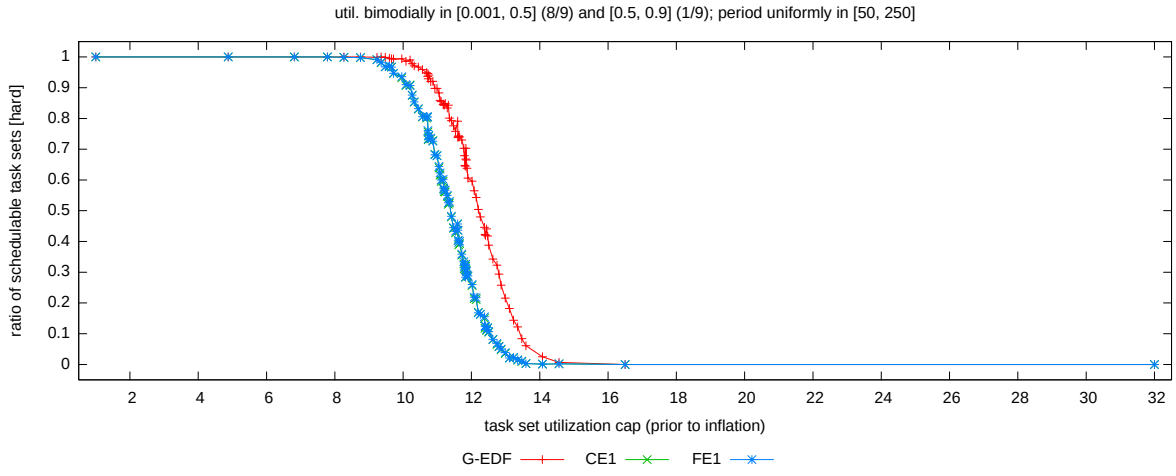

(c)

Figure 79: Comparison of CE1 and FE1 (coarse- vs. fine-grained queues) in terms of hard schedulability of task sets with bimodal light per-task utilizations and **(a)** short, **(b)** moderate, and **(c)** long periods. These graphs correspond to Fig. 19.

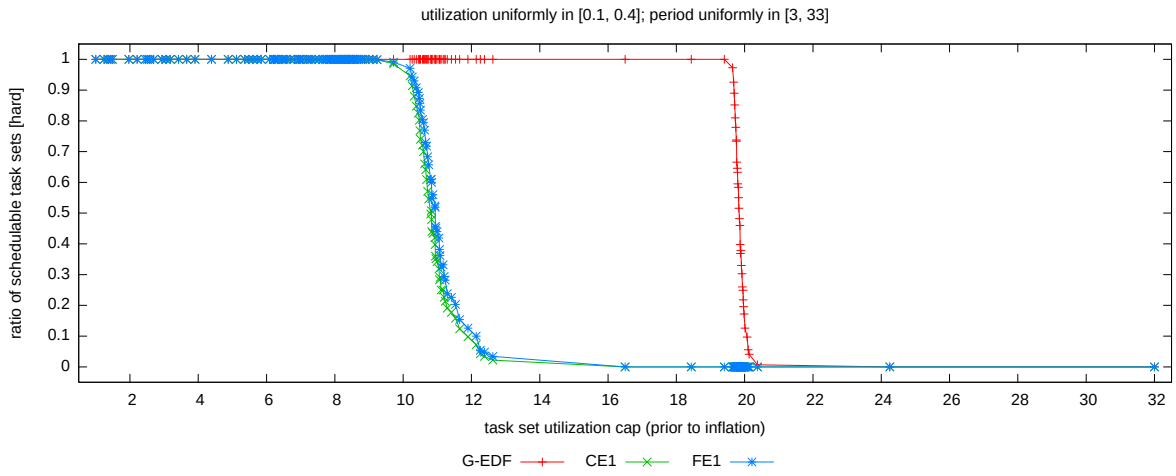

(a)

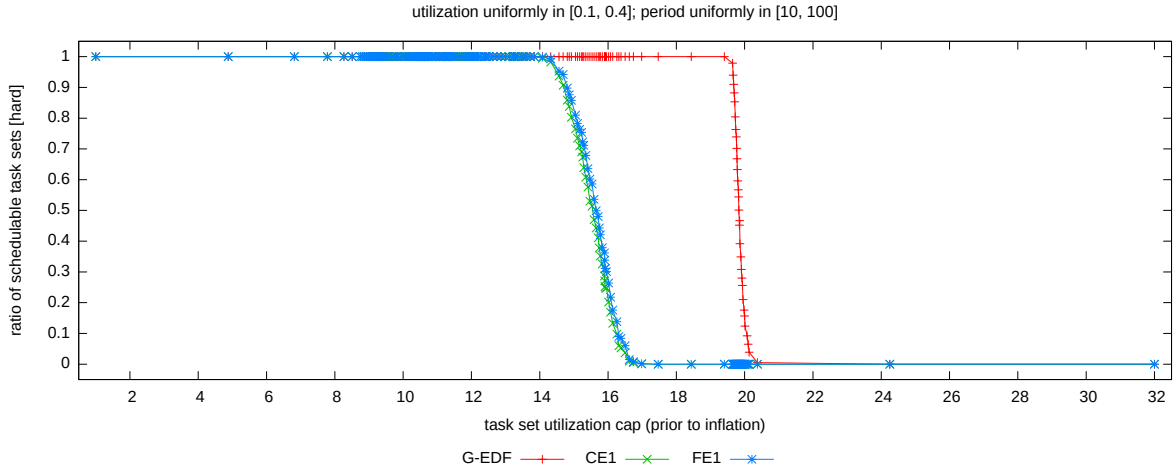

(b)

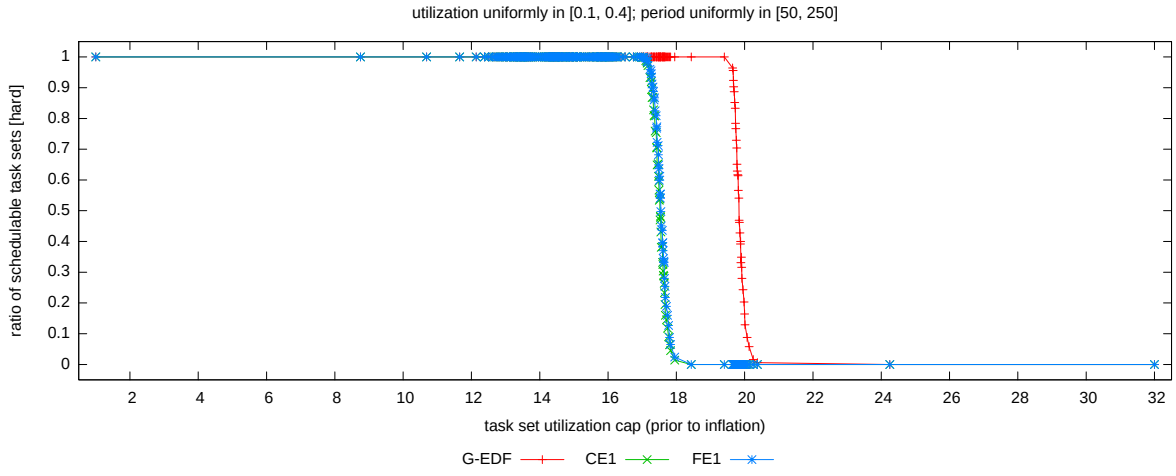

(c)

Figure 80: Comparison of CE1 and FE1 (coarse- vs. fine-grained queues) in terms of hard schedulability of task sets with uniform medium per-task utilizations and **(a)** short, **(b)** moderate, and **(c)** long periods. These graphs correspond to Fig. 20.

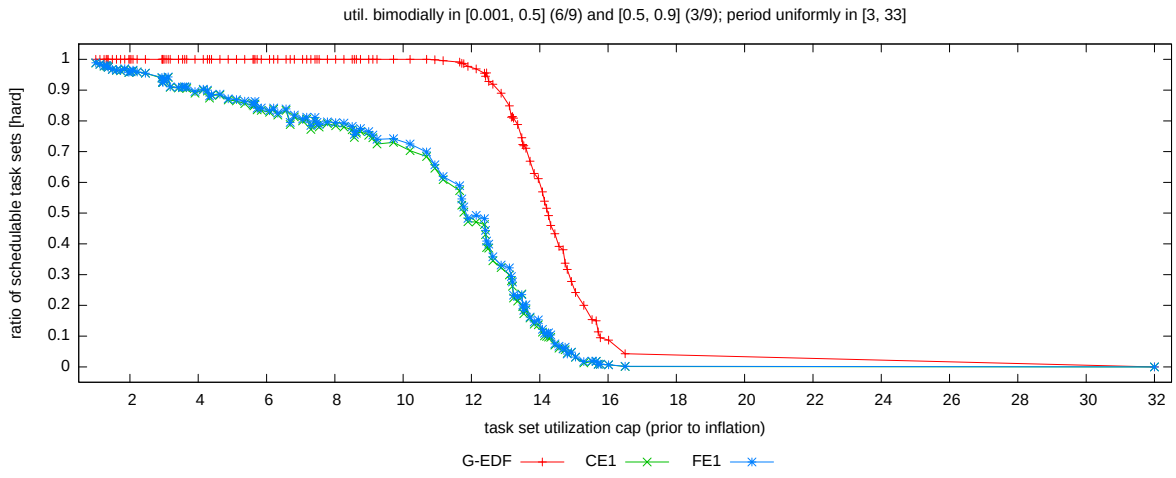

(a)

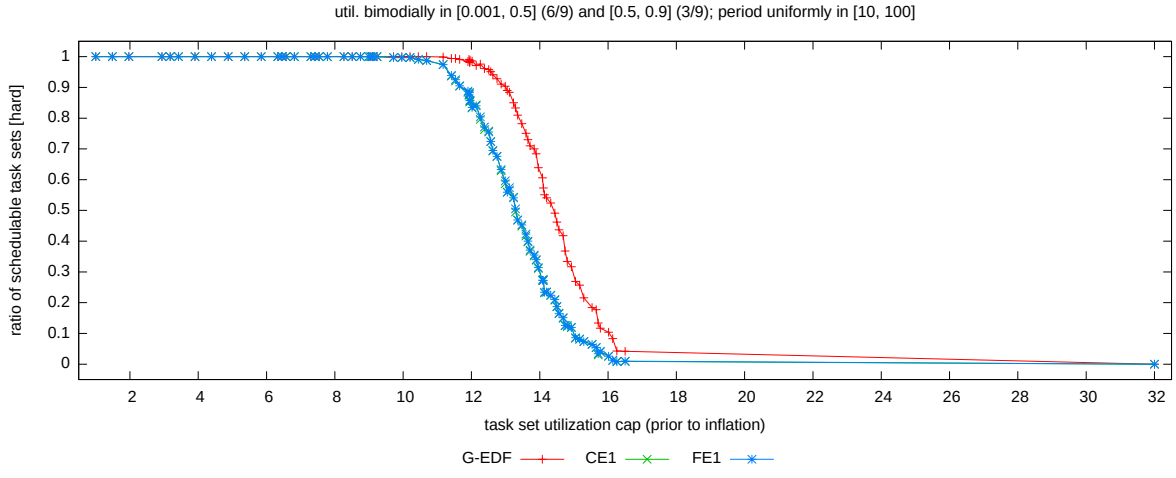

(b)

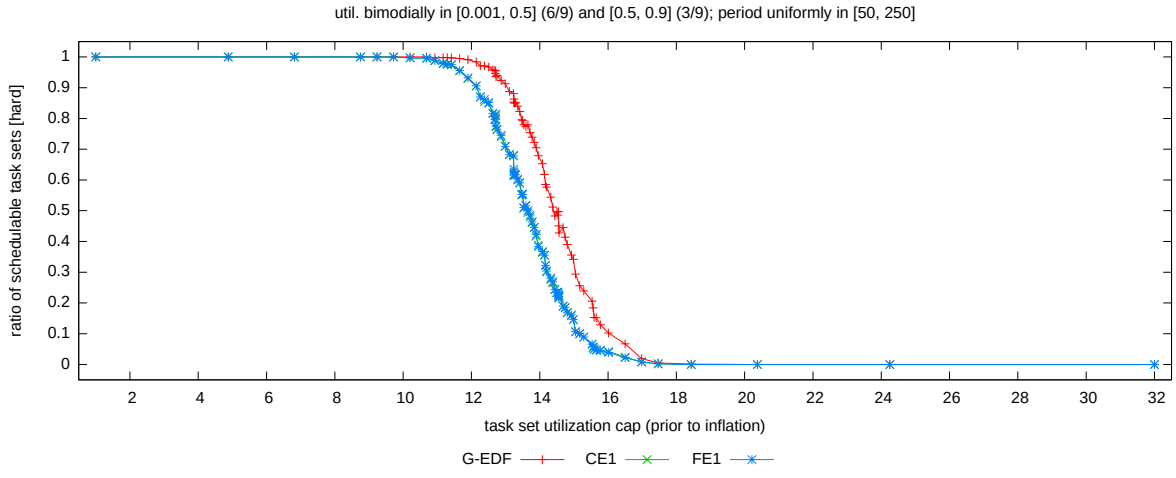

(c)

Figure 81: Comparison of CE1 and FE1 (coarse- vs. fine-grained queues) in terms of hard schedulability of task sets with bimodal medium per-task utilizations and **(a)** short, **(b)** moderate, and **(c)** long periods. These graphs correspond to Fig. 21.

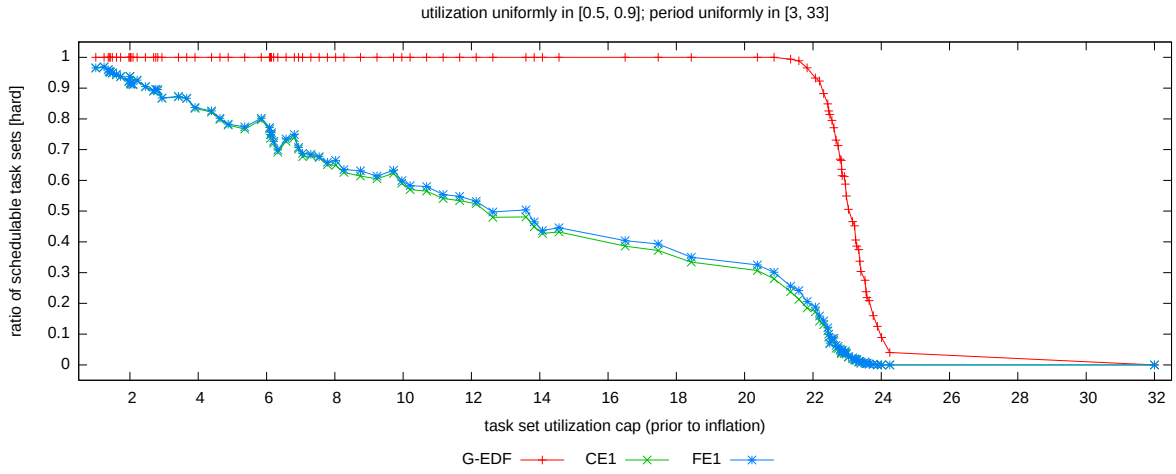

(a)

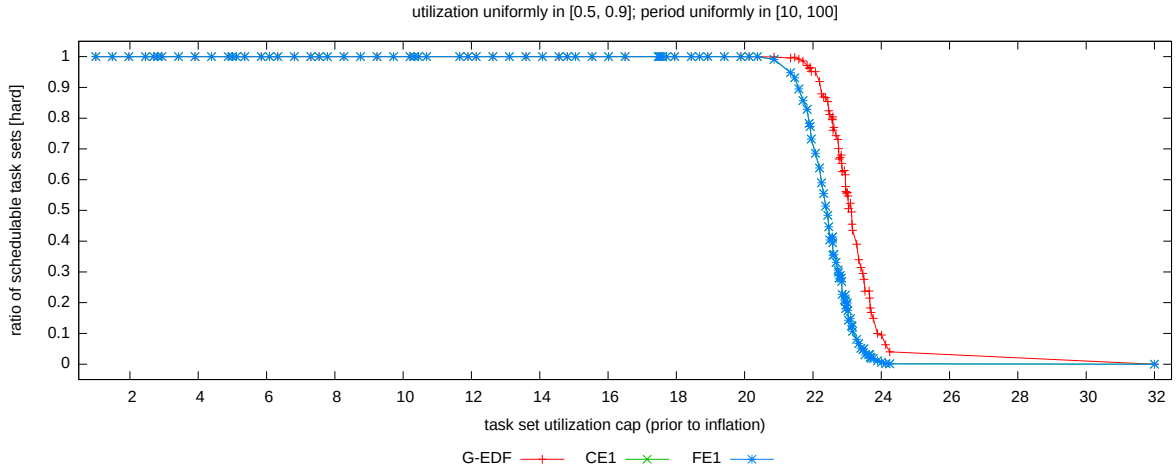

(b)

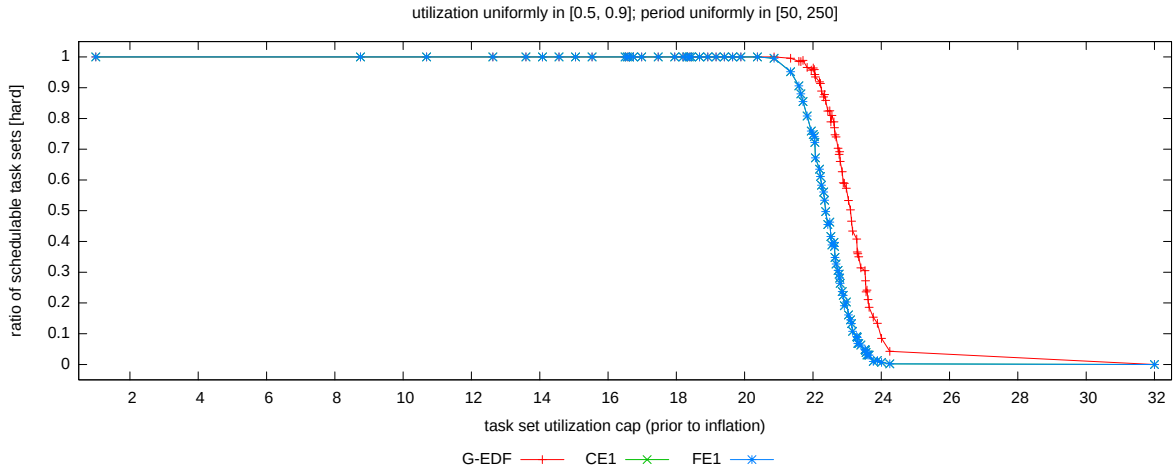

(c)

Figure 82: Comparison of CE1 and FE1 (coarse- vs. fine-grained queues) in terms of hard schedulability of task sets with uniform heavy per-task utilizations and **(a)** short, **(b)** moderate, and **(c)** long periods. These graphs correspond to Fig. 22.

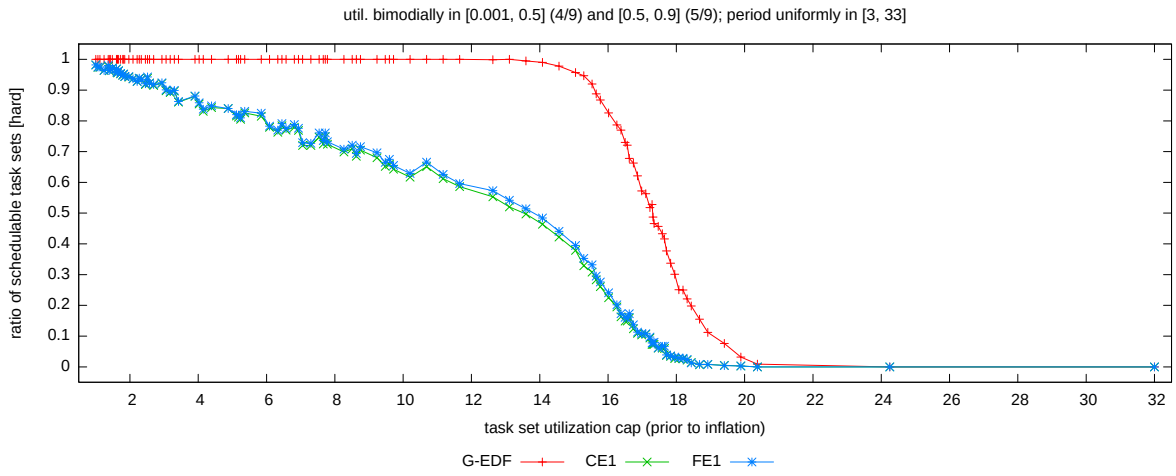

(a)

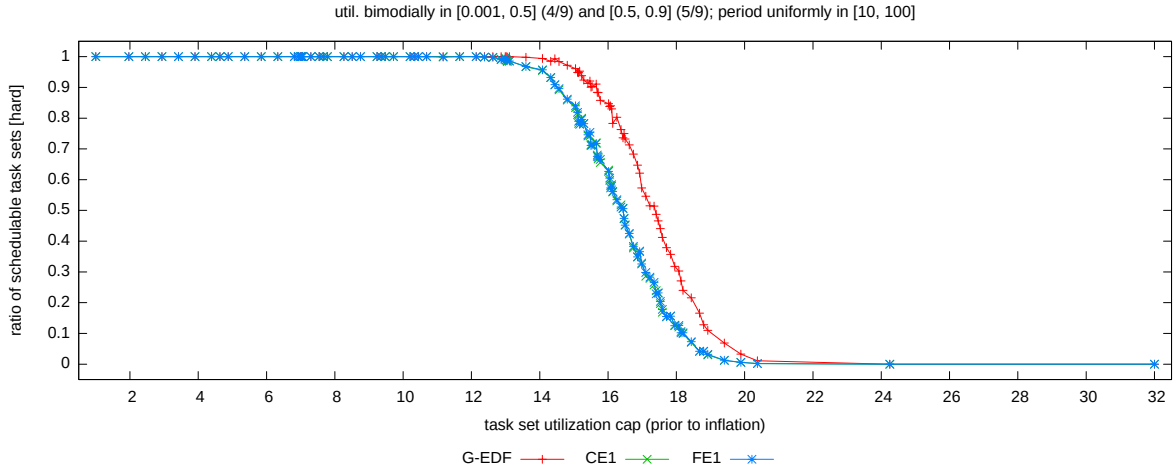

(b)

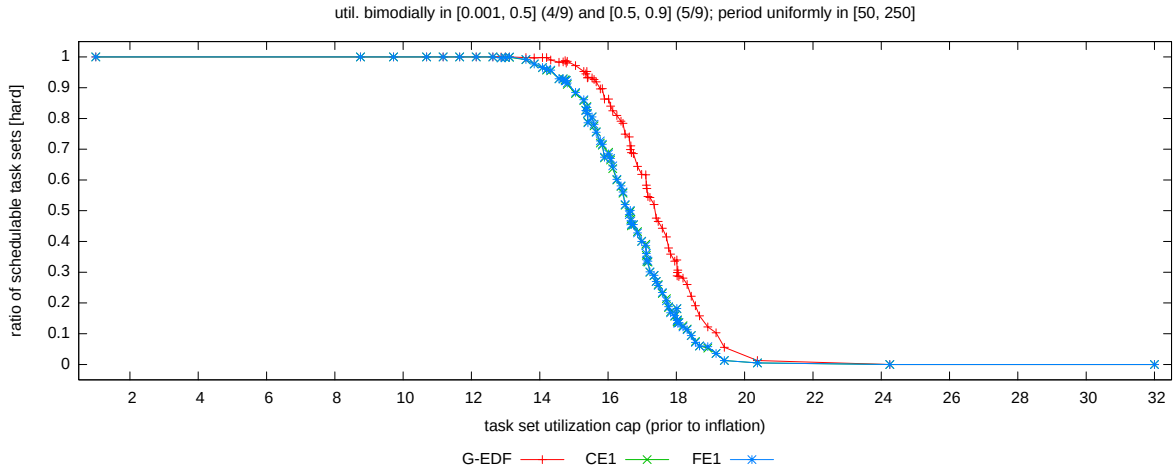

(c)

Figure 83: Comparison of CE1 and FE1 (coarse- vs. fine-grained queues) in terms of hard schedulability of task sets with bimodal heavy per-task utilizations and **(a)** short, **(b)** moderate, and **(c)** long periods. These graphs correspond to Fig. 23.

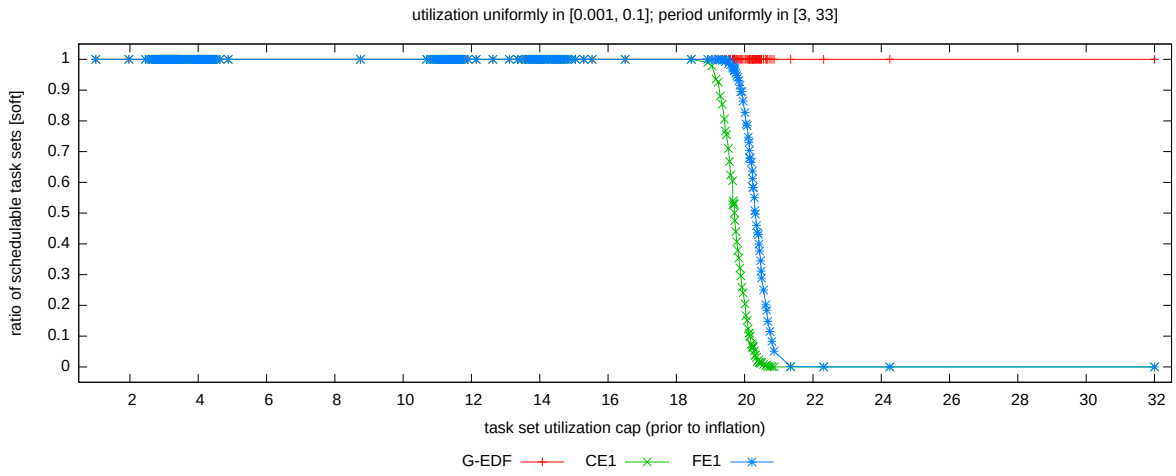

(a)

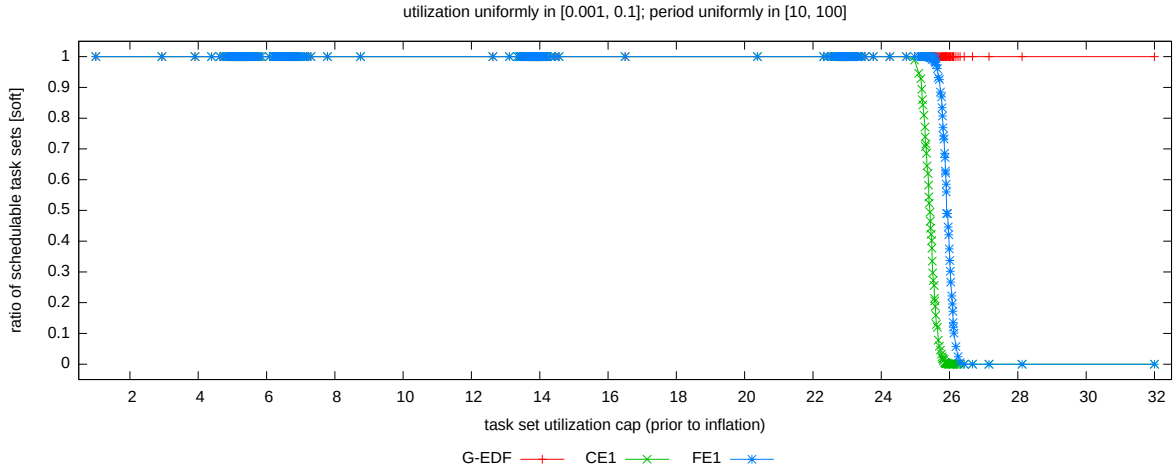

(b)

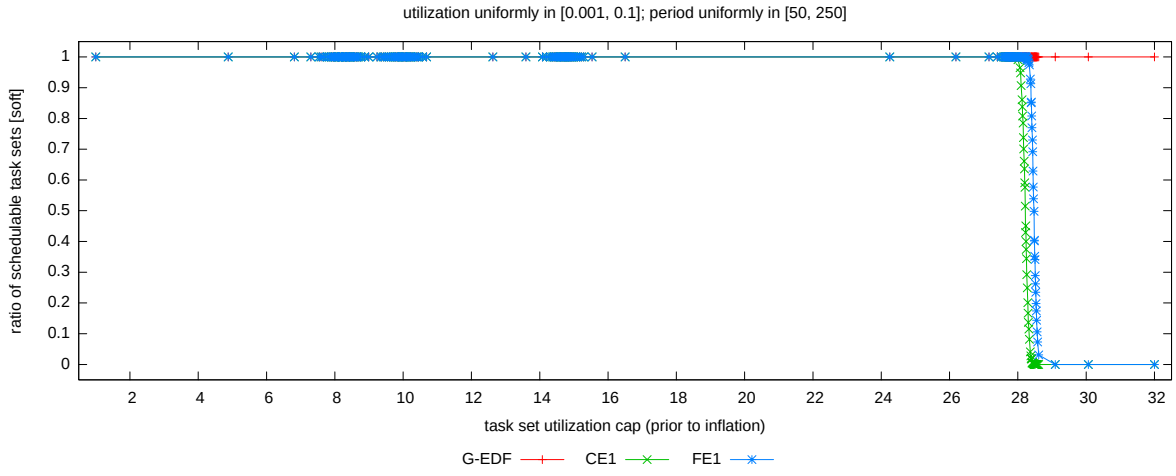

(c)

Figure 84: Comparison of CE1 and FE1 (coarse- vs. fine-grained queues) in terms of soft schedulability of task sets with uniform light per-task utilizations and **(a)** short, **(b)** moderate, and **(c)** long periods. These graphs correspond to Fig. 24.

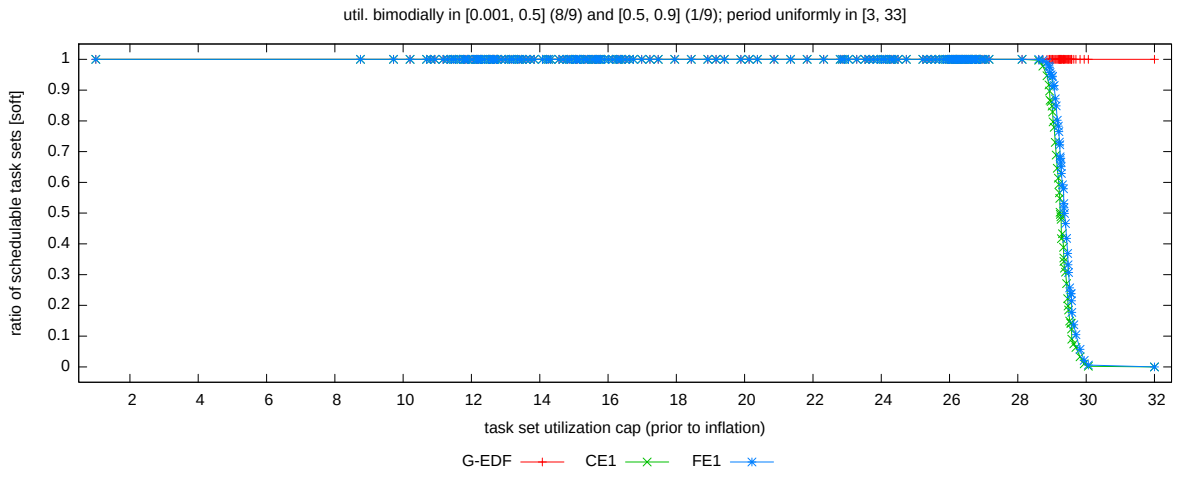

(a)

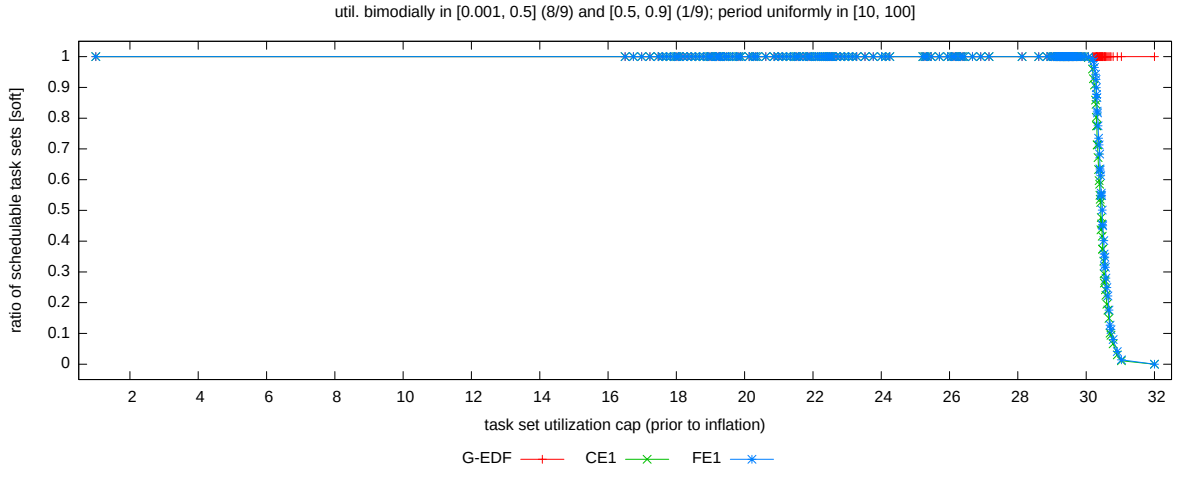

(b)

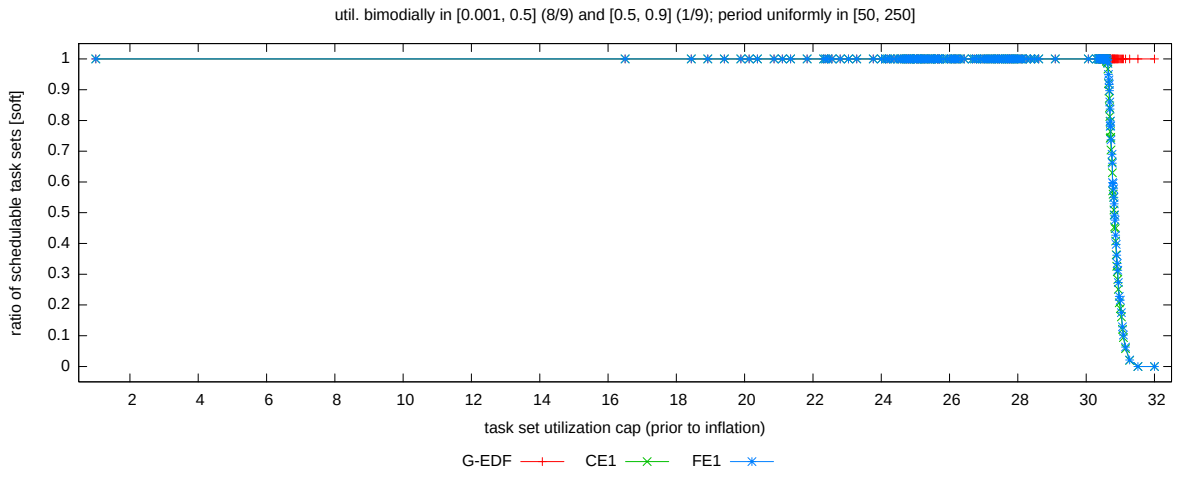

(c)

Figure 85: Comparison of CE1 and FE1 (coarse- vs. fine-grained queues) in terms of soft schedulability of task sets with bimodal light per-task utilizations and **(a)** short, **(b)** moderate, and **(c)** long periods. These graphs correspond to Fig. 25.

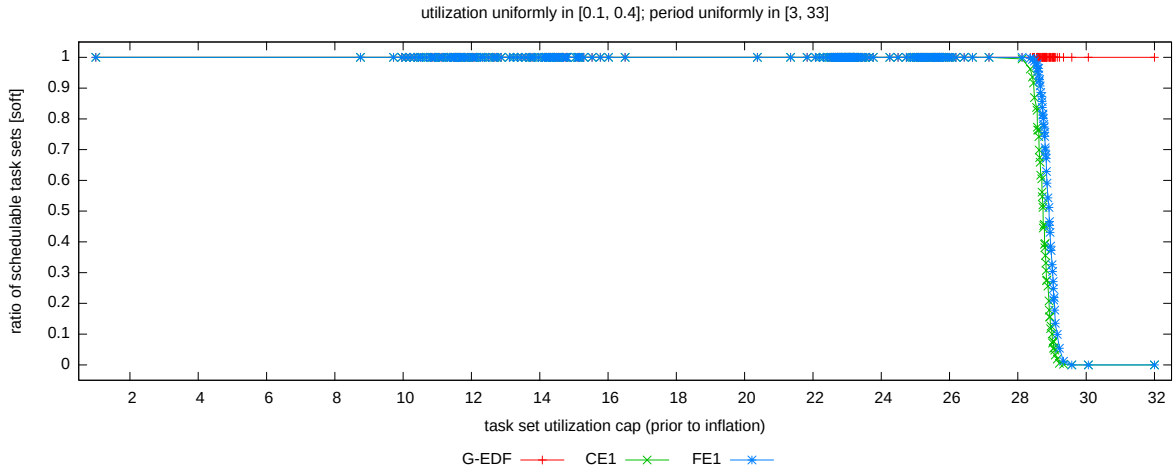

(a)

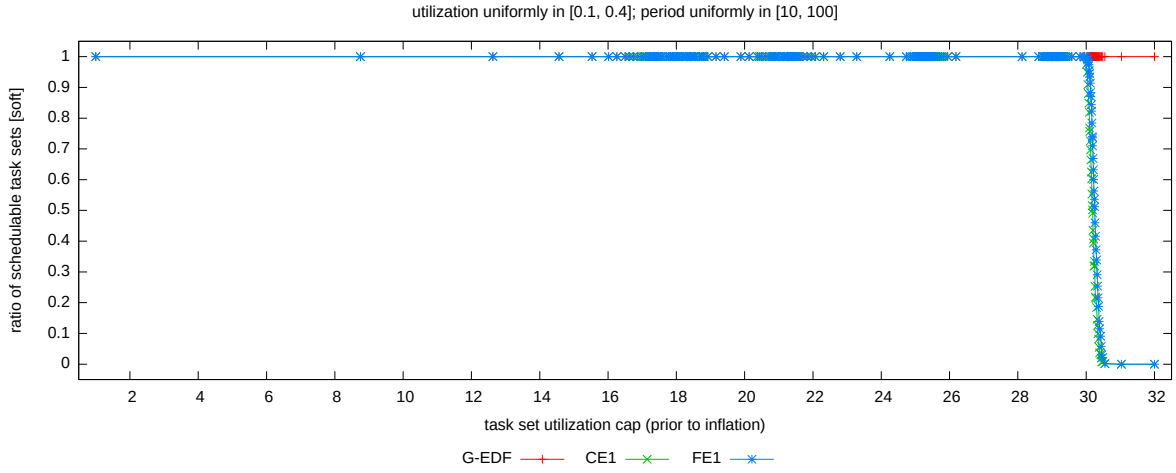

(b)

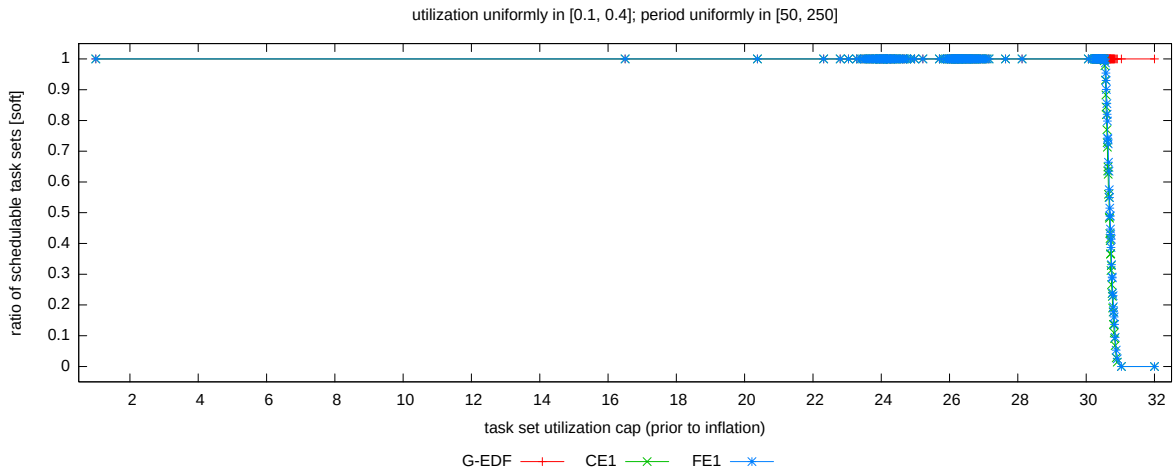

(c)

Figure 86: Comparison of CE1 and FE1 (coarse- vs. fine-grained queues) in terms of soft schedulability of task sets with uniform medium per-task utilizations and **(a)** short, **(b)** moderate, and **(c)** long periods. These graphs correspond to Fig. 26.

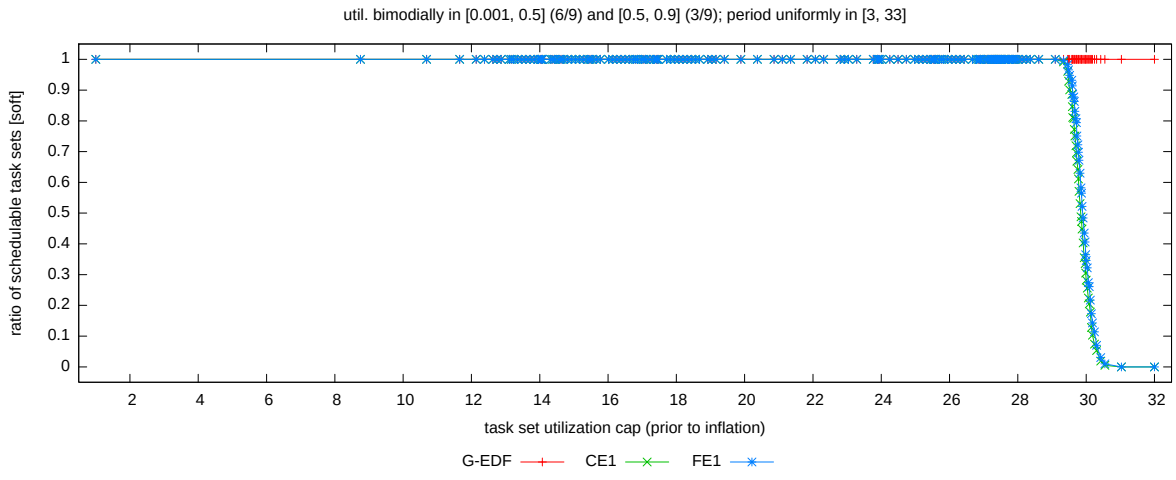

(a)

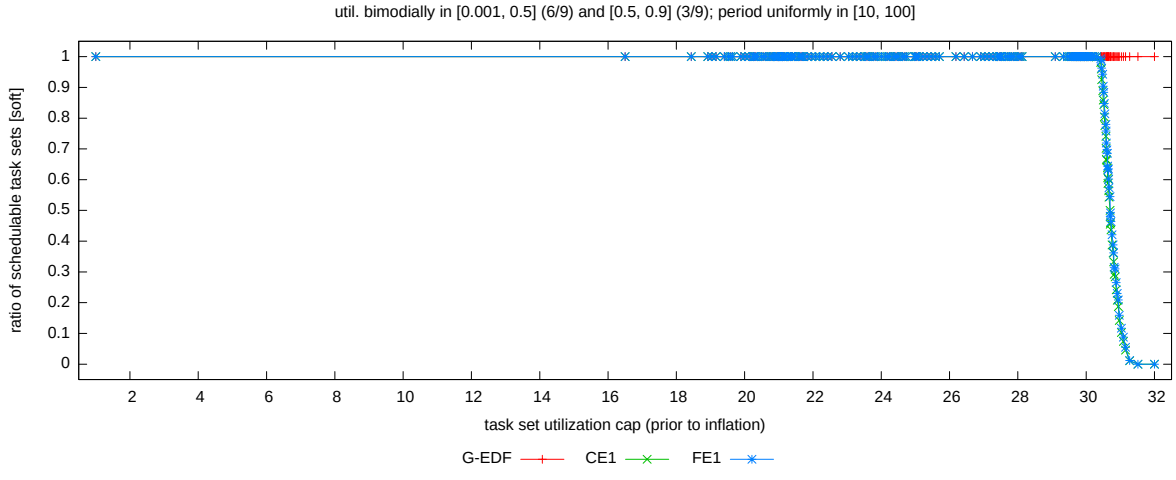

(b)

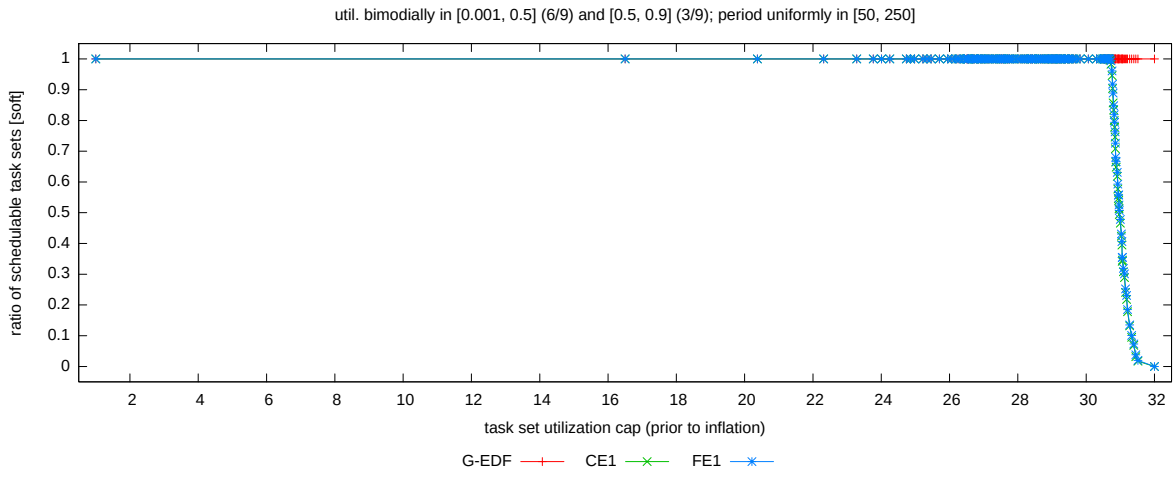

(c)

Figure 87: Comparison of CE1 and FE1 (coarse- vs. fine-grained queues) in terms of soft schedulability of task sets with bimodal medium per-task utilizations and **(a)** short, **(b)** moderate, and **(c)** long periods. These graphs correspond to Fig. 27.

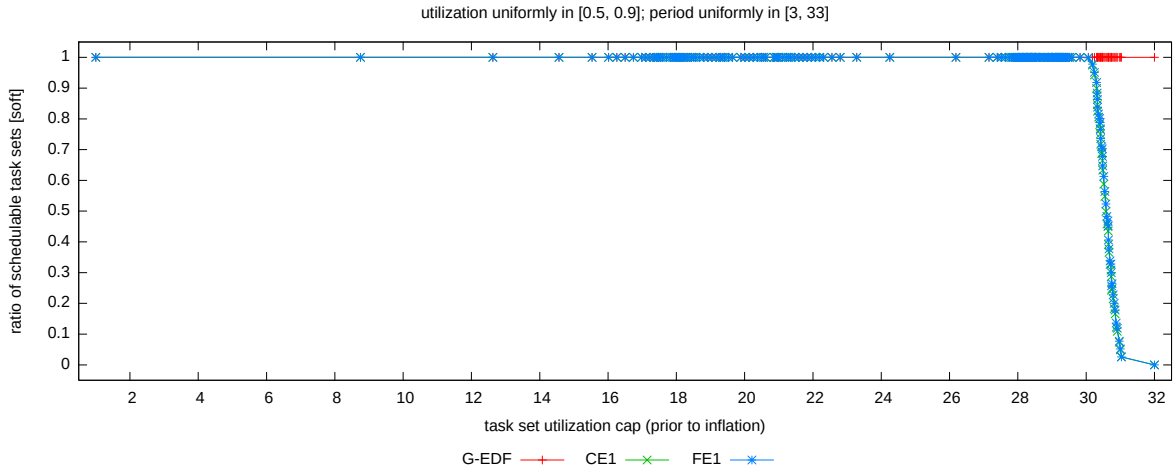

(a)

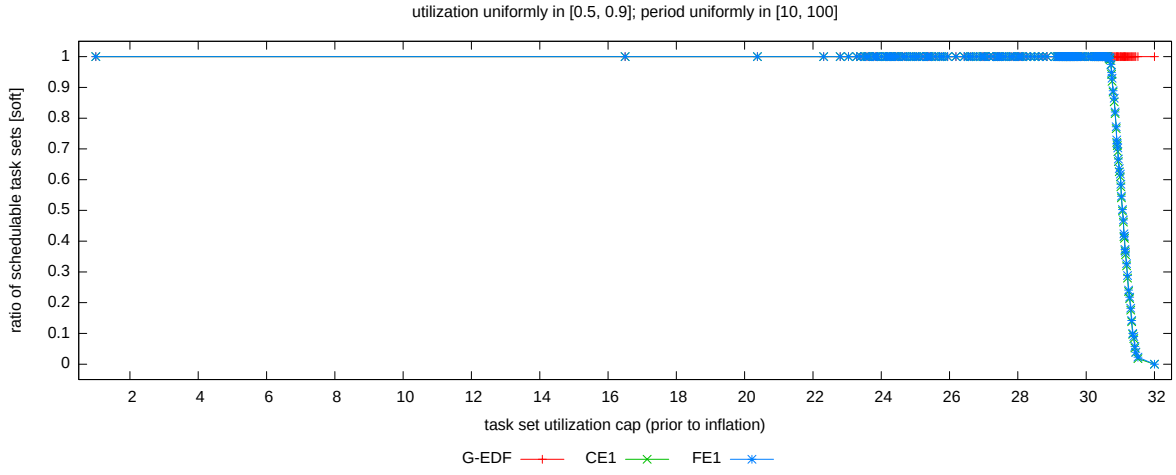

(b)

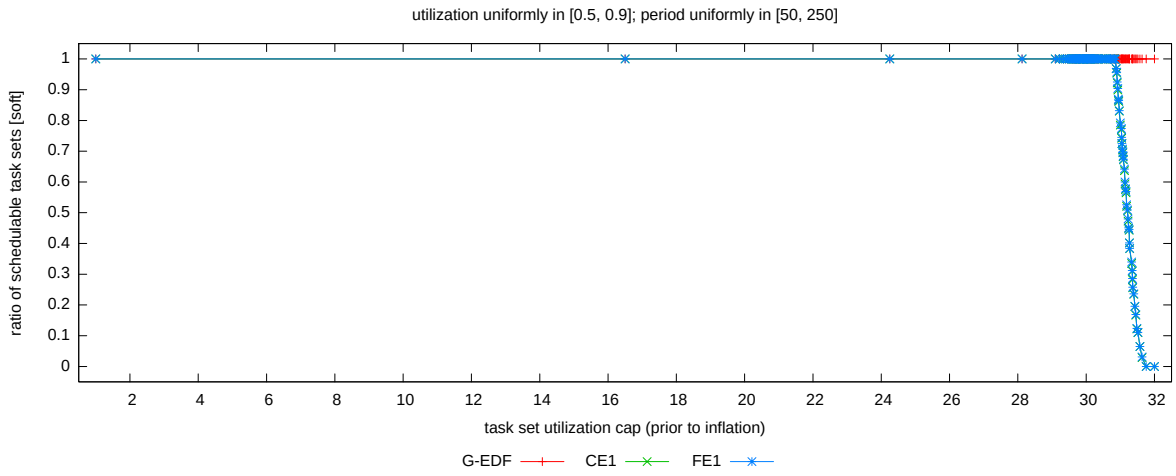

(c)

Figure 88: Comparison of CE1 and FE1 (coarse- vs. fine-grained queues) in terms of soft schedulability of task sets with uniform heavy per-task utilizations and **(a)** short, **(b)** moderate, and **(c)** long periods. These graphs correspond to Fig. 28.

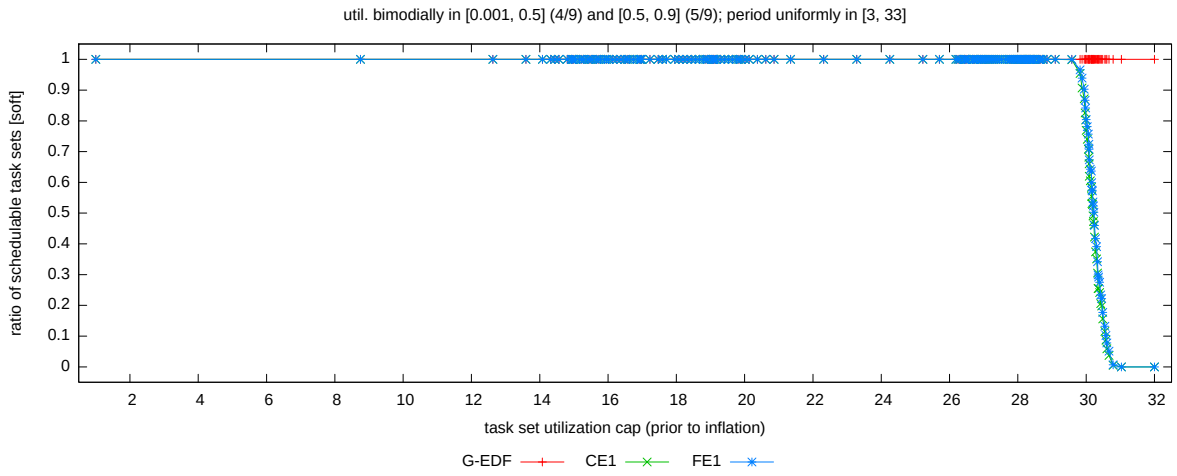

(a)

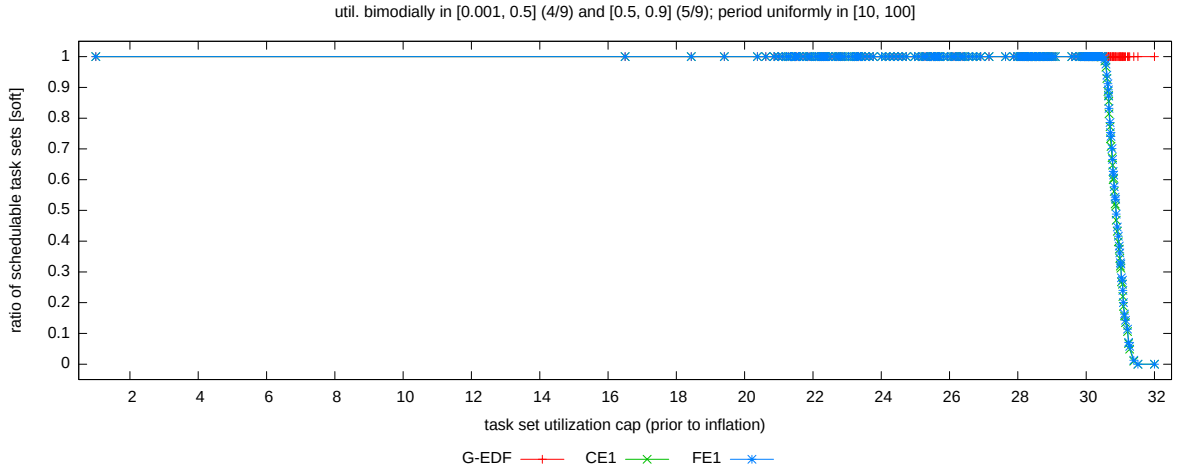

(b)

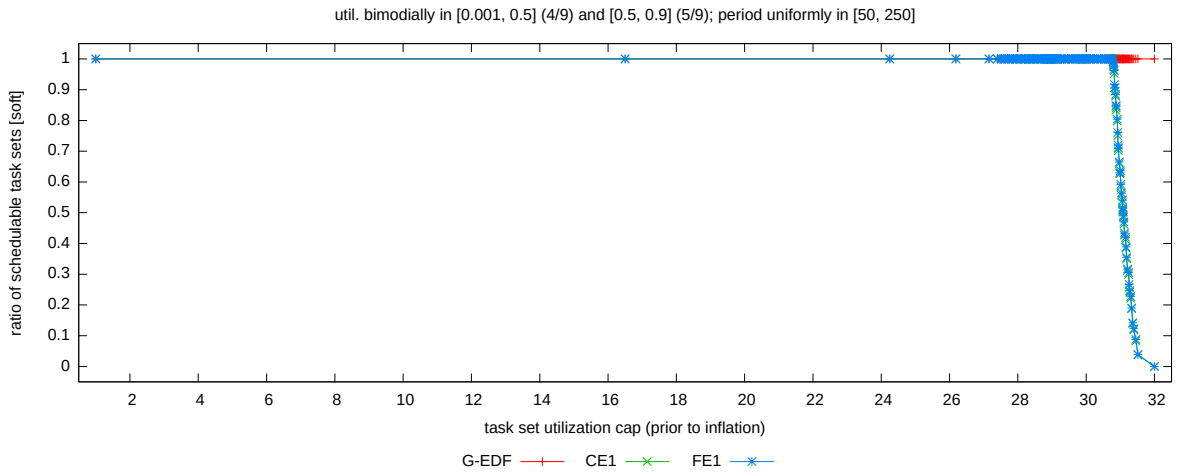

(c)

Figure 89: Comparison of CE1 and FE1 (coarse- vs. fine-grained queues) in terms of soft schedulability of task sets with bimodal heavy per-task utilizations and **(a)** short, **(b)** moderate, and **(c)** long periods. These graphs correspond to Fig. 29.

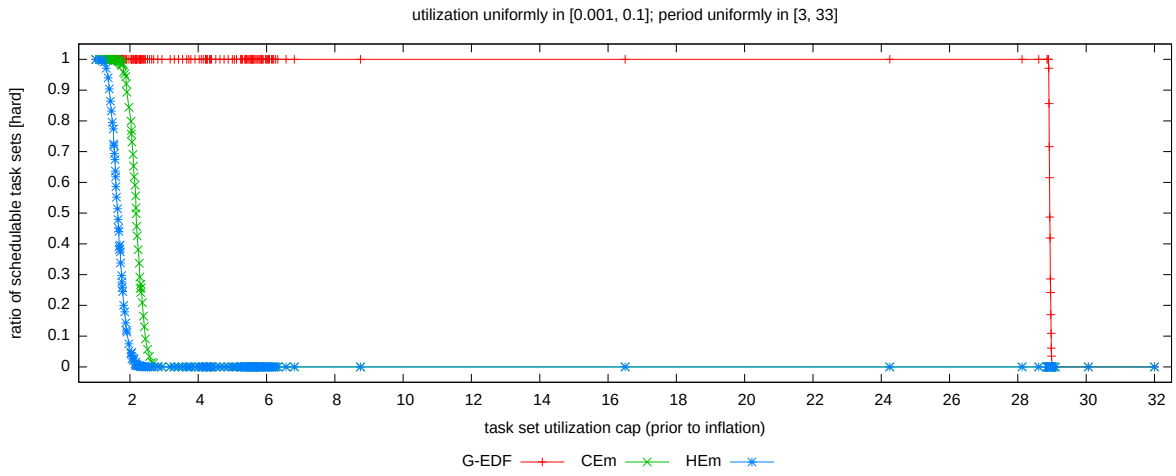

(a)

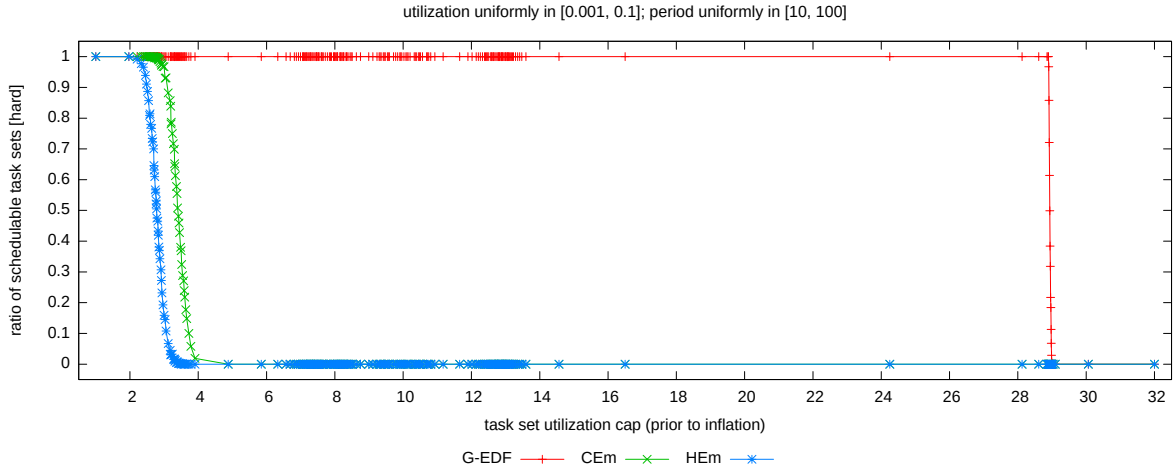

(b)

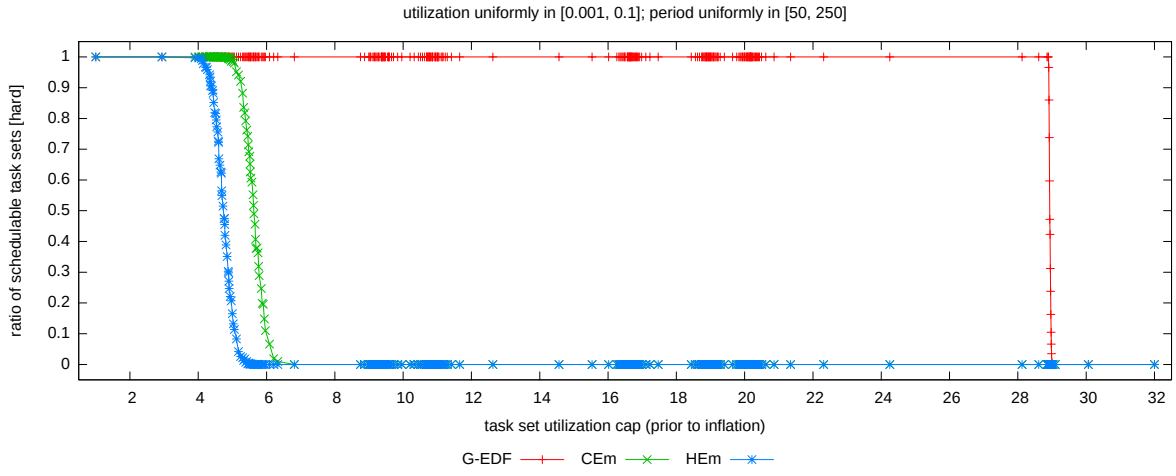

(c)

Figure 90: Comparison of CEm and HEm (coarse-grained vs. hierarchical queues) in terms of hard schedulability of task sets with uniform light per-task utilizations and **(a)** short, **(b)** moderate, and **(c)** long periods. These graphs correspond to Fig. 18.

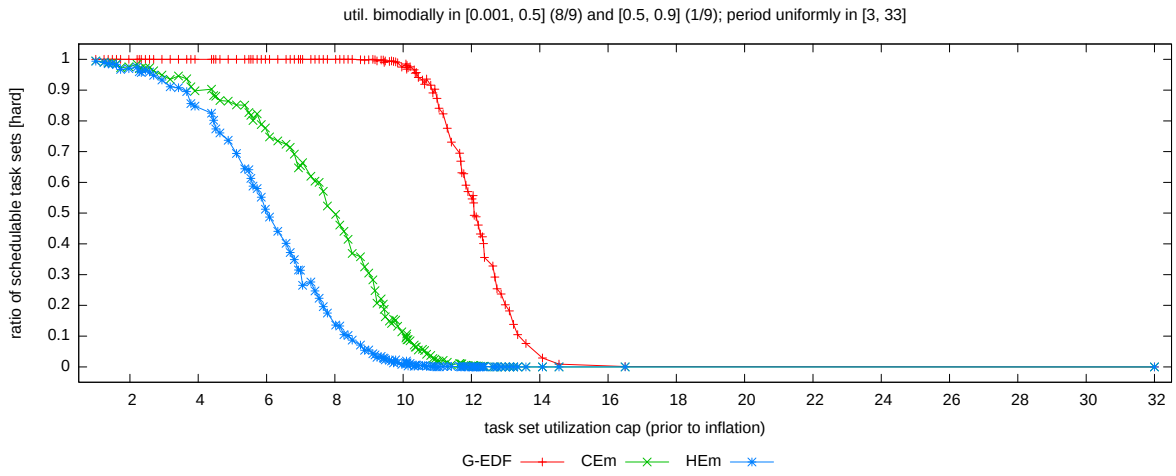

(a)

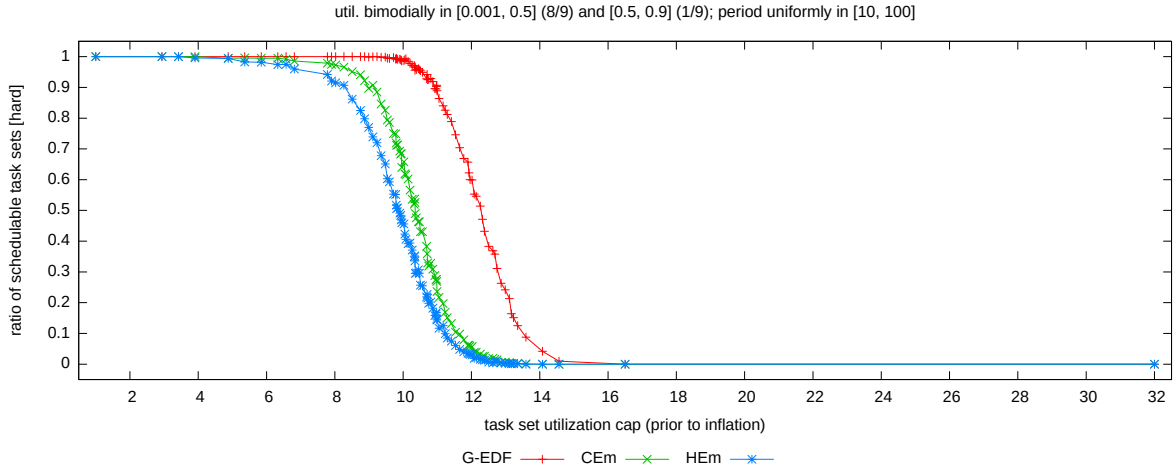

(b)

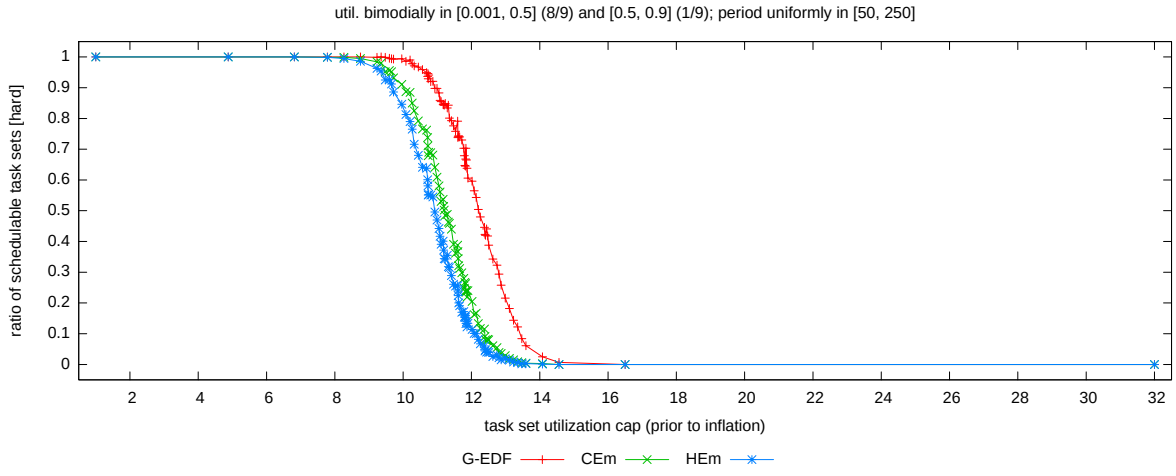

(c)

Figure 91: Comparison of CEm and HEm (coarse-grained vs. hierarchical queues) in terms of hard schedulability of task sets with bimodal light per-task utilizations and **(a)** short, **(b)** moderate, and **(c)** long periods. These graphs correspond to Fig. 19.

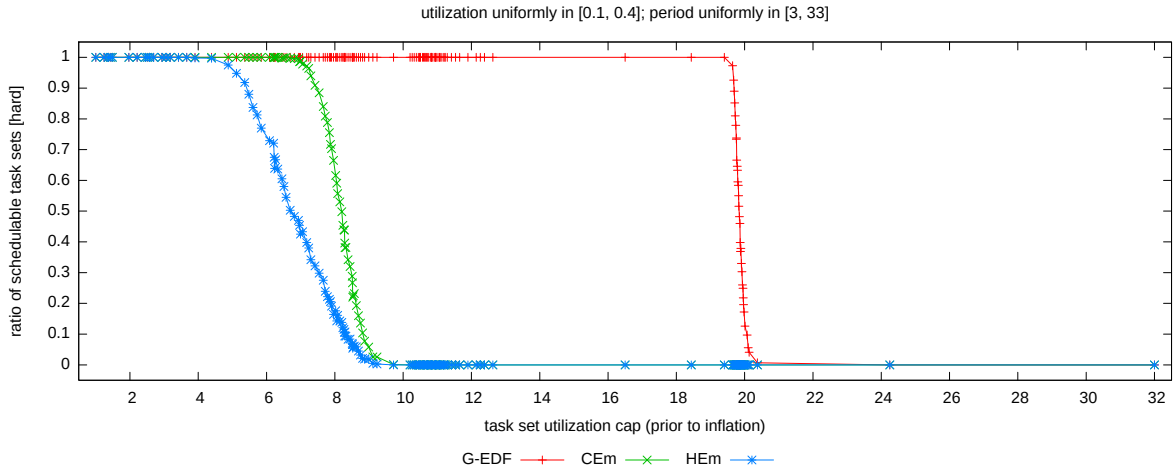

(a)

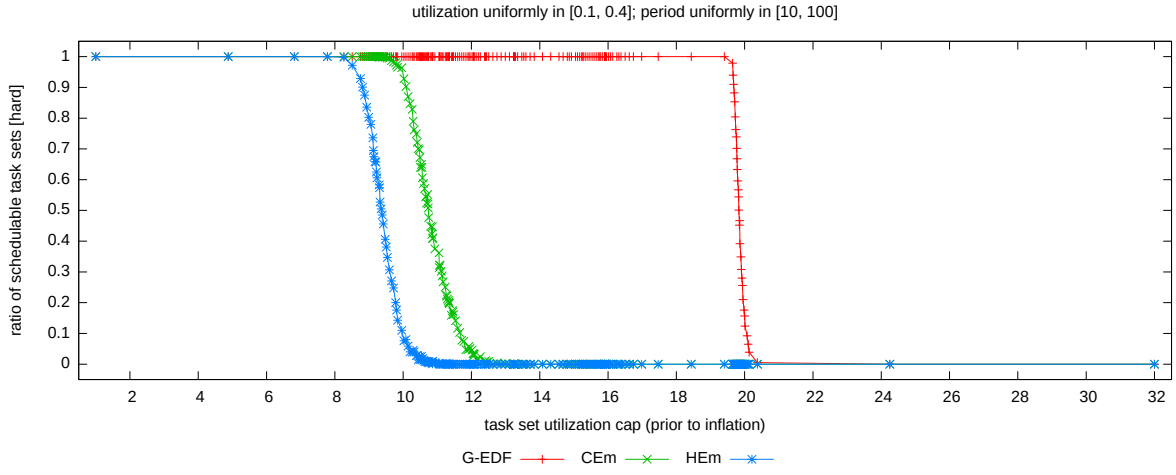

(b)

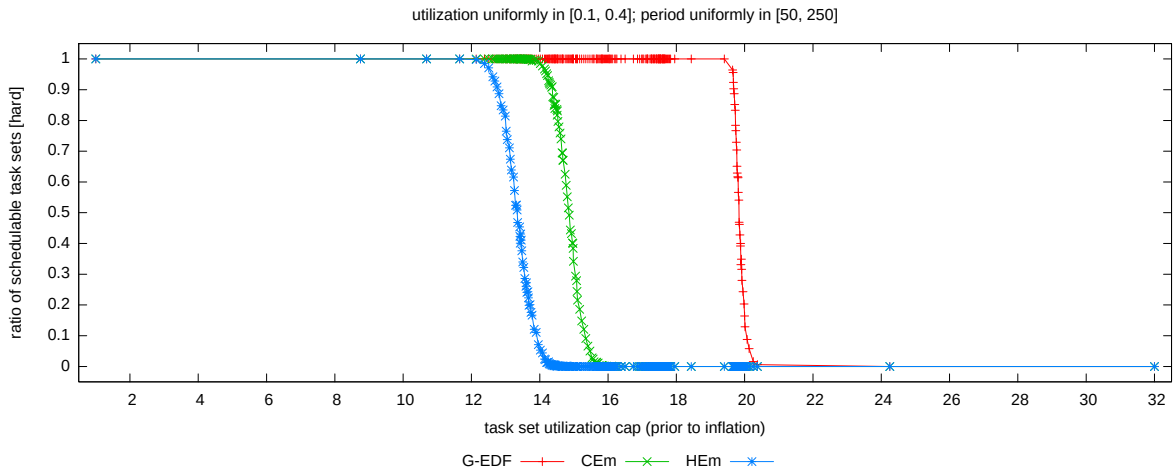

(c)

Figure 92: Comparison of CEm and HEm (coarse-grained vs. hierarchical queues) in terms of hard schedulability of task sets with uniform medium per-task utilizations and **(a)** short, **(b)** moderate, and **(c)** long periods. These graphs correspond to Fig. 20.

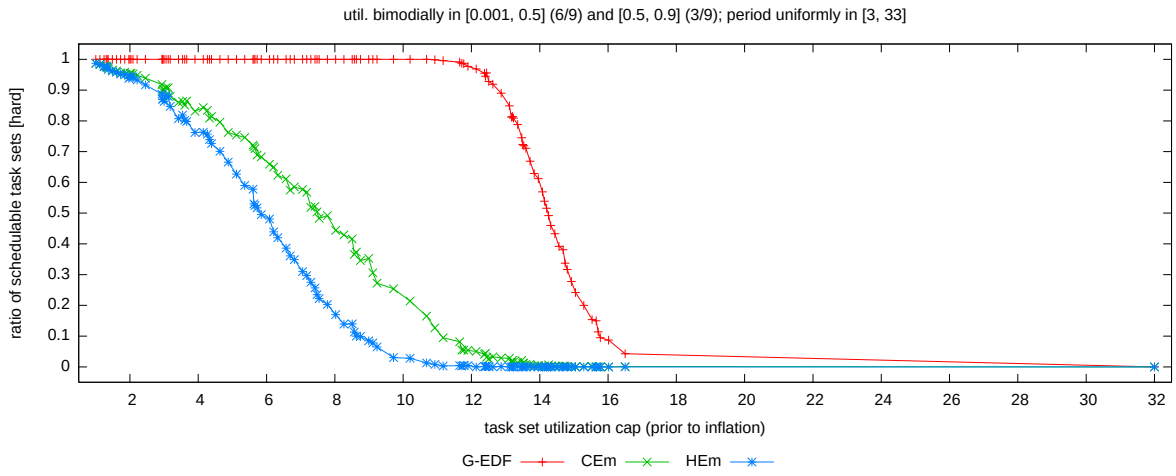

(a)

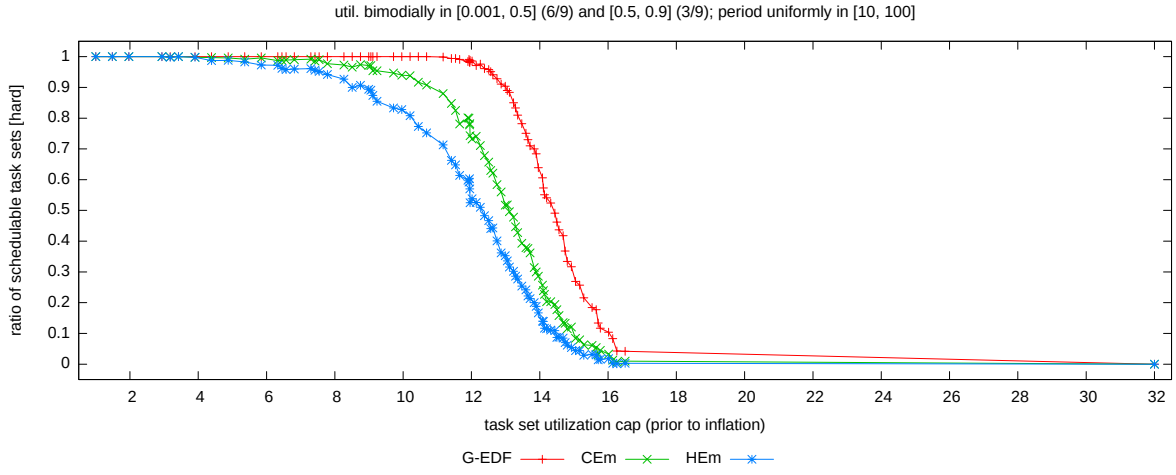

(b)

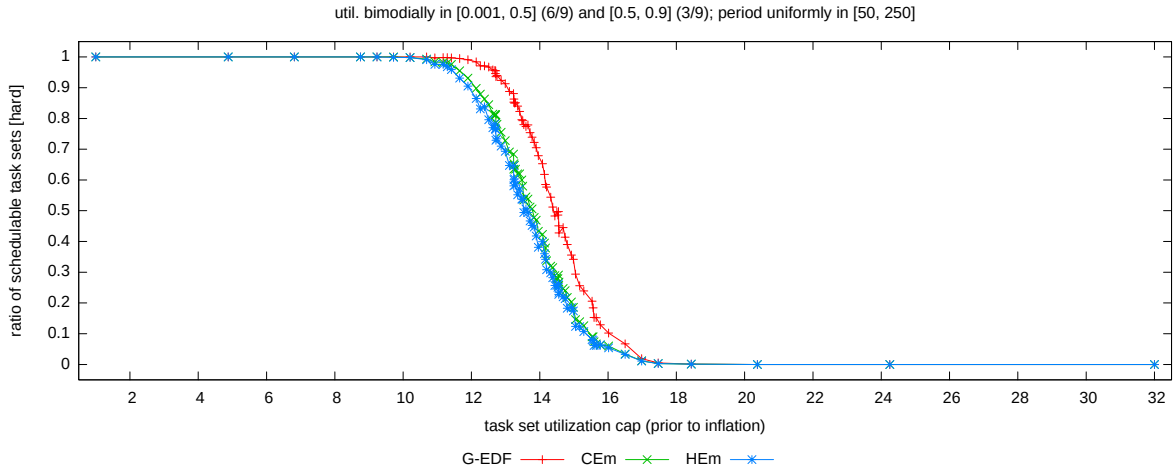

(c)

Figure 93: Comparison of CEm and HEm (coarse-grained vs. hierarchical queues) in terms of hard schedulability of task sets with bimodal medium per-task utilizations and **(a)** short, **(b)** moderate, and **(c)** long periods. These graphs correspond to Fig. 21.

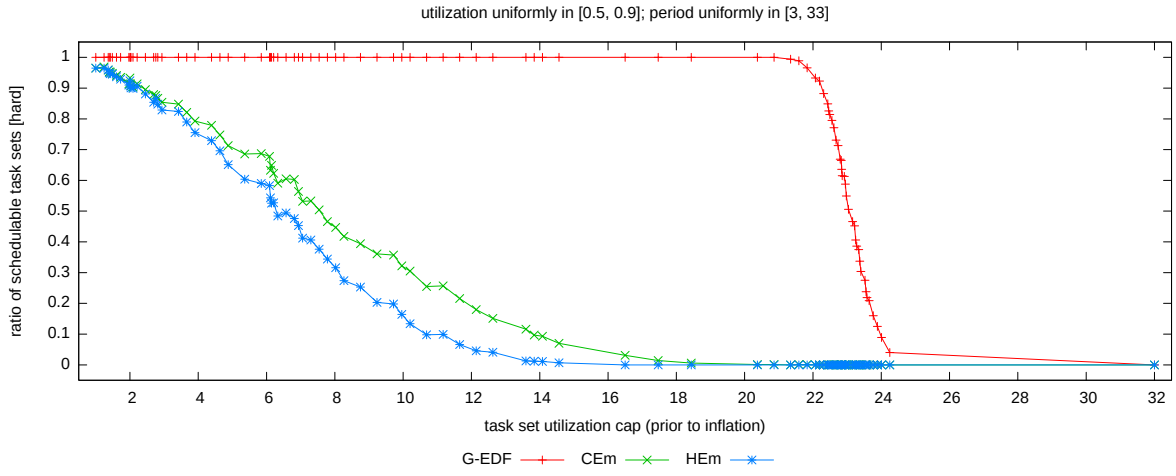

(a)

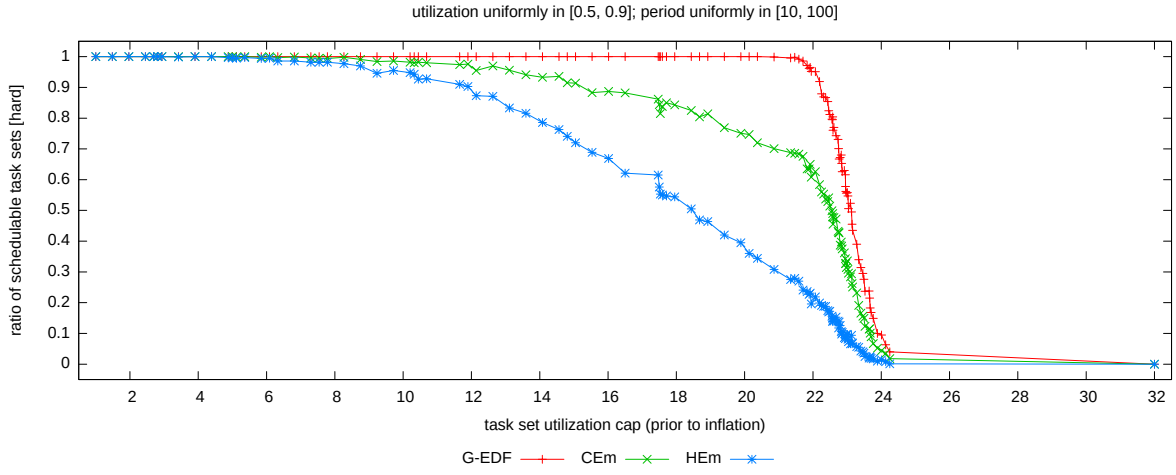

(b)

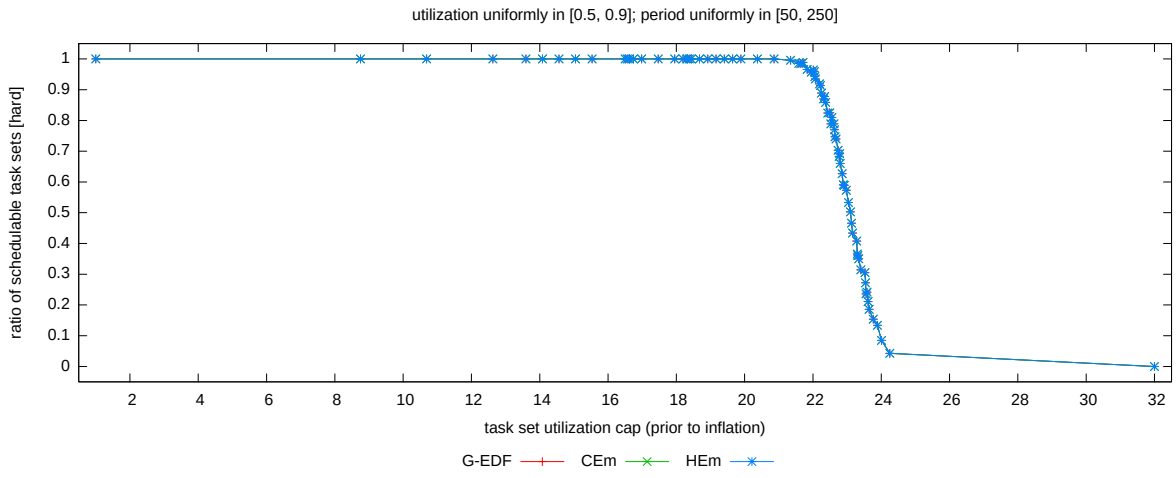

(c)

Figure 94: Comparison of CEm and HEm (coarse-grained vs. hierarchical queues) in terms of hard schedulability of task sets with uniform heavy per-task utilizations and **(a)** short, **(b)** moderate, and **(c)** long periods. These graphs correspond to Fig. 22.

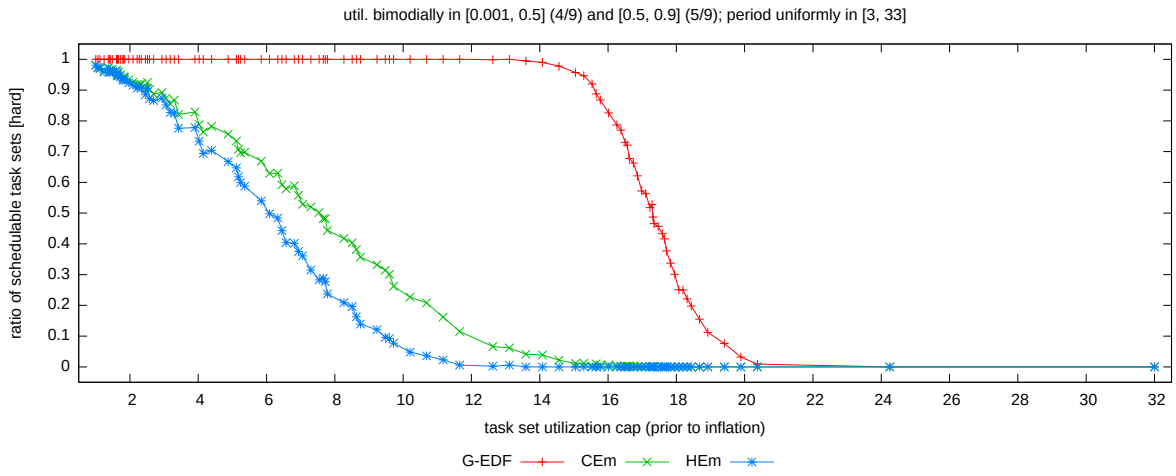

(a)

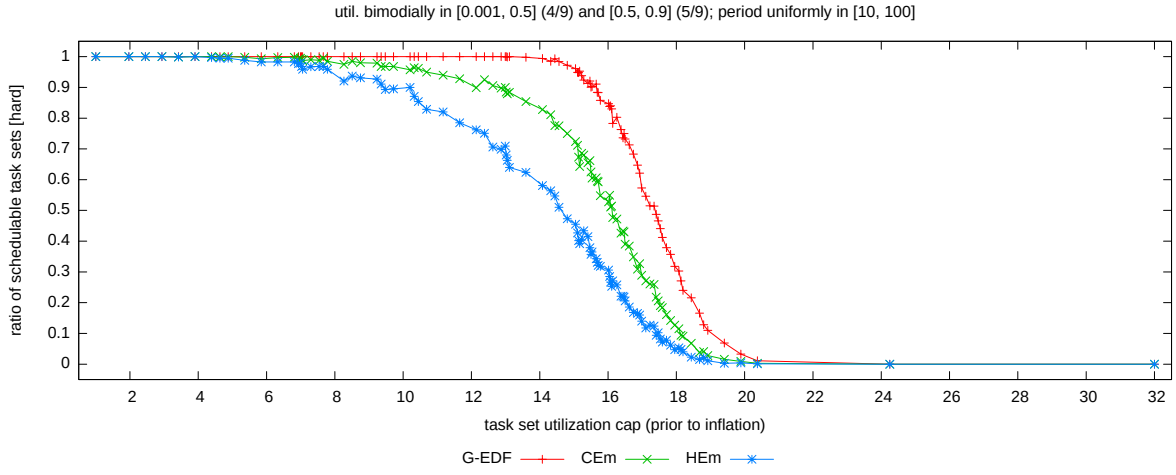

(b)

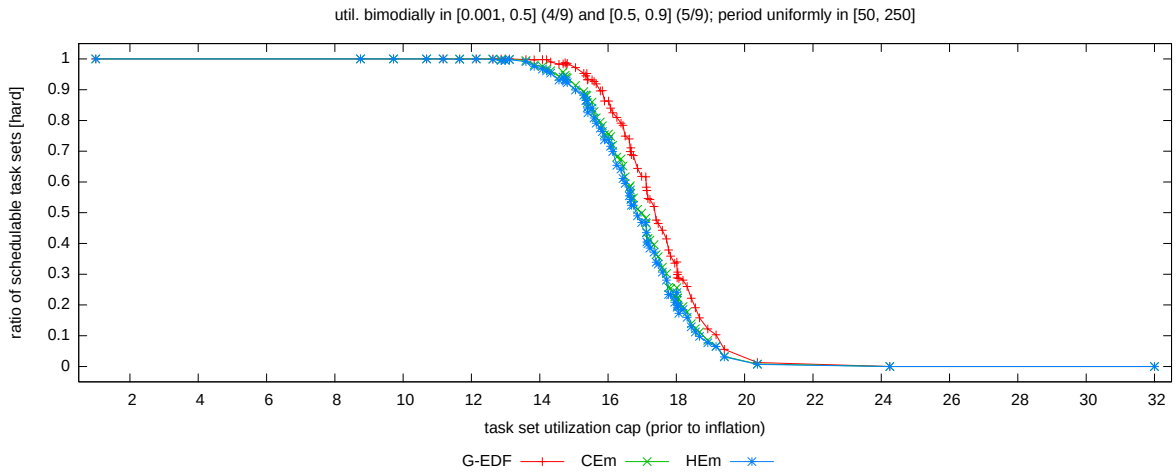

(c)

Figure 95: Comparison of CEm and HEm (coarse-grained vs. hierarchical queues) in terms of hard schedulability of task sets with bimodal heavy per-task utilizations and **(a)** short, **(b)** moderate, and **(c)** long periods. These graphs correspond to Fig. 23.

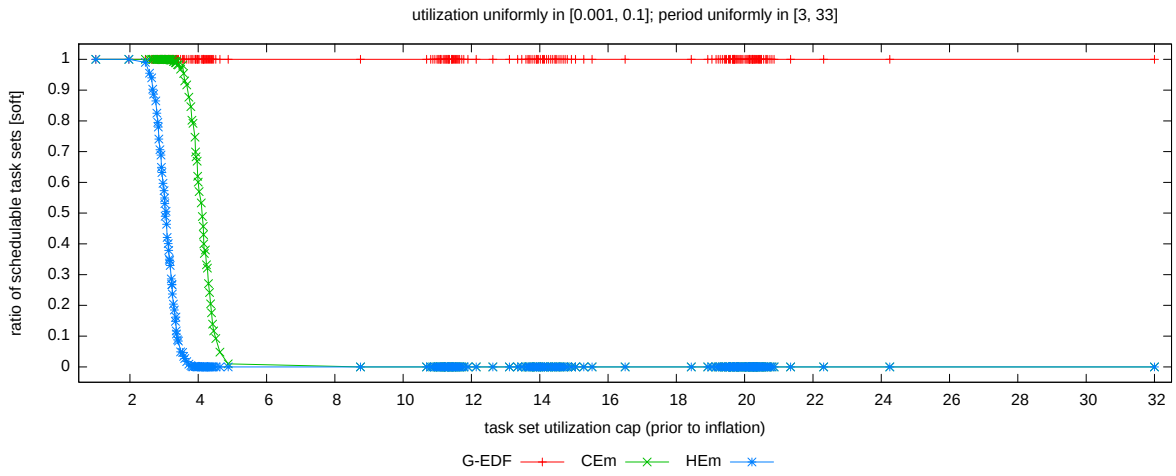

(a)

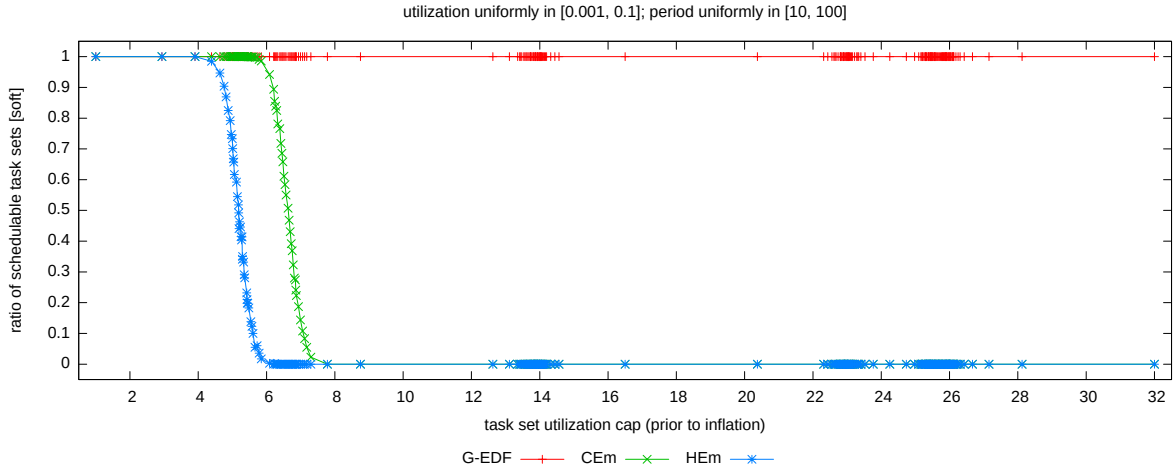

(b)

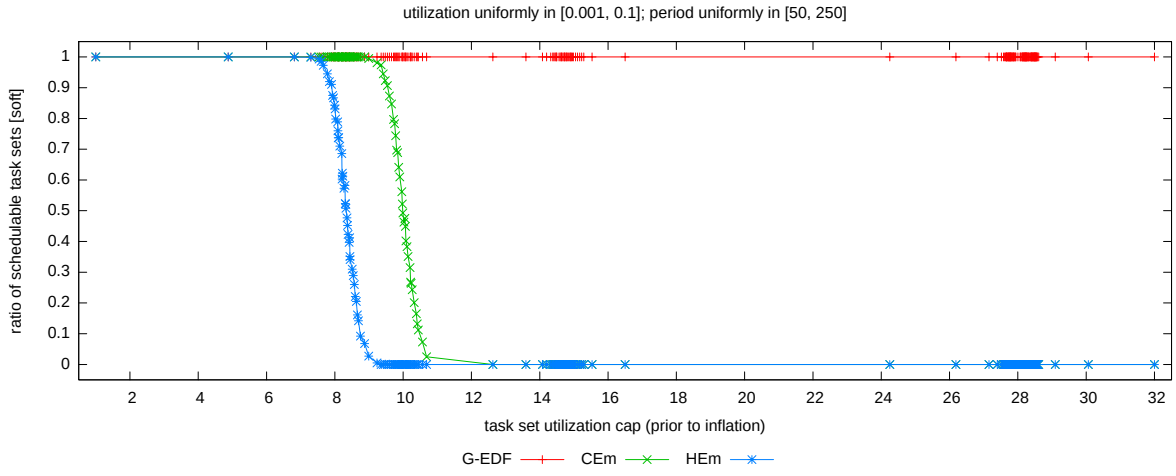

(c)

Figure 96: Comparison of CEm and HEm (coarse-grained vs. hierarchical queues) in terms of soft schedulability of task sets with uniform light per-task utilizations and **(a)** short, **(b)** moderate, and **(c)** long periods. These graphs correspond to Fig. 24.

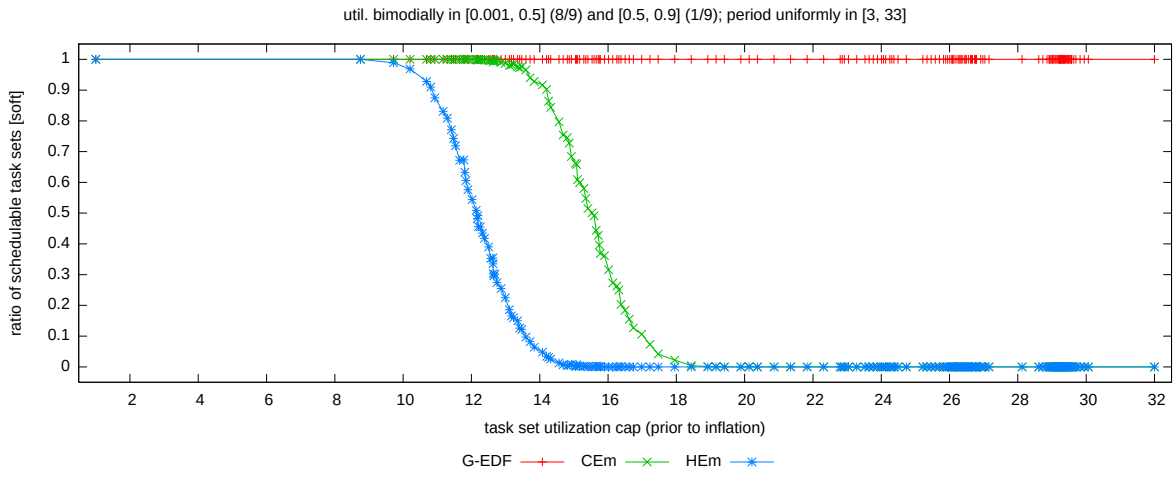

(a)

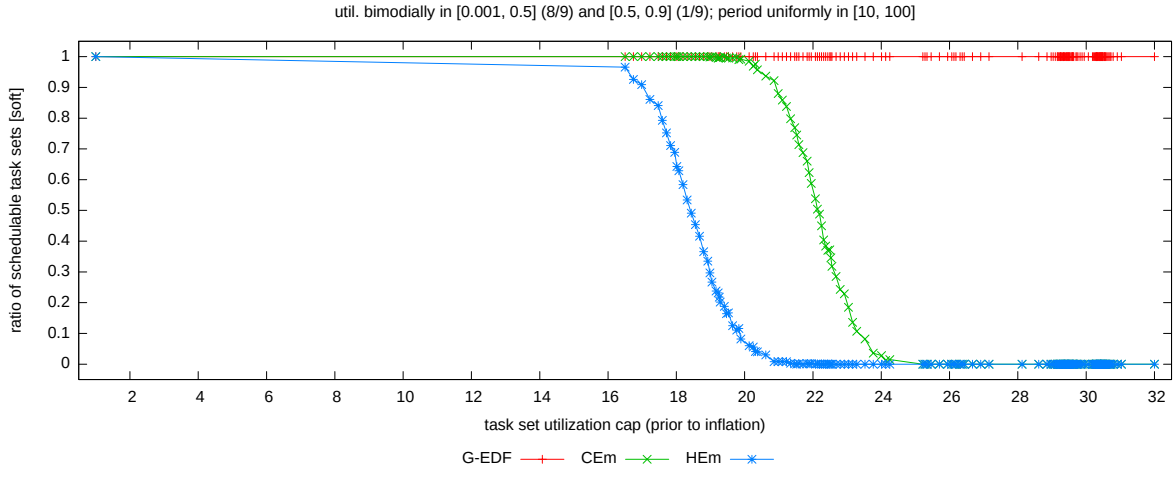

(b)

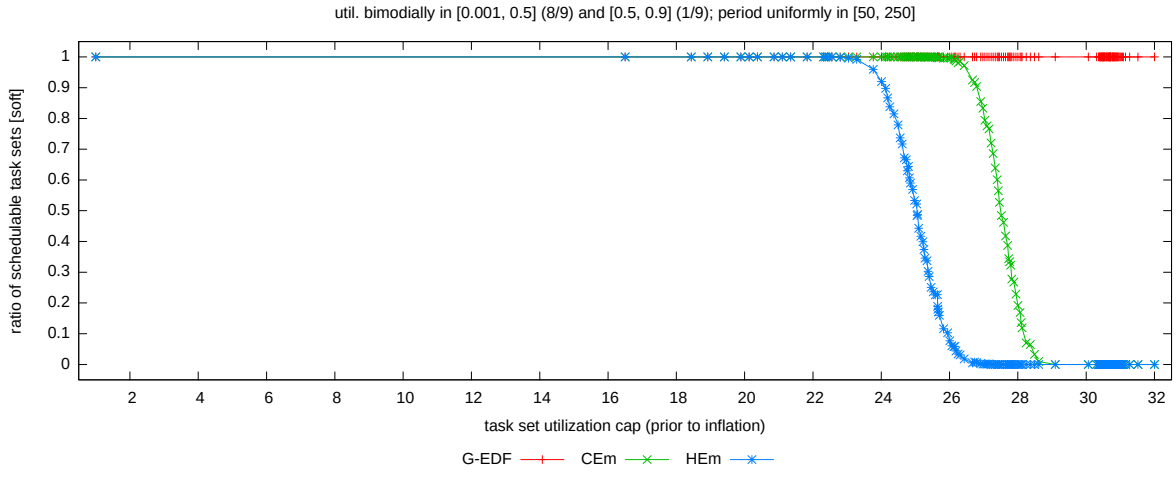

(c)

Figure 97: Comparison of CEm and HEm (coarse-grained vs. hierarchical queues) in terms of soft schedulability of task sets with bimodal light per-task utilizations and **(a)** short, **(b)** moderate, and **(c)** long periods. These graphs correspond to Fig. 25.

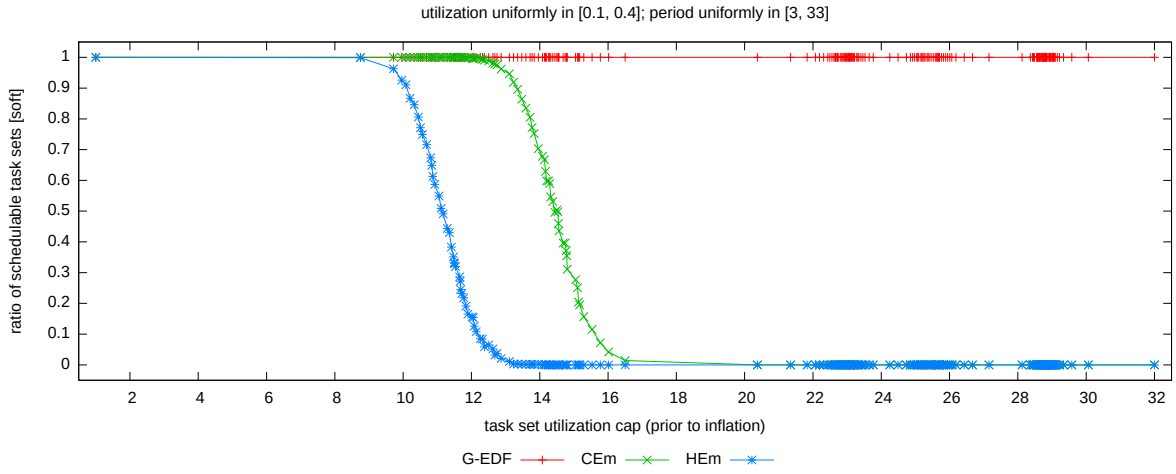

(a)

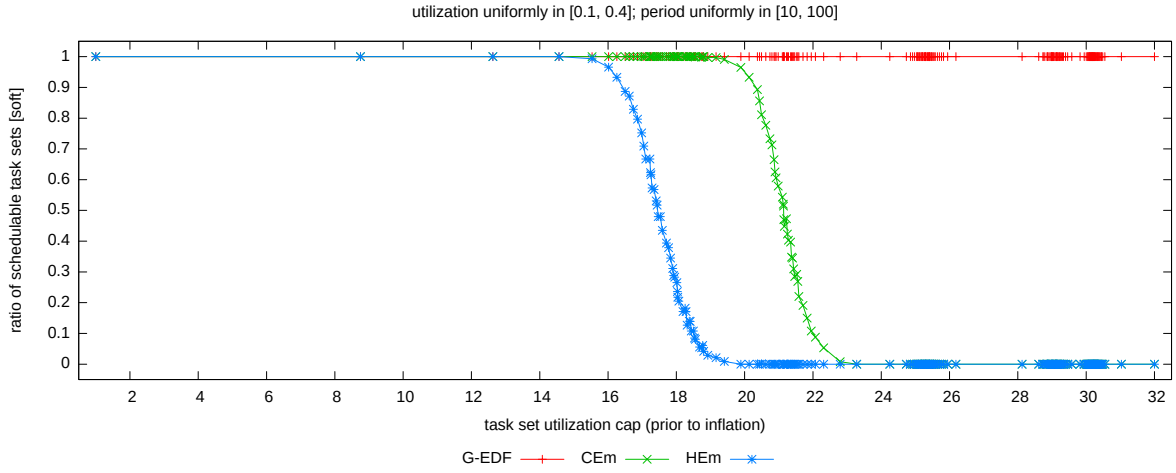

(b)

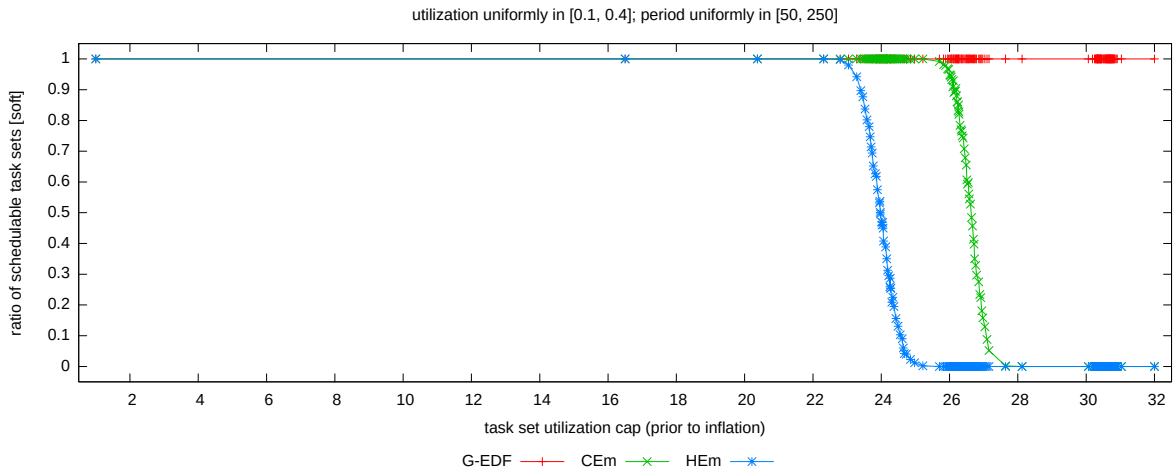

(c)

Figure 98: Comparison of CEm and HEm (coarse-grained vs. hierarchical queues) in terms of soft schedulability of task sets with uniform medium per-task utilizations and **(a)** short, **(b)** moderate, and **(c)** long periods. These graphs correspond to Fig. 26.

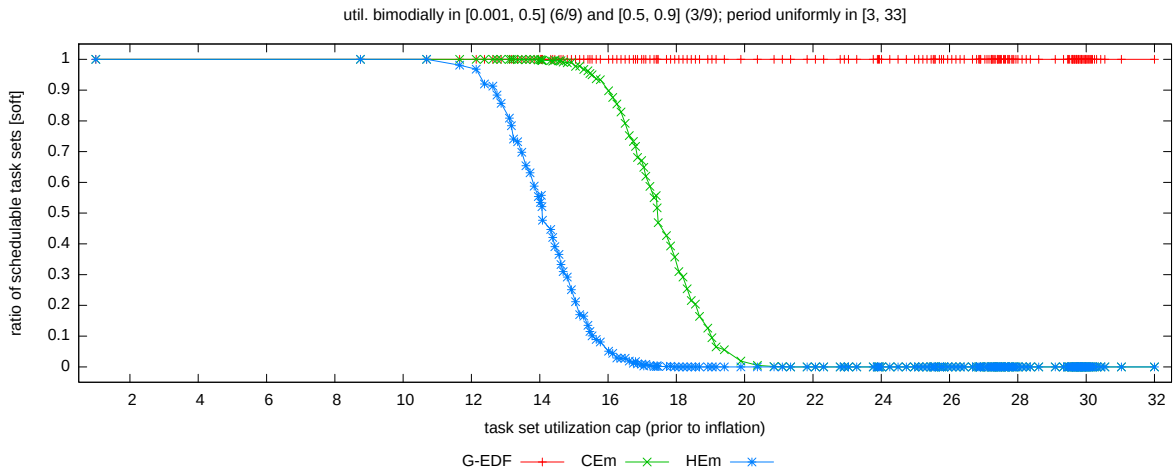

(a)

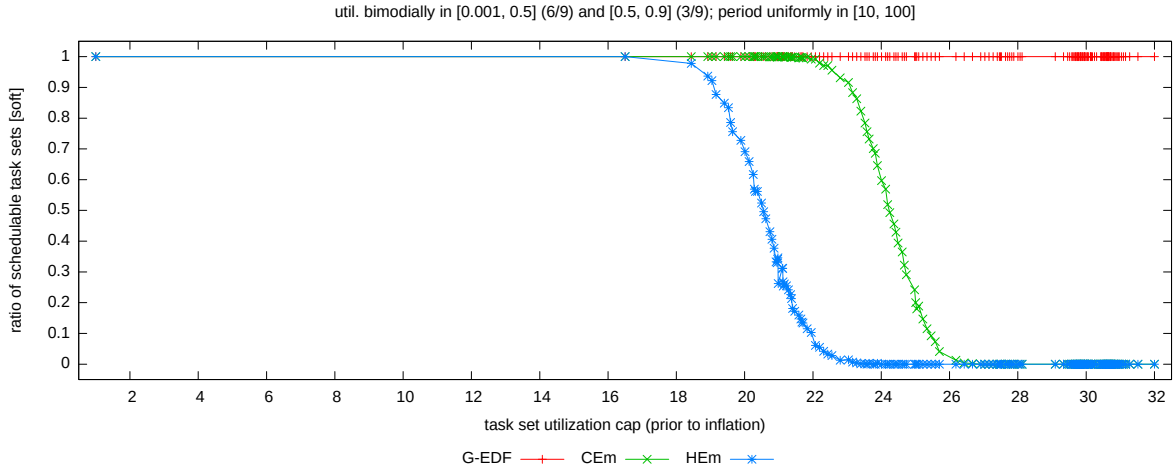

(b)

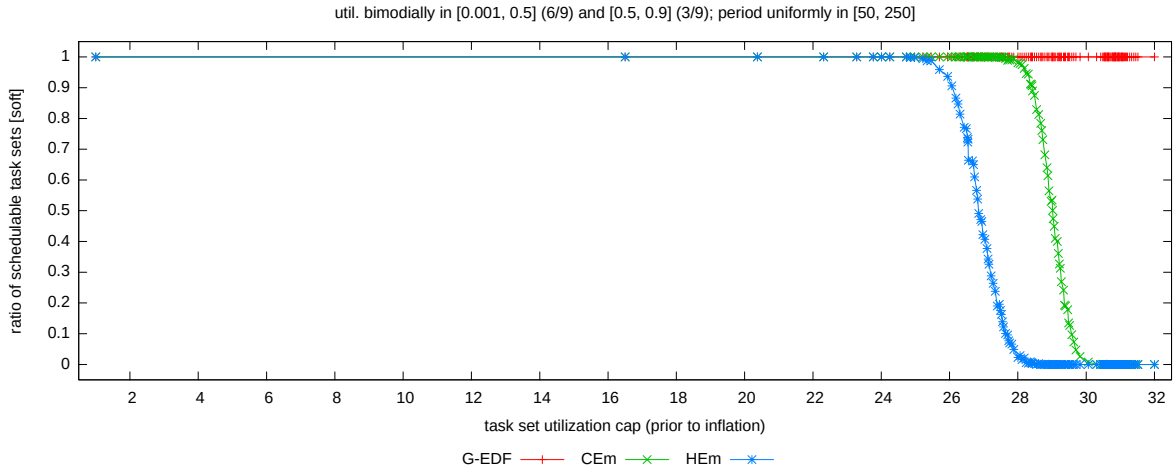

(c)

Figure 99: Comparison of CEm and HEm (coarse-grained vs. hierarchical queues) in terms of soft schedulability of task sets with bimodal medium per-task utilizations and **(a)** short, **(b)** moderate, and **(c)** long periods. These graphs correspond to Fig. 27.

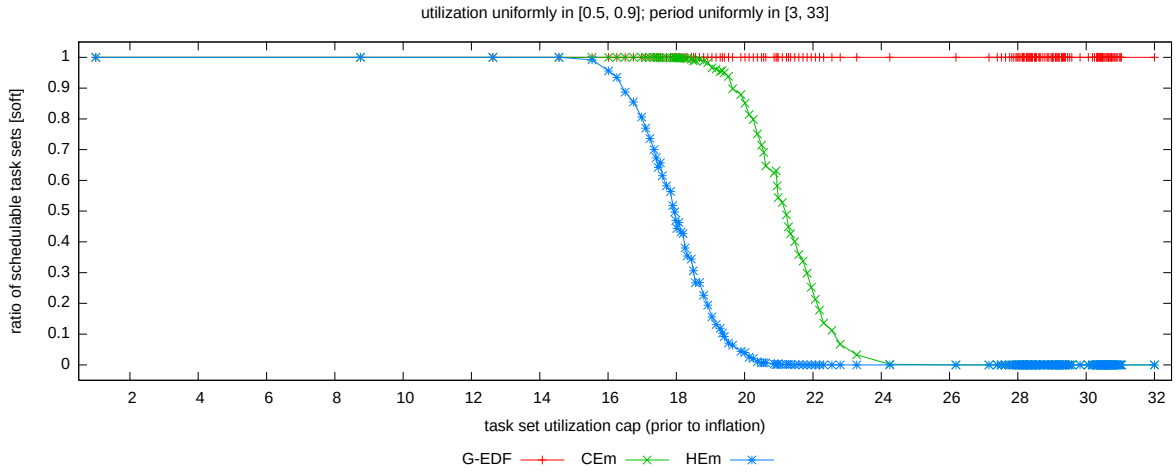

(a)

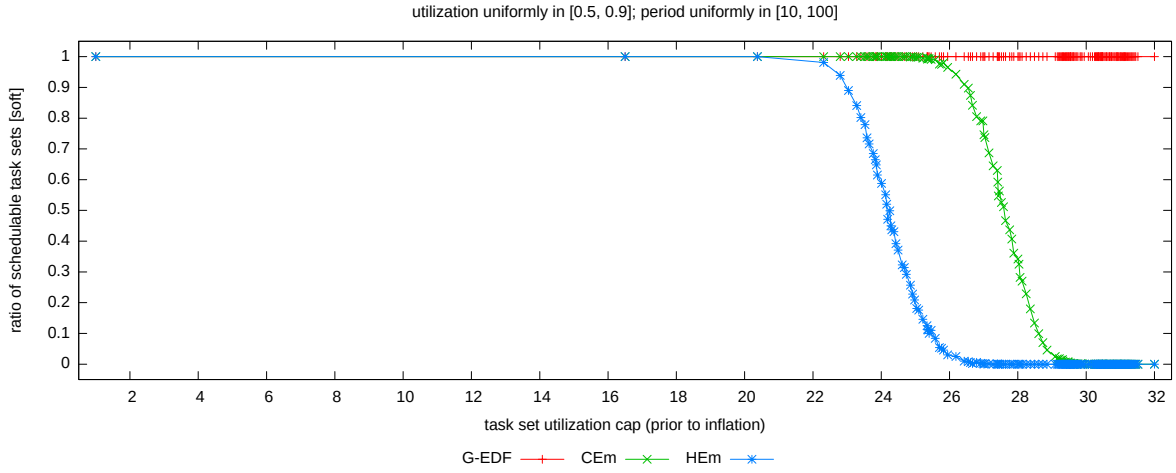

(b)

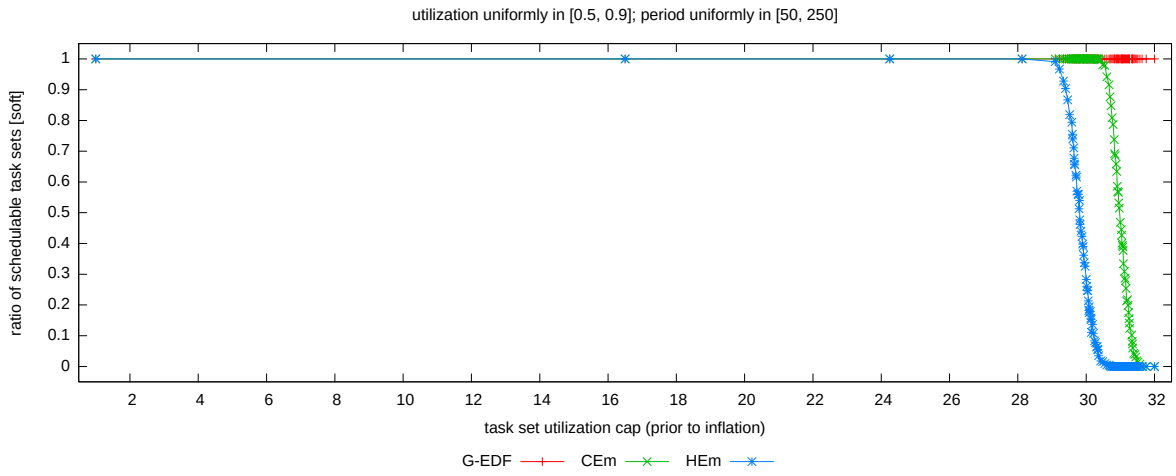

(c)

Figure 100: Comparison of CEm and HEm (coarse-grained vs. hierarchical queues) in terms of soft schedulability of task sets with uniform heavy per-task utilizations and **(a)** short, **(b)** moderate, and **(c)** long periods. These graphs correspond to Fig. 28.

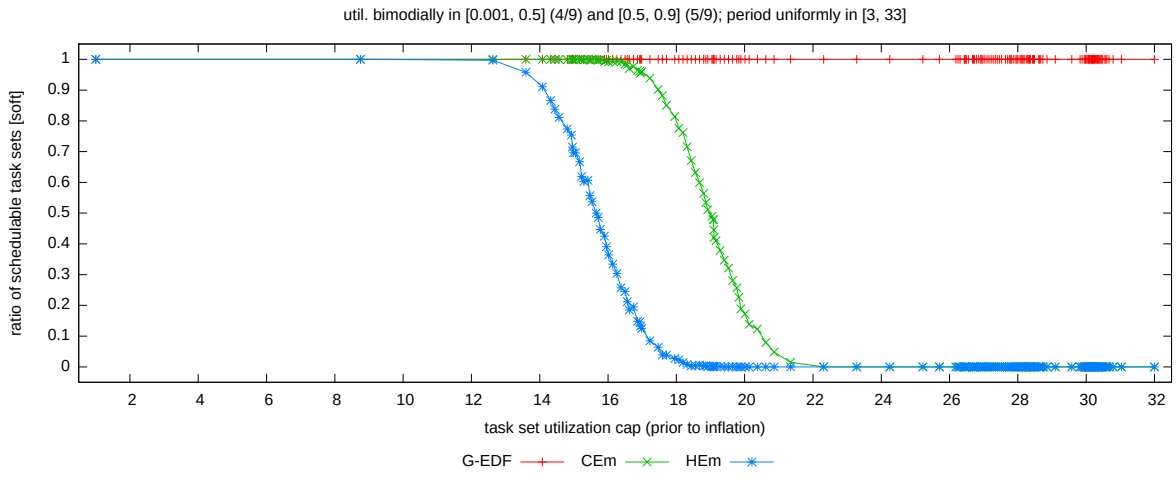

(a)

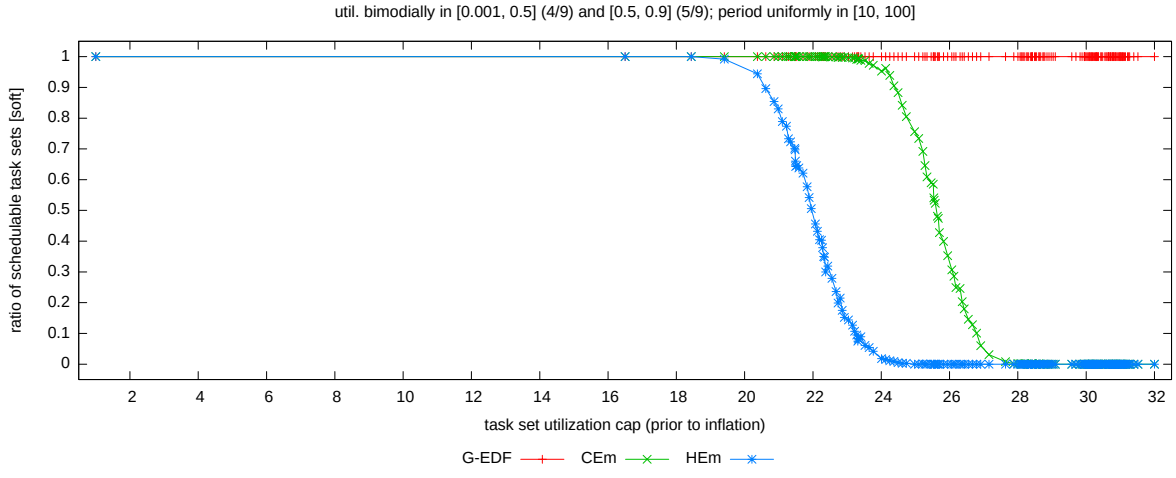

(b)

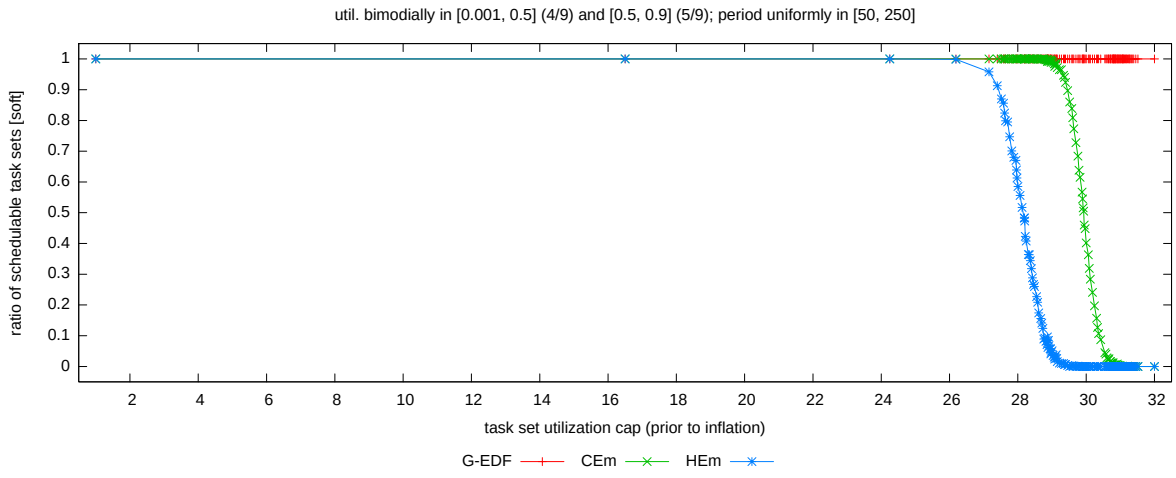

(c)

Figure 101: Comparison of CEm and HEm (coarse-grained vs. hierarchical queues) in terms of soft schedulability of task sets with bimodal heavy per-task utilizations and **(a)** short, **(b)** moderate, and **(c)** long periods. These graphs correspond to Fig. 29.

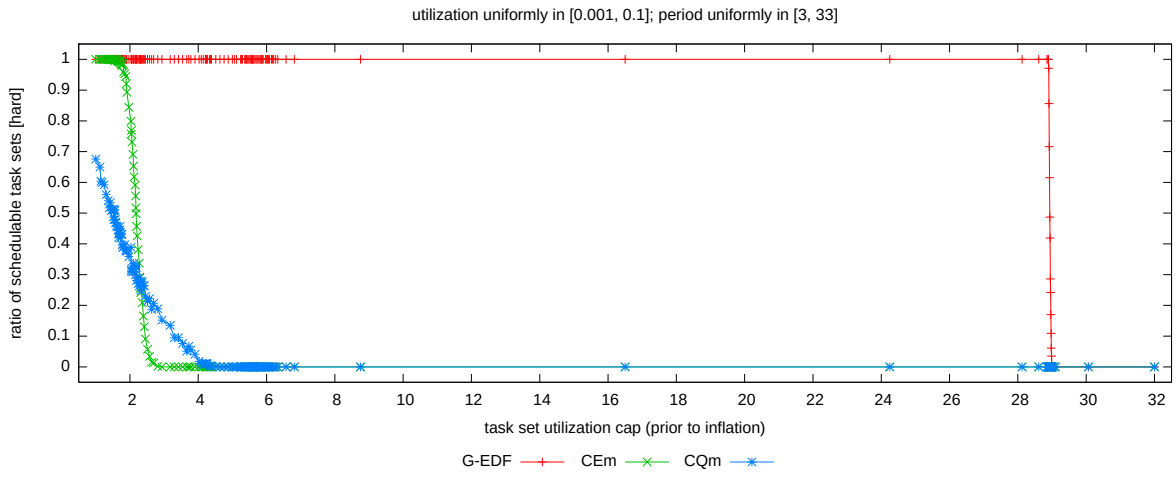

(a)

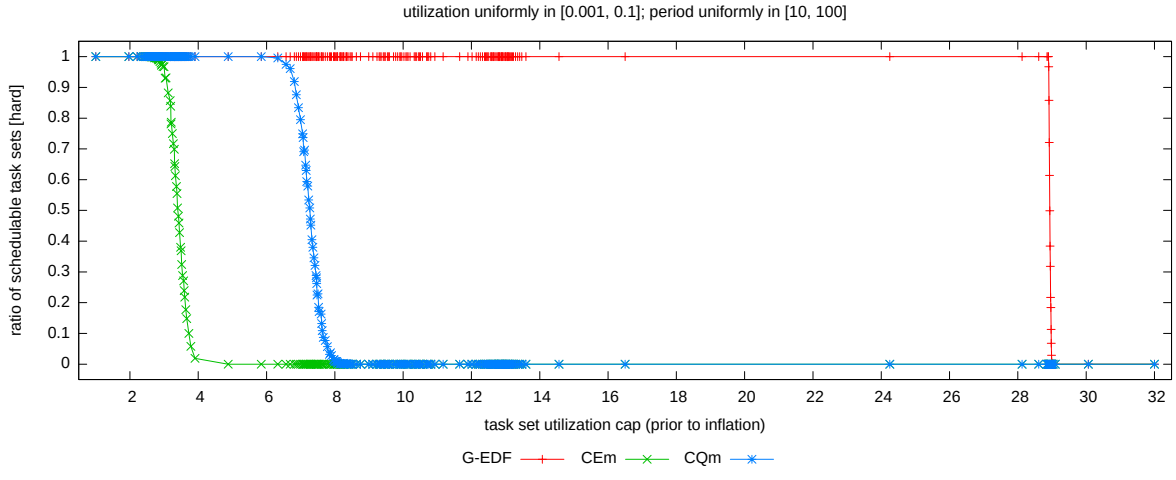

(b)

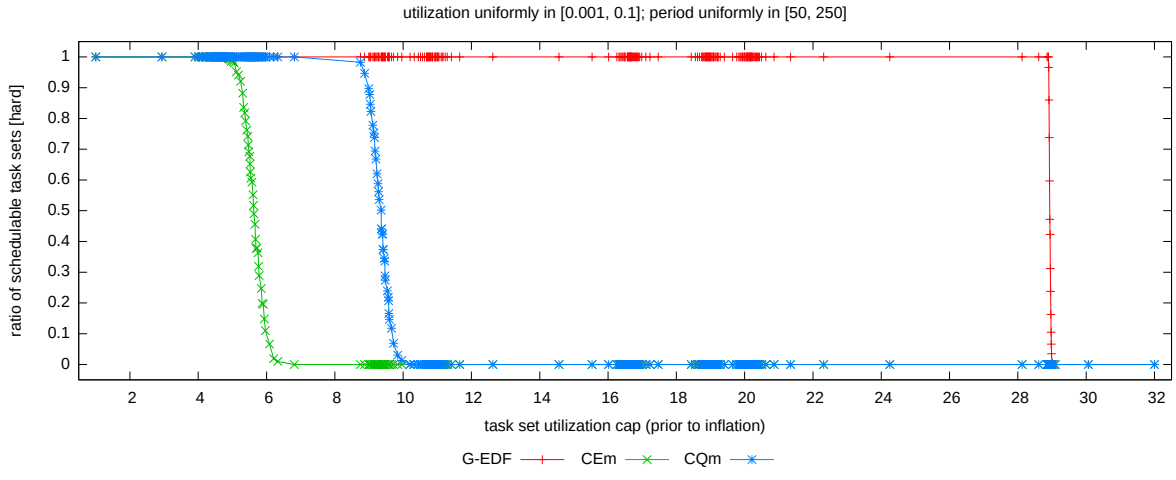

(c)

Figure 102: Comparison of CEm and CQm (event- vs. quantum-driven scheduling) in terms of hard schedulability of task sets with uniform light per-task utilizations and **(a)** short, **(b)** moderate, and **(c)** long periods. These graphs correspond to Fig. 18.

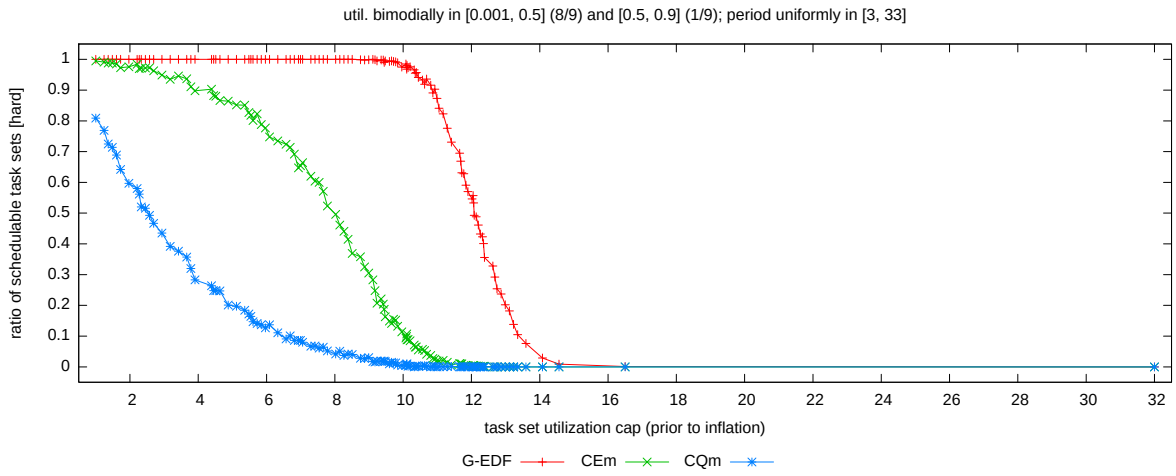

(a)

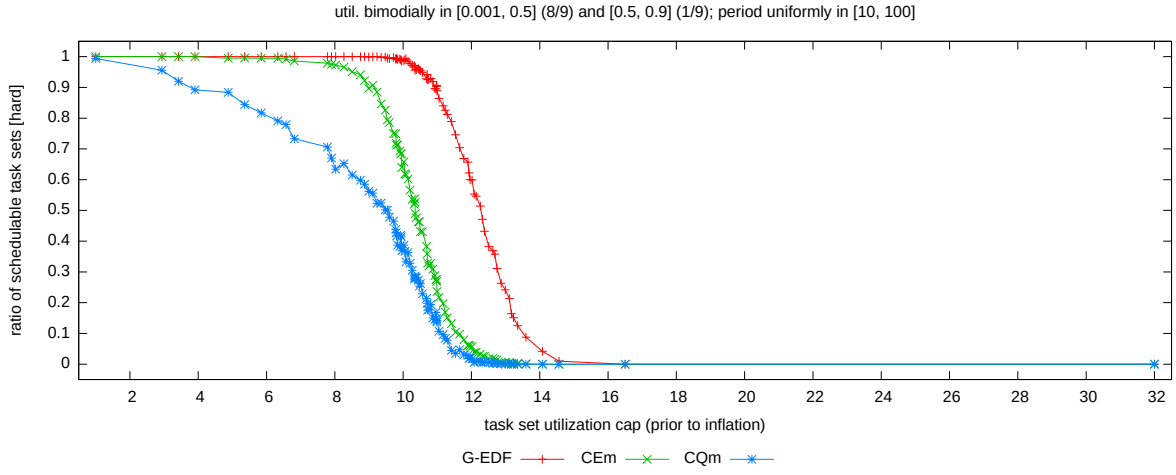

(b)

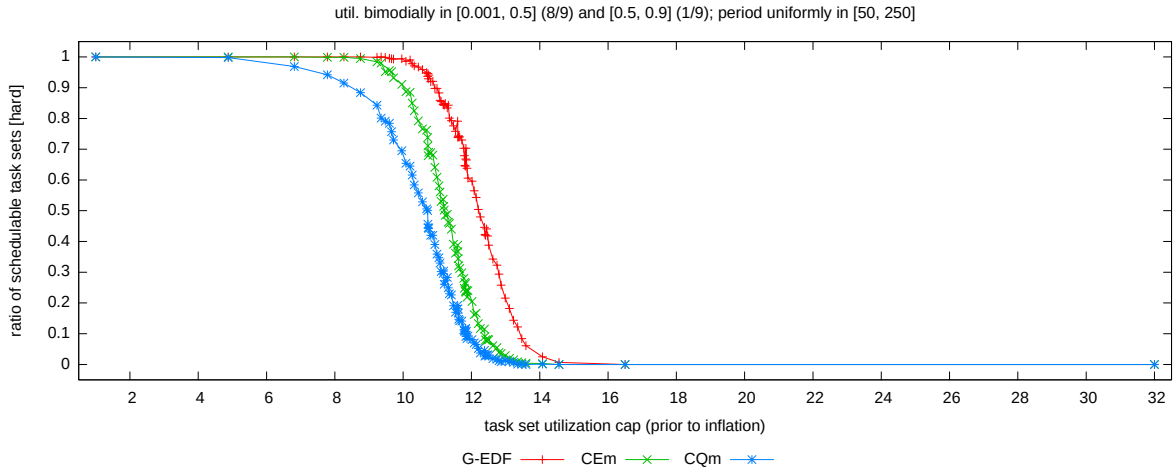

(c)

Figure 103: Comparison of CEm and CQm (event- vs. quantum-driven scheduling) in terms of hard schedulability of task sets with bimodal light per-task utilizations and **(a)** short, **(b)** moderate, and **(c)** long periods. These graphs correspond to Fig. 19.

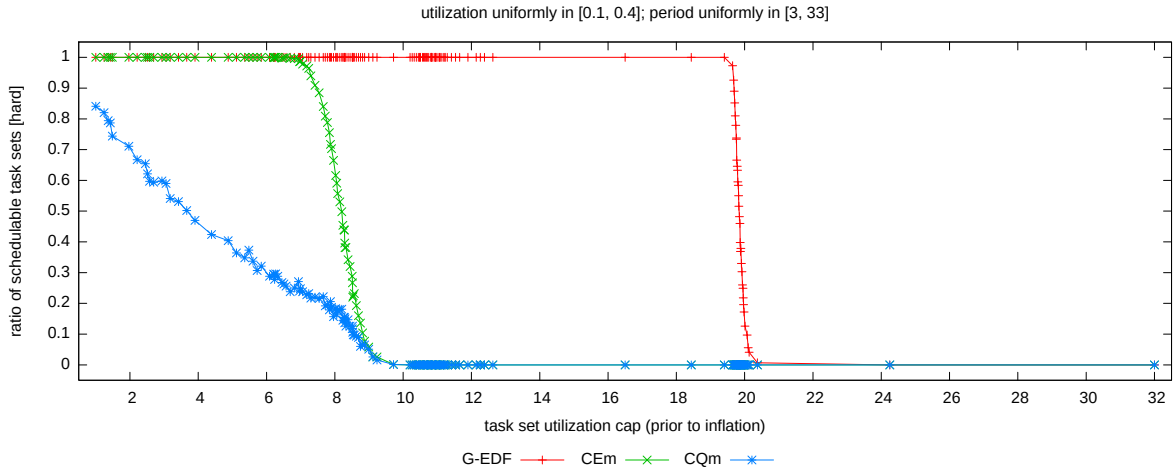

(a)

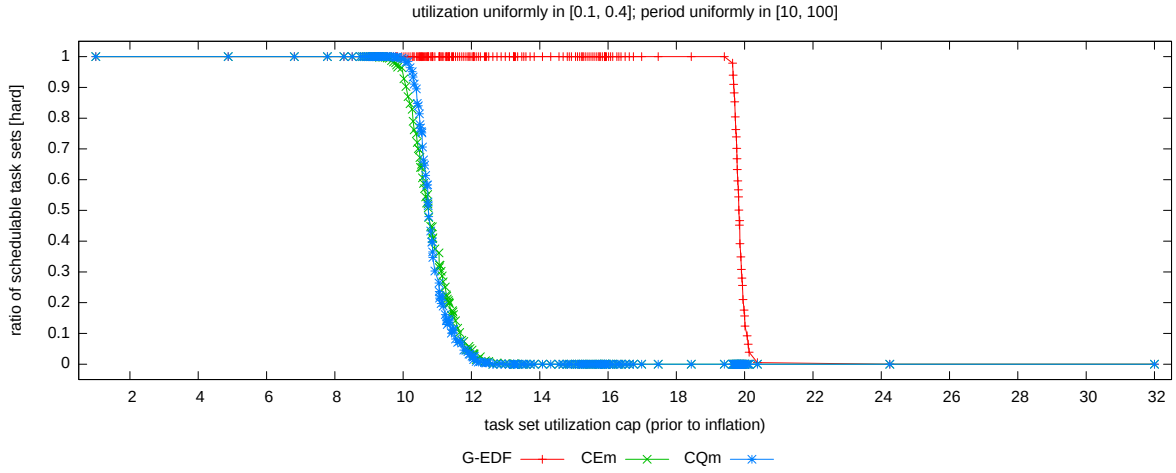

(b)

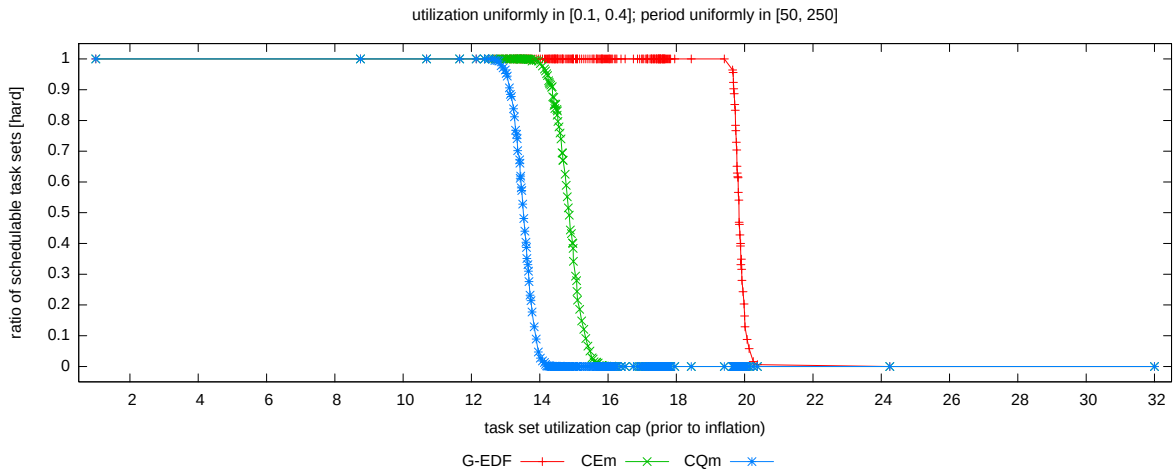

(c)

Figure 104: Comparison of CEm and CQm (event- vs. quantum-driven scheduling) in terms of hard schedulability of task sets with uniform medium per-task utilizations and **(a)** short, **(b)** moderate, and **(c)** long periods. These graphs correspond to Fig. 20.

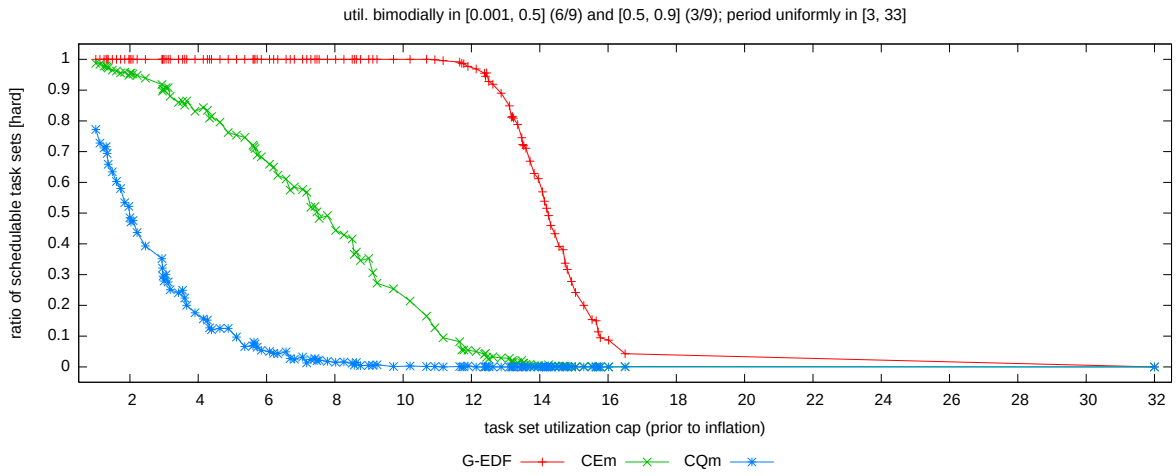

(a)

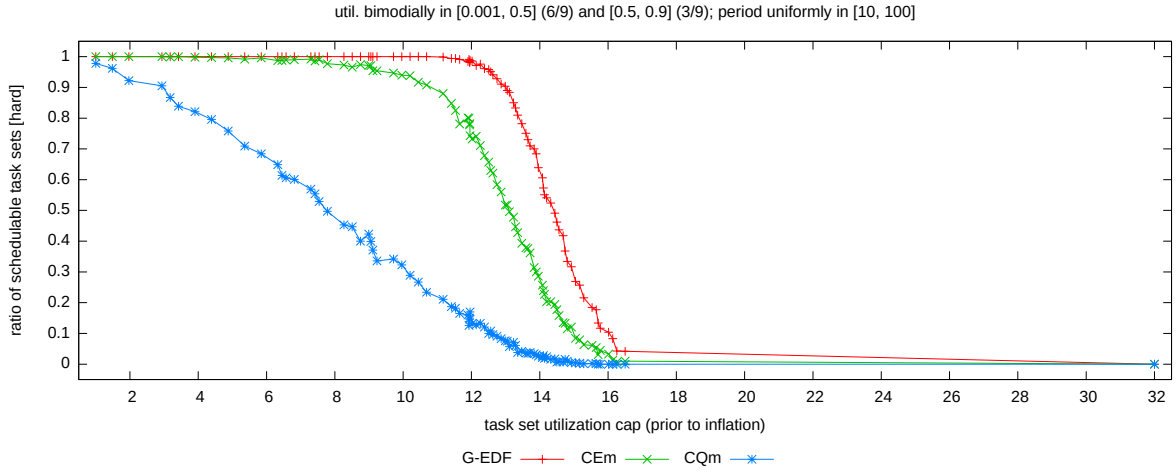

(b)

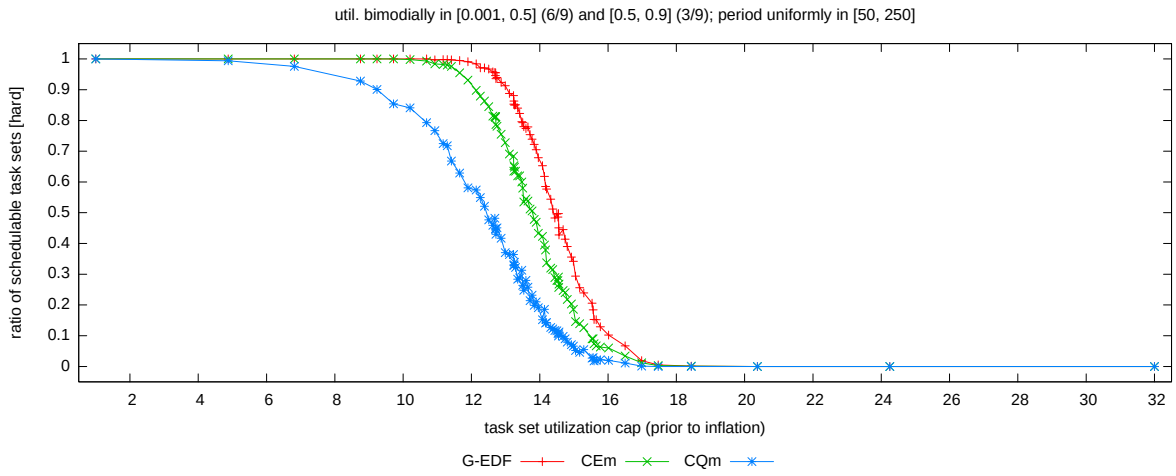

(c)

Figure 105: Comparison of CEm and CQm (event- vs. quantum-driven scheduling) in terms of hard schedulability of task sets with bimodal medium per-task utilizations and **(a)** short, **(b)** moderate, and **(c)** long periods. These graphs correspond to Fig. 21.

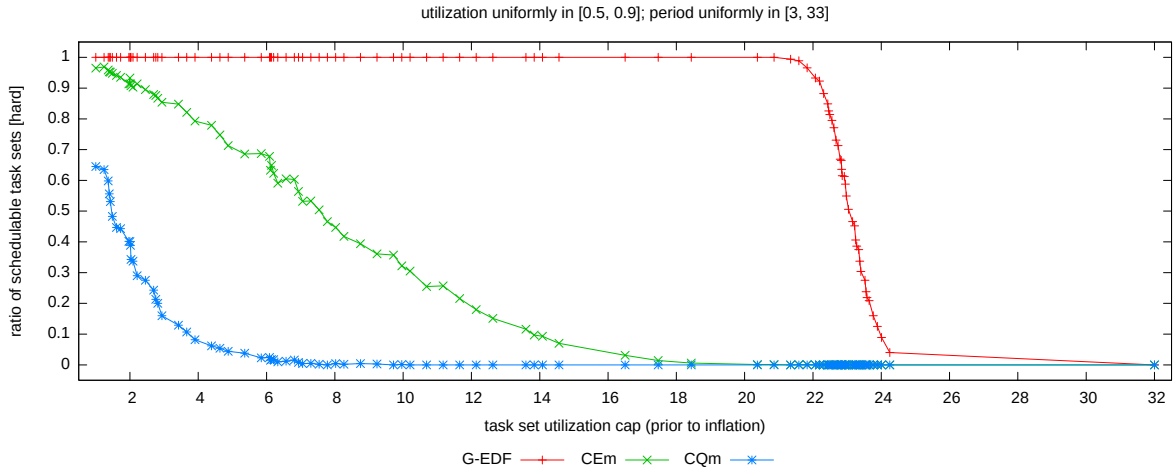

(a)

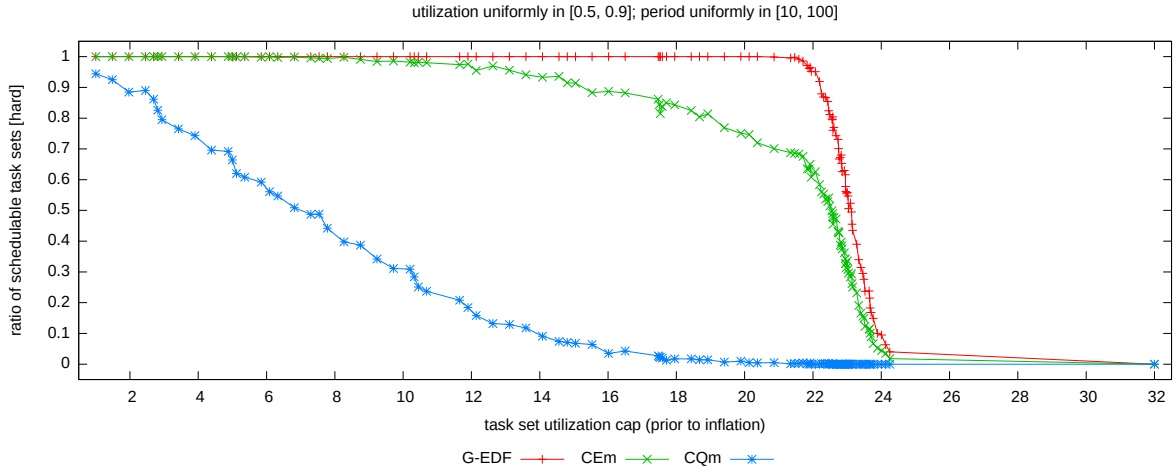

(b)

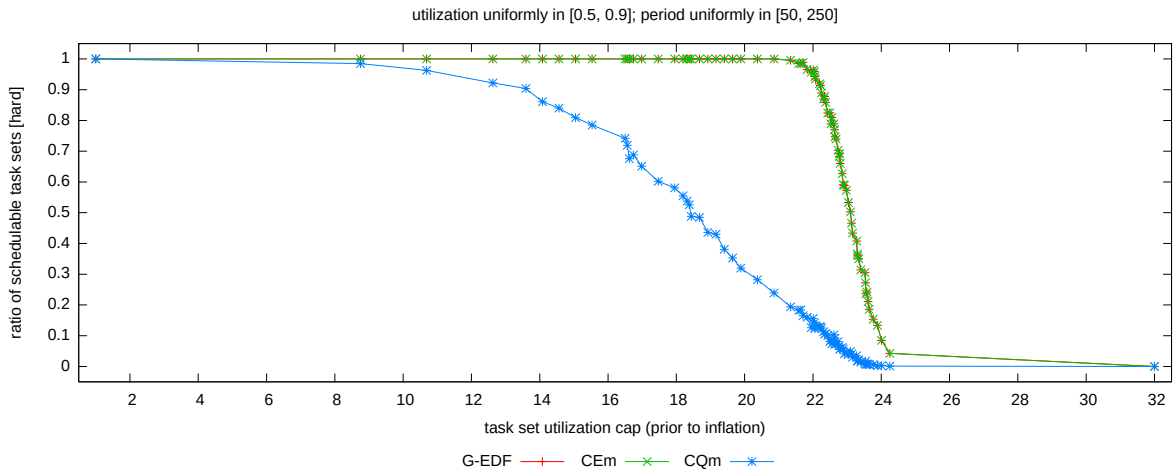

(c)

Figure 106: Comparison of CEm and CQm (event- vs. quantum-driven scheduling) in terms of hard schedulability of task sets with uniform heavy per-task utilizations and **(a)** short, **(b)** moderate, and **(c)** long periods. These graphs correspond to Fig. 22.

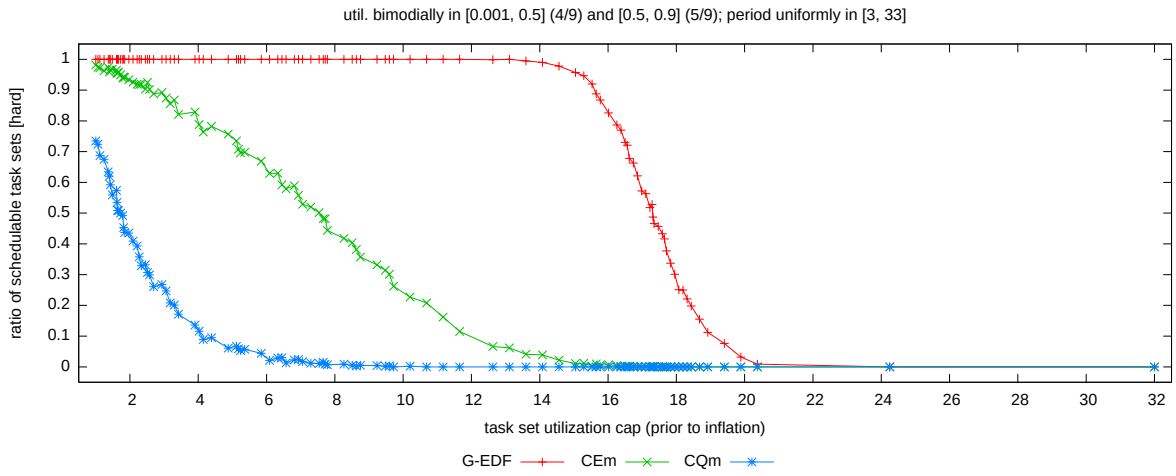

(a)

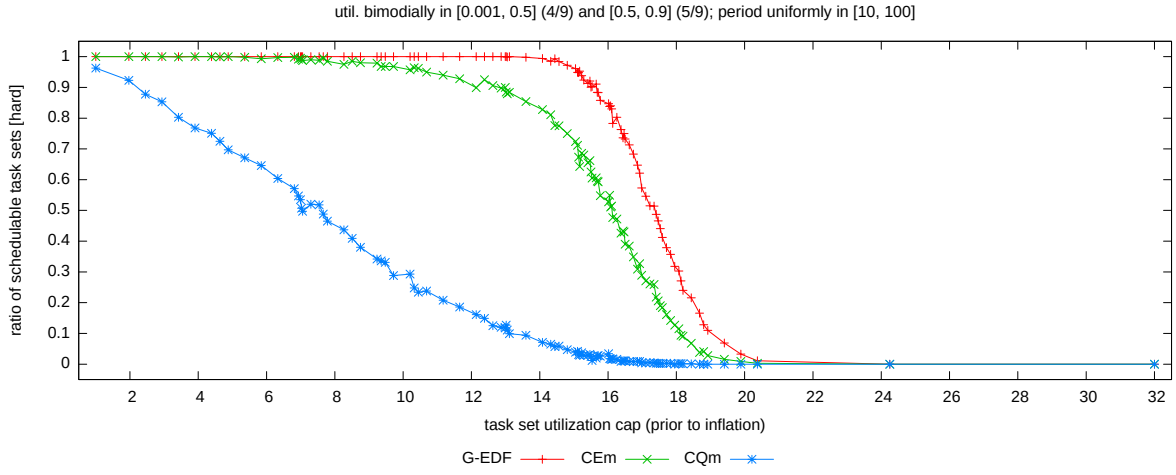

(b)

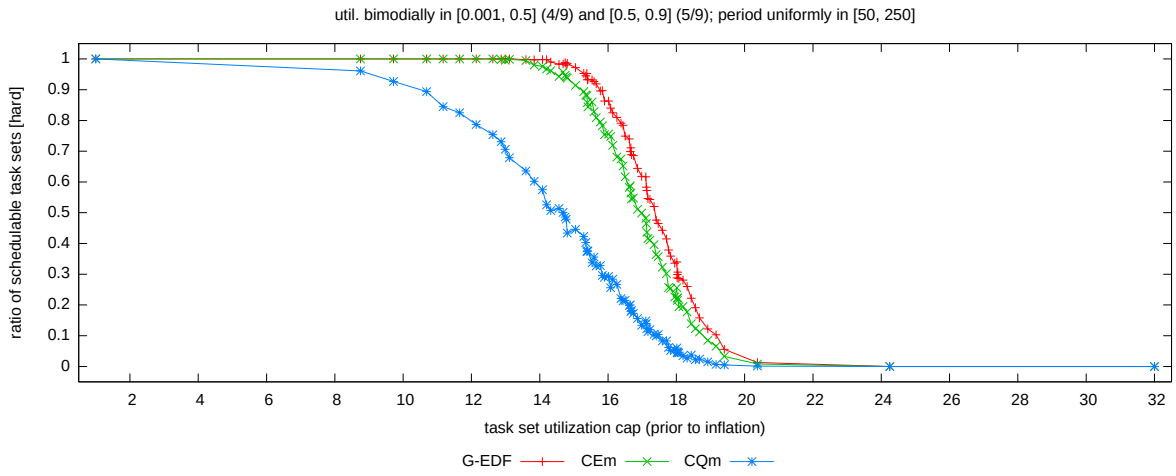

(c)

Figure 107: Comparison of CEm and CQm (event- vs. quantum-driven scheduling) in terms of hard schedulability of task sets with bimodal heavy per-task utilizations and **(a)** short, **(b)** moderate, and **(c)** long periods. These graphs correspond to Fig. 23.

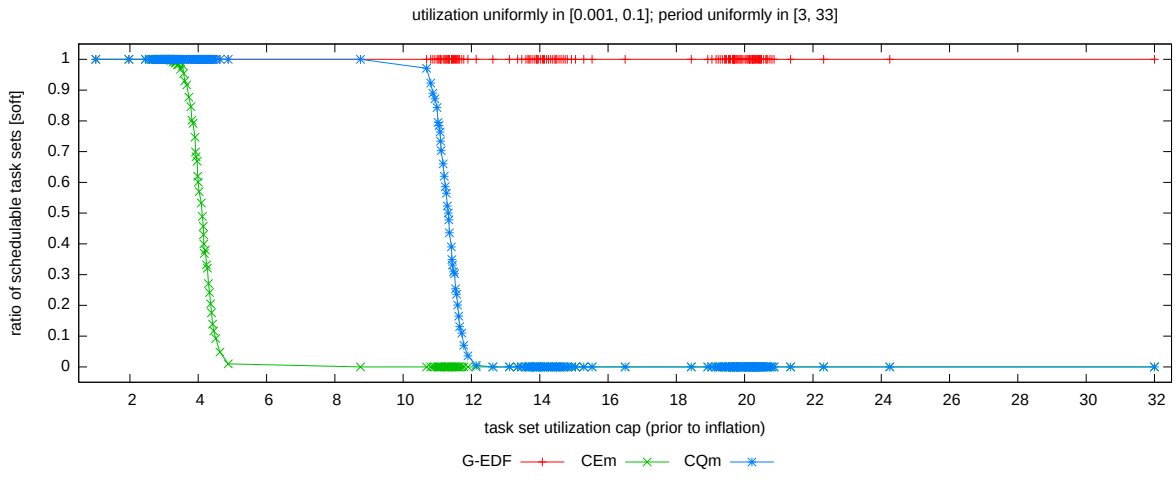

(a)

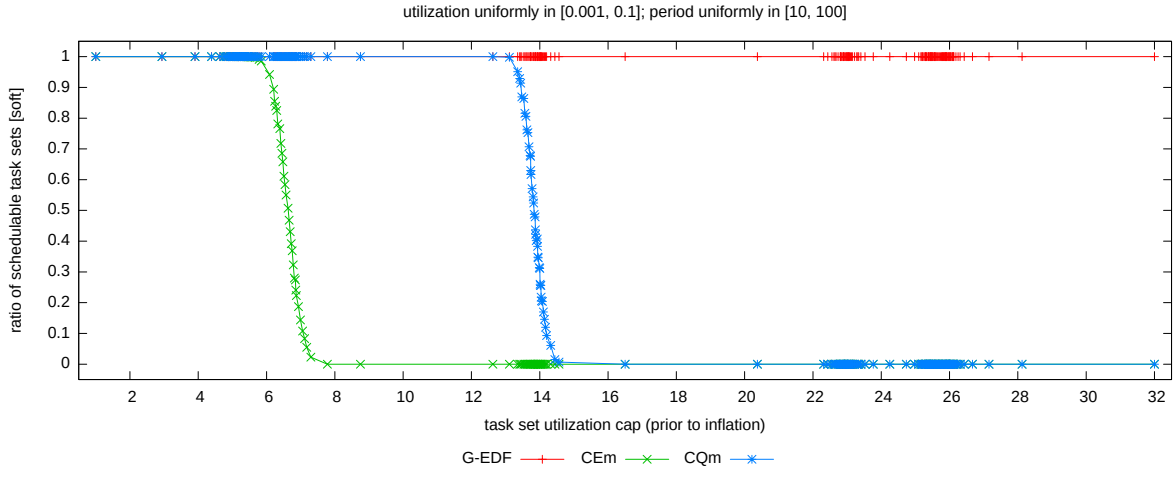

(b)

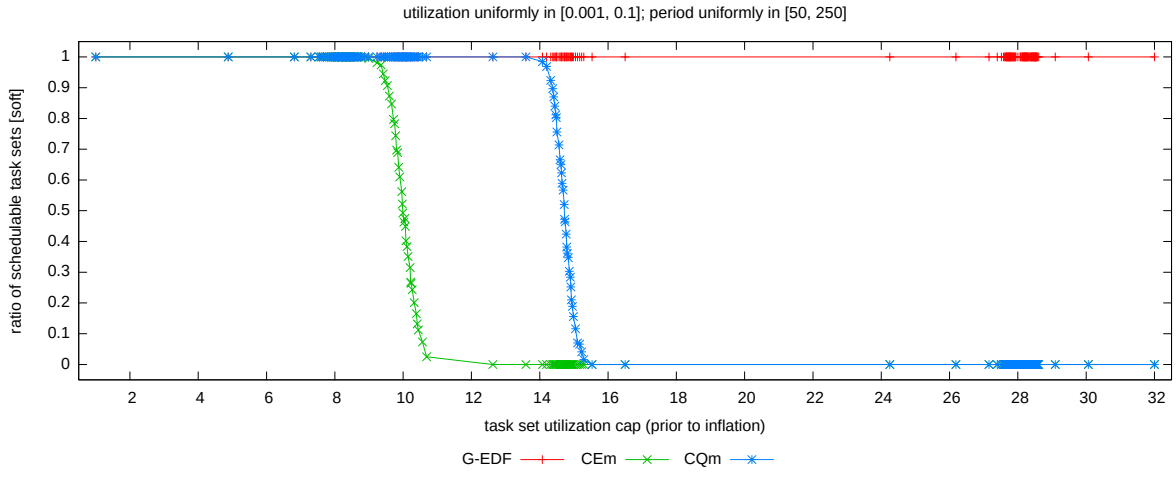

(c)

Figure 108: Comparison of CEm and CQm (event- vs. quantum-driven scheduling) in terms of soft schedulability of task sets with uniform light per-task utilizations and **(a)** short, **(b)** moderate, and **(c)** long periods. These graphs correspond to Fig. 24.

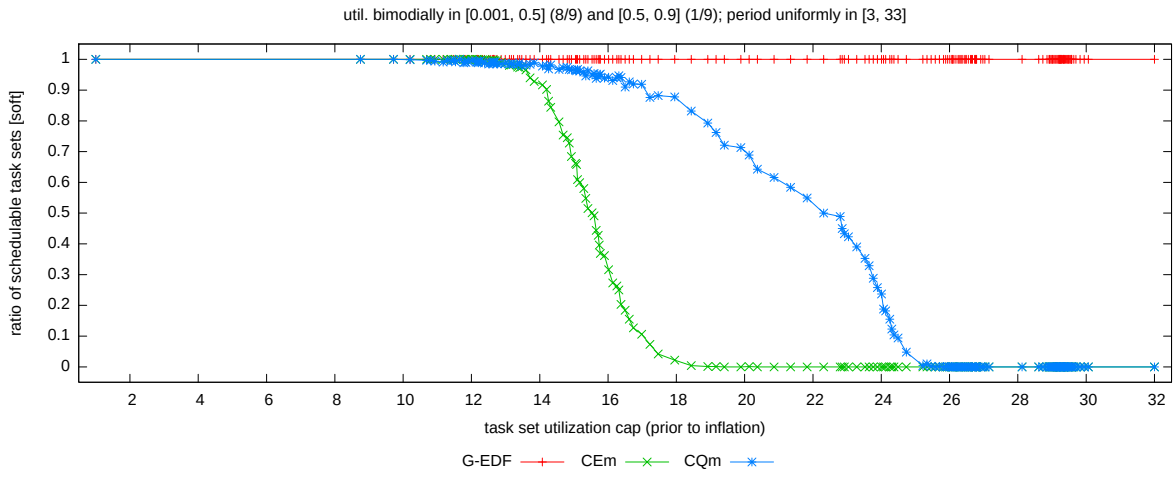

(a)

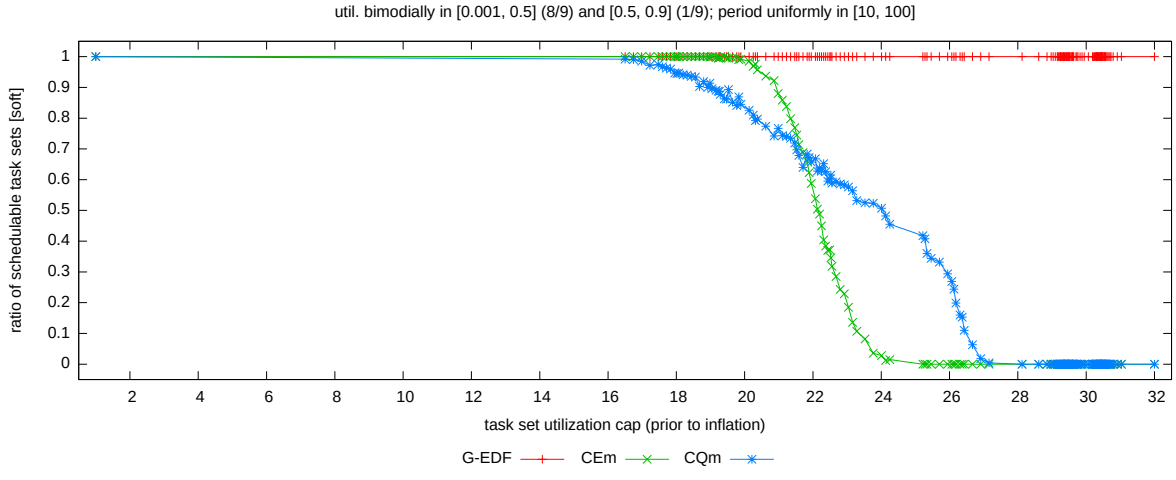

(b)

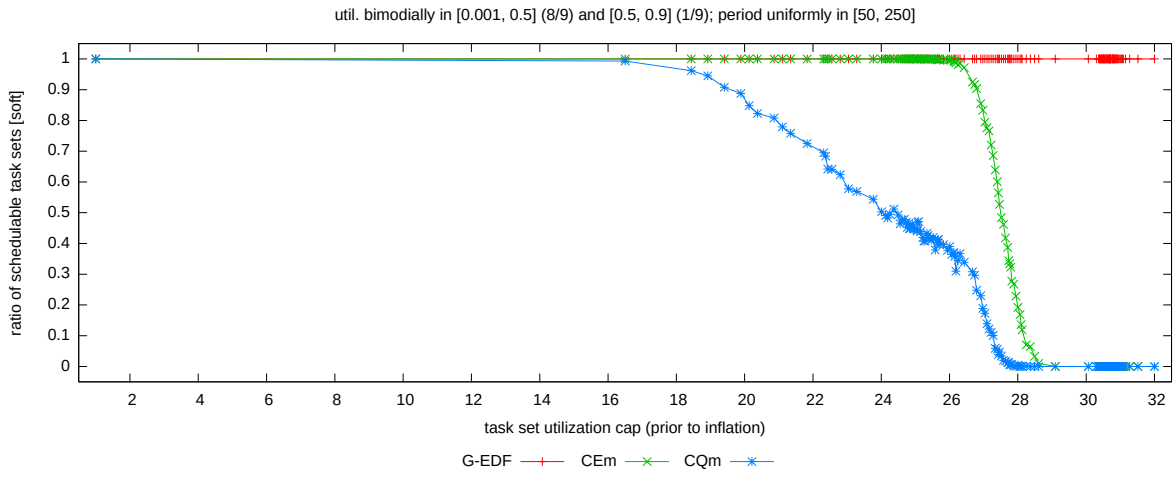

(c)

Figure 109: Comparison of CEm and CQm (event- vs. quantum-driven scheduling) in terms of soft schedulability of task sets with bimodal light per-task utilizations and **(a)** short, **(b)** moderate, and **(c)** long periods. These graphs correspond to Fig. 25.

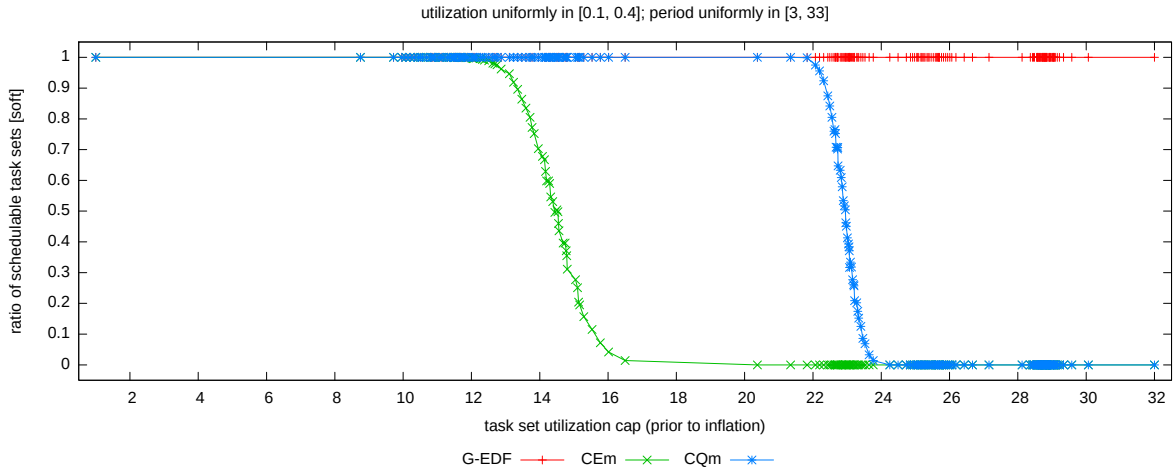

(a)

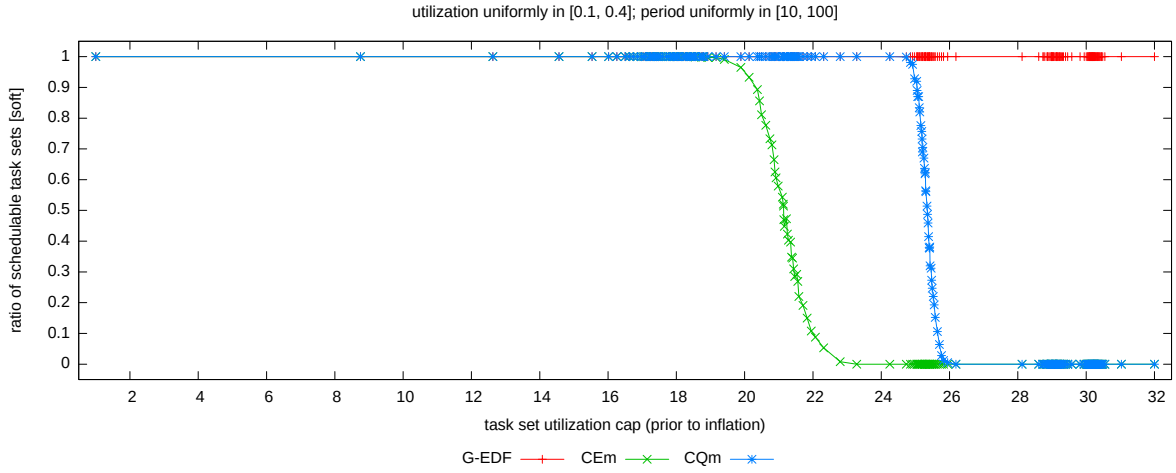

(b)

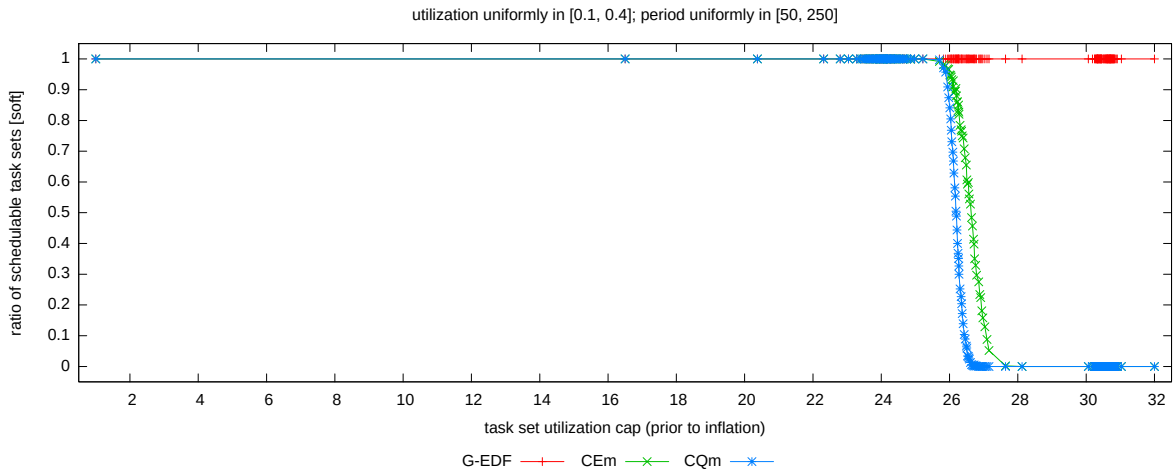

(c)

Figure 110: Comparison of CEm and CQm (event- vs. quantum-driven scheduling) in terms of soft schedulability of task sets with uniform medium per-task utilizations and **(a)** short, **(b)** moderate, and **(c)** long periods. These graphs correspond to Fig. 26.

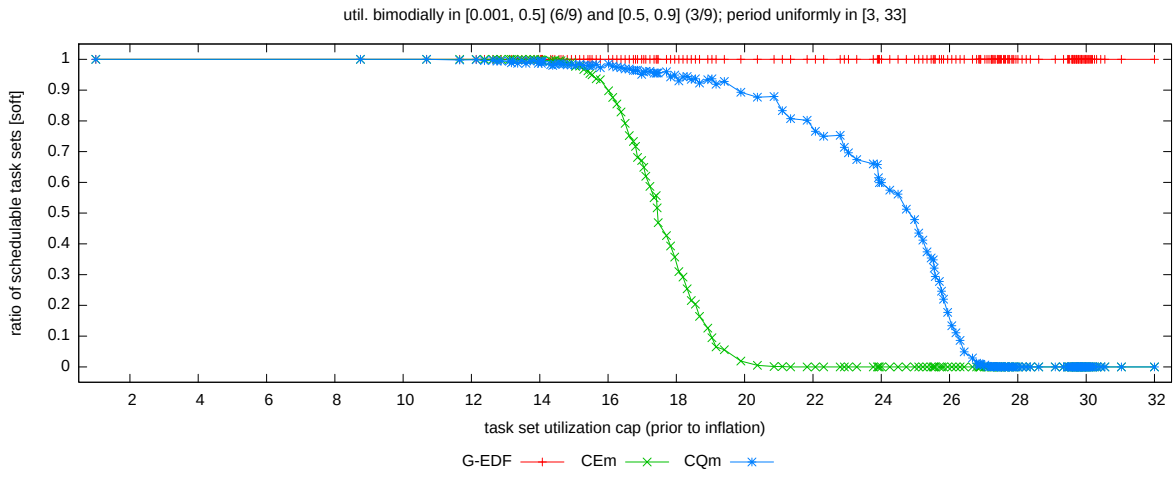

(a)

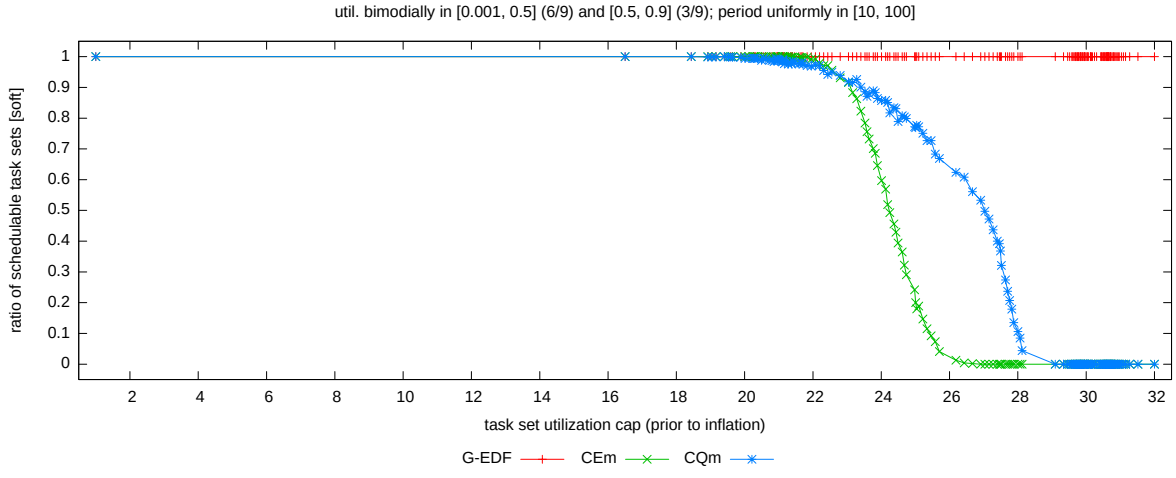

(b)

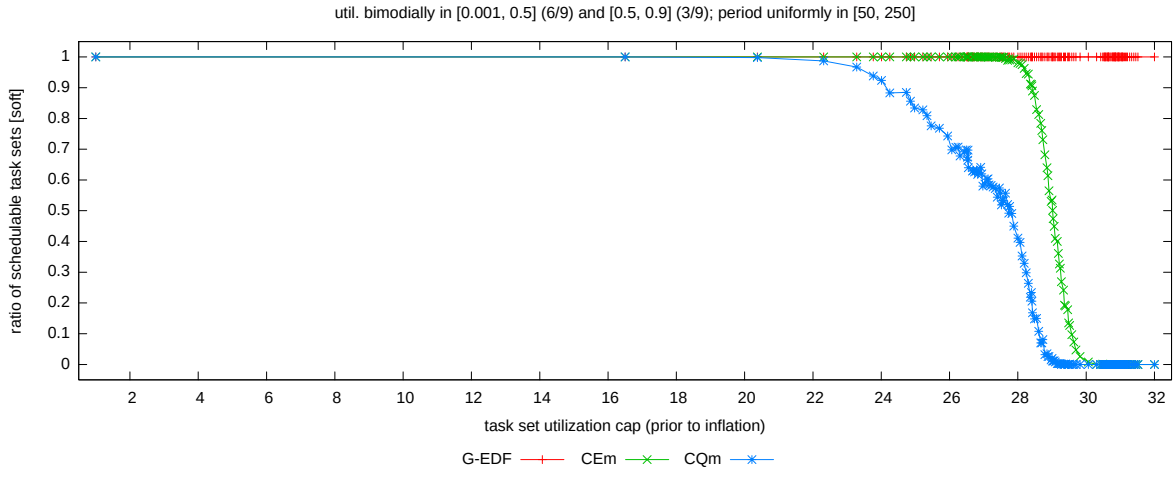

(c)

Figure 111: Comparison of CEm and CQm (event- vs. quantum-driven scheduling) in terms of soft schedulability of task sets with bimodal medium per-task utilizations and **(a)** short, **(b)** moderate, and **(c)** long periods. These graphs correspond to Fig. 27.

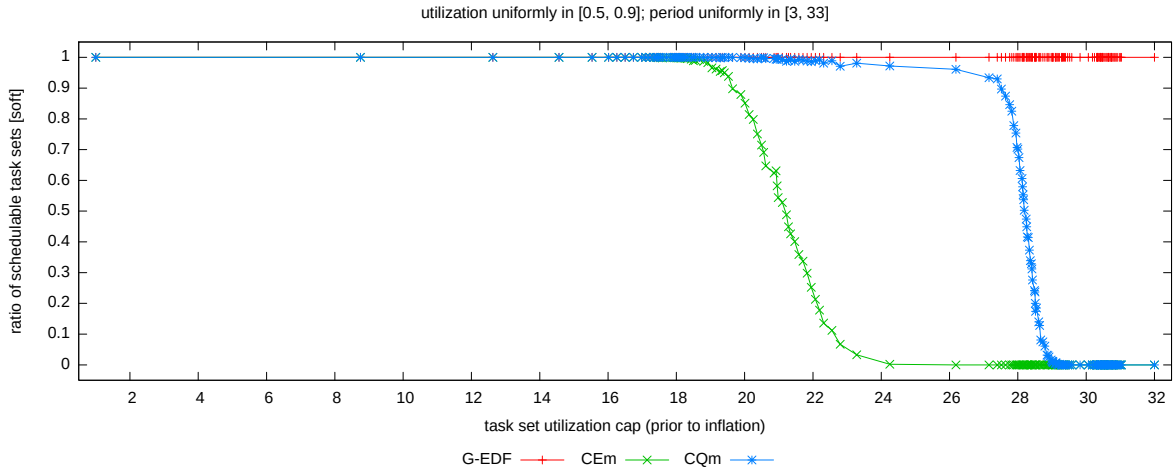

(a)

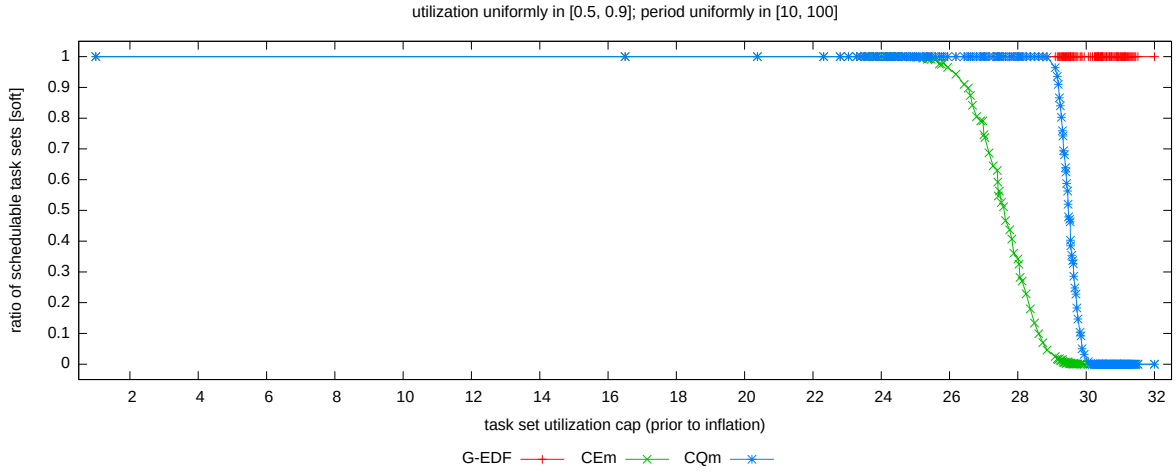

(b)

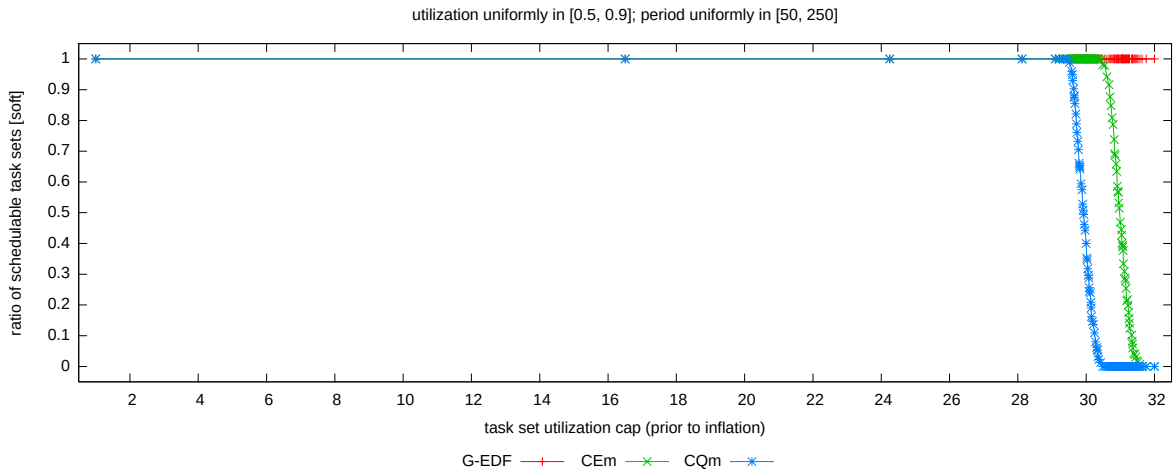

(c)

Figure 112: Comparison of CEm and CQm (event- vs. quantum-driven scheduling) in terms of soft schedulability of task sets with uniform heavy per-task utilizations and **(a)** short, **(b)** moderate, and **(c)** long periods. These graphs correspond to Fig. 28.

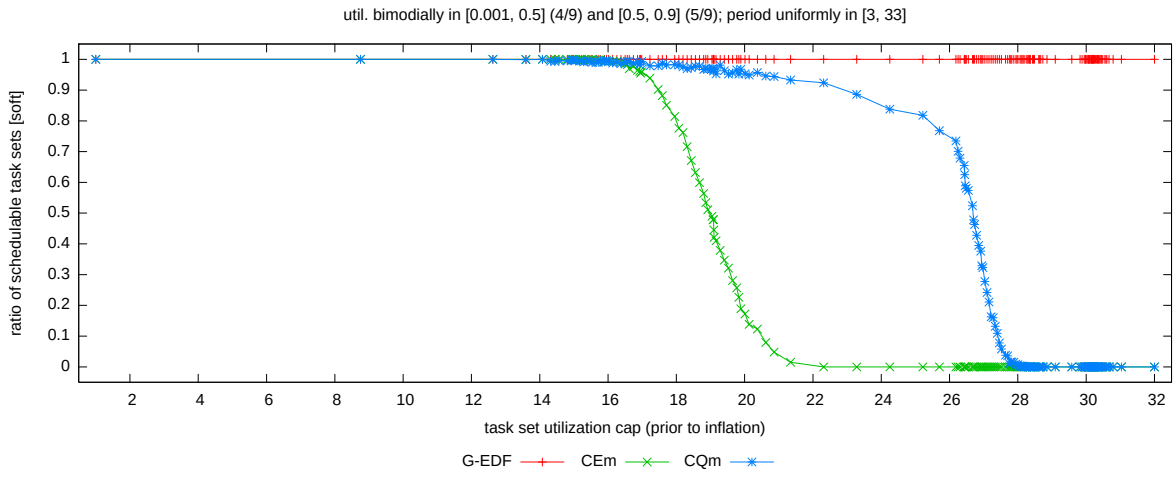

(a)

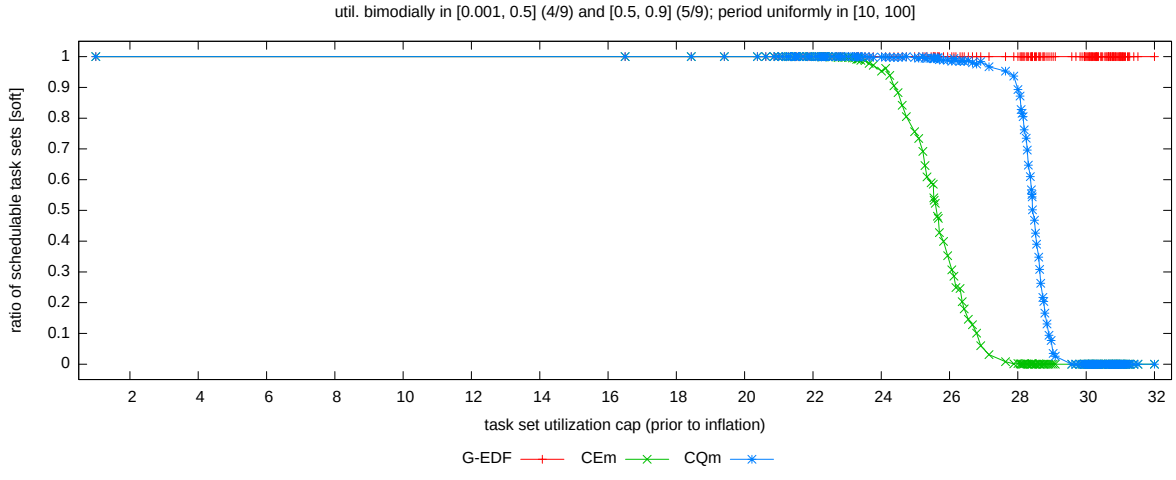

(b)

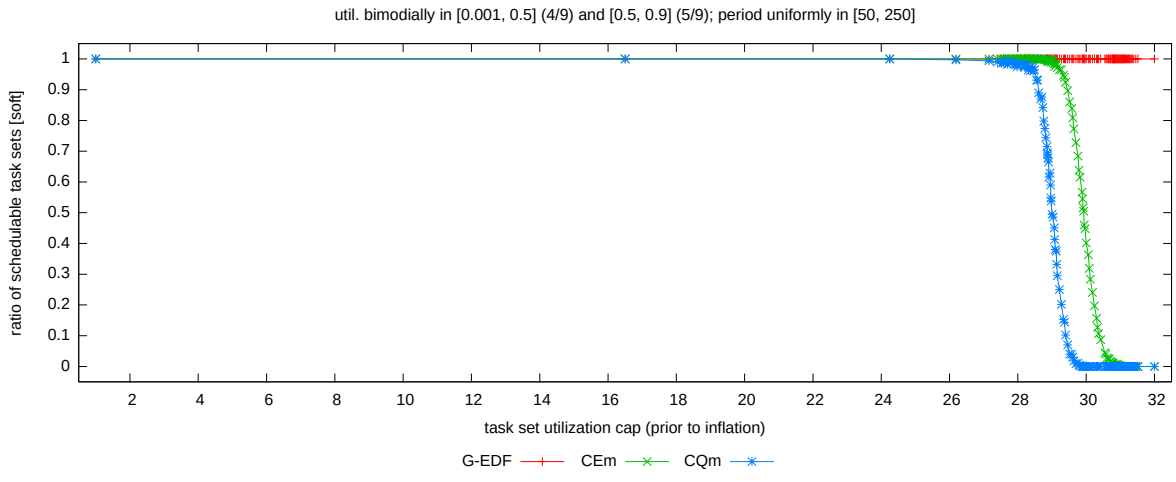

(c)

Figure 113: Comparison of CEm and CQm (event- vs. quantum-driven scheduling) in terms of soft schedulability of task sets with bimodal heavy per-task utilizations and **(a)** short, **(b)** moderate, and **(c)** long periods. These graphs correspond to Fig. 29.

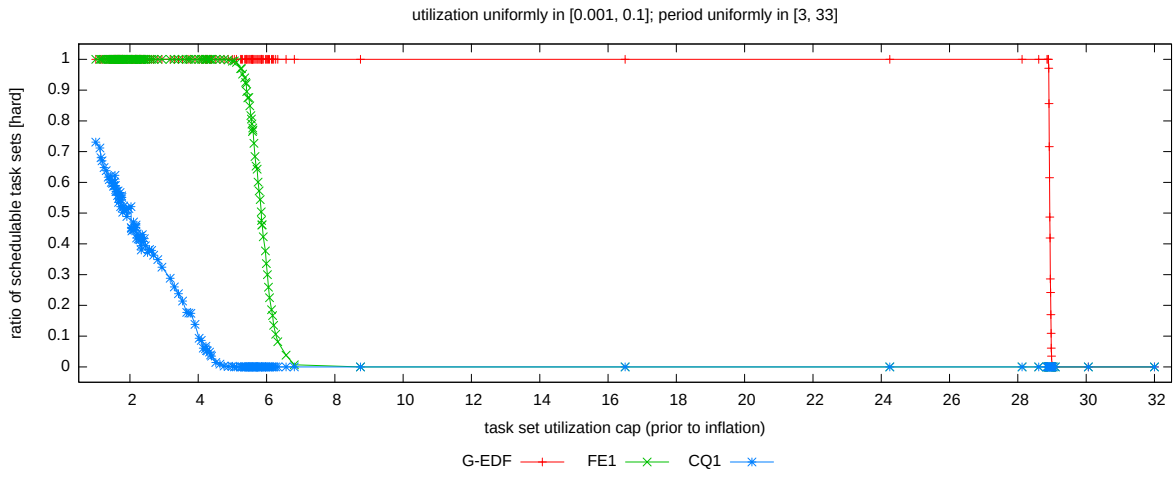

(a)

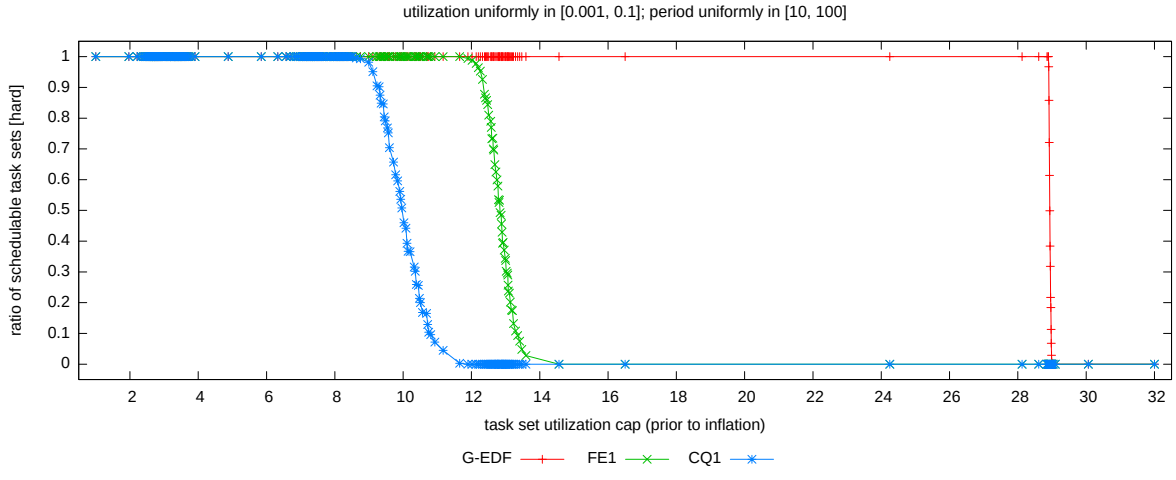

(b)

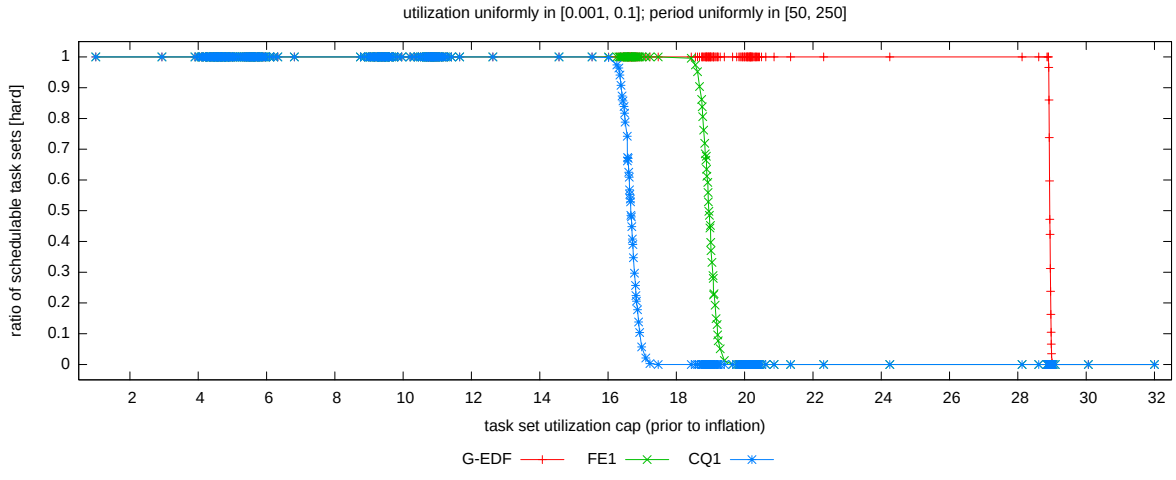

(c)

Figure 114: Comparison of FE1 and CQ1 (event- vs. quantum-driven scheduling) in terms of hard schedulability of task sets with uniform light per-task utilizations and **(a)** short, **(b)** moderate, and **(c)** long periods. These graphs correspond to Fig. 18.

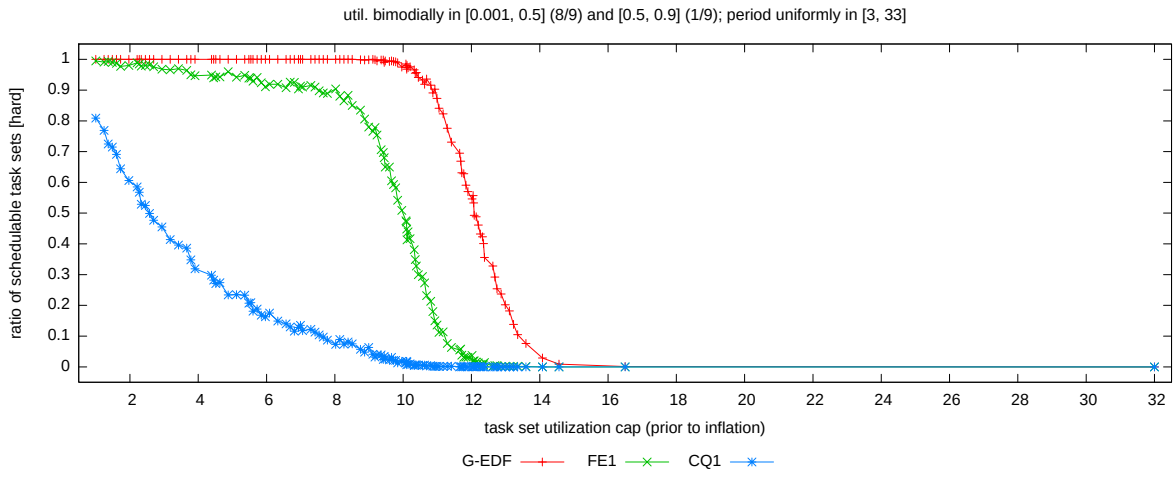

(a)

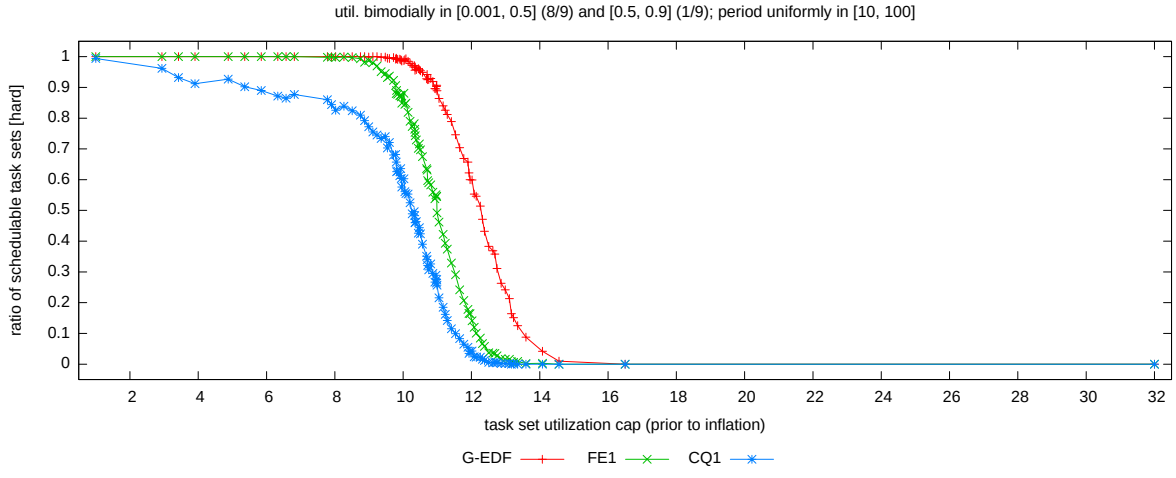

(b)

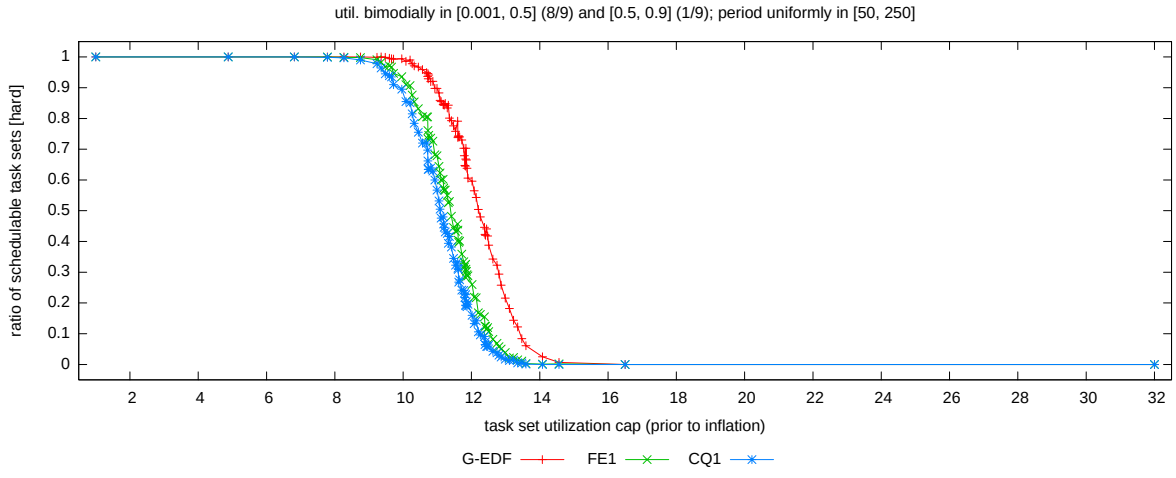

(c)

Figure 115: Comparison of FE1 and CQ1 (event- vs. quantum-driven scheduling) in terms of hard schedulability of task sets with bimodal light per-task utilizations and **(a)** short, **(b)** moderate, and **(c)** long periods. These graphs correspond to Fig. 19.

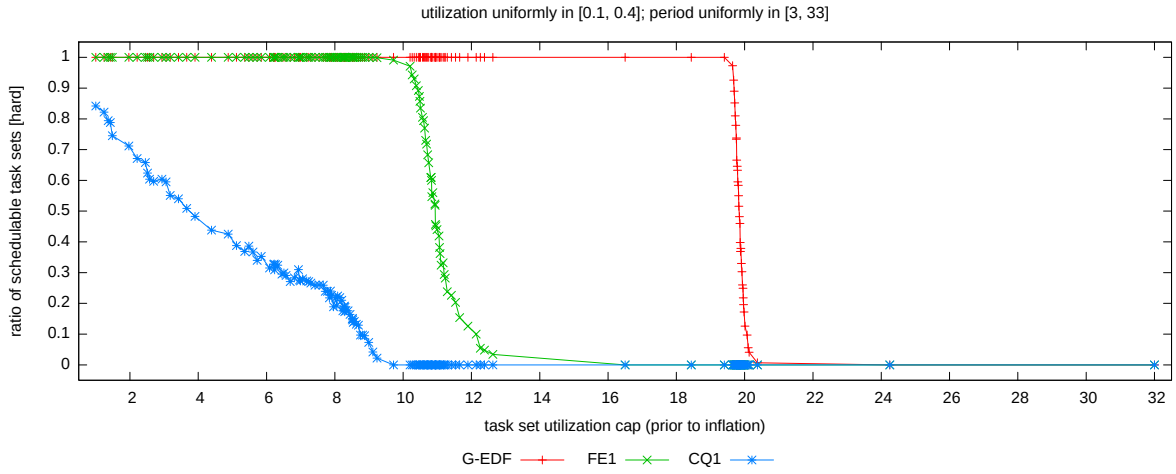

(a)

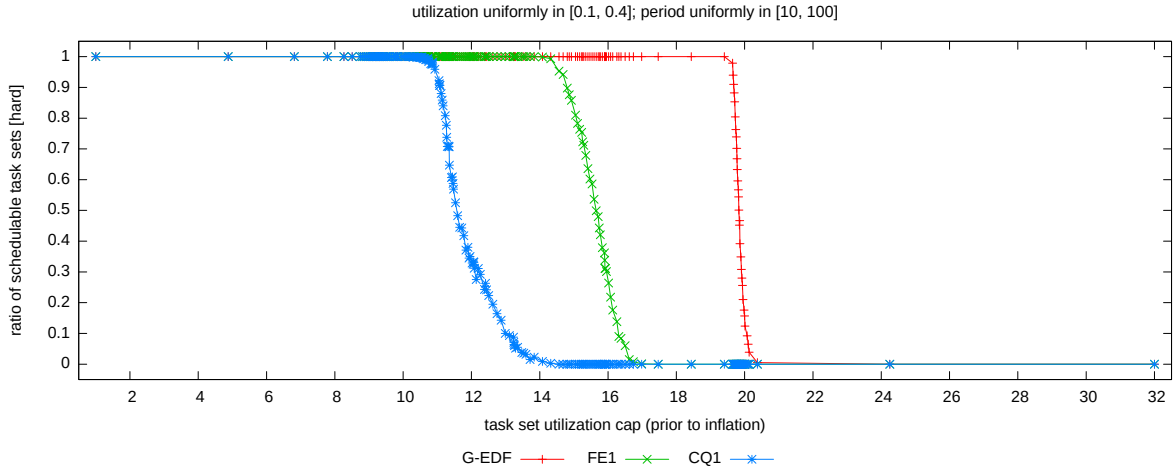

(b)

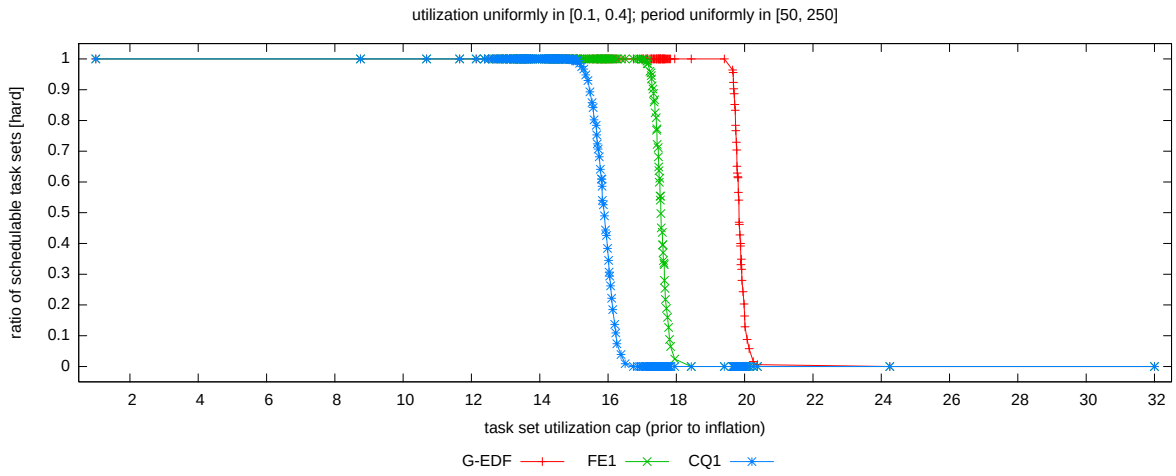

(c)

Figure 116: Comparison of FE1 and CQ1 (event- vs. quantum-driven scheduling) in terms of hard schedulability of task sets with uniform medium per-task utilizations and **(a)** short, **(b)** moderate, and **(c)** long periods. These graphs correspond to Fig. 20.

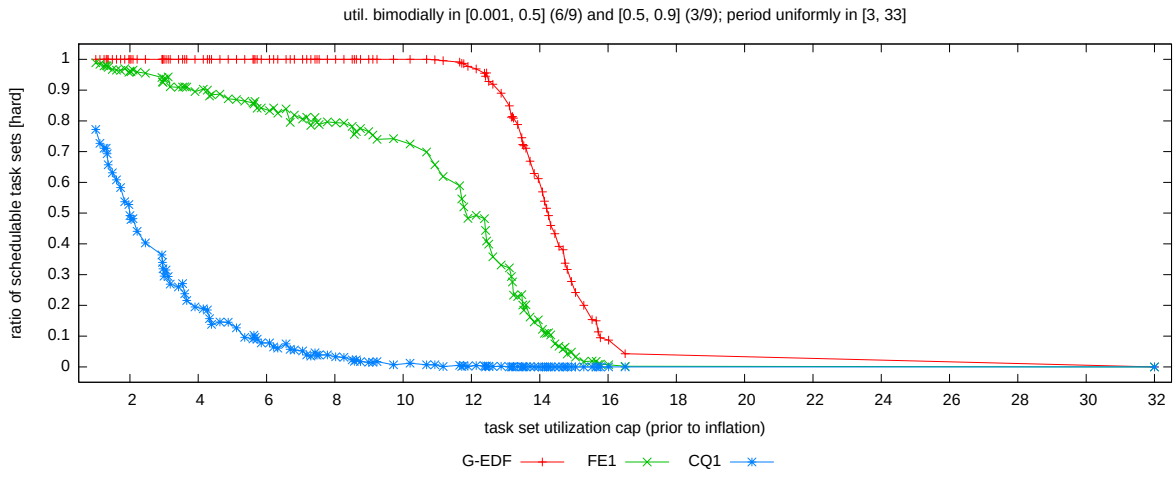

(a)

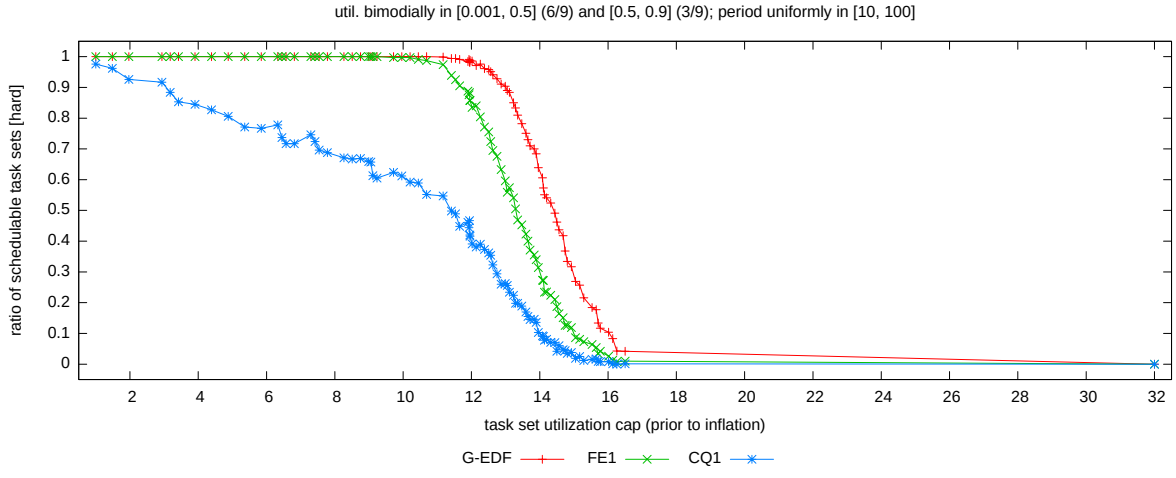

(b)

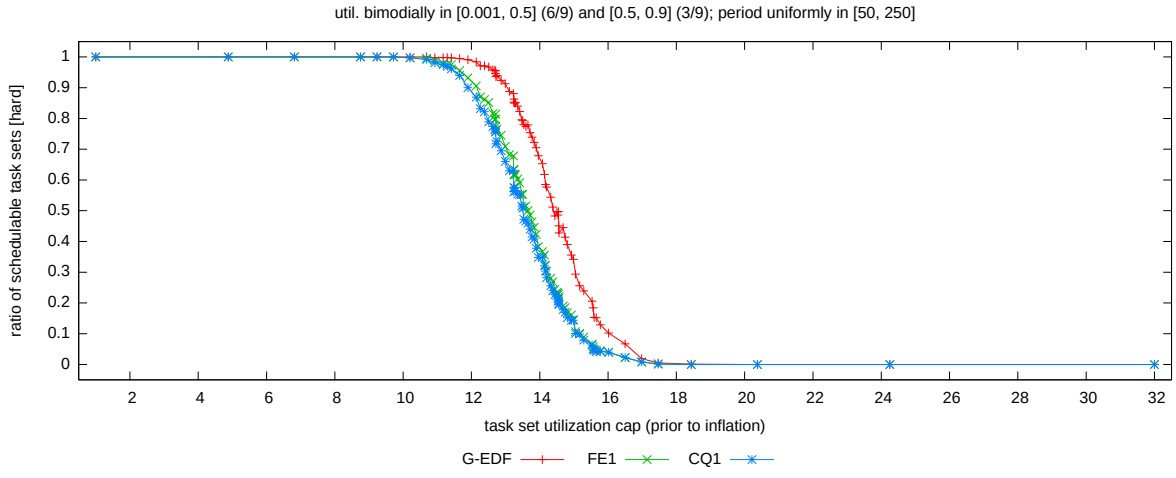

(c)

Figure 117: Comparison of FE1 and CQ1 (event- vs. quantum-driven scheduling) in terms of hard schedulability of task sets with bimodal medium per-task utilizations and **(a)** short, **(b)** moderate, and **(c)** long periods. These graphs correspond to Fig. 21.

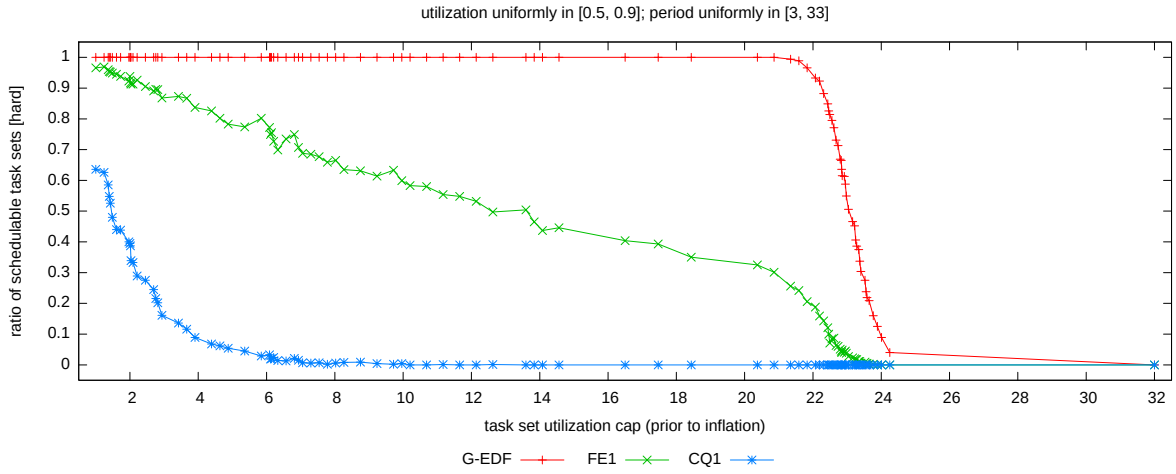

(a)

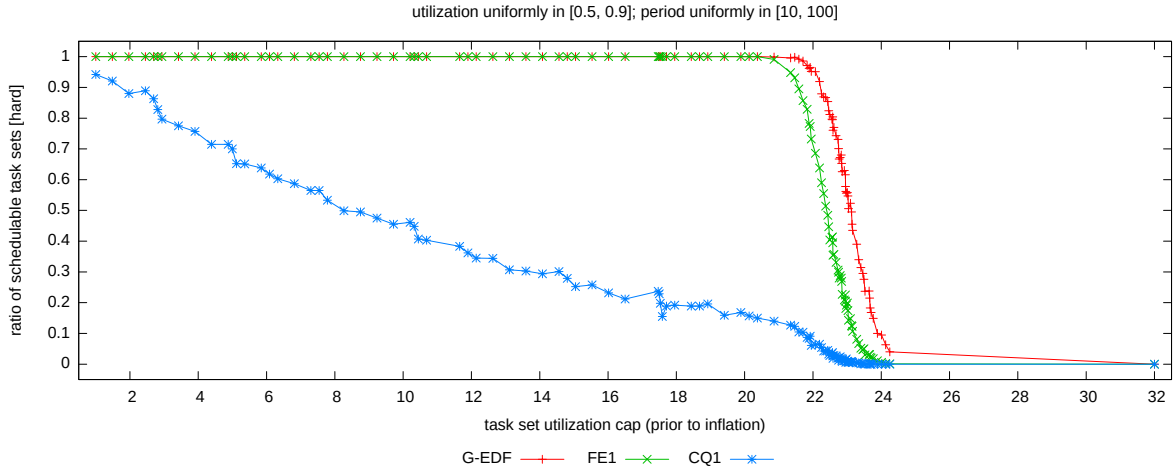

(b)

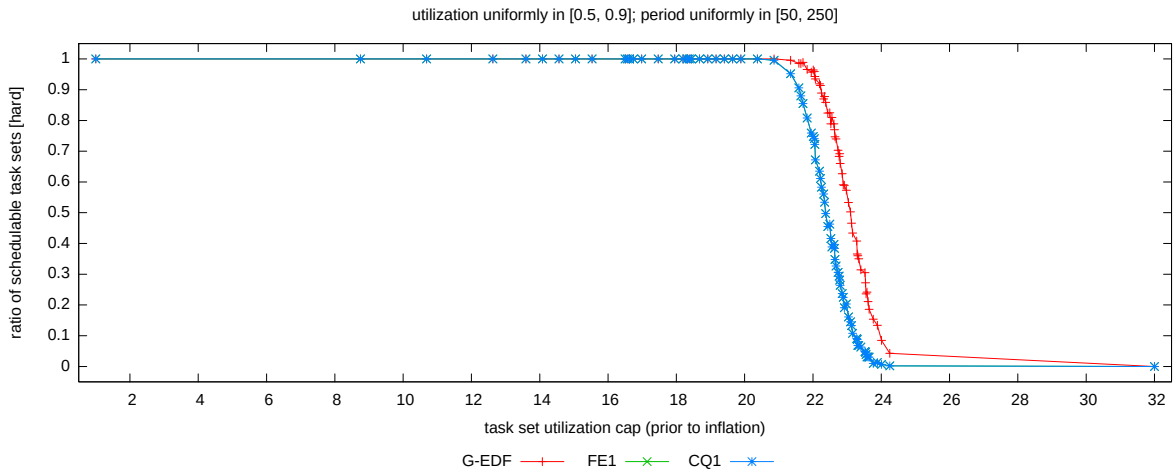

(c)

Figure 118: Comparison of FE1 and CQ1 (event- vs. quantum-driven scheduling) in terms of hard schedulability of task sets with uniform heavy per-task utilizations and **(a)** short, **(b)** moderate, and **(c)** long periods. These graphs correspond to Fig. 22.

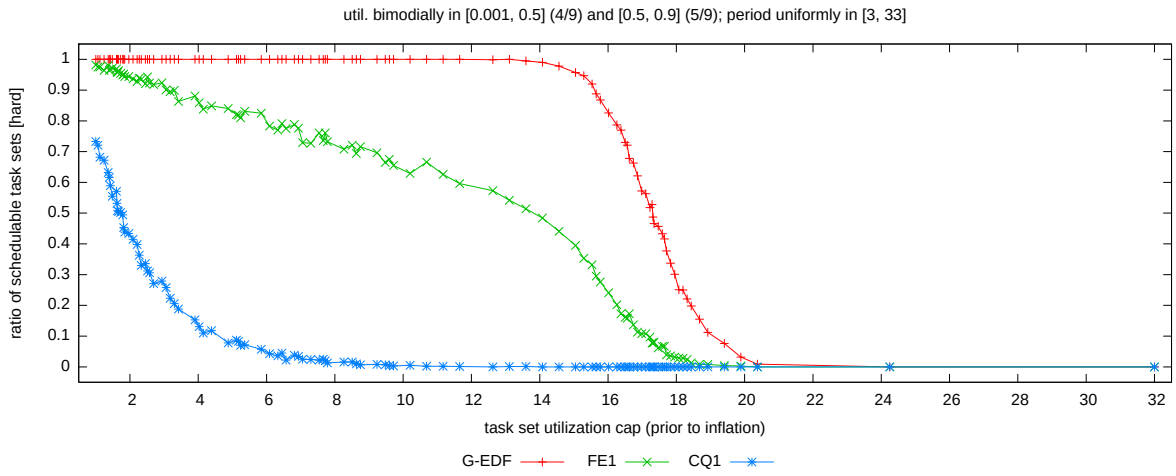

(a)

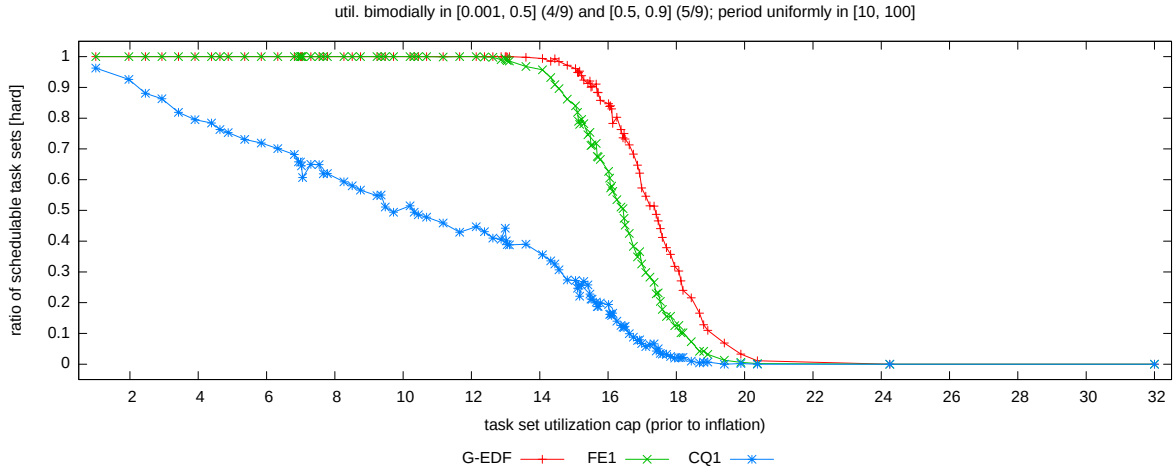

(b)

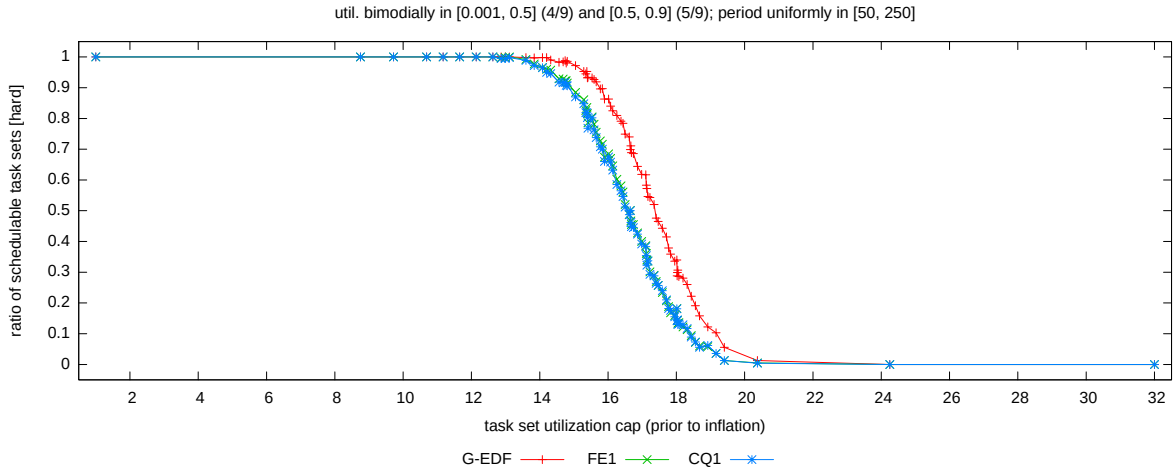

(c)

Figure 119: Comparison of FE1 and CQ1 (event- vs. quantum-driven scheduling) in terms of hard schedulability of task sets with bimodal heavy per-task utilizations and **(a)** short, **(b)** moderate, and **(c)** long periods. These graphs correspond to Fig. 23.

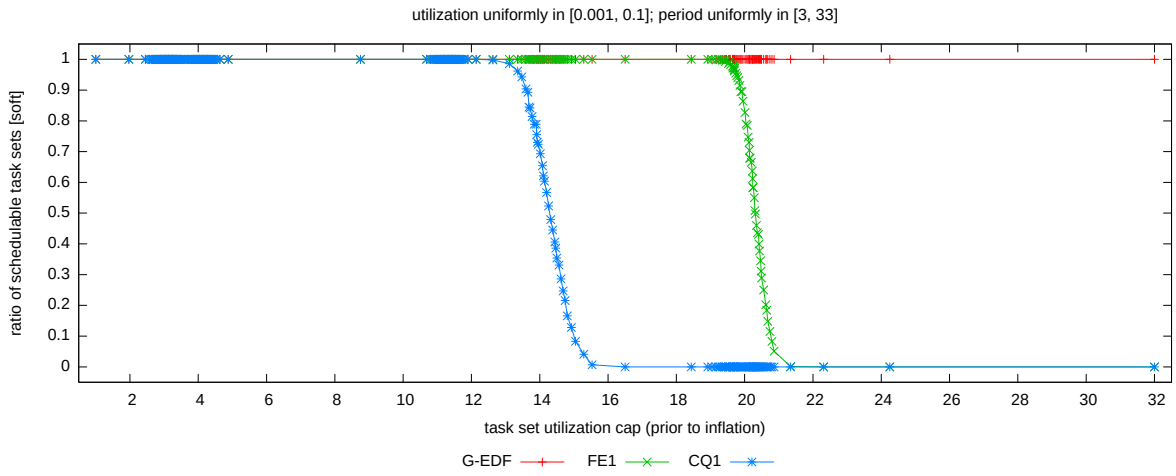

(a)

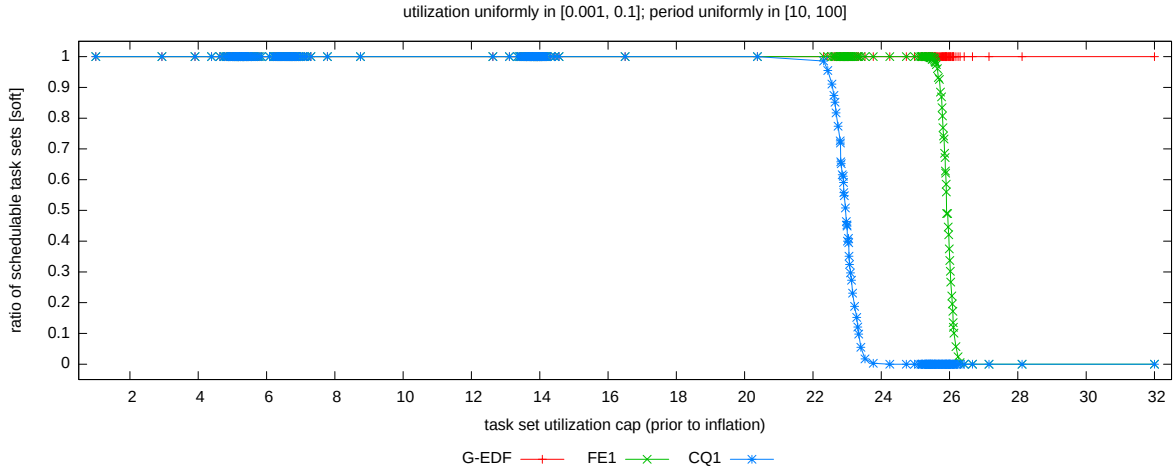

(b)

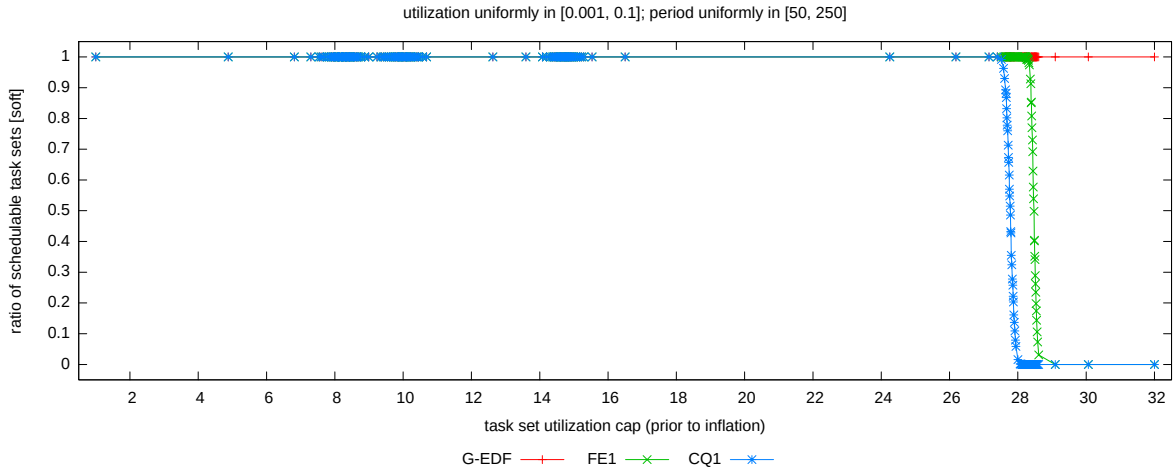

(c)

Figure 120: Comparison of FE1 and CQ1 (event- vs. quantum-driven scheduling) in terms of soft schedulability of task sets with uniform light per-task utilizations and **(a)** short, **(b)** moderate, and **(c)** long periods. These graphs correspond to Fig. 24.

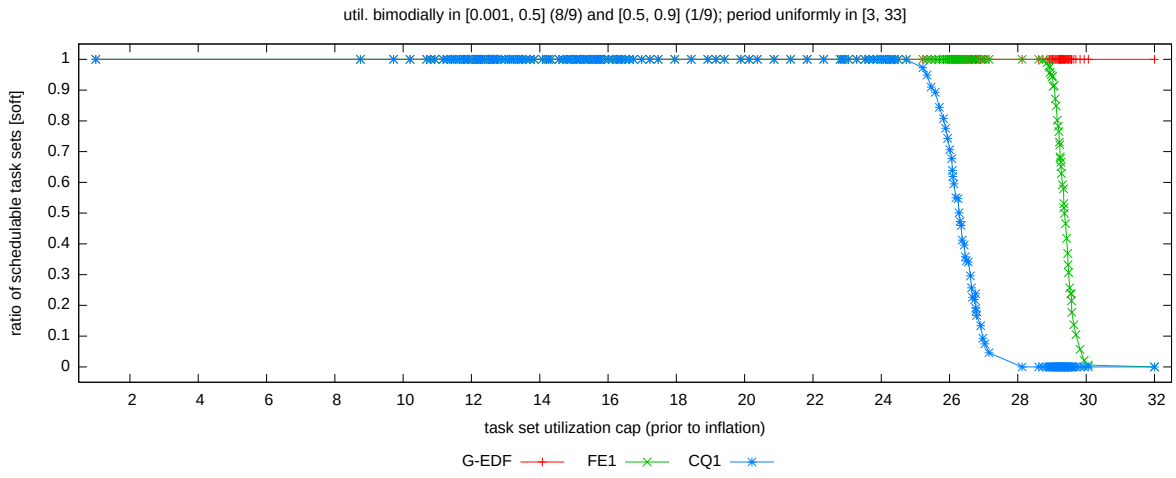

(a)

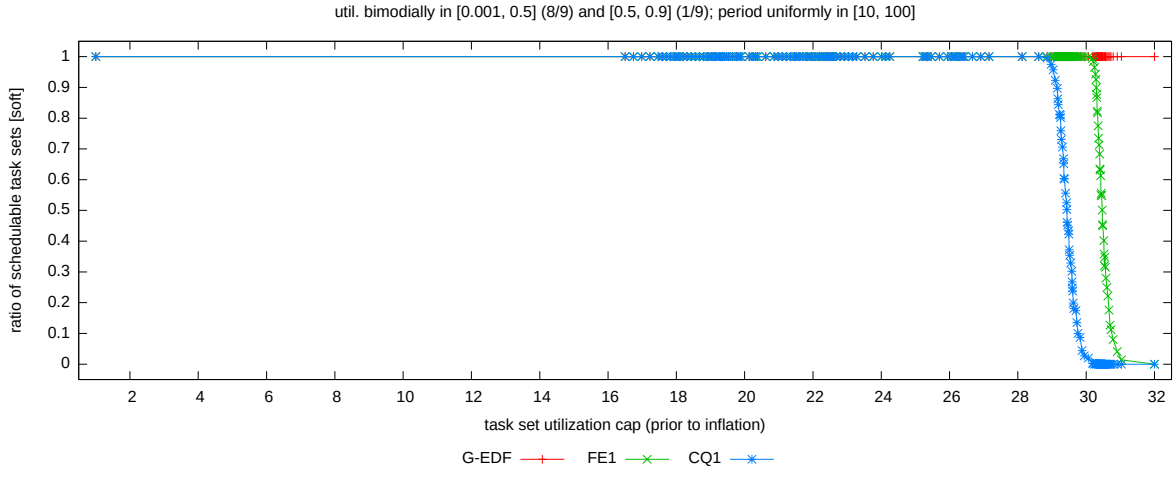

(b)

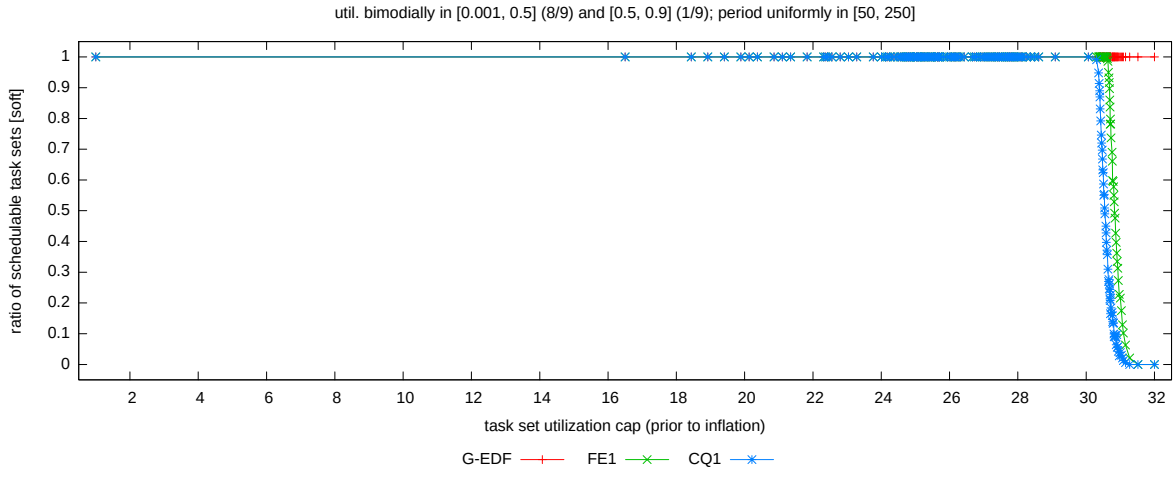

(c)

Figure 121: Comparison of FE1 and CQ1 (event- vs. quantum-driven scheduling) in terms of soft schedulability of task sets with bimodal light per-task utilizations and **(a)** short, **(b)** moderate, and **(c)** long periods. These graphs correspond to Fig. 25.

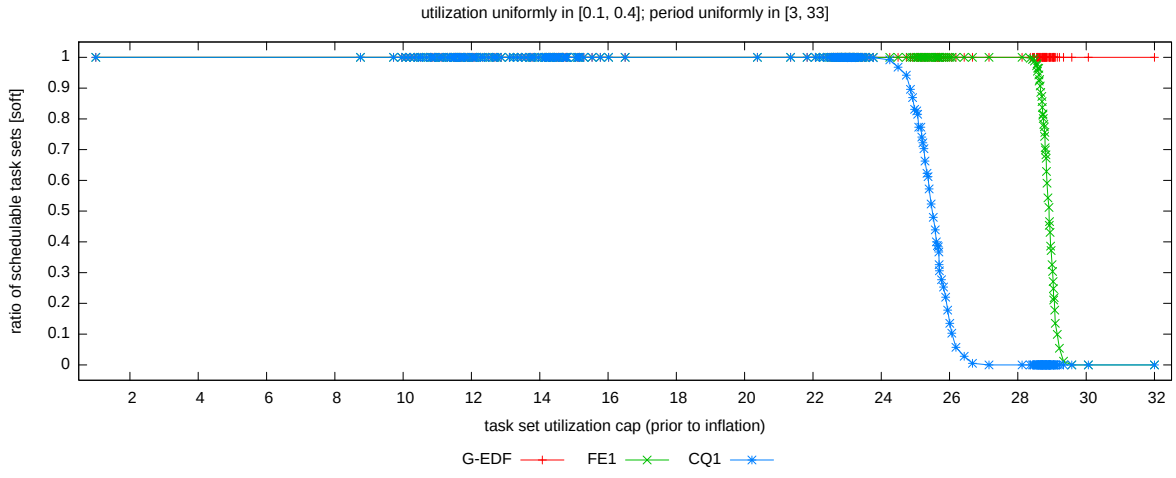

(a)

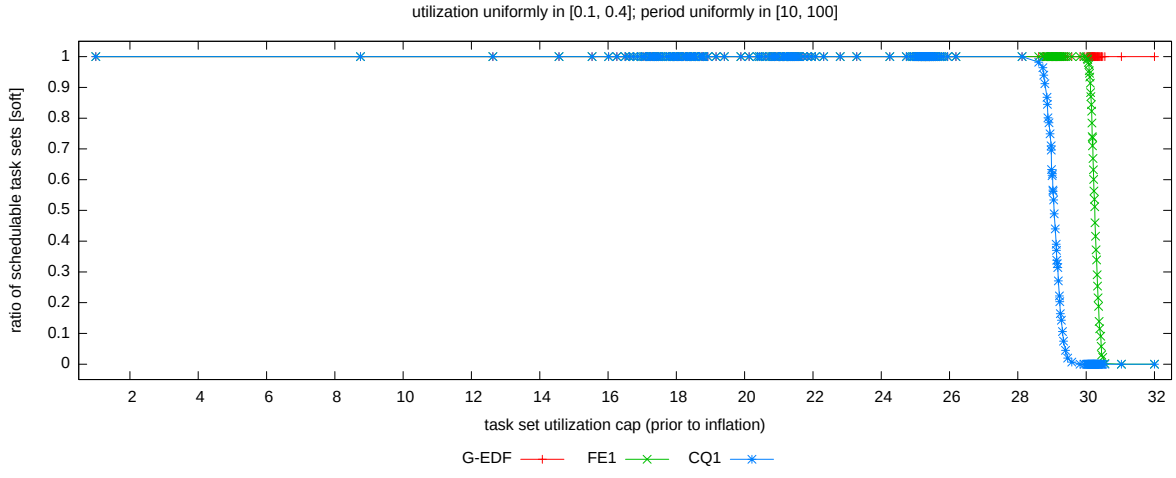

(b)

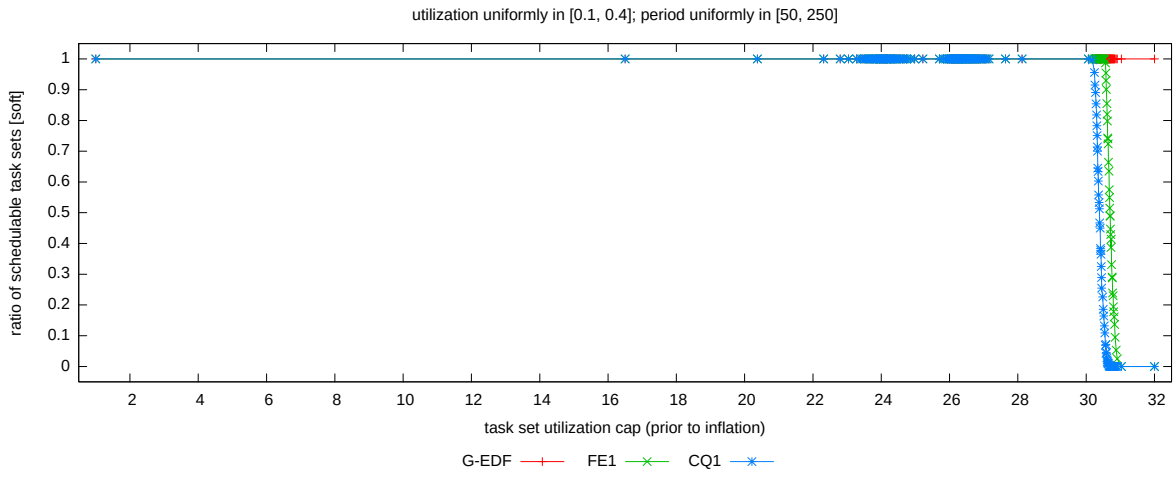

(c)

Figure 122: Comparison of FE1 and CQ1 (event- vs. quantum-driven scheduling) in terms of soft schedulability of task sets with uniform medium per-task utilizations and **(a)** short, **(b)** moderate, and **(c)** long periods. These graphs correspond to Fig. 26.

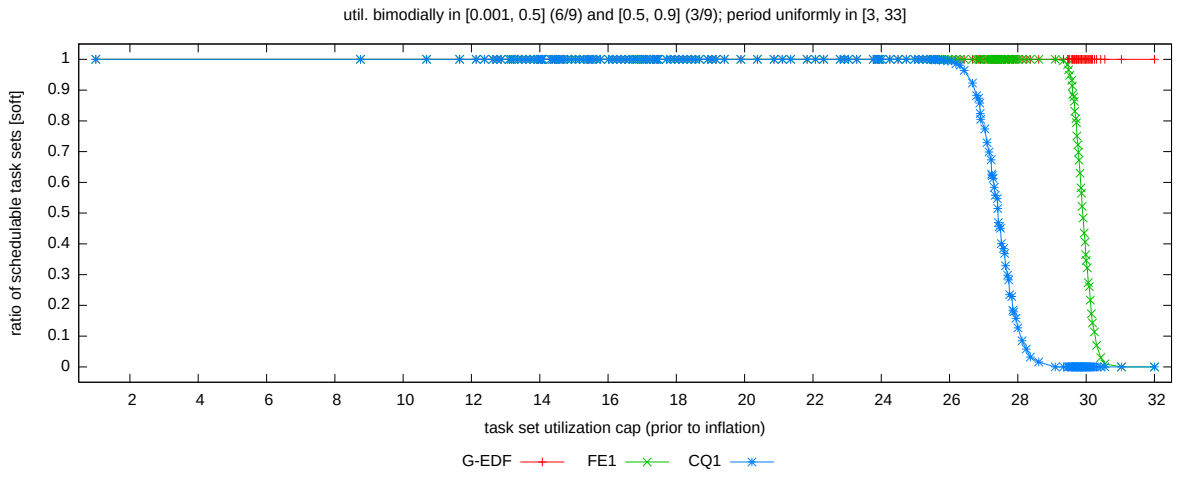

(a)

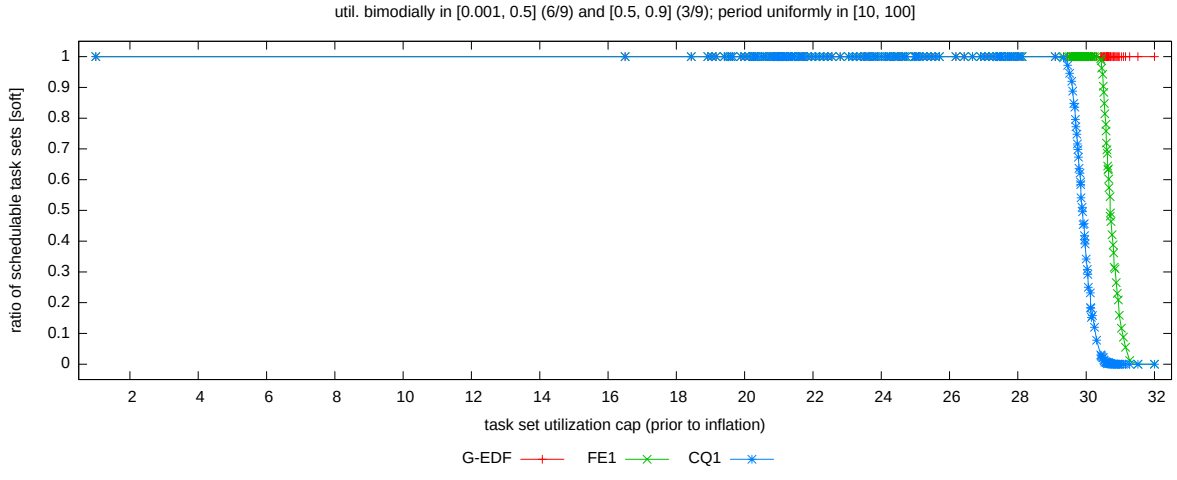

(b)

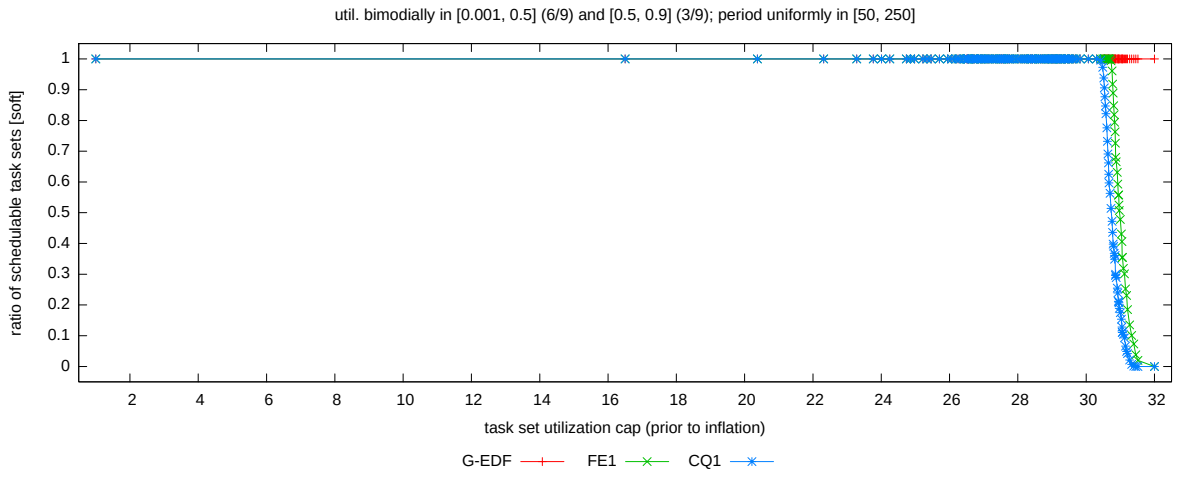

(c)

Figure 123: Comparison of FE1 and CQ1 (event- vs. quantum-driven scheduling) in terms of soft schedulability of task sets with bimodal medium per-task utilizations and **(a)** short, **(b)** moderate, and **(c)** long periods. These graphs correspond to Fig. 27.

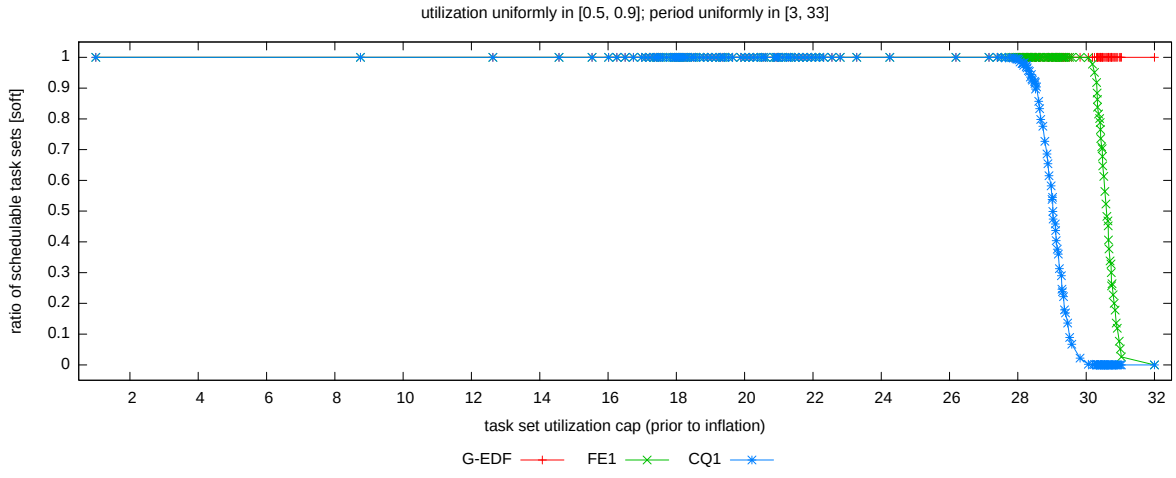

(a)

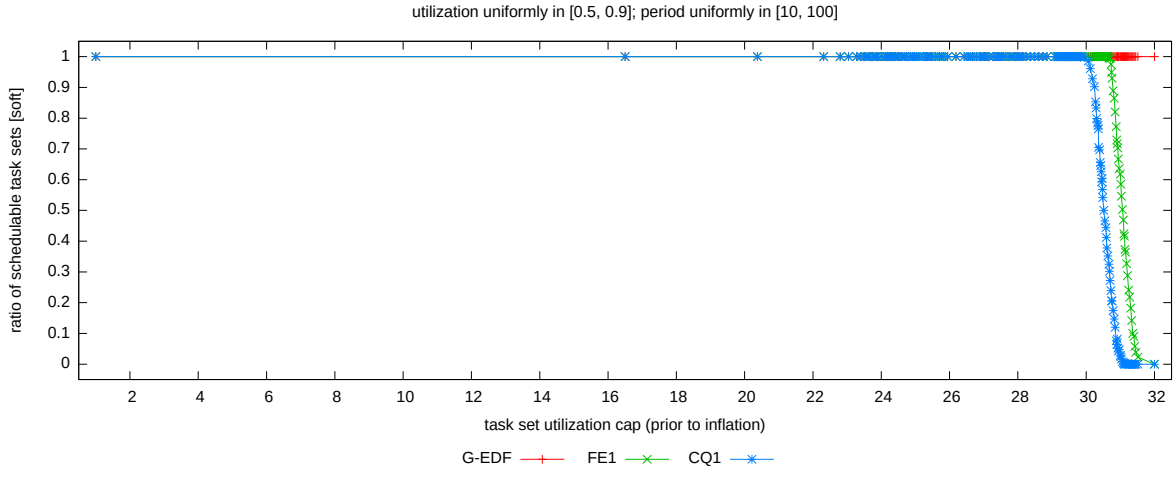

(b)

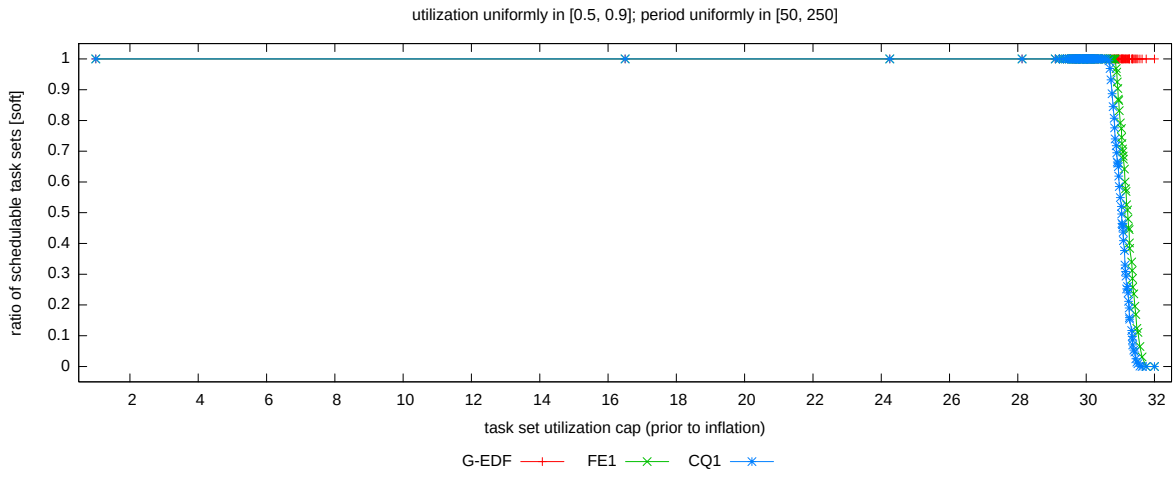

(c)

Figure 124: Comparison of FE1 and CQ1 (event- vs. quantum-driven scheduling) in terms of soft schedulability of task sets with uniform heavy per-task utilizations and **(a)** short, **(b)** moderate, and **(c)** long periods. These graphs correspond to Fig. 28.

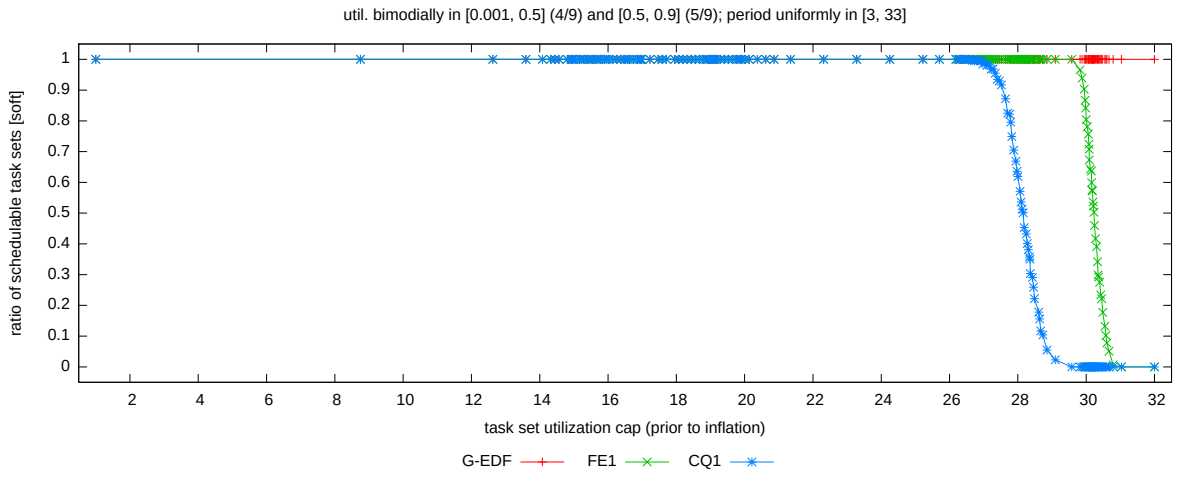

(a)

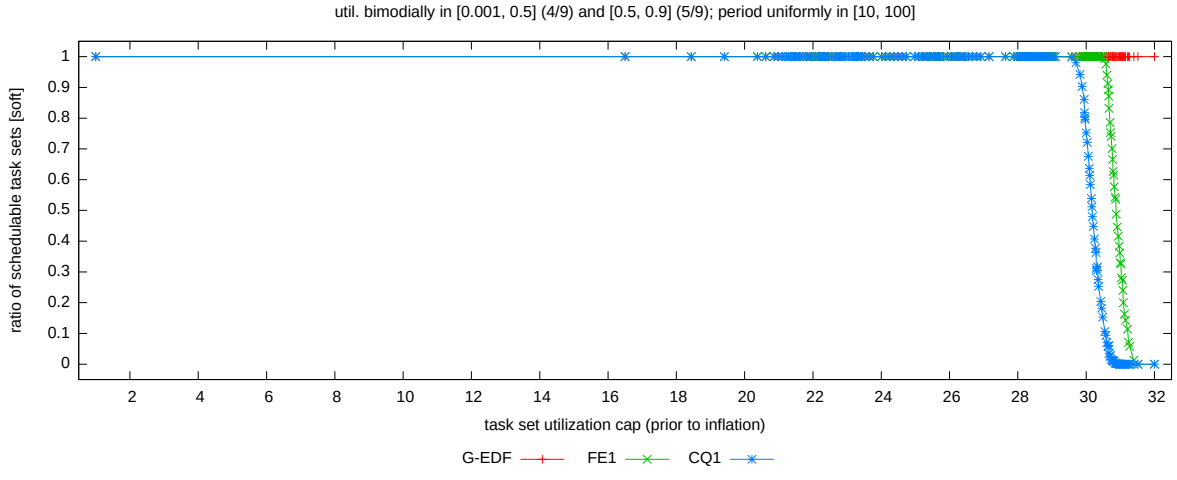

(b)

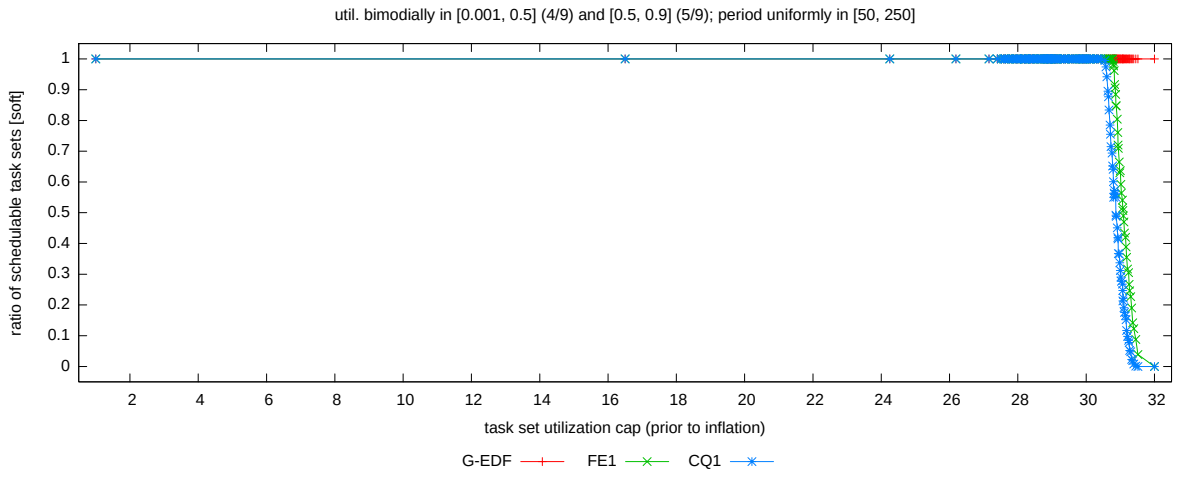

(c)

Figure 125: Comparison of FE1 and CQ1 (event- vs. quantum-driven scheduling) in terms of soft schedulability of task sets with bimodal heavy per-task utilizations and **(a)** short, **(b)** moderate, and **(c)** long periods. These graphs correspond to Fig. 29.

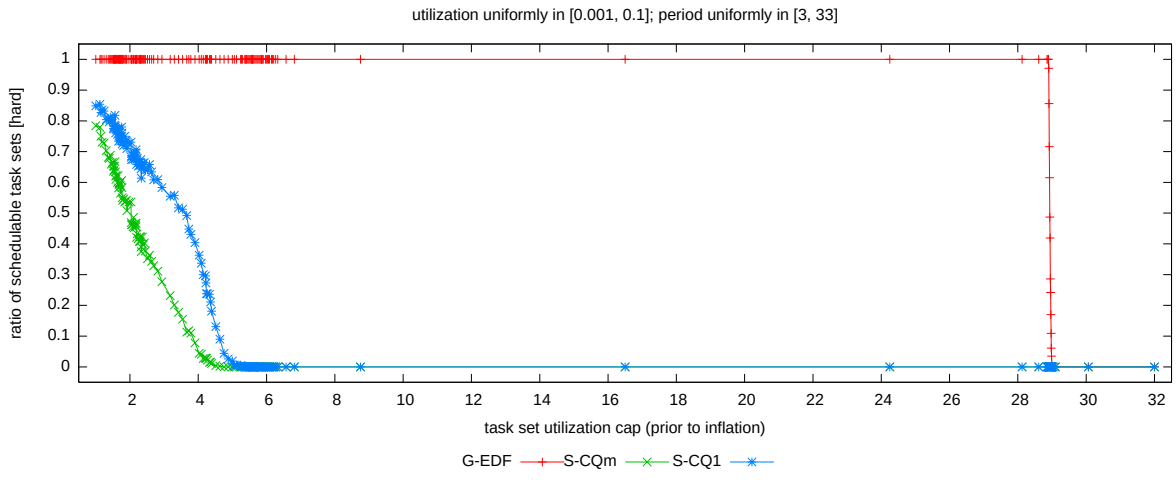

(a)

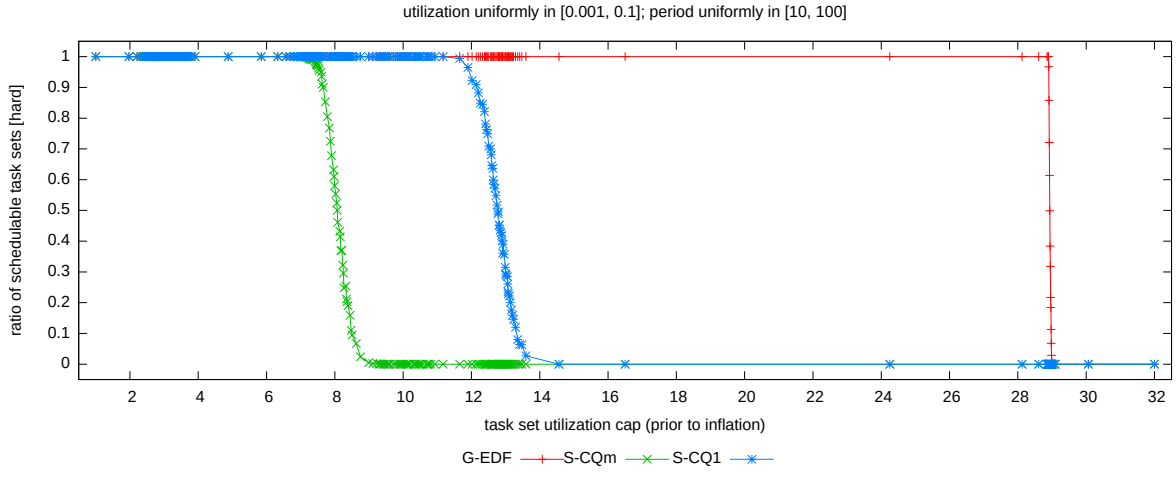

(b)

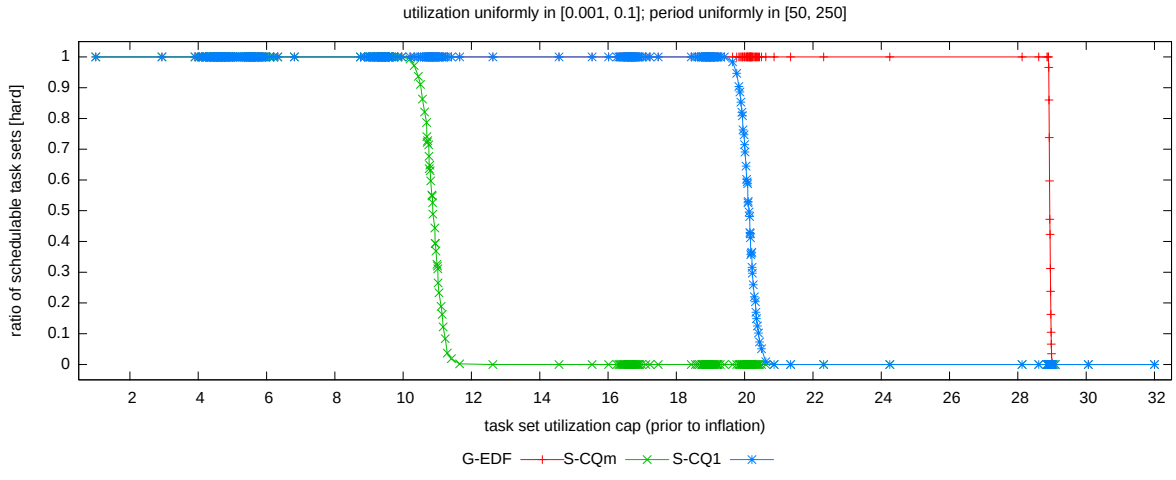

(c)

Figure 126: Comparison of S-CQm and S-CQ1 (global vs. dedicated interrupt handling) in terms of hard schedulability of task sets with uniform light per-task utilizations and **(a)** short, **(b)** moderate, and **(c)** long periods. These graphs correspond to Fig. 18.

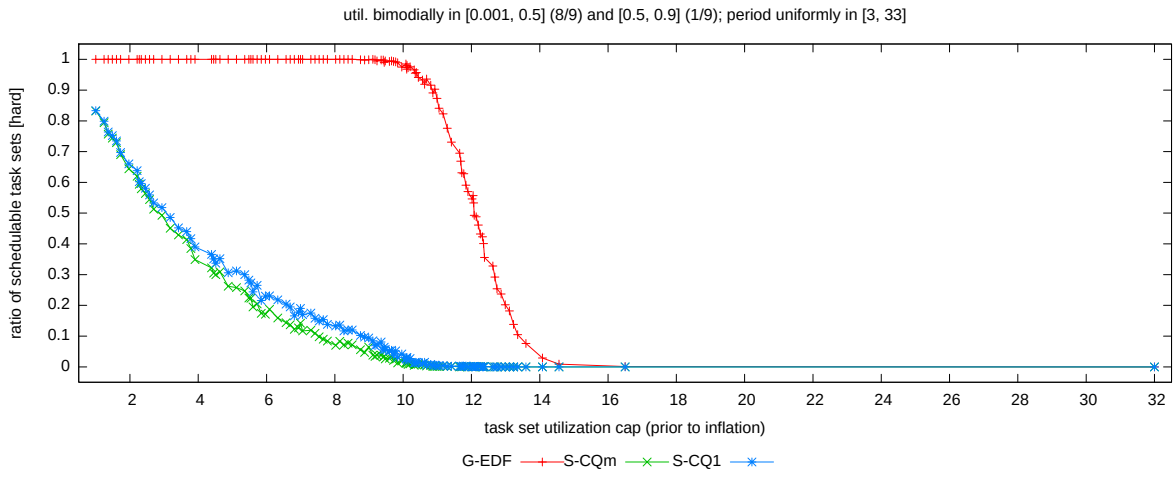

(a)

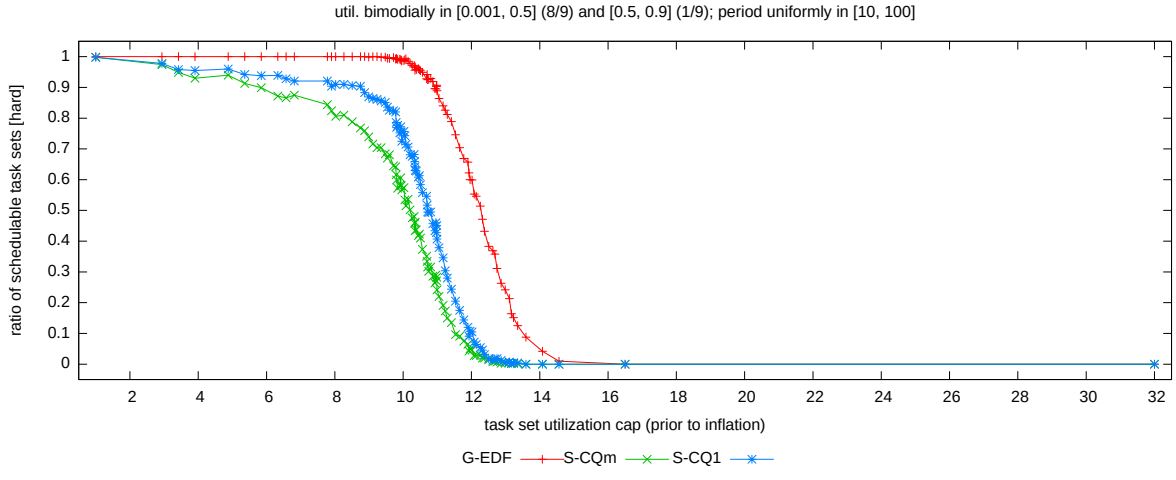

(b)

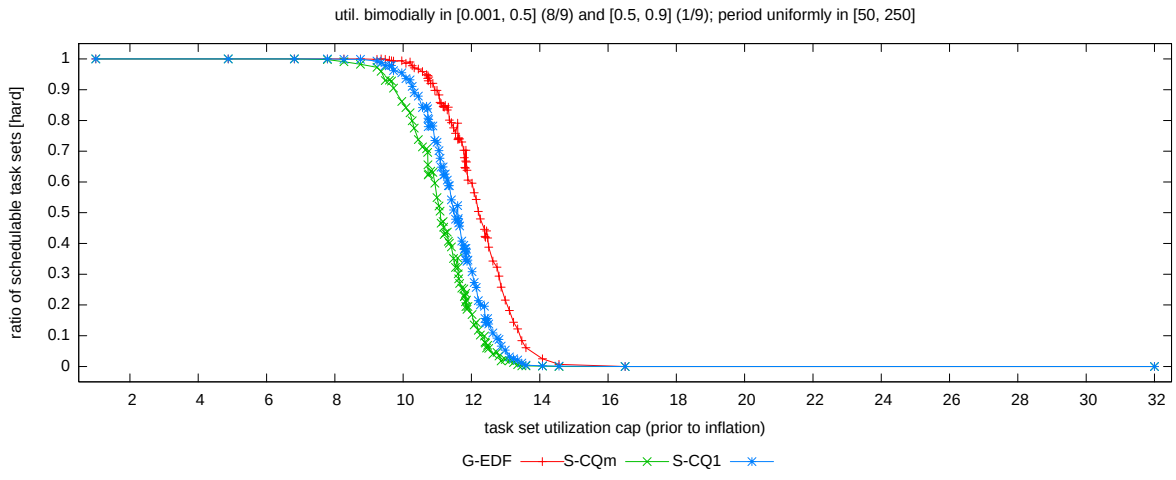

(c)

Figure 127: Comparison of S-CQm and S-CQ1 (global vs. dedicated interrupt handling) in terms of hard schedulability of task sets with bimodal light per-task utilizations and **(a)** short, **(b)** moderate, and **(c)** long periods. These graphs correspond to Fig. 19.

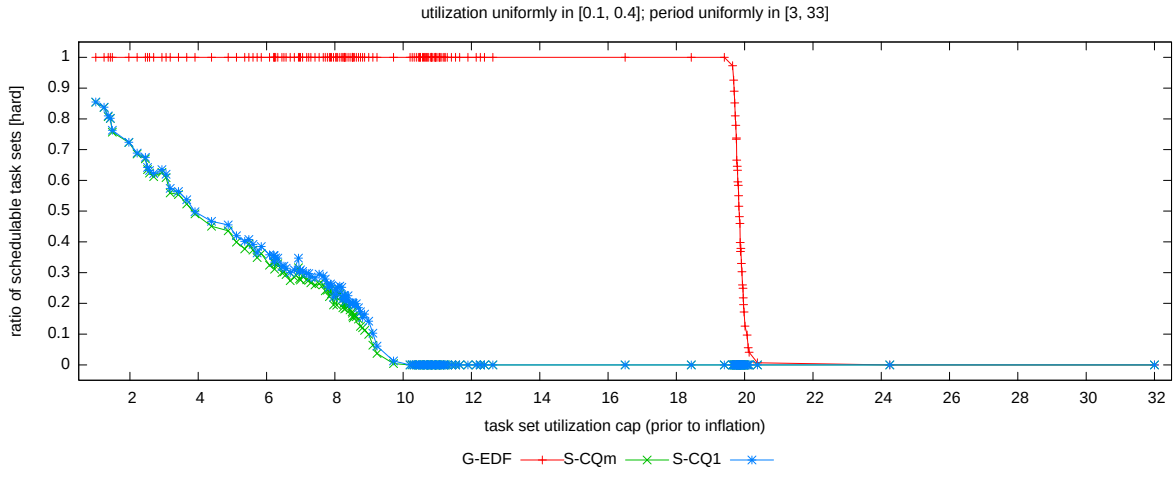

(a)

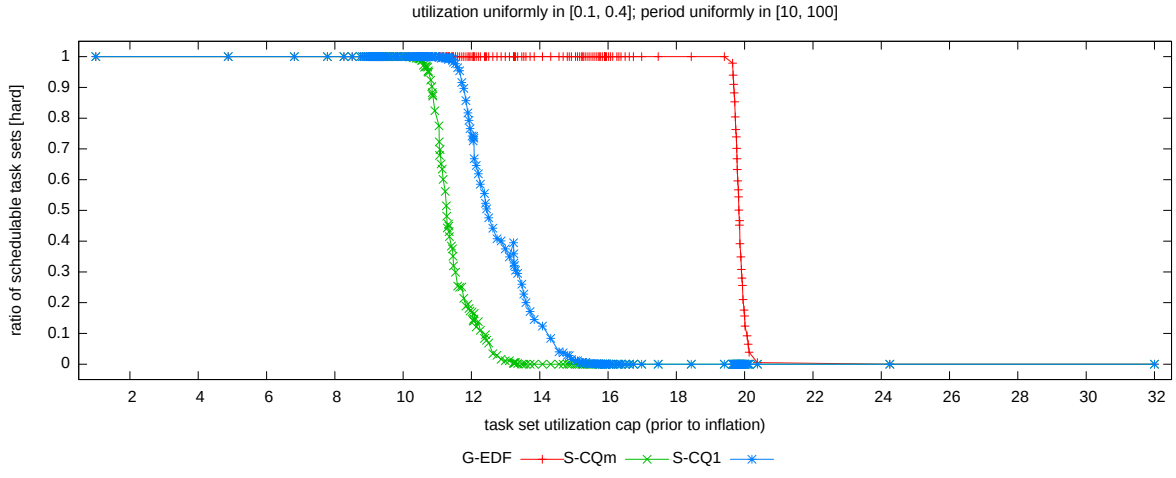

(b)

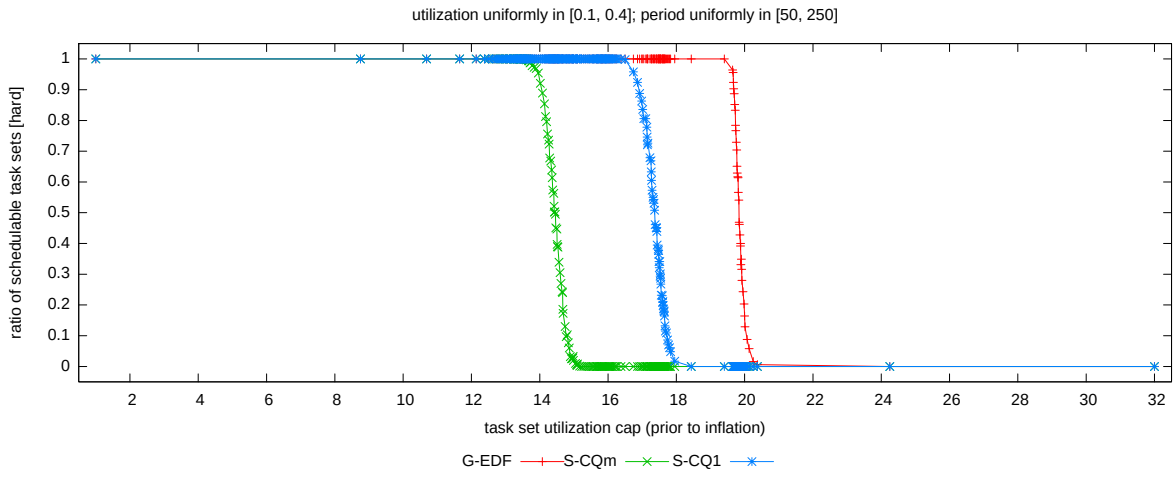

(c)

Figure 128: Comparison of S-CQm and S-CQ1 (global vs. dedicated interrupt handling) in terms of hard schedulability of task sets with uniform medium per-task utilizations and **(a)** short, **(b)** moderate, and **(c)** long periods. These graphs correspond to Fig. 20.

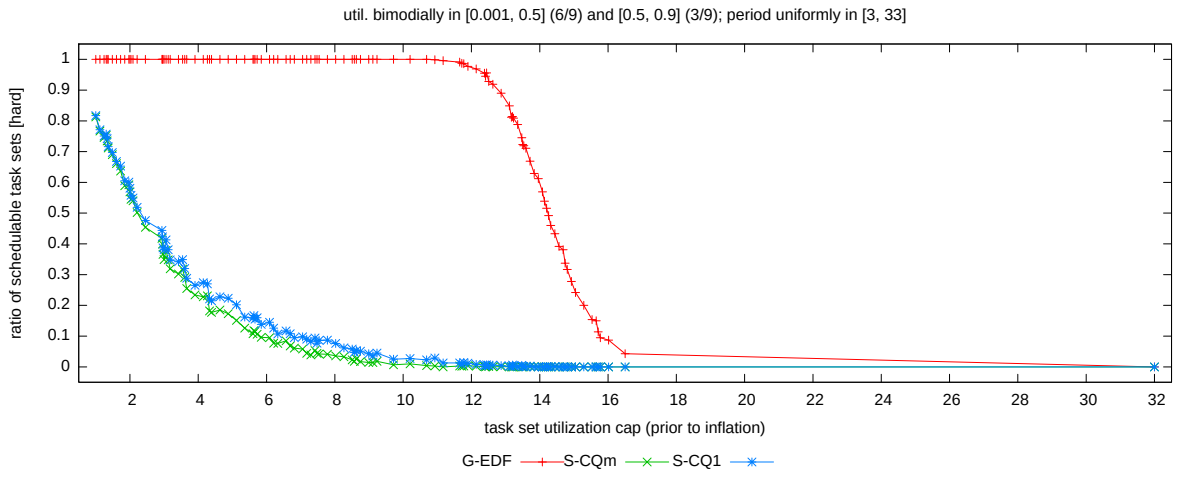

(a)

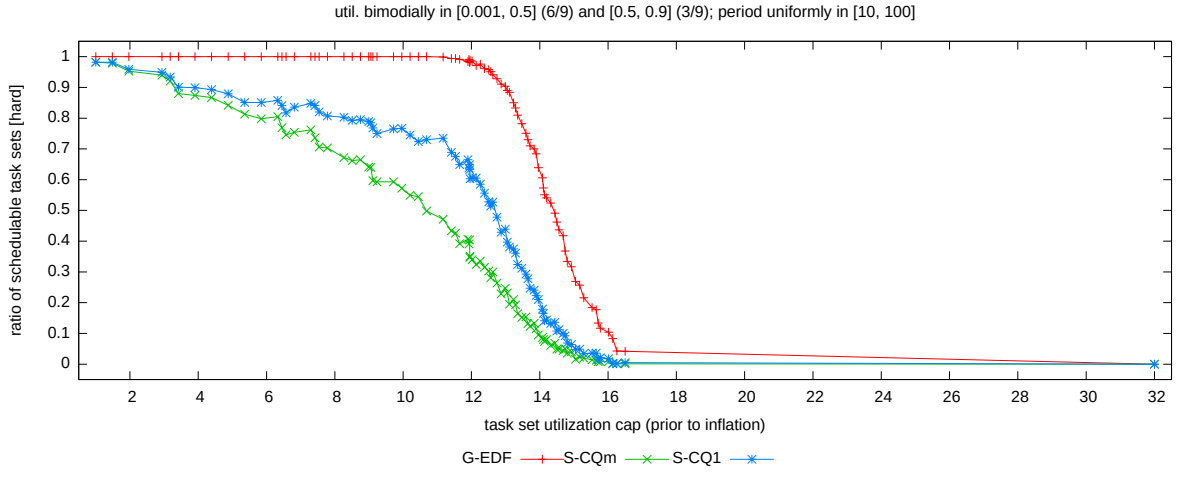

(b)

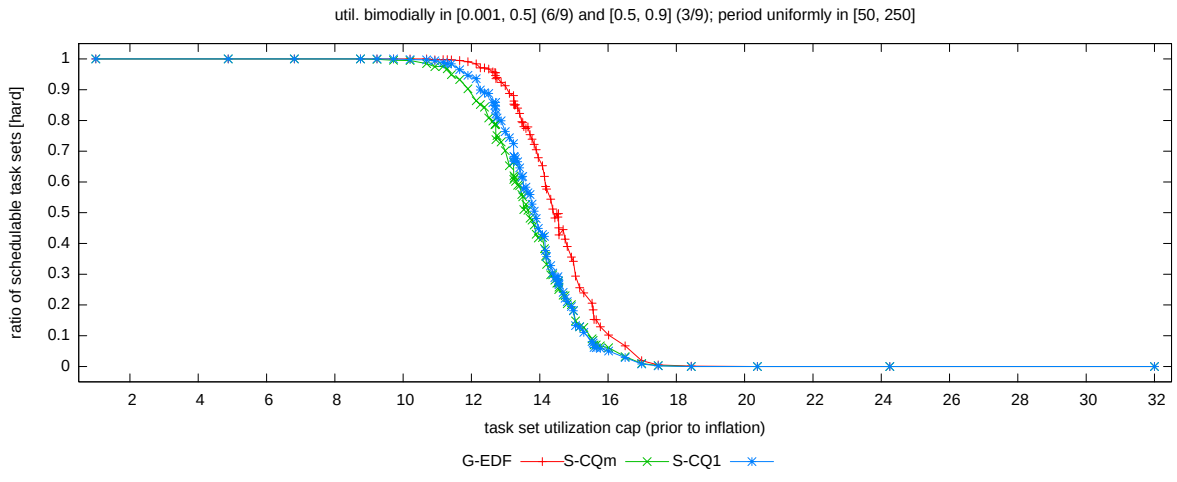

(c)

Figure 129: Comparison of S-CQm and S-CQ1 (global vs. dedicated interrupt handling) in terms of hard schedulability of task sets with bimodal medium per-task utilizations and **(a)** short, **(b)** moderate, and **(c)** long periods. These graphs correspond to Fig. 21.

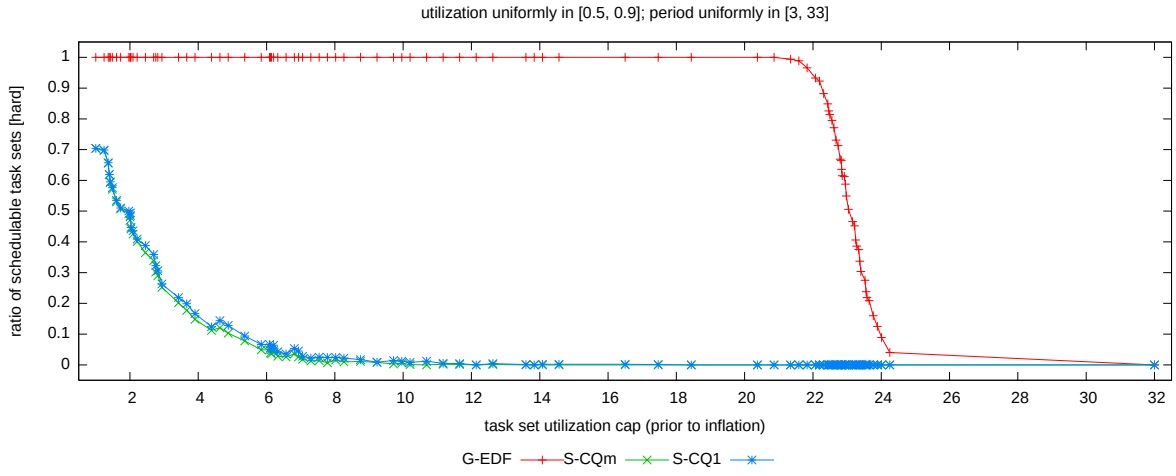

(a)

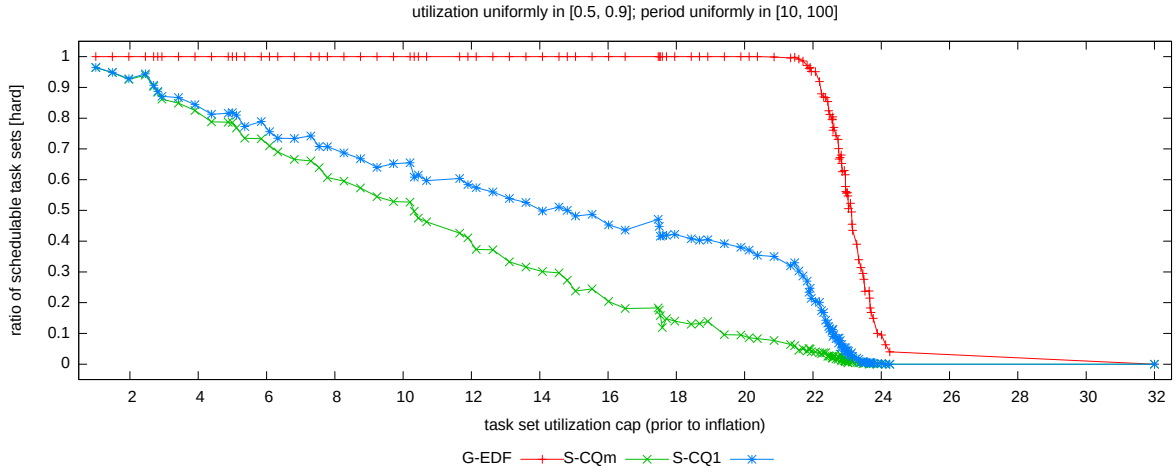

(b)

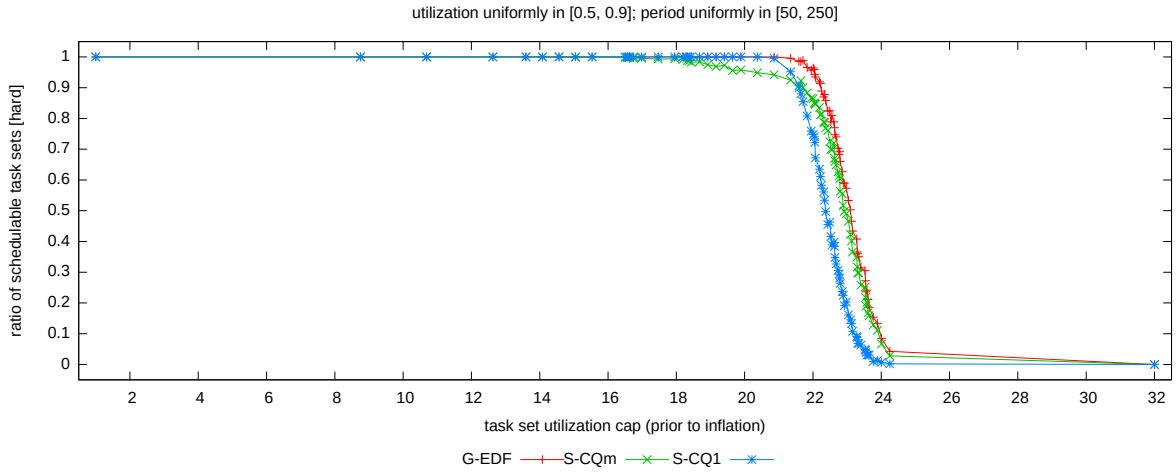

(c)

Figure 130: Comparison of S-CQm and S-CQ1 (global vs. dedicated interrupt handling) in terms of hard schedulability of task sets with uniform heavy per-task utilizations and **(a)** short, **(b)** moderate, and **(c)** long periods. These graphs correspond to Fig. 22.

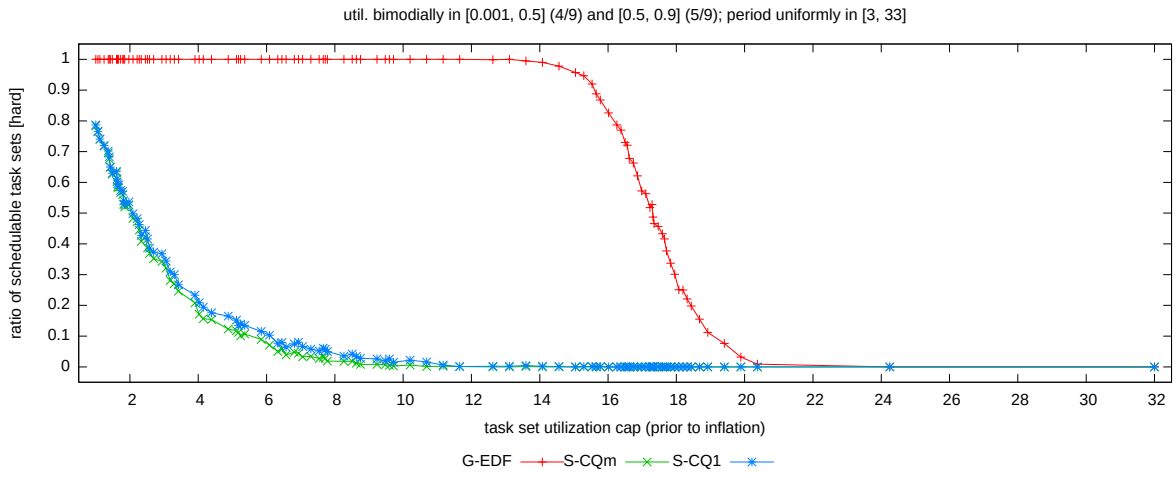

(a)

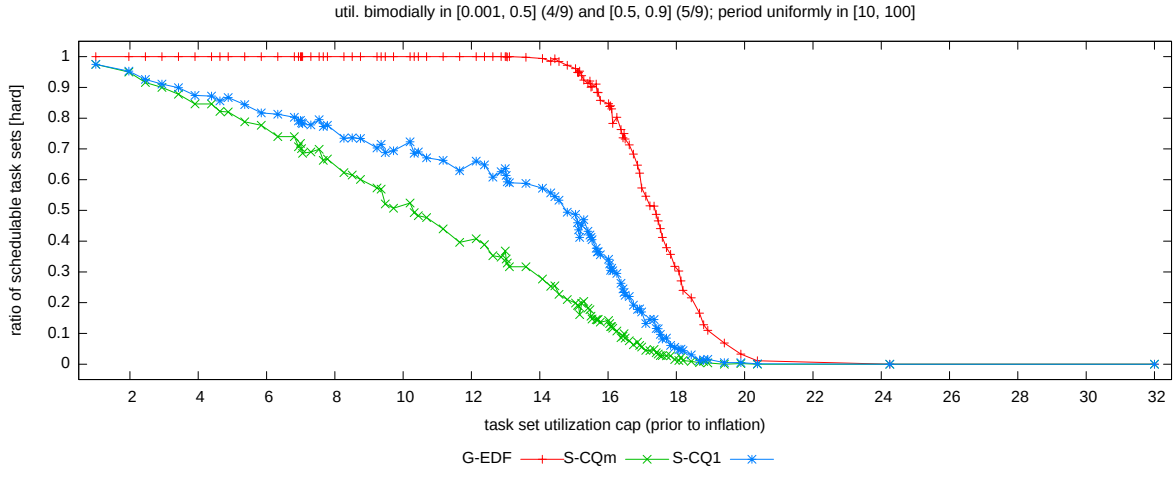

(b)

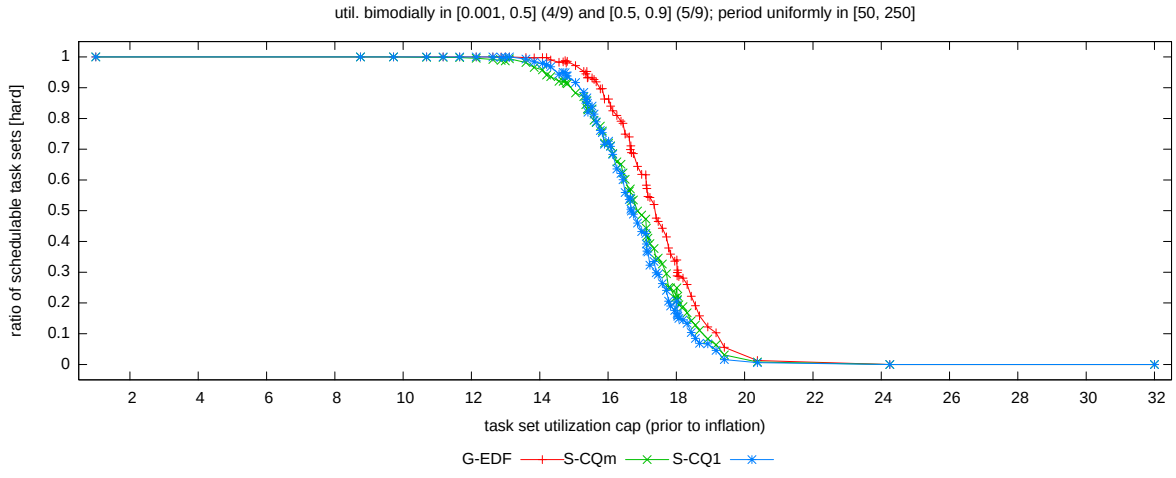

(c)

Figure 131: Comparison of S-CQm and S-CQ1 (global vs. dedicated interrupt handling) in terms of hard schedulability of task sets with bimodal heavy per-task utilizations and **(a)** short, **(b)** moderate, and **(c)** long periods. These graphs correspond to Fig. 23.

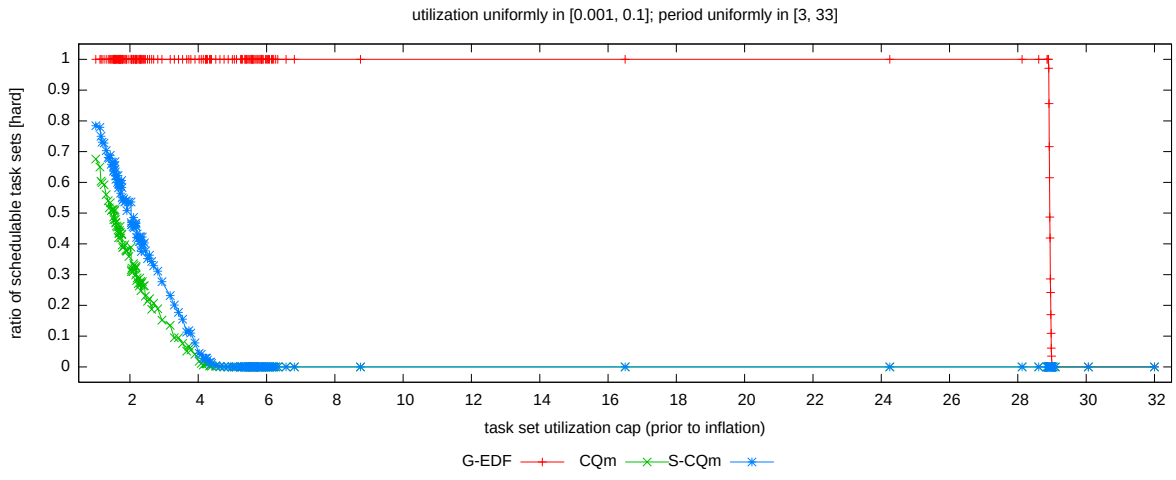

(a)

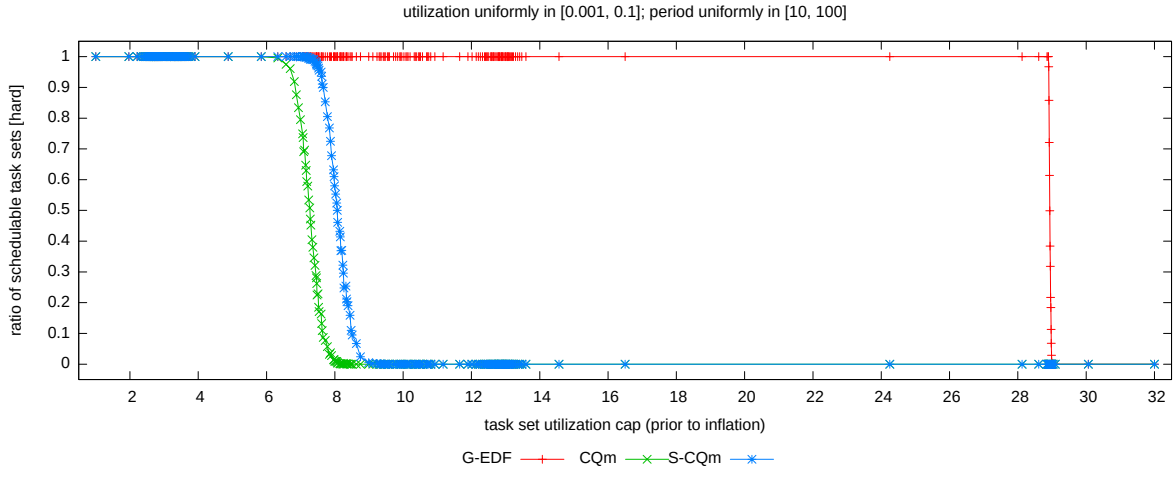

(b)

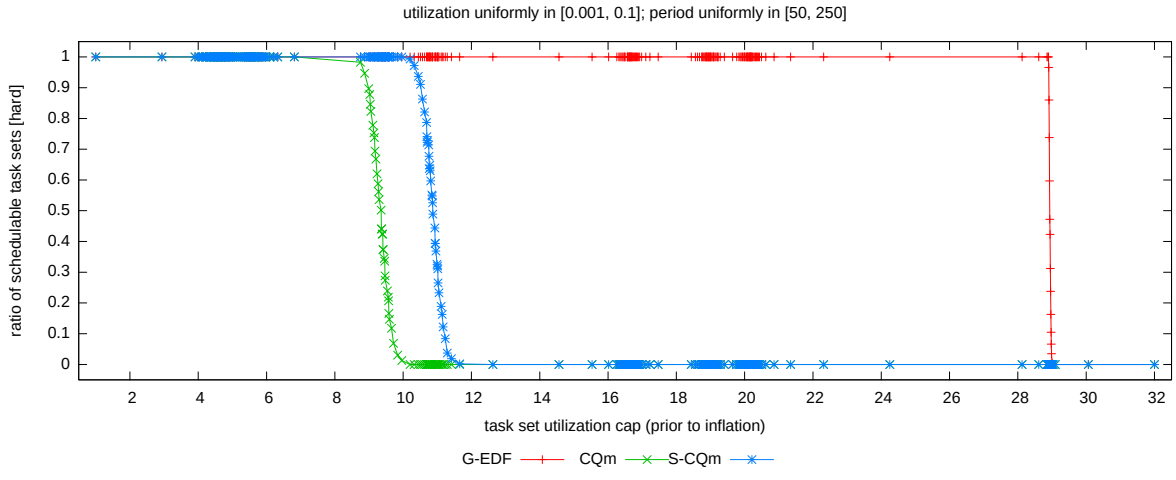

(c)

Figure 132: Comparison of CQm and S-CQm (aligned vs. staggered quanta) in terms of hard schedulability of task sets with uniform light per-task utilizations and **(a)** short, **(b)** moderate, and **(c)** long periods. These graphs correspond to Fig. 18.

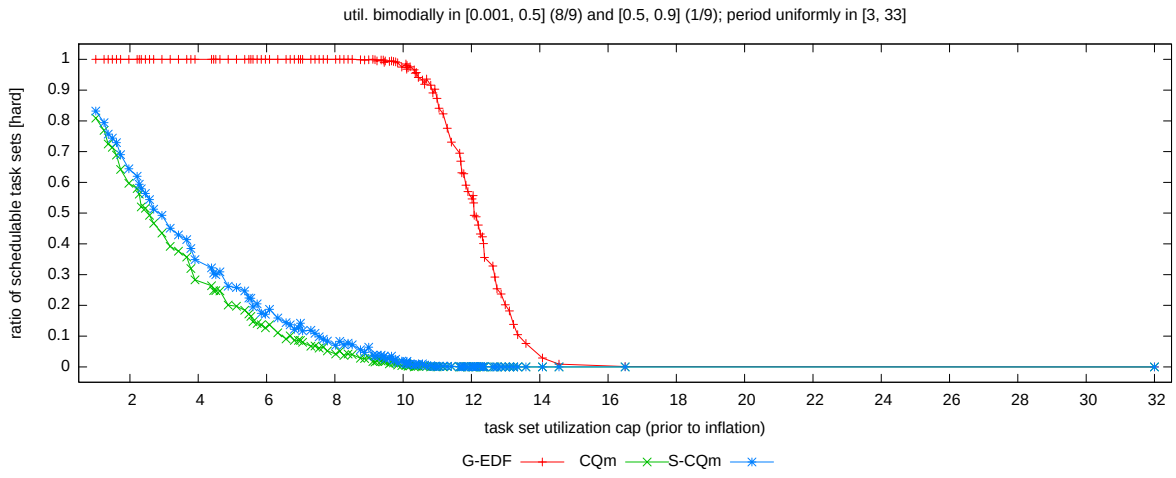

(a)

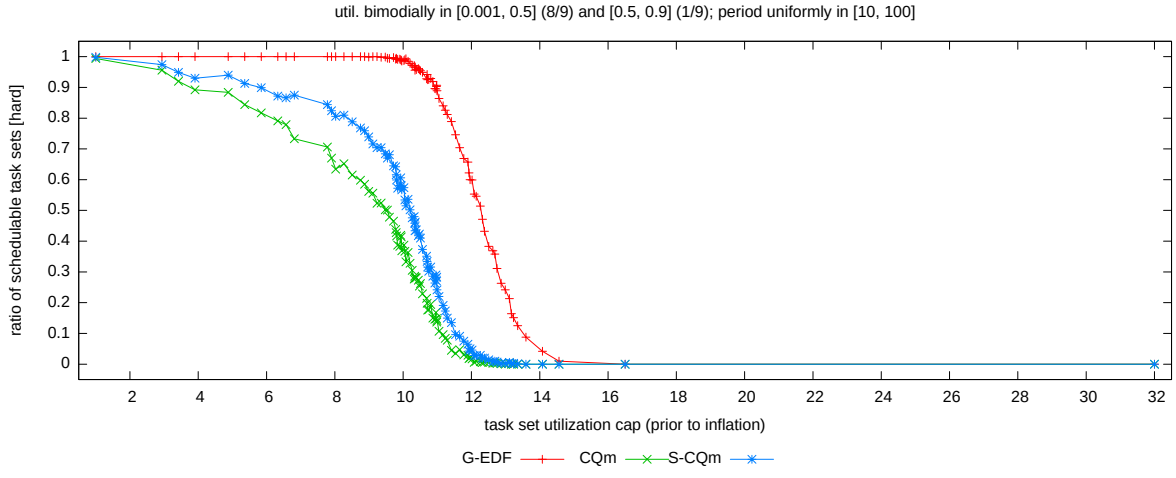

(b)

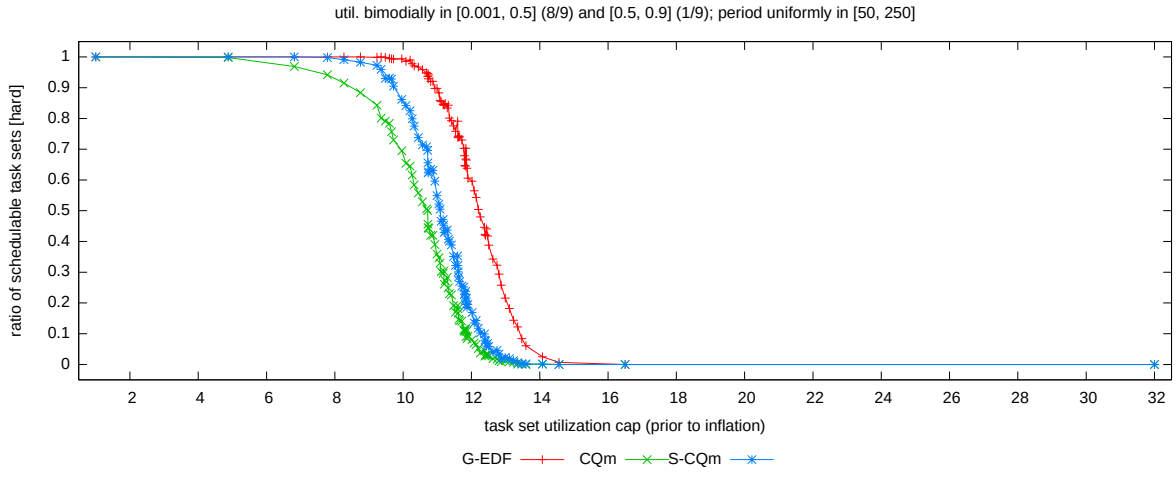

(c)

Figure 133: Comparison of CQm and S-CQm (aligned vs. staggered quanta) in terms of hard schedulability of task sets with bimodal light per-task utilizations and **(a)** short, **(b)** moderate, and **(c)** long periods. These graphs correspond to Fig. 19.

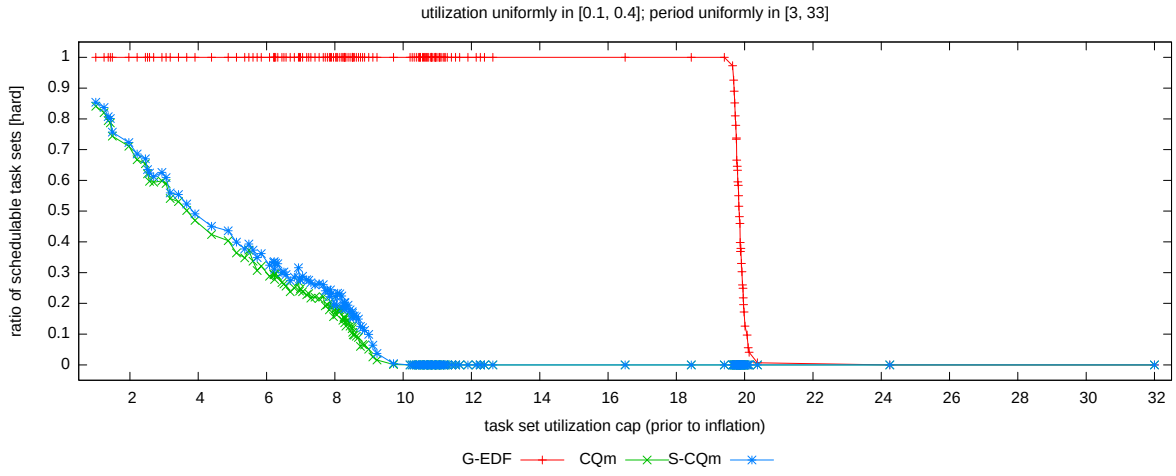

(a)

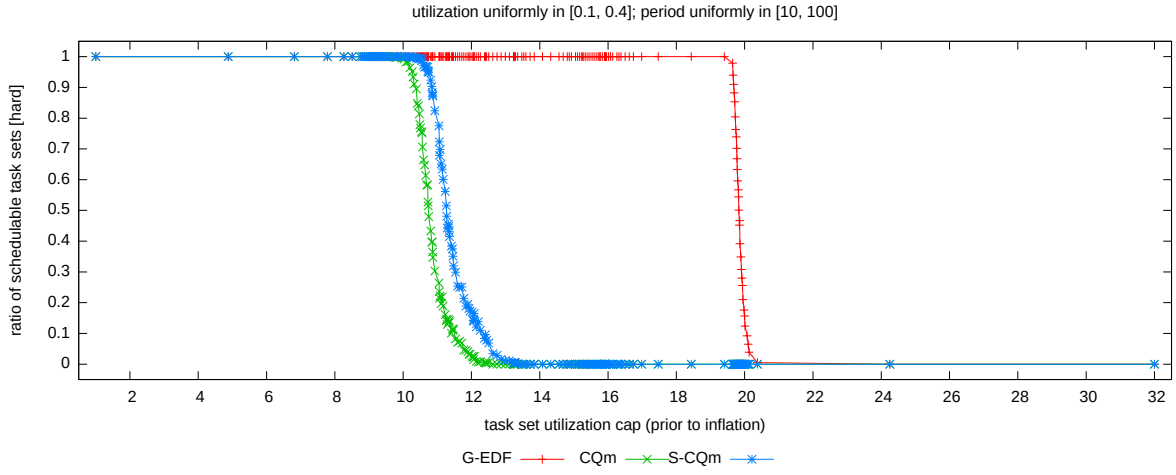

(b)

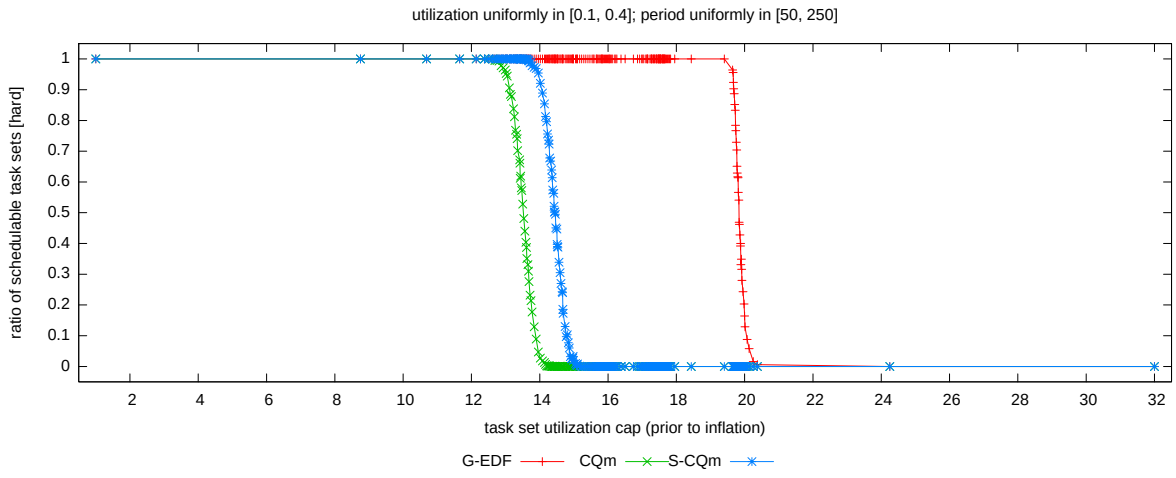

(c)

Figure 134: Comparison of CQm and S-CQm (aligned vs. staggered quanta) in terms of hard schedulability of task sets with uniform medium per-task utilizations and **(a)** short, **(b)** moderate, and **(c)** long periods. These graphs correspond to Fig. 20.

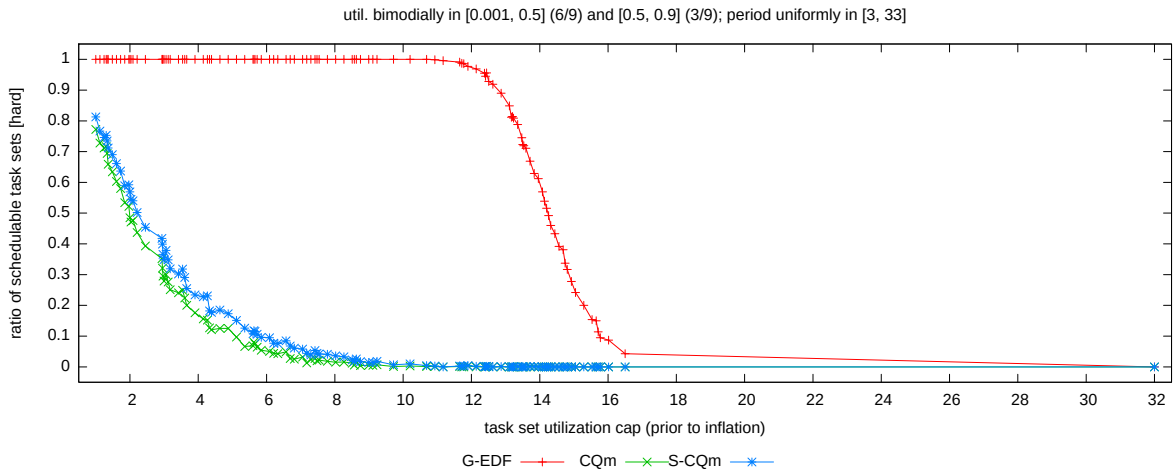

(a)

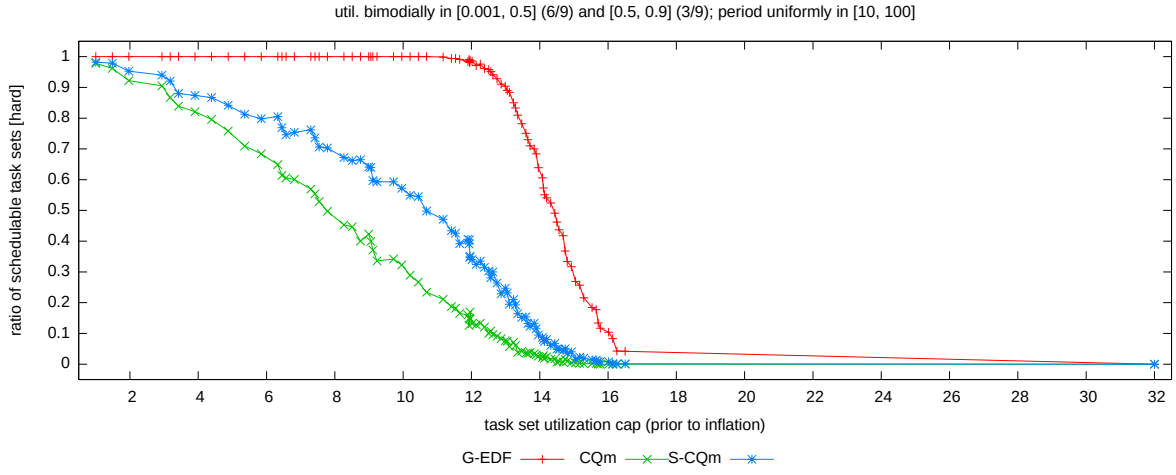

(b)

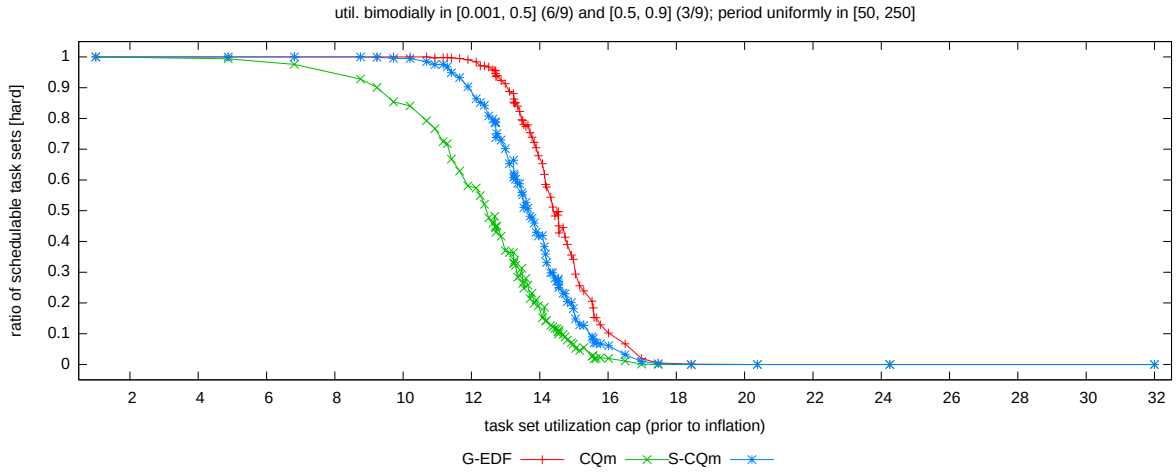

(c)

Figure 135: Comparison of CQm and S-CQm (aligned vs. staggered quanta) in terms of hard schedulability of task sets with bimodal medium per-task utilizations and **(a)** short, **(b)** moderate, and **(c)** long periods. These graphs correspond to Fig. 21.

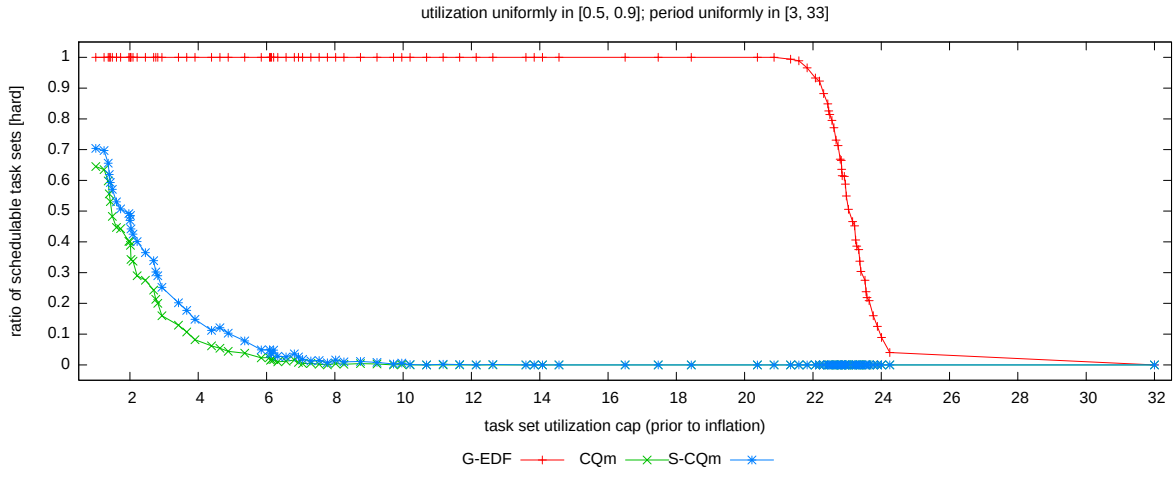

(a)

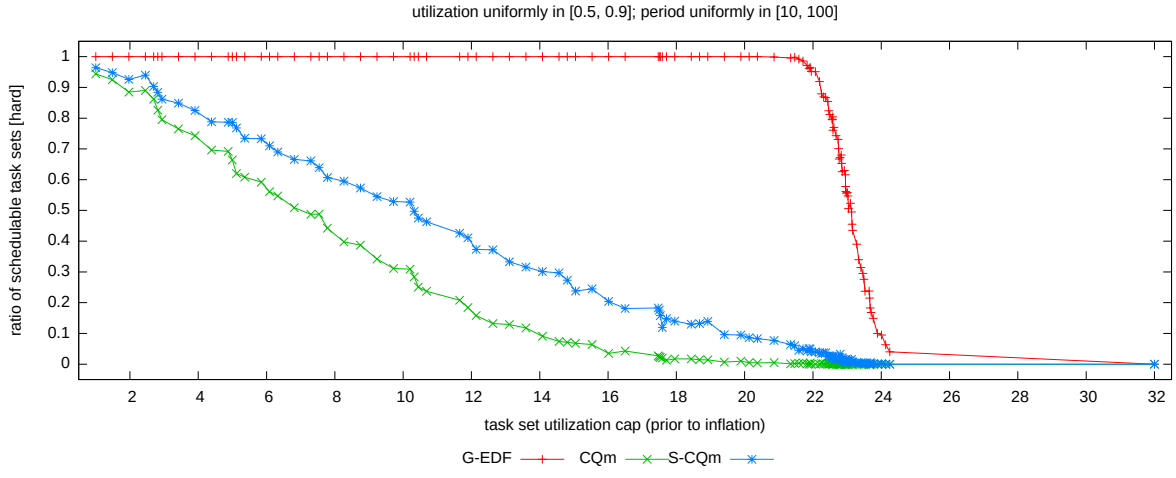

(b)

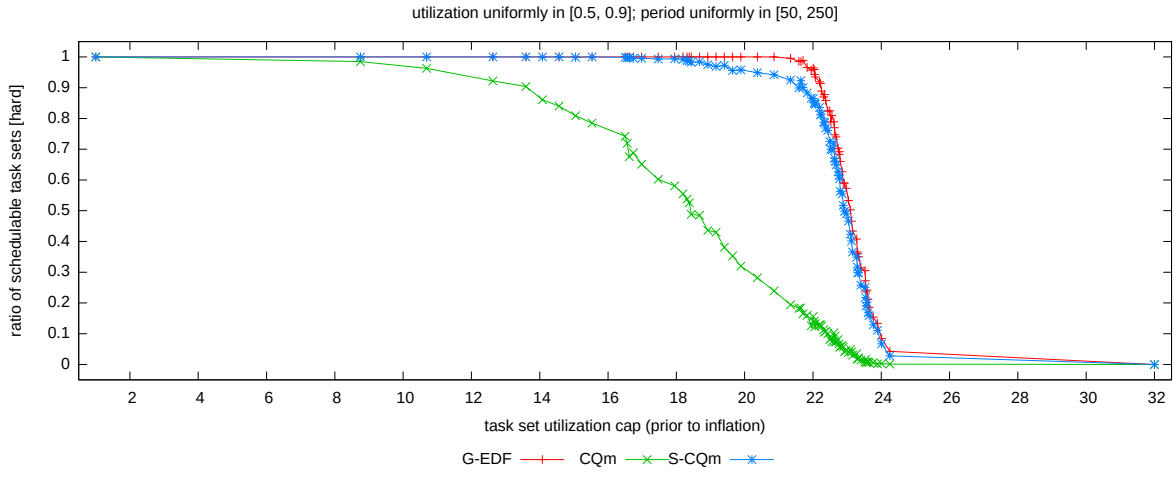

(c)

Figure 136: Comparison of CQm and S-CQm (aligned vs. staggered quanta) in terms of hard schedulability of task sets with uniform heavy per-task utilizations and **(a)** short, **(b)** moderate, and **(c)** long periods. These graphs correspond to Fig. 22.

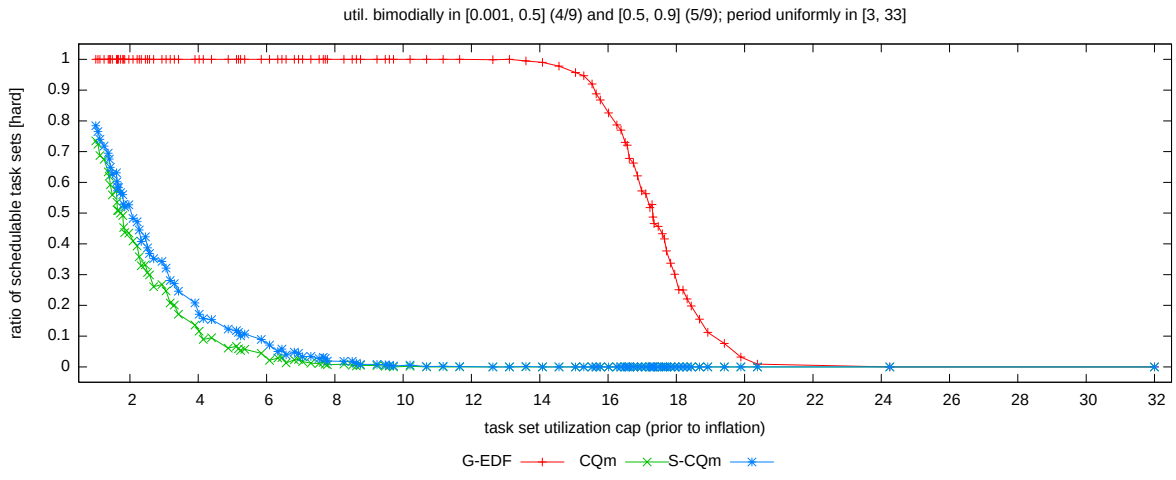

(a)

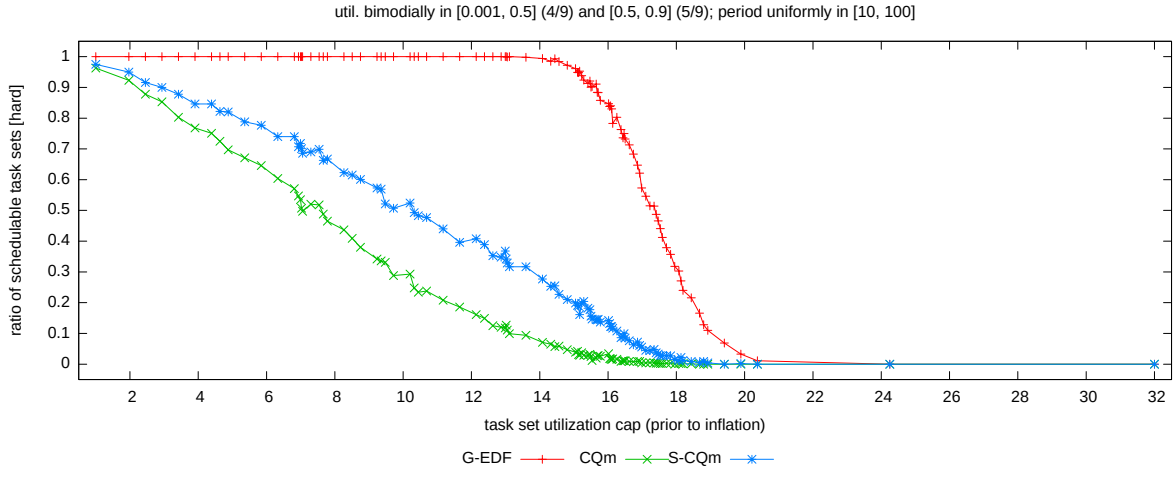

(b)

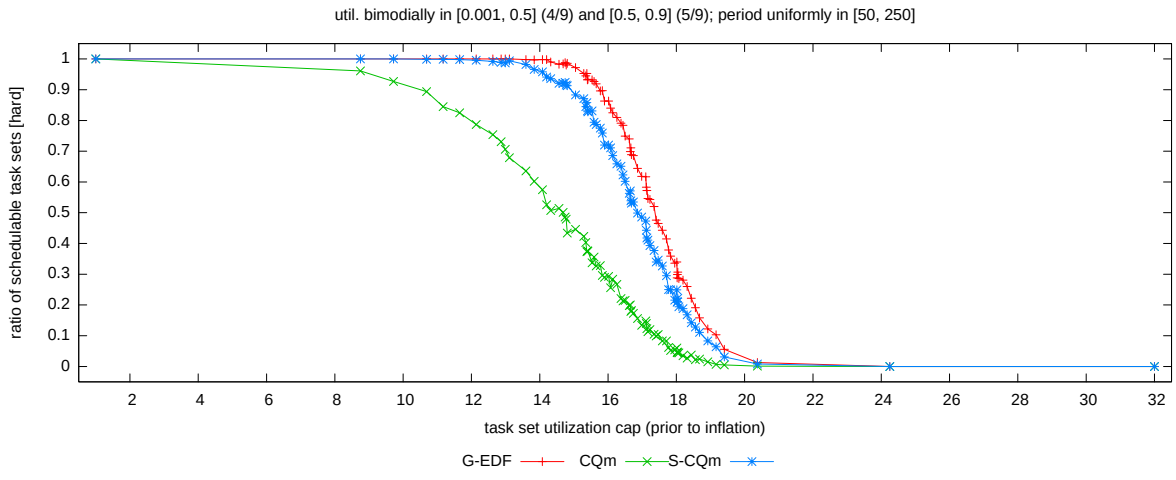

(c)

Figure 137: Comparison of CQm and S-CQm (aligned vs. staggered quanta) in terms of hard schedulability of task sets with bimodal heavy per-task utilizations and **(a)** short, **(b)** moderate, and **(c)** long periods. These graphs correspond to Fig. 23.

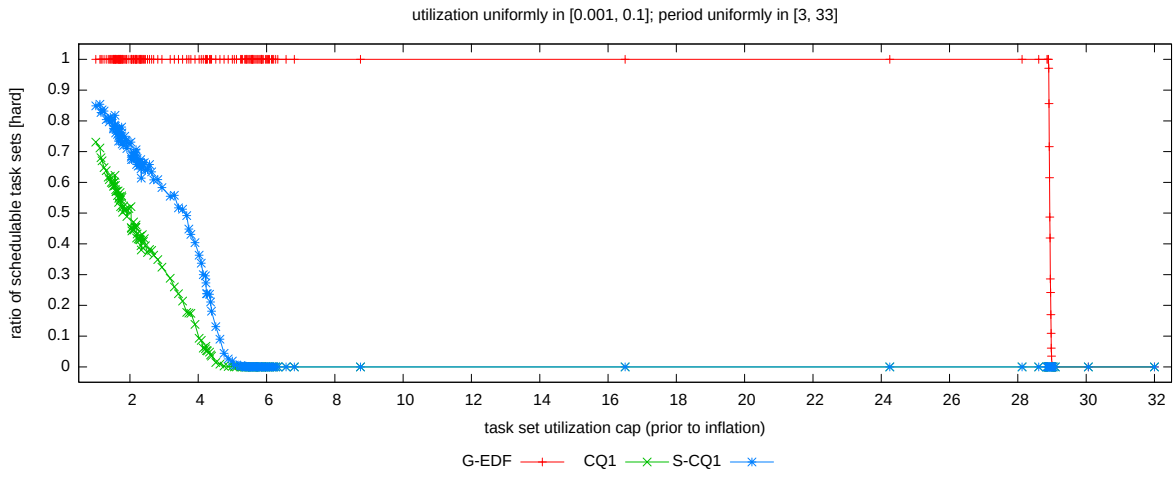

(a)

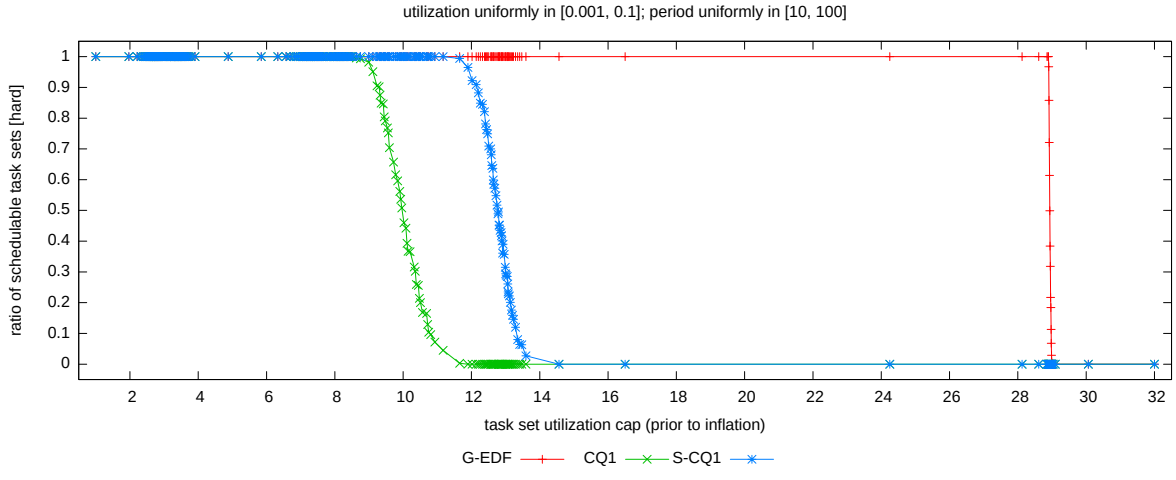

(b)

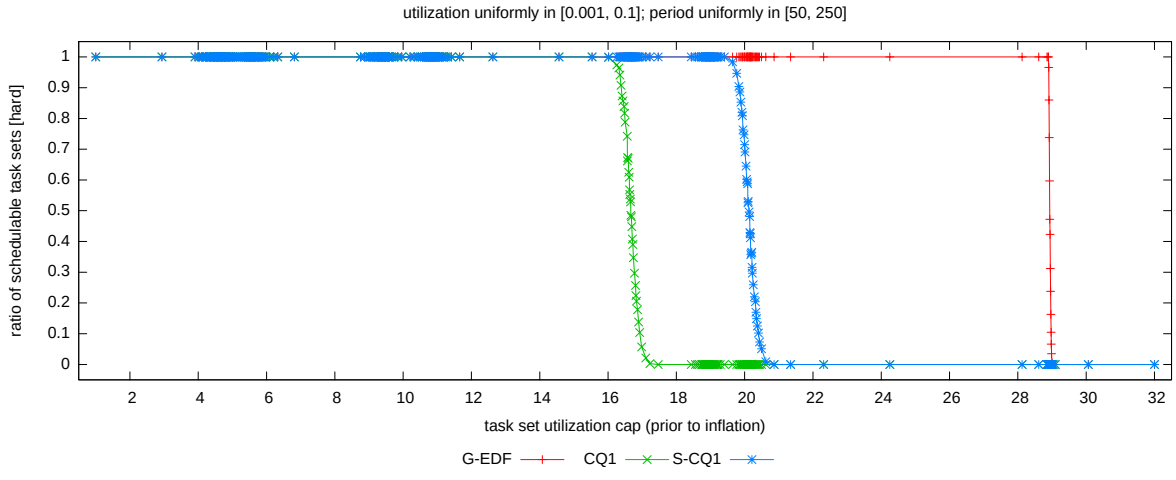

(c)

Figure 138: Comparison of CQ1 and S-CQ1 (aligned vs. staggered quanta) in terms of hard schedulability of task sets with uniform light per-task utilizations and **(a)** short, **(b)** moderate, and **(c)** long periods. These graphs correspond to Fig. 18.

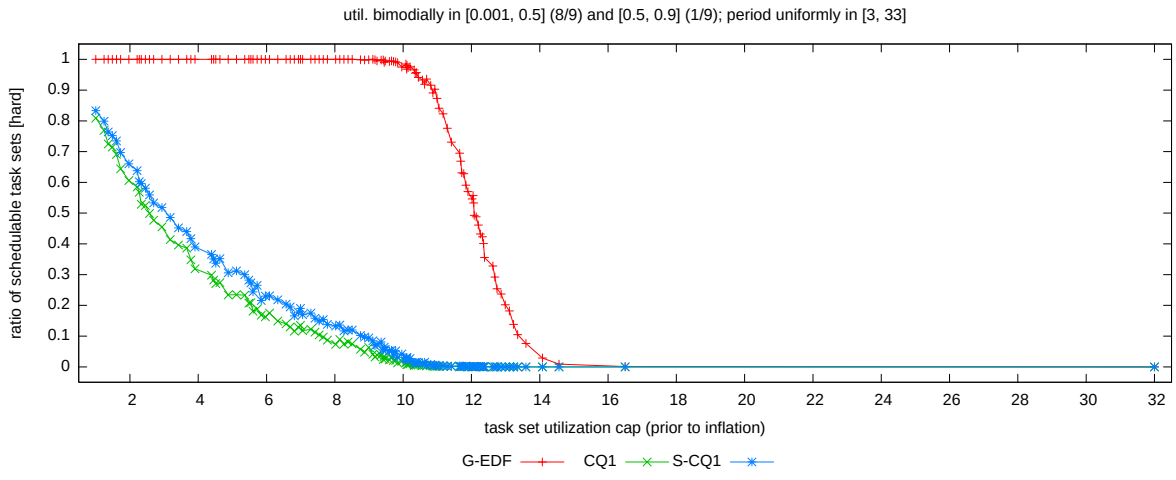

(a)

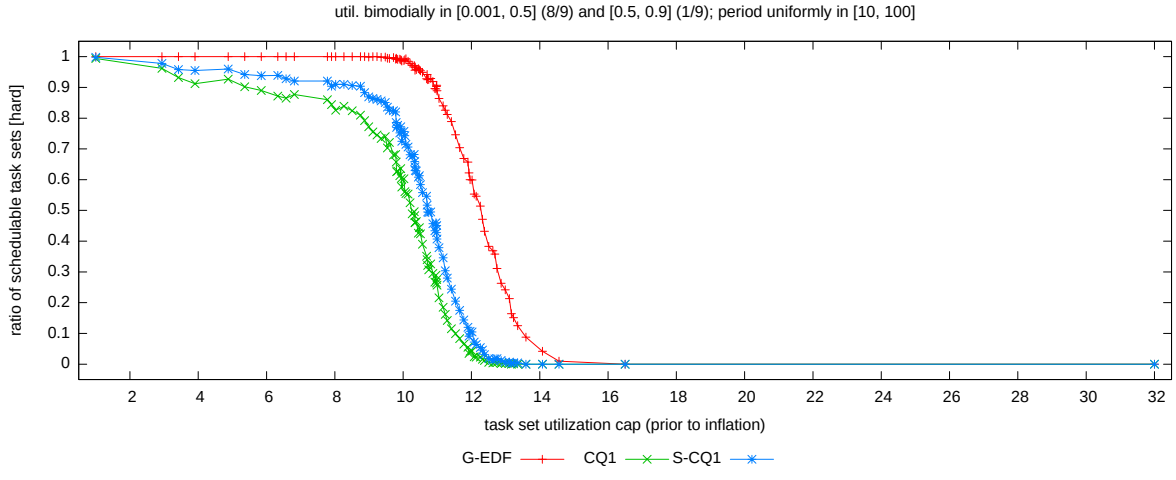

(b)

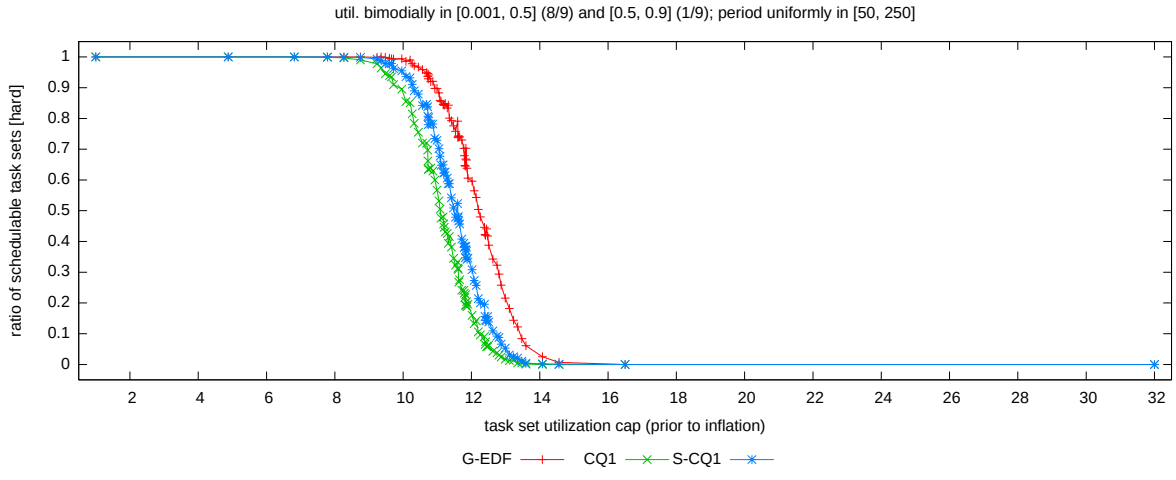

(c)

Figure 139: Comparison of CQ1 and S-CQ1 (aligned vs. staggered quanta) in terms of hard schedulability of task sets with bimodal light per-task utilizations and **(a)** short, **(b)** moderate, and **(c)** long periods. These graphs correspond to Fig. 19.

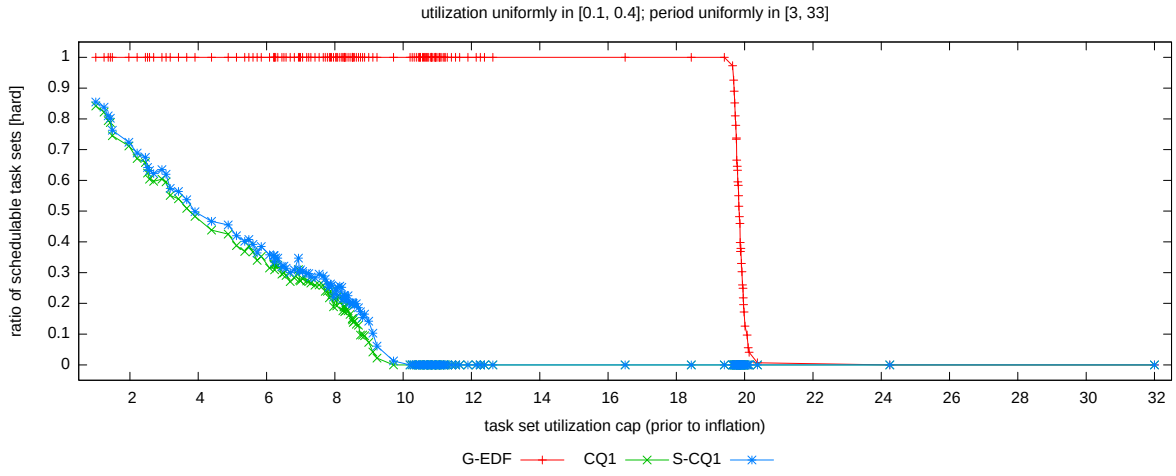

(a)

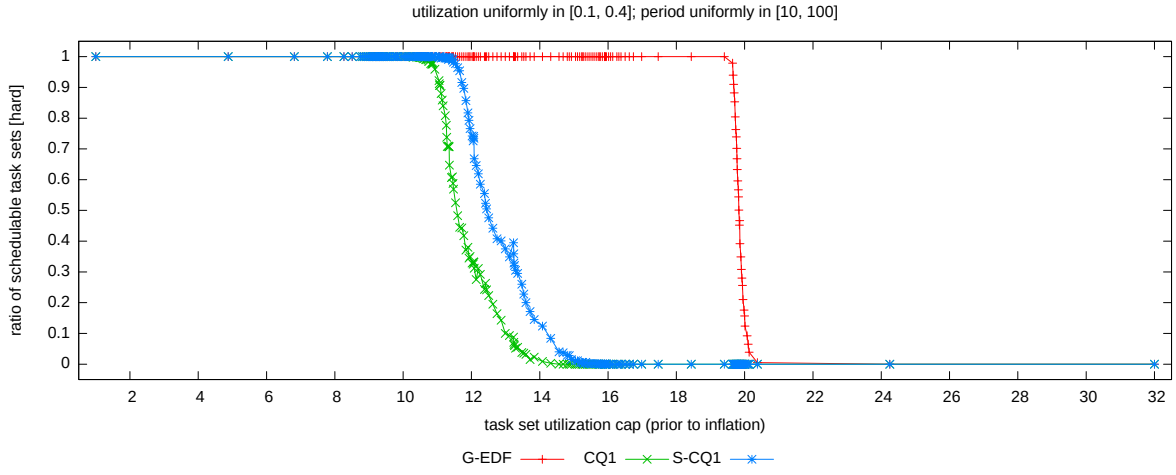

(b)

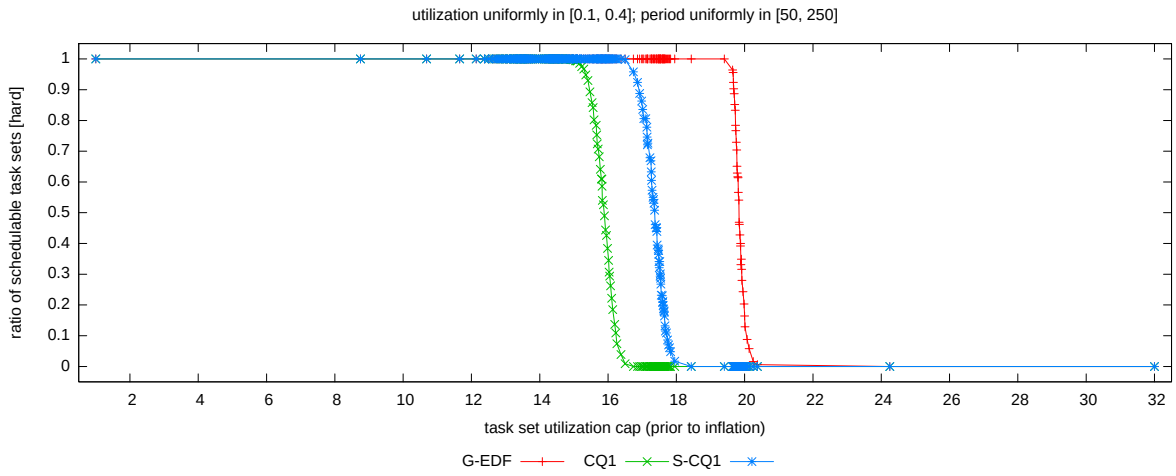

(c)

Figure 140: Comparison of CQ1 and S-CQ1 (aligned vs. staggered quanta) in terms of hard schedulability of task sets with uniform medium per-task utilizations and **(a)** short, **(b)** moderate, and **(c)** long periods. These graphs correspond to Fig. 20.

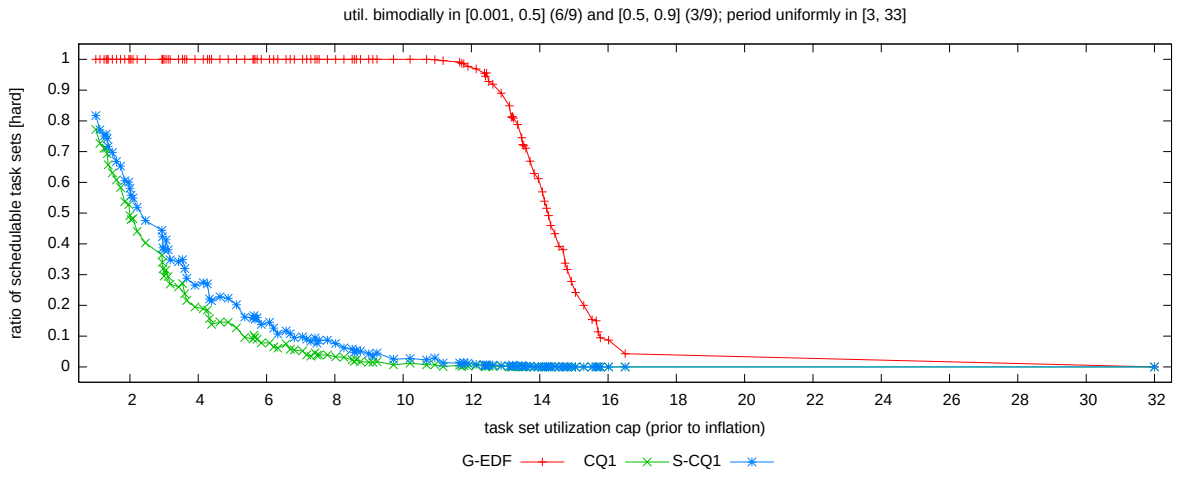

(a)

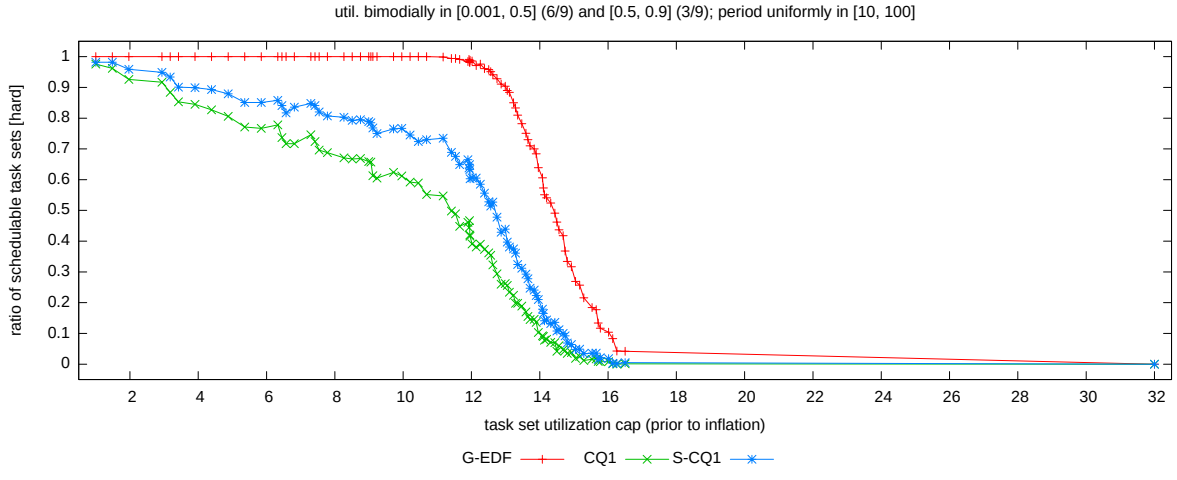

(b)

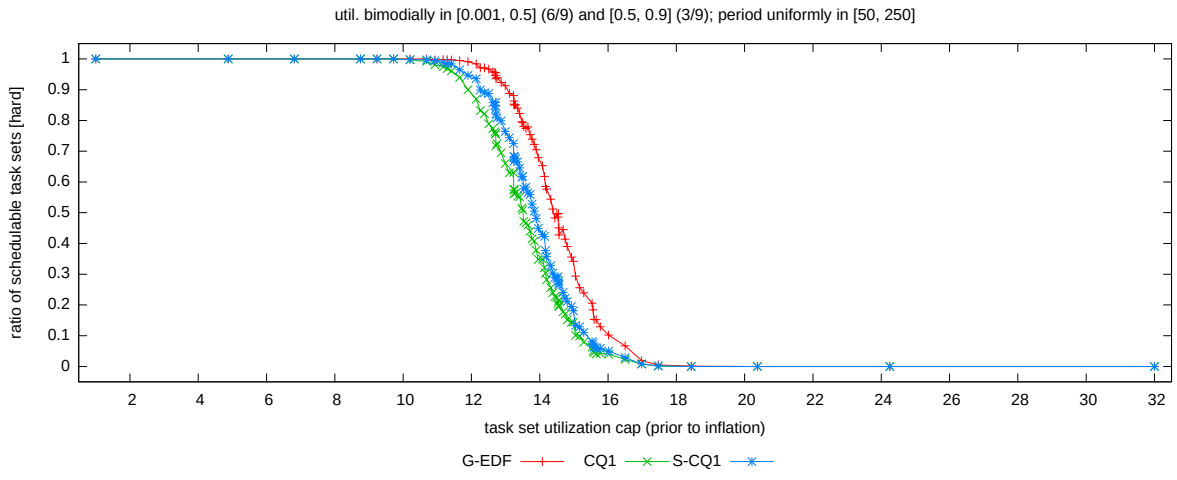

(c)

Figure 141: Comparison of CQ1 and S-CQ1 (aligned vs. staggered quanta) in terms of hard schedulability of task sets with bimodal medium per-task utilizations and **(a)** short, **(b)** moderate, and **(c)** long periods. These graphs correspond to Fig. 21.

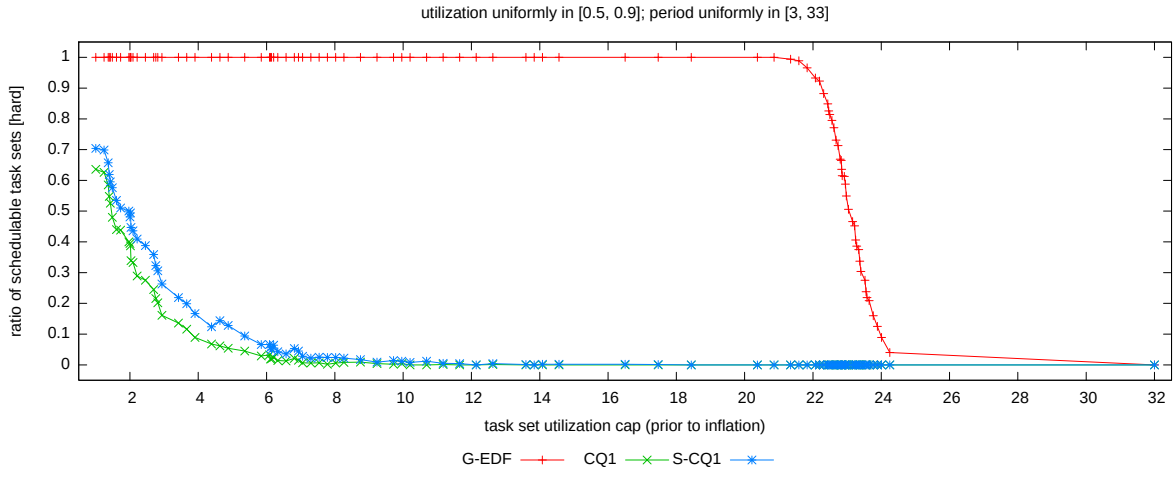

(a)

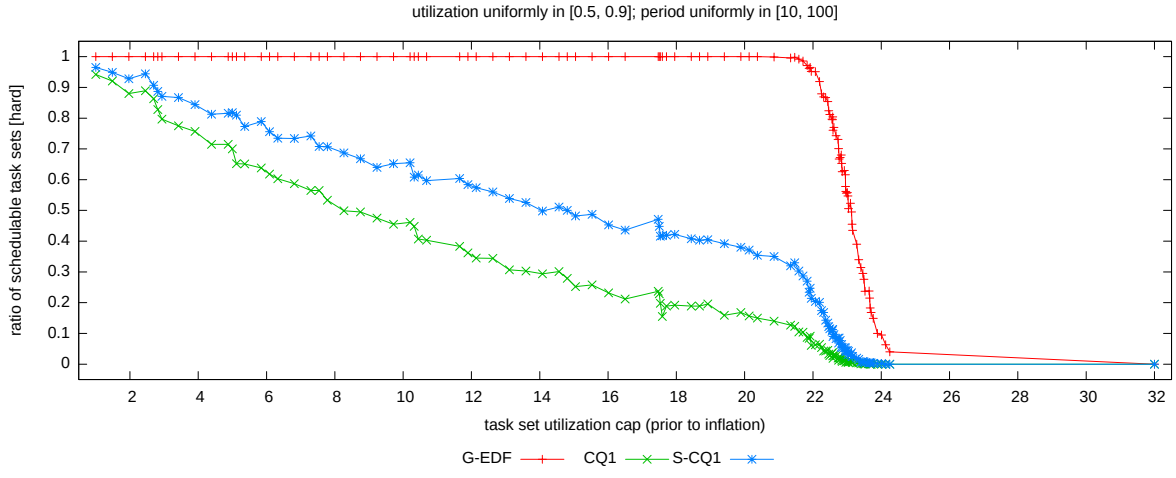

(b)

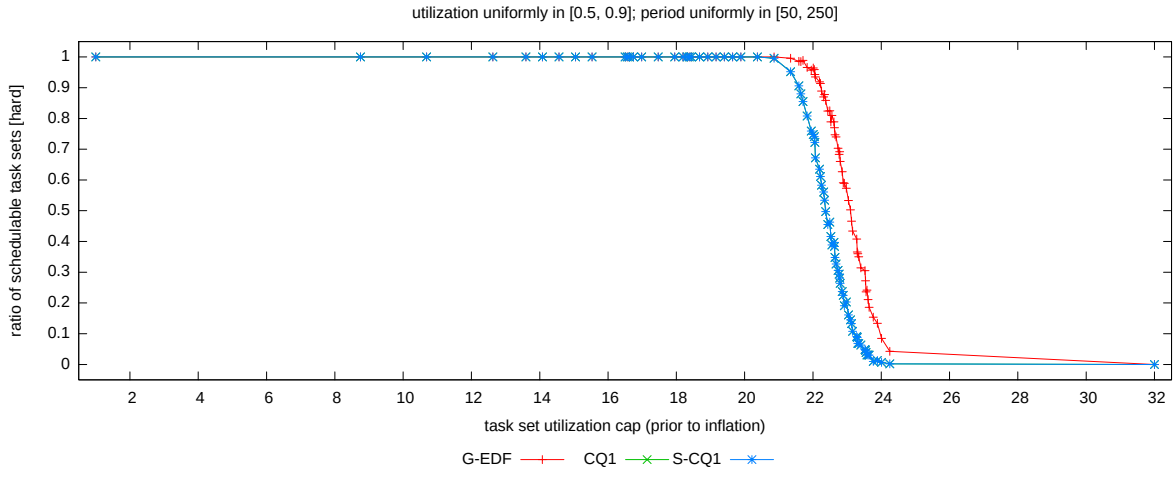

(c)

Figure 142: Comparison of CQ1 and S-CQ1 (aligned vs. staggered quanta) in terms of hard schedulability of task sets with uniform heavy per-task utilizations and **(a)** short, **(b)** moderate, and **(c)** long periods. These graphs correspond to Fig. 22.

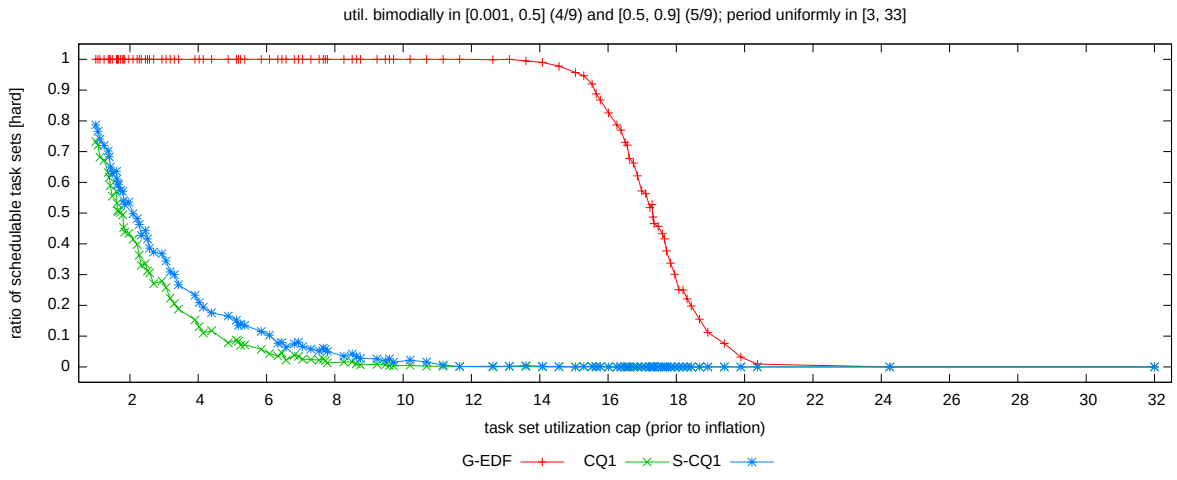

(a)

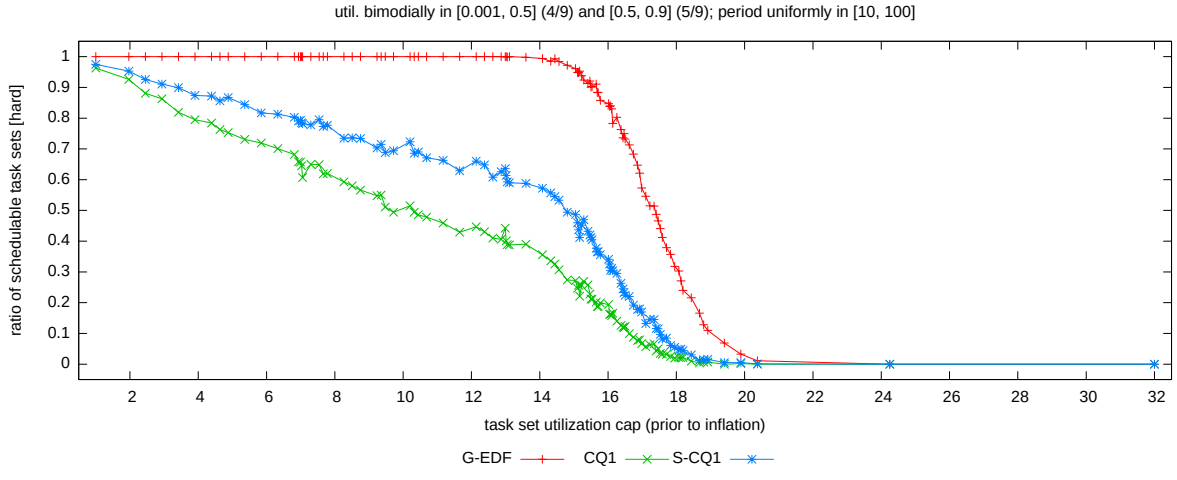

(b)

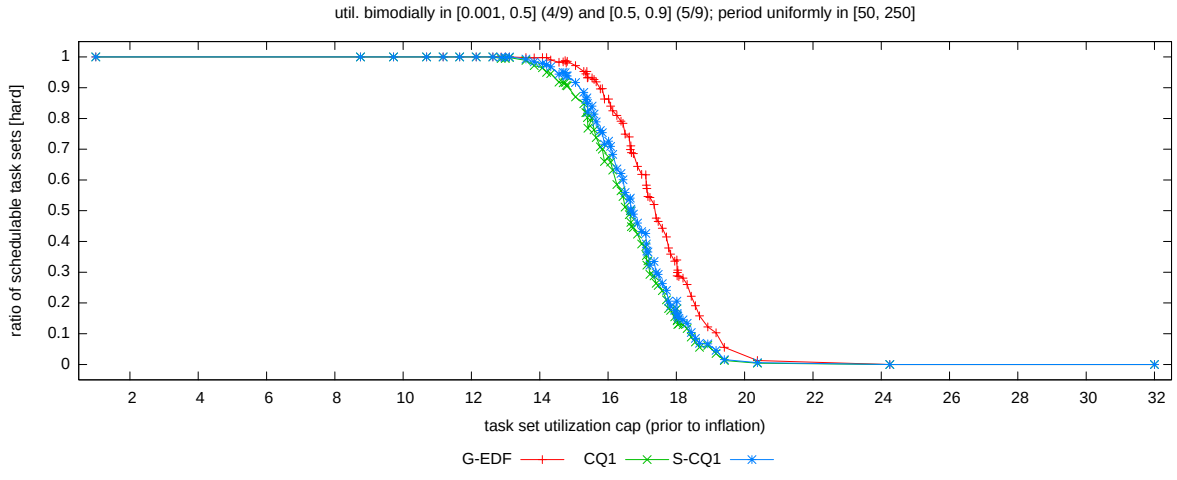

(c)

Figure 143: Comparison of CQ1 and S-CQ1 (aligned vs. staggered quanta) in terms of hard schedulability of task sets with bimodal heavy per-task utilizations and **(a)** short, **(b)** moderate, and **(c)** long periods. These graphs correspond to Fig. 23.

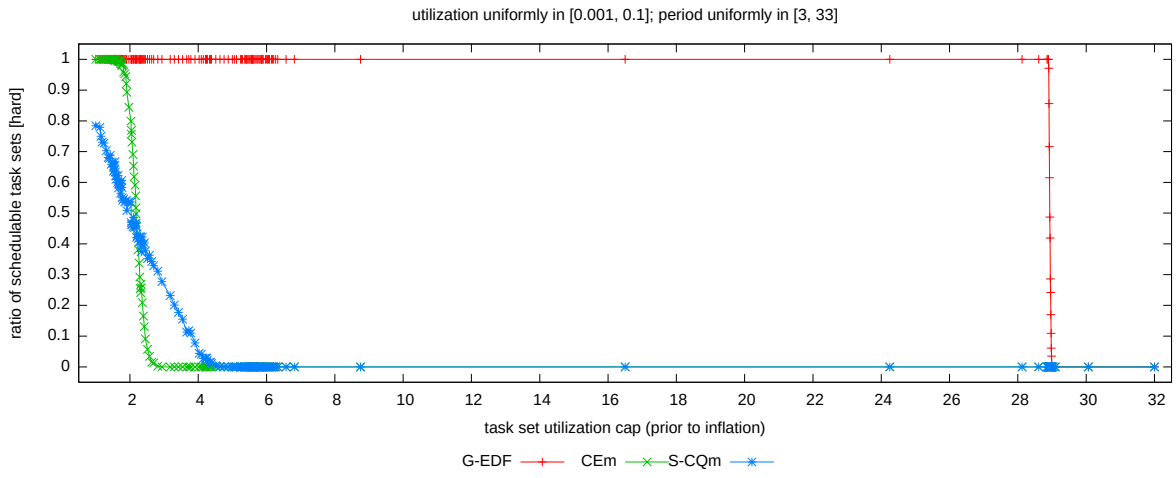

(a)

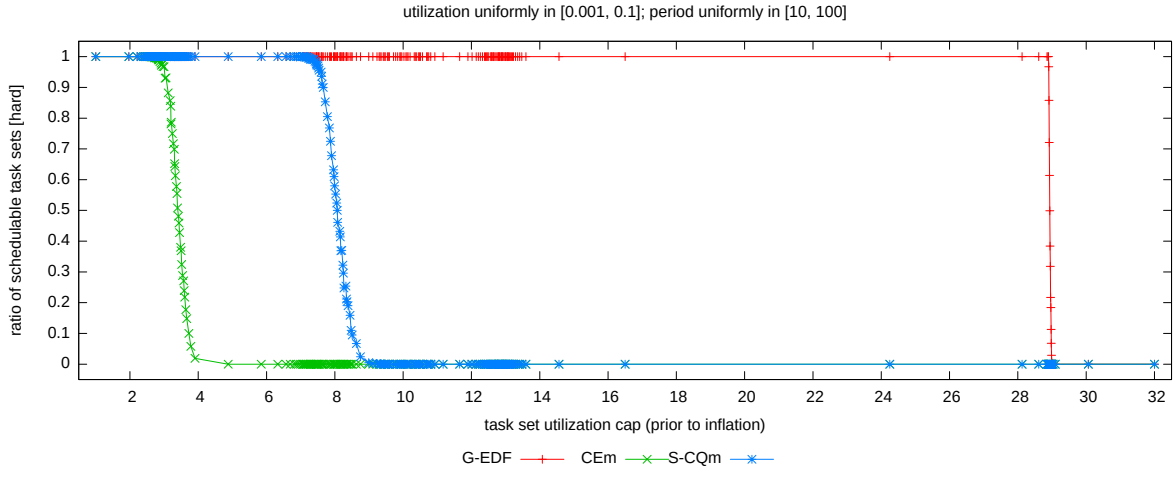

(b)

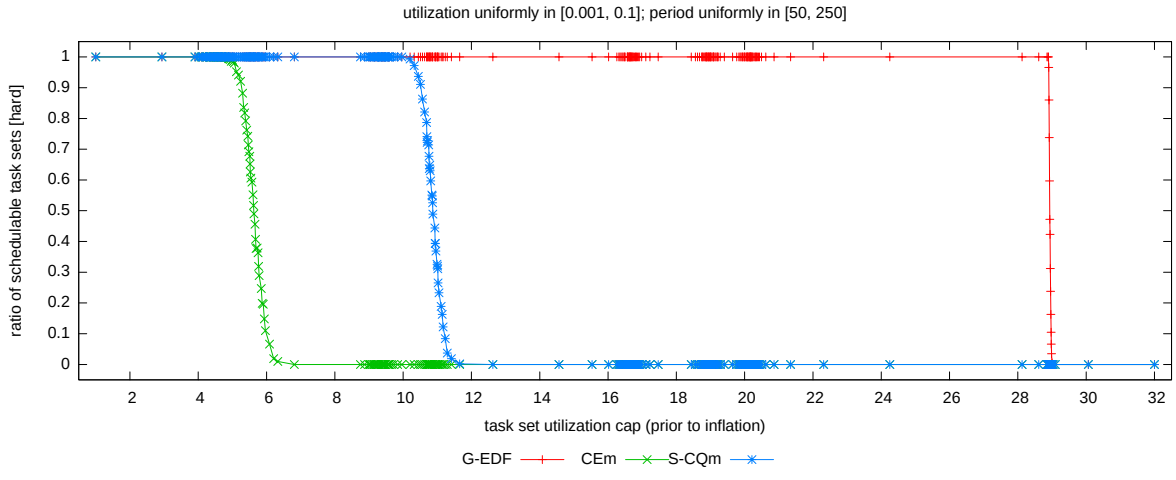

(c)

Figure 144: Comparison of CEm and S-CQm (event- vs. quantum-driven scheduling) in terms of hard schedulability of task sets with uniform light per-task utilizations and **(a)** short, **(b)** moderate, and **(c)** long periods. These graphs correspond to Fig. 18.

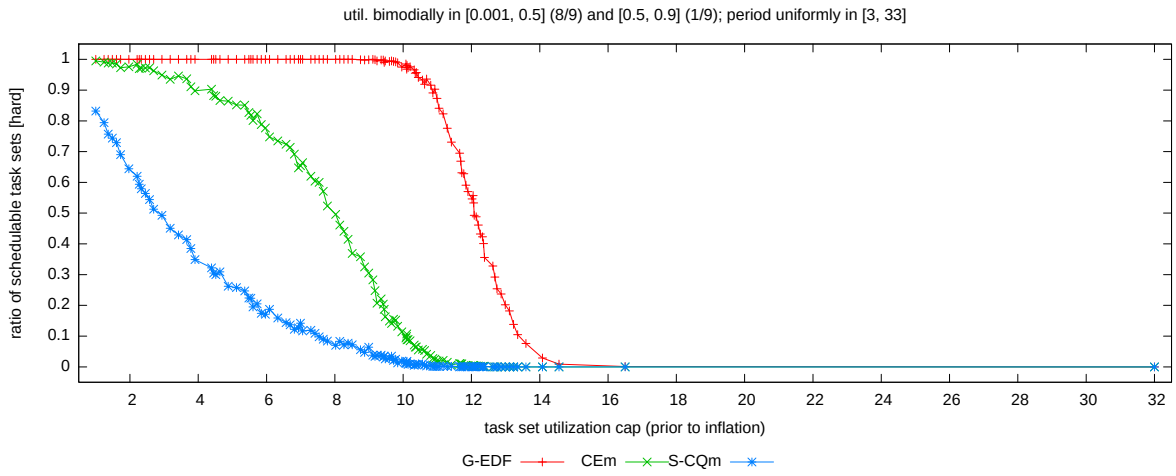

(a)

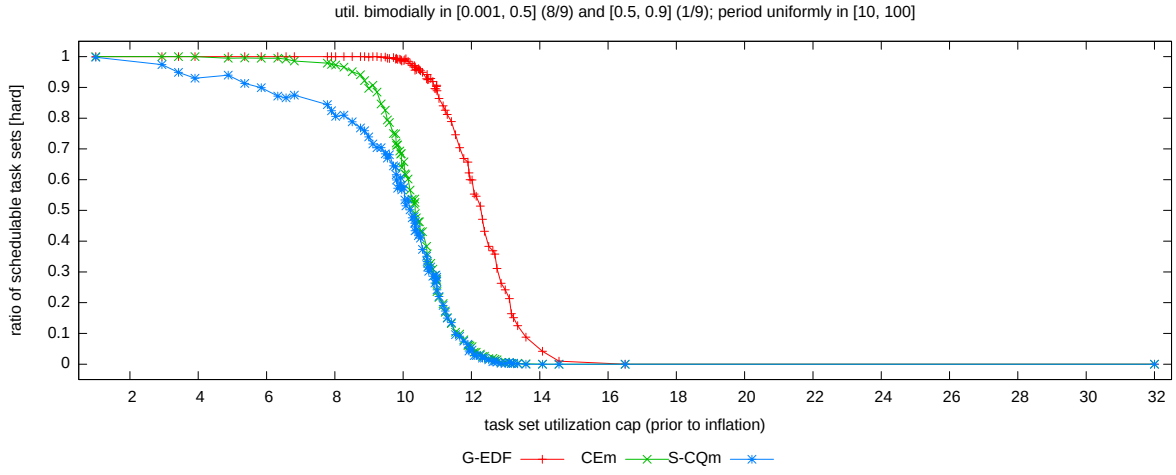

(b)

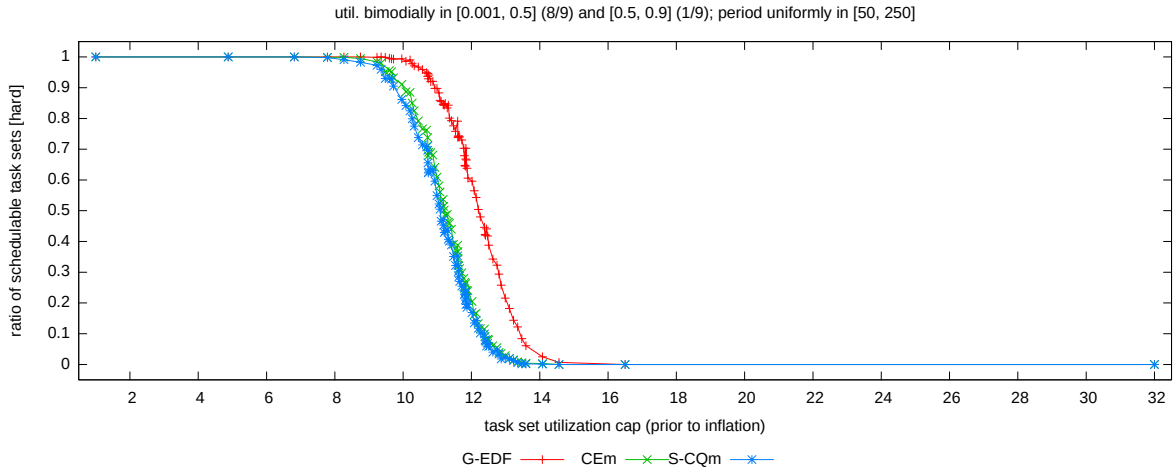

(c)

Figure 145: Comparison of CEm and S-CQm (event- vs. quantum-driven scheduling) in terms of hard schedulability of task sets with bimodal light per-task utilizations and **(a)** short, **(b)** moderate, and **(c)** long periods. These graphs correspond to Fig. 19.

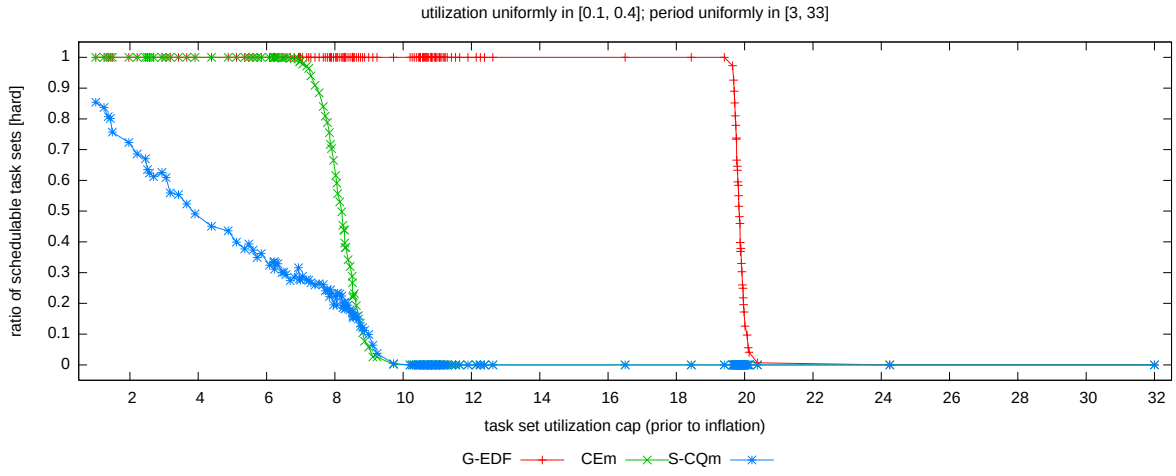

(a)

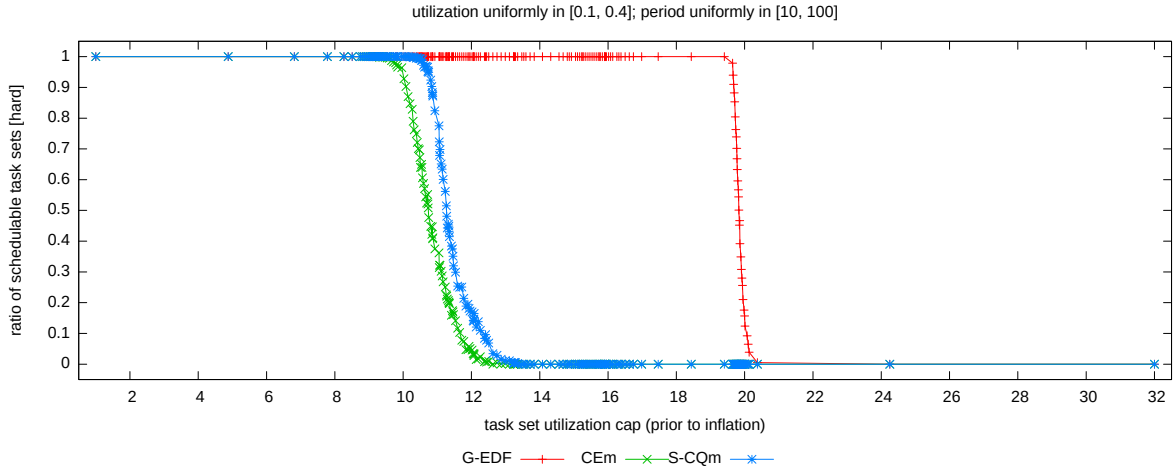

(b)

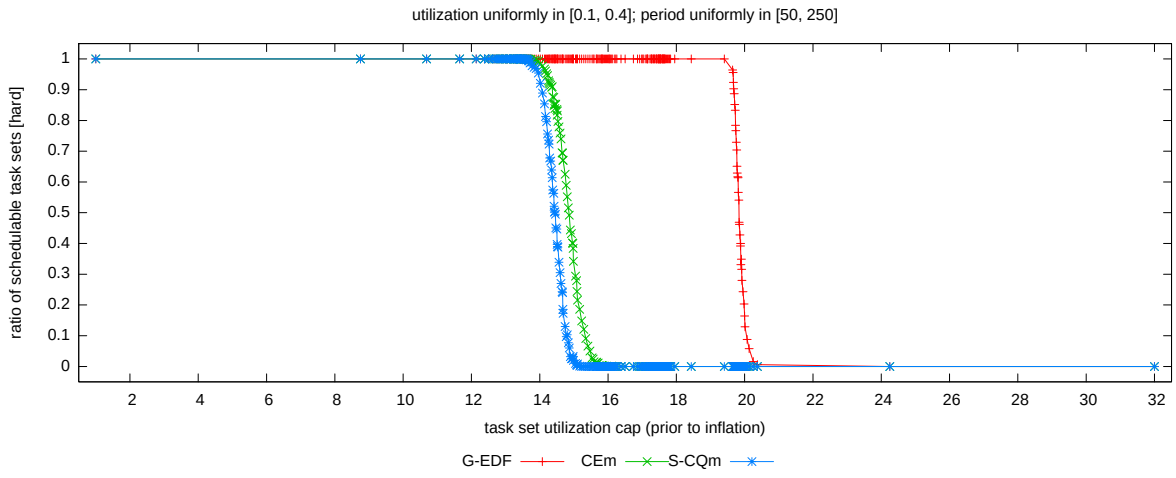

(c)

Figure 146: Comparison of CEm and S-CQm (event- vs. quantum-driven scheduling) in terms of hard schedulability of task sets with uniform medium per-task utilizations and **(a)** short, **(b)** moderate, and **(c)** long periods. These graphs correspond to Fig. 20.

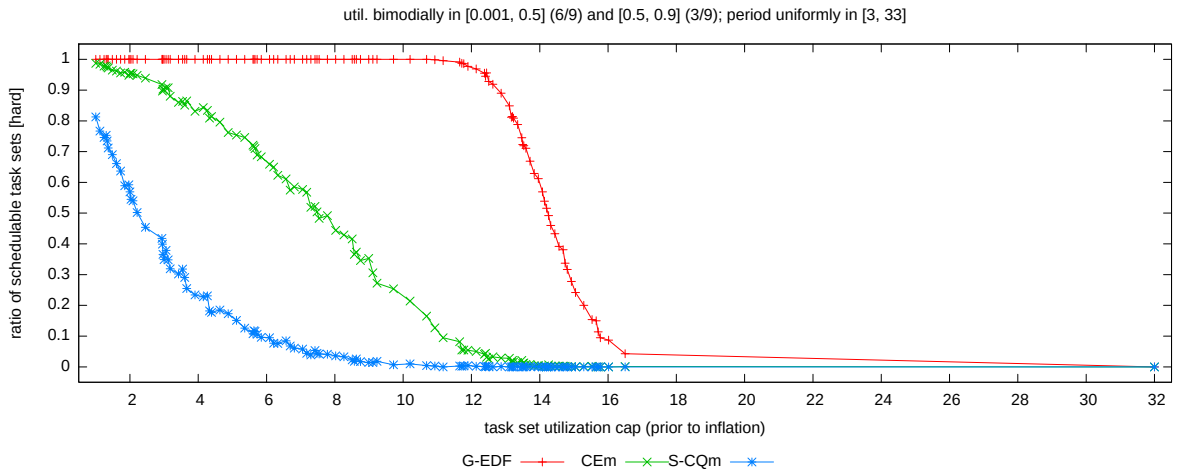

(a)

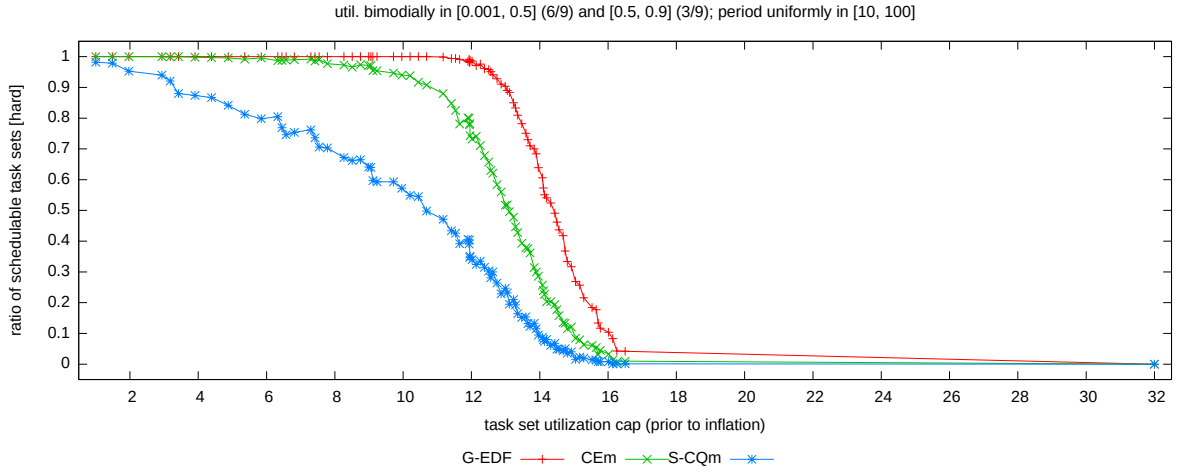

(b)

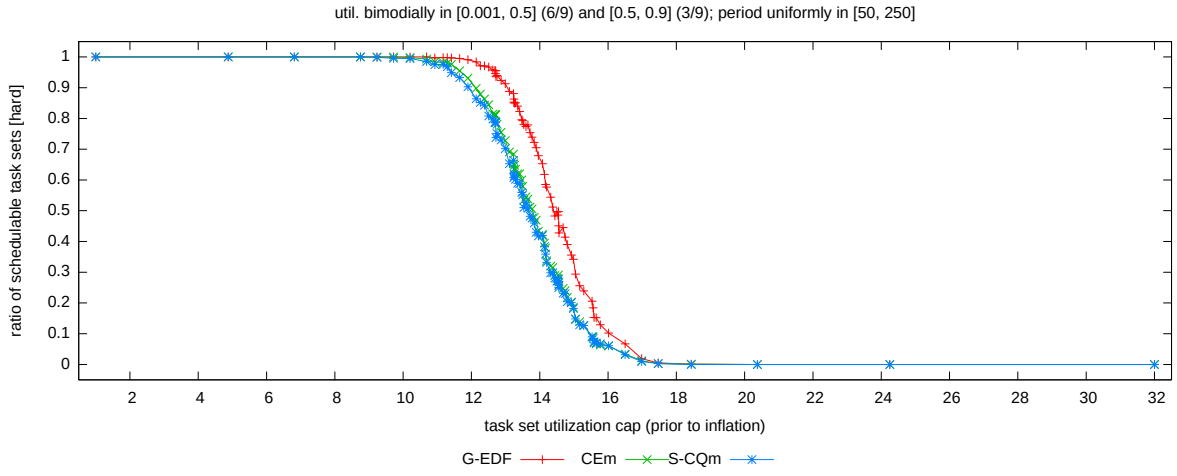

(c)

Figure 147: Comparison of CEm and S-CQm (event- vs. quantum-driven scheduling) in terms of hard schedulability of task sets with bimodal medium per-task utilizations and **(a)** short, **(b)** moderate, and **(c)** long periods. These graphs correspond to Fig. 21.

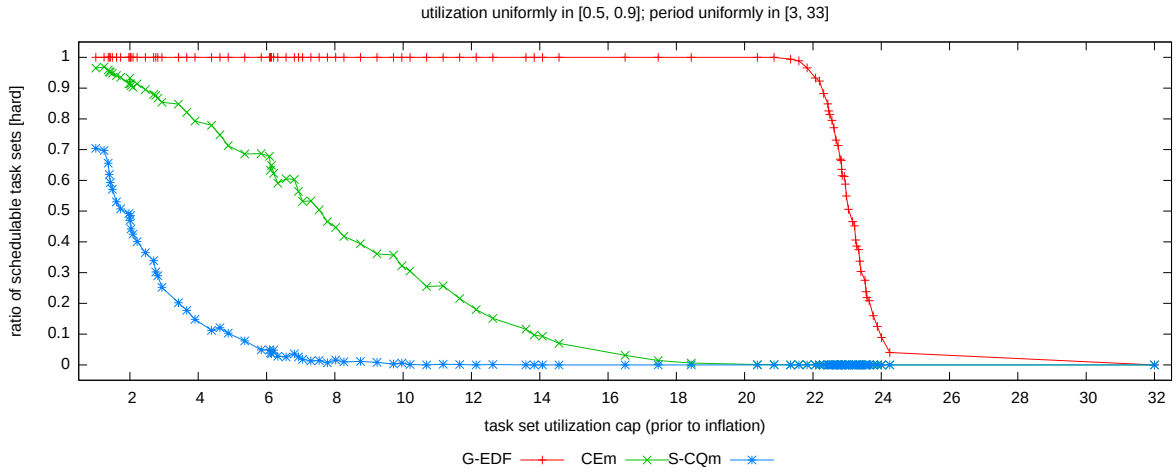

(a)

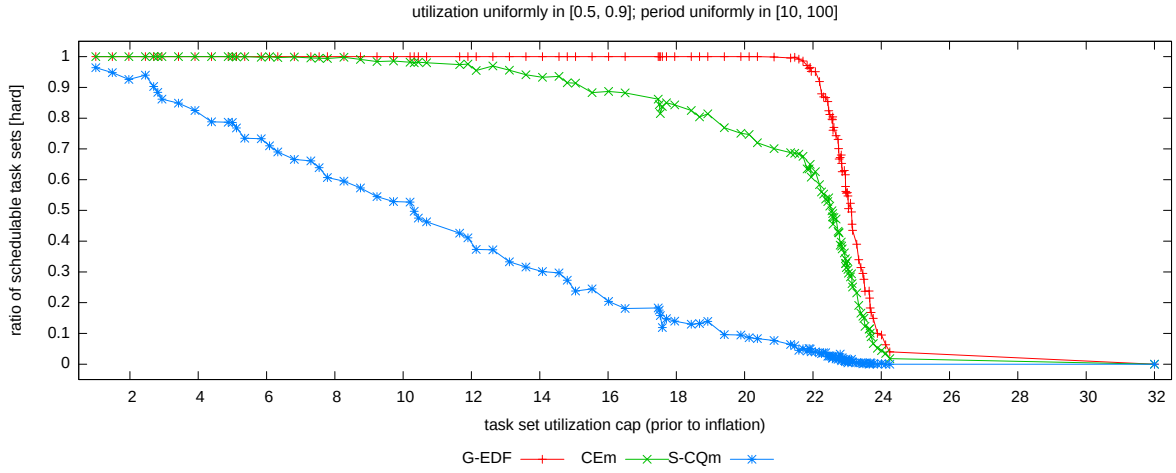

(b)

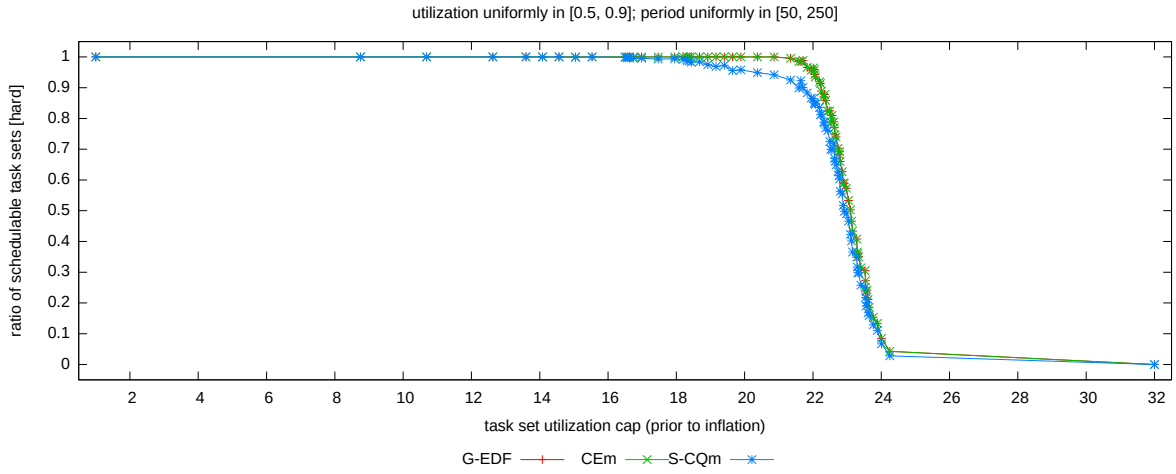

(c)

Figure 148: Comparison of CEm and S-CQm (event- vs. quantum-driven scheduling) in terms of hard schedulability of task sets with uniform heavy per-task utilizations and **(a)** short, **(b)** moderate, and **(c)** long periods. These graphs correspond to Fig. 22.

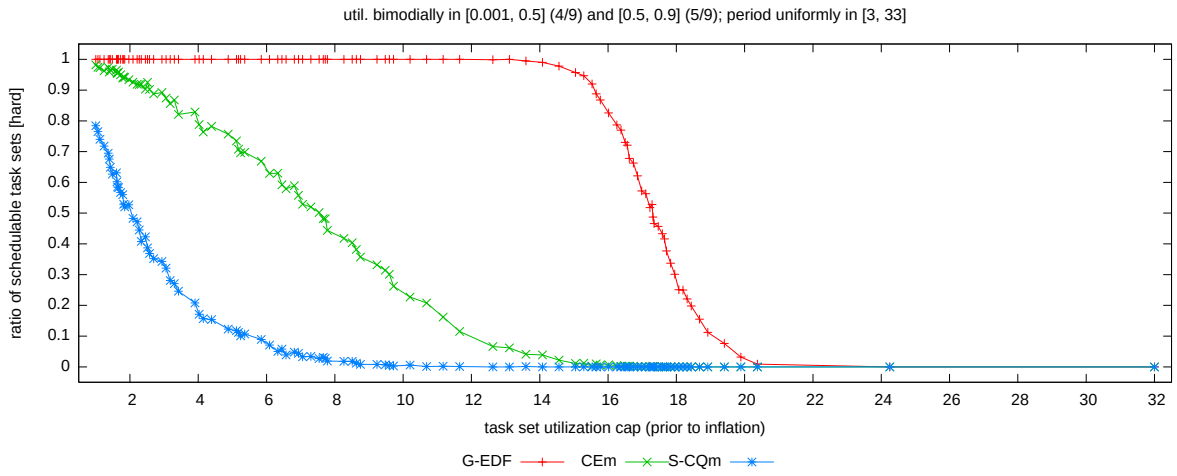

(a)

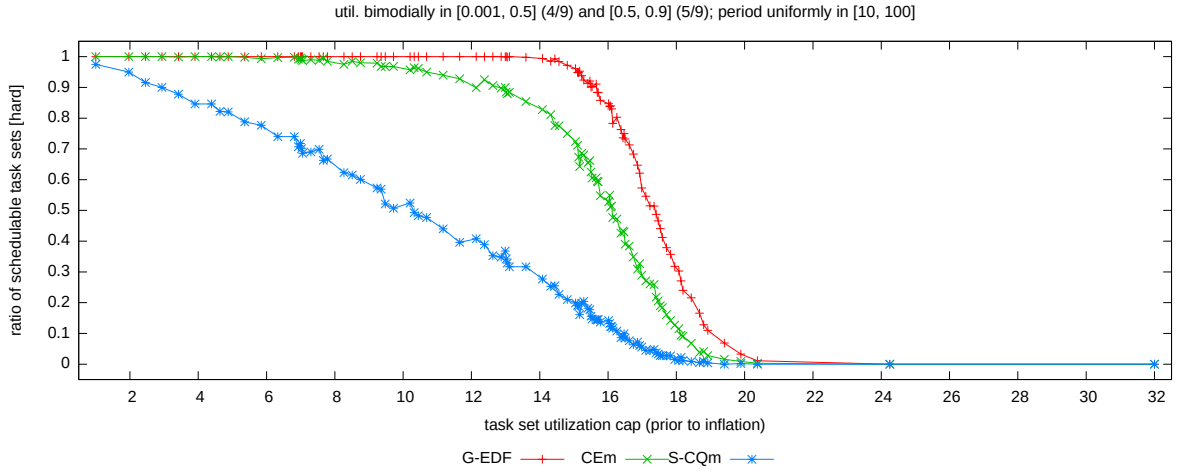

(b)

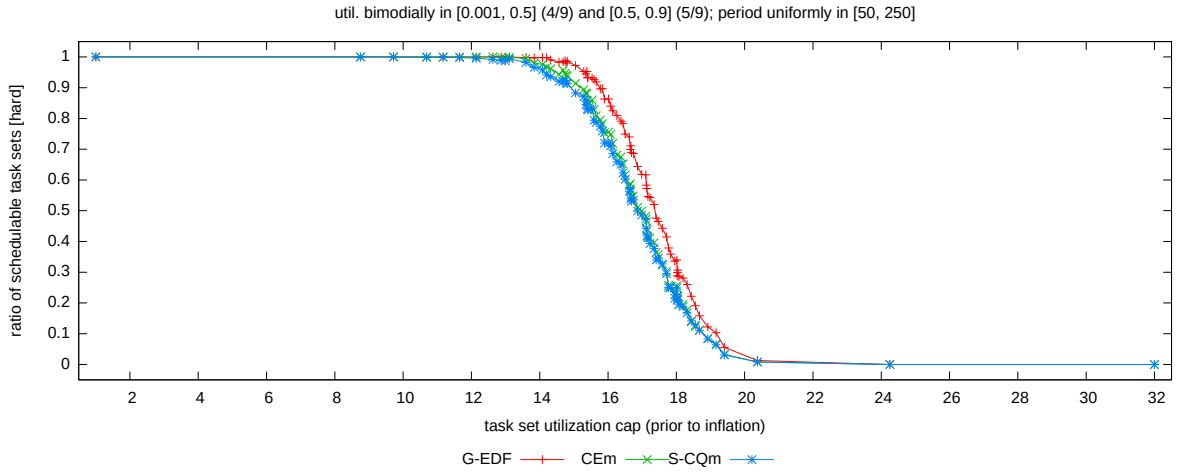

(c)

Figure 149: Comparison of CEm and S-CQm (event- vs. quantum-driven scheduling) in terms of hard schedulability of task sets with bimodal heavy per-task utilizations and **(a)** short, **(b)** moderate, and **(c)** long periods. These graphs correspond to Fig. 23.

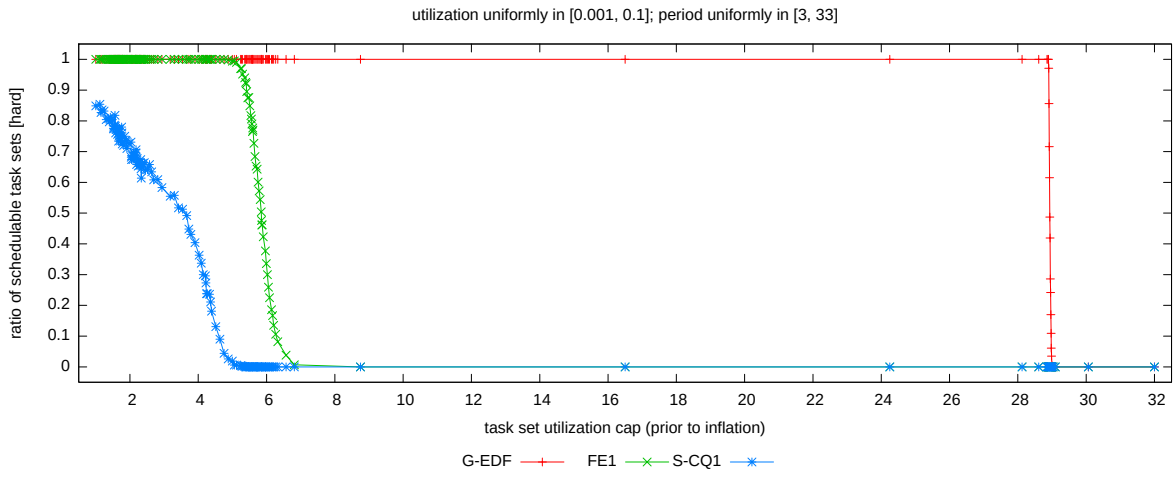

(a)

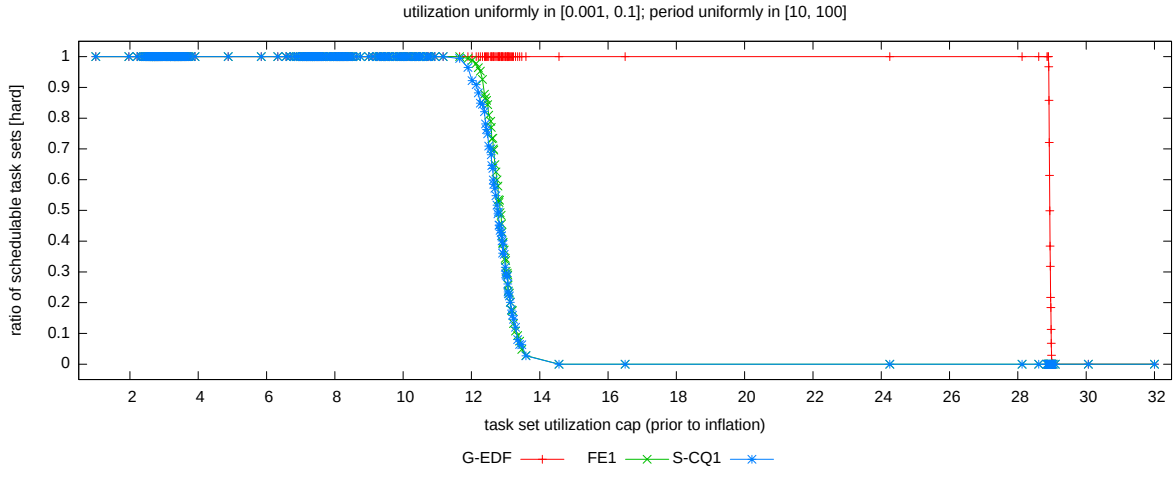

(b)

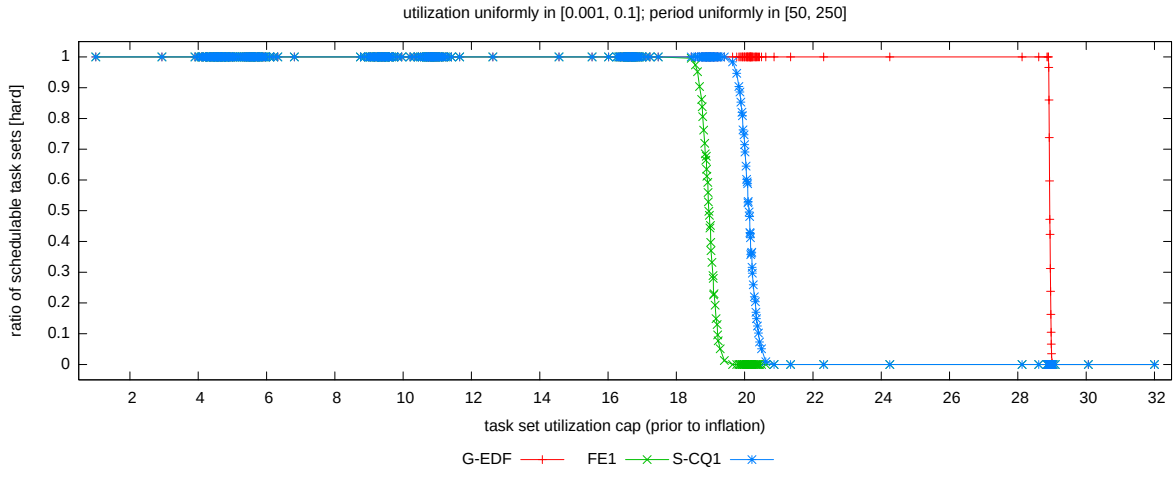

(c)

Figure 150: Comparison of FE1 and S-CQ1 (event- vs. quantum-driven scheduling) in terms of hard schedulability of task sets with uniform light per-task utilizations and **(a)** short, **(b)** moderate, and **(c)** long periods. These graphs correspond to Fig. 18.

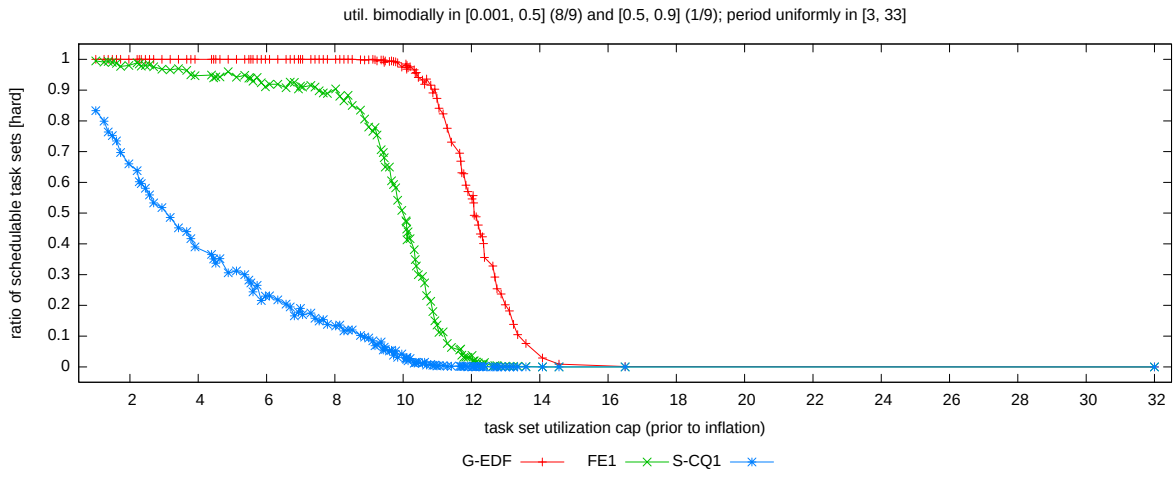

(a)

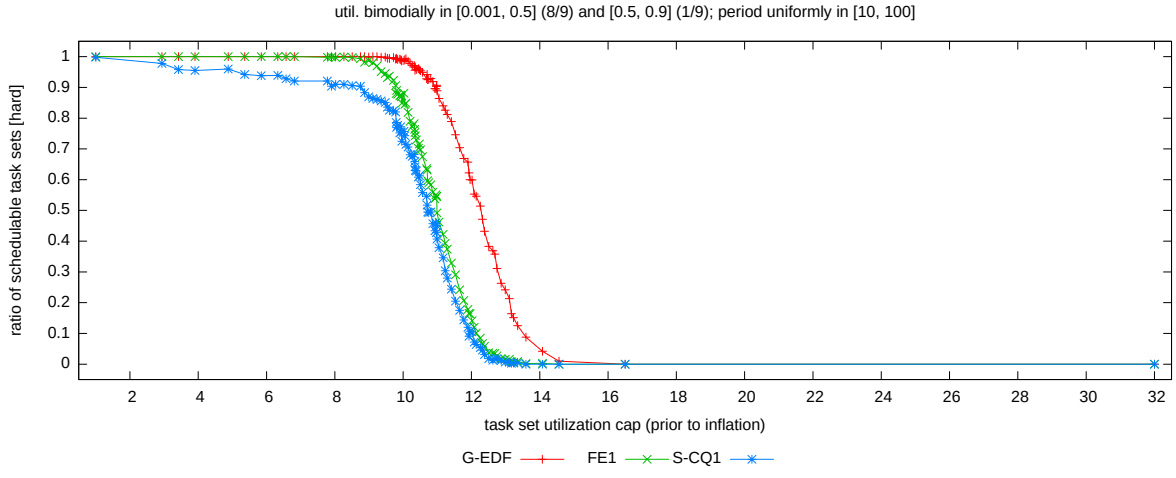

(b)

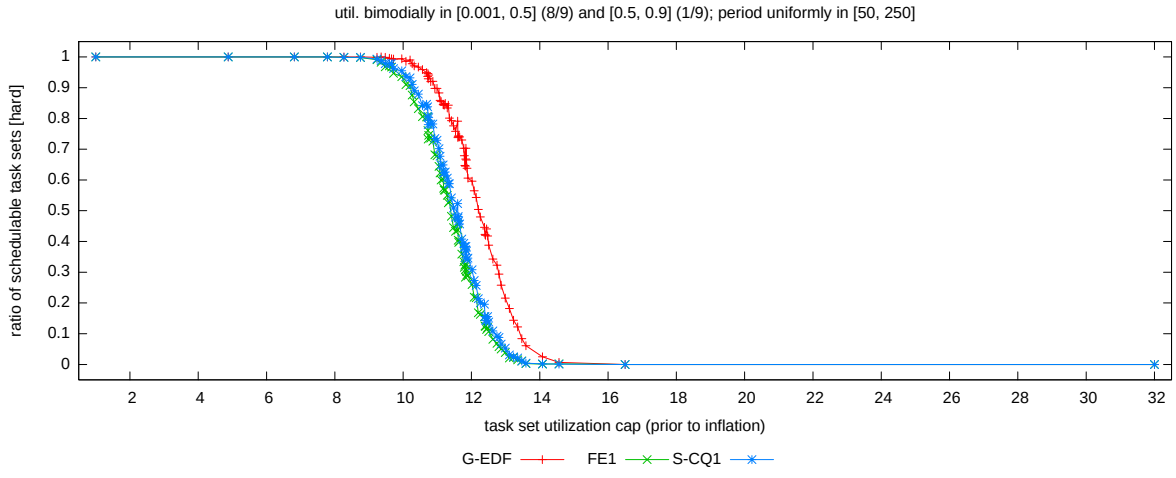

(c)

Figure 151: Comparison of FE1 and S-CQ1 (event- vs. quantum-driven scheduling) in terms of hard schedulability of task sets with bimodal light per-task utilizations and **(a)** short, **(b)** moderate, and **(c)** long periods. These graphs correspond to Fig. 19.

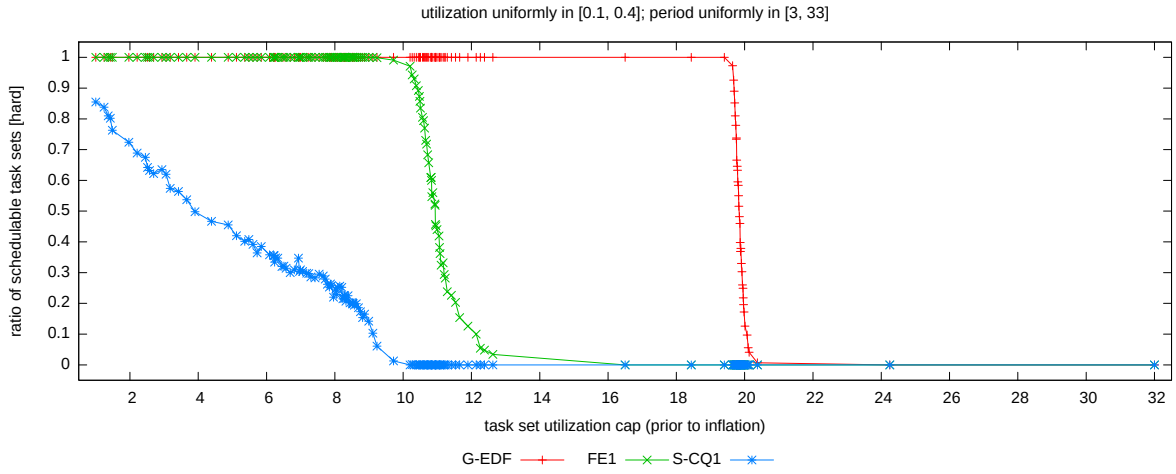

(a)

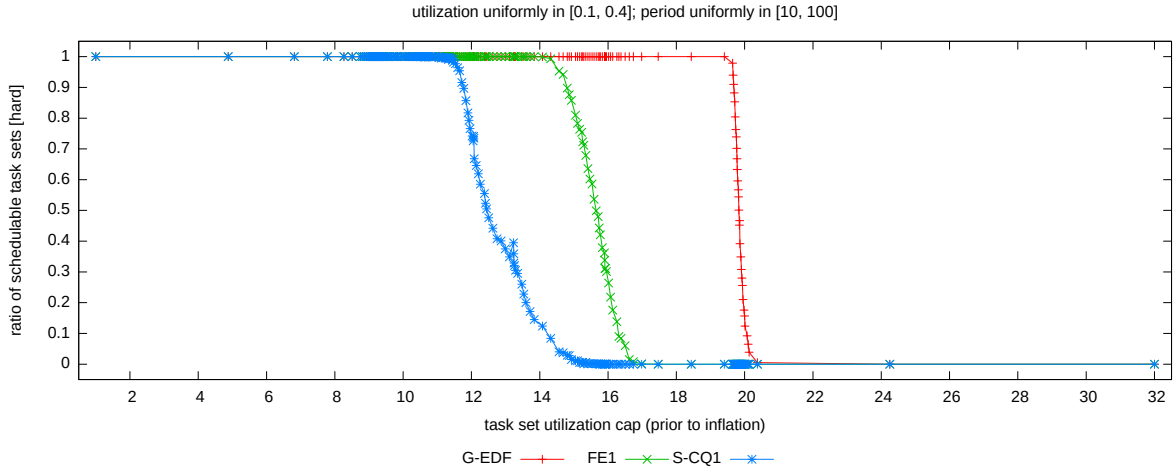

(b)

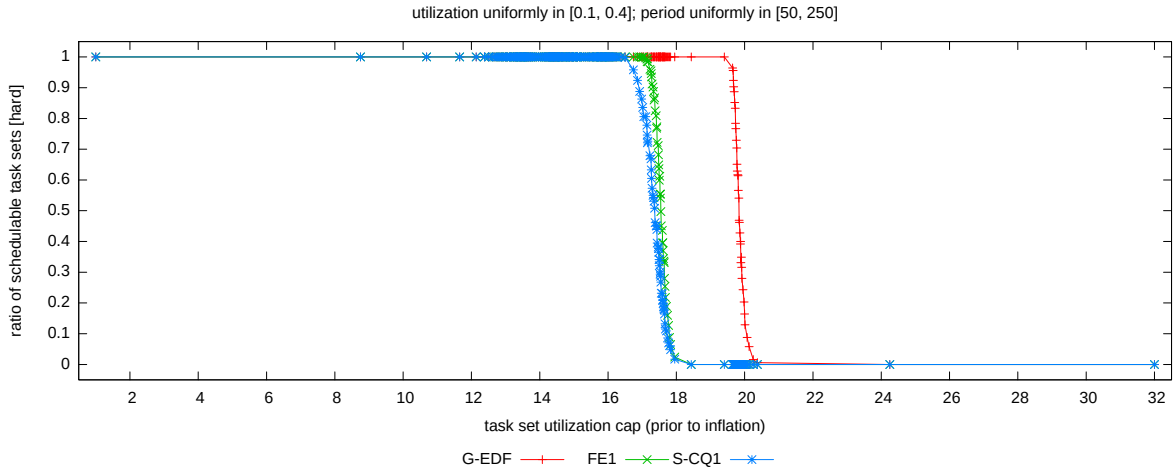

(c)

Figure 152: Comparison of FE1 and S-CQ1 (event- vs. quantum-driven scheduling) in terms of hard schedulability of task sets with uniform medium per-task utilizations and **(a)** short, **(b)** moderate, and **(c)** long periods. These graphs correspond to Fig. 20.

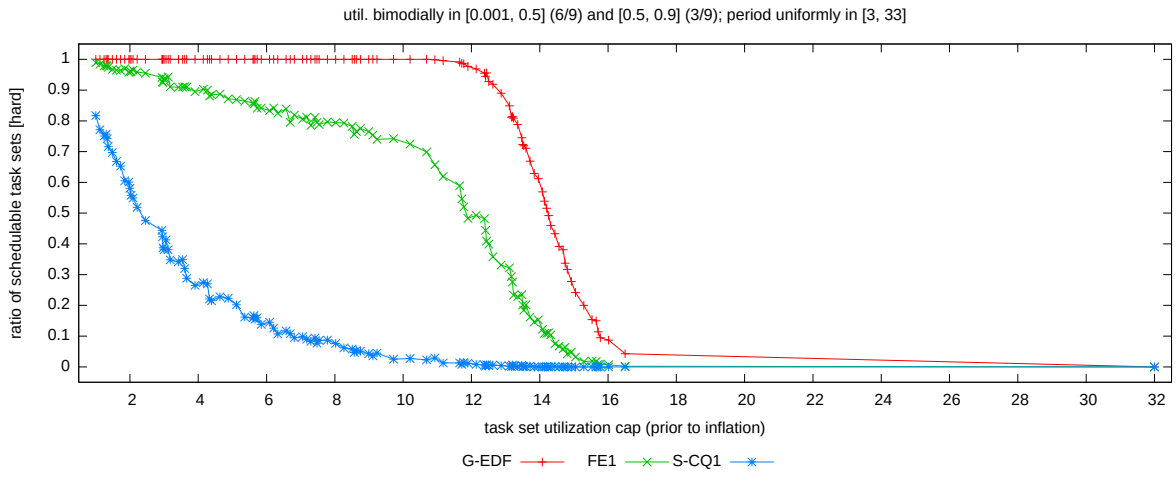

(a)

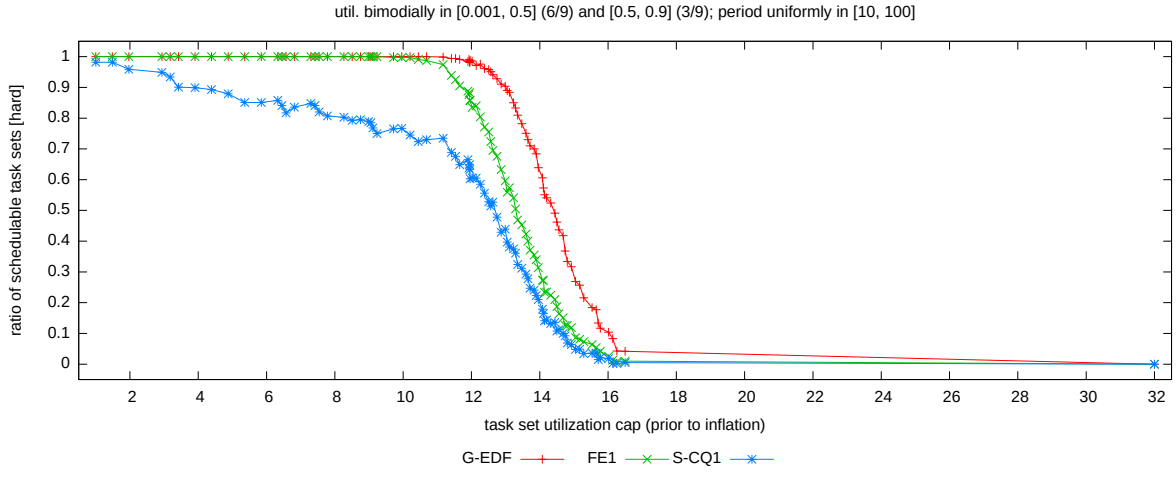

(b)

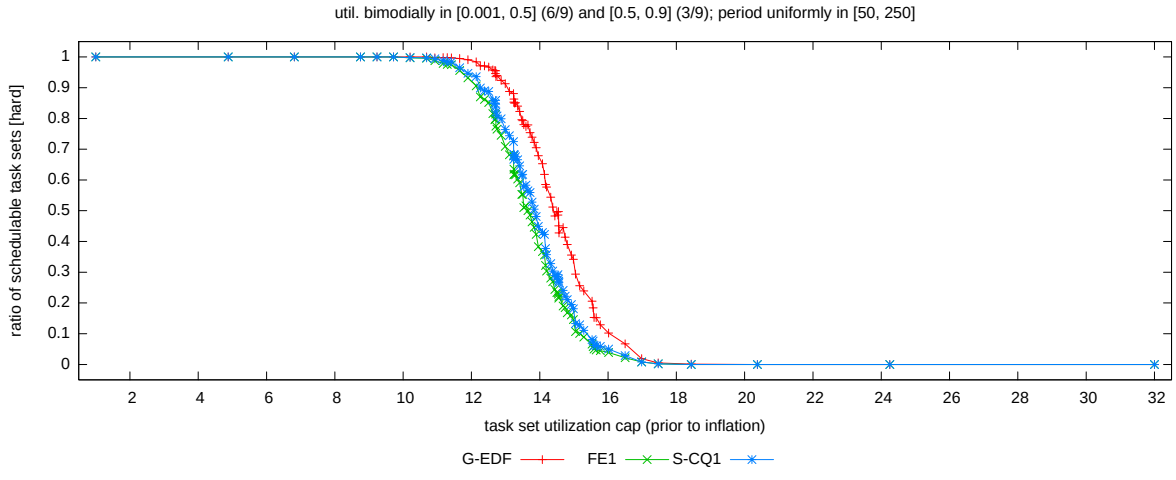

(c)

Figure 153: Comparison of FE1 and S-CQ1 (event- vs. quantum-driven scheduling) in terms of hard schedulability of task sets with bimodal medium per-task utilizations and **(a)** short, **(b)** moderate, and **(c)** long periods. These graphs correspond to Fig. 21.

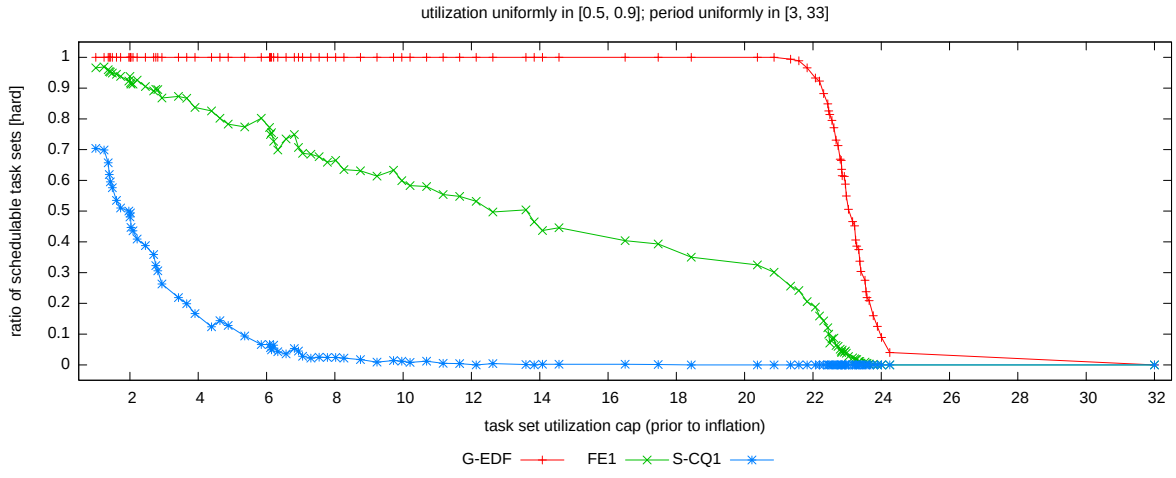

(a)

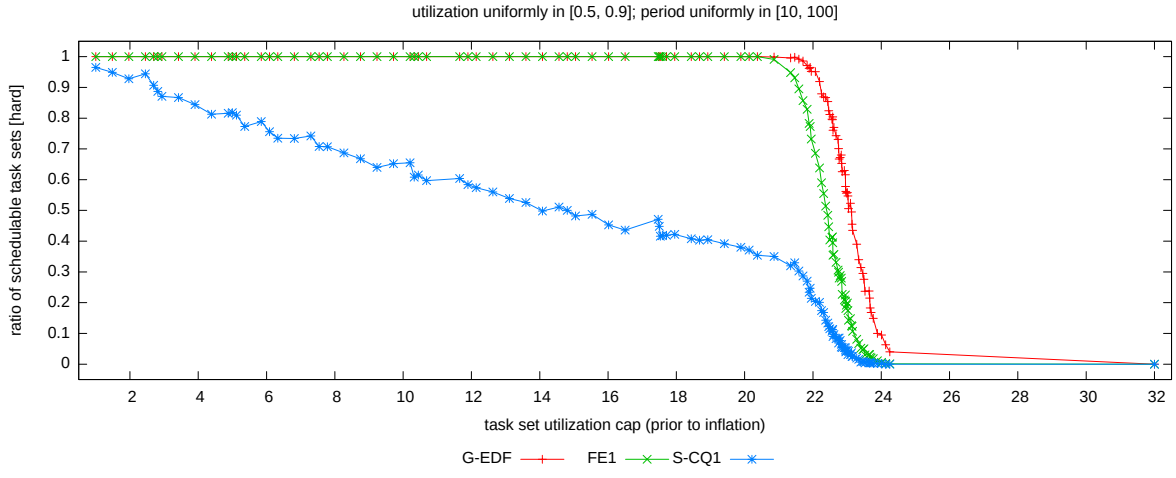

(b)

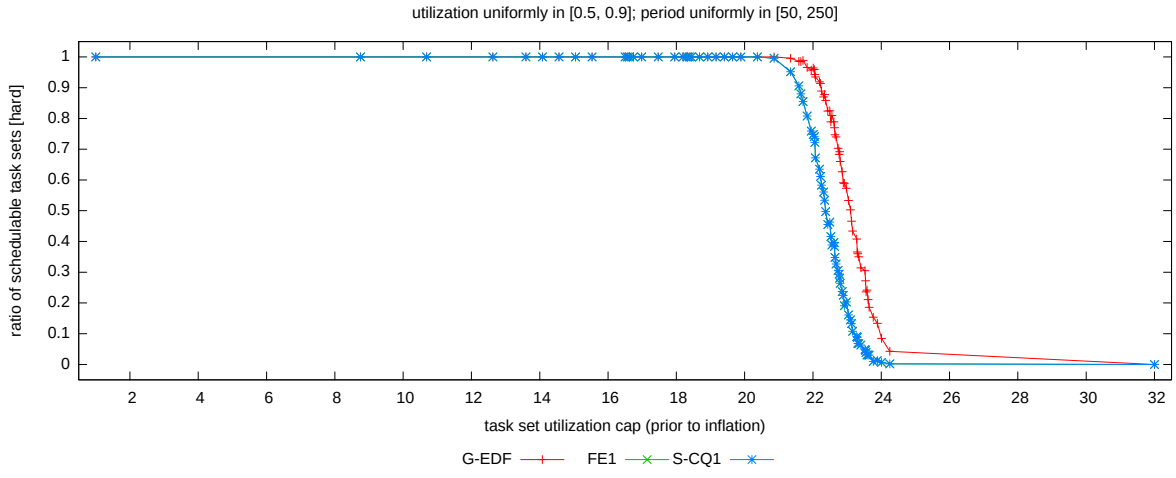

(c)

Figure 154: Comparison of FE1 and S-CQ1 (event- vs. quantum-driven scheduling) in terms of hard schedulability of task sets with uniform heavy per-task utilizations and **(a)** short, **(b)** moderate, and **(c)** long periods. These graphs correspond to Fig. 22.

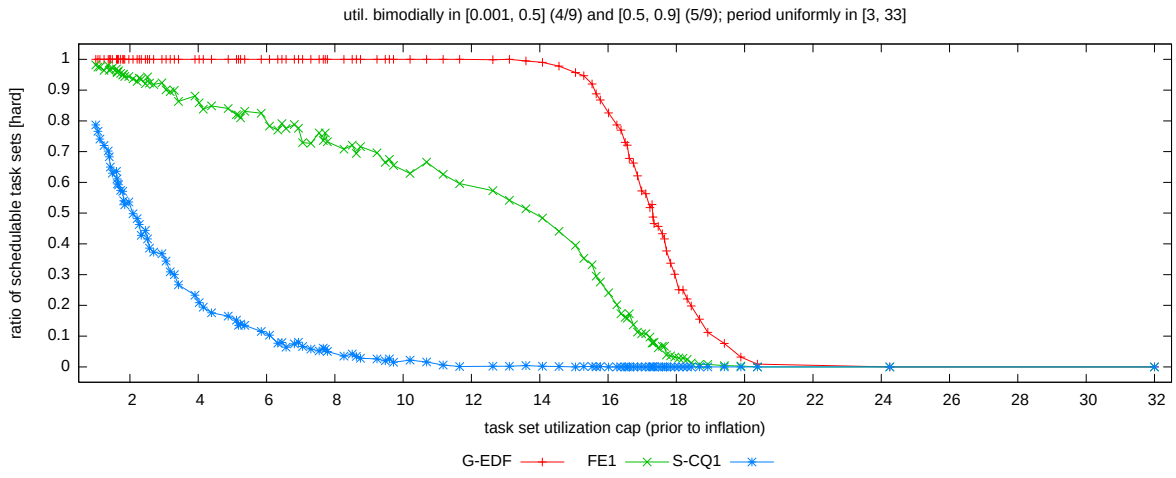

(a)

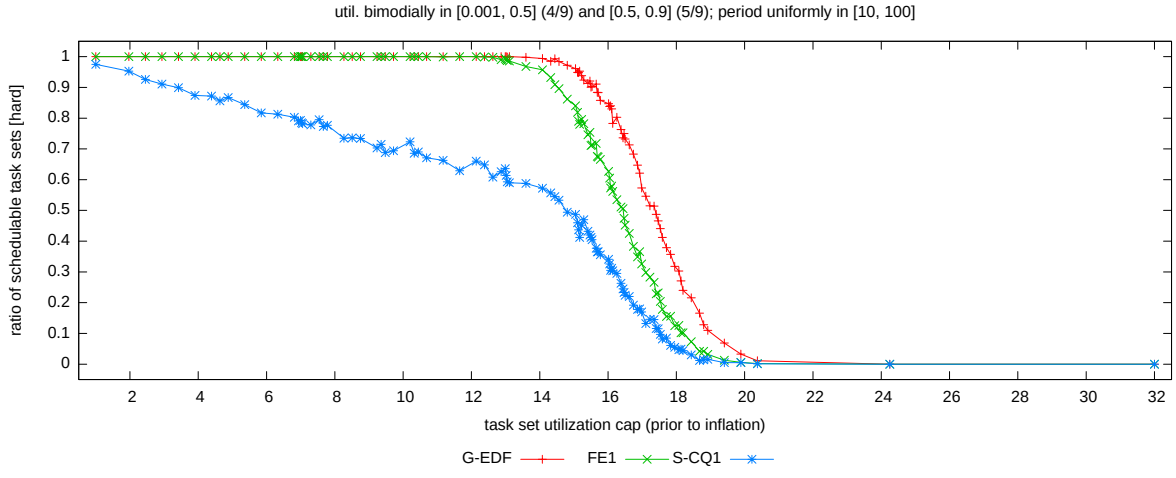

(b)

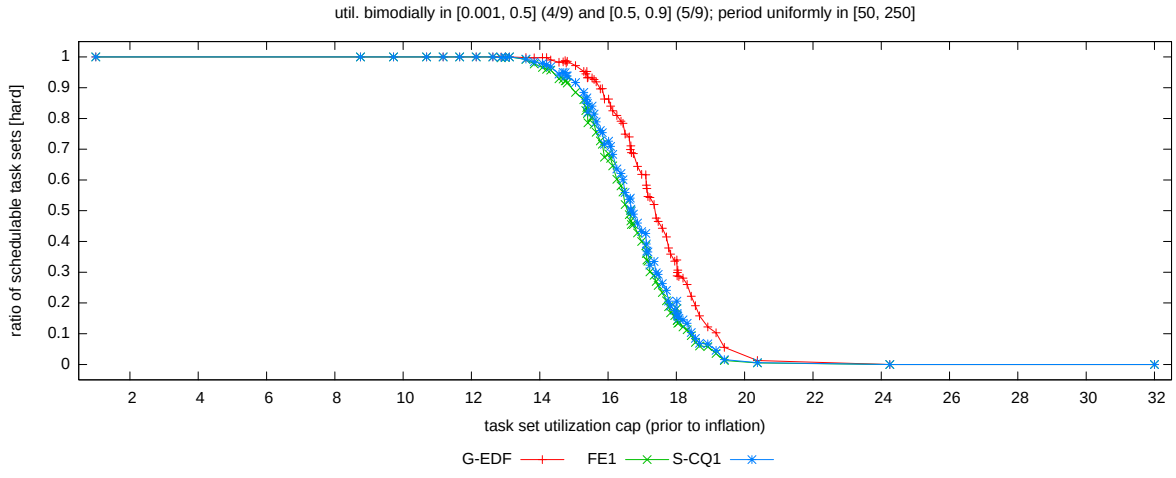

(c)

Figure 155: Comparison of FE1 and S-CQ1 (event- vs. quantum-driven scheduling) in terms of hard schedulability of task sets with bimodal heavy per-task utilizations and **(a)** short, **(b)** moderate, and **(c)** long periods. These graphs correspond to Fig. 23.